PSO 7171 - Oxyfuel Combustion for below zero CO2 emissions

Toftegaard, Maja Bøg; Brix, Jacob; Hansen, Brian Brun; Putluru, Siva Sankar Reddy; Montgomery, Melanie; Hansen, Kim G; Fisker, Dennis; Jensen, Peter Arendt; Glarborg, Peter; Jensen, Anker Degn

Publication date:
2011

Document Version
Publisher's PDF, also known as Version of record

PSO 7171 – Oxyfuel Combustion for below zero CO_2 emissions

Maja B. Toftegaard, Jacob Brix, Brian B. Hansen, Siva Reddy Putluru, Melanie Montgomery, Kim G. Hansen, Dennis Fisker, Peter Arendt Jensen, Peter Glarborg, Anker D. Jensen

May 2011

Department of Chemical and Biochemical Engineering
Technical University of Denmark
Building 229
DK-2800 Kgs. Lyngby
Denmark

Preface

This report describes the work carried out in the PSO project "PSO 7171 – Oxyfuel combustion for below zero CO_2 emissions". The work has been conducted in collaboration between the Departments of Chemical and Biochemical Engineering (CHEC, KT) and Mechanical Engineering (MEK) at the Technical University of Denmark, DONG Energy Power, and Vattenfall. The following people have participated:

DONG Energy Power: Maja Bøg Toftegaard, Bo Sander, Dennis Fisker, Kim Granly Hansen, Søren Lovmand Hvid, Thomas Paarup Pedersen, Willy van Well

Vattenfall: Melanie Montgomery, Karen Pantleon (DTU-MEK), Ole Biede, Marie Anheden, Karin Eriksson

CHEC, DTU-KT: Jacob Brix, Weigang Lin, Brian Brun Hansen, Siva Reddy Putluru, Thomas Wolfe, Workshop, Jan Erik Johnsson, Peter Arendt Jensen, Peter Glarborg, Anker Degn Jensen

Students: Bjørn Maribo-Mogensen, 50 p MSc (KT), Rolf Ringborg, 20 p BSc (KT), Rogelio Rodriguez, 30 p MSc (KT), Jesper Grossman/Morten Petersen, 2*20 p BSc (KT), Magdalena Rogowska, 30 p MSc (MEK)

The project coordinator, Anker Degn Jensen, would like to thank for fruitful cooperation with Energinet.dk, and in particular research administrator Jesper Bergholdt Sørensen.

The project has been run in close cooperation with the PSO project 10069 Advanced Diagnostics of Oxyfuel Combustion Processes. The results of this project have led to improved understanding of the phenomena that was explored in the present project.

Within the project a number of papers, conference contributions, and PhD theses have been produced. Below is a list of the work:

Papers:

Brix, J., Jensen, P.A. and Jensen, A.D. 'Coal devolatilization and char conversion under Suspension fired conditions in O_2/N_2 and O_2/CO_2 atmospheres, Fuel, 2010, **89**, pp. 3373–3380.

Brix, J., Jensen, P.A. and Jensen, A.D., 'Modeling char conversion under suspension fired conditions in O_2/N_2 and O_2/CO_2 atmospheres', Fuel, 2011, **90**, pp. 2224–2239.

Brix, J., Petersen, M.S., Glarborg, P., Jensen, P.A. and Jensen, A.D. 'Coal char reactivity: A thermogravimetric study on chars obtained in O_2/N_2 and O_2/CO_2 in an entrained flow reactor under suspension fired conditions and in a TGA, submitted to Fuel.

Brix, J., Toftegaard, M., Jensen, P.A., Glarborg, P., Jensen, A.D. 'Oxy-fuel forbrænding af fossile brændsler', Dansk Kemi, 2009, 90, p. 14-15.

Hansen, B.B., Fogh, F., Knudsen, N.O. and Søren Kiil, 'Performance of a Wet Flue Gas Desulfurization Pilot Plant under Oxy-Fuel Conditions', Industrial and Engineering Chemistry Research, 2011, dx.doi.org/10.1021/ie1022173.

Toftegaard, M.B., Brix, J., Jensen, P.A., Glarborg, P. and Jensen, A.D. 'Oxy-fuel combustion of solid fuels', Progress in Energy and Combustion Science, 2010, **36**, pp. 581-625.

Anders Hjörnhede, Melanie Montgomery, Martin Bjurman, Pamela Henderson, Alexander Gerhardt, 'Preliminary experiences with material testing at the oxyfuel pilot plant at schwarzepumpe', 9th Liege Conference : Materials for Advanced Power Engineering 2010, Proceedings, pp. 1220-1236.

Conference contributions:

Brix, J., Jensen P.A. and Jensen, A.D. 'Oxyfuel combustion of solid fuels', work in progress poster, 32nd Symposium (International) on Combustion, 2008, 3-8 august, Montreal, Canada.

Jacob Brix, Peter Arendt Jensen, Peter Glarborg, Anker Degn Jensen, 'Char Conversion under Suspension Fired Conditions in O_2/N_2 and O_2/CO_2 Atmospheres', 2011, Swedish-Finnish Flame Days, January 26-27, Piteå Havsbad Conference Hotel, Piteå, Sweden (oral).

Jacob Brix, Peter Arendt Jensen, Anker Degn Jensen, 1st Oxyfuel Combustion Conference, Coal Devolatilization and Char Conversion in Oxy-Fuel Combustion, Cottbus, Germany, 8-11 September 2009 (poster).

PhD Theses:

Jacob Brix, Oxyfuel combustion of solid fuels, PhD thesis, Department of Chemical and Biochemical Engineering, Technical University of Denmark, 2011.

Maja B. Toftegaard, Oxyfuel Combustion of Coal and Biomass, PhD thesis, Department of Chemical and Biochemical Engineering, Technical University of Denmark, 2011.

Abstract

The reduction of CO_2 emissions is of highest concern in relation to limiting the anthropogenic impacts on the environment. Primary focus has gathered on the large point sources of CO_2 emissions constituted by large heat and power stations and other heavy, energy-consuming industry. Solutions are sought which will enable a significant reduction of the anthropogenic CO_2 emissions during the transformation period from the use of fossil fuels to renewable sources of energy. Carbon capture and storage (CCS) has the potential to significantly reduce CO_2 emissions from power stations while allowing for the continuous utilisation of the existing energy producing system in the transformation period. Oxyfuel combustion is one of the possible CCS technologies which show promising perspectives for implementation in industrial scale within a relatively short period of time. Oxyfuel combustion deviates from conventional combustion in air by using a mixture of pure oxygen and recirculated flue gas as the combustion medium thereby creating a flue gas highly concentrated in CO_2 making the capture process economically more feasible compared to technologies with capture from more dilute CO_2 streams. This project has investigated a number of the fundamental and practical issues of the oxyfuel combustion process by experimental, theoretical, and modelling investigations in order to improve the knowledge of the technology. The subjects investigated cover: general combustion characteristics of coal and biomass (straw) and mixtures thereof, formation and emission of pollutants, ash characteristics, flue gas cleaning for SO_2 by wet scrubbing with limestone and for NO_x by selective catalytic reduction (SCR), corrosion of boiler heat transfer surfaces, operation and control of large suspension-fired boilers, and the perspectives for the implementation of oxyfuel combustion s a CO_2 sequestration solution in the Danish power production system. Regarding the fundamental combustion characteristics (combustion, emissions, and ash), the project has not identified any disqualifying characteristics. On the contrary, oxyfuel has the potential to improve fuel burnout and significantly reduce NO_x emissions compared to conventional combustion in air. However, the significantly increased levels of CO_2, H_2O, CO (and SO_2) within the boiler will have a negative effect on the risk of corrosion through a number of mechanisms such as carburisation (CO_2 and H_2O), water wall corrosion due to reducing conditions (CO), and both high- and low-temperature sulphur-induced corrosion (SO_2/SO_3). Both the wet flue gas desulphurisation and the selective catalytic reduction process for NO_x removal have shown satisfying performance in oxyfuel atmospheres. At the same time, process calculations have shown that it is possible to retrofit an existing boiler to oxyfuel combustion. Different configurations; cold and hot recirculation of flue gas; are possible each with differences in the associated uncertainty, necessary level of process re-design, and reductions in the plant efficiency. It was generally seen that the configuration with the highest level of re-design, i.e. hot recirculation of flue gas, provided the possibility of the highest electrical efficiency but also the largest number of technical challenges. Generally, it has been concluded that it would be beneficial to mainly apply the oxyfuel technology to new-build plants rather than as a retrofit solution. In that respect, it is unlikely that oxyfuel power plants are commissioned in Denmark before 2020. However, in order to meet the very strict demands for the reduction of CO_2 emissions within EU by 2050 application of oxyfuel combustion capture at power stations burning CO_2 neutral fuels (biomass) could be an advantageous solution due to the associated, negative CO_2 emissions.

Table of Contents

APPENDIX C
Jacob Brix, Peter Arendt Jensen, and Anker Degn Jensen. Coal Devolatilization and Char Conversion under Suspension Fired Conditions in O_2/N_2 and O_2/CO_2 Atmospheres. Fuel, 2010, 89, pp. 3373–3380.

APPENDIX D
Jacob Brix, Morten Storgaard Petersen, Jesper Banke Grossmann, Peter Glarborg, Peter Arendt Jensen, and Anker Degn Jensen. Coal Char Reactivity: A Thermogravimetric Study on Chars Obtained in O_2/N_2 and O_2/CO_2 in an Entrained Flow Reactor Under Suspension Fired Conditions and in a TGA. Submitted to Fuel, 2011.

APPENDIX E
Jacob Brix, Peter Arendt Jensen, and Anker Degn Jensen. Modeling Char Conversion under Suspension Fired Conditions in O_2/N_2 and O_2/CO_2 Atmospheres. Fuel, 2011, 90, pp. 2224–2239.

APPENDIX F
Brian B. Hansen, Folmer Fogh, Niels Ole Knudsen, and Søren Kiil. Performance of a wet flue gas desulphurisation pilot plant under oxy-fuel conditions. Industrial and Engineering Chemistry Research, 2011, dx.doi.org/10.1021/ie1022173.

APPENDIX G
Putluru Siva Sankar Reddy, Jan Erik Johnsson, Rolf Ringborg, and Anker Degn Jensen. SCR catalyst performance under oxyfuel conditions. CHEC Research centre, Department of Chemical and Biochemical Engineering Technical University of Denmark. 2010.

APPENDIX H
Melanie Montgomery. Literature survey: Potential corrosion problems in oxyfuel environments, December 2008.

APPENDIX I
Anders Hjörnhede, Melanie Montgomery, Martin Bjurman, Pamela Henderson, and Alexander Gerhardt. Preliminary experiences with material testing at the oxyfuel pilot plant at Schwarzepumpe, 9th Liege Conference: Materials for Advanced Power Engineering 2010, Proceedings

APPENDIX J
Dennis Fisker. Oxyfuel combustion for below zero CO_2 emission, Procesteknisk rapport. DONG Energy, July 2010.

APPENDIX K
Kim Granly Hansen. Oxyfuel combustion for below zero CO_2 emission, CFD report. DONG Energy, March 2011.

1 Introduction

Global warming is probably the largest environmental challenge of our time. The main reason for global warming is suggested to be the increased levels of greenhouse gases, most importantly carbon dioxide, in the atmosphere. The main source for anthropogenic carbon dioxide emissions is the combustion of fossil fuels and hence, due to the fact that power plants constitute large point sources of CO_2 emissions, the power and heat producing sector is facing a continuously increasing demand to reduce its emissions of CO_2. Even though renewable energy is becoming increasingly important, the change of technologies and the transformation of the energy supply infrastructure is a slow process and the world will depend on fossil fuels for energy supply for a long time to come.

Coal is the most abundant fossil fuel with widespread resources all over the world. Nevertheless, coal will only be an option for the future if it is possible for reduce the emissions of CO_2 in a cost-efficient manner. Besides the continuous work related to increasing the fuel conversion efficiency in power plants and switching to fuels with lower fossil carbon content than coal which both will decrease the CO_2 emissions on a longer timeframe, technologies are sought which will enable a near elimination of the emission of CO_2 from the existing fleet of power plants in the transitional period.

Danish power plants are among the world champions in efficient use of coal and, additionally, significant experience has been collected on co-combustion of fossil fuels (mainly coal) and biomass in suspension-fired units. By combining fossil fuel/biomass co-fired processes (or possibly even pure biomass combustion) with CO_2 separation and storage the result becomes a net extraction of CO_2 from the atmosphere, potentially reversing the global warming.

Three main technology tracks for CO_2 capture from power plants have been identified. The processes are shown schematically in Figure 1-1.

Post-combustion capture collects CO_2 by scrubbing a conventional flue gas stream dilute in CO_2 (about 14 vol%). The dilution makes this a rather expensive approach. Pre-combustion capture is coupled to gasification and is as such not applicable as a retrofit solution to the existing fleet of suspension-fired boilers. In an oxyfuel power plant the combustion takes place in an atmosphere of pure oxygen and recirculated flue gas producing a flue gas that mainly consists of water and CO_2 since nitrogen has been eliminated from the combustion medium. The high concentration of CO_2 in the flue gas stream makes it economically more feasible to sequester CO_2 for subsequent deposition or exploitation than what is the case for post-combustion capture. However, at present, techno-economic studies have not identified any significant differences in the overall operating expenses between the post-combustion and oxyfuel combustion capture technologies. However, oxyfuel combustion capture holds the potential of significant reductions in the operating expenses if novel air separation technologies could be implemented.

The oxyfuel technology introduces large changes to the power plant layout compared to the post-combustion process which is a tail-end solution. More research on the oxyfuel technology is thus needed in order to fully clarify the impacts of its application. A main area of interest is the changes to the combustion process due to the change from air as oxidant to the mixture of oxygen and recirculated flue gas. The changes to the combustion process will have implications on the entire power plant cycle and there is a lack of knowledge on many fundamental and practical issues of the oxyfuel combustion process.

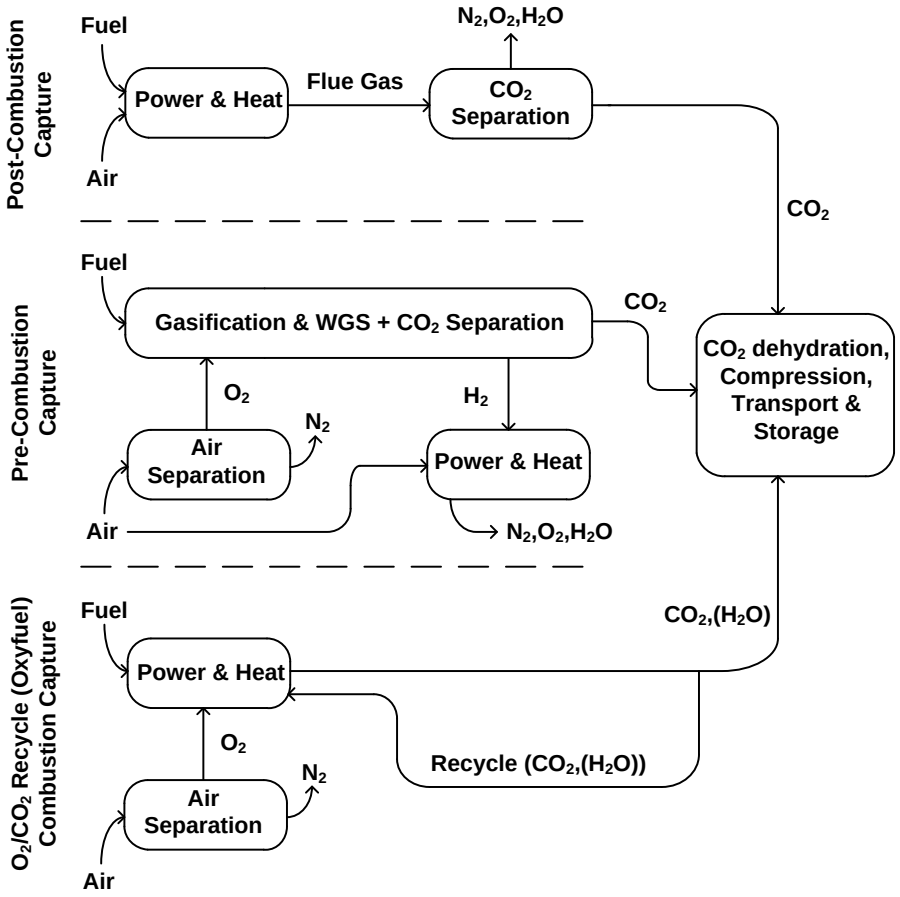

Figure 1-1: Possible, overall plant configurations for the three main categories of carbon capture technologies.

1.1 Project Objectives

The purpose of this project is through lab and pilot scale experiments and modelling to increase the knowledge on oxyfuel combustion. The investigations focus on three different areas: (1) combustion chemistry, (2) materials and corrosion, and (3) plant operation and control. More specifically, the following subjects have been investigated:

1. General combustion characteristics of coal-biomass mixtures in an atmosphere of O_2/CO_2 with focus on the influence of excess oxygen and high CO_2 levels on burnout.
2. Formation and emission of pollutants (CO, NO_X, and SO_2) as a function of excess oxygen. For NO and SO_2 the influence of flue gas recirculation is of particular interest since SO_2 may be captured by ash and NO will be reburned in the flame zone. This will lead to overall lower emissions.
3. Ash characteristics – with emphasis on the chemical composition and the fate of potassium and chlorine during biomass co-firing.
4. Flue gas cleaning for SO_2 (wet FGD) and NO_X (SCR) in an atmosphere with high CO_2 concentration.

5. Corrosion of boiler heat transfer surfaces in gas atmospheres relevant to oxyfuel combustion and increased creep exposure due to changed flue gas temperature distribution.
6. Operation/control of a large suspension-fired boiler using the oxyfuel process with focus on the changes compared to air combustion on heat uptake, the minimum and maximum load, gas flow pattern, and the possibility to change between oxyfuel combustion and air combustion.
7. Furthermore, an overview of the perspectives of oxyfuel combustion for CO_2 sequestration in the Danish power production system will be provided.

The investigation of the general combustion characteristics of pure coal, pure straw, and coal-straw mixtures have been investigated both theoretically and experimentally. A literature study on the state-of-the-art of the oxyfuel process has been published in the review journal Progress in Energy and Combustion Science and is enclosed in Appendix A. Experimentally, the combustion aspects in 1) and 2) have been investigated in two different experimental setups; a 5 kW_{th} entrained flow solid fuel combustor and a pilot scale 30 kW_{th} swirl burner. The swirl burner was likewise applied in the investigations on ash characteristics. Chapters 2 and 3 summarise the work performed on the two setups.

The effect of the high CO_2 concentrations on the FGD and SCR processes is reported in chapters 4 and 5. Chapter 6 provides the results of the theoretical and experimental work performed on identifying potential, additional corrosion mechanisms during oxyfuel combustion compared to air-firing. The model-based investigations on operation and control of an oxyfuel boiler are given in chapters 7 and 8. The evaluation of the perspectives for the application of oxyfuel combustion in the Danish power production system is given in Chapter 9.

2 Introducing Biomass in Carbon Capture Power Plants: Coal and Biomass Combustion in Air and Oxyfuel Atmospheres – Experimental Investigations in a Swirl Burner

The oxyfuel combustion process introduces several changes to the power plant configuration. Most important, the main part of the flue gas is recirculated to the boiler and mixed with pure oxygen. The oxidant thus contains little or no nitrogen and a near-pure CO_2 stream can be produced by cooling the flue gas to remove water. The change to the oxidant composition compared to combustion in air will induce significant changes to the combustion process.

The results reported here cover five important aspects with respect to the operation of a power plant, both the conventional air-blown type and oxyfuel combustion plants:

(1) Combustion fundamentals, including in-furnace temperature profiles and burnout;
(2) Emissions of polluting species (NO, SO_2, and CO);
(3) Quality of residual products, here only fly ash is considered;
(4) Slagging and fouling, focusing on the deposit formation propensities and deposit composition for different fuels at different operating conditions;
(5) Process economics, targeting the area of an oxyfuel power plant with the largest potential of reducing operating expenses – the oxygen demand.

The above areas have been investigated experimentally in a once-through, 30 kW_{th} semi-technical scale setup which simulates combustion in suspension-fired boilers, see Figure 2-1. Four different fuels have been applied; a pulverized, bituminous Colombian coal; pulverized, Danish cereal straw pellets; and two coal/straw blends with straw shares of 20 and 50 wt%. The fuels have been burned in air and synthetic O_2/CO_2 mixtures simulating recirculation of dry flue gas in an oxyfuel power plant. For more information, see Appendix B.

2.1 Combustion Fundamentals

A match of flue gas temperature profiles and burnout efficiency was obtained for combustion of the bituminous coal in air and a 30 % O_2/CO_2 mixture at an oxygen level of 5 % in the dry, exit flue gas. At these conditions the burnout efficiency was sufficiently high (> 99.5 %) in order for the fly ash to be comparable to fly ash from full-scale power plants.

Co-firing coal with straw and combustion of pure straw yields significant changes to the combustion conditions compared to the case with pure coal as fuel. For very high straw shares (> 50 %) the flue gas temperature decreases significantly due to delayed ignition and hence, the flame length increases significantly, as observed from in-flame CO measurements. The occurrence of large straw particles (originating from straw nodes) travelling almost unconverted through the experimental setup leads to a decrease in burnout efficiency, from 99.5 to 98.9 % for combustion in air and from 99.8 to 99.3 % during oxyfuel combustion. This corresponds to changes in fly ash carbon contents from 5.0 wt% (coal/air) to 20.7 wt% (straw/air) and from 2.6 wt% (coal/oxyfuel) to 12.5 wt% (straw/oxyfuel), see Figure 2-2.

In-flame peak CO levels of 10 vol% have been measured during oxyfuel combustion of coal, straw and a coal/straw blend with a straw share of 50 wt%.

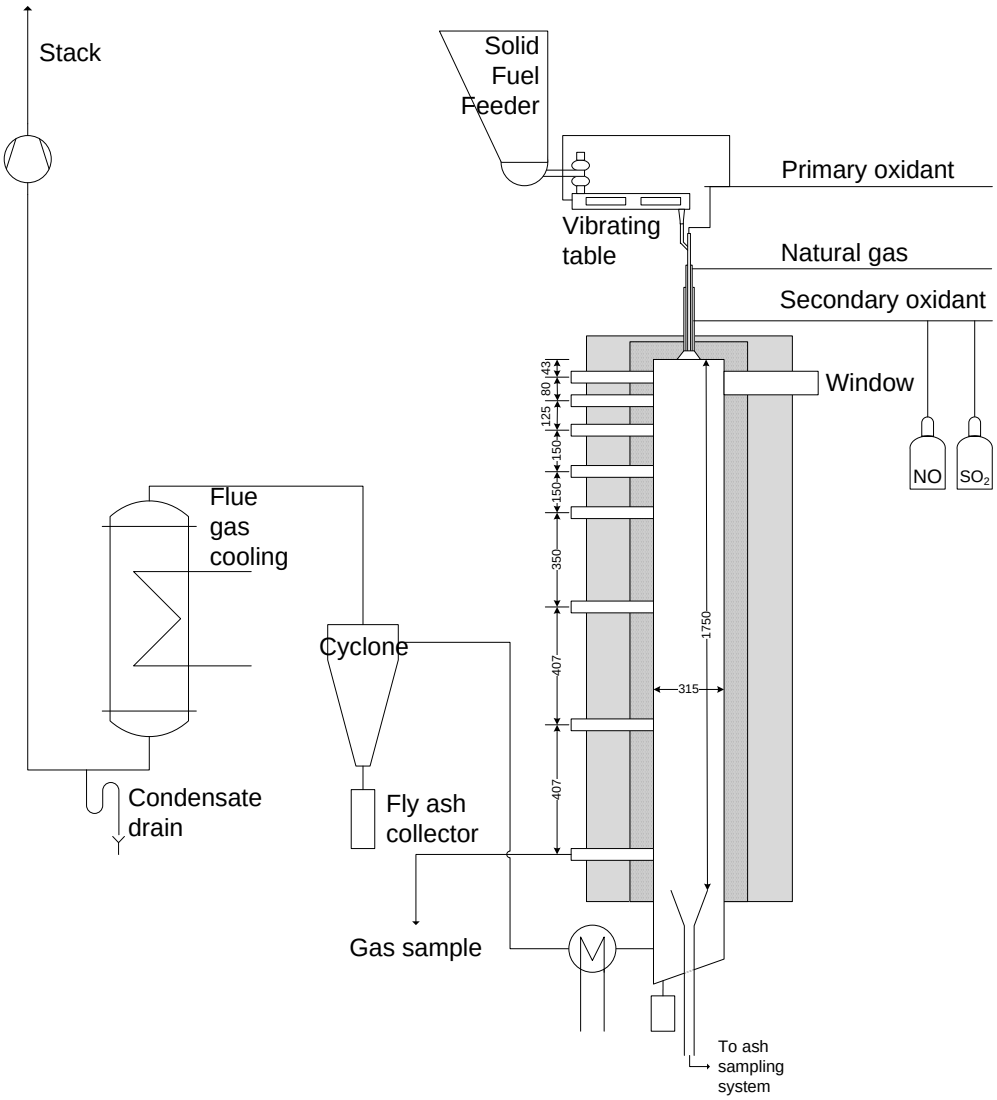

FIGURE 2-1: Schematic of the 30 kW swirl burner setup.

2.2 Emissions

Whereas no significant change to the CO and SO_2 emissions are associated with the change in combustion atmosphere, the emission rate of NO was reduced 35 % on average during oxyfuel combustion compared to the conventional air-firing. Three mechanisms were suggested to explain this reduction; increased internal NO reduction due to reduced dilution of NO in the gas phase, increased reduction of NO over char promoted by high CO levels in the flame, and the influence of high concentrations of CO_2 on the radical pool promoting reduction of NO when fuel and oxidant are mixed at oxidizing conditions.

Also, the change in fuel type affects the emission rates of NO and SO_2. For a given combustion atmosphere increasing the straw share of the fuel reduces both NO and SO_2 emission rates, see Figure 2-3. For NO this is in accordance with the decreasing Fuel-N content with increasing fuel straw share. At the same time, the Fuel-N to NO conversion ratio increases with decreasing Fuel-N content due to the lower reduction of NO in the gas phase from other gaseous N-containing species. The relative difference in the NO emission between

air and oxyfuel combustion increases with increasing fuel straw share which is a further benefit of oxyfuel combustion. The reduced emission of SO_2 with increasing fuel straw share is a consequence of a higher availability of water soluble potassium in fly ash and deposits capable of capturing SO_2 from the gas phase.

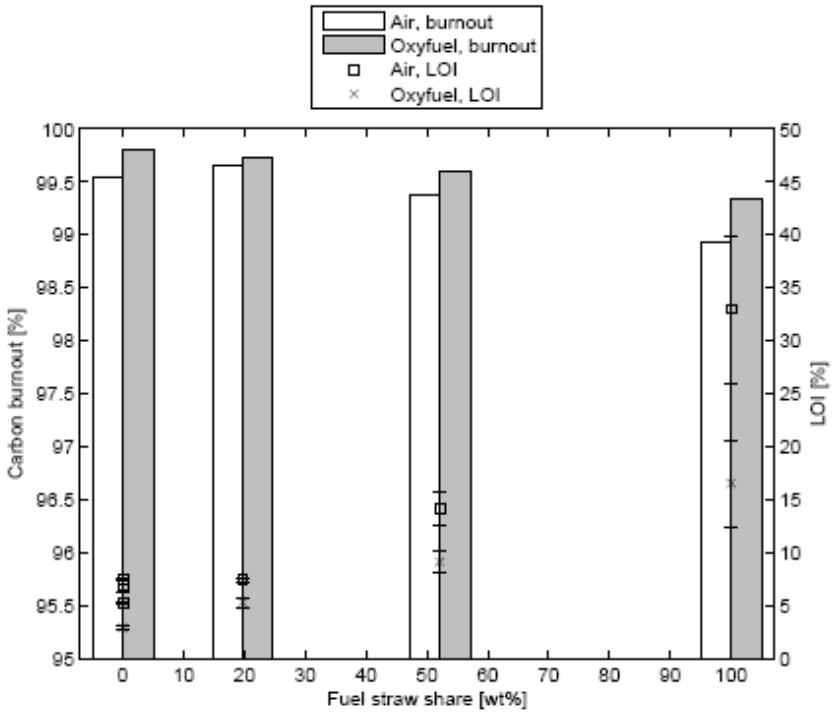

FIGURE 2-2: Calculated carbon burnout and loss-on-ignition analysis of fly ash as function of fuel straw share. Comparison of air and oxyfuel environments at the reference operating conditions. The error bars correspond to two standard deviations on the LOI analysis

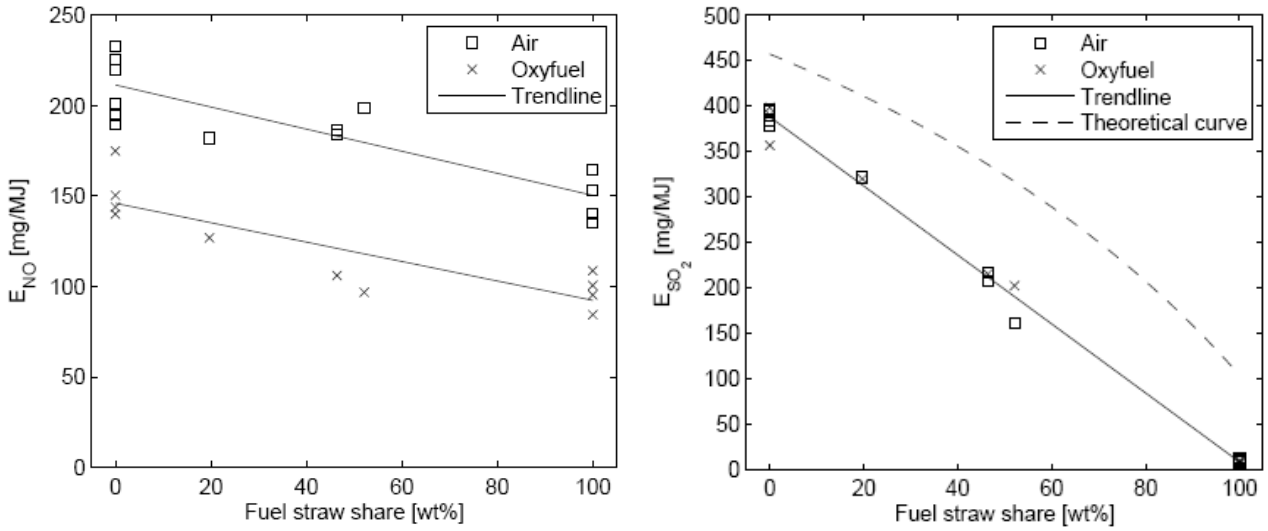

FIGURE 2-3: Emission rates of NO (left) and SO_2 (right) as a function of the weight based straw share of the fuel. Comparison of air and oxyfuel environments at the reference operating conditions.

The effect of the plant configuration, i.e. the position of the withdrawal of flue gas for recirculation downstream of the boiler, on the emission of NO and SO_2 was investigated for combustion of pure coal. Recirculation of untreated flue gas was simulated by doping NO and SO_2 to the oxidant in different amounts. The results showed that about 75 % reduction of the NO emission rate compared to air-firing could be obtained while the presence of high levels of SO_2 within the boiler will increase the capture of sulphur (SO_3) in the fly ash and deposits by up to 100 %, see Figure 2-4. Even so, less than 5 % of the recirculated SO_2 is removed from the gas-phase due to capture by solid phases.

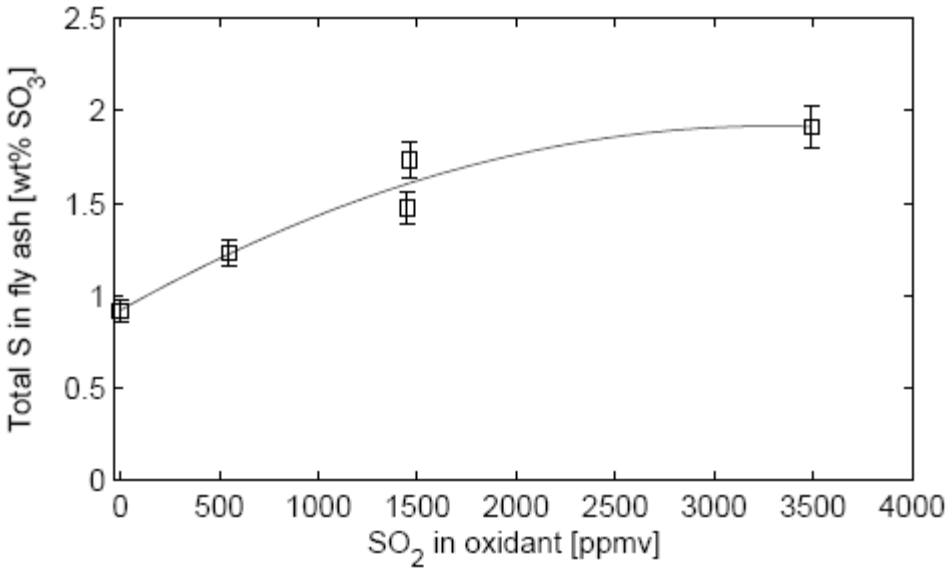

FIGURE 2-4: Relation between the total amount of sulphur captured in fly ash, measured as SO_3, and the concentration of SO_2 in the oxidant. Error bars correspond to two times the standard deviation in the analysis. The data have been fitted with a second order polynomial trend line.

2.3 Fly Ash Quality and Deposit Formation

One of the main concerns regarding the oxyfuel combustion technology is the risk of compromising the fly ash quality with respect to its applicability as an additive in concrete production. In this respect, the most often suggested plant configuration with recirculation of flue gas prior to desulphurization induces a risk of increasing the amount of sulphur in the fly ash above the permissible level of 3 wt% SO_3. The results obtained in this work show that simulating a recirculation of SO_2 to the boiler yielded an increase of about 60 % in the amount of sulphur captured in the fly ash from combustion of coal (@1500 ppm SO_2 at the inlet, see Figure 2-4). The applied coal has relatively low sulphur content (0.62 wt%, as received) and even with the increased retention (1.6 wt% SO_3 in the fly ash), the requirements could be met with considerable margin.

Co-firing of coal with straw has significant effects on the fly ash quality. Compared to the applied coal the straw has a markedly different content of K, Ca, Al, S, and Cl. A considerable increase in the corrosion potential is observed due to formation of water soluble alkali and alkali earth sulphates and chlorides in the ash with increasing straw share above 20 wt%, see Figure 2-5.

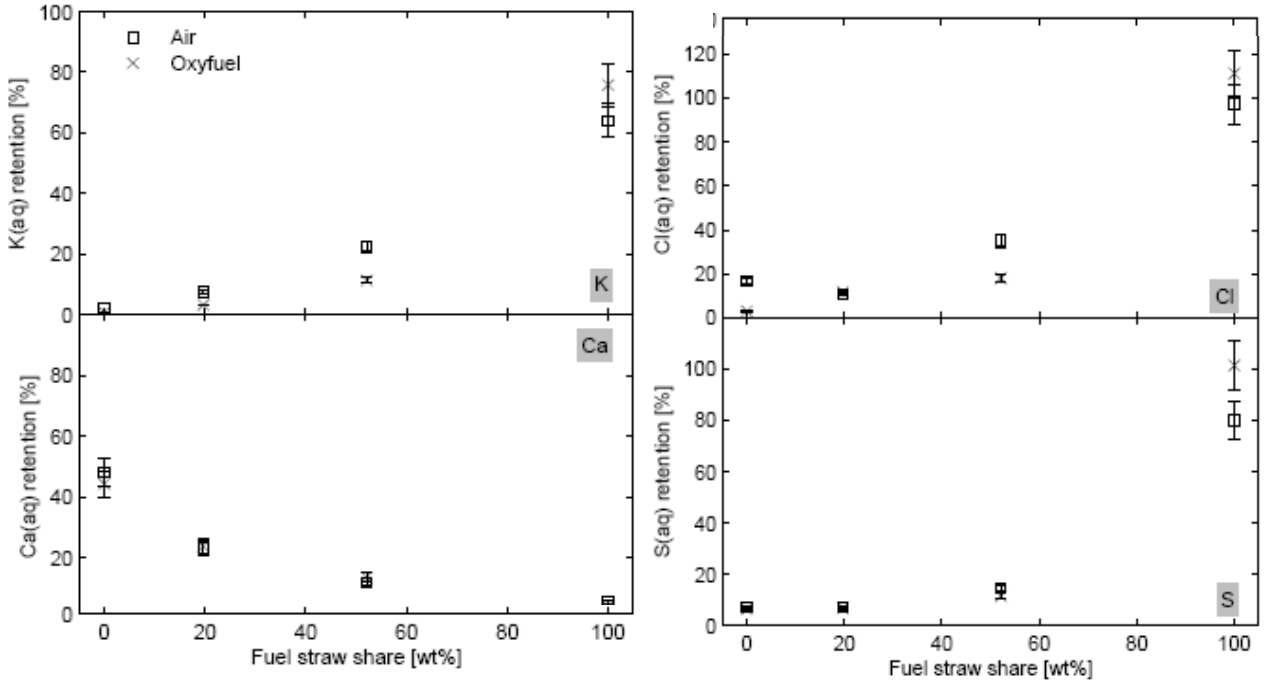

FIGURE 2-5: Capture of K, Ca, Cl, and S in water soluble form in fly ash as percentage of the amount of the element fed with the fuel and as a function of the weight based straw share of the fuel. Comparison of air and oxyfuel environments at the reference operating conditions.

A comparison of the fly ash data from this work to data from full-scale boilers co-firing coal and straw showed good agreement with respect to the capture of potassium in water soluble form in the fly ash. However, deviations were observed with respect to the degree of sulphation of the fly ash with full-scale plants achieving a higher amount of K_2SO_4 in the fly ash than the semi-technical setups applied in this work and reported in literature.

Similar deposition propensities have been found for co-firing coal with 20 to 50 wt% straw in each combustion atmosphere. However, significantly increased flux to the deposit probe was observed for combustion of pure straw. The deposit also became more sintered and difficult to remove. The change from combustion in air to oxyfuel combustion increased the deposition rate, most likely due to higher flue gas temperatures at the sampling position. High in-furnace levels of SO_2 during oxyfuel combustion lead to increased sulphation of coal deposits.

2.4 Process Economics

The production of near-pure oxygen for oxyfuel power plants constitutes the single-largest penalty to the operating expenses. An investigation was made which showed that it is possible to reduce the excess oxygen level during combustion, and hence the operating costs, by increasing the concentration of oxygen at the burners. For example, the oxygen excess could be reduced to 2.4 % in the exit flue gas at an inlet O_2 concentration of 50 vol% while obtaining a burnout of 99.6 % during pure straw combustion. The change to the oxidant composition therefore did not compromise the fuel burnout and further did not increase the emission rates of NO and SO_2. It did, however, induce significant changes to the in-furnace temperature profile, i.e. higher near-burner temperatures, and increased the rate of deposition of ash on cooled

surfaces. Further investigations are needed in order to determine the potential of this strategy for reducing the operating expenses for the oxyfuel process.

2.5 Implications for Oxyfuel Combustion

An incentive to the execution of the work described in this summary was to investigate whether any show-stoppers regarding the oxyfuel combustion technology could be identified. A number of critical aspects were found from which the potential changes to the combustion conditions have been investigated experimentally. The main concerns were associated with the risk of increased fire-side corrosion and the risk of a reduction in fly ash quality due to the significant changes to the composition of the flue gas with higher levels of CO_2, H_2O, and potentially SO_2/SO_3.

The results from this work has not brought forth any disqualifying characteristics of the oxyfuel combustion process rendering it unsuited for implementation as carbon capture technology in suspension-fired power plants. On the contrary, increased burnout and lower NO emission rates were observed during oxyfuel combustion compared to combustion in air in the applied experimental setup.

3 Modelling Suspension Fired Combustion in O_2/CO_2 and O_2/N_2 Atmospheres

This summary and its associated appendices describe the development of a comprehensive single particle combustion model, which has been validated against data on char conversion obtained under suspension fired conditions in an Entrained Flow Reactor (EFR) under O_2/N_2 and O_2/CO_2 atmospheres. Kinetic parameters used in the modelling are found from ThermoGravimetric Analyzer (TGA) experiments on char formed under suspension fired conditions in the EFR.

3.1 EFR Experiments

EFR experiments in O_2/N_2 and O_2/CO_2 were performed using the reactor shown schematically in Figure 3-1. Reactor temperatures and inlet O_2 concentrations between 1173 – 1673 K and 5 – 28 vol. % were used. Gas atmospheres were created by mixing bottled gases, except for air, which was supplied by a compressor. Particle sampling and gas analysis for O_2, CO_2 and CO were done at each sampling position.

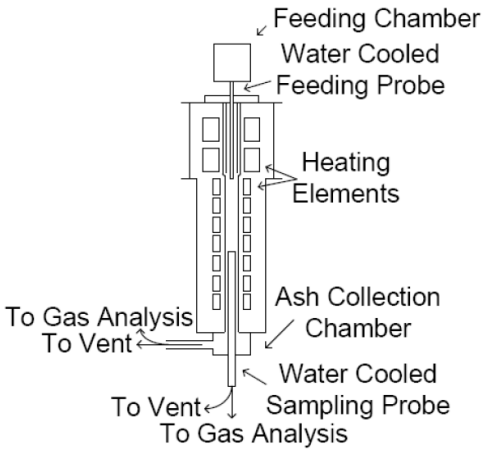

FIGURE 3-1: Schematic illustration of the isothermal electrically heated entrained flow reactor used in the experiments. Gas atmospheres were made by mixing bottled gases, except when combustion was carried out in air, which was supplied from a compressor. The water cooled sampling probe can be operated across the entire reaction zone, enabling sampling at residence time covering the entire devolatilization and combustion process. By adjusting the suction during particle sampling it was ensured that particles were sampled iso-kinetically from a well defined section of the laminar flow profile.

The degree of char conversion at each sampling position was found by ash tracing and devolatilization experiments were conducted at each experimental temperature to correct the char mass balance for volatile weight loss.

The experiments showed no effect of CO_2 gasification during devolatilization and char conversion. At 1573 K and 1673 K the lower diffusion coefficient of O_2 in CO_2 was however found to lower char conversion rate compared to O_2/N_2 due to external mass transfer limitations. A detailed description of the experiments and the data treatment can be found in Appendix C.

3.2 TGA Experiments

TGA experiments were performed at 5 vol. % O_2 using char sampled in the EFR as fuel. Combustion experiments were initially carried out in both N_2 and CO_2 based atmospheres to evaluate the influence of carrier gas. As the carrier gas was not found to have an influence when the process was taking place in zone I all experiments presented were conducted in N_2/O_2. Gasification experiments were also conducted at 80 vol% CO_2 in N_2. In all experiments, 1 – 1.5 mg sample was converted at a heating rate of 5 K/min as these

conditions were found to ensure completely intrinsic char conversion. Details of the experiments can be found in Appendix D.

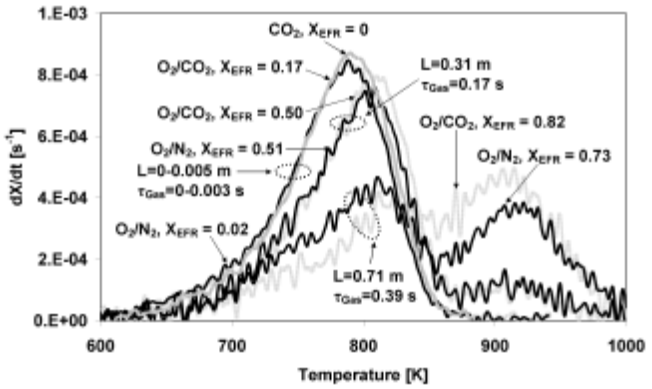

FIGURE 3-2: Combustion reactivity of EFR char obtained from devolatilization at 1173 K in CO_2 and by combustion at 1173 K in 27.7 – 27.9 vol. % O_2 in N_2 or CO_2. A TGA heating rate of 5 K min^{-1} has been used to reach a maximum temperature of 1123 K in 5 vol. % O_2 and 95 vol. % N_2. Sample masses were within 1.2 – 1.5 mg.

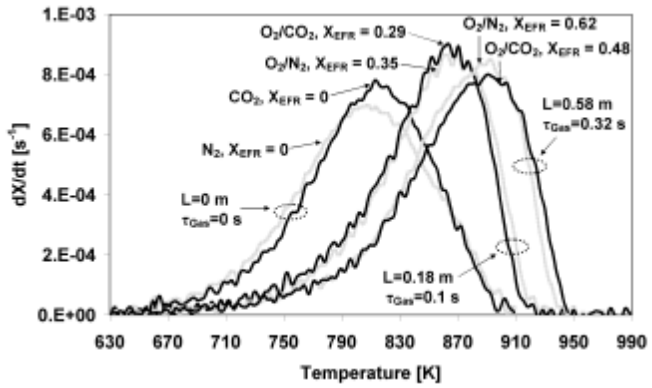

FIGURE 3-3: Combustion reactivity of EFR char obtained from devolatilization at 1673 K in N_2 and CO_2 and from combustion at 1673 K in 3.1 – 3.2 vol. % O_2 in N_2 or CO_2. A TGA heating rate of 5 K min^{-1} has been used to reach a maximum temperature of 1123 K in 5 vol. % O_2 and 95 vol. % N_2. Sample masses were within 1.2 – 1.5 mg.

Figure 3-2 and figure 3-3 show reactivity profiles of chars sampled in the EFR at 1173 K and 1673 K with inlet O_2 concentrations in CO_2 of 28 and 5 vol%, respectively.

Both figure 3-2 and figure 3-3 show no differences between EFR chars prepared in O_2/N_2 and O_2/CO_2, a conclusion that is supported by all TGA reactivity profiles that can be used for similar comparisons (see Appendix D). In figure 3-2 two peaks are seen in the reactivity profiles for the partly converted char samples (X>0.5 => char conversion > 50 %). These peaks indicate the existence of char phases of distinctively different reactivity and they will be addressed further when discussing the results of modelling. From reactivity profiles of EFR chars formed by devolatilization at temperatures between 1173 K and 1673 K a number of Arrhenius plots were made for both combustion and gasification. From these plots it was found that significant deactivation, affecting only the combustion rate, took place as EFR temperatures used for devolatilization increase. As a result of this the kinetic expression in eq. 1 was found to describe both combustion and gasification using the kinetic parameters in Table 3-1.

$$k = k_0^* \cdot \exp\left(\frac{E_D}{R \cdot T^*}\right) \cdot \exp\left(\frac{-E_A}{R \cdot T}\right) \qquad \textbf{Eq. 1}$$

In eq. 1 k_0^* is the pre-exponential factor, E_D is the energy of deactivation, T^* is the highest temperature experienced by the particle at any point in its life time, and E_A is the energy of activation.

TABLE 3-1: Intrinsic kinetic parameters used in eq. 1

Species/Property	n	E_D [kJ mol^{-1}]	E_A [kJ mol^{-1}]	k_0* [kg m^{-2} s^{-1} (mol m^{-3})$^{-0.5}$]
O_2	0.5	20.5	137.5	1.44
CO_2	0.5	0	230.8	7.33

3.3 Modelling

A COal COmbustion MOdel (COCOMO) has been developed to simulate suspension fired combustion of coal char in O_2/N_2 and O_2/CO_2. The model encompasses the three different particle morphologies; cenospheres, network- and dense chars, each distributed between six discrete particle sizes and it relies on eq. 1 and Table 3-1 to describe combustion and gasification rates of the char. Details of the model can be found in Appendix E.

COCOMO shows a high degree of accuracy when it is used to predict char conversion rates in both O_2/N_2 and O_2/CO_2, which is illustrated in figure 3-4 for conversion profiles obtained a reactor temperature of 1373 K and different inlet concentrations of O_2 and in figure 3-5 that show the accuracy of the model for all data points used for validation.

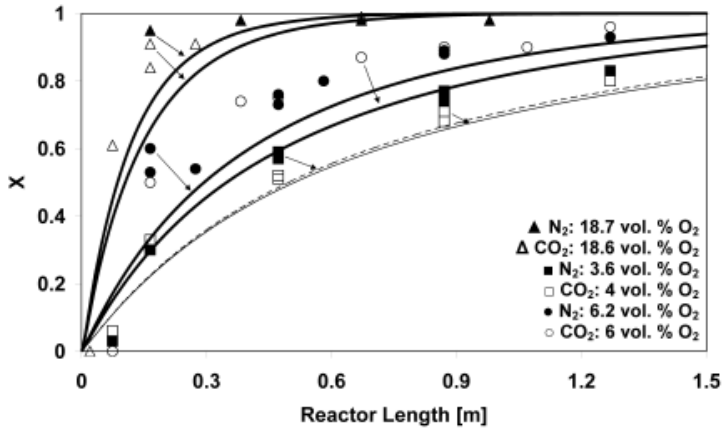

FIGURE 3-4: COCOMO profiles and experimental profiles obtained at 1373 K in N_2 and CO_2. The O_2 concentrations are the averages of the local concentrations at each sampling position. λ ~ 2.3 – 9.8.

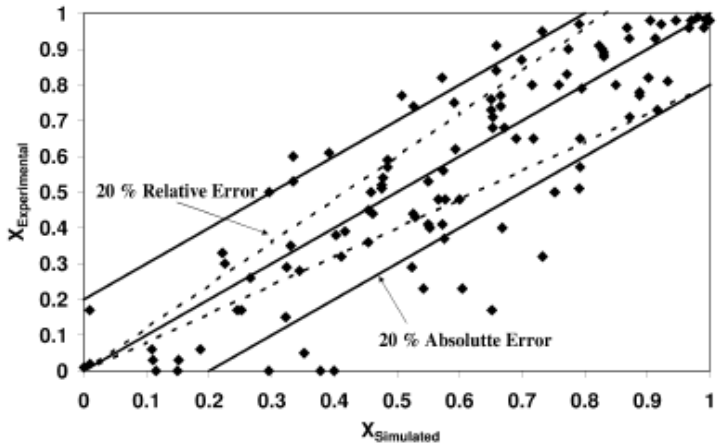

FIGURE 3-5: Comparison between COCOMO and experimental data. The experimental data covers reactor temperatures between 1173 K – 1673 K and inlet O_2 concentrations between 5 and 28 vol. % corresponding to stoichiometric values between 2 and 15.

In figure 3-5 it can be seen that COCOMO has large errors in the prediction of some of the experimental data, for the case of low degrees of char conversion. The reason for this links back to the two peaks in the reactivity profiles in figure 3-2. It was found from simulation under the conditions in figure 3-2 (1173 K, 28 vol. % O_2 at the inlet) that some particle classes reached excessively high temperatures close to 1800 K, some with heating rates as high as 20000 K s^{-1}. This can be expected to lead to a secondary devolatilization and further char deactivation, possibly as a result of "char cluster" phase formation, where heavy products of secondary devolatilization adsorbs/adhere to the chars mineral phase, causing a heterogeneous deactivation of the particle. Scanning Electron Microscopy (SEM) did also reveal non reactive particle at high overall degrees of char conversion. As COCOMO is programmed to treat char deactivation as homogeneous, depending only on temperature, the two phase behaviour is not captured, leading to erroneous predictions of the overall conversion rate. A second and last source of prediction errors is caused by a delayed heterogeneous ignition at low O_2 concentrations (5 vol. % at the inlet) and low reactor temperatures (1173 K and 1273 K). This is not captured by COCOMO that assumes an onset of heterogeneous ignition once simulation is started. Further discussion of the modelling results can be found in Appendix E.

3.4 Conclusions

The governing conclusions of this work are stated below. Elaboration on experimental findings and calculations, leading to the conclusions can be found in details in App. C-E.

No differences were found in volatile weight loss when O_2/N_2 was replaced with O_2/CO_2 under otherwise similar conditions (App. C).

No differences in char morphology and intrinsic reactivity were found between chars formed and partly consumed in O_2/N_2 and O_2/CO_2 in the EFR (App. C and D).

A COal COmbustion MOdel (COCOMO) was developed, which adequately describes coal char conversion in O_2/N_2 and O_2/CO_2. The model relies on intrinsic kinetic parameters for combustion and gasification found in a TGA using chars formed under suspension fired conditions in the EFR (App. D and E).

The CO_2-gasification reaction was not found to be important during neither devolatilization nor char conversion (App. C and E). This conclusion relates specifically to the applied bituminous coal under the tested conditions. For more reactive coal types such as lignite of biomass, or at higher temperatures it is not unlikely that CO_2 gasification may play a role. As shown in Appendix E the CO_2 gasification reaction may catch up to the O_2 reaction which is limited by external diffusion under these conditions.

When char combustion takes place at high temperatures (1573 K and 1673 K) the lower diffusion coefficient of O_2 in CO_2 compared to N_2 was found to lower the conversion rate (App. C and E).

4 Performance of a wet flue gas desulphurisation pilot plant under oxy-fuel conditions

The worldwide combustion of coal, oil and other fossil fuels emits NO_x, SO_2, particles and anthropogenic CO_2 (i.e. caused by human activity). In modern power plants, NO_x, SO_2, and particles are efficiently removed, while CO_2 remains a challenge. Oxy-fuel firing is, however, a promising technology that should enable the capture and storage of anthropogenic CO_2 emissions from large stationary sources such as power plants and heavy industry. Unresolved issues concerning a high energy demand for air separation and CO_2 compression, determination of the optimal recycle location of flue gas, the flue gas cleaning steps required (SO_2, NO_x and particles), and the impact of an oxy-fuel flue gas on the cleaning steps, exist. To achieve the goal of capture and storage of CO_2, with as low concentrations of impurities as possible, and thereby reach close to zero CO_2 emissions from fossil fuel fired power plants, a continued highly efficient operation of the wet FGD process, as well as other flue gas cleaning processes, is an important requirement.

The aim of this work was to study the performance of the limestone-based wet flue gas desulphurisation (FGD) process, in a pilot scale plant, under operating conditions corresponding to oxy-fuel firing. The investigated operating conditions include flue gas composition (7 and 90 % CO_2), pH (5.0 and 5.4), flue gas flow rate (3.5 and 17.5 $Nm^3\ hr^{-1}$), slurry temperature (44 and 53 $^{\circ}C$) and 10 mM adipic acid addition. The most important output parameters were the overall degree of desulphurisation and the residual limestone concentration in the gypsum slurry.

Pilot-scale experiments quantified that the introduction of a flue gas with 90 vol. % CO_2, at a holding tank pH of 5.4, reduced the limestone dissolution rate significantly and thereby increased the residual, particulate limestone concentration in the gypsum slurry from 4.0 to 6.2 g per litre slurry relative to a base-case (air-firing) experiment with a flue gas CO_2 concentration around 7 vol. %. The degree of desulphurisation furthermore increased from 91 to 94 % due to the higher residual limestone concentration/absorber pH (increased from ~3.5 to ~4.0). The addition of 10 mM adipic acid to the slurry was not sufficient to return the increased concentration of residual limestone to the base case (air-firing) level, but a higher absorber pH (~4.5) and an additional increase in desulphurisation degree, from 94 % to 97 %, was obtained. Using a holding tank pH of 5.0 (no adipic acid) returned both parameters to the levels observed in the base-case experiment. The prolonged flue gas residence time (i.e. increased liquid/gas ratio) of the two experiments with low flue gas flow rates, yielded very high total desulphurisation degrees, making a distinction between the two experiments (44.4 vs 53.3 $^{\circ}C$) impossible. However, the SO_2 removal down through the absorber indicates a decreased performance at elevated temperatures.

The full description of the work is provided in Appendix F.

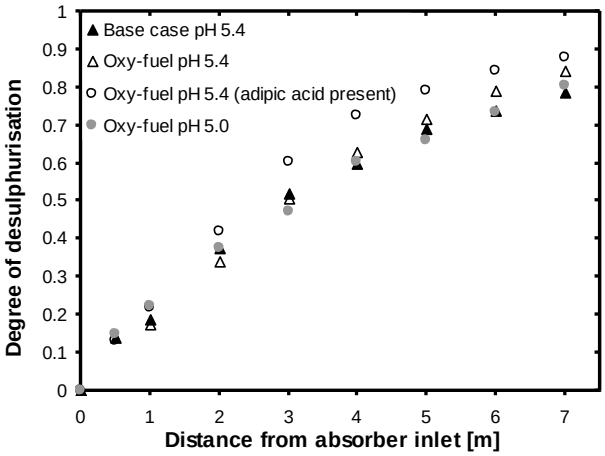

FIGURE 4-1: Degree of desulphurisation (±0.01) as a function of distance from absorber inlet in the pilot plant for air-firing (pH of 5.4) and oxy-fuel experiments with and without adipic acid (pH of 5.0 and 5.4)

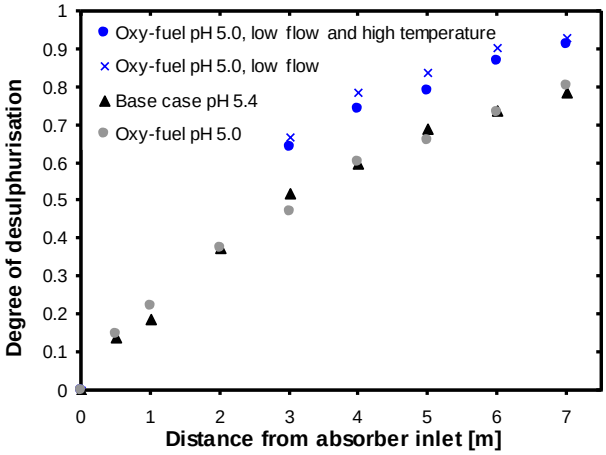

FIGURE 4-2: Degree of desulphurisation (±0.01) as a function of distance from absorber inlet in the pilot plant for air-firing (pH of 5.4) and oxy-fuel experiments with decreased flue gas flow rates (pH of 5.0)

5 SCR catalyst performance under oxyfuel conditions

5.1 Introduction

The oxyfuel combustion process differs from air combustion in several ways such as high concentrations of CO_2 and water in the flue as well as increased levels of SO_2/SO_3 if recirculation is before the desulfurization plant. Furthermore, the use of pure oxygen in the combustion process is costly, and so lowering of the combustion stoichiometry is attractive from an economic point of view. This, however, will lead to low oxygen concentrations in the flue gas and possibly increased CO levels.

In this part of the project an introductory, experimental investigation has looked into some of the influences that oxyfuel combustion has on SCR performance: The influence of CO_2 as carrier gas, influence of low oxygen concentration, and the ability of the SCR catalyst to act as an oxidation catalyst for CO.

5.2 Experimental

The following section will briefly describe the experimental setup. The reactor was made from quartz and was supplied with gas from cylinders controlled by MFCs (mass flow controllers) while being placed in an electrically heated furnace. The gas enters the reactor in the bottom of the oven and is then led through the outer tube into the inner tube where the catalyst was placed, seen in Figure 5-1. The gas then exits the reactor and is led to the analyzer through a traced tube.

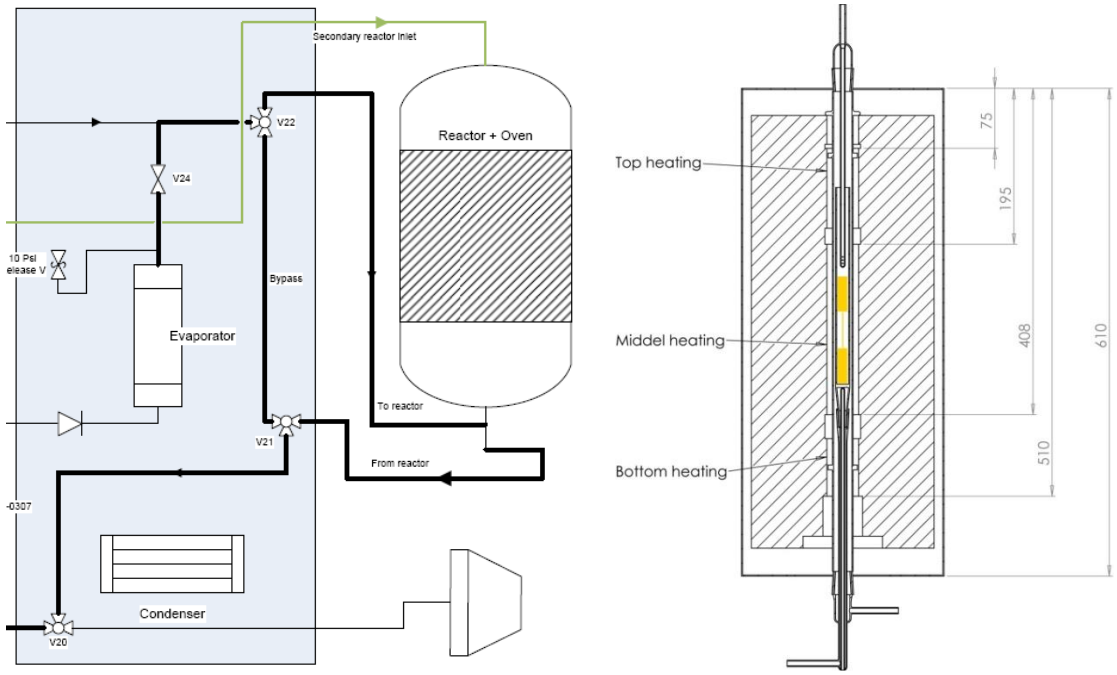

FIGURE 5-1: Left: Reactor setup, the bold black line is traced. Green line contains NH_3. Right: Reactor with catalyst packing.

5.2.1 Catalyst composition

Vanadium based catalyst plates were supplied by Haldor Topsoe. The composition of the catalyst mass base is approx. 1.2% V_2O_5, 7% WO_3 and the rest TiO_2 (anatase) and fiber. Fiber material consists primarily of SiO_2

and also alumina and calcium to a lesser extent. The dimensions of the catalyst plates are 1.7 x 1.7 cm^2. A typical catalyst mass used in the experiments was approx. 0.3 grams.

5.2.2 SCR activity measurements

The SCR activity measurements were carried out at atmospheric pressure in a fixed-bed quartz reactor loaded with 200 mg of fractionized (180-300 µm) catalyst powder sample or 1.7 x 1.7 cm^2 catalyst plate sample. The reactant gas composition was adjusted to 415 ppm NO, 500 ppm NH_3, 5% O_2, 2.3% H_2O and balance N_2 (92.6%) for conventional SCR conditions. For oxyfuel conditions it was 415 ppm NO, 500 ppm NH_3, 5% O_2, 2.3% H_2O, N_2 (7.6%) and balance CO_2 (85%). The total flow rate was maintained at 3 l/min (ambient conditions). During the experiments the temperature was increased stepwise from 200 to 400 °C while the NO and NH_3 concentrations were continuously monitored by an ABB gas analyzer. The catalytic activity is represented as the first-order rate constant ($m^3/kg \cdot s$):

$$k' \cdot \tau = \ln(1 - x) \tag{1}$$

5.3 Results and Discussion

5.3.1 Diffusivity

One possible influence of exchanging N_2 with CO_2 is a lower diffusion coefficient of the reactant molecules (NO/NH_3). Table 5-1 shows theoretically calculated values of the diffusion coefficient of NO in either N_2 or CO_2. It can be seen that the diffusion coefficient of NO in N_2 is 9.4 - 13.3% larger compared to that of NO in CO_2.

TABLE 5-1: Theoretically calculated bulk diffusitivity of NO

Temperature	D_{NO,N_2}	D_{NO,CO_2}	Difference
$[°C]$	$\left[\frac{m^2}{s}\right] \cdot 10^{-5}$	$\left[\frac{m^2}{s}\right] \cdot 10^{-5}$	$[\%]$
200	4.65	4.03	13.3
250	5.36	4.71	12.1
300	6.25	5.63	9.96
350	7.20	6.51	9.59
400	8.20	7.43	9.38

5.3.2 Comparison of SCR Activity

Figure 5-2 shows that the activity of the catalytic plate is lower in the CO_2 environment compared to the N_2. At low temperatures the difference in activity is the largest while it gradually is reduced as the reaction temperature is increased. The figure also shows how the catalyst is influenced by mass transfer limitations

at higher temperatures, T > 300 °C. Overall there is a 7-18% lower activity in the CO_2 environment as compared to N_2. This decrease in SCR activity can be divided into two mechanisms:

1. Physical effects
2. Chemical effects

Regarding physical effects it seems there is a close correlation between activity and bulk diffusion. The difference in bulk diffusion of around 10% agrees reasonably well with the loss of activity at high temperature where the reaction on the plates is severely influenced by diffusion limitations. The influence of CO_2 seems slightly higher at low temperature where diffusion limitations play a minor role. This could indicate that CO_2 also has a chemical effect, for example adsorption at the active sites. At higher temperature the CO_2 desorbs and only the effect of diffusion remains.

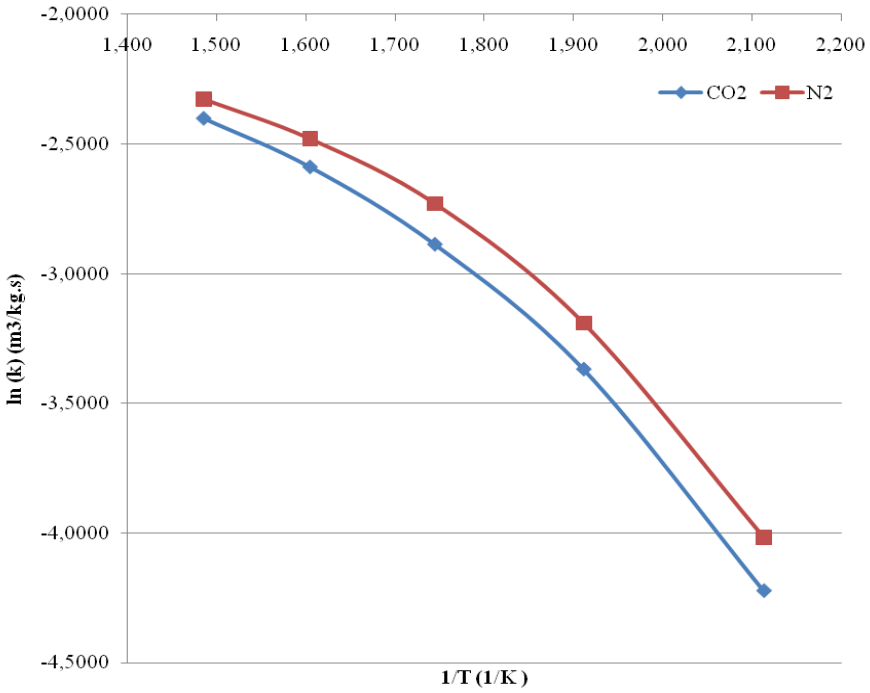

FIGURE 5-2: Arrhenius plot for plate catalysts with dimensions 1.7 x 1.7 cm, temperatures ranging from 200 to 400 °C, total flow 3 L/min.

To test this further, additional experiments were made with powdered catalyst where diffusion limitations were absent. It was found that at high temperature there is no difference between CO_2 and N_2 while the difference remains at low temperature. These observations support the picture described above, i.e. a chemical effect of CO_2 at low temperature (adsorption on active sites) and a slower diffusion of NO/NH_3 in CO_2 which becomes evident a high temperature where the reaction is diffusion limited.

5.3.3 Investigation of oxygen dependency in CO_2 environment

A series of experiments on the influence of oxygen concentration has been conducted. The experimental results can be seen in Figure 5-3 as the first order rate constant for NO reduction. A significant decrease in activity is seen when the oxygen concentration is below about 3000 ppmv, but above about 5000 ppmv the

influence of changing the oxygen concentration is very small. Calculated curves from a kinetic model describing the influence of oxygen are also shown.

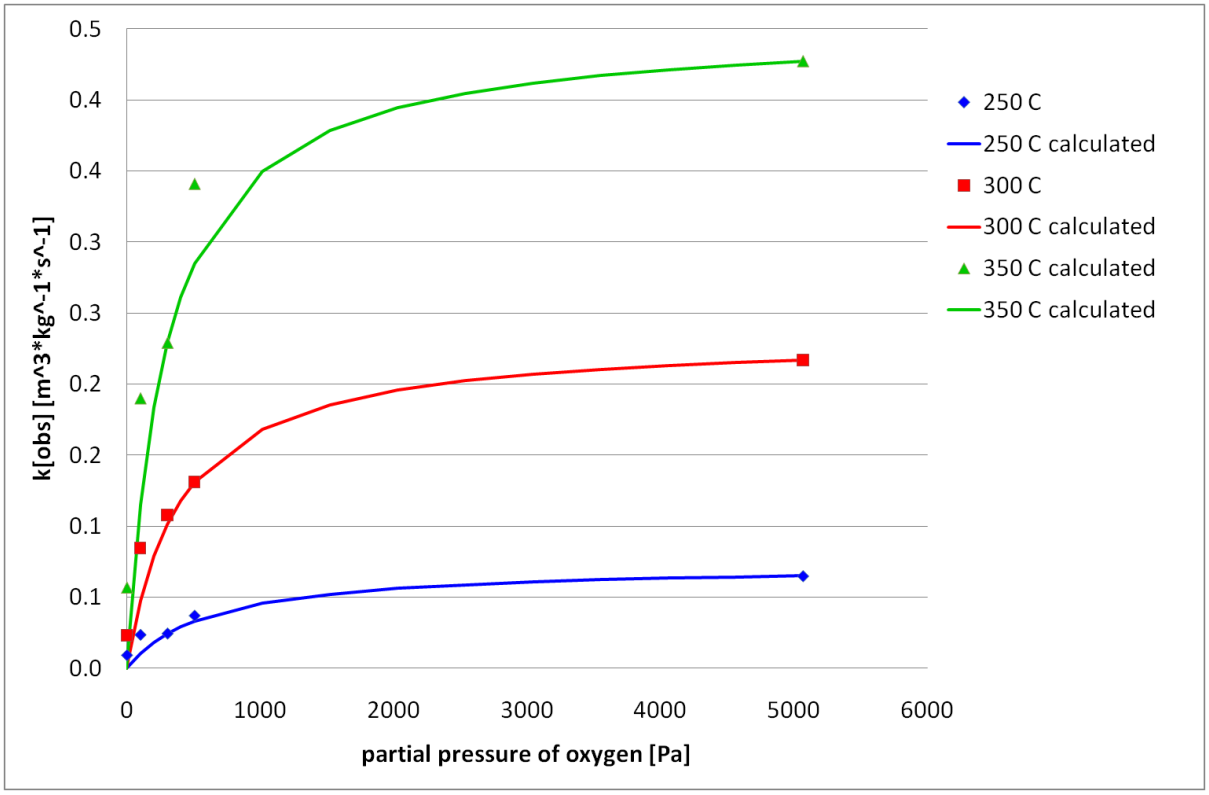

FIGURE 5-3: k[obs] vs. partial pressure of oxygen and model of how the oxygen influences the activity.

5.3.4 CO oxidation ability of SCR catalyst

It is know that under oxyfuel conditions CO_2 contains approximately 90% of the dry flue gas volume. CO_2 at high partial pressure and high flame temperatures can dissociate into CO and O_2 and it would be useful if the SCR catalyst could carry out the oxidation of CO if this has not occurred prior to the flue gas reaching the SCR unit.

CO oxidation measurements were carried out at atmospheric pressure in a fixed-bed quartz reactor loaded with 200 mg of fractionized (180-300 µm) catalyst powder sample or 1.7 x 1.7 cm^2 catalyst plate sample. The reactant gas composition was adjusted to 500 ppm CO, 500 ppm CO_2, 5% O_2, 2.3% H_2O and balance N_2 (92.6%). The total flow rate was maintained at 3 L/min (ambient conditions). During the experiments the temperature was increased stepwise from 200 to 400 °C while the CO, CO_2 and O_2 concentrations were continuously monitored by ABB gas analyzer. The SCR catalyst did not show any CO oxidation ability both in powder and plate catalyst experiments under these experimental conditions.

5.4 Conclusions

Three aspects of the different flue gas composition of oxy-fuel combustion compared to normal air-combustion on the operation of the selective catalytic reduction of NO_x have been investigated: The influence of a high CO_2 concentration, the influence of a low O_2 concentration as would be beneficial from a process economic point of view and finally the possibility of using the SCR catalyst as an oxidation catalyst for a potentially increased CO level in the flue gas.

It was found that the activity of the typical industrial V_2O_5-WO_3/TiO_2 SCR catalyst is about 10 % lower when the carrier gas is CO_2 corresponding to oxyfuel conditions compared to when the carrier gas is N_2. At high temperature the difference is due to increased diffusion limitations of the reacting species, NO and NH_3, in CO_2 compared to N_2, while at low temperature the further, percentual decrease in activity is speculated to be due to adsorption of CO_2 on the catalyst active sites. The catalyst activity is optimal when the oxygen concentration is above about 5000 ppmv, but below this level the rate decreases fast with decreasing oxygen concentration. Finally, it was found that the catalyst is inactive for CO oxidation.

Overall, the performed investigations do not indicate any problems for the SCR process in oxy-fuel flue gases.

6 Potential corrosion problems in oxyfuel environments

6.1 Introduction

This part of PSO 7171 seeks to give a realistic assessment of materials problems that could be encountered during the process of oxyfuel firing.

In oxyfuel firing, fuel combustion occurs with oxygen and not air and the resulting flue gas will be mainly CO_2 and H_2O. In addition there may be recirculation of about 2/3 of the flue gas, thus any trace elements in the flue gas will with time build up in concentration. This could be important with respect to the amount of sulphur within the flue gas. The higher content of CO_2 in the flue gas makes it more cost effective to recapture CO_2 after combustion.

A literature survey was completed in 2008 identifying some of the areas of potential corrosion problems (Appendix H) A M.Sc. project by Magdalena Rogowska has been conducted in 2010 under the supervision of Karen Pantleon (DTU Mekanik). In the M.Sc. report the literature has been updated and laboratory exposures in oxy-carburising gas environments have been conducted so that a better understanding of pertinent corrosion mechanisms is given. This has been followed by additional laboratory exposures to verify the mechanisms considered in the M.Sc. report as well as work on preparation of an article. The M.Sc. report and the report on the additional work can be supplied by contact to DTU Mekanik. Vattenfalls actual experiences with corrosion in the Schwarze Pumpe pilot plant are also included for information (Appendix I).

6.2 Summary of Literature

With oxyfuel firing in the boiler, flue gas will consist of approx 60% CO_2 and 30% H_2O with the SO_2 concentration also increasing threefold due to recirculation of the flue gas. The O_2 content will be similar to conventional firing. Actual values have been measured in the Schwarze Pumpe plant (Appendix I). However these values will depend on coal type, variations in firing mode, and variations in burner design.

TABLE 6-1: Typical flue gas compositions for air- and oxyfuel-firing.

	Measurements in dry gas after ESP					H_2O Vol. % in flue gas	Fly-ash SO_3 mg/kg
	CO_2 Vol %	O_2 Vol%	CO mg/Nm^3	SO_2 mg/Nm^3	NOx mg/Nm^3		
Air-firing	13	6	7	1600	300	8	46 $\pm$ 9
Oxyfuel	95	6.8	2.5	7000	1600	30	77 $\pm$ 18

Oxyfuel combustion results in higher CO_2 and H_2O concentrations as well as higher SO_2 concentrations if the flue gas is recirculated before desulphurisation. Since the oxygen level is similar to that in conventional firing, it could be anticipated that the same protective oxides formed during conventional firing can also be formed during oxyfuel firing as the partial pressure of oxygen would be sufficiently high.

Literature reveals that high CO_2 and H_2O concentrations in the gas phase result in increased oxide thickness compared to a high O_2 content. In general, a protective duplex oxide of magnetite and iron chromium spinel is formed. However, to what extent there is carburisation depends on different alloys. In environments with combinations of CO_2 and H_2O, carburisation is observed in the underlying alloy for ferritic steels and carbides are also present within the oxide.

Increasing SO_2 in the flue gas results in oxidation and sulphidation to various degrees. The rates of reaction are significantly higher than with pure oxygen due to sulphides being incorporated in the scale. Sulphides are not as protective as oxides and lead to faster diffusion rates. Increased SO_2 will also lead to an increased sulphate presence within the deposit that can result in slightly higher corrosion rates. This can be equivalent to using a coal with higher sulphur content, or co-firing with biomass where more sulphate is present in the deposit.

Recirculation of gases and the presence of high CO_2 levels could give rise to areas with reducing conditions within the boiler. With conventional firing, reducing conditions have been observed on the furnace wall near the burners especially if low-NO_x burners and staged firing has been implemented. Thus, much experience exists concerning reducing conditions during low-NOx operation. The following factors are known to have an influence on waterwall corrosion in conventional firing.

- Fuel: Cl, S
- Flue gas: O_2, CO, H_2S
- Deposition of FeS- and/or carbon-rich (unburnt) particles
- Flame contact
- Changing between oxidising and reducing atmosphere
- Heat flux
- Metal temperature

Even if the flue gas was run through a FGD before recirculation to remove sulphur, there would still be a higher level of CO during combustion which may pose problems. It is the authors opinion based also on the preliminary results from Schwarze Pumpe that it is here there will be problems in the oxyfuel plant. Since the use of oxygen is so expensive, there will be the incentive to use the least amount of oxygen possible and this could affect the amount of waterwall corrosion.

The increased SO_2 and H_2O levels will probably result in problems in the “air” preheater region where dew point corrosion can occur. The most important acid dew point is that for sulphuric acid as this is considerably higher than for water. In an environment with SO_2, SO_3, and water, sulphuric acid could condense on the tubes. SO_2 has a dew point below that of water but can react with oxygen to produce SO_3 which has a dew point above that of water. Figure 6-1 shows how the dew point temperature changes with SO_3 and water vapour content.

Thus, it is not only the SO_3 concentration that affects dew point corrosion but also the increased water vapour concentration from 9 % in conventional firing to 30 % in oxyfuel firing. The corrosion rate is highest just below the dew point where the SO_3 concentration is high in the condensate present as a film on metallic surfaces. As the temperature decreases, the corrosion rate decreases as the acid is diluted.

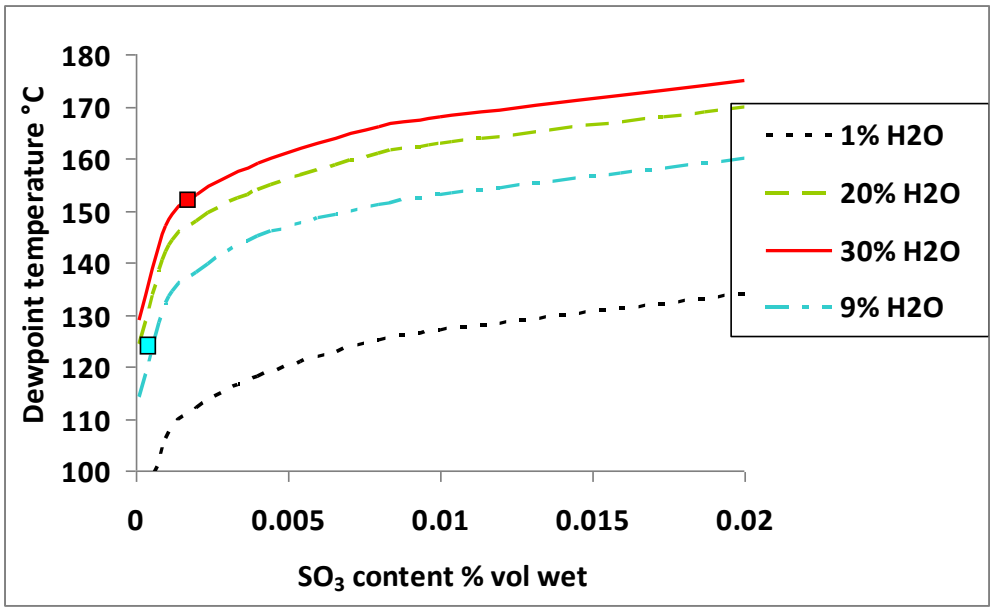

FIGURE 6-1: Dew point temperature depending on SO_3 and water vapour content (taken from Appendix I)

6.3 M.Sc. Exam Project and Further Work:

The motivation for undertaking the M.Sc. project to investigate carburization was that some specimens exposed in Vattenfall regi at the Brandenburg Technical University oxyfuel test facility revealed precipitation (believed to be carburization) which was difficult to explain based on the literature available. Sanicro 28 (a high alloyed steel) revealed precipitations which could be carburization whilst other lower alloyed steels showed no sign of carburization. Due to this result, a M.Sc. project was started to specifically look at this steel and compare it to lower alloyed steels.

Corrosion investigations of two austenitic stainless steels (Sanicro 28, TP347HFG) and a martensitic steel (X20CrMoV121) in carbon containing oxidising environment at 700 °C for 167h and for selected samples 334h were undertaken in the laboratory facilities at DTU-Mekanik. Samples were exposed to three mixtures of gases: CO_2, CO_2-46%H_2O, and air. In addition to the gas atmosphere, also the influence of sample geometry on the corrosion behaviour was examined. Real steel tubes utilised in power plants were used and therefore the influence of curved (concave, convex) versus flat surfaces was of interest. In the laboratory, usually flat surfaces which have a carefully prepared surface finish are used. However, in the plant, the tubes are as received and in the case of oxyfuel it is fireside corrosion thus the convex surface which is relevant. Comparison between these surfaces gives an important link between laboratory investigations and power plant exposures and to what extent results from plane surface can be used to predict behaviour on the curved surfaces of tubes.

Results showed that the oxidation and carburization behaviour of investigated materials was very much influenced by the gas atmosphere. During exposure in CO_2 and CO_2-46%H_2O all steels formed localised or continuous double oxide scale, whereas more protective Cr-rich surface scales developed during air exposure. The morphology and phase composition of the oxide scales were the same in CO_2 as in CO_2-46%H_2O. Moreover, investigations revealed that composition (especially Cr content) and microstructure of the tested materials had an impact on their corrosion resistance. Oxide scales formed for the investigated materials had different morphology and consequently the oxidation rate was found to be the lowest for

Sanicro 28, moderate for TP347H FG, and highest for X20CrMoV121. When exposing the materials to CO_2 and CO_2-46%H_2O they experienced precipitations believed to be carburization. However, precipitations assumed to be carburization were detected only beneath locations where a double oxide scale had formed. The martensitic steel was difficult to assess as there are a large amount of carbides in the original microstructure, and no significant change in microstructure could be observed.

Exposure of Sanicro 28 in air revealed the presence of precipitations both on the convex and concave surfaces. It is believed that these precipitations are due to the presence of both sigma phase and carbides and are not caused by the carbon content within the gas. Thus sometimes the presence of precipitates is not an indication of carburisation due to carbon containing gases but evolution of the microstructure due to heat treatment. In addition, the results from Sanicro 28 and TP347H FG showed that the oxidation behaviour differed on curved surfaces compared to flat faces. In all cases, the oxidation rate was highest on the concave surface. However, it is still unclear whether the difference in formation of oxide scales was influenced by the different samples geometry (curved vs. flat surfaces) or by different surface preparation prior to heat treatments.

Further experiments were conducted as a continuation to this MSc project. It was hoped that the identification of phases within the precipitation zone would be possible but this has not yet been accomplished. Thus there is no positive identification of a carbide rich zone, only circumstantial evidence such as precipitations present after etching. Some of the precipitations observed for Sanicro 28 could be due to sigma phase. Specimens were exposed at 600 °C in CO_2, 700 °C in CO_2 and 700 °C in CO_2+ 46% H_2O + 1%O_2. At 600 °C, there was little sign of precipitation within the steel although there is a duplex oxide present on TP347H FG. This could indicate that longer exposure times are required at 600 °C to see the precipitations present at 700 °C or that the precipitations are due to other phases which are more stable at 700 °C such as sigma phase. This work confirmed the finding that precipitations believed to be carburization occurs primarily due to the presence of a duplex oxide. The presence of water vapour makes the oxide more susceptible to “carburization”. Even if the duplex oxide is not as apparent as in the case of Sanicro 28, the presence of water vapour results in precipitations. These experiments have shown clearly that the austenitic steels could be susceptible to precipitations at higher temperatures. The presence of 1% O_2 in the gas phase was not enough to promote a Cr rich oxide layer on the TP347H FG steel and increased precipitation was also observed.

6.4 Concluding remarks

This work identifies corrosion problems with oxyfuel combustion based on the literature survey and the subsequent laboratory experiments and pilot plant testing results published by Vattenfall. Although there has been an amount of experience with steam oxidation and carbon dioxide and sulphur dioxide, the amount of experience with these components together is limited. The increased sulphur dioxide presence will probably result in sulphate rich deposits similar to those in co-firing. There is the added possibility of carbon deposition within the alloy and oxide and this is observed from laboratory exposures at 700 °C. It is indicated that the presence of water vapour induces a duplex oxide which is more penetrable to carbon ingress from the environment. Thus H_2O+CO_2 have a negative synergistic effect on the corrosion rate. The addition of 1% O_2 is not enough to yield a chromium rich oxide. The laboratory experiments have also indicated that there are differences between the curved and flat surfaces of the tube, where the concave surface results in higher oxidation rates. The difficulties of assessing carburisation are also highlighted as

carbon is difficult to analyse for especially on curved surfaces, and the presence of precipitations are not necessarily a sign of carburisation due to oxyfuel conditions.

It is also suggested that potential problems with water wall corrosion will be likely. This is based on the fact that during coal firing, reducing conditions are sometimes observed on the waterwalls, and an indication of increased corrosion has also been observed by Vattenfall.

With respect to low temperature corrosion, dew point corrosion will be a problem due to the higher concentration of SO_3 and H_2O in the gas phase. Indications of this have also been observed by Vattenfall.

7 Potentials and Consequences when Retrofitting an Existing Power Station Unit to Oxyfuel Combustion

7.1 Introduction

The purpose of this process technology study is to establish the potential and consequences of retrofitting an existing power station unit to oxyfuel combustion on the basis of experience with detailed calculations of DONG Energy's power stations both in terms of boiler and turbine.

The key issues of the operation and control study are:

- To determine the expected performance and efficiency of an oxyfuel retrofit
- To describe the necessary plant alterations/new components
- To describe and thoroughly calculate process coupling
- To analyse furnace and combustion using CFD to validate the calculations and improve the process model, see Chapter 8
- To determine alternative process couplings
- To optimise boiler performance.

This study focuses on retrofit of existing plants. The current design of the boiler; firing system, furnace size and heating surface geometry, is therefore maintained.

The main report, Appendix J, contains a detailed, technical description and documentation of all calculations. This executive summary summarises the assumptions, key results at full load, and the conclusion.

7.2 Boundary conditions

The process technology study focuses on necessary plant alterations and an assessment of the potential and performance of oxyfuel combustion. A number of boundary conditions have been laid down in advance to form the basis of consistent calculations:

Power station unit to be studied.
Studstrup Power Station, unit 4 (SSV4) has been selected as the case study. The unit is coal dust-fired in a double-pass Benson boiler equipped with deNOx and desulphurisation plant. The boiler is fairly representative of DONG Energy's boilers and will provide us with an indication of the challenges generally resulting from a retrofit to oxyfuel.

Oxygen factory
The oxygen factory, producing the pure O_2 for oxyfuel combustion, is considered an external unit and therefore not included in the process optimisation. The production of pure O_2 requires significant power capacity. The power demand is represented in the heat balances as an independent auxiliary consumption and is deducted from the performance of the unit. The power demand is assumed to be constant at 160kWh/kh O_2 irrespective of unit load. This estimate is based on information obtained from oxygen suppliers at several conferences.

Coal
All calculations are based on a coal type representative of all the coal types fired at SSV4. The heating value (LHV) = 25.17MJ/kg.

Turbine cycle
The turbine cycle is included in the model calculation, but no optimisation for oxyfuel is performed.

Calculation scope
The calculations only assess the impact on the unit performance and efficiency. No financial conditions such as investments or operating costs are included.

7.3 Short plant description

The convoy units Studstrup Power Station 3 and 4 are built as conventional CHP plants. Unit 4 was commissioned in 1985. The units are conventional coal-fired steam turbine plants with condensate and feedwater preheating as well as steam extraction for district heating production. Straw co-firing has been established, and after commissioning the units have been equipped with desulphurisation and deNOx plants.

7.4 Calculations

To analyse the consequences of a retrofit to oxyfuel at SSV4, calculations of three process couplings have been performed:

1. Reference model with air combustion
2. SSV4 – retrofit to oxyfuel basis coupling
3. Oxyfuel combustion with hot recirculation before desulphurisation.

This summary contains a general description of the three process couplings, results and comparison of full load results and description of critical process conditions and components. See the full report, Appendix J, for part load calculations, detailed process description and optimisation calculations. Heat balances of all three process couplings across the entire load range are included as an appendix to the full report.

All process calculations are performed in DONG Energy's in-house process calculation tool Mopeds. In Mopeds overall models of boiler and turbine cycles are made, which is essential to an assessment of the impact of significant alterations on the performance of a unit. Over the years, Mopeds has proved to be a reliable tool for process calculations which very accurately match the calculations performed by turbine and boiler suppliers.

7.4.1 Reference on air

The reference is set as air combustion with operating range and performance as is.

Process design
The total process at SSV4 is described to form the basis of the assessment of the retrofit to oxyfuel combustion. The overall flows are discussed based on model drawings, and technical descriptions of key components affected by a retrofit to oxyfuel are provided.

Boiler

The boiler is a dual-pass boiler with a nominal steam generating capacity of 286kg/s.

The boiler has the following nominal data:

Steam flow	286kg/s
Steam pressure HP/IP	245/45 bar
Steam temperature HP/IP	540/540°C

Figure 7-1 shows a graphic boiler model with state variables. Blue lines represent feed water, red lines represent HP steam and pink lines represent IP steam for reheating. The boiler is equipped with flue gas recirculation where cold flue gas after the air preheater is returned to the furnace. To maintain a nominal IP temperature of 540°C, approx 51kg/s flue gas must be recirculated. This means that at optimum control, no water is injected into the reheater steam.

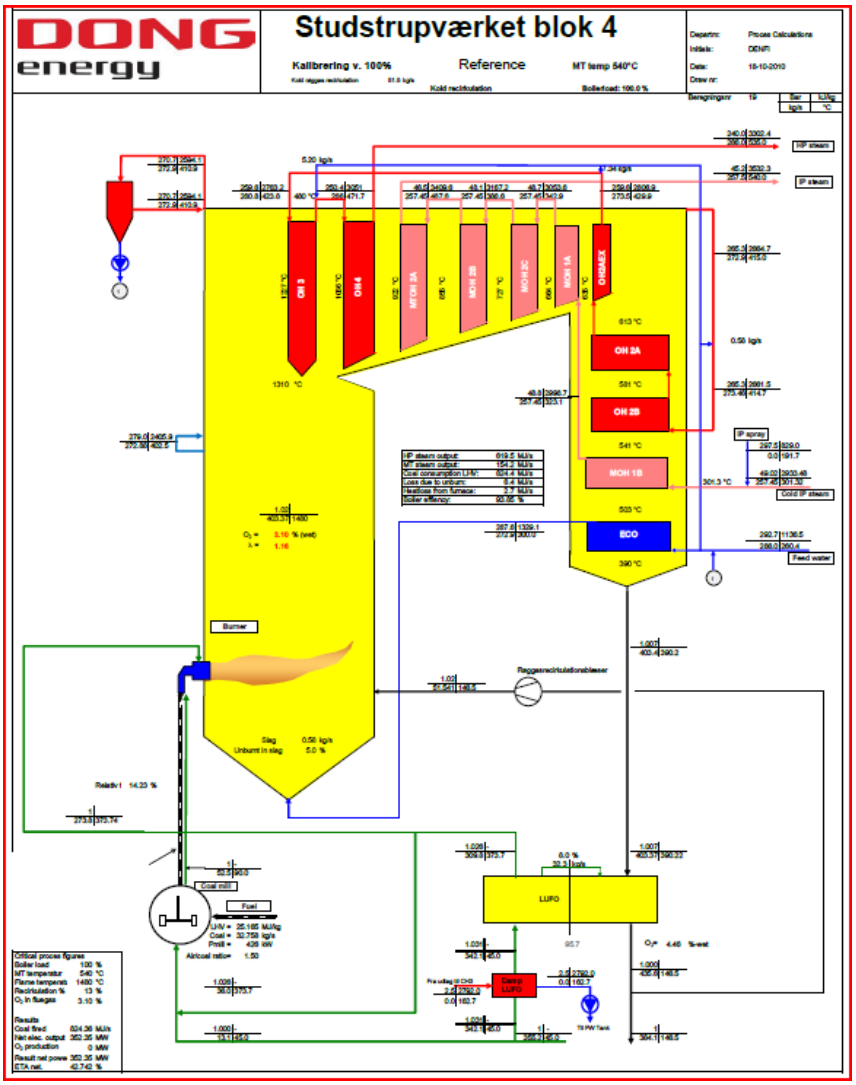

FIGURE 7-1: Graphic boiler model

Turbine cycle
The unit is an extraction plant with an operating range from full condensing mode to full back-pressure operation, i.e. maximum district heating production at current boiler load. During district heating production, steam for the district heating exchanger is extracted before the LP turbine. For further details, please see the main report.

7.4.2 Key boiler components
Listed below are the boiler components, the design of which directly affects the process interfaces in a retrofit to oxyfuel combustion. This facilitates commenting of practical conditions and description of technical challenges.

Air preheater
SSV4 is equipped with a trisector Ljungström air preheater. At retrofit to oxyfuel this design provides the possibility of having different gas compositions in the existing air ducts to the boiler.

Desulphurisation plant
The desulphurisation plant at SSV is of the SDAP-producing type. The desulphurisation degree is approx 90%. Flue gas cooling in the desulphurisation plant is 20 °C above saturation.

Coal mills
The coal is ground into coal dust in the coal mill and dried by means of primary air.

Flue gas recirculation
SSV4 is equipped with flue gas recirculation. The cold flue gas is recirculated after the air preheater and is fed to the boiler. Due to the cold recirculation, the boiler's efficiency is affected by the recirculation flow. During operation, the recirculation flow is adjusted according to the steam temperature at the IP outlet.

7.5 SSV4 – retrofit to oxyfuel basis coupling
The process coupling in the basis solution at retrofit of SSV4 is established to achieve a technically viable solution. A number of potential couplings and variations have been evaluated to reach a basis coupling which is good in terms of the process and addresses the most important technical challenges. The process is based on a number of assumptions:

1. O_2 in the furnace – potentially high local O_2 concentration near the burner.
2. Recirculation after desulphurisation – limited increased concentration of SO_2/SO_3.
3. Primary air to coal mills – dry CO_2 is required.
4. Flue gas flow is increased significantly – fans and ducts to be adjusted.

7.5.1 Basis coupling oxyfuel retrofit
The boiler's water and steam sides are unchanged both in terms of design and flow. A detailed description of the process coupling can be found in the main report. The overall Mopeds model of SSV4 has been rebuilt and adjusted to the basis coupling, and the load range was subsequently verified.

All known temperature limitations for materials in walls and superheaters are met in the calculations.

Optimisation of oxyfuel basis coupling

For the basis coupling, potential optimisation through a temperature increase at the furnace outlet to maximum and a reduction of the total O_2 discharge from the boiler have been investigated. Both initiatives improve the performance at oxyfuel retrofit but require further initiatives at retrofit of the boiler.

7.5.2 Oxyfuel combustion with hot recirculation before desulphurisation

Recirculation of flue gas before the air preheater results in a simpler process and improved utilisation of the energy in the flue gas. The concept must be compared to the basis coupling where cold flue gas is recirculated after the desulphurisation plant. The comparison is made at 100% boiler load with the following boundary conditions:

- O_2 in furnace as basis coupling.
- Dry CO_2 for primary air preheater sector and coal mills.
- Recirculation flow determined by an IP temperature of 540°C.

7.5.2.1 Process coupling for hot recirculation

The hot flue gas is recirculated before the air preheater by means of a fan located in a hot and dirty environment. This concept is known from DONG Energy plants. The flow through the air preheater is significantly reduced at the hot flue gas side where only flue gas for CO_2 purification passes the air preheater and at the cold side where only dry CO_2 is heated for the coal mills.

7.6 Results

All results – full load as well as partial load – and supporting heat balances are included in the main report. Verification of the three concepts at full load has resulted in the following:

		Reference air	Cold recirculation	Hot recirculation
Boiler load	%	100	100	100
IP temperature	°C	540	540	540
Temperature furnace	°C	1480	1371	1382
Recirculation %	%	13	67	67
O_2 in flue gas	%	3.1	3.1	3.1
Results				
Coal fired	MJ/s	824.4	827.6	810.2
Net elec. output	MW	352.3	352.2	352.8
O_2 production	MW	0.0	40.7	39.6
Result net power	MW	352.3	311.5	313.2
ETA net.	%	42.7	37.6	38.7

In addition to the calculated reduction resulting from retrofit to oxyfuel combustion, the cost of capture and compression of CO_2 must be included to obtain the correct efficiency. Internal DONG Energy documents reveal that this results in a further reduction of the efficiency by approx 3.5-4.5 percentage points.

Critical issues in the process couplings for oxyfuel retrofit
Two conditions in relation to the basis coupling described must be investigated further:

The O_2 concentration around the burners is assumed to be higher than the resulting O_2 concentration at the boiler outlet. In consultation with burner suppliers, it must be clarified if this necessary flow control may be obtained throughout the operating range and if burnout using oxyfuel is satisfactory.

Temperature at desulphurisation plant inlet
The potential of increased cooling of the flue gas before desulphurisation must be investigated as the current high temperatures are close to the plant's limit and thereby may present a limitation to the operation. The limitation is caused by increased sulphuric acid dew-point temperature when using oxyfuel.

For hot recirculation before the desulphurisation plant, increased concentrations of SO_2/SO_3 are also critical due to the increased risk of corrosion.

Necessary plant alterations
As the basis coupling for oxyfuel retrofit at SSV is based on the use of existing components and plants to the highest degree practicable, some mechanical components must either be upgraded or replaced. The most important components are:

- ID fans and cold or hot recirculation fan
- O_2 heater
- Heat transfer surface for cooling of flue gas
- Ducting for dry CO_2 for the mills.

The scope of the duct work greatly depends on whether the unit after retrofit is to use oxyfuel alone or both air and oxyfuel. The concept for start-up is not included in this analysis.

7.7 Conclusion

Two concepts for retrofit of SSV4 to oxyfuel combustion have been calculated in Mopeds. The model and the results for combustion and furnace have been verified using a CFD model of the boiler's first pass, see Chapter 8.

Using the assumptions made for process coupling of energy consumption to oxygen production, the efficiency of the entire unit (SSV4) at full load is reduced from 42.7% to 37.6% in the basis coupling. Please note that the efficiency is further reduced when consumption for capture and compression is included.

The basis coupling may be introduced with the least possible uncertainty and minimum re-design of the process. The most important challenges are high local O_2 concentration in the burner zone and the possibility of maintaining steam temperatures without introducing corrosion problems.

Hot recirculation of flue gas provides the possibility of improving the overall performance but not without technical challenges and a recirculation fan critical to oxyfuel operation located in a hot and dirty environment. Without an actual optimisation of the hot recirculation, an improvement of little more than 1% is achieved.

Parameter variations in the recirculation flow also shows the weaknesses of retrofit to oxyfuel compared to a new plant optimised for oxyfuel combustion. Optimising the boiler's heat transfer surface outfit and choice of materials may probably result in improved performance, and a turbine cycle may be designed for potential steam temperatures. Seen as the investment in the oxygen factory is significant even compared to that of a power station unit, it is considered to be beneficial with a plant designed optimised for oxyfuel combustion.

8 Evaluation and Validation of Zero-Dimensional Boiler Model by Three-Dimensional CFD Simulations

As a part of a study of retrofitting of an existing Benson type boiler to oxy-fuel combustion a number of three-dimensional CFD calculations of the coal-fired SSV4 boiler have been performed. The overall study has the goal to evaluate the feasibility of retrofitting a conventional coal-fired boiler to operate at oxy-fuel conditions in order to reduce CO_2 emissions. An in-house steady-state heat and mass balance calculator, MOPEDS, is used to perform calculations at different boiler loads for conventional combustion of coal in atmospheric air. Calculations are then performed at oxyfuel conditions, to investigate any changes in the heat uptake within the boiler. Special emphasis is given to flue gas recirculation and reheater temperature levels.

Since the models in MOPEDS are zero-dimensional, CFD is used to validate the models. It is expected that the better representation of the real boiler geometry in a CFD model will give better results for radiant heat transfer in the furnace.

The CFD calculations are performed in ANSYS FLUENT. Modelling of coal combustion is done using the Discrete Phase Model, DPM, in Fluent. The model follows an Euler-Lagrange approach where the gas phase is modelled as a continuous phase solving the Reynolds-averaged Navier-Stokes equations. The coal is modelled by a representative number of discrete particles that are tracked through the computational domain using a Lagrangian model. The two phases are coupled and interchange momentum, heat and mass.

In order to test the sensitivity of the model to the particle field, a number of simulations are performed where the entire particle source field in a converged solution is replaced by a new one. Iterations are then continued until a new converged solution is obtained. The investigation supports the evaluation of the changes inside the boiler after shifting from air to oxy-fuel combustion.

The CFD model has been calibrated to match the heat uptake in the furnace known from process calculations and operation of the plant. After calibration has been completed, calculations have been performed at oxyfuel conditions. These calculations have been compared to MOPEDS calculations for Oxyfuel.

The results from the CFD calculations show that the change in heat uptake in the furnace is smaller when exchanging the particle source field than the change in heat uptake when shifting from conventional air combustion to oxy-fuel combustion. The variation in heat uptake with different particle source fields is around 10 MW, whereas the heat uptake in the furnace changes with 45 to 50 MW. A comparison between MOPEDS calculations and the CFD model is shown in Table 8-1.

TABLE 8-1: Comparison of furnace heat uptake for CFD calculations and the MOPEDS calculations.

	Air	Oxy-fuel
MOPEDS	295 MW	260 MW
CFD	300 MW	255 MW

The difference between the CFD cases compared to the ones predicted with MOPEDS is not significant. So it is concluded that MOPEDS is an adequate tool, compared to CFD, to model any changes in the combustion process when operating at oxy-fuel conditions as long as one is mainly interested in the main temperature levels and heat fluxes within the boiler.

9 Perspectives of oxy-fuel combustion for CO_2 sequestration in the Danish power production

The project has shown that generally (not addressing the gas cleaning step) there are only limited technical barriers in the application of oxyfuel combustion in power plants - mainly corrosion issues need to be resolved further. The conducted literature review indicated that capturing CO_2 through oxy-fuel combustion can be competitive to the other two methods for capturing CO_2: post-combustion capture and pre-combustion capture. The results show furthermore that it is technical possible to retrofit existing power plants to oxyfuel-combustion, but they also show that retrofitting an existing power plant will imply a number of constraints that may affect the efficiency of such an oxyfuel power plant negatively. Therefore, it seems most likely that oxy-fuel combustion capture will be applied to new power plants especially designed for this concept while post-combustion capture will be applied at existing power plants. This view is in accordance with the fact that almost all planned CCS-demonstration projects around the world on existing power plants will apply post-combustion capture and only a very few work towards retrofitting plants with oxy-fuel combustion.

As the building of new power plants is not foreseen in Denmark in the near future (until 2020), oxy-fuel combustion will not be applied in the near future in the Danish power production. It is very difficult to foresee the possibilities of applying oxyfuel-combustion in the Danish power production in the longer term as it among others will depend on the role that thermal power plants will play in the Danish future power system, on whether CCS will be applied as tool for decreasing CO_2 emissions or as tool for supplying CO_2 for Enhanced Oil Recovery in the North Sea.

The project has also shown that oxy-fuel combustion can both be applied to the combustion of coal, of biomass and the co-combustion of coal and biomass. Oxy-fuel combustion of biomass will lead to power production with negative CO_2 emissions. This may become important in the long term towards 2050, as several scenario studies show that Europe will need these CO_2-negative technologies in order to meets its goals for very low CO_2-emissions in 2050.

Next to the application on biomass, there are a number of less mature developments within oxy-fuel combustion that may become important in the long-term: concepts where gas is combusted in pure oxygen, oxy-fuel combustion in Circulated Fluidized Bed boilers, Chemical Looping Combustion where metal-oxides are used as oxidant instead of oxygen and membrane technologies for producing oxygen that require much less power than the conventional cryogenic technologies.

10 Summary and Conclusions

Oxyfuel combustion, i.e. combustion in a mixture of oxygen and recirculated flue gas (carbon dioxide and water vapour), has gained great focus as one of the possible and promising technologies for carbon capture from power plants. The change from conventional air-firing to oxyfuel combustion would necessitate a considerable rebuild/redesign of both existing and new power plants. This, in combination with the significant changes to the combustion process caused by the change in the overall composition of the combustion medium, lays the ground for the need to generally improve the fundamental knowledge on oxyfuel combustion.

The purpose of this project has thus been to investigate oxyfuel combustion of coal and biomass by laboratory and pilot scale experiments and theoretical work/modelling within the areas:

- General combustion characteristics
- Ash characteristics
- Corrosion of boiler heat transfer surfaces
- Flue gas cleaning for SO_2 (wet FGD) and NO_x (SCR) in an atmosphere with high CO_2 concentration
- Operation/control of large suspension fired boilers using the oxyfuel process

The experimental investigations on the general combustion characteristics and the characteristics of ash have been performed in two setups; a 5 kW entrained flow reactor and a 30 kW swirl burner reactor. The fuels applied were a bituminous, Columbian coal and Danish, cereal straw. The corrosion and flue gas cleaning aspects have likewise been investigated in laboratory and pilot scale setups. The work on operation and control has solely been approached by modelling.

The results presented in this report have shown that it is possible to obtain combustion characteristics (flame temperature profiles, volatile weight loss, intrinsic reactivity of char, etc.) during oxyfuel combustion similar to those found for air-firing when the inlet oxygen concentration in the $O_2/CO_2(+H_2O)$ combustion medium is increased to about 30 vol%. For a given furnace size and similar flue gas oxygen levels, oxyfuel showed superior to air combustion by increasing the fuel burnout. The difference in burnout efficiency between air and oxyfuel combustion increases with an increasing straw share during coal/straw co-firing. This is mainly suggested to be due to the increased importance of the about 50 % longer residence time during oxyfuel combustion (smaller flue gas volume) when the flame length increases with increasing straw share. Due to the high temperatures in the flame and the higher reactivity of straw compared to coal, it is not unlikely that gasification could also contribute to increase the difference in fuel conversion efficiency for increasing straw share. A model (COCOMO) describing coal char conversion in O_2/N_2 and O_2/CO_2 atmospheres was developed. The model was validated against experimental data for a wide range of conditions and showed satisfying agreement.

Oxyfuel combustion likewise showed superior to air combustion by significantly decreasing NO_x emissions. In once-through setups (corresponding to no NO_x in the recirculated flue gas) the average decrease in the NO emission rate was 35 % whereas the emission rate decreased up to 75 % when simulation of recirculation of NO through the burner was performed. At otherwise similar combustion conditions, emissions of CO and SO_2 did not differ from the values found during combustion in air. However, when SO_2 recirculation was simulated about 5 % of the recirculated SO_2 was captured in solid phases, fly ash and

deposits, leading to a slightly decreased emission rate. For the investigated bituminous coal the sulphur content in the fly ash increased about 60 % during simulated recirculation of SO_2. This increase did, however, not compromise the fly ash quality with respect to its usability for cement and concrete production. Sulphur retention in deposits will likewise increase with increasing in-furnace SO_2 levels.

No difference in ash characteristics could be identified between air and oxyfuel combustion due to the otherwise similar combustion conditions. During coal/straw co-firing an increase in the fuel straw share was observed to significantly increase the retention of water soluble K, Cl, and S in the fly ash. For pure straw combustion almost 100 % capture of Cl and S in the ash was determined while about 60-80 % of the potassium was present as water soluble salts. The increase in K, Cl, and S in fly ash and deposits leads to a considerable increase in the corrosion potential compared to combustion of pure coal when the fuel straw share is increased above 20 wt%.

Generally, a change from air combustion to oxyfuel combustion has been observed to lead to increased desulfurization efficiency. However, the amount of residual limestone in the gypsum product may increase due to the high gas-phase level of CO_2.

No problems regarding the SCR process for NO_x reduction have been observed during the experimental tests performed. The activity of the typical, industrial V_2O_5-WO_3/TiO_2 catalyst is about 10 % lower at oxyfuel conditions compared to the air reference. The difference is mainly due to the reduced diffusivity of the reacting species, NO and NH_3, in CO_2 compared to N_2. The reduction reaction is typically diffusion limited. A similar percentage difference was observed at low temperature indicating adsorption of CO_2 on the active sites of the catalyst. In order to achieve full activity of the catalyst, the flue gas oxygen level should be above about 5000 ppmv.

The significant increase in CO_2 concentration within the boiler during oxyfuel combustion could lead to carbon deposition within the boiler tubes. H_2O in high concentrations will produce an oxide layer which is more penetrable than the oxide layer formed during conventional combustion in air where the flue gas H_2O level is lower. The combination of high levels of both CO_2 and H_2O in oxyfuel flue gas has a negative synergistic effect on the corrosion rate of boiler heat transfer surfaces. The high levels of CO within the radiating section of the boiler will induce a significantly increased risk of water wall corrosion. This concern is believed to one of the most important regarding corrosion risks during oxyfuel combustion.

Process calculations have shown that it is possible to redesign an existing boiler to the oxyfuel combustion process while maintaining the critical steam temperatures. The efficiency loss for the basis coupling with cold flue gas recirculation downstream of the desulphurization plant and disregarding the loss associated with the capture and compression steps was 5.1 % points (from 42.7 % to 37.6 %). Hot recirculation of the flue gas could improve the process. However, this is associated with further technical challenges.

Generally, it has been concluded that it would be beneficial to mainly apply the oxyfuel technology to new-build plants rather than as a retrofit solution. In that respect, it is unlikely that oxyfuel power plants are commissioned in Denmark before 2020. However, in order to meet the very strict demands for the reduction of CO_2 emissions within EU by 2050 application of oxyfuel combustion capture at power stations burning CO_2 neutral fuels (biomass) could be an advantageous solution due to the associated, negative CO_2 emissions.

Appendices

Progress in Energy and Combustion Science 36 (2010) 581–625

Contents lists available at ScienceDirect

Progress in Energy and Combustion Science

journal homepage: www.elsevier.com/locate/pecs

Oxy-fuel combustion of solid fuels

Maja B. Toftegaard [a,b], Jacob Brix [a], Peter A. Jensen [a], Peter Glarborg [a], Anker D. Jensen [a,*]

[a] Department of Chemical and Biochemical Engineering, Technical University of Denmark, DK-2800 Kgs. Lyngby, Denmark
[b] DONG Energy, Kraftvaerksvej 53, DK-7000 Fredericia, Denmark

ARTICLE INFO

Article history:
Received 15 May 2009
Accepted 10 February 2010
Available online 31 March 2010

Keywords:
Carbon capture and storage
Oxy-fuel combustion
Coal
Biomass
Emissions

ABSTRACT

Oxy-fuel combustion is suggested as one of the possible, promising technologies for capturing CO_2 from power plants. The concept of oxy-fuel combustion is removal of nitrogen from the oxidizer to carry out the combustion process in oxygen and, in most concepts, recycled flue gas to lower the flame temperature. The flue gas produced thus consists primarily of carbon dioxide and water. Much research on the different aspects of an oxy-fuel power plant has been performed during the last decade. Focus has mainly been on retrofits of existing pulverized-coal-fired power plant units. Green-field plants which provide additional options for improvement of process economics are however likewise investigated. Of particular interest is the change of the combustion process induced by the exchange of carbon dioxide and water vapor for nitrogen as diluent. This paper reviews the published knowledge on the oxy-fuel process and focuses particularly on the combustion fundamentals, i.e. flame temperatures and heat transfer, ignition and burnout, emissions, and fly ash characteristics. Knowledge is currently available regarding both an entire oxy-fuel power plant and the combustion fundamentals. However, several questions remain unanswered and more research and pilot plant testing of heat transfer profiles, emission levels, the optimum oxygen excess and inlet oxygen concentration levels, high and low-temperature fire-side corrosion, ash quality, plant operability, and models to predict NO_x and SO_3 formation is required.

Contents

* Corresponding author. Tel.: +45 4525 2841; fax: +45 4588 2258.
E-mail address: aj@kt.dtu.dk (A.D. Jensen).

0360-1285/$ – see front matter © 2010 Elsevier Ltd. All rights reserved.
doi:10.1016/j.pecs.2010.02.001

1. Introduction

The world, and especially the developing countries such as China and India, is facing an increasing growth in the demand for electrical power [1,2]. New power plants are thus being constructed at a considerable rate in order to keep up with this demand [1–3]. The majority of the recently constructed and planned power plants, on a world-wide basis, are coal-fired [1,2]. Coal is a cheaper and more abundant resource than other fossil fuels such as oil and natural gas while at the same time being a very reliable fuel for power production [4,5].

In the developed countries an increasing part of the energy consumption is being produced from renewable sources of energy; wind, biomass, solar, hydro power, etc. [1]. The main purpose of the shift from a fossil fuel based production to renewable energy is to decrease the emission of greenhouse gases. Especially the emission of CO_2 from the combustion of fossil fuels has gained great focus in recent years in connection with the discussions of global warming. Since the beginning of the industrialization in the late part of the 18th century the amount of CO_2 in the atmosphere has increased sharply from about 280 to 380 ppm [6], see Fig. 1.

Table 1 lists the current and projected CO_2 emissions, in Gton carbon per year, from power generation (both electricity and heat) [1]. Both the emissions and the coal share of the emissions are seen to increase toward 2030 for the world as a whole. Even though the CO_2 emissions are seen to increase within Europe the percentage increase is much less pronounced than for the rest of the world and the coal share of the emissions is expected to decrease. Despite the fact that the ultimate goal for most countries is to phase out all fossil fuels in heat and power production as well as in the transport sector, the share of renewable energy sources increases only slowly and the world will depend on fossil fuels for many years to come. A rapid move away from fossil fuels could result in great conflicts concerning water and land use between biomass for energy production, food production, and forestation [7] as well as in serious disruption to the global economy [8]. The latter is mainly caused by the long lifetime of the energy supply infrastructure. In the transitional period, technologies are sought which will enable the continuous usage of fossil fuels but at the same time eliminate the emission of CO_2.

1.1. Carbon capture and storage

Since power plants constitute large point sources of CO_2 emission the main focus is related to their operation. Currently,

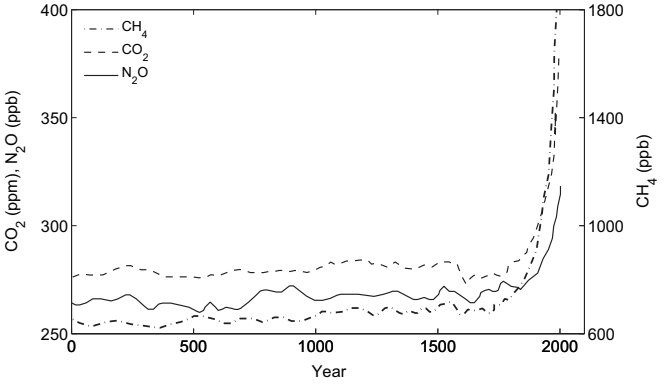

Fig. 1. Development in the concentrations of important long-lived greenhouse gases in the atmosphere over the last 2000 years. The increases in concentrations since about year 1750 are attributed to human activities in the industrial era. Data taken from [6].

Table 1
Estimated CO_2 emissions from power generation (Gton C/year). The numbers in parenthesis indicate the percentage coal share of the emissions. Data taken from [1].

Region	2005	2015	2030
World	3.0 (72)	4.0 (74)	5.1 (74)
European Union	0.38 (70)	0.39 (66)	0.42 (61)

several possible technologies are being investigated which will enable the so called Carbon Capture and Storage (CCS) from power plants [5,8–14]. Both researchers in universities and other research institutions, most manufacturers of boilers and other power plant related equipment, and many power companies are active. CCS will act as a complimentary technology to the ongoing work related to increasing fuel efficiency and the change toward fuels with lower fossil carbon content, e.g. natural gas and/or biomass. As indicated by the term CCS, the elimination of CO_2 emissions include two consecutive operations:

1. Capture of CO_2 from the power plant flue gas
2. Storage of the CO_2 (incl. transport to storage site)

The estimated cost of separation, capture, and compression of CO_2 (point 1) from power plants or other point sources accounts for around 75% of the total cost of a geologic sequestration process [11,15–17].

1.2. Carbon storage technologies overview

The disposal technology should ensure a complete elimination of the CO_2 from the earth's carbon cycle in order to stabilize the CO_2 concentration in the atmosphere. Two types of disposal are defined: sequestration (permanent disposal) or storage (disposal for a significant time period) [7]. These terms are often interchanged in the sense that time periods of more than the order of 10,000 years are considered permanent. Possible storage methods suggested include injection in e.g. depleted oil and gas reservoirs, coal beds, deep saline aquifers, etc. [7,11,17–24]. The estimated storage potential for the suggested options is given in Table 2.

When CO_2 is injected below the caprock in oil and gas reservoirs as well as deep saline aquifers it is first trapped by static and hydrodynamic mechanisms. Secondary trapping mechanisms begin operating over time and act to immobilize the CO_2 in the reservoir, thereby significantly limiting the risk of leakage [7,15,24–26]. This type of storage is considered secure even in the initial injection phase where the secondary trapping mechanisms contribute only minimally [7].

The large storage potential in deep aquifers without structural traps is only obtainable if the traps are not required for secure storage during the initial phases [19]. Even without this storage volume the remaining sites offer storage capability for potentially the next many hundred of years [19,22], see more below. According to Table 2 the estimated retention time in the underground storage sites is 10^5–10^6 years. The retention time for storage in combination with enhanced oil recovery (EOR) differs between authors and ranges from only 10s of years [20,19] to permanent disposal [7].

Table 2
Estimated storage capacities and retention times for CO_2 in different types of sinks on a world-wide basis. Data taken from [7,17–22].

Sink	Storage capacity (Gton C)	Retention time (years)
Enhanced Oil Recovery (EOR)	20–65	10–10^6
Deep aquifers with structural traps	30–650	10^5–10^6
Deep aquifers without structural traps	~14,000	10^5–10^6
Depleted oil and gas wells	130–500	10^5–10^6
Coalbeds	40–260	10^5–10^6
Ocean disposal	400–1200	500–1000

Because of the limited retention times and the great risks of explosive release of CO_2 back into the atmosphere and/or an alteration of the ocean chemistry in the near vicinity of the disposal sites [7] ocean disposal is regarded a less attractive storage solution.

A comparison of the estimated CO_2 emissions from power production, Table 1, and the estimated storage capacities in EOR and saline aquifers, Table 2, yields between 75 and 6000 years of storage on a world-wide basis (2.5 Gton C/year stored). This calculation is based on the fact that due to small size and remote location of many utility plants only a limited fraction of these emissions can be captured and stored cost-effectively. Baes et al. [18] estimate this fraction to be around 50%. CCS is generally not anticipated as a permanent solution to the elimination of anthropogenic CO_2 emissions from electricity and heat generation. The lower limit of 75 years of storage capacity should thus be sufficient in order for the industry to change almost entirely toward renewable sources of energy.

1.3. Carbon capture technologies overview

The identified technologies for carbon capture can be divided into four main categories [5,11,12,23,27–30], described briefly below. Fig. 2 shows the main operations concerned with the post-, pre-, and oxy-fuel combustion technologies.

Post-combustion capture: CO_2 is separated from the flue gas of conventional pulverized-coal-fired power plants. The separation is typically performed via chemical absorption with monoethanolamine (MEA) or a sterically hindered amine (KS-1) [23,31–35]. Amine absorption is a proven technology in the process industry [23,34,36,37]. The demonstrated scale of operation is, however, significantly smaller than the typical size of power plants [34] and serious penalties to the plant efficiency exist at the current state of development [5,8,12,16,34,38–43]. The anticipated drop in the net efficiency of the power plant is about 10–14% points [41,34]. Some current research projects investigate the possibility of developing

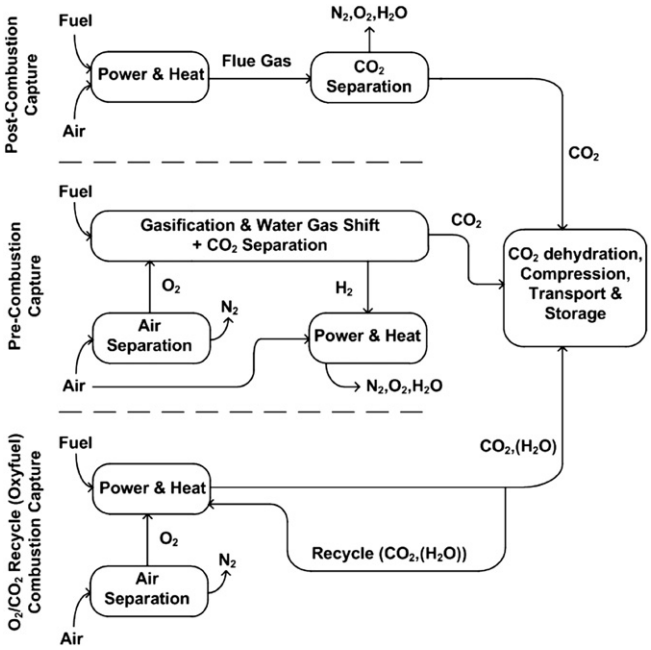

Fig. 2. Possible, overall plant configurations for the three main categories of carbon capture technologies. Adopted from [10].

more efficient absorbents [35]. More on the technology can be seen in [5,8,13,29,44–47].

The chilled ammonia process in which an aqueous solution of ammonia constitutes the absorbent has shown promising reductions in energy consumption in laboratory studies, up to 50%, compared to the MEA process [42]. The process benefits from low operating temperatures and precipitation of ammonium bicarbonate (NH_4HCO_3) yielding a higher CO_2 loading of the absorbent.

Retrofit to existing plants for both process types is considered relatively simple since the capture unit can be added downstream of the boiler and flue gas cleaning systems without any significant changes to the original plant [8,45]. There are, however, strict requirements for removal of SO_2 and NO_2 from the flue gas prior to the CO_2 capture since these components react irreversibly with the absorbent leading to its degradation.

Pre-combustion capture: Also termed fuel decarbonisation. The process is typically suggested to be used in connection with Integrated Gasification Combined Cycle (IGCC) power plants where it is termed IGCC–CCS. Coal gasification is applied to obtain a gas (syngas) containing CO, CO_2, and H_2. The CO is transformed into CO_2 by the water-gas shift reaction and can then be separated from the remaining hydrogen containing gas before this is combusted in a gas turbine. Alternatively, H_2 can be separated from the syngas and the CO combusted in an O_2/CO_2 atmosphere [48]. Some techno-economic calculations [11,30,36,49,50] show that IGCC has promising process economics and plant efficiency characteristics. However, high capital costs are associated with plant construction and IGCC plants are generally much more complicated systems than suspension-fired boilers [51,37]. Only few electricity producing IGCC units exist [29,50,52–54], none of which are equipped with CCS. As a consequence of the few plants and limited operating experience along with the highly integrated nature of the plants compared to the more matured, conventional pulverized-coal-fired power plants, the demonstrated availability for IGCC is significantly less (80–85% versus ~96%, respectively) [5,30,37,50,52,55]. IGCC–CCS is not a viable option for retrofit of existing pf plants [30,51,56,57].

Oxy-fuel combustion: By eliminating molecular nitrogen from the combustion medium the flue gas will consist mainly of CO_2 and water. The plant configuration typically suggested involves flue gas recirculation to the burners to control the flame temperature to within the acceptable limits of the boiler materials. Implementation of the oxy-fuel combustion technology in existing pulverized-coal-fired power plants will induce a larger change of the plant configuration when comparing to the post-combustion absorption processes mentioned above. This is mainly due to the fact that the combustion chemistry is altered by substituting recycled flue gas (mainly CO_2 and water) for nitrogen in the oxidizer. Several of the earlier techno-economic assessment studies indicate that oxy-fuel combustion should be the most energy and cost efficient of the carbon capture technologies [9,16,38,58–63]. This conclusion is mainly based on assumptions of greater boiler efficiency caused by a smaller flue gas volume and the reduced need for flue gas cleaning, i.e. deNO_x and desulphurization, including the derived decrease in capital and operating costs. It is suggested that SO_x and NO_x can be stored along with CO_2 in the geospheric sinks [8,12,64,65]. Typically, no experimental validation of these assumptions has been performed. Whether co-storage of SO_x and NO_x is politically acceptable is, however, questionable.

The main disadvantage of the oxy-fuel combustion technology is the need for almost pure oxygen. The available large-scale technology for air separation is based on cryogenic distillation which will impose a very large energy penalty on the plant [65]. The expected efficiency drop is about 7–11 percent points, or about 15–30% of the generated electricity (net power output), depending on the initial plant efficiency [5,8,12,16,27,29,43,58,59,66–69].

Emerging technologies: Technologies such as membrane separation, chemical looping combustion, carbonation–calcination cycles, enzyme-based systems, ionic liquids, mineralization, etc. impose the possibility to drastically reduce the cost of electricity and the energy penalty concerned with carbon capture from power plants. The papers by Eide et al. [70], Abu-Khader [28], Hossain and de Lasa [71], and Figueroa et al. [14] provide broad overviews of these technologies and their current state of development.

The choice of technology will depend on several factors. First and foremost the economy and the expected development in plant efficiency is of importance. The maturity, expected availability, operating flexibility, retrofit or green-plant built, local circumstances, utilities preferences, etc. will likewise have to be taken into account. No general acceptance of superiority of one of the presented technologies over the others exists. Several techno-economic studies also indicate that with the current knowledge on the technologies no significant difference in cost within the limits of precision of the applied cost estimates can be determined between amine absorption capture, coal-based IGCC type capture, and oxy-fuel combustion capture [5,8,22,57,66,67,72].

Because of the large changes induced in the power plant by the implementation of oxy-fuel combustion, more research is needed to fully clarify the impacts of the introduction of this technology. Many laboratory scale investigations of the technology have been performed within the last two decades and it is generally accepted that it is possible to burn coal and natural gas in an O_2/CO_2 atmosphere. On the other hand, it is likewise recognized that much work still remains in obtaining sufficient insight into the effects on e.g. emissions, residual products such as fly ash, flue gas cleaning, heat transfer, etc.

In 2005, Wall and coworkers [4] published a literature review on the oxy-fuel combustion technology. The work was updated in the broader CCS review by Wall [5] in 2007. The reviews focused mainly on combustion fundamentals, overviews of research groups and their experimental facilities, techno-economic assessments of the technology, and research needs.

The amount of literature on the oxy-fuel technology has increased drastically over the latter years and significant new information is thus now available. The objective of the present review has been to summarize the current knowledge status on the oxy-fuel combustion technology. The current review has two focuses. (1) The possible advantages and challenges associated with retrofitting of existing pulverized-coal-fired power plants to the oxy-fuel combustion technology as well as considerations regarding green-field plants. (2) The reported results from laboratory- and semi-technical scale experiments regarding the combustion process fundamentals, including the flue gas composition and residual products.

2. The oxy-fuel combustion technology and retrofit implications

2.1. Process overview

In open literature, oxy-fuel combustion with recirculation of flue gas was proposed almost simultaneously by Horn and Steinberg [58] and Abraham et al. [60] in the early eighties. Abraham et al. proposed the process as a possible mean to produce large amounts of CO_2 for Enhanced Oil Recovery (EOR) whereas Horn and Steinberg had in mind the reduction of environmental impacts from the use of fossil fuels in energy generation. As such, the technology received renewed interest in the mid-90s in connection with the re-emerging discussions of global warming caused by increased CO_2 levels in the atmosphere [12].

Oxy-combustion can in principle be applied to any type of fuel utilized for thermal power production. The research interests have

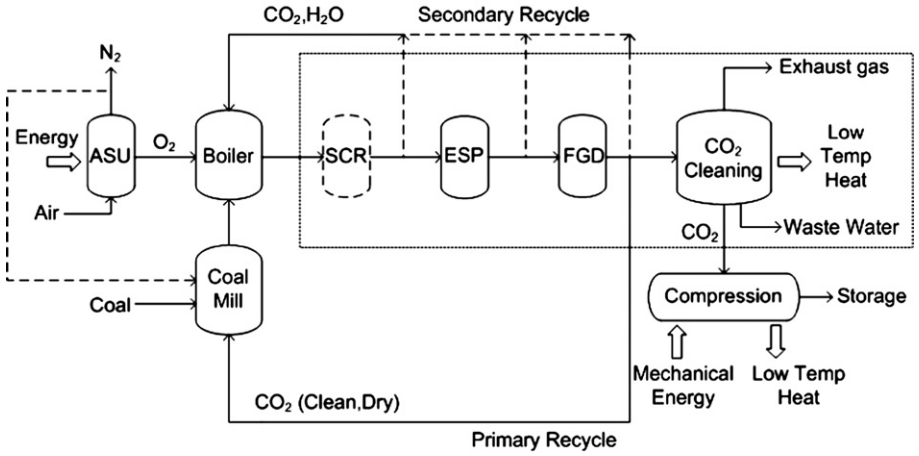

Fig. 3. Possible configuration of an oxy-fuel power plant. ASU: Air Separation Unit, SCR: Selective Catalytic Reduction reactor (deNOx), ESP: Electrostatic Precipitator, FGD: Flue Gas Desulphurization. Energy inputs and low-temperature-heat outputs new to the plant in case of a retrofit are indicated.

mainly been focused on coal and natural gas since these are the most abundant fuels. For these specific fuels the technology is typically termed oxy-coal and oxy-natural gas combustion, respectively. Application of CCS through oxy-combustion of biomass or blends of coal and biomass will result in a possible mean of extracting CO_2 from the atmosphere and thereby possibly inverting the presumed anthropogenic caused changes to the climate [11,23,30].

As indicated in Section 1.3 a shift from conventional air-firing to oxy-fuel combustion in a power plant will induce multiple changes to the plant configuration. Fig. 3 provides a sketch of a coal-fired oxy-fuel plant with indications of the major process steps and the necessary energy inputs and low-temperature-heat outputs new to the plant when retrofitting an existing coal-fired unit. The sketch covers the original state-of-the-art plant with boiler, coal mills, and flue gas cleaning equipment. The final processing of the CO_2 stream, i.e. the removal of water and the non-condensible gases like O_2, N_2, Ar, etc. to meet the requirements regarding purity of the CO_2 stream, as well as the air separation unit (ASU) and the compression step for the CO_2 stream before it is transported to the storage site are new to the plant. The discussion in the coming sections is based on the assumption that an underground geological formation, a saline aquifer, is used as storage site. The type of storage will have an impact on the oxy-fuel process, especially the flue gas purification units, through the quality criteria for the CO_2 stream.

Table 3 provides the results of our calculation on the approximate daily flows in and out of a 500 MW_e oxy-fuel combustion power plant. The calculations are based on a state-of-the-art electrical efficiency of 46% of the conventional plant (supercritical steam parameters, LHV basis) [49] with a 10 percent point decrease due to oxy-fuel operation. The used reference coal is a high-volatile bituminous coal from Colombia see Table 4 for its properties. The oxygen is assumed to have a purity of 100%, in order to simplify the calculations. The combustion is performed in a mixture of 30% O_2 in CO_2 with an oxygen excess of 10%, corresponding to an oxygen concentration of 3% in the dry recycle stream. The recycle ratio for the dry flue gas is 0.75. As a preliminary assumption, the condenser will remove 100% of the water in the flue gas. The CO_2 capture efficiency is ~92%. The remainder of CO_2 is vented to the atmosphere together with the non-condensable gas species in the exhaust gas from the CO_2 cleaning unit. Generally, between 90 and 95% capture efficiency is expected for oxy-fuel plants [30].

The survey of the implications of retrofitting for oxy-fuel combustion in the next sections will be starting at the point of delivery of the sequestration-ready CO_2. The discussion will proceed with the auxiliary units new to the plant and end up with the original parts of the power plant. In order to limit the survey, the discussions, when relevant, will refer to plants utilizing bituminous and/or sub-bituminous coals. Specific aspects regarding lignite fired plants are excluded.

Table 3
Approximate mass streams in a 500 MW_e oxy-fuel combustion power plant with an electric efficiency of 36% on a net heating value (LHV) basis.

Stream	Mass Flow (ton/day)
Oxygen in	9700
Coal in	4400
Waste water (from condenser)	2000
Exhaust gas	1100
CO_2 for sequestration	10,300
N_2 from ASU	31,800

2.2. CO_2 purity requirements

The exact requirements to the quality of the CO_2 stream for different storage scenarios are not yet fully clarified [30,73–75].

Table 4
Properties for El Cerrejon bituminous coal (Colombian).

LHV, as received (MJ/kg)	27.09
Moisture, as received (wt%)	5.0
Proximate analysis (wt%, dry)	
Ash	10.1
Volatile	36.7
Fixed carbon (by difference)	53.2
Ultimate analysis (wt%, daf)	
C	80.70
H	5.41
N	1.69
S	0.73
O (by difference)	11.47
Ash composition (wt%, dry)	
Al	10.89
Ca	1.58
Fe	5.05
K	1.78
Mg	1.39
Na	0.59
P	0.08
Si	26.73
Ti	0.53
O (by difference)	51.37

Table 5
Suggested CO_2 quality specifications from different sources.

Parameter	Modest quality, aquifer storage	High quality, on-shore storage	U.S. Specifications	Saline formation
	Anheden et al. [76]		Lee and Miller [77]	Fout [78]
Pressure	110 bar	110 bar	–	150 bar
Temperature	50 °C	50 °C	<50 °C	–
CO_2	>96 vol%	>96 vol%	>95%	Not limited[b]
H_2O	<500 ppm	<50 ppm	<480 ppmv	150 ppmv
N_2, Ar	<4 vol%[a]	–	<4%	Not limited[b]
O_2	<4 vol%[a]	<100 ppm	<10 ppm	<100 ppmv
SO_2	<200 mg/Nm^3	<50 mg/Nm^3	–	<3 vol%
H_2S	–	–	<10–200 ppm	<1.3 vol%
NO_x	–	–	–	Uncertain
NH_3	–	–	–	Not limited
CO	–	–	–	Not limited
CH_4	–	–	–	<0.8 vol%
HC's	–	–	<5%	<5 vol%
H_2	–	–	–	Uncertain
Glycol	–	–	<0.04 ppmv	–

[a] Sum of N_2, O_2, and Ar should be <4 vol%.
[b] No limit but the impacts on compression power and equipment cost need to be considered.

However, Table 5 provides a number of suggestions for purity requirements found in the literature.

Some authors lay down different criteria for different storage sites [76,78], the differences mainly being associated with the content of water, oxygen and SO_2. Lee and Miller [77] comment on the individual limits with respect to e.g. the minimum miscibility pressure (CO_2, hydrocarbons, and N_2), the risk of corrosion (O_2, water), as well as materials (temperature), operations (glycol), and safety (H_2S). Anheden [76] likewise identifies the aspects which should be taken into account when determining the individual limits. These aspects come down to operational issues, storage integrity, environmental aspects during the full lifetime of the capture and storage chain, health and safety aspects, legal aspects, and economic considerations. The authors state that the requirements arising from exposure limits in case of leakage to air put the strictest restrictions to the process and are, at the same time, the easiest to quantify. The exact requirements will most probably be determined for each individual case of capture and storage.

Jordal and coworkers [10,74] considered the optimum specifications with respect to technical and economical considerations. Not surprisingly, the optima differed. For economic reasons, the preferable option is to co-store as many of the impurities; SO_x, NO_x, non-condensable gas species, and water, as possible. This will reduce the plant investment and operating costs of the process. The disadvantage could be the requirement for more expensive materials in e.g. compressors and pipelines to withstand the potentially severely corrosive environment. There is, however, an economic optimum for the non-condensables (N_2, O_2, NO, CO, H_2, CH_4, Ar, etc.) since co-storage of these species will increase energy and reservoir size requirements as well as capital and operating expenses in the transport chain with an amount proportional to their concentrations [24,73,74]. At the same time the non-condensible gas species will entail an energy and capital penalty when removed from the CO_2 stream [73,74]. Technically, there are two general issues which should be considered. First, the purity requirements for transport and storage with respect to corrosion and the risk of structural changes within the storage formations caused by impurities in the CO_2 stream. Secondly, the limitations to the present best available technology for flue gas cleaning, i.e. particle removal, water condensation, dehydration, SO_x removal and removal of non-condensible gas species, and how to minimize the loss of CO_2 to the atmosphere during the purification process. It is obvious that the technical considerations will set both the lower and upper limits to the purity requirements.

SO_2 receives the largest amount of interest with respect to the effect of contaminants on the structure of storage formations. A typical assumption regards the possibility of co-storing the SO_2 together with the CO_2 because of very similar physical and chemical properties at supercritical conditions [10,58,65,67,75,79]. However, even small amounts of SO_2 may cause problems due to the risk of calcium sulphate formation and thus a decreasing porosity of the reservoir rock [26,75,79,80]. Oxygen could likewise lead to the formation of precipitations [74]. On the other hand, if the concerns regarding SO_2 in the storage formations prove to be insignificant there would obviously be a possible economic benefit from combined capture and storage of CO_2 and SO_2 [80]. The current state of flue gas cleaning on modern power plants involves ~85% removal of NO_x, ~98% removal of SO_2, and ~99.8% removal of particulates [68,30]. The fact that only a finite percentage of the SO_2 is removed with the current best available technology elucidates the importance of identifying the correct purity demands through e.g. field tests since these may have a significant impact on the plant configuration, operating conditions and operating costs [43,64]. Besides the chemical effects of impurities in the CO_2 on the reservoir rock, CO_2 itself has the potential to alter the mechanical properties of the rock [26,17]. Especially calcite ($CaCO_3$) precipitation which can cement the reservoir around the injection well and render further injection impossible should be taken into consideration.

With respect to transportation the greatest concern involves the water content in the CO_2 stream [27,64,73,75]. In the presence of water, CO_2 can cause so called sweet corrosion [26,17]. Water vapor and CO_2 in the presence of liquid water can likewise form solid ice-like crystals known as hydrates [64,73,79,80]. Concurrent presence of both water and SO_2 (incl. H_2S) in the CO_2 stream will increase the risk of sulfuric acid corrosion. If the flue gas is dehydrated to a dew point 5 °C below the temperature required for transport conditions, the sulphur dioxide will behave almost as carbon dioxide in the supercritical state and the two gases should not cause any corrosion problems [26,79,80]. Others report no risk of corrosion at a dew point of less than −60 °C [66]. A requirement for a very low water content in the CO_2 is thus present. This can most likely not be achieved by condensation alone and drying by e.g. absorption in a recyclable dehydrant (triethylene glycol) in combination with the last compression step, see Section 2.3, will be necessary [43,65,74,79].

Some researchers believe that all the limiting factors regarding purity of the CO_2 stream arise from compression and transportation requirements [67,73,74]. In this respect, the demand of dryness is crucial.

Another aspect regarding the concentrated CO_2 stream is the legislative classification. This will depend on the content of contaminants such as H_2S, sulphur oxides, NO_x, hydrocarbons, etc. Significant quantities of these elements could mean that the stream should be regarded as a hazardous waste [7,19,64,73,74,80]. This could eventually lead to difficulties with respect to locating suitable storage sites or a large penalty concerned with the purification.

2.3. CO_2 processing

Assuming that CO_2 transportation should be in pipelines, the CO_2 must be conditioned to both pipeline and reservoir specifications, as described in the above section. Moreover, the stream must be compressed to a high enough pressure to overcome the frictional and static pressure drops and deliver the CO_2 at the storage site without risking flashing of gas anywhere in the process [73,75].

The typically suggested conditions of the CO_2 stream at the delivery point includes the following ranges of pressures and temperatures; 80–200 bar and 0–50 °C [8,11,25,27,41,56,67,74,81–84]. There is, however, a preference for 100–110 bar and a temperature above the critical value (31.1 °C), see Fig. 4. At these conditions the CO_2 is in the supercritical state, even though the presence of impurities will increase the critical pressure of the mixture compared to that of pure CO_2 [67].

2.3.1. Compression step

Compression of gases is a highly energy demanding process. This step will induce one of the larger penalties to the plant efficiency in oxy-fuel operation when comparing to conventional air-firing. Generally, ~2–3% point decreases in electrical efficiency, directly associated with the compression step, have been reported [5,16,50,66,67]. Factors such as compressor efficiency, the amount of impurities in the CO_2-rich stream, and opportunities for integration with the remaining plant will influence the power consumption [65,85].

Since no specific new problems are expected with respect to the compression of CO_2, no demonstration programs are considered to be required [66].

2.3.2. Removal of water and non-condensable gas species

Many existing boilers were not designed to be leak tight and may be difficult to retrofit to oxy-fuel operation where air ingress should be avoided. It is generally reported very difficult to totally avoid air ingress into even small laboratory and pilot scale burners [12,16,63,86–91] and in real size plants it will be almost impossible [62,83,92,93]. The amount of work put into tightening the boiler and flue gas passages will thus be a trade off with the power consumption of the compression unit. Air-fired boilers operate at negative gauge pressure for obvious safety reasons. To avoid air ingress in oxy-fuel boilers one could consider operation at positive gauge pressure. It is, however, questionable whether the avoidance of air ingress can counterbalance the enhanced risk of severe CO and CO_2 poisoning of the boiler surroundings and the necessary safety systems to avoid casualties [83]. The amount of air leaking into the boiler and flue gas ducts is believed to constitute around 3% of the flue gas mass flow (1% in boiler and 2% in ESP) [5,40,67,94] for a new-build plant. As the ingress of air typically increases over time, older boilers can have air in-leakage rates of 8–16% [65,67]. Significant air ingress will reduce the CO_2 concentration in the flue gas and thus result in increased costs for CO_2 cleaning since the non-condensable gases most likely must be removed before (or during) compression. According to Tan et al. [12] the air ingress level should be limited to about 3% in large-scale plants to obtain CO_2 concentrations in the flue gas which will enable an economical treatment of the CO_2 stream.

This additional need for clean-up, besides air separation, is potentially a significant drawback of the oxy-fuel technology compared to e.g. post-combustion capture with amine absorption which has only one purification step [95]. When the oxy-fuel technology was first proposed purification of the CO_2 was not discussed and has most likely not been considered necessary.

The purity of the oxygen for combustion will likewise be a trade off between the ease of liquefaction of the flue gas and the power requirement for the air separation [61,62,67]. Nakayama et al. [61] performed an investigation regarding the combined power requirement for air separation and CO_2 liquefaction under the assumption of no air ingress into the system. Fig. 5 shows the relationship between purity of feed oxygen and power consumption for a plant with a gross capacity of 1000 MW_e. According to the figure, an oxygen purity of 97.5% will require the lowest overall power consumption. Purities greater than this leads to a significant increase in the air separation energy consumption which the decreased consumption in the liquefaction step cannot counterbalance. Others report optimum purities of 95% [8,43,62,66,67,83,95] taking into account the effect of air ingress. At an oxygen purity of 95% obtained by cryogenic distillation, the

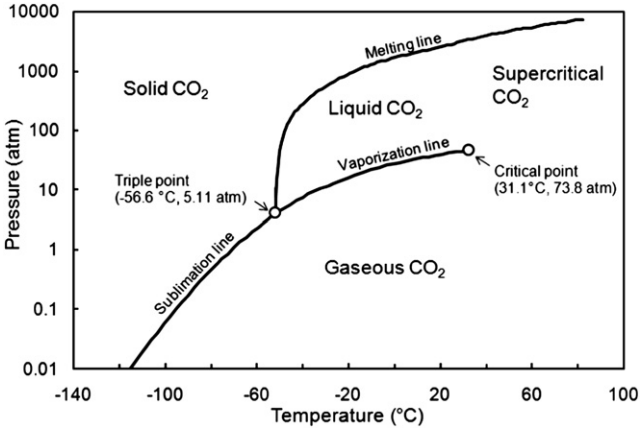

Fig. 4. Phase diagram for CO_2.

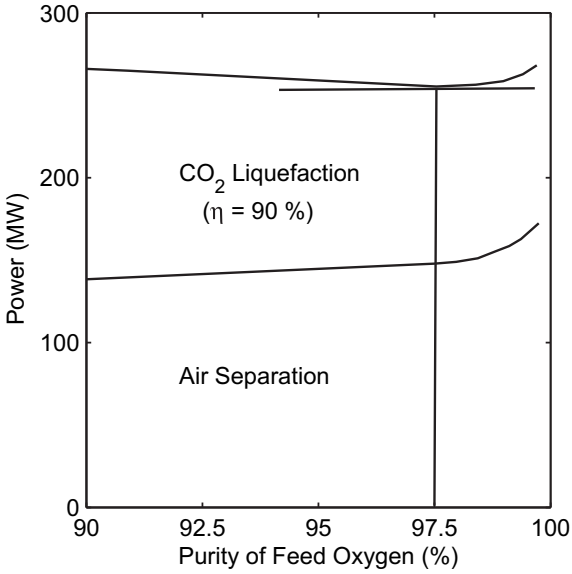

Fig. 5. Theoretical relationship between the purity of oxygen fed to the burners and the power consumption for air separation and CO_2 liquefaction in a 1000 MW_e (gross) plant. Data taken from [61].

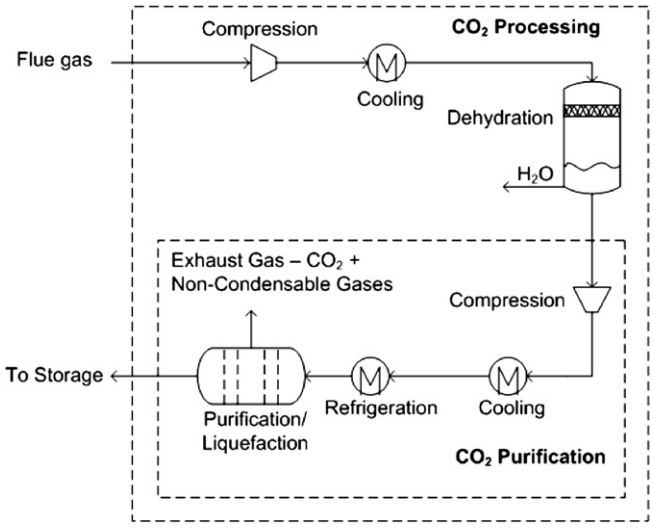

Fig. 6. Possible process scheme for CO_2 processing and purification, i.e. removal of non-condensable gas species, in an oxy-fuel power plant. Adapted from [85].

remaining impurities present will be argon (3–4 mol%) and nitrogen (1–2 mol%) [67,68]. The almost complete avoidance of nitrogen is beneficial with respect to also reducing NO_x emissions.

Fig. 6 illustrates in more detail suggestions to the CO_2 processing and purification steps in an oxy-fuel plant. It is possible that an initial dehydration of the flue gas is performed in combination with the flue gas cleaning step before the initial compression in order to reduce the total flue gas volume and thus costs and equipment size.

After condensation of water vapor, the CO_2 stream will have a purity of about 70–95% depending on oxygen purity, oxygen excess, and air ingress into the boiler [4,8,16,40,43,67,91,92,96]. The condensation process will likewise serve to remove water-soluble gas phase components as well as other species with higher boiling points than CO_2 [74]. Some CO_2 will dissolve in the water and cause a loss in the capture efficiency if not regenerated [74]. If the major part of the flue gas water content is removed at relatively high temperatures and low pressures the loss of CO_2 can be kept low [74].

The flue gas processing and purifications system will produce three streams as indicated in Fig. 6; The CO_2 stream for compression and sequestration, an exhaust gas containing mainly the non-condensable gas species (Ar, N_2, O_2, CO, NO_x) and some CO_2 depending on technology, see more below, and a waste water stream originating from the condensed water.

The exhaust gas stream, around 10–20% of the dry flue gas by volume, is vented to the air. Its composition depends on the chosen cleaning process but is assumed to be about half CO_2 and half N_2, O_2, and Ar. Aspelund and Jordal [73] state that the loss of CO_2 to the exhaust stream for a one column system will be 1:1, i.e. 1 mol of CO_2 per mole of non-condensable gas.

Depending on the plant configuration, especially whether a desulphurization plant is installed, the waste water stream could be very acidic (sulfuric acid, hydrocloric acid, etc.) and thus extremely corrosive (pH 1.5–3) [10,67,92,97]. The flue gas purification unit should thus be designed acid-proof [82,10] as well as the flue gas pathway [10] due to the risk of low-temperature acid corrosion. Additionally, a fraction of the CO_2 (due to its solubility in water) and a large part of the particles remaining after the ESP will be captured in the waste water stream. This stream therefore requires further processing before disposal. This is expected to occur with methods already commercially available [10].

The gas purification unit could e.g. be a flash [40,10] or a distillation unit [27,74,92] since CO_2 forms non-azeotropic mixtures with impurities such as N_2, O_2, and Ar [85]. The thermodynamic properties of the CO_2 stream fed to the purification unit will be affected by its content of impurities (N_2, O_2, Ar, NO_x, and SO_2). Possible ranges of impurity concentrations are: Ar (0–5%), N_2 (0–15%), O_2 (0–7%), and SO_2 (0–1.5%). The changes are mainly affecting the dew and bubble points, heat capacity as well as the enthalpy and entropy. This again will have an impact on the operating conditions, energy consumption, configuration, and separation performance of the purification system [85]. Generally, removal of SO_2 in a flash or distillation system is not preferable since it has a large, negative impact on product purity and energy requirements for even small impurity levels [85] since the thermodynamic properties are very close to that of CO_2.

The basic principle in the flash and distillation units is to utilize the differences in boiling point for the different species to separate them. Fig. 7 shows a comparison between the performances of the two purification systems. The figure reveals that for the same recovery rate and feed compositions the distillation process requires less energy and produces a slightly higher-purity CO_2 stream than the flash process. This has likewise been reported by Aspelund and Jordal [73,74].

The typical CO_2 recovery for oxy-fuel plants is reported at ~90% [12,30,40,43,67]. 100% capture was expected theoretically in one of the earlier studies of the technology [59], under the assumption that the entire flue gas stream could be sequestered in the ocean.

A possibility exists that the initial flue gas cleaning and the CO_2 processing steps can be combined in one process unit. This is interesting in the case that desulphurization is neglected within the recycle loop. Air Products Inc. has proposed a process that removes both non-condensable impurities as well as Hg, essentially all SO_x

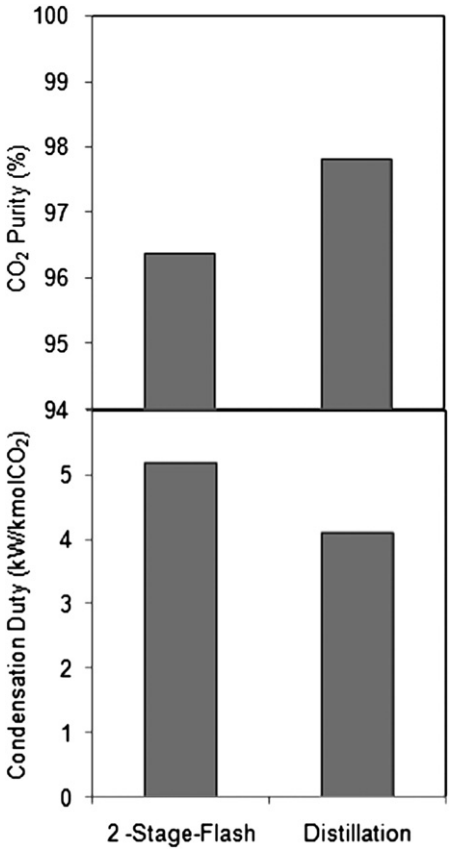

Fig. 7. Performance comparison between 2-stage flash and distillation column based on simulations. The CO_2 recovery rate is 92.15% and the feed compositions (in mol%) to the purification units are CO_2: 76, O_2: 6, N_2: 15, Ar: 2.5, and SO_2: 0.5. Adopted from [85].

and about 90% of the NO_x through the production of waste water containing sulfuric and nitric acid [98].

This compression and purification process has been initially tested in mid-2008 [98]. The tests have confirmed the potential of the process. However, further tests are necessary to gain further understanding of the chemical mechanisms and the kinetics [98]. This is expected to be performed at the Vattenfall Schwarze Pumpe pilot plant [99]. The process should likewise be evaluated against well proven deNO_x and desulphurization technologies [67,43].

2.4. Air separation

The air separation unit provides the oxygen for the combustion. The current state of technology development necessitates the application of a cryogenic distillation unit. No other mature technologies exist which can be applied for the necessary size of operation [40,59,65,79,80,82,93,100], see Fig. 8. At the same time, because of mechanical size limitations it will be necessary to build more cryogenic air separation units to operate in parallel. The largest cryogenic ASU plant currently operating (2008) produces 4500 t/d, but design studies for a 7000 t/d have been performed [65]. As seen from Table 3 the oxygen requirement for a 500 MW_e plant is between 9000 and 10,000 t/d, indicating the need for 2–3 parallel ASU plants.

Cryogenic distillation consumes high amounts of energy in the form of electricity. Preliminary calculations indicate that this operation alone requires about 60% of the power consumption for carbon capture and reduces the overall efficiency of the power plant by about 7–9 percentage points [8,10,16,40,43,50,67]. Major improvements are thus required to yield a more efficient oxygen production. It is not likely to find these improvements within the cryogenic technology [62,65,67] and thus alternative technologies like e.g. ion transport membranes (ITMs) should be investigated further. However, it is possible that some synergies can be obtained from an integration of the ASU's with the power plant, i.e. by using the low-temperature heat from the ASU intercoolers for e.g. feed water heating [93].

The availability of the oxygen plant is crucial to the power plant operation. Typical availabilities of 98–99% and only limited time for maintenance are reported from suppliers [65,67]. Another important requirement is the ability to follow the load changes of the power plant. According to Xu et al. [43] the maximum ramp rate for an ASU is 3%/min. The boiler, however, can generally be operated at a ramp of up to 6%/min. At the same time, ASU's are only able to operate at 60–100% load [82,43] and show rather poor efficiencies below 80%. In combination, this gives rise to some operational difficulties, which should be investigated further.

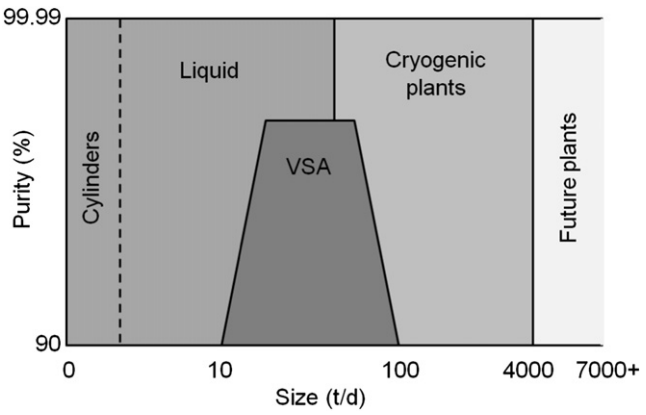

Fig. 8. Oxygen supply technologies. Selection as a function of quantity (tonnes per day) and required purity. Cylinders and Liquid: Continuous delivery from manufacturers in either cylinders or for own storage vessel. VSA: Vacuum Swing Adsorption. Future plants could be either cryogenic or based on other technologies, such as e.g. membranes. Adapted from [65].

The introduction of a liquid oxygen storage could provide a solution in which the difference between demand and production during positive load changes in the boiler is taken from the storage and vice versa during decreases in the boiler load [43,92,99]. The storage facility also makes it possible to shift to air-firing mode within a relatively short amount of time without risking boiler trips in case of unexpected ASU shut-down. Even without the load changing challenges, it may be beneficial to decouple the ASU and power plant by introducing oxygen storage. In that way, the liquid oxygen could provide a means of energy storage in periods with high electricity production from e.g. wind mills. The safety issues related to a liquid oxygen storage on a power plant site should be assessed thoroughly however in order to evaluate its applicability. Preliminary studies by Xu et al. [43], suggest to install a tank with a 500 tonne capacity for liquid oxygen at 2.5 bar (about −175 °C), corresponding to approximately 1.5 h of operation of their 413 MW_e, net, oxy-fuel reference plant.

For economic reasons it should be considered whether the massive amount of almost pure nitrogen, ~31,800 t/d at low temperature, could be applied for a purpose in the plant or elsewhere.

2.5. Flue gas recirculation

The oxygen for combustion is mixed with recycled flue gas to moderate flame temperatures and obtain a boiler heat transfer profile similar to that of air-firing in the case of retrofit. Typically, between 60 and 80% of the flue gas is recycled to the boiler [4,5,8,10,43,66–68,79,80,101,102].

As shown in Fig. 3 two recycle streams will be necessary. The primary recycle is used for fuel transport and corresponds to the primary air in conventional units. It will be about 20% of the total amount of combustion air (RFG + O_2) [67]. The secondary stream will constitute the equivalent to the secondary, tertiary, and overfire (if necessary) air flows when oxygen has been added.

A study performed by Kather et al. [68] determined that the temperature of the recirculated flue gas should be between 200 and 350 °C in order to take into account the operation of an ESP and flue gas fan, among others.

2.5.1. Positioning of recycle streams

2.5.1.1. Primary recycle. A general consensus exists that the primary recycle stream must be cooled, scrubbed, dried and then reheated to about 250 °C or more before entering the mills [66–68,83,101]. The obvious choice is thus as indicated in Fig. 3 to take this stream after the first condensation step during the flue gas processing.

The reheating is necessary in order for the stream to be able to dry the coal and carry the moisture at the typical mill exit temperature of 60–90 °C [67,68]. If the drying capacity of the primary recycle gas is too small the wet coals will clog the mills. Scrubbing of the flue gas ensures removal of SO_2 which would induce corrosion in the mills due to condensation of sulfuric acid at temperatures below 150–160 °C [103]. Xu et al. [43] suggest adding a bypass from upstream the ESP outlet to increase the temperature of the recycle streams approximately 5 K in order to avoid moisture condensation along the recycling ductwork.

2.5.1.2. Secondary recycle. Several options exist for the position where the secondary recycle stream is taken. The dashed lines in Fig. 3 indicate these possibilities. Depending on the actual position the heat and water contents along with the concentration of

pollutants (NO_x, particles, SO_x, etc.) will vary. Even though several reports on oxy-fuel combustion conclude that both deNO_x and desulphurization can be eliminated due to co-sequestration of the impurities with the CO_2 [60,61,67] this is not necessarily possible in practice, see Section 2.2. Most probably, the power plant should be able to run in air-firing mode without capture, at least during start-up and shut-down, and thus also needs the flue gas cleaning equipment to obey the legislation regarding emissions. There is, however, the possibility of by-passing the SCR and FGD plants during oxy-fuel operation. It will still be necessary to remove the particulates to avoid accumulation of solids in the boiler and to prevent the flue gas recirculation fan and gas passages from unnecessary wear due to erosion.

Even though oxy-fuel combustion provides the opportunity of highly reduced emissions of NO_x [4,12,16], it is doubtful if the legislations concerning emissions can be fulfilled without some degree of NO_x removal for all future power plants. During start-up and shut-down which most likely will occur at air-firing conditions NO_x removal is likewise regarded necessary. It is possible that the SCR plant can be run at reduced efficiency during oxy-fuel combustion and that operating costs thus can be reduced. The SCR is typically positioned at high-dust conditions. By passing as large an amount as possible of the flue gas around the SCR it is possible to significantly enhance the catalyst lifetime. Even though ammonia is not added to the flue gas, its passage through the SCR catalyst will reduce the catalyst lifetime. It is likely that the extra cost related to the bypass will be counterbalanced by the reduced cost for change of catalyst may be even with an overall saving. An alternative option is the production of a concentrated liquid waste water stream containing both NO_x and SO_x [66] which can be treated to avoid pollutant emissions to the air, see Section 2.3.2.

The acid gases such as sulphur oxides, HCl, and HF are not reduced through the same mechanisms as NO_x in the boiler. Recirculating the flue gas before desulfurization will result in up to an about 3–4 times increase of the sulphur (and chloride) levels in the boiler [4], see Table 6. Since both sulphur and chloride are potentially corrosive this significant increase can cause problems in the boiler components when firing medium to high sulphur containing coals [43]. Significantly increased levels will likewise have a negative impact on a wet desulphurization plant. The change corresponds to firing coals with excessive amounts of S, Cl, F, etc.

Sulphur retention in fly ash is another area of concern. Significantly increased retention can lead to problems utilizing the fly ash for cement and concrete production. The upper limit for sulphur in fly ash used for concrete is 3 wt% measured as SO_3 [104]. The limiting value for sulphur in fly ash used in cement production is not regulated by standards but rather determined individually between the cement manufacturer and the fly ash producer. However, the limit is usually not less strict than for concrete purposes. Utilization of fly ash from power plants is becoming increasingly important [105]. The potential risk of contaminating the fly ash with excessive amounts of sulphur is thus very critical to the configuration of an oxy-fuel power plant. In conclusion, the secondary recycle stream will most likely have to be taken downstream of some sort of desulphurization process whether it be a conventional wet FGD plant or another process.

The water content in the secondary recycle could potentially have an impact on the combustion characteristics and the general plant performance and efficiency [102]. This is mainly a consequence of the differences in thermodynamic properties, e.g. heat capacity, between CO_2 and water vapor. The effect of wet and dry recycle streams on in-furnace temperatures, ignition, emissions, etc. are discussed in more detail in Section 3. This section will focus on the plant configuration aspects of a wet versus a dry flue gas recycle.

Nakayama et al. [61] proposed five different plant configurations covering both wet and dry recycle, see Fig. 9. The configurations differ in the position of the recycle path and the oxygen preheater. Changing the position of these units will have an impact on the size of both the preheater, the electrostatic precipitator (ESP), and the flue gas cooling unit. The choice of a wet versus a dry recycle will influence the gas recirculation fan (GRF) as will the possibility of recirculating fly ash to the boiler (system A). In relation to the gas recirculation fan, a dry recycle is most favourable since it induces less wear of the fan. On the other hand, a dry recycle will require

Table 6
Example of the effect of recycle strategy on SO_2 concentration in the flue gas, based on 1000 ppmv without recycle. Data taken from [4].

Fraction of total flue gas recycled	Sulphur concentration in flue gas
0.7	3110
0.6	2370
0.5	1920
0.4	1650
0.3	1390
0.2	1230
0.1	1080
0	1000

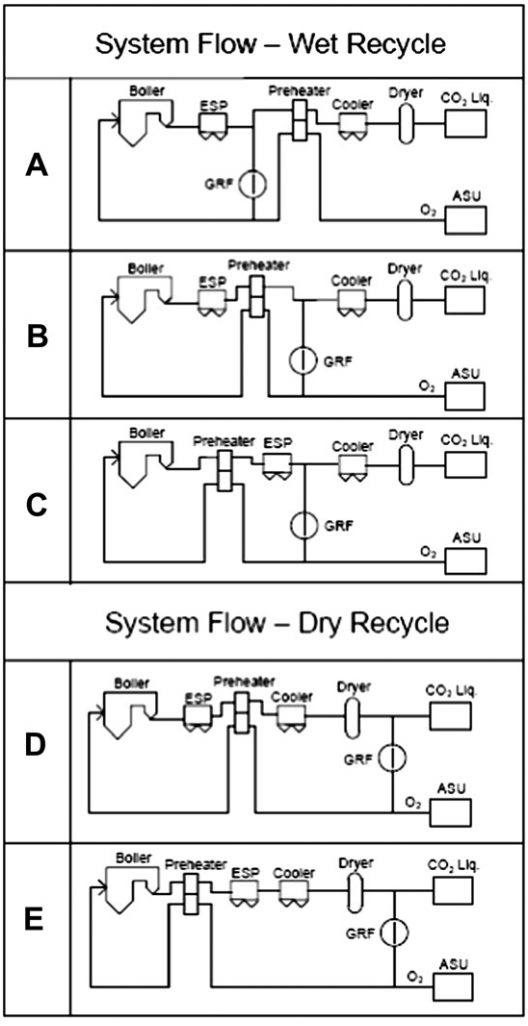

Fig. 9. Different, possible configurations for oxy-fuel combustion with either dry or wet recirculated flue gas. The suggested configurations do not include process units for removal of NOx and SO_2. ASU: Air Separation Unit; GRF: Gas Recirculation Fan, ESP: Electrostatic Precipitator. Adopted from [61].

approximately four times larger capacities of the preheater, cooling, and drying units compared to the wet recycle case.

Nakayama et al. [61] concluded that a wet recycle taken after the ESP and oxygen preheater (system B) was the most promising configuration. The evaluation is based solely on theoretical considerations and no experiments were performed to test the effect of wet and dry recycle on the combustion process. The suggested configurations include only particle removal for flue gas cleaning, not deNO$_x$ nor desulfurization since these were not considered necessary to obtain the required purity of the CO_2 stream. The investigation likewise neglects the fact that some of the recycled flue gas should be used in the coal mills as transport and drying gas.

Dillon et al. [66] likewise assess different recycle arrangements considering both a primary and secondary recycle stream. All of their five arrangements did, however, have the same conditions for the primary recycle, the only difference being the type of equipment for reheating. The authors arrived at a wet, reheated secondary recycle as being the most advantageous option.

As described in Section 2.2, mixtures of CO_2 and H_2O are known from the oil and gas industry to cause potential corrosion problems in piping. Corrosion in the flue gas recirculation ducts in case of temperatures below the water dew point is thus an issue that should be addressed when designing an oxy-fuel plant.

For security and availability reasons, Hellfritsch et al. [82] suggest that the flue gas recirculation should consist of multiple independent paths (e.g. 4 of 25% each).

In relation to retrofit of an existing power plant the exact benefits and disadvantages concerned with each of the possible plant configurations regarding secondary recycle position and its water content should be clarified in order to choose the most optimal solution. For green-field plants it is possible that a specific concept could prove to be generally accepted.

2.5.2. Oxygen addition

2.5.2.1. Primary stream. Fig. 3 indicates that no oxygen is added to the primary recycle before entering the mills. This is mainly due to safety reasons [83]. The highest possible temperature in the coal mills is 120 °C. This limit is set according to materials considerations. In N_2 there is no risk of explosions in the mills if the oxygen concentration is below 12%. The use of air during operation in conventional plants can thus be considered a safety risk and is handled through safety precausions. Due to a suggested, inhibitory effect of CO_2 on explosions it is possible that the O_2 level in the mixture sent through the mills can be raised to above 21% without inducing a risk of explosion [67]. No data are available however.

Even though it is theoretically possible to have relatively high oxygen concentrations in the primary recycle without risking an explosion, some authors advise against it [67]. In practical power plant operation, mills are continually brought in and out of operation to meet the changes in electricity demands. This provides a possibility of transient mismatches between recycle and oxygen flows and thus significant variations in the oxygen concentration. Additionally, equipment failures in control valves, recycle fans, etc. are considered severe security risks [67]. The risk of obtaining significantly higher oxygen concentrations than the safe limit in the coal mills and induce an explosion from ignition of coal dust is thus profound.

With respect to NO_x formation, it is likely that limiting the oxygen concentration in the primary oxidant stream is beneficial since a fuel-rich flame core will be formed. The only concern could thus be flame stabilization. Some preliminary results obtained by IFRF [88,12] suggest, however, that satisfactory ignition and flame stabilization is obtainable when all oxygen is introduced with the secondary oxidant stream. It should be noted that oxygen corresponding to the excess amount, approximately 3 vol%, will be present in the primary recycle.

2.5.2.2. Secondary stream. If no oxygen is added to the primary recycle the entire amount should be mixed into the secondary stream. Due to the risk of spontaneous ignition of dust in the recycle stream there will most probably be an upper limit to the concentration of oxygen in this stream as well. If this limit is exceeded it will be necessary to inject oxygen either directly through the burners or the over-fire ports [83].

Mixing of the oxygen stream into the recycled flue gas cannot be considered unproblematic with the amounts relevant for a power plant. It is crucial that the resulting oxidant stream has a homogeneous composition in order to maintain stable burner operation and prevent safety hazards due to injection of large amounts of pure oxygen to the furnace. Generally, it is very important to minimize the risk of having pure oxygen present together with combustibles anywhere in the system. It is questionable if nozzle injection of one stream into the other without e.g. a static mixer will be satisfactory. In the Schwarze Pumpe pilot plant static mixers are used to ensure proper mixing of oxygen and flue gas [106,94]. Some researchers are addressing alternative equipment which will allow proper mixing in the flue gas ducts [91].

Table 7 summarizes the advantages and disadvantages associated with the different options for oxygen introduction to the boiler. Either way the oxygen addition to the boiler is performed it is most likely that new (or modified) burners will need to be developed to obtain efficient and stable combustion in an oxy-fuel plant [67,107–109].

2.6. Operation of conventional flue gas cleaning equipment

In case it is necessary to include both desulfurization and deNO$_x$ in an oxy-fuel combustion power plant the operation and performance of these units in atmospheres with high CO_2 concentrations should be clarified. These aspects of oxy-fuel combustion seem to be an overlooked area in the research since most investigations neglect these basic units in the plant configuration. Most of those who actually do include these units [4,10,63,80,82] assume that they can operate with exactly the same or even better settings, throughput, and economics as in a conventional plant.

2.6.1. Desulphurization

The largest uncertainties regarding operation concerns the desulfurization plant. Below, the series of reactions occurring during the process in a wet plant are provided. First, SO_2 is dissolved in the aqueous phase producing hydrogen sulfite, (1). Simultaneously, limestone ($CaCO_3$) is dissolved releasing CO_2, (2) and (3). The hydrogen sulfite is oxidized to sulphate in the irreversible reaction given by (4). Finally, gypsum ($CaSO_4 \cdot 2H_2O$) is produced by the reaction between calcium and sulphate ions, (5).

$$SO_2 + H_2O \rightleftharpoons HSO_3^- + H^+ \quad (1)$$

$$CaCO_3 + 2H^+ \rightleftharpoons Ca^{2+} + HCO_3^- + H^+ \quad (2)$$

$$Ca^{2+} + HCO_3^- + H^+ \rightleftharpoons Ca^{2+} + H_2O + CO_2 \quad (3)$$

$$HSO_3^- + 0.5O_2 \rightarrow SO_4^{2-} + H^+ \quad (4)$$

$$SO_4^{2-} + Ca^{2+} + 2H_2O \rightleftharpoons CaSO_4 \cdot 2H_2O \quad (5)$$

Since the wet desulfurization process rely on limestone emitting CO_2 during the conversion equilibrium limitations could arise due

to the high CO_2 concentration in the flue gas. Likewise, the oxidation of HSO_3^- to SO_4^{2-}, (4), in the desulfurisation plant is performed with air in conventional units. Application of air to oxy-fuel desulfurisation would induce an undesirable dilution of the CO_2 with nitrogen [68,101,110]. Instead, a portion of the secondary oxidant stream or alternatively pure oxygen could be directed to the desulfurisation unit. The consequences of each of the three possibilities should be investigated. An other alternative could be to construct the desulphurization plant in such a way that the SO_2 absorption and the oxidation occur in two separate units [68,76,94,110]. In that case air can be used as oxidizer without the risk of reducing the CO_2 concentration in the flue gas.

In the case of a wet recycle the flue gas entering the flue gas desulphurization unit will contain significantly higher amounts of water vapor than in a conventional plant. Even in the case of a dry recycle, the water vapor concentration will increase due to less dilution. The increase in water concentration could lead to an increase of the equilibrium temperature of the gypsum/limestone suspension and thereby influence the kinetics of the desulphurization process. A higher temperature of the suspension could thus lead to a reduction in the degree of desulphurization due to a decrease of the solubility of SO_2.

Studies performed by Air Liquide Inc. together with The Babcock & Wilcox Company in the 30 MW_{th} test facility located in Alliance, Ohio [91,51] revealed no noticeable change in the performance of a conventional wet FGD scrubber. Similar conclusions were obtained by Oryshchyn et al. [111] from laboratory-scale experiments.

Due to the fact that only few results on desulphurization in oxy-fuel atmospheres have been published, this is an area of the oxy-fuel process which needs further attention.

The gypsum produced should likewise meet certain quality requirements, see Table 8. The high partial pressure of CO_2 in the gas phase could limit the dissolution of the limestone in the solution and thus potentially increase the amount of residual limestone in the gypsum. This could cause problems in the further utilization of the gypsum and would influence process economics negatively.

2.6.2. NO_x removal

The concerns regarding removal of NO_x from the flue gas stream are much less than for desulphurization. However, it will still be necessary to verify the performance of e.g. an SCR unit, which is the typical choice for large power plants, if the NO_x reduction obtained during the oxy-fuel combustion is not adequate. An increase in the CO_2 concentration above the catalyst is not considered to have an effect on performance. The possibly increased levels of both SO_2 and SO_3 in the flue gas do, however, impose a risk for reduced performance. SO_3 in the flue gas is known to form sticky and corrosive ammonium bisulfate when NH_3 is added [113]. Increasing the SO_3 level will likewise increase the dew-point temperature for ammonium bisulfate. If the SCR operating temperature falls below the dew point, especially during low load operation, severe clogging of the catalyst must be expected. Additionally, the catalyst acts as an oxidizer and will convert part of the SO_2 content of the flue gas to SO_3 increasing the risk of ammonium bisulfate formation [113].

Table 8
Selected quality requirements for gypsum produced by wet desulphurization of flue gas [112].

Parameter	Value [wt%]
Purity	>95
Residual limestone	<4
Moisture	<10

2.6.3. Particulate removal

As Suriyawong et al. [114] state, the collection efficiency of particulate removal devices is size dependent. Since oxy-fuel combustion shows the ability of altering the size distribution of ash particles, see Section 3.5, the performance of the electrostatic precipitator (ESP), which is the most common particulate removal system in large-scale power plants, will be subject to changes. For both ultrafine (<100 nm) and sub-micrometer (100 nm < d_p < 1 μm) sized ash particles the penetration (1 − collection efficiency) depends on particle size due to different charging effects and these particles are thus not effectively captured.

A potential change in the size distribution of the fly ash from oxy-fuel combustion is not the only aspect of relevance for ESP performance. The flue gas composition could likewise impose a change in the ion production rate within the ESP and thus lead to a change in collection efficiency. Suriyawong et al. [114] have found that for ESP's with positive coronas it is necessary to increase the applied voltage to obtain similar collection efficiencies in oxy-fuel plants as for air-fired plants. However, when negative coronas are used, there is only an insignificant effect of the ESP performance from the change in flue gas composition in the oxy-fuel plant.

Based on equilibrium calculations Schnurrer et al. [115] conclude that the increased SO_3 content in the flue gas is expected to improve the performance of the ESP. This is caused by lower ash resistivity as a result of deposition of sulphate species on the fly ash.

2.6.4. Potential improvements for a green-field plant

For a green-field plant there could be an incentive for applying a hot ESP as the first flue gas cleaning unit downstream of the boiler. The hot ESP is generally considered too costly for air-blown units. Removal of the particulates as the first step will, however, yield the possibility of applying a low-dust SCR downstream of the ESP with low catalyst degradation compared to the more conventional high-dust option. The secondary recycle can then potentially be taken in between the ESP and SCR, which additionally reduces the necessary size of the SCR unit. In order to control the sulphur accumulation in the system and thus prevent

Table 7
Advantages and disadvantages associated with the different options for oxygen addition to recirculated flue gas.

Option	Advantage(s)	Disadvantage(s)
Before coal mills	(1) Sufficient space in recirculation duct to ensure adequate mixing (2) The stream to the mills will be drier than without oxygen (3) With oxygen in primary stream burner design is expected to be closer to that for conventional air burners	(1) Risk of zones with very high-oxygen concentrations if mixing is inadequate and thereby increased risk of combustion/explosions in mills (2) Primary stream will be cooled due to the low temperature of the oxygen
After mills, before burners	(1) No risk of explosion in mills (2) Possible to obtain the same oxygen concentration in the burner as is the case for operation on air	(1) Significant risks are associated with the injection of nearly pure oxygen into a high temperature stream of coal and flue gas
Directly in burners (either pure oxygen lance or with the secondary stream)	(1) No risk of explosion in mills or flue gas ducts (2) No expenses for mixing in primary stream (3) Oxygen lance provides increased control of the mixing of oxygen and fuel in the near-burner zone	(1) Burner design has to be re-thinked (2) Limited capacity for coal drying in mills

both corrosion and ammonium bisulfate degradation of the SCR catalyst due to high SO_3 levels, a desulphurization unit prior to the SCR should be installed.

The major advantage concerned with the change of sequence of the flue gas cleaning units is to reduce the size of the equipment due to the fact that the flue gas volume is reduced with about 60–80% after the secondary recycle has been taken. In the suggested configuration, the desulphurization unit will, however, not be reduced in size. A disadvantage is that if a wet FGD (the conventional choice) is installed before the SCR, additional cooling and reheating will be necessary. These operations will reduce the plant efficiency.

2.7. Boiler and steam cycle

The oxy-fuel boiler is subject to relatively extensive changes regarding chemistry compared to the case of air-firing. The two main, combustion related properties that change during oxy-fuel combustion are [5]:

- Gas radiative properties
- Gas heat capacity

Substituting CO_2 (+water vapor) for N_2 in the oxidant results in a larger specific heat capacity compared to air, see Table 9. Firing with the same ratio between oxygen and 'inerts' will thus result in a lower flame temperature [118–122] and difficulties in stabilizing the flame [12,123]. In order to obtain a stable flame and the same adiabatic flame temperature in oxy-fuel experiments as in air combustion overall oxygen concentrations between 25 and 42 vol% have been reported necessary [87,97,116,118,120–122,124–126]. The span is somewhat dependent on the coal type and the typical values reported for bituminous coals are 28–35%.

CO_2 and water vapor are radiating species as opposed to N_2. The radiative heat flux in the flame zone originating from the gas phase is thus expected to increase in oxy-fuel combustion compared to air-firing at comparable gas phase temperatures. The radiative heat flux from solid particles (soot, char, and ash) depends on a number of parameters. Radiation from ash particles depends mainly on the particle temperature whereas radiation from soot and char is influenced by the mixing characteristics of the flame, local O_2, CO_2, and H_2O concentrations, and temperature.

In coal flames radiation from soot can dominate the heat transfer in the radiative section. The formation rate of soot can be very sensitive to the mixing of fuel and oxidizer in diffusion flames. The near-burner flow dynamics are expected to change in oxy-fuel combustion compared to air-firing due to the changes in flow rates through the burners if conventional burners for air-firing are used. Soot formation and hence the radiation intensity is thus expected to change as well.

2.7.1. Burner operation and flame stabilization

Increasing the oxygen concentration to achieve similar adiabatic flame temperatures to that of air operation is the obvious solution to obtain stable combustion. With this approach the total volumetric flow through the burners and boiler is reduced compared to air-firing because of the overall lower amount of 'inerts'. In order to keep the coal particles in suspension, it has been suggested that the primary flow must have the same linear velocity as in air-firing [83], typically 17 m/s as minimum [116]. Since the density of CO_2 likewise is higher than for N_2, see Table 9, the mass flow ratio of primary to secondary flows through the burner inlets is increased. This could create an imbalance in the burner aerodynamics compared to air-firing and thus have an impact on ignition, flame shape, and mixing [116]. It is possible that the minimum velocity will depend on the density of the primary stream. A lower value than used in air-firing could then prove to be adequate for oxy-fuel combustion. This would have to be tested in larger-scale setups.

Besides increasing the oxygen concentration to obtain stable combustion, other suggestions have been made:

Liu and Okazaki [127] suggested to stabilize the flame by recirculating additional heat with the flue gas while maintaining an air-like composition of the oxidant. In connection with the application of Ion Transfer Membranes (ITM) for air separation they likewise suggested heat recirculation to obtain stable combustion with oxygen concentrations down to about 15 vol% in the burner inlet. Utilization of ITM membranes will require relatively low oxygen concentrations in the oxidant in order to achieve sufficient driving force in the air separation. The authors claimed that the recirculation of heat should not affect the plant efficiency negatively. There has been no reports of experiments with this approach in larger scale.

Another alternative approach is taken by Toporov et al. [107,108] who work on changing the burner design in order to obtain stable flames at low oxygen concentrations in the O_2/CO_2 oxidant mixture. This approach is likewise to enable the use of ITM membranes for air separation instead of a cryogenic unit and thus reduce the penalty on the plant efficiency from about 8 to between 3 and 5% [108]. In order to obtain stable operation their aim is to provide the necessary heat to compensate for the higher heat capacity of the oxidant and the heat used for the endothermic gasification reactions taking place in the near-burner region from the post-flame zone. This is done by promoting under-stoichiometric conditions near the burner region ($\lambda = 0.6$) and having a strong internal recirculation zone to lead hot combustion products back into the burner quarl. A burner design was obtained which allowed stable operation with just below 21% oxygen in the oxidant and an overall stoichiometry of $\lambda = 1.3$. The drawback of this concept is an increase in the recirculation rate of flue gas. However, this is believed to be fully offset by the reduction in power demands for the air separation process [107,108].

2.7.2. Heat uptake

Existing boilers have been carefully designed to match the radiative and convective heat transfer properties of the air-fired combustion process. Especially important is the distribution of heat transfer between the furnace chamber (evaporation) and

Table 9
Properties of gases at 1123 °C and atmospheric pressure [116,117].

	H_2O	O_2	N_2	CO_2	Ratio CO_2/N_2
Density (ρ) [kg/m^3]	0.157	0.278	0.244	0.383	1.6
Thermal conductivity (k) [W/m K]	0.136	0.087	0.082	0.097	1.2
Specific heat capacity (c_p) [kJ/kmol K]	45.67	36.08	34.18	57.83	1.7
Specific heat capacity (c_p) [kJ/kg K]	2.53	1.00	1.22	1.31	1.1
Heat sink (ρc_p) [kJ/m^3 K]	0.397	0.278	0.298	0.502	1.7
Dynamic viscosity (μ) [kg/m s]	5.02e-05	5.81e-05	4.88e-05	5.02e-05	1.0
Kinematic viscosity (ν) [m^2/s]	3.20e-04	2.09e-04	2.00e-04	1.31e-04	0.7
Mass diffusivity of O_2 in X ($D_{O_2/X}$) [m^2/s]	–	–	1.7e-04	1.3e-04	0.8

convective part (superheating) but the maximum heat flux to the furnace walls is also important.

The choice of recycle ratio, i.e. the fraction of the total flue gas flow which is recirculated to the boiler, and thus the oxygen concentration in the oxidant affects the heat transfer by controlling the flame temperature and the volume flow through the boiler [65]. The radiative heat transfer is mainly determined from the flame temperature and the gas radiative properties, whereas the convective heat transfer is determined mainly by the Reynolds and Prandtl numbers, the thermal conductivity, and the temperature of the flue gas passing the superheater banks. Fig. 10 shows the connection between the recycle ratio and the adiabatic flame temperature and flue gas volume. In this respect, the flue gas volume is a rough indicator for the convective heat transfer. It is seen that recycle ratios of either 0.61 or 0.76 yield conditions corresponding to air-firing (with $\lambda = 1.15$), although only for one of the parameters. It is thus not possible to simultaneously obtain both an adiabatic flame temperature and a volumetric flue gas flow through the boiler similar to that of air combustion. Section 3.2 will assess the subject of heat transfer in more detail.

2.7.3. Oxygen excess

It is important to note that excess oxygen for oxy-fuel combustion carries a much greater penalty than in the air-firing case and that the power consumption in the ASU is directly proportional to the amount of oxygen lead to the boiler [95]. A reduction in the oxygen excess would thus benefit both the ASU and CO_2 compression train power demands [66,68,81,95]. In modern power plants the air excess is typically 15–20% ($\lambda = 1.15$–1.2) [68,103,128] corresponding to about 3 vol% O_2 in the dry flue gas. The excess is predominantly determined by the uncertainty in the coal mass flow to each burner. By introducing more efficient monitoring of the coal flow to each burner and thus a better control of the oxidizer and fuel flows, it should be possible to reduce the required oxygen excess during oxy-fuel combustion to no more than 10% [68]. At 10% excess oxygen and an oxidizer containing 30% O_2 the dry flue gas O_2 concentration will likewise be about 3 vol%.

Theoretical considerations regarding the second law efficiency of gas-fired power plants equipped with either oxy-fuel combustion or post-combustion capture have been conducted by Simpson and Simon [95]. Their computations showed that oxy-fuel combustion becomes more favourable with respect to efficiency than post-combustion systems as the oxygen excess level is decreased.

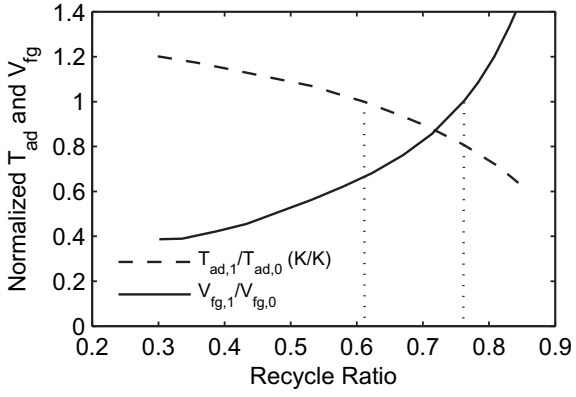

Fig. 10. Theoretical considerations on the effect of flue gas recycle ratio on adiabatic flame temperature, T_{ad}, and flue gas volume, V_{fg}. The reference values, $T_{ad,0}$ and $V_{fg,0}$, are for air combustion. Data taken from [88].

2.7.4. Fire-side corrosion

The change in the composition of the combustion medium in oxy-fuel combustion could potentially give rise to increased risk of corrosion. The increased levels of CO_2, H_2O, and SO_2 are expected to change the corrosion potential of the flue gas. Both aspects regarding metal surface oxidation and corrosion under deposits due to changes in deposit compositions are important to investigate [129–131]. Regarding deposits, especially the co-existence of sulphates and carbonates within the deposits could be critical to the boiler tube surfaces [131]. The aspect of carburization of Cr-containing steels due to high partial pressures of CO_2 could likewise constitute a challenge to materials lifetimes due to brittleness.

Pirón Abellán et al. [132] studied the oxidation of martensitic steels (Cr-containing alloys) in different CO_2 and H_2O-containing atmospheres at temperatures between 550 °C and 700 °C in a laboratory setup. They found significant carburization in high CO_2 containing atmospheres. They expect the carburization to be governed primarily by the permeability of the protective oxide layer toward CO_2. However, the authors show that the presence of water vapor will limit the transport of CO_2 through the oxide layer and thus the extent of carburization. The exposure atmospheres contained no O_2 and the consequence of the presence of excess oxygen on the obtained results will need to be examined to fully clarify the effect of the change from air-firing to oxy-fuel combustion on fire-side corrosion.

2.7.5. Aspects regarding green-field plants

The above discussions are based on the case of a retrofitted conventional air-fired plant to oxy-fuel conditions. For a green-field plant it will be possible to refine the boiler design. The adoption of conditions similar to those of air-firing is not necessarily the most optimal for an oxy-fuel combustion plant. A major target will be a significant reduction or even complete elimination of the rate of external flue gas recirculation. Instead, control of the flame temperature can be obtained from internal recirculation in the boiler [10]. This will likewise have a positive impact on the residence time and thus the burnout of the char particles. The possible avoidance of the external recirculation will reduce the size of the boiler and thus the boiler capital cost significantly [10]. At the same time, efficiency loss due to thermal radiation to the environment and the electricity demand for the flue gas recirculation fans will be reduced.

Maintaining the external recycle is likewise an option. Instead of matching the flame temperature to air-like conditions it would be possible to shift heat transfer to higher temperature throughout the entire boiler, leading to less entropy loss. Higher combustion temperature may lead to more efficient combustion with better burnout at reduced oxygen excess levels. Higher oxygen concentration will at the same time require less flue gas recirculation and thus a smaller volume flow through the boiler.

2.8. Summary

The present section has discussed the effects of retrofitting a suspension-fired power plant to oxy-fuel operation. A number of new process units are necessary; an air separation facility to provide the combustion process with almost pure oxygen, ducts and fans for external recirculation of flue gas to the burners in order to control flame temperatures, and a CO_2 processing facility including a flue gas condensation unit, compressors, and a purification unit to remove non-condensable species from the product stream.

The review of the literature has shown that even though the cost and efficiency penalties associated with the technology are significant, oxy-fuel combustion of pulverized coal is technically and economically feasible for retrofitting of existing power plants. At the

same time, oxy-fuel combustion for CO_2 recovery and sequestration is a competitive power generation technology in relation to post-combustion capture with amines. However, a number of critical aspects regarding the technology and plant configuration have been identified, as listed below. These are the issues which should be investigated in further detail to ensure that the technology is in fact a useful alternative to air-firing and post-combustion capture.

Plant availability: The risk of lowering the availability of the plant due to the introduction of the additional auxiliary equipment could be crucial to implementation.

Plant efficiency: With the currently available cryogenic technology for large-scale oxygen production the efficiency penalty for an oxy-fuel power plant is significant. Besides alternative air separation technologies, it is necessary to investigate additional measures that will allow the improvement of the electrical efficiency. Reduced oxygen surplus during combustion and a high steam cycle efficiency would have a positive effect on the efficiency.

Load changes: The relatively low gradients for load change in the air separation unit compared to those for the thermal cycle could provide a problem with respect to operation of the plant in a system with a large amount of decentralized, non-constant electricity sources, e.g. wind mills. In a world with an increasing fraction of the electricity produced by variable sources, central power plants will be required to run with frequent changes in the load to adjust to the demand for electricity. Additionally, the inability of current air separation units to run at low load without major penalties to the efficiency will require several oxygen plants running in parallel, as well as some sort of storage/buffer capacity.

Enhanced purification: The potential need for two purification steps, i.e. both the air separation unit and the pre-compression purification due to leakage of air into the flue gas ducts, could be a major disadvantage to the process. Post-combustion, in comparison, only requires the amine absorption step. The exact requirements for the final CO_2 quality are still to be determined and they will dictate the plant configuration with respect to the different purification units.

Flue gas recycle: The optimal positioning of the flue gas recycle withdrawal points has not been identified. The choice could have a large impact on both operation, economics, and plant maintenance related to corrosion issues.

Combustion process: The significant changes to the combustion process, including the potential effects on heat uptake, fly ash quality and fire-side corrosion likewise provide a challenge.

Several of the above aspects are difficult to examine either theoretically or during small-scale tests. The information and experience obtained from the operation of a larger-scale demonstration plant will greatly improve the knowledge of the process.

The majority of issues regarding the combustion process is, on the other hand, possible to clarify in smaller scale experiments. Much work has already been performed in this area including heat uptake and burner stability measurements as well as aspects regarding coal particle ignition, burnout, flame propagation, radiating properties of the flame, boiler efficiency, and changes in emission levels. In fact, most of the literature related to oxy-fuel combustion is concerned with the combustion chemistry and emissions.

In addition to the changes in the combustion, issues related to corrosion are also very relevant for the evaluation of the process. Because of the increased concentration of CO_2 and perhaps SO_2 in the flue gas, the risk of enhanced high temperature corrosion compared to conventional air-firing is present.

3. Oxy-fuel combustion fundamentals

The following subsections summarize the work performed on oxy-fuel combustion fundamentals by different researchers and reported in the open literature. The assessment will focus on chemical aspects connected to the boiler and other issues directly related to the combustion, e.g. convective and radiative heat transfer, corrosion, and emissions.

3.1. Research groups and experimental facilities

Tables 10 and 11 provide an overview of the different groups active within oxy-fuel combustion research. The groups have been divided according to the scale and type of their experiments, i.e. whether they run combustion experiments with flue gas recirculation in semi-technical scale or in once-through, laboratory-scale reactors.

Included in the tables is information on the most important parameters for the experiments; maximum reactor temperature, oxygen concentration, fuel type, and oxygen excess, as well as an interpretation of the aim of the research performed by each group.

3.2. Heat and mass transfer effects

The present section covers aspects of the effects of operating parameters such as oxidizer composition and oxygen excess levels on flame temperature and heat transfer in the boiler.

As described in Section 2.7 the differences in the radiative and thermo-physical properties of CO_2 and N_2, see Table 9, affect the combustion process through alterations of the temperature and mass transfer properties of the gas phase. As a consequence, the heat uptake in a boiler will likewise change compared to that of a conventional air-fired plant.

3.2.1. Flame and gas phase temperatures

Croiset et al. [120] report the results of combustion of two different coals in air and different mixtures of O_2 and CO_2 in the 0.3 MW oxy-fuel combustion facility at CANMET. The coals tested were a Canadian western sub-bituminous coal (Highvale) and a US eastern bituminous coal. Temperatures along the centre-line have been measured with a suction pyrometer for air-firing and 21, 28, 35, and 42 vol% O_2 in CO_2, see Fig. 11. The experiments have been performed with an oxygen excess between 1.46 (21% O_2) and 1.3 (35% O_2) for the Highvale coal. For the Eastern bituminous coal the oxygen excess was between 1.2 (28% O_2) and 1.1 (42% O_2), corresponding to 5% oxygen in the flue gas (dry). The data in the lower figure show that for the 21% O_2 case a direct substitution of N_2 for CO_2 in the oxidant leads to a considerably lower temperature in the flame zone, a decrease of up to about 300 °C, caused by the higher specific heat capacity of CO_2 compared to N_2. By increasing the oxygen concentration it is possible to obtain flame and gas phase temperature profiles almost similar to those obtained from conventional combustion in air. The necessary oxygen concentration is somewhat dependent on the type of coal, ~35% for the bituminous coal and ~31% for the sub-bituminous coal. Based on additional experiments the authors conclude that up to 5% nitrogen in the combustion medium has no significant effect on flame temperatures. Comparable results regarding the effect of oxygen concentration on flame temperature have been reported by Wang et al. [118], Liu et al. [121], and Tan et al. [122], among others.

Experiments in a 1.2 MW burner at Ishikawajima-Harima Heavy Industries Co. Ltd. (IHI) [119] explored the effect of wet (16 wt% H_2O) and dry primary recycle (for coal transportation) on furnace temperature and flame stability, see Fig. 12. During the experiments the flow rate and composition of the secondary recycle was kept constant. It was found that drying the flue gas increased the gas temperature near the burner by about 150 °C for the same volumetric gas flow rate and thus helped stabilizing the flame by improving ignition stability. The heat capacity of water

Table 10
Oxy-fuel combustion research groups working in pilot scale and semi-technical scale with flue-gas recirculation.

Group	Ref.	Test unit [MW_{th}]	Unit description	Inlet O_2 [vol%]	Recycle: wet/dry	Coal type	Aim of work (interpretation of the authors)
Vattenfall	[133,94,106,134, 92,99]	30	Down-fired boiler, single burner	Max 40	Dry PFGR/ wet SFGR	Lignite, Bituminous, Biomass	Schwarze Pumpe pilot plant. Investigate the entire technology chain of an oxy-fuel combustion power plant in an industrial relevant pilot scale.
B&W and Air Liquide	[91,51,131,135]	30	B&W Clean Environment Development Facility	–	–	Bituminous, Sub-bituminous, Lignite	Verification of process parameters for full-scale design.
ANL	[118,86]	3	Tower furnace, single swirl burner	22–40	Wet/dry	Sub-bituminous	Determine practical feasibility of the oxy-fuel process from combustion and heat transfer data.
IFRF	[88,12]	2.5	Horizontal furnace, air staged swirl burner	21–26	Wet	Bituminous	Implementation of oxy-firing
B&W	[63]	1.5	Pilot scale boiler, air staged combustion system	21–25	Dry	Sub-bituminous	Feasibility of oxy-firing. Process performance, pollutant formation.
IHI	[87,119,136–139, 116,115,128]	1.2	Vertical, down-fired furnace, swirl burner	27	Wet/dry	5 Bituminous	Implementation of oxy-firing. Direct injection of O_2. Ignition characteristics. Effect of load changes. Ash impacts.
E.ON	[140–142]	1.0	Combustion Test Facility	Max 24	Wet	3 Bituminous	Combustion characteristics, coal ash transformation and deposition, corrosion (50 h tests).
IVD	[143–148]	0.5	Vertical furnace, swirl burner	27–30 (dry basis)	Wet	Bituminous, Lignite	Identification of variations in combustion behaviour. Impact on facility components other than furnace. Continuous operation for ~100 h.
CANMET	[120,97,89,149,150, 9,151,122]	0.3	Vertical combustor, down-fired swirl burner	28–42	Wet/dry	Bituminous, Sub-bituminous, Lignite, NG	Emissions from oxy-fuel combustion. Modelling tool validation. Burner and boiler design.
Doosan Babcock	[72,152,98]	0.16	Vertical furnace, down-fired low-NO_x burner	–	Dry	6 Bituminous	NO_x Reduction Test Facility (NTRF). Demonstration of oxy-fuel combustion. Supply of flue gas for test of novel flue gas cleaning process.
Chalmers	[123,90,153–156]	0.10	Down-fired furnace, swirl burner	25–29	Dry	Lignite, Propane	Cause of NO_x reduction. Gas-phase reactions. Firing strategies for NO_x reduction. Radiation.
CIRCE	[157]	0.10	Bubbling Fluidized Bed combustor	20–40	Wet	2 Sub-bituminous, wood, olive residues	Technical feasibility of oxy-fuel combustion of blends of coal and biomass.
TU Dresden	[101,110]	0.05	Vertical reactor, down-fired burner	20–30	–	Lignite	Investigation of combustion related parameters. Validation of CFD model. Production of flue gas for flue gas cleaning test pilot.

Table 11
Overview of oxy-fuel combustion research groups working in once-through laboratory-scale reactors.

Group	Ref.	Test unit [kW_{th}]	Unit description	Max T [°C]	Inlet O_2 [vol%]	λ	Fuel type	Aim of work (interpretation of the authors)
Tokyo	[158,127,159]	–	Flat flame burner	1177	21	0.7–1.2	Anthracite/CH_4	Cause of NO_x reduction. Investigate concept of heat recirculation.
Nagoya	[96,160,161]	–	Quasi-1D EFR	1300	20–100	0.7–3.3	3 Bituminous, Semi-Anthracite	Influence of λ, O_2 concentration, temperature, and type of coal with and without initial NO_x.
Nagoya	[109]	145	Bench-scale vertical furnace	> 3000	85–88	0.9–1.1	Sub-bituminous	Verify lab-scale results for high-oxygen concentration oxy-fuel combustion with respect to NO_x emission and fuel burnout. Burner design.
Leeds	[162,121]	20	Down-fired coal combustor	1350	21, 30	1.2	7 Bituminous	Comparison between air- and oxy-firing. Sensitivity to different fuels.
IVD	[163,164,143–148,165]	20	EFR	1400	21, 27, 35	1.15	4 Bituminous, Lignite	Comparison between air- and oxy-firing. Effectiveness of air-staging. Sulphur emissions formation.
Sandia	[166,126,167,168]	–	Optical EFR facility	1730	6–36	–	Bituminous, Sub-bituminous	Ignition devolatilization, and combustion rate of pulverized coal particles.
Sandia	[169]	–	Multi-Fuel Combustor (MFC)	1350	12–36	6.67	Bituminous/NG	NO_x formation mechanism.
TU Munich	[170,171]	200	Side-fired furnace	–	Up to 50	0.3–4	NG	Proof-of-concept for controlled staging in oxy-fuel combustion.
DTU	[172–174]	–	Laminar Flow Reactor	1527	0.05–0.4	0.25–8	CH_4	Investigate chemical effects of high concentrations of CO_2. Dependence of presence of NH_3 and NO.
BYU	[124,175,176]	–	Multi-fuel Flow Reactor (MFR), laminar	1627	21–37	0.75–1.05	2 Bituminous, Sub-bituminous	NO_x formation and reduction.
TU Aachen	[177]	25	Gas Combustion Chamber	900	14–21	1.15	CH_4	Stabilization of flameless combustion with low O_2 concentrations.
TU Aachen	[107,108,178,179]	100	Lab Scale Oxy-coal Test Rig	1250	19–30	1.3	2 Lignite, 3 Bituminous	Burner design for stable oxy-fuel combustion at low O_2 concentrations. NO_x emissions comparison between flameless and flame combustion.
CSIC	[180]	–	Entrained-Flow Reactor	1100	21–35	0.75–4	2 Bituminous, Anthracite, Semi-anthracite, Biomass	Ignition and burnout of coal/biomass blends.
Northeastern Uni.	[181]	4.2	Laminar-flow Drop-tube Furnace	1327	20–100	–	Bituminous, Lignite, Synthetic char	Comparison between air- and oxy-firing. Volatile flame and char burning phenomena. Effect of particle size.
Huazhong	[182,183,125]	–	Drop-Tube Furnace	1500	20–40	–	5 Bituminous	Ash formation. Comparison between air- and oxy-firing.
ECN	[184]	–	Lab-scale Combustion Simulator	1450	25–28	–	Coal, 2 Biomasses	Coal/biomass blends. Effect of different burner zone residence times on burnout, emissions, and fouling.
Utah (UU)	[185]	29	U Furnace	1550	21	1.15	3 Bituminous, Sub-bituminous, Lignite	Fate of char-N during both air- and oxy-fuel firing.
Utah (UU)	[186]	100	Oxy-Fuel Combustor	1088	21–30	1.15	Bituminous	Provide data for validation of coal-jet ignition model.
Washington Uni. in St. Louis	[117,114]	–	Tubular furnace	1200	20–50	–	Sub-bituminous	Understand effect of oxy-fuel combustion on sub-micrometer particle formation and mercury speciation.
Pennsylvania State Uni.	[187]	–	Drop-Tube Reactor	1550	21–30	1.25	2 Bituminous	Char burnout and CO emissions investigations.

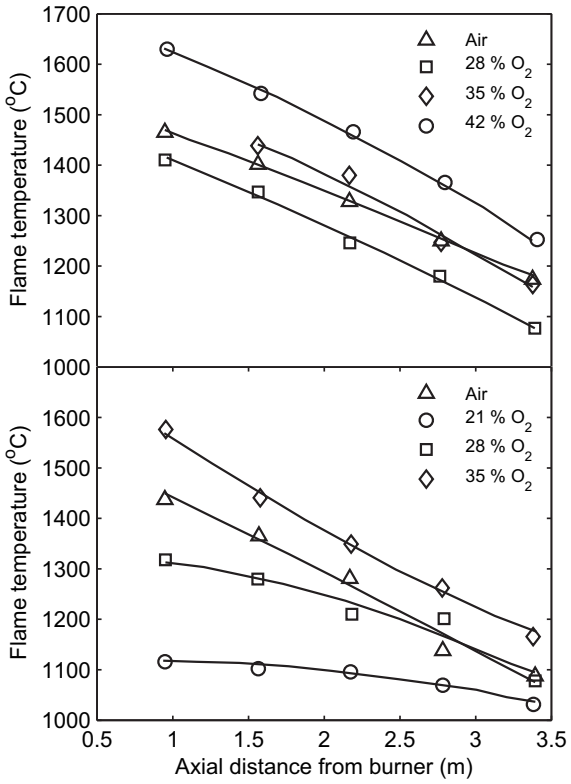

Fig. 11. Top: Centre-line axial temperatures for U.S. eastern bituminous coal burned in different O_2/CO_2 mixtures. The oxygen excess yields a dry flue gas O_2 concentration of 5%. Bottom: Centre-line axial temperatures for Canadian western sub-bituminous coal (Highvale) coal burned in different O_2/CO_2 mixtures. The oxygen excess was between 1.46 (21% O_2) and 1.3 (35% O_2) corresponding to approximately 8% O_2 in the dry flue gas. Both set of data are obtained in the CANMET 0.3 MW combuster operated at a firing rate of 0.21 MW. Data taken from [120].

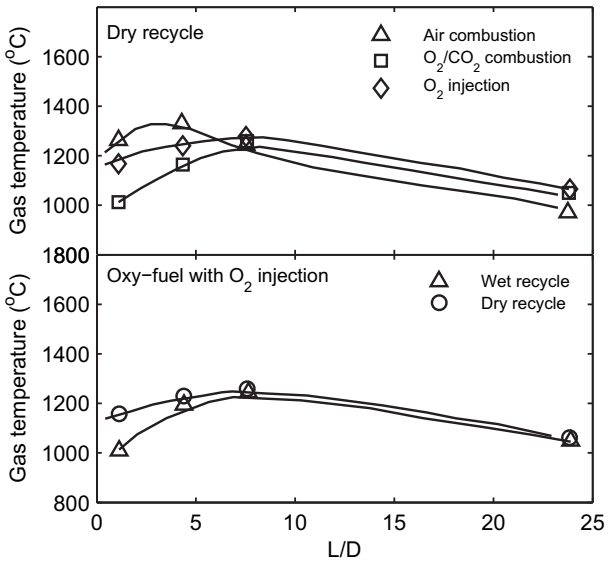

Fig. 12. In-flame gas temperature profiles along burner axis in the IHI 1.2 MW burner for a low-volatile bituminous coal (coal A). The overall oxygen concentration in the combustion gas is 27 vol% (30 vol% in the secondary stream). Top: Effect of pure oxygen injecting through burner in the case of a dry primary recycle stream. Bottom: Effect of wet and dry primary recycle stream in the case of direct oxygen injection. Wet flue gas contains 16 wt% H_2O. Data taken from [119].

vapor is significantly lower than that of CO_2, see Table 9. Taking only this factor into account, the presence of water vapor in the recycle would act to increase the flame temperature, i.e. the opposite effect of what was observed. These findings thus suggest that factors such as radiation and endothermal radical formation (O, OH, H, etc.) dominate the temperature effect of water vapor in the recycle.

Injection of pure oxygen through the centre of the burner likewise increased the gas temperature in the near-burner area compared to a similar experiment with the same O_2/CO_2 ratio in the oxidant but without separate oxygen injection.

3.2.2. Radiative and convective heat transfer

As mentioned in Section 2.7, it is essential to match the flame and heat transfer characteristics for oxy-fuel combustion to those for air-firing in case of a boiler retrofit. In order not to reduce plant efficiency or induce operational difficulties, the ratio between radiative and convective heat transfer should be maintained similar to that of air-firing as well [12].

3.2.2.1. Overall heat transfer. Experiments performed by IFRF [88,12] have shown that a recycle ratio of 0.58 (26 vol% O_2) yields radiative and convective heat transfer rates similar to those of air-firing in their experimental setup. The observed, optimum recycle rate is marginally lower than the theoretically determined value, see Fig. 10, which is caused by some degree of air leaking into the boiler and the fact that pure CO_2 was used for fuel transportation [88].

Investigations of the possible differences between wet and dry recycle has been performed by the Argonne National Laboratory [86], see Fig. 13. The experiments showed that the optimal $(CO_2 + H_2O)/O_2$ molar ratio is different in each case. The ratio yielding the same overall heat uptake changed from 3.25 (equal to a recycle ratio of 0.68 or 23.8 vol% O_2 at the burner inlet) for the wet case to 2.6 (recycle ratio of 0.63 or 27 vol% O_2 at the burner inlet) for the dry case. The optimum recycle ratios were likewise validated at reduced load and with a bituminous coal. Wall et al. [128] saw a similar difference between wet and dry recycle. Their values were 28% and 35% for wet and dry recycle, respectively. The difference suggests that the absolute concentration of water vapor in the boiler has a significant effect on overall heat transfer efficiency. The exact reason for this influence is not clear and modelling could provide indications to the influence from different factors such as radiation, thermo-chemical properties of the gases, etc.

3.2.2.2. Radiative heat transfer. The main contributor to the heat transfer from a flame from conventional fuels is thermal radiation [4,5]. The radiating species considered for pulverized-coal-fired systems are H_2O, CO_2, CO, SO_2, soot, char, and ash particles [65,86,128,188].

The presence of higher concentrations of CO_2, H_2O, and SO_2 in oxy-fuel combustion will increase the non-luminous radiation [65]. Payne et al. [86] and Khare et al. [116] estimated gas emissivities in both air- and oxy-fuel atmospheres. Even though their estimates are not in exact agreement, they generally find a difference of 0.1 between the two types of environments, e.g. from 0.45 in air to 0.55 in oxy-fuel [116,128].

Because of the higher concentrations of H_2O and CO_2 in the furnace and their higher gas emissivities compared to nitrogen, the radiative heat transfer in the boiler will exceed that of conventional air-firing for the same adiabatic flame temperature [4,5,128,155]. In order to obtain the required heat transfer profile in both the radiative and convective passes a slightly lower oxygen concentration than required to reach a comparable adiabatic flame temperature should thus be chosen [4,5,128]. Typical results suggests a decrease of the oxygen concentration of 2–3 vol%. The use of the adiabatic

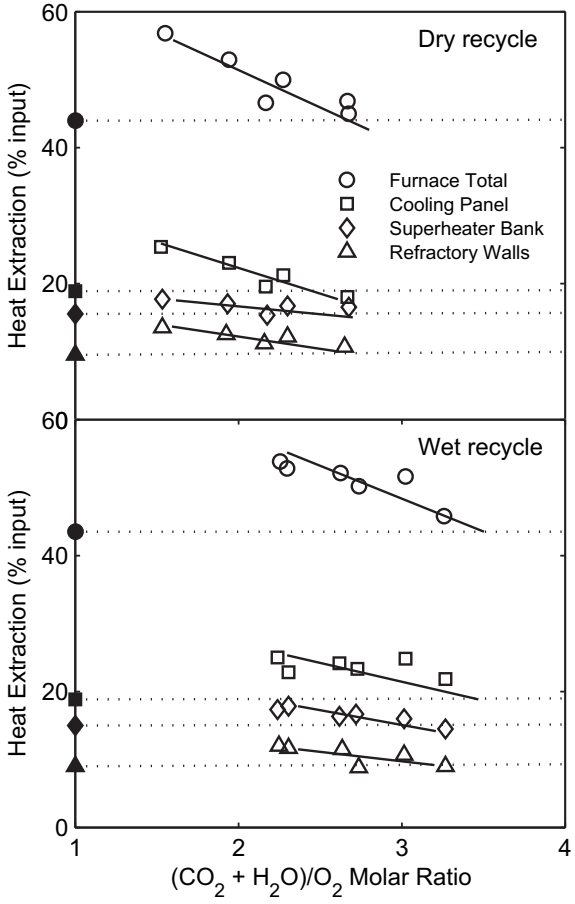

Fig. 13. Heat extraction in different furnace sections of a 3 MW_{th} setup as function of the $(CO_2 + H_2O)/O_2$ molar ratio in the flue gas for dry recycle and wet recycle. For the dry case the recycled flue gas contains 5% residual H_2O due to lack of efficiency in the water removal system. Solid symbols correspond to experiments in air. The coal tested is sub-bituminous (Black Thunder). Data taken from [86].

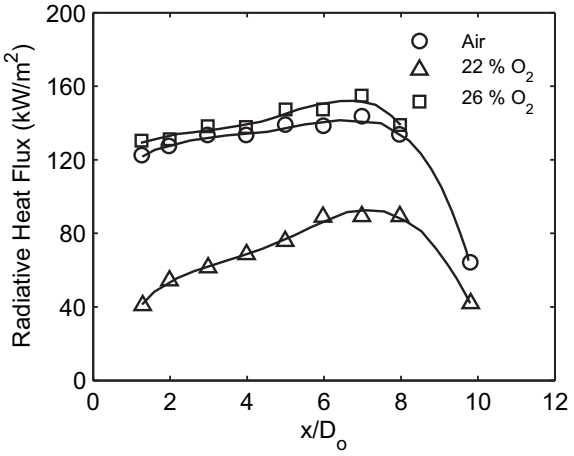

Fig. 14. The effect of recycle ratio on the net radiative heat flux along the IFRF 2.5 MW furnace operated with wet flue gas recirculation. Results obtained for a bituminous coal during air combustion and oxy-fuel combustion with oxygen concentrations of 22% and 26% at the inlet. These oxygen concentrations correspond to recycle ratios of 0.73 and 0.58, respectively. Data taken from [88].

flame temperature as a rough indicator of radiative heat transfer characteristics is thus altered compared to air-firing [88,12].

Fig. 14 shows the radiative heat transfer profiles for three different coal flames; the air-firing case, as well as oxy-fuel flames with overall oxygen concentrations in the oxidant of 22 and 26 vol %. The experiments are performed in the IFRF 2.5 MW_{th} furnace. It is seen that 26% O_2 in the oxidant yields a profile very similar to that of air-firing, as expected. At the same time, the inlet oxygen concentration of 26% was reported to yield in-flame gas composition trends, combustion performance, flame length, and flame stability comparable to normal air operation.

Experiments on oxy-fuel combustion of propane [153,155] have revealed an up to 30–60% increase in the flame radiation intensity (27% O_2) at peak levels compared to air-firing. At the same time, the gas temperature levels are generally slightly lower for the oxy-fuel case. The authors observed that the increased gas emissivity due to enhanced CO_2 concentrations could not account for the entire difference. Further investigations showed that the in-flame soot volume fraction increased when shifting to oxy-fuel conditions [153]. Due to the lower volumetric flow rates and higher fuel concentration compared to oxidant in the oxy-fuel combustion the concentration and residence time of soot precursors in the near-burner region are increased. The formation of soot will thus be promoted [155]. These mechanisms for a gaseous fuel most probably also apply to volatiles combustion in coal-fired operation. The relative effect of an enhanced soot formation from volatiles on overall radiation from a solid-fuel flame is not known and could thus be the subject of future research.

Shaddix and Molina [168] measured the soot cloud size for a bituminous and a sub-bituminous coal in both N_2 and CO_2-based combustion media. Fig. 15 show the results for the bituminous coal. Generally, oxy-fuel combustion leads to larger soot cloud formation compared to the nitrogen based experiments at equivalent oxygen concentrations, confirming the results from Andersson et al. [153,155]. For increasing oxygen partial pressure the soot cloud size decreases for both types of combustion atmospheres.

The effect of in-flame particulates on flame radiative properties is mainly a function of their total mass and temperature. The absolute amount of ash does not change between air- and oxy-firing operation for equal fuel input. The amount of soot in the flame can, on the other hand, change drastically with changes in the near-burner flow dynamics. Changes in the burnout rate of char can likewise affect the location of heat transfer by radiation in the flame zone.

Besides experiments on propane, Andersson et al. [188] conducted radiation intensity measurements in air- and oxy-fuel flames burning lignite. They found that the shift in combustion medium resulted in only a negligible increase in the total radiation intensity at comparable gas phase temperatures. Due to gas-particle overlaps and the fact that particle radiation dominates in solid-fuel flames the effect of increased gas emissivity is limited. Regarding the gas phase, the authors concluded, however, that operating with a wet flue gas recycle would have a much larger impact on radiation intensity in large-scale boilers than the increase in CO_2 partial pressure. This observation is in line with that of Nozaki et al. [119].

3.2.2.3. Convective heat transfer. The increase in both density and heat capacity of the flue gas from increased concentrations of CO_2 and water vapor will increase the heat transfer in the convective section of the boiler [4,5] (for the same volumetric flow and entering temperature as during air-firing). However, in order to obtain an adequate temperature and heat uptake in the radiative section the flue gas flow is reduced due to the necessary increase in oxygen concentration. The resulting heat transfer rate in the convective section is not necessarily reduced in comparison with air-fired conditions as a consequence of the reduced flue gas flow rate. The convective heat transfer is a function of the Reynolds number, the Prandtl number, and the thermal conductivity of the

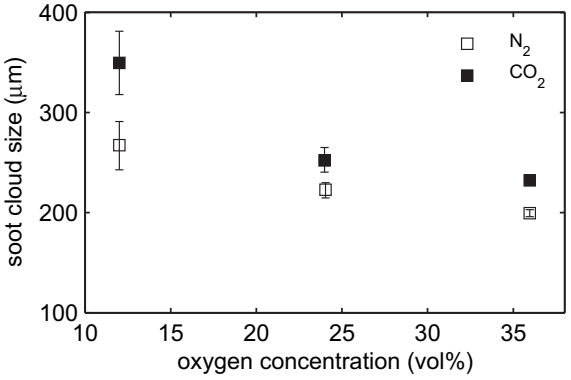

Fig. 15. Variation of characteristic soot cloud size during devolatilization of Pittsburgh coal (high-volatile bituminious) for different gas compositions in the Sandia optical EFR facility. Error bars represent 95% statistical error. Data taken from [168].

flue gas. All of the above will change with the change in flue gas composition and the flue gas temperature associated with the shift from air-firing to oxy-fuel combustion. Whether the resulting heat transfer rate in the convective section will match that of the air-firing case is dependent on the specific case. Simulations would be a valuable tool in the evaluation.

3.3. The combustion process

3.3.1. Devolatilization and ignition

Volatiles constitute a major fraction of the combustible matter of most coals used for power generation. The combustion of volatiles releases heat which is important for ignition, local stoichiometries, and pollutant emissions [172]. The differences in properties for N_2 and CO_2 presented in Table 9 suggest that devolatilization and ignition in oxy-fuel combustion will occur at different rates than for combustion in air if CO_2 is substituted directly for N_2.

Shaddix and Molina [126,168] studied the effects of the presence of CO_2 and enhanced oxygen concentrations on the devolatilization and ignition of pulverized Pittsburgh (high-volatile bituminous) and Black Thunder (sub-bituminous) coals in a laminar flow reactor. Fig. 16 shows estimated values of particle devolatilization and ignition times for the Pittsburgh coal at 1700 K in different gas mixtures. From the data it is concluded that the exchange of CO_2 for N_2 does not significantly affect the devolatilization time for this particular type of experiment. From a consideration of heating an inert particle, the authors reason that for a fixed gas phase temperature the only factor that influences the initial heating of a particle is the thermal conductivity [126,168]. As seen from Table 9 the ratio between the thermal conductivity of CO_2 and that of N_2 is close to one at 1400 K. Hence, the initial heating profile of particles in each atmosphere will effectively be similar. Since coal devolatilization is an endothermic process with a rate that is strongly dependent on particle temperature and heating rate the specific conditions of the reported experiments suggest that there should be no difference between the different atmospheres, as observed. The result is, however, only valid for the case of equal gas phase temperatures, regardless of the gas phase environment. For a practical boiler this assumption is not necessarily satisfied.

As the oxygen concentration increases the devolatilization as well as the ignition occur more rapidly. In earlier work on air combustion Murphy and Shaddix [166] proposed the increase in the devolatilization rate with increasing oxygen concentration to be the result of (1) a closer proximity of the volatiles flame to the coal particle, and (2) a higher temperature of the volatile flame. Furthermore, modelling considerations suggested increasing

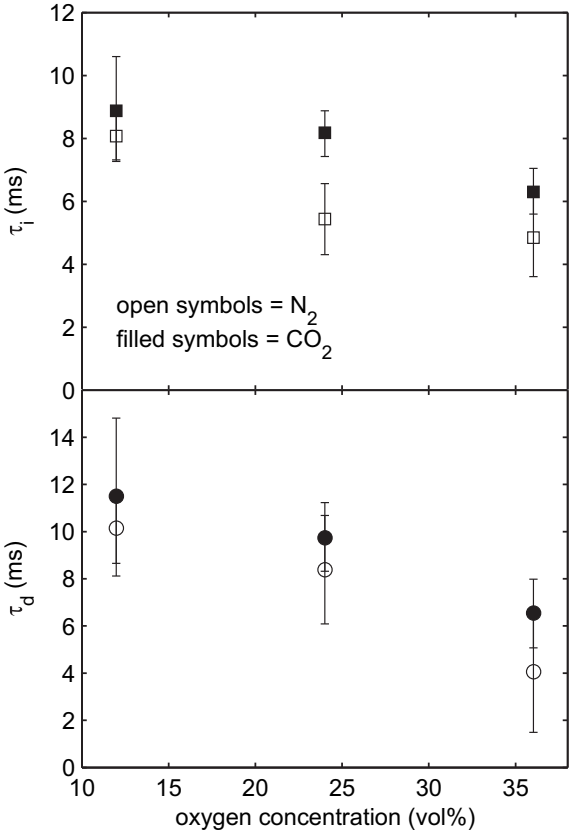

Fig. 16. Variation of ignition delay (τ_i) and devolatilization (τ_d) times for Pittsburgh coal burned in different gas mixtures in the optical EFR at Sandia National Laboratories. The data is based on images collected with an ICCD camera. Vertical bars represent the statistical error. Ignition delay was defined as the time elapsed from particle injection into the reactor to the time when 50% of the images correspond to devolatilization. Data taken from [168].

kinetic control for increasing oxygen concentrations. At a low oxygen partial pressure and high temperature, oxygen transport through the gas film surrounding the particles will be rate limiting. At increasing oxygen partial pressures and constant temperature the kinetic rate will remain almost constant whereas the rate of gas film transport will increase linearly with the pressure.

The differences in particle ignition times observed in Fig. 16 is a consequence of the differences in transport properties of the surrounding gas, the combustion heat release, and the reactivity of the local fuel-oxidizer mixture [126,168]. Generally, increasing the mixture reactivity and heat release will decrease the ignition time, whereas an increase in the product of density and heat capacity (the heat sink, ρC_p) leads to an increase in the ignition time. The heat sink for CO_2 is substantially larger than for N_2, see Table 9, leading to an increase in ignition time for similar oxygen levels. Kiga et al. [136], Kimura et al. [87], and Liu et al. [121] have observed similar delays in the ignition of coal particles when burning in an atmosphere of 21% O_2 in CO_2. Increasing the oxygen concentration will increase the characteristic reaction rate of the local mixture and thus decrease the ignition time [126,168,189]. Changing from 24 to 36% O_2 is seen to have a large, absolute effect on the oxy-fuel mixture. Comparing the results for air- and oxy-fuel combustion reveals that it should be possible to obtain similar devolatilization and ignition properties for oxy-fuel combustion as for conventional air-firing.

Suda et al. [190] measured the flame propagation velocity with respect to different coal concentrations, coal types, and ambient gas compositions in a microgravity facility. Fig. 17 shows the observed

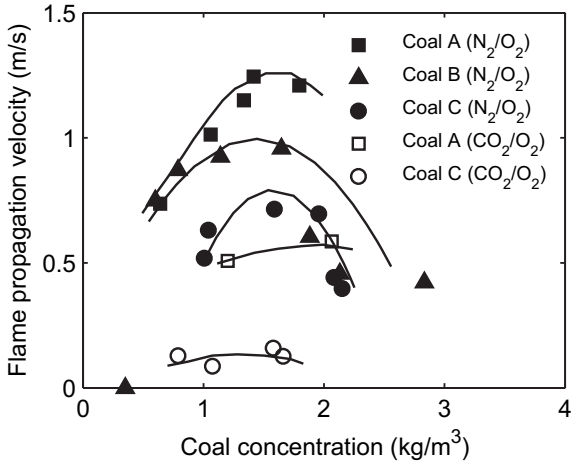

Fig. 17. Effect of coal concentration on the flame propagation velocity for three different coals; A, B, and C. Measurements are performed in a microgravity facility. The coals differ in their volatile matter contents. Coal A has the highest amount (46.0 wt%), followed by coal B (36.2 wt%) and then C (32.9 wt%), all on an "as received basis". Coal particle diameters: 53–63 μm, O_2 concentration: 40% by volume. Data taken from [190].

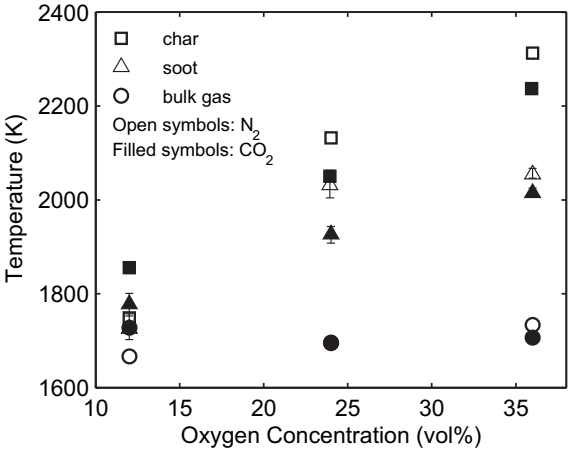

Fig. 18. Variation of characteristic soot cloud and char combustion temperature, during devolatilization and subsequent char combustion in different O_2/N_2 and O_2/CO_2 mixtures. The fuel is a Pittsburgh coal (bituminous) and the experiments are performed in the Sandia EFR facility. Error bars represent 95% statistical error. Data taken from [168].

effect of each parameter. The coal type is seen to have a significant effect on the flame propagation speed in both enriched air- and oxy-fuel environments. Each case operates with 40 vol% O_2 in the oxidizer. The difference in coal type is mainly a matter of the volatile content of each coal. The speed is seen to increase with increasing volatile matter content. For a given coal in a given environment an optimum in the propagation speed exists with respect to the coal concentration. The optimum concentration is seen to be approximately similar for all data series. According to the authors, this particle concentration corresponds to an inter-particle distance roughly equal to the flame radius of a single, burning particle [190].

3.3.2. Volatile and char burnout

Besides the impact from exchanging N_2 with CO_2 on the devolatilization and ignition of coal particles the burnout of both char and volatiles is expected to be affected.

The coal burning process is typically limited by both chemical kinetics and external diffusion (Zone II conditions). At 1400 K the diffusivity of O_2 in CO_2 is only about 75% of that in N_2. The lower diffusivity will thus reduce both the burning and heat generation rates for the coal particles [169]. At the same time, the diffusivity is a strong function of temperature. Hence, the effect of the enhanced heat capacity of CO_2 and the associated decrease in flame temperature for similar oxygen concentration in oxy-fuel and air combustion will further reduce the burning rate. Fig. 18 shows trends in ambient gas phase as well as soot cloud and char combustion temperatures for different combustion media obtained by Shaddix and Molina [168] in their EFR facility. At equal oxygen concentrations and gas phase temperatures combustion in O_2/N_2 mixtures generally yield higher temperatures of both soot clouds and char than in O_2/CO_2 mixtures.

The consumption rate of volatiles in oxy-fuel combustion is likewise expected to be slower than in air due to the lower diffusivity of small hydrocarbons in CO_2 compared to N_2 [122,126,168].

In retrofit respects, burnout in oxy-fuel combustion with comparable adiabatic flame temperatures as in air is expected to improve. This is because of the higher oxygen partial pressure experienced by the burning fuel, possible gasification by CO_2 (and H_2O), and longer residence times due to the lower gas volumetric flows [5,128]. Other researchers claim that excess CO_2 in the vicinity of the burning particle could alter the reaction equilibrium and slow down the burning rate [117]. However, that conclusion is based on a simplified analysis.

3.3.2.1. Burnout times. Bejarano and Levendis [181] have conducted a series of experiments with non-intrusive optical multi-colour pyrometry measurements of volatile flame and char burning phenomena in single particle environments. Fig. 19 illustrates average temperatures and burnout times measured for a high-volatile bituminous coal. The data indicate an effect of exchanging N_2 for CO_2 and the effect of varying the O_2 concentration in the oxidizer. The lower diffusivity of O_2 in CO_2 compared to N_2 is the major cause of reducing the burning rate during char combustion [167]. Generally, it is seen that an oxygen mole fraction of 0.3–0.35 yields similar temperature and burnout data for oxy-fuel combustion compared to combustion in air. By comparing the measured and calculated burnout times shown in the figure, Bejarano and Levendis [181] conclude that the char combustion for both air- and oxy-fuel combustion occurs in Zone II.

Wang et al. [118] have shown a significant increase in char burnout rate when increasing the oxygen concentration in O_2/CO_2 combustion from 21 to 29%. Similar results were found by Naredi and Pisupati [187] from drop-tube experiments on bituminous coals with 21% and 30% oxygen in the oxidant. Tan et al. [12] refer to studies performed by Takano and coworkers in the IHI 1.2 MW swirl burner which gave similar results. Moreover, a marked reduction in unburned carbon in the fly ash with increasing oxygen level was observed.

In general, the reported investigations have shown that increasing the oxygen concentration in the oxidant for oxy-fuel combustion can compensate for the larger specific heat of CO_2 compared to N_2. Comparable burnout times are thus achievable.

3.3.2.2. Gasification reactions. Both CO_2 and H_2O may contribute to the burnout of char particles through gasification reactions, (6) and (7), when these species are present in high concentrations at high temperature [191,166] and the oxygen excess, λ, is significantly lower than 1.

$$C + CO_2 \rightleftharpoons 2CO \quad (6)$$

$$C + H_2O \rightleftharpoons CO + H_2 \quad (7)$$

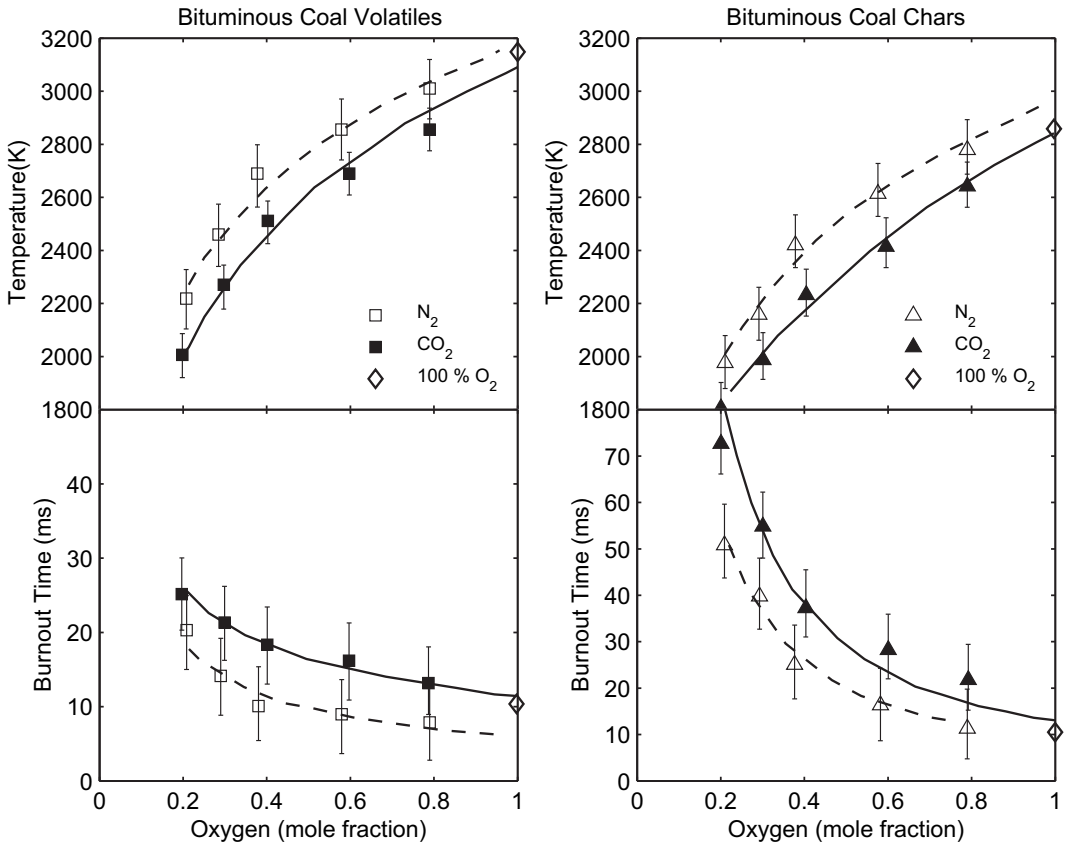

Fig. 19. Average particle temperatures (top row) and burnout times (bottom row) for a high-volatile-A bituminous Pittsburgh #8 coal (45–53 μm) burning in O_2/N_2 and O_2/CO_2 in a laminar-flow drop-tube reactor at $T_{furnace} = 1400$ K. The temperatures shown correspond to ~50% burnout times for each phase. Error bars correspond to one standard deviation, σ. Data taken from [181].

In low-temperature regions (400–900 °C) gasification does not play a role. This is due to a much lower rate of reaction for gasification with CO_2 compared to O_2-combustion at these conditions [192].

Results presented by Wall et al. [139,128] indicate that the volatile yield is higher during oxy-fuel combustion than in air. They attribute it to gasification. However, Borrego and Alvarez [193] found the opposite trend during their experiments.

Due to the conflicting results, the possible influence of gasification reactions during oxy-fuel combustion is an area which needs further investigations.

3.3.2.3. Effect of coal properties. Liu et al. [162] investigated the burnout efficiency compared to combustion in air for a range of bituminous coals in their 20 kW swirl burner, see Fig. 20. Even though the burnout efficiency differs between the samples it is always higher for combustion in 30% O_2/70% CO_2 than in air. Generally, the increase in burnout efficiency is between 0.5 and 2%. An examination of the coal characteristics has not revealed any obvious correlation between the burnout efficiency and the proximate or ultimate analysis. The reason for the differences within each coal type is suggested to be the higher oxygen concentration combined with similar temperatures for the oxy-fuel tests. The authors stress that gasification and longer residence times of the burning particles in the combustion chamber could also contribute to the higher burnout efficiency observed [162].

Fig. 21 shows the results of the work performed on burnout characteristics of different coals by Arias et al. [180]. The burnout of both coals show similar trends with changes in the stoichiometry. At fuel-lean conditions the burnout asymptotically approach a value of 100%. It is seen that the burnout of the high-volatile coal generally is a little lower than for the low-volatile coal. This is contrary to what was expected since the high-volatile coal should be more reactive. However, there may be significant uncertainties in the experimentally determined burnout, particularly because of alkali metal volatilization and possible ash carbonization from CO_2. For both coals the overall lowest burnout is, as expected, observed for oxy-fuel combustion with a low oxygen content.

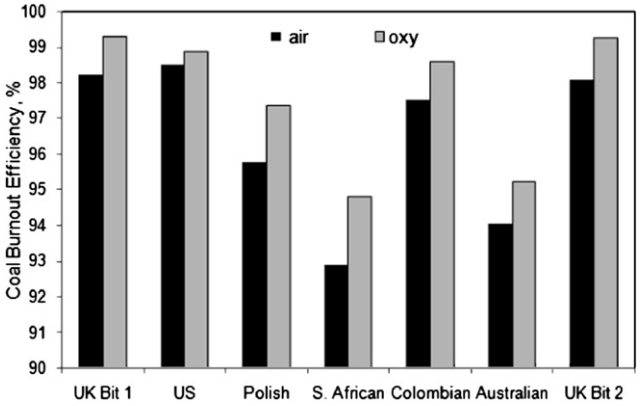

Fig. 20. Effect of combustion media on coal burnout efficiency for seven different bituminous coals. Results obtained in a 20 kW down-fired swirl burner. The coals are burned at $\lambda = 1.2$ in air and a mixture of 30% O_2 in CO_2 (oxy). Data taken from [162].

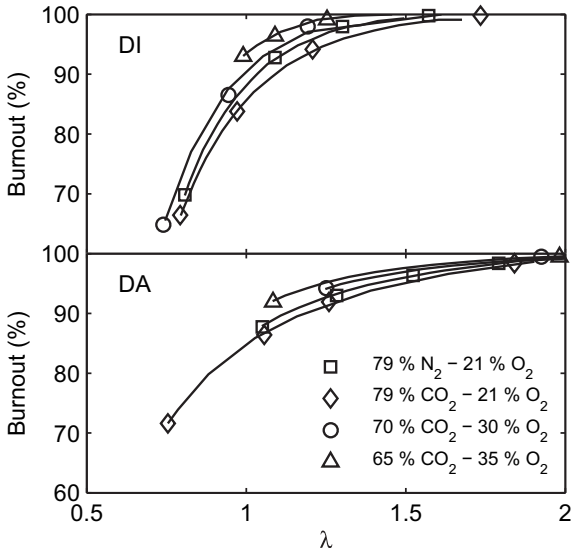

Fig. 21. Effect of gas atmosphere and stoichiometry on burnout of a low- and a high-volatile coal (DI and DA, respectively). The experiments are performed in an entrained-flow reactor. Data taken from [180].

3.3.2.4. Particle size effects. An investigation of the effect of particle size (45–53 and 75–90 μm) on volatiles and char temperatures has been performed by Bejarano and Levendis [181]. Given that the actual data and the measurement uncertainty has not been stated, the results given in Fig. 22 show only small or insignificant differences between the investigated particle size ranges.

The burnout times for the char particles are seen to depend on the particle size. As expected, the larger the particles the longer the burnout times. The effect of particle size is seen to be more significant in an oxy-fuel environment. A plausible explanation could be the lower diffusivity in CO_2 compared to N_2. Comparable results have been obtained by Huang et al. [189] from experiments in a TG thermal analyser.

3.3.2.5. CO. At high partial pressure and high temperature CO_2 can dissociate into CO and O_2 through the strongly endothermic reaction, (8), [172].

$$CO_2 \rightleftharpoons CO + 0.5O_2 \quad (8)$$

In the flame zone in oxy-fuel combustion both of the above conditions are present. Gasification of carbon, reaction (6) and (7), could likewise contribute to increase in the production of CO during oxy-fuel combustion. However, among researchers there is a difference in opinion on whether it is the thermal dissociation, [175], or the gasification reactions, [149], that play the dominant role in the significant increase in CO concentration in the flame compared to air-firing.

An even more important pathway to the increase in CO concentrations in the flame zone of oxy-fuel flames could be the reaction between CO_2 and H radicals, see reaction (9). The increased level of CO_2 induces a possible alteration of the composition of the O/H radical pool during oxy-fuel combustion due to the competition between O_2 and CO_2 for H radicals, (9) and (10) [172,194].

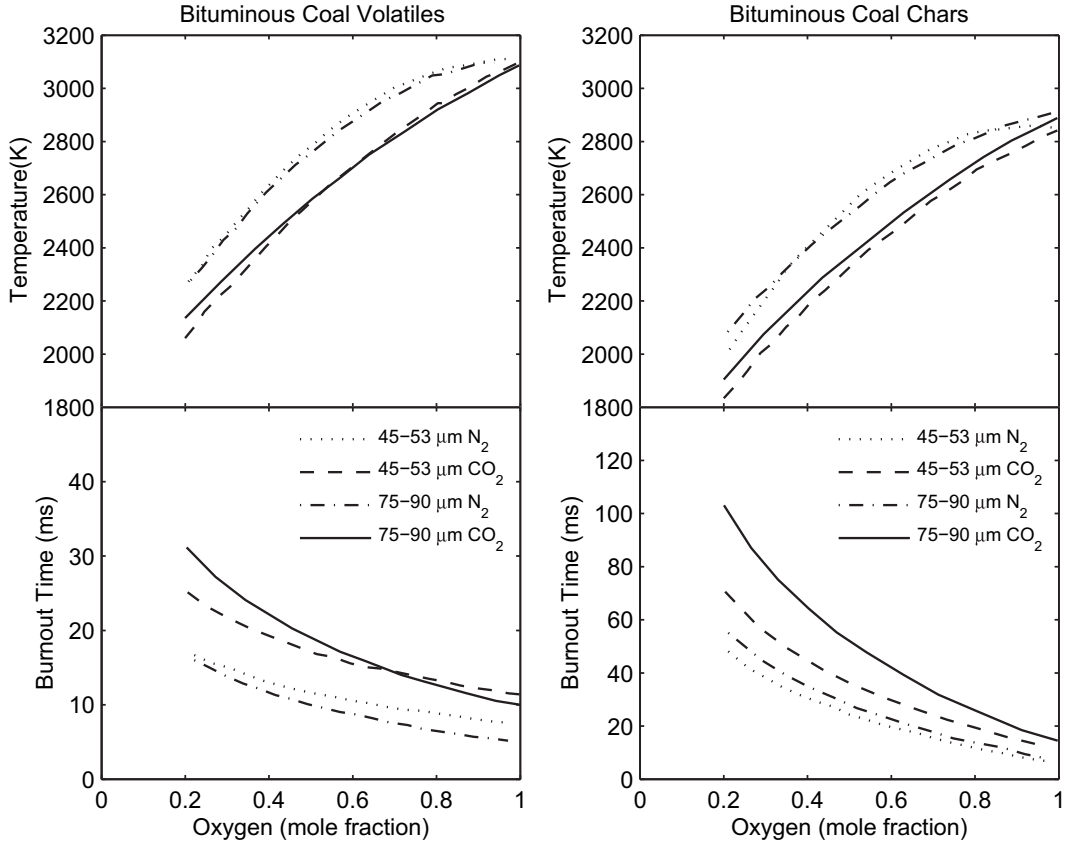

Fig. 22. Trends in average temperatures (top row) and burnout times (bottom row) for a high-volatile-A bituminous Pittsburgh #8 coal of two different size cuts (45–53 and 75–90 μm) burning in O_2/N_2 and O_2/CO_2 in a laminar-flow drop-tube reactor at $T_{furnace} = 1400$ K. The temperatures shown corresponds to ca. 50% burnout. Data taken from [181].

$$H + CO_2 \rightleftharpoons CO + OH \quad (9)$$

$$H + O_2 \rightleftharpoons O + OH \quad (10)$$

Due to the high partial pressure of CO_2 in oxy-fuel combustion the ratio of OH to both O and H will increase and the total amount of radicals is expected to decrease compared to air-blown combustion. Besides the reaction with H radicals, reaction of CO_2 with CH_2 radicals will likewise contribute to enhance the concentration of CO in the flame zone [172,194–196].

Whether the emission of CO from oxy-fuel combustion is larger than from air-firing has been subject to investigation. Because of its severe toxicity it is important that oxy-fuel combustion does not lead to an increased CO emission. Wang et al. [118] report no significant difference in the CO concentration levels both within the latter part of the flame zone and in the exhaust from a 3 MW_{th} horizontal furnace for both air- and oxy-fuel combustion experiments with comparable flame temperatures. A five time increase in the CO level within the flame was expected however based on a modelling study. For an oxy-fuel experiment with an air-like composition of the oxidant the CO concentration in the flame zone was expected to be slightly larger than for air combustion based on modelling. The observed values for the oxy-fuel experiment were lower than calculated. All experiments yielded full burnout of CO before the exhaust.

Experiments performed in the IFRF 2.5 MW_{th} furnace by Woycenko et al. [88] show significantly increased CO levels within the flame zone. Still, the combustion of CO has completed before the furnace exit and no significant CO emission is observed. Similar results were obtained by Scheffknecht and coworkers [164,148] and Liu et al. [121] even when the excess oxygen level was slightly higher for the latter oxy-fuel test. Changing the oxygen concentration from 30 to 21% increased the CO emission from 34 to 200 ppmv, due to delayed ignition and lower peak temperature.

Experiments on natural gas combustion performed by Glarborg and coworkers [172–174] indicate that the high levels of CO_2 in oxy-fuel atmospheres prevent complete oxidation of fuel (CO) to CO_2 at high temperatures even when excess oxygen is present. However, the effect is most pronounced at fuel-rich or stoichiometric conditions. There is no indication that high CO_2 levels influence CO oxidation at low temperatures when oxygen is in excess and hence there should be no increased risk of high CO emissions from a gas-fired oxy-fuel plant if mixing of fuel and oxidant is adequate.

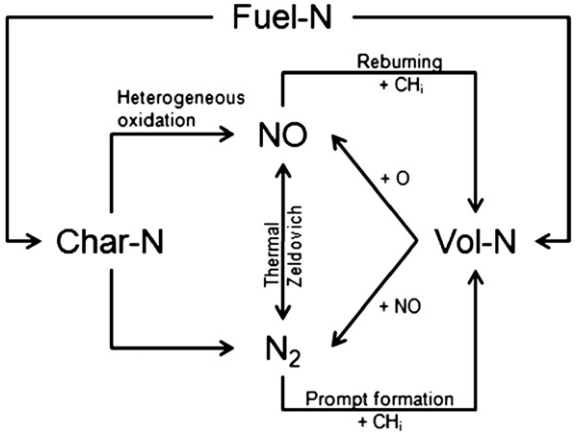

Fig. 23. The overall mechanism of NO formation and reduction. Vol-N is an intermediate gaseous compound, e.g. HCN or NH_3.

3.3.2.6. Summary. The difference in the thermo-chemical properties of N_2 and CO_2 affects the combustion process. At 21% O_2 in CO_2 devolatilization, ignition, and burnout proceeds at a lower rate than in air. However, increasing the oxygen concentration in the oxy-fuel environment to about 30% to obtain the same adiabatic flame temperature as in air yields similar devolatilization, ignition, and combustion rates as seen in air combustion. At comparable adiabatic flame temperatures oxy-fuel combustion is reported to yield improved burnout of char. This is most likely due to longer residence times and higher partial pressures of oxygen in the vicinity of the burning particles. Even though contribution of gasification by CO_2 and/or H_2O to the increased burnout is suggested several times in literature, it is questionable if this effect is of significant importance for the conversion of the fuel.

CO levels in the flame zone are generally reported to increase significantly in oxy-fuel combustion compared to air-firing. Even though the high CO_2 levels prevent CO from being oxidized at high temperatures complete conversion is expected when excess oxygen is present during cool-down of the flue gas.

3.4. Gaseous pollutants emissions

The following subsections discuss the reported knowledge on the most important gaseous emissions besides CO from oxy-fuel combustion; NO_x, SO_2, and SO_3. Trace elements in the gaseous phase, e.g. Hg, Cd, As, and Se, are likewise treated. No results have been published regarding emissions of HCl and HF.

3.4.1. NO_x

3.4.1.1. NO_x formation. In conventional air combustion the generally accepted pathways for NO_x formation are the following three mechanisms [197–199], see e.g. Fig. 23:

Thermal: Thermal NO formation results from N_2 and O_2 reacting at high temperatures (above 1500 °C) to form NO. The mechanism involves three reactions, known as the extended Zeldovich mechanism.

$$N_2 + O \rightleftharpoons NO + N \quad (11)$$

$$O_2 + N \rightleftharpoons NO + O \quad (12)$$

$$N + OH \rightleftharpoons NO + H \quad (13)$$

Prompt: Prompt NO is formed when hydrocarbon radicals in fuel-rich zones attack molecular nitrogen to form cyanide species, which subsequently form NO when oxidized. These reactions can take place at temperatures lower than is required for thermal NO formation.

Fuel: Fuel NO is derived from nitrogen in the fuel reacting through either volatile-N or char-N. Nitrogen released with the volatiles further decomposes into cyanide and amine species. These intermediate species may react to produce N_2 or NO, depending on the conditions. Char-N reacts through heterogeneous reactions and intermediate CN species to eventually produce NO or N_2. Detailed understanding of the reaction pathways for the conversion of char-N has not been established and is still an area of active research. The split between NO and N_2 on an overall level depends on factors such as the nitrogen content of the coal, its rank and volatility, as well as the stoichiometry.

It is generally assumed that up to 20% of the total NO_x formed from pulverized coal combustion in air is due to thermal NO_x and about 80–100% is derived from fuel-N while the prompt NO_x mechanism is negligble, depending on the quantity of fuel-bound nitrogen species [199]. The low level of molecular nitrogen in oxy-fuel combustion will

suppress the formation of thermal and prompt NO_x and hence potentially lower the overall NO_x emission rate.

The general conclusion in published literature is that the amount of NO_x emitted from an oxy-fuel plant can be reduced to somewhere between one-third and half of that from combustion in air [51,63,87,88,91,97,119,120,128,162]. However, the application of an oxygen concentration higher than 21% to obtain adequate flame temperatures could result in an enhancement of fuel-NO_x formation [122].

The potential for reducing the NO_x emissions from a power plant considerably compared to air-firing [4,200] has been one of the key drivers in oxy-fuel combustion research, particularly in USA [5] and thus, NO_x chemistry has been one of the most heavily investigated areas within the oxy-fuel combustion technology. Normann et al. [201] have recently published a review on emission control of nitrogen oxides from oxy-fuel combustion.

The potential for a significant decrease in NO_x formation is mainly important for oxy-fuel power plants with a configuration of the flue gas clean-up train which releases the impurities, including NO_x, to the atmosphere. If instead a CO_2 cleaning process is chosen which captures NO_x and produces e.g. nitric acid the NO_x formation rate is of less importance although it will affect process economics. In any case, if NO_x formation can be reduced without significant negative consequence to the remaining combustion process it is desirable.

3.4.1.2. Mechanism for the reduction of NO_x during oxy-fuel combustion. The majority of homogeneous NO_x chemistry is taking place in the devolatilization and near-flame zone. The implications of oxy-fuel combustion on the homogeneous NO_x formation and destruction are therefore likely to be alterations in equilibria and reaction pathways caused by higher concentrations of CO_2 and NO_x in this part of the furnace. If the recycled flue gas is wet the higher partial pressure of H_2O will likewise interfere through its influence on radical formation and destruction. The enhanced levels of CO_2 and NO_x are also expected to affect the heterogeneous formation and reduction of NO. In addition to chemical effects, changes in the mixing patterns between fuel and oxidizer are likely to affect the nitrogen chemistry. In the following, these mechanisms for reduction of NO_x in oxy-fuel combustion are discussed.

Effect of the increased NO concentrations (reburning): Recirculation of NO with the flue gas through the burner would be expected to lead to a considerable reduction of the nitrogen oxides emission through processes similar to those of reburning. Reburning is a chemically complex process in which nitric oxide is abated using fuel as reducing agent [202]. The process involves partial oxidation of the reburning fuel under fuel-rich conditions, reduction of NO by reaction with fuel fragments, and subsequent conversion of the intermediate nitrogenous species.

The reduction of NO may involve the following types of reaction:

1. NO_x is reduced to cyanide and amine intermediates by reaction with hydrocarbon radicals, formed from the volatiles released from the coal particles in the early flame zone.
2. NO_x is converted to N_2 through reactions with other reactive nitrogen species (XN), such as cyanides and amines. The XN species may be formed either from from the hydrocarbon-NO reactions or from release of N-volatiles in the early flame.
3. NO_x is converted to N_2 by heterogeneous reactions on char or soot.

From experiments performed in a small-scale laboratory reactor, Okazaki and Ando [158] evaluated the relative impact of these mechanisms for NO reduction. They concluded that reburn type reactions, i.e. reactions of recycled NO_x with hydrocarbons, is the dominant mechanism in reducing NO_x emissions and that it accounts for 50–80% of the decrease in NO observed in oxy-fuel combustion. Reactions of NO_x with N-volatiles were estimated to contribute 10–50% to the NO reduction. The reduction of NO on char in oxy-fuel combustion was found to be of minor importance, but their results may be biased by the choice of a char with a low reactivity (formed from anthracite).

Effect of the low N_2 concentration: At a very low concentration of N_2 in the oxidizer, the thermal NO_x formation mechanism can be disregarded since the oxy-fuel combustion atmosphere will be oversaturated with NO at all times [123,156]. For this reason the Zeldovich reactions will be reversed and serve to convert NO to N_2.

A modelling study using detailed chemical kinetics on oxy-fuel combustion of lignite performed by Andersson et al. [90] indicates that while the formation of NO from fuel-N is the same or even slightly higher for oxy-fuel combustion compared to combustion in air, the destruction mechanisms at oxy-fuel conditions are enhanced compared to air conditions, leading to an overall reduction in the NO emission. At high temperatures (>1500 °C), the near-elimination of molecular nitrogen in oxy-fuel combustion facilitates reduction of NO by the Zeldovich mechanism. In order to obtain an effective reduction of NO by the reverse Zeldovich mechanism, a sub-stoichiometric combustion and/or an insignificant amount of air ingress into the furnace is required (air-staging to promote long enough residence time) [156]. At the same time, applying a wet flue gas recycle will increase the NO_x reduction potential [156].

Effect of the increased CO_2 concentration: Only few studies have been reported on the impact of high CO_2 concentrations on the nitrogen chemistry in oxy-fuel combustion. Mendiara and Glarborg [174,173] investigated the implications of the alterations to the radical pool as described in Section 3.3.2 on NO formation and destruction. They considered oxidation of methane doped with either NH_3 (used to simulate volatile-N) [174] or NO [173] in a laminar flow reactor. According to their results, CO_2 acts to promote NO formation from volatile-N under fuel-rich conditions whereas it inhibits NO at both stoichiometric and fuel-lean conditions. At low oxygen concentrations formation of NO is favoured by the increase in OH-concentration. At conditions with oxygen excess, the reduced formation of NO is caused by the limitation of the O/H radical pool, particularly O. In reburning, a high concentration of CO_2 had only a small impact on the NO reduction efficiency under reducing conditions, while at stoichiometric conditions CO_2 slightly enhanced removal of NO.

Okazaki and Ando [158] pointed to the increased importance of reduction of NO_x on char surfaces due to reaction with CO. The CO levels increase because of the high CO_2 concentration as described in Section 3.3.2. The promoting effect of CO on NO_x reduction on char is well documented [199,203–206], but this mechanism is mostly important at fluidized bed conditions [198], i.e. at temperatures well below those characteristic of pulverized fuel combustion.

A change in selectivity of the release of char-N to NO has been suggested by Park et al. [207]. They investigated nitrogen release from pulverized bituminous coal char during the reaction with O_2, CO_2, and H_2O using Ar as carrier gas in a fixed bed flow reactor. Their experiments showed that increasing the concentration of CO_2 in an H_2O and O_2 free environment reduced the char-N to NO release ratio. In contrast to gasification with H_2O, no HCN or NH_3 were measured when CO_2 was the reactant. These experiments thus suggest that the increased levels of CO_2 during oxy-fuel char combustion may suppress the formation of NO and its precursors.

Effect of changes to the flame and fuel/oxidizer mixing pattern: Implementation of oxy-fuel combustion may bring about changes in the flame structure and the fuel/oxidizer mixing pattern. These

changes will depend on the burner geometry and the degree of recirculation and the composition of the flue gas.

Mackrory et al. [124,175] identify the following mechanisms that may enhance NO_x reduction in oxy-fuel combustion:

- Less secondary oxidizer entrainment into the burner's recirculation zone due to a more detached flame, i.e. reduced oxygen availability and limited initial NO formation.
- Temperature increase in the fuel-rich zone will increase the rate of NO destruction. At higher temperatures the conversion of volatile-N proceeds faster toward N_2 than NO.
- Reduced NO formation from char since more fuel-N is released with the volatiles.
- Indirect effects through changes in reaction rates (combustion) and temperatures from the enhanced importance of gasification reactions.

Their overall conclusion is that faster NO destruction in oxy-fuel combustion appears to be at least partially due to the higher CO and NO concentrations.

3.4.1.3. Summary of reported, experimental results. Table 12 provides a summary of the reported results on NO_x emission from oxy-fuel combustion in setups with flue gas recirculation compared with that from air-firing. Most of the experiments yield a decrease in the NO_x emission rate during oxy-fuel combustion. However, some experiments show an increase which is suggested to be caused by the fact that the mechanism of fuel-NO_x formation is very sensitive to the method with which oxygen and fuel is mixed in the flame [122,124,151]. As oxy-fuel burners are typically adopted from air-firing principles the resulting fluid dynamics of the flame can be disadvantageous with respect to NO_x emissions even though the flames are stable.

In the following sections the reported results on NO_x emissions from oxy-fuel combustion are divided according to the effects of different operating conditions and design aspects. Results from both once-through laboratory reactors and setups with flue gas recirculation are included. In each section a further subdivision is made, separating the different types of experimental setups, i.e. EFR type experiments from swirling flames. The underlying mechanisms of NO_x formation and destruction do not change between setup types. However, scaling effects and the fact that mixing of fuel and oxidizer in larger burners is crucial to NO_x formation will influence the absolute levels of NO_x emitted. A direct comparison of small laboratory-scale setups and larger swirl burners with respect to NO_x concentrations and emission rates is thus not possible. A clear example of this is the experiments performed by Hasatani et al. [161,109]. They burned a sub-bituminous Indonesian coal in an oxy-fuel environment with oxygen concentrations between 85 and 88 vol% in both an entrained-flow reactor [161] and in a 145 kW_{th} vertical furnace [109]. They observed NO_x concentrations of 4700 ppm and 1500 ppm, respectively, for otherwise similar combustion conditions.

3.4.1.4. Effects of changes in the oxygen concentration, oxygen excess, flue gas recycling ratio, and gas phase temperature. Experiments on NO_x emissions from oxy-fuel combustion of a high-volatile bituminous coal in the IFRF 2.5 MW_{th} furnace were performed in the early nineties by Woycenko et al. [88]. As shown in Fig. 24 they observed considerably higher NO_x concentrations during oxy-fuel combustion with 26 vol% O_2 in the oxidant than in the air-firing case. However, the total mass of NO_x formed per energy input of coal [mg/MJ], also termed the emission rate, was significantly lower in the oxy-fuel case which was assigned to the near-elimination of thermal NO_x formation and reburning of recirculated NO_x.

Further experiments showed that an increase of the concentration of oxygen in the oxidant, and thus the flame temperature, yielded an increase in both the flue gas NO_x concentration and the emission rate. The increase in oxygen concentration was performed by decreasing the flue gas recycle ratio. Similar trends of reduced

Table 12
Summary of NO_x emission results from experiments in pilot scale and semi-technical scale with flue-gas recirculation.

Author(s)	Fuel input (MW)	Inlet O_2, Oxy (%)	Emission (mg/MJ)	Conversion ratio (%)	Conclusion(s)
Payne et al. [86]	3	Dry: 28 wet: 24	Air: 560 Oxy, dry: 160 Oxy, wet: 95	–	NO_x formation is reduced by approximately 70% for dry recycle and 80% for wet recycle compared to air-firing.
Woycenko et al. [88]	2.1	26	Air: 320 Oxy: 50–150	Air: 30 Oxy: 5–14	NO_x formation is lower in oxy-coal combustion with flue-gas recirculation than in air case.
Châtel-Pélage et al. [63]	1.5	25	Air: 100–175[a] Oxy: 25–55	–	Potential for drastic NO_x reduction of up to 60–70%
Kimura and coworkers [87,119]	1.2	27	Air: 340 Oxy: <90	Air: 30–33 Oxy: <8	NO_x conversion ratio in oxy-fuel combustion is significantly lower than that in normal air combustion because the recycled NO_x is rapidly reduced to HCN or NH_3 in the combustion zone (reburning).
Scheffknecht and coworkers [144]	0.5	27–30	Air: 90–350[b] Oxy: 55–325	–	NO_x emission rate increases for increasing burner stoichiometry and is always higher for air combustion than oxy-fuel combustion for comparable operation conditions.
Croiset and coworkers [120,97]	0.21	28, 35, 42	Air: 340 Oxy: 100–210	Air: 35[c] Oxy: 10–22	High NO_x concentration inside the furnace but lower NO_x emission rate with the flue gas than for air-firing.
Chui et al. [150,151]	0.21	28	Air: 110 Oxy: 62–150	Air: 14 Oxy: 8–19	NO_x formation is strongly dependent on burner design, i.e. the near-burner flow field. NO_x emission from oxy-fuel combustion can change from lower to higher than in the air-firing case.
Tan et al. [122]	0.21	35	Air: 211–269 Oxy: 68–233	Air: 21–31 Oxy: 8–24	NO_x emissions dependent on coal type. Lignite, sub-bituminous, and bituminous coals tested. Specially designed burner for oxy-firing significantly reduces the NO_x emission rate.
Andersson et al. [90]	0.1	25, 27, 29	Air: 150 Oxy: 40–50	Air: 24 Oxy: 7–8	The reduction in NO emissions for oxy-fuel combustion is due to an increased destruction of formed and recycled NO compared to air-firing. The conversion of fuel-N to NO is similar or even slightly higher during oxy-fuel combustion than in air.

[a] The interval reflects the variation between $\lambda = 0.68$ and 1.2 for the air tests and $\lambda = 0.85$–1.05 for oxy-fuel tests.
[b] The interval reflects the variation between $\lambda_{burner} = 0.75$ and 1.15 for both the air- and oxy-fuel tests.
[c] Conversion made using coal HHV.

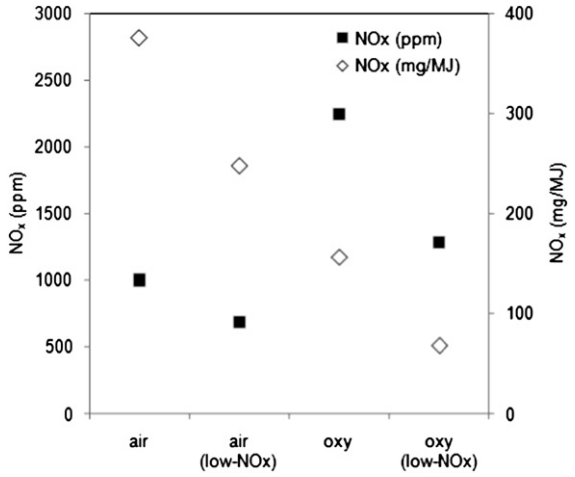

Fig. 24. NO emissions and flue gas concentrations for air-firing and oxy-fuel combustion (oxy) with and without low-NO_x burner technology. The fuel, a high-volatile bituminous coal (Göttelborn), is burned in the IFRF 2.5 MW_{th} furnace. The combustion is performed at an overall stoichiometry of $\lambda = 1.15$ and the inlet oxygen concentration in the oxy-fuel experiments is 26%, corresponding to a recirculation ratio of 0.58. The NO_x concentration is in the dry flue gas and is normalized to 0% O_2. Data taken from [88].

NO_x emission rates during oxy-fuel combustion compared to air-firing have been reported for different fuels in laminar flow reactors [174], entrained-flow reactors [96,160,161,169], and swirling flames [72,90,97,120,121,164].

According to Hu et al. [161] there are two opposing factors influencing NO_x formation and reduction in coal combustion; the oxidation of fuel-N by oxygen and other oxidizing species, and the reduction of NO_x by reducing agents, such as hydrocarbons from pyrolysis and resident char. They have performed a series of experiments in their entrained-flow reactor analysing the influence of oxygen concentration, oxygen excess, and gas phase temperature to clarify the importance of each parameter on NO_x formation and destruction. Fig. 25 shows, as expected, that the NO_x concentration generally increases with increasing oxygen concentration, partly due to decreased dilution, and shows a peak at near stoichiometric conditions. The NO_x emission rate (bottom row), however, increases approximately linearly near $\lambda = 1$ when changing from fuel-rich to fuel-lean conditions. At high oxygen excess for all oxidant compositions the NO_x emission rates approach asymptotic values. Increasing the gas phase temperature results in both increasing NO_x concentrations and emission rates for all stoichiometric values. As accentuated in Fig. 26 for a temperature of 1273 K, it is likewise seen that the emission rate yields a slight peak at around 50% O_2 in the oxidizer, however most significantly for fuel-lean conditions. Hu et al. [96] state that this phenomenon is a consequence of the concentration of reducing agents increasing proportionally to the increase in O_2 concentration (decreasing recycle ratio). At low oxygen concentrations (<50 vol%) they thus assume oxidation to dominate and NO_x emissions to increase with increasing O_2 concentration. For O_2 concentrations above 50%, reduction by reducing species should play the dominant role and NO_x emissions decrease with increasing O_2 concentration [96].

The concentration of reducing agents does undoubtedly contribute to the behaviour in Fig. 26 but other factors may likewise contribute. As the oxygen concentration is increased the reaction between char and oxygen proceeds faster which will result in higher particle temperatures. The fractional conversion of char-N to NO has been reported to increase initially with temperature [199] until the point where the oxygen-char reaction approaches the diffusion limited regime. A further increase in particle temperature

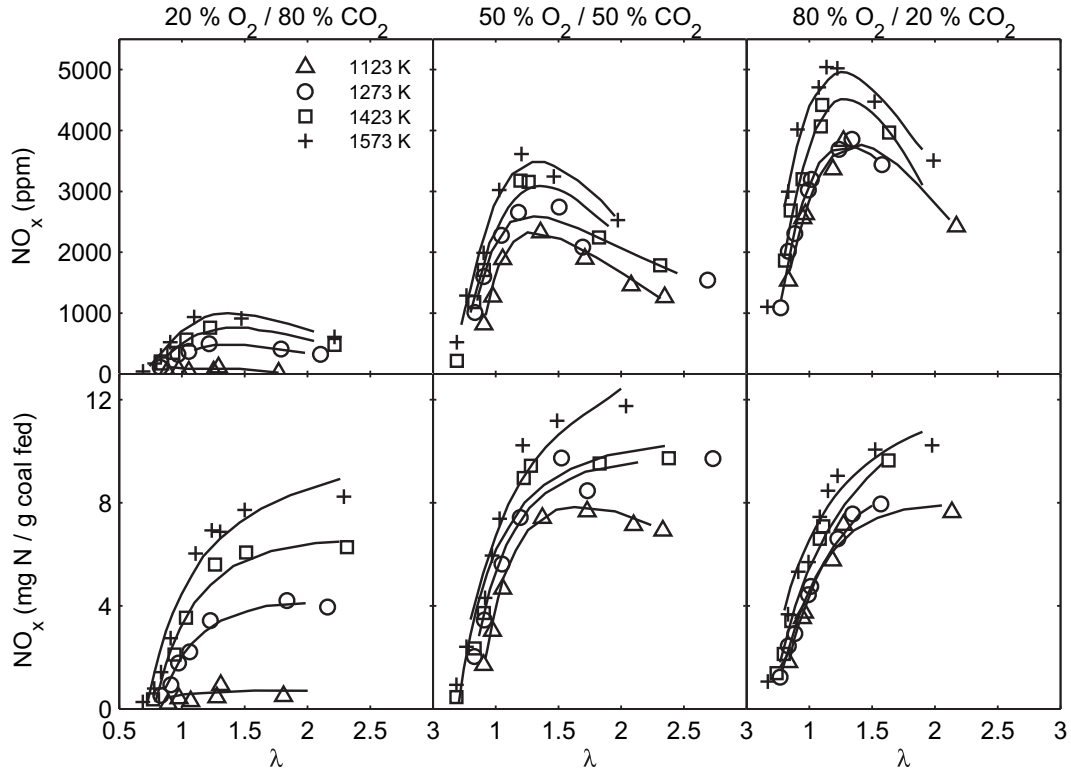

Fig. 25. NO_x emission versus stoichiometric ratio and temperature at different O_2 concentrations for CO_2-based oxidizers. Experiments performed on a bituminous coal in an entrained-flow reactor with a coal flow rate of up to 180 g/h. The NO_x concentrations in ppm are given as measured. Data taken from [96].

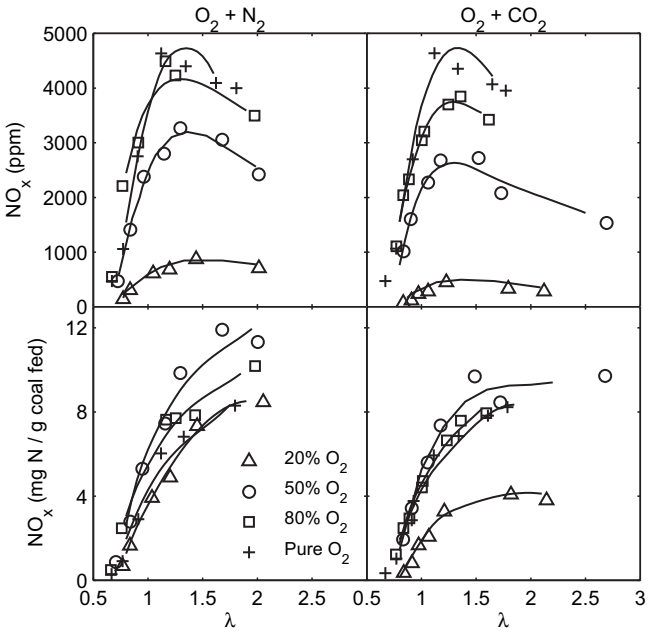

Fig. 26. NO_x emissions as a function of stoichiometric ratio at different O_2 concentrations for N_2 and CO_2-based inlet gases at 1273 K. Experiments performed on a bituminous coal in an entrained-flow reactor with a coal flow rate of up to 180 g/h. The NO_x concentrations in ppm are given as measured. Data taken from [96].

will mainly increase the rate of NO reduction by char [199], in fact what is observed from the data in the figure.

Nozaki et al. [119] showed that air- and oxy-fuel combustion of a low-volatile bituminous coal yielded similar NO_x profiles in their 1.2 MW burner with flue gas recirculation, even though NO_x was recirculated to the burner during oxy-fuel firing. The experiments were performed with fixed firing rate and excess oxygen conditions at the burner. Measurements of HCN and NH_3 along the burner axis showed significantly increased levels of NH_3 in oxy-fuel combustion compared to air-firing, see Fig. 27. The authors concluded that NO_x recycled with the flue gas is reduced primarily to NH_3 and N_2 in the early part of the flame. Experiments with direct oxygen injection in the burner revealed a significant increase in the HCN concentration in the flame zone. Nozaki et al. [119] assume this to be caused by increased devolatilization arising from a higher flame temperature compared to the oxy-fuel case without direct oxygen injection. Air-firing and oxy-fuel combustion without oxygen injection yielded similar HCN profiles even though the flame temperatures were significantly different. Based on the described observation, oxy-fuel combustion leads to higher concentrations of the intermediate cyano and amine species in the NO_x formation mechanism in the flame zone compared to air-firing. At the same time, oxy-fuel combustion yields similar concentrations of NO_x in the exhaust gas compared to air-firing and thus reduced NO_x emission rates due to the lower volume of flue gas.

3.4.1.5. Effect of flue gas composition. Most laboratory-scale experiments on oxy-fuel combustion are performed in once-through reactors, where the recirculated flue gas is simulated by pure CO_2. It is relevant to compare the results of once-through experiments to those with flue gas recirculation to clarify whether there are significant differences which should be accounted for.

The experiments reported by Croiset and coworkers [97] yield a 40–50% decrease in NO_x emission rates when flue gas is recycled, compared to once-through runs, see Fig. 28. The experiments were performed in the CANMET 0.3 MW_{th} vertical combustor facility at

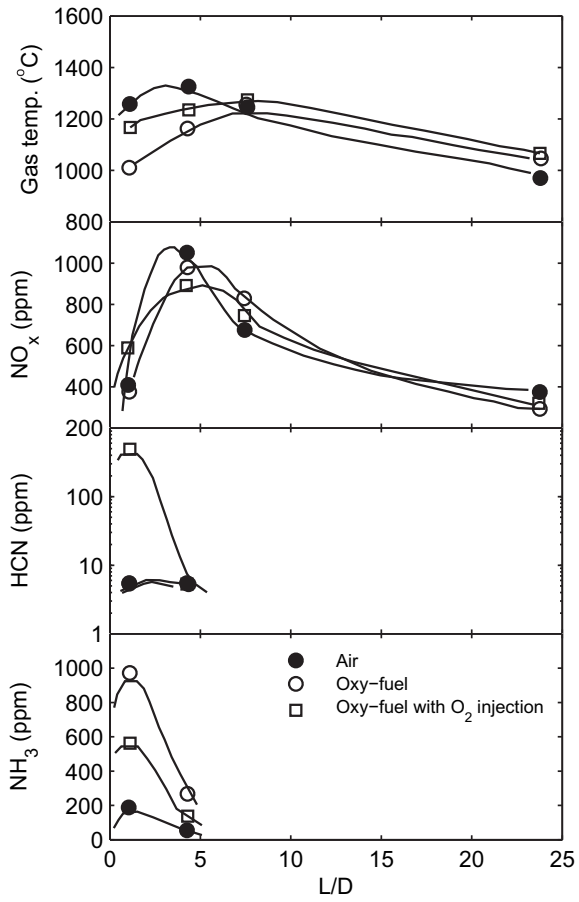

Fig. 27. Gas temperature, NO_x, HCN, and NH_3 concentrations along the burner axis for air combustion, oxy-fuel combustion, and oxy-fuel combustion with direct oxygen injection through the burner in the IHI 1.2 MW furnace. O_2 concentration is 0% in primary stream, 30% in secondary stream, and thus 27% overall. The coal is low-volatile bituminous (Coal A) and the recycle streams are dry. Data taken from [119].

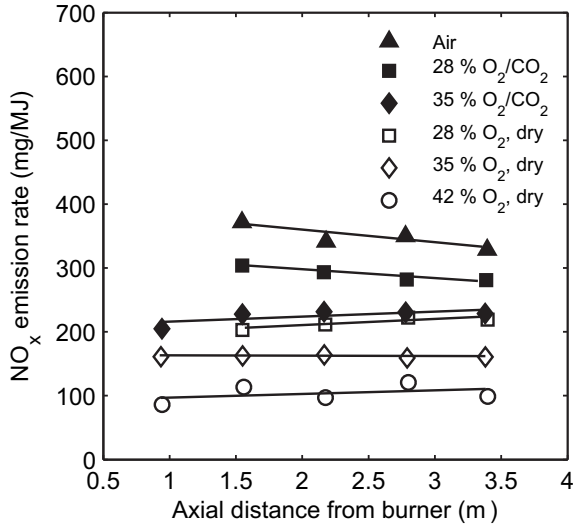

Fig. 28. Centre-line axial NO_x concentration (shown as the emission rate) for a US eastern bituminous coal burned in the CANMET 0.3 MW_{th} vertical combustor facility at a firing rate of 0.21 MW with 5 vol% excess oxygen in the dry flue gas. Comparison of air combustion as well as oxy-fuel experiments with flue gas recycle (open symbols) and once-through runs (O_2/CO_2, filled symbols). Oxy-fuel experiments with flue gas recycle are provided for the case with a dry recycle stream (O_2, dry). The recirculation ratios are 0.63 (28% O_2), 0.51 (35% O_2), and 0.40 (42% O_2). Data taken from [97].

a firing rate of 0.21 MW with 5 vol% excess oxygen in the dry flue gas. Oxygen concentrations in the inlet of 28, 35, and 42% were tested.

The results reported in the literature generally show that combustion in air yields the highest NO_x emissions, oxy-fuel combustion based on synthetic gas mixtures ($CO_2 + O_2$) yields lower emission rates at comparable conditions, whereas oxy-fuel combustion with recirculation of flue gas yields the lowest emission rates.

Wet versus Dry Recycle: Payne et al. [86] observed that the reduction efficiency of NO_x through reburning in a 3 MW_{th} oxy-fuel sub-bituminous coal flame appeared to be higher when a wet instead of a dry recycle was applied. The reduction was 80% and 70%, respectively, compared to results obtained for air-blown combustion. During the experiments the flue gas oxygen concentration and the firing rate were fixed.

Nozaki et al. [119] likewise investigated the effect of wet and dry flue gas recycle for the primary flow, i.e. the flow for coal transportation, in their 1.2 MW_{th} burner. The experiments were performed with fixed firing rate and excess oxygen at the burner. Fig. 29 shows measurements of gas phase temperature as well as NO_x, HCN, and NH_3 concentrations along the burner axis. The NO_x concentration in both experiments peaks at the same level, although the formation of NO_x is shifted further down the reactor in the case of a wet, primary recycle. This can be attributed to the significant reduction in flame temperature in the first measurement point. At the same time, both the HCN and NH_3 concentrations are markedly higher for the dry recycle compared to the wet. This is likewise attributable to the differences in temperature profiles and hence the effect on the homogeneous gas phase chemistry dominating NO_x formation in the flame zone.

Initial NO_x Concentration: As indicated in Section 3.4.1.2 it is likely that high NO_x concentrations at the onset of both devolatilization and char combustion will limit the formation of further NO in the flame.

Liu et al. [162] determined the difference in reduction efficiency for experiments on a bituminous coal with 500 and 1000 ppmv NO_x in the oxidant O_2/CO_2 mixture in their 20 kW swirl-stabilized once-through burner setup. They saw that the change in reduction efficiency between the two levels of NO_x was less than 1% and thus within the experimental uncertainty. For their specific operating conditions, the NO_x concentration in the oxidant was thus not a limiting parameter in the reduction process.

Based on experiments in air, Spinti and Pershing [185] have shown that the apparent conversion of char-N to NO_x is a strong function of the initial NO_x level at the onset of char combustion in the range of 0–900 ppm NO_x on a dry basis. Likewise, the excess oxygen level affected the conversion rate, see Fig. 30. To remove the effect of volatile-N to NO_x conversion during the experiments the authors burned premade chars in methane. The char particles were withdrawn from a pulverized-coal flame just after devolatilization was terminated. For the conditions tested, increasing the initial NO_x concentration had a greater effect on the reduction of the apparent conversion of char-N to NO_x than decreasing the oxygen excess level. In air combustion which is the case for the described experiments, a high initial NO_x level translates to a high conversion of volatile-N to NO_x. This will have a negative impact on the process through an increase of the overall NO_x emission rate. In oxy-fuel combustion a high initial NO_x concentration at the base of the flame will most likely almost entirely originate from the recirculated flue gas. The apparent conversion of char-N to NO_x during oxy-fuel combustion could thus decrease as the concentration of NO_x in the oxidant increases, e.g. due to a reduced recycle ratio.

Fig. 31 shows computations of the total NO_x emission as a function of the conversion of volatile-N to NO_x and the fraction of coal-N released during devolatilization in air. It is seen that the lowest overall emission rate is achieved when the volatile-N to NO_x

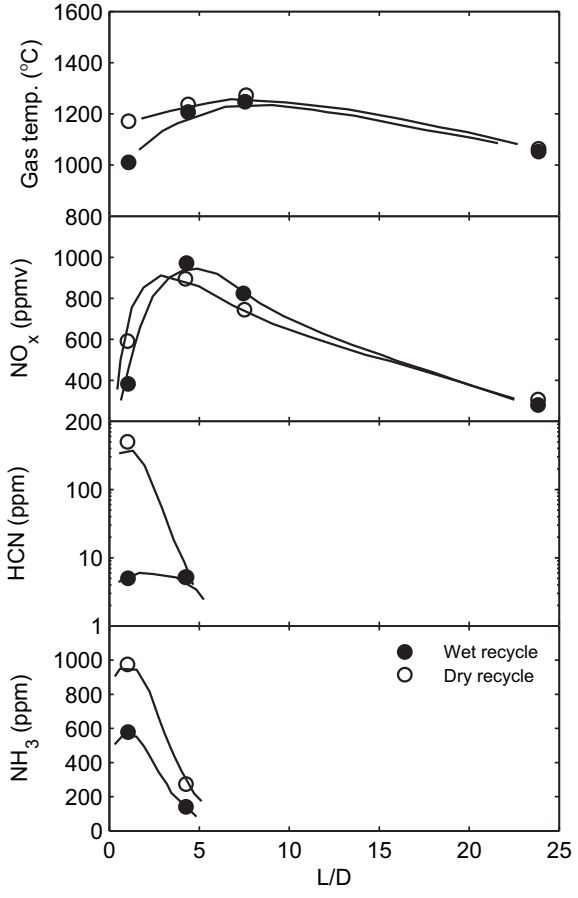

Fig. 29. Effect of wet versus dry recycle of primary gas on gas temperature, NO_x, HCN, and NH_3 concentrations along the burner axis in the IHI 1.2 MW furnace. The setup is operated in oxy-fuel mode with direct O_2 injection through the burner and with a low-volatile bituminous coal (Coal A). Data taken from [119].

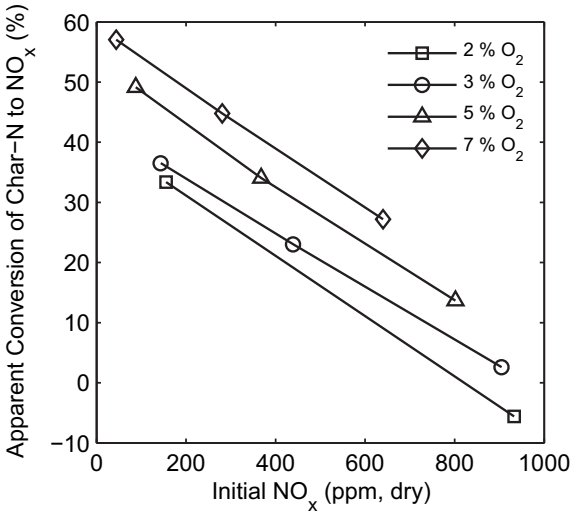

Fig. 30. Comparison of the effects of excess O_2 and of initial gas phase NO_x concentration on the conversion of char-N to NO_x for an Illinois #6 coal char combusted in air in a 29 kW furnace. Data taken from [185].

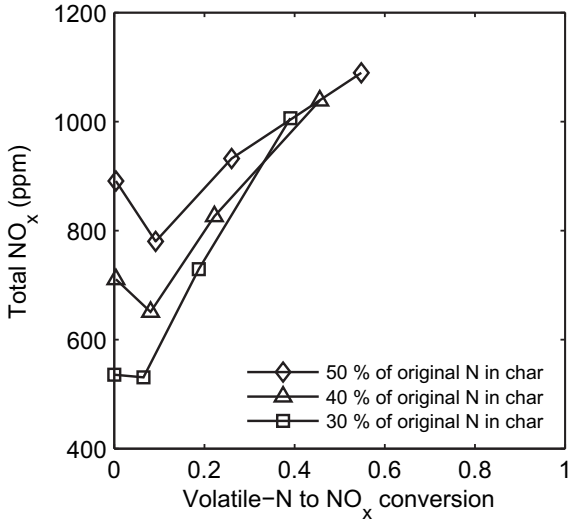

Fig. 31. Estimated NO_x emissions from Illinois #6 coal combusted in air. Results are based on modelling. Data taken from [185].

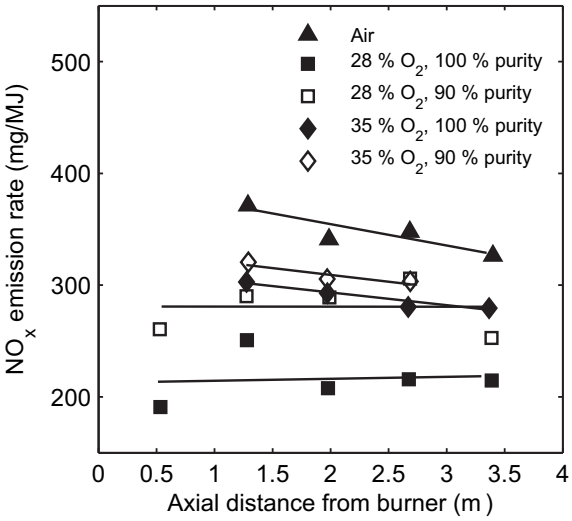

Fig. 32. Centre-line axial NO_x concentration (shown as the emission rate) for a US eastern bituminous coal. Comparison of air combustion and once-through (O_2/CO_2) oxy-fuel experiments with different oxygen purities in the CANMET 0.3 MW_{th} vertical combustor facility. The experiments were performed at a fixed firing rate of 0.21 MW and with an excess oxygen level corresponding to 5 vol% O_2 in the dried flue gas. Data taken from [120].

conversion is low and as much of the coal-N content as possible is released with the volatiles. The governing assumption applied in the modelling was that char-N to NO_x conversion decreases with increasing initial NO_x level during combustion.

Based on the observations above it seems that a high concentration of NO_x in the recirculated flue gas could increase the reduction rate of NO_x in the flame and thus lead to a further reduction of the emission rate.

3.4.1.6. Effect of oxygen purity and air penetration. Croiset et al. [120] have determined the NO_x emission rates from air-firing and once-through oxy-fuel combustion experiments of a US eastern bituminous coal with two different oxygen purities, 90 and 100% (remaining is N_2). The experiments were performed in the CANMET 0.3 MW combustion facility at a firing rate of 0.21 MW and with temperature profiles as shown in Fig. 11. As expected, the NO_x emission rate increases with decreasing oxygen purity, see Fig. 32. The difference between data obtained with an oxygen purity of 90% and 100% in the experiments with an oxygen concentration of 28% versus those obtained with 35% oxygen at the inlet is quite significant. There is, however, no obvious explanation to the deviations.

The data indicate that a less clean inlet O_2/CO_2 mixture (increased N_2 content) or air entrainment near the burners may give rise to increased NO_x emission due to thermal NO formation.

3.4.1.7. Influence of oxidant staging. The use of oxidant staging in oxy-fuel combustion as a primary measure to reduce NO_x emissions introduces a necessity for optimization due to the fact that the oxidant stream will contain NO_x.

Liu et al. [121,162] have investigated the effect of staging on the reduction of NO_x emissions from both air and oxy-fuel combustion in a once-through reactor. The authors focused on the effect of staging and NO_x recycling position on the reduction of recycled NO_x. Fig. 33 shows their results for the bituminous coal, Polish Blend. It is obvious that both the combustion media, air or oxy-fuel, the operating mode, with or without staging, and the NO recycling location influences the reduction efficiency. Focusing on the position where NO_x is recycled there is no significant difference between the primary and secondary oxidant streams, which both are introduced through the burner. The tertiary stream constitutes the staging stream. Recycling of NO_x through the tertiary stream markedly reduces the reduction efficiency, down to the range of 44–54% [162] as also shown by Scheffknecht and coworkers [144,148,164] in comparable experiments.

For a commercial oxy-fuel plant NO_x would be present in all oxidant streams. The use of over-fire air would then potentially decrease the rate of reduction of NO_x. On the other hand, a significant fraction of the NO_x present in the recycled flue gas will be

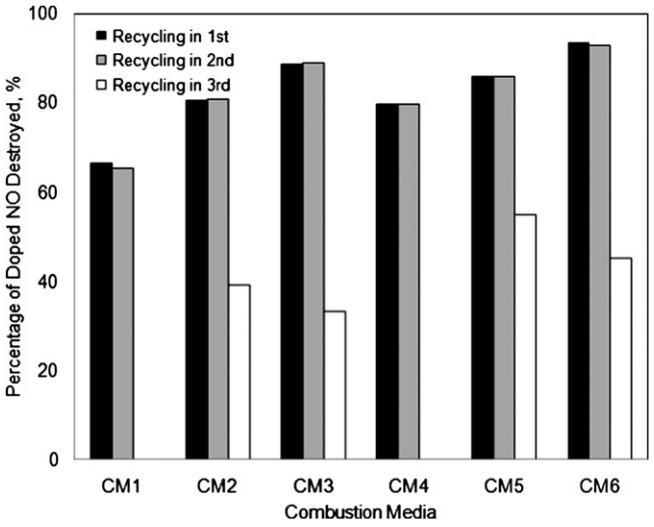

Fig. 33. Effects of combustion medium, staging position, and oxidant stream chosen for NO recirculation (doping) on the reduction efficiency of recycled NO. Experiments are performed on a bituminous coal, Polish Blend, in a 20 kW swirl-stabilized once-through burner setup. Five percent of NO in N_2 was added and mixed to the different streams of oxidants to simulate the NOx recycle. The concentration of the simulated recycled NO was in the range of 500–700 ppmv. 1st, 2nd, and 3rd refer to primary, secondary, and tertiary oxidant streams. The recycling locations (injection of the tertiary oxidant stream), Level 1 and 2, are 570 and 880 mm downstream of the burner, respectively. CM1: 1st & 2nd – Air, $\lambda = \lambda_{burner} = 1.20$; CM2: 1st & 2nd – Air, $\lambda = 1.20$, $\lambda_{burner} = 0.80$, Level 1; CM3: 1st & 2nd – Air, $\lambda = 1.20$, $\lambda_{burner} = 0.80$, Level 2; CM4: 1st & 2nd – 30% O2/70% CO_2, $\lambda = \lambda_{burner} = 1.20$; CM5: 1st & 2nd – 30% O_2/70% CO_2, $\lambda = 1.20$, $\lambda_{burner} = 0.80$, Level 1; CM6: 1st & 2nd – 30% O_2/70% CO_2, $\lambda = 1.20$, $\lambda_{burner} = 0.80$, Level 2. Data taken from [162].

introduced through the burners and thus experience fuel-rich conditions for a longer period of time. The optimum degree of over-fire oxidant still remains to be determined and would, at the same time, be dependent on the burner design.

3.4.1.8. Coal properties. The effect of coal properties on the formation and reduction of NO_x in oxy-fuel combustion has been investigated by several researchers. In entrained-flow reactor type experiments both Hu et al. [161] and Shaddix and Molina [169] have observed increasing NO_x emission with decreasing rank of the coals. The coals investigated range from semi-anthracite over high-volatile bituminous to sub-bituminous. Shaddix and Molina [169] attributed the trend to the higher volatile content, higher char combustion temperature, and the lower fuel-N content for the lower ranking coals.

Mackrory and Tree [175] have observed that the difference between the NO_x emissions in air- and oxy-fuel combustion in their laminar flow reactor increases with the rank of the coal. Their observations are based on experiments performed with one sub-bituminous coal and two high-volatile bituminous coals, Illinois # 6 and Pittsburgh # 8.

Seven different bituminous coals were investigated in a 20 kW swirl-stabilized once-through burner setup by Liu et al. [162]. The authors measured the coal-N to NO conversion ratio between oxy-fuel combustion with 30% O_2 in CO_2 and in air. Their data showed no clear correlation between the conversion ratio and the coal rank, volatile matter, nitrogen content, etc. Instead, as shown in Fig. 34, there seems to be a dependence of the char reactivity. Increasing reactivity leads to a relatively larger conversion of coal-N to NO at oxy-fuel conditions. This could be attributed to the observation of Liu et al. [162] that reactive coals produced slightly higher temperatures in the combustion zone. According to Liu et al. this will promote NO_x formation at the fuel-lean conditions at which the tests have been run. For the less reactive coals more unburnt char exists in the flame zone which may promote reduction of the previously formed NO_x.

A large portion of the recycled NO_x in an oxy-fuel plant could be NO_2 due to oxidation of NO in the downstream processes [160,161]. Fig. 35 shows the results of interchanging NO for NO_2 in the synthetic, recycled flue gas applied in the entrained-flow reactor experiments by Hu et al. [160,161] for two different coals. For the high-volatile coal, Prima, the figure demonstrates no significant differences between the two species with respect to the stoichiometric ratio. However, for the medium-volatile coal, Datong, the reduction efficiency in the fuel-lean region is markedly lower for NO_2 than for NO. There are some uncertainties regarding the specific mechanism for the reduction of NO_2 in the flame [160,161] even though suggestions to direct reduction via free radicals or through initial conversion to NO have been given. The results by Hu et al. [160,161] indicate that the volatile matter in the coal has a dominant effect.

Fig. 36 shows burner axis profiles of gas temperature, as well as NO_x, HCN, and NH_3 concentrations for two different coals burned in air and oxy-fuel environments (O_2 concentration of 27 vol% at inlet) in a 1.2 MW_{th} furnace [119]. The coals differ in their volatiles content. It is obvious from the peaks in the temperature profiles that the low-volatile coal (A) ignites further downstream than the medium-volatile coal (B). The gas phase temperature just outside the burner mouth ($L/D = 0$) for the two coals thus differs by approximately 200 °C. For each coal, the NO_x concentration profile is very similar regardless of the combustion environment. It must thus be the coal properties determining the NO_x formation, with the low-volatile coal producing more NO_x. This observation is contrary to the results presented above. It is likewise seen that the coal volatile content has an impact on the HCN and NH_3 profiles. They report that the coal with the higher volatiles content forms significantly more HCN during combustion than the low-volatile coal which on the other hand produces a very high concentration of ammonia in the early flame zone during oxy-fuel combustion.

The limited investigations of the influence of coal properties on NO_x formation during oxy-fuel combustion indicate that the relative production of NO_x at oxy-fuel conditions compared to when combustion is performed in air increases with increasing reactivity of the coal char. The effect could be caused by a greater sensitivity to char combustion temperature of the NO_x formation mechanism in an oxy-fuel environment than in air.

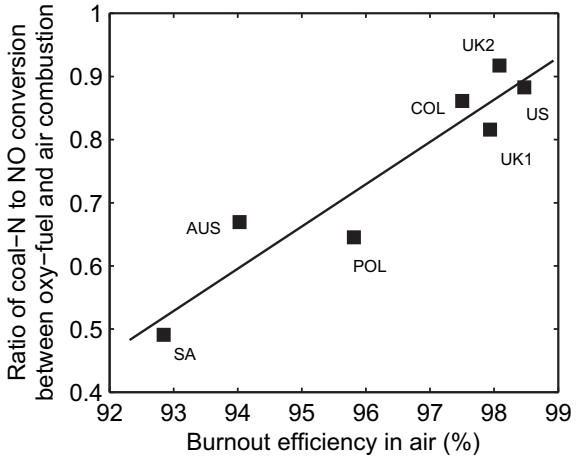

Fig. 34. The dependence of the ratio of coal-N to NO_x conversion between coal combustion in 30% O_2/70% CO_2 and coal combustion in air on the coal burnout efficiency in air for seven different bituminous coals. Experiments are performed in a 20 kW swirl-stabilized once-through burner setup with an overall stoichiometric value of 1.2. SA: South African, AUS: Australian, POL: Polish Blend, COL: Colombian, UK1(2): UK Bituminous 1 (or 2), US: US Blend. Data taken from [162].

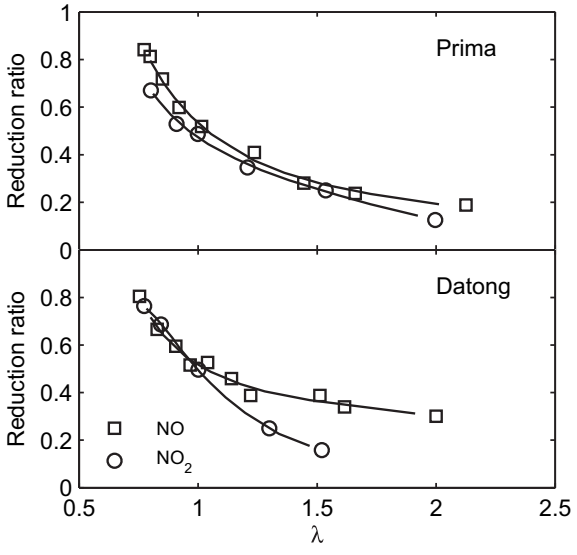

Fig. 35. Reduction ratios of recycled NO and recycled NO_2 as a function of stoichiometry obtained in an entrained-flow reactor. The reduction ratio at a given stoichiometry is obtained from the difference in NO_x emission between an experiment with and without recirculation of NO_x. The operating conditions are: recycling ratio of 0.4; $T = 1373$ K; fixed residence time of 2 s; concentration of NO_x in the inlet gas of 1000 ppm for recycled-NO_x experiments. Prima: high-volatile bituminous Indonesian coal; Datong: medium-volatile bituminous Chinese coal. Data taken from [161].

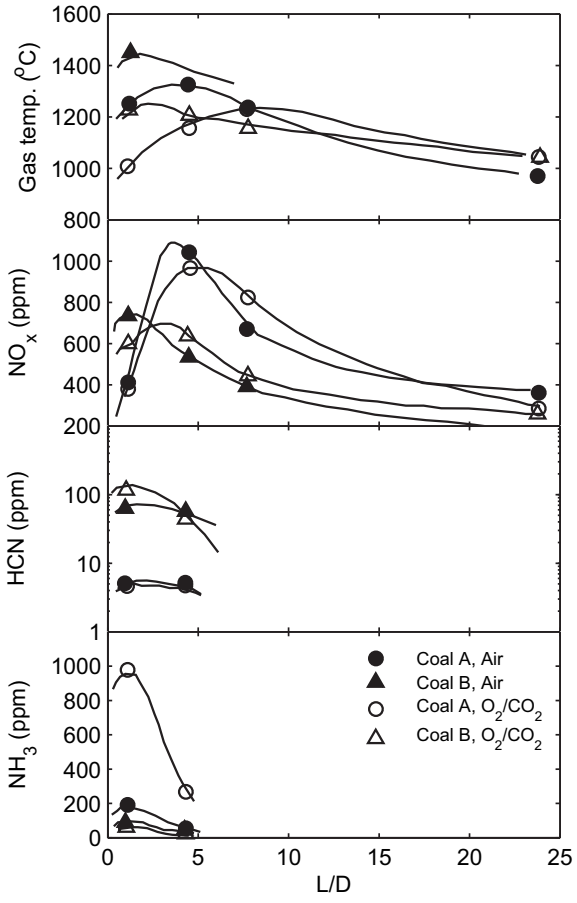

Fig. 36. Effect of coal volatiles content on gas temperature, NO_x, HCN, and NH_3 concentrations along the burner axis in a 1.2 MW furnace. Coal A, low-volatile bituminous, 26.1% volatile matter. Coal B, medium-volatile bituminous, 41.2% volatile matter. O_2 concentration is 0% in primary stream, 30% in secondary stream, and 27% overall at inlet, $\lambda = 1.2$. The recirculated flue gas in the oxy-fuel experiments contains up to 200 ppm NO_x. Data taken from [119].

3.4.1.9. Effect of burner configuration for swirling flames. Fig. 24 showed that exchanging a conventional burner for a low-NO_x burner in oxy-fuel combustion yielded a 56% reduction in the NO_x emission rate. Thus, NO_x formation in oxy-fuel combustion depends on the burner configuration and especially the flow field in the near-burner zone, just as is the case during conventional air combustion.

Experiments performed by Chui et al. [150] in the CANMET 0.3 MW vertical combustor research facility show that NO_x emissions are highly dependent on the burner swirl number, i.e. flow dynamics. Increasing the swirl number from 1 to 2 decreases the NO_x formation by 34%. However, for the range of swirl numbers applied in the experiments NO_x emissions during oxy-fuel combustion was higher than for air-firing, 140–150 versus 110 mg/MJ. This was true for both burner configurations tested. Because of safety limitations, the amount of oxygen mixed into the secondary oxidizer stream was restricted to 28% on a dry basis. For the same reason, the primary stream contained little or no oxygen. To obtain the necessary overall oxygen concentration during combustion a portion of the total oxygen demand was injected as pure oxygen through a special annuli in the burners. The burners provided stable flames but the injection of pure oxygen caused the release of volatiles and fuel-N from the Canadian sub-bituminous coal tested to occur in the O_2-rich portion of the flame. An improved burner design subsequently tested by Chui et al. [151] reduced the NO_x emission down to 40 mg/MJ at oxy-fuel conditions and improved the remaining combustion characteristics as well.

Due to the strong influence from the near-burner flow field on NO_x emissions from swirling flames it will be difficult to transfer the results from the changes to the specific burner configurations obtained by Chui et al. [150,151] to a general trend for other oxy-fuel burners.

Based on experiments regarding char-N to NO_x conversion and modelling investigations, Spinti and Pershing [185] suggest the following measures in order to obtain the largest possible reduction in NO_x emissions. (*i*) a burner which yields a fuel-rich flame core, (*ii*) high temperatures during devolatilization, and (*iii*) a char oxidation zone with temperatures as low as possible in combination with low excess O_2 and adequate residence time for char burnout at the lower gas temperatures. This is not different from the case of air-firing. However, because of the changes in mass flow rates in the primary and secondary inlets, see Section 2.7.1, the optimal burner design for oxy-fuel combustion is not necessarily similar to that developed for conventional air-firing.

3.4.2. SO_x

Sulphur emissions and the effect on ash properties and boiler-tube corrosion in oxy-fuel combustion from significantly increased levels of gas-phase-S in the boiler have received increasing attention in the recent years.

There have been contradictory observations on the SO_2 emissions from oxy-fuel combustion. Some researchers experimentally show a decrease when comparing to combustion in air [88,96,97,128,136,138] whereas others on the basis of either experiments [121,113] or equilibrium calculations [149] report no differences.

Kiga et al. [136] reported oxy-fuel experiments performed in the IHI 1.2 MW_{th} combustion facility with recirculation of dry flue gas. The investigations showed that the conversion of the coal sulphur content, measured as the amount of S in the outlet divided by the amount going in with the coal, decreased markedly in oxy-fuel combustion compared to air-firing operation. Even though the authors were not able to close the mass balance for sulphur the results indicated that the major part of the difference could be attributed to removal of S through condensation as H_2SO_4 in low-temperature ducts and by retention in ash particles.

Zheng and Furimsky [149] modelled the formation of SO_2 and SO_3 based on equilibrium considerations during both air- and oxy-fuel combustion. They found that practically all of the sulphur content in coals is released as SO_2 and SO_3 irrespectively of the combustion medium, as CO_2 plays an insignificant role for the release compared to oxygen. With respect to recycle ratio and oxygen excess, their simulations yielded an increased amount of SO_3 with an increase in the amount of available oxygen.

Generally, the disagreements observed between experimental findings and the computations based on equilibrium modelling are expected to be a consequence of computations reflecting conditions immediately after combustion and not accounting for changes occurring further downstream. Another plausible explanation is the fact that some of the processes could be kinetically controlled, e.g. the heterogeneous reactions controlling retention of S in ash and other deposits, a fact that is not captured in the simulations.

Table 13 provides a summary of the results on SO_2 emissions from semi-technical and pilot scale experiments with flue gas recirculation.

In the following sections the reported results on SO_2 emissions from oxy-fuel combustion are divided according to the effects of different operating conditions and design aspects. The subject of boiler-tube corrosion due to the presence of sulphur in the flue gas is likewise treated.

Table 13
Summary of SO_2 emission results from experiments in pilot scale and semi-technical scale with flue-gas recirculation.

Author(s)	Fuel input (MW)	Inlet O_2, Oxy (%)	Emission (mg/MJ)	Conversion ratio	Conclusion(s)
Woycenko et al. [88]	2.1	26	Air: 645 Oxy: 375–418	Air: 100% Oxy: 60–67%	The conversion ratio of fuel-S into SO_2 is lower for oxy-fuel combustion than air.
Wall et al. [138,128]	1.2	27	Air: 150–416 Oxy: 100–291	Air: 63–83% Oxy: 40–53%	Lower SO_2 emission in oxy-fuel than in air, level dependent on coal type. Increased SO_3 concentrations increases acid dew point from ~ 133 to ~ 156 °C.
Croiset and coworkers [120,97]	0.21	28, 35	Air: 300–320 Oxy: 260–275	Air: 91% Oxy: 56–65%	SO_2 emissions independent of wet and dry recycle even though removal through condensate was expected. Drop in conversion rate attributed to conversion to SO_3 and/or retention in ash and deposits. Coal sulphur content most important factor to determine SO_x emission.
Tan et al. [122]	0.21	35	–	–	SO_2 emission rates slightly lower for oxy-fuel combustion than in air even though the concentration was 3–4 times higher in the oxy-fuel case.
Scheffknecht and coworkers [144,145,147]	0.5	27–30	–	Air: –Oxy: 96–100%	Negligible reduction of SO_2 in the radiative section of a boiler. Higher SO_2 concentrations yields higher H_2S formation in fuel-rich zones. Calcium-rich coals show greater tendency to capture S.

3.4.2.1. Effects of changes in the oxygen concentration, oxygen excess, flue gas recycling ratio, and gas phase temperature. Hu et al. [96] focus on the effect of oxidizer composition, stoichiometry, and flame temperature in their investigations of SO_2 emissions in an entrained-flow reactor with a coal feed rate up to 180 g/h. They encountered the highest conversion ratios at or near stoichiometric conditions, see Fig. 37. The decrease in S conversion at fuel-rich conditions is assumed to be due to retention in unburned coal and formation of other, reduced S-containing species (e.g. H_2S, COS, and CS_2). These species were not measured. The reduction in SO_2 emissions at fuel-lean conditions compared to stoichiometric conditions has not been explained but could partly be due to increased conversion to SO_3.

According to Liu et al. [121] SO_2 emissions are not significantly affected by the use of staging or changes in the combustion media.

3.4.2.2. Effect of the composition of the recirculated flue gas. Croiset and coworkers [120,97] reported experiments regarding SO_2 emissions from the combustion of a US eastern bituminous and a Canadian sub-bituminous (Highvale) coal in the 0.3 MW CANMET oxy-fuel combustion facility. Fig. 38 shows SO_2 emission rates for air-fired experiments, once-through experiments (synthetic flue gas denoted O_2/CO_2), and dry flue gas recycle (O_2, dry) experiments. The data for the bituminous coal in the figure show similar emission rates for experiments with air and the synthetic O_2/CO_2 mixture. For the recycle experiments with 28 and 35 vol% O_2, however, the emission rates were slightly lower.

Comparing gas phase concentrations instead of emission rates reveal that the measured SO_2 concentrations in the burner during oxy-fuel combustion with a recycle fraction of about 60 vol% were approximately 3 times higher than for air-firing [97]. The theoretical increase in the SO_2 concentration was about a factor of 4. The authors concluded that the conversion of sulphur into SO_2 was independent of oxygen concentration and that retention in ash and/or further oxidation into SO_3 could explain the difference. Ash analysis showed that less than 3% of the initial S-content in the coal was

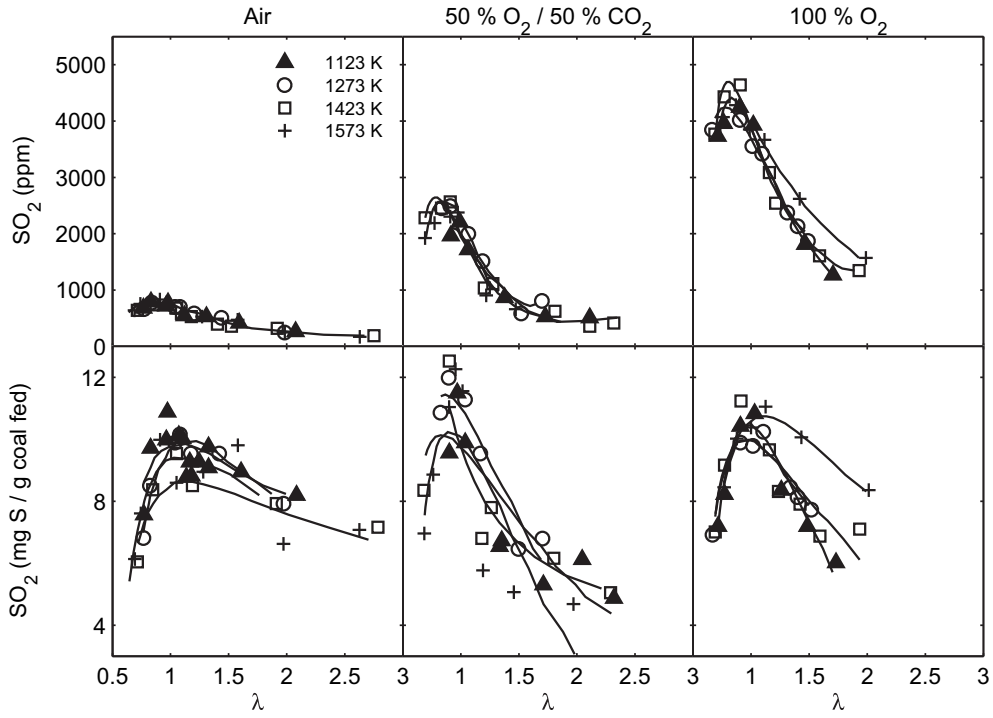

Fig. 37. SO_2 emissions versus stoichiometric ratio and temperature at different O_2 concentrations for N_2 and CO_2-based oxidizers. Experiments are performed in an entrained-flow reactor with a coal feed rate of up to 180 g/h. The SO_2 concentrations in ppm are given as measured. Data taken from [96].

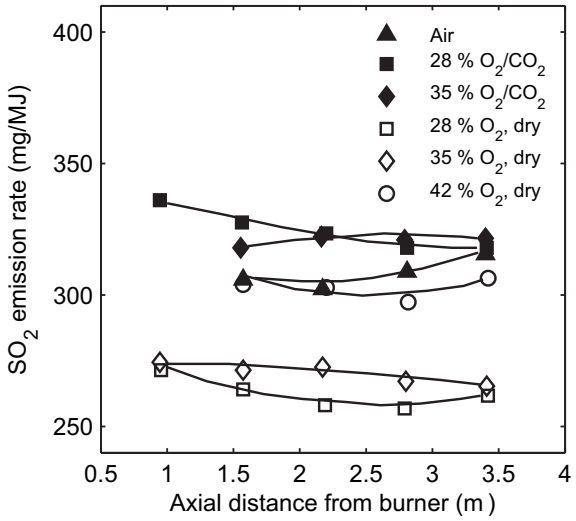

Fig. 38. Centre-line axial SO_2 concentration (shown as the emission rate) for an Eastern bituminous coal burned in the CANMET 0.3 MW vertical combustor research facility at a firing rate of 0.21 MW with 5 vol% excess oxygen in the dry flue gas. Comparison of air combustion as well as oxy-fuel experiments with flue gas recycle (open symbols) and once-through runs (O_2/CO_2, filled symbols). Oxy-fuel experiments with flue gas recycle are provided for the case with a dry recycle stream (O_2, dry). The recirculation ratios are 0.63 (28% O_2), 0.51 (35% O_2), and 0.40 (42% O_2). Data taken from [97].

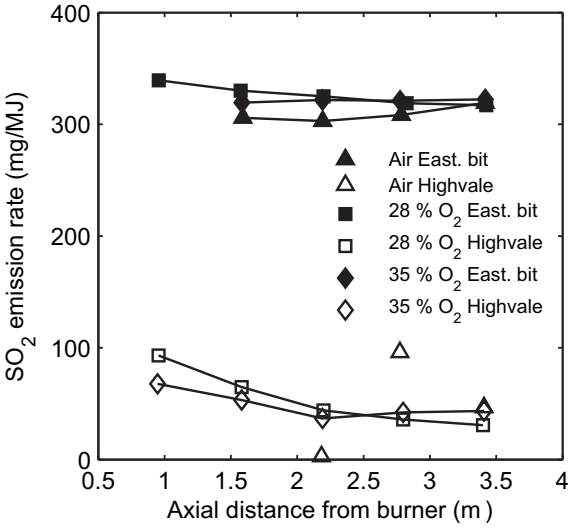

Fig. 39. Centre-line axial SO_2 emission rate. Comparison of Highvale sub-bituminous and US eastern bituminous coals. The experimental setup is the CANMET 0.3 MW vertical combustor research facility operated in once-through mode at a firing rate of 0.21 MW with 5 vol% excess oxygen in the dry flue gas. Data taken from [120].

present in the ash. However, the condensed water did have a sulphate content of above 3000 mg/L and a pH between 2 and 3. The high sulphate concentration in the condensate indicates high SO_3 levels in the flue gas. In the work by Mönckert et al. [147] the sulphur retention in calcium containing coals is shown to increase with increasing SO_2 concentration in the recycled flue gas. This is due to the formation of $CaSO_4$.

Experimental runs with wet flue gas recycle were likewise performed by Croiset and Thambimuthu [97] but showed no significant difference to the dry case. The authors, however, expected a lower emission rate for the latter case since some SO_2 should be removed with the waste water during the flue gas condensation.

3.4.2.3. Effect of coal sulphur content. Comparing the data in Fig. 39 leads to the conclusion that the specific SO_2 emissions are almost exclusively dependent on the coal type, i.e. sulphur content. The Eastern bituminous coal has a sulphur content of 0.96 wt% (dry basis) whereas the sub-bituminous coal (Highvale) contains 0.24 wt% (dry basis) [120]. The relative differences due to changes in combustion medium and oxygen concentration are thus negligible in this context.

3.4.2.4. The SO_2 to SO_3 conversion and sulphur-induced corrosion. In later work from CANMET, Tan et al. [122] reported further results on the conversion of SO_2 to SO_3 in the flue gas. They showed that the conversion was about 5% whereas it is typically between 1 and 5% in conventional air-firing systems [113,122,147] depending on the combustion conditions and the sulphur content of the coal. These values have likewise been found by Scheffknecht and coworkers [145]. Klostermann [113] and Mönckert et al. [147] report that SO_3 formation is promoted by both high oxygen and high water levels in the flue gas. In the case of a flue gas recycle without prior SO_2 removal the amount of SO_3 in the boiler can thus reach high values (up to about 85 ppmv [147]) and thus increase the risk of sulphur corrosion in the regions of the system which operate below the acid dew point.

Because of the potentially higher SO_3 concentrations in the flue gas, the acid dew point will increase accordingly [115,138,145,147,148]. Increases of about 20–40 °C from ~130 to ~160 °C have been reported [113,138,145]. Schnurrer et al. [115] found a similar trend from their thermo-chemical equilibrium calculations. An earlier formation of sulfuric acid in the flue gas ducts will increase the risk of flue gas side corrosion in the low-temperature parts considerably. Schnurrer et al. suggest using a dry flue gas recycle to decrease the concentration of water in the flue gas and thus the amount of acid that can form.

Scheffknecht and coworkers [144,145,147,148] investigated the impact of recirculation of SO_2 (by doping the oxidant stream in their 20 kW EFR) on the transformation of SO_2 in the radiant section of a boiler. They found only a negligible reduction in the concentration of the recycled SO_2. However, high concentrations of SO_2 in the furnace was found to increase the concentration of H_2S in the fuel-rich regions for both air- and oxy-fuel firing conditions, see Fig. 40, inducing a higher risk of corrosion. The H_2S to SO_2 ratio in the oxy-fuel experiments were lower than in air even though the absolute concentration was higher.

3.4.2.5. In-boiler desulphurization. In a series of papers Liu and coworkers [127,208,209] address the ability of oxy-fuel combustion

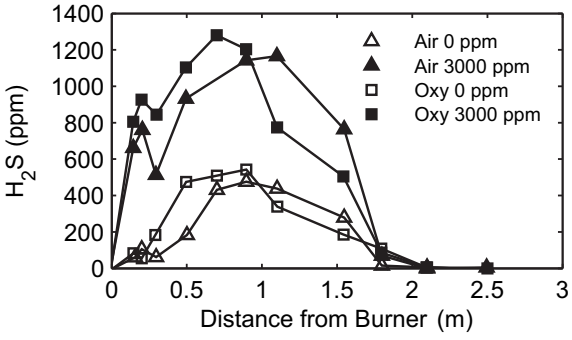

Fig. 40. H_2S concentration profiles along burner axis for air- and oxy-fuel combustion experiments on lignite. The experiments were performed in an 20 kW entrained-flow reactor with and without doping of the oxidizer with 3000 ppm SO_2. Data taken from [144].

to drastically reduce the emissions of SO_2 from combustion of coal. They suggest in-boiler desulphurization by injection of limestone. The combination of both high SO_2 and CO_2 partial pressures should ensure high reactivity of the limestone toward SO_2. The authors explain the increased reactivity by two factors: (1) high SO_2 limits $CaSO_4$ decomposition and (2) high CO_2 limits decarbonisation of limestone before sulphation whereby direct sulphation of limestone without decarbonisation is favoured. The direct sulphation will minimize the diffusion resistance through the solid phase (no pore clogging) and hence a larger part of each limestone particle will participate in the desulphurization reaction.

Even though the experiments show significantly increased reactivity of the limestone toward SO_2 for a sulphur containing flue gas recycle compared to conventional air-fired conditions, this strategy is not likely to be adopted in power plants which produce fly ash for cement and concrete production due to the associated mixing of gypsum and fly ash.

3.4.2.6. Summary. The substitution of N_2 by CO_2 in oxy-fuel combustion does not affect the release of sulphur from the coal during combustion. However, the increased oxygen partial pressure necessary to maintain an appropriate flame temperature increases the formation rate of SO_3. During operation with a flue gas recycle without SO_2 removal the SO_2 and thus the SO_3 levels in the boiler and flue gas ducts increase significantly which will enhance the risk of sulphur-induced corrosion at both high and low temperatures. High in-boiler concentrations of sulphur oxides can likewise increase retention of S in the fly ash. Increased retention will reduce the SO_2 emission rate but could at the same time yield problems with further utilization of the fly ash in cement and concrete production.

3.4.3. Trace elements

The subject of trace element emissions during oxy-fuel combustion is generally seen to have drawn minor attention compared to other of the fundamental combustion issues investigated. Because of the scarcity of published results within this area of research none of the results described below have been confirmed by other research groups.

According to the equilibrium calculations performed by Zheng and Furimsky [149] the Hg-, Cd-, As-, and Se-containing emissions are only insignificantly affected by the combustion medium. However, in case of incomplete elimination of these species in the flue gas cleaning equipment situated before the flue gas recycle point elevated concentrations will occur in the boiler and thus in the flue gas stream to be treated before sequestration.

Suriyawong et al. [117] measured the mercury emission from air- and oxy-fuel combustion of a sub-bituminous coal in a laminar reactor and determined the ratio between the elemental and oxidized forms. Fig. 41 shows their results.

The data lie within typically agreed intervals of sub-bituminous coals, i.e. 10–20% of the total mercury emissions are in the oxidized states with the remainder in the elemental state. The concentrations measured are within the range of uncertainty of the mercury content in the coals which indicate that burning coal at oxy-fuel conditions does not have a significant effect on neither the vaporization nor the speciation at the furnace exit.

At CANMET, ongoing research addresses mercury removal technologies for oxy-fuel combustion [9].

3.5. Ash and deposition chemistry

The transformations of coal mineral matter during combustion are significantly affected by the temperature and the gas phase composition surrounding the coal particles [125]. The change in combustion atmosphere and the potential change in local particle temperature between oxy-fuel combustion and air-fired combustion may thus have an effect on the ash formation mechanisms and hence the ash composition and quality.

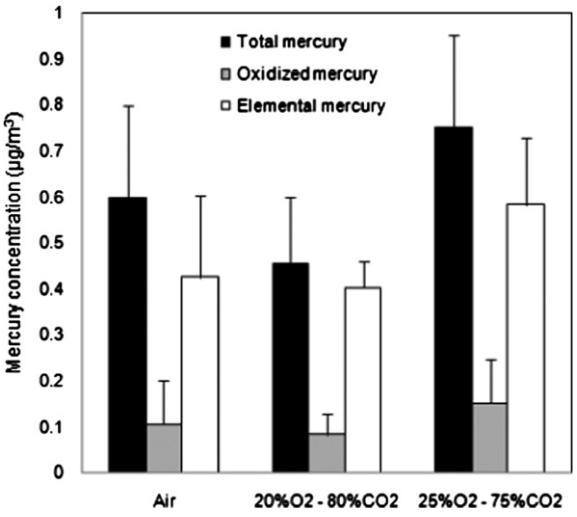

Fig. 41. Mercury concentration measured at the furnace exit of a laminar reactor. Experiments are performed with a sub-bituminous coal in air and for two O_2/CO_2 mixtures with a fixed reactor temperature of 1200 °C. The total Hg concentration is divided into the fraction consisting of metallic (elemental) Hg and the oxidized forms. Data taken from [117].

3.5.1. Particle formation mechanisms

Fig. 42 shows the mineral transformation and particle formation pathways for both fine (sub-micrometer, mode around 0.1 μm) and coarse particles during coal combustion. There are two pathways for the formation of sub-micrometer particles; (1) direct vaporization of volatile metals, e.g. Na, Pb, Cd, and Hg, which react in the gas phase and subsequently nucleate or condense on the surface of existing particles; (2) non-volatile species like e.g. silica oxides can be reduced to sub-oxides, e.g. as in reaction (14). These sub-oxides have a lower melting point and are devolatilized and rapidly reoxidized in the gas phase causing an oversaturated mixture.

$$MeO_x + CO \rightleftharpoons MeO_{x-1} + CO_2 \quad (14)$$

Particle formation occurs mainly through nucleation whereas growth is dominated by condensation and collision mechanisms. The sub-micrometer particle formation mechanisms are complex functions of such factors as coal type, combustion temperature, fuel to oxidizer ratio, and residence time. This is likewise the case for the resulting particle size distributions [117].

Coarse ash particles are formed from the non-volatile mineral inclusions in the coal which are not released as sub-oxides. These inclusions can coalesce and form a glassy matrix or remain in their original state if the temperature does not exceed their melting points [117].

The main fraction of the fines will consist of spherical particles due to their origin from gas phase species. On the other hand, the shapes of the coarse particles may vary from spherical or near-spherical to irregular, depending mainly on the char particle temperatures during combustion, i.e. whether they have been melted.

3.5.2. The effects of gas composition on particle formation

Combustion at oxy-fuel conditions with an air-like composition of the oxidant will result in a lower adiabatic flame temperature and hence a reduction of the coal burning rate compared to combustion in air, see Sections 2.7, 3.2, and 3.3. The vaporization of both volatile metals and metal sub-oxides as well as the particle

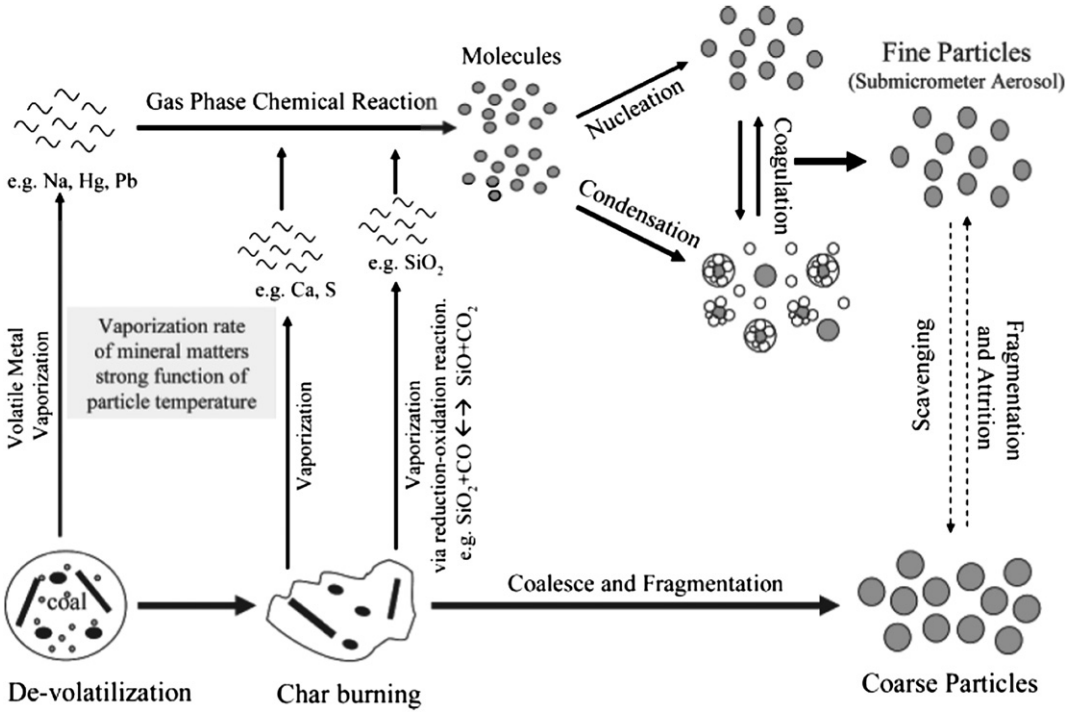

Fig. 42. Mineral transformation and particle formation pathways during coal combustion [117].

formation rates will thus be significantly smaller, as observed by Suriyawong et al. [117] and Sheng and coworkers [125,182,183]. From their investigations, Suriyawong et al. found that the ratio between fine and coarse particles shifted significantly toward fewer sub-micrometer particles in this particular oxy-fuel case. The mean size of the fine particles likewise became smaller because the particles have less time to grow when ignition and combustion is delayed, see Fig. 43. The bottom part of the figure shows the amount of various elements in the fine ash. It is generally observed that a smaller amount of ash forming elements have vaporized from the coal in the case of oxy-fuel conditions causing the lower number concentration. At the same time, the ratios between the different elements have changed. Particularly calcium and iron are released to the gas phase to a much lesser extent than in air. Suriyawong et al. [117] explain this phenomenon in the way that the increased concentration of CO_2 in the bulk gas will shift the sub-oxides formation equilibrium toward the oxides, see reaction (14), and thus reduce the formation of sub-micrometer particles through this pathway. The reduced particle surface temperature is, however, of significant importance. Sheng et al. [182] likewise determined the compositions of their ashes. They observed a similar shift in the ratio between volatile and less volatile species in the sub-micron ash for oxy-fuel combustion with an air-like oxidant composition. Increasing the oxygen concentration diminished the difference between air and oxy-fuel combustion. Differences in the oxygen concentration and thus the combustion temperature of the coal and char particles can alter the distribution between the main phases slightly, as more or less of the included minerals melt into a glass phase [183,125].

Increasing the O_2 concentration in CO_2 from 20 to 50% increases the particle surface temperature during combustion from 1772 K to 2679 K [117]. As a result, the particle size distribution of the sub-micrometer-sized fraction of ash particles is shifted toward larger sizes, see Fig. 44.

Sheng et al. [183] observed the same trend for their Chinese coals. They likewise concluded that the temperature difference between air and oxy-fuel combustion with 20% O_2 in CO_2 might alter the particle fragmentation and coalescence mechanisms in addition to lowering the ash vaporization rate. However, the particle number concentration in the less than 50 nm range does not change.

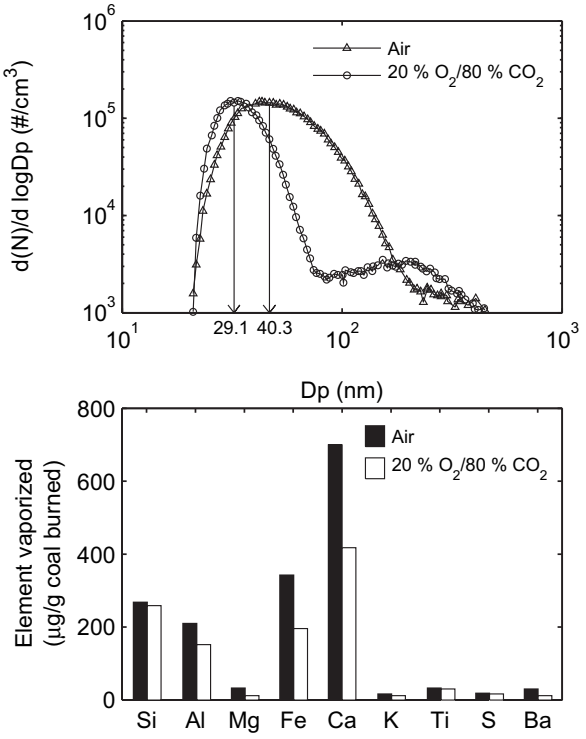

Fig. 43. Top: Sub-micrometer particle size distribution from air and 20% O_2/80% CO_2 combustion of a sub-bituminous coal obtained in a laminar flow reactor with a fixed temperature of 1200 °C. Bottom: Measured elemental compositions in sub-micrometer-sized ash from the same experiments. Data taken from [117].

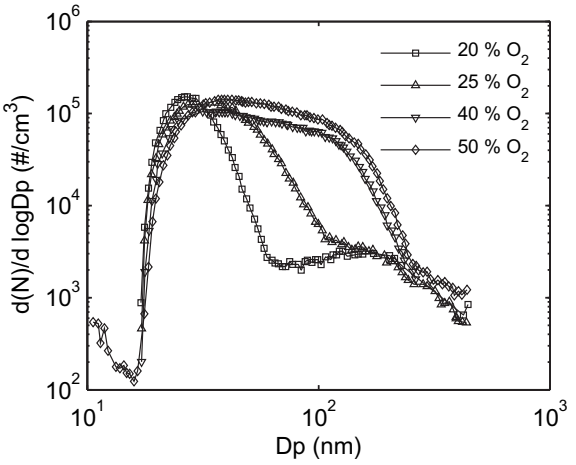

Fig. 44. Sub-micrometer particle size distributions for oxy-fuel combustion at different O_2 concentrations obtained from combustion of a sub-bituminous coal in a laminar flow reactor with a fixed temperature of 1200 °C. Data taken from [117].

According to Suriyawong et al. [117] this is due to the fact that the nucleation and condensation mechanisms are competing. Below a critical concentration of small particles vaporized species tend to nucleate. Above this limit condensation dominates leading to growth in particle size instead of particle number concentration.

Comparing Figs. 43 and 44 leads to the conclusion that increasing the oxygen concentration in oxy-fuel combustion from 20% to between 25 and 40% will produce a particle size distribution similar to that obtained in air for the small size fraction of ash particles. Experiments reported by Wall et al. [138,128] confirm this observation.

A modelling study by Krishnamoorthy and Veranth [210] investigated the effect of particle size, bulk gas composition, and in-furnace temperature during oxy-fuel combustion on the vaporization of metal sub-oxides from the burning char due to locally reducing conditions within the particles. Fig. 45 shows the ratio between CO and CO_2 as a function of radius in a char particle burning in atmospheres of varying CO_2 concentrations.

The results indicate that increasing the CO_2 level in the bulk gas significantly decreases the CO/CO_2 ratio inside the particles even though the absolute concentration of CO increases. Based on equilibrium considerations considering reaction (14) a shift from air-blown to oxy-fuel combustion should thus impose decreased vaporization of refractory oxides from the coal mineral phase during combustion.

3.5.3. Ash quality

To the power plants which sell their coal fly ash for cement or concrete production the quality of the ash in this respect is crucial. Especially the sulphur content of the ash is a critical parameter, the limiting value for S is 3 wt% measured as SO_3, as described in Section 2.5.1.2. Significantly increased sulphur retention compared to the level which is normal in air-fired operation will make the fly ash useless as a substitute for cement in concrete production. This is due to sulphates reacting with the other components in the concrete matrix after hardening. The result is an expansion of the mineral phase and thus fatal cracks in the structure.

The results published by Farley [72] indicate that the fly ash from oxy-fuel combustion of coal should be "equally acceptable for cement manufacturing as those arising from conventional air-firing". However, the paper provides no reference to the specific restrictions on the fly ash composition applying in the UK by which the above statement cannot be assumed applicable to the regulations and conditions in other countries without further verification.

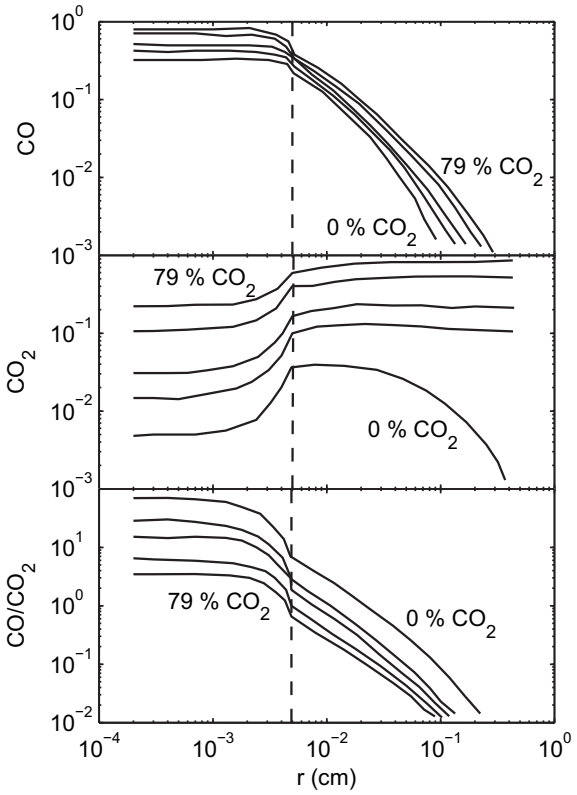

Fig. 45. CO and CO_2 partial pressures (atm) and the CO/CO_2 ratio as a function of radius from the centre of a particle through the boundary layer. Vertical dotted line corresponds to the surface of the particle. The data are for a 100 μm char particle burning in a furnace with walls at 1750 K and 0, 10, 20, 50, and 79 vol% CO_2 in the bulk gas. The O_2 concentration in the bulk gas is 20 vol% for all simulations. The remainder of the bulk gas consist of 1% H_2O and the difference is N_2. Note that the position of the legends in the figure showing the CO/CO_2 ratio has been corrected compared to the original figure in [210].

Wall et al. [138] report similar compositions and melting behaviour of both fly and bottom ashes obtained from air and oxy-fuel combustion. The coal with the highest calcium content showed a slightly increased concentration of sulphur. During the experiments emphasis was reported to be on generating the same temperature and heat transfer conditions, i.e. by operating with 27% O_2 on a wet basis in the oxidizer. From their experiments Sheng and Li [125] reported a small increase in the content of limestone due to the higher partial pressure of CO_2 at oxy-fuel conditions compared to air-firing.

For a flue gas recycle without prior sulphur removal the sulphur level in the boiler could increase with a factor of up to 4–5. This significant increase will induce a risk of enhanced sulphur retention in the fly ash [12,115,128,145]. Lowering the flame temperature in the boiler will also increase the possibility of SO_2 retention in ash [12]. Maier et al. [145] state that retention of sulphur in ash does not take place in the radiant section of a boiler due to the temperature being above the 1150 °C where sulphate salts are stable. However, in the convective section the temperature will be lower and the ash will be able to capture sulphur compounds.

Experiments by Croiset et al. [97] on a US eastern bituminous coal have shown that the retention is generally low, i.e. only about 2–3% of the initial S-content in the coal is present in the ash. A later investigation showed that the retention of sulphur in the fly ash is very dependent on the alkaline and alkaline earth content of the ash [122]. For a sub-bituminous coal with a highly alkaline ash they observed that nearly 14% of the initial sulphur content of the coal

was retained in the ash. It is suggested that it is the SO_3 in the flue gas that is retained through sulphate salts.

Based on the above, a possible solution could be to restrict the power plants to operate on only low alkaline and/or low sulphur bituminous and sub-bituminous coals and thereby limit the changes in the sulphur content of the fly ash from oxy-fuel combustion. This is however not a desirable restriction for the plant owners as it will reduce the operability of the plants.

The question of ash quality, especially the risk of increased sulphur retention, is still a potential risk for the application of oxy-fuel combustion as a carbon capture technology. The risk is largest for the most frequently proposed process design where flue gas is recycled before the desulphurization plant.

3.5.4. Depositions, slagging, and fouling

Early studies on ash deposition, slagging, and fouling at the ANL 3 MW_{th} pilot scale furnace referred by Payne et al. [86] showed that there were no identifiable differences between air-firing and oxy-fuel combustion. However, Glarborg and Bentzen [172] state that the high CO levels in the near-burner region could promote increased corrosion and slagging. Similarly, Schnurrer et al. [115] saw from their equilibrium calculations that the formation of deposits potentially could occur at furnace wall temperatures 30–60 °C higher than what is seen during conventional combustion in air. This may alter the position of deposits and thus potentially necessitate a relocation of soot blowers, etc. At the same time, they expect oxy-fuel combustion to provide a higher propensity for slagging and fouling caused by increased amounts of molten and solid alkali sulphates.

Experiments conducted by Mitsui Babcock Energy, ltd on a 160 kW_{th} test facility in Renfrew, UK [72], likewise included studies into the impact of oxy-fuel combustion on slagging and fouling. Inserting a deposition probe into the combustion chamber led to the observation of a slightly faster rate of deposition compared to air-firing. The temperature of the probe has not been stated by the author. At the same time the deposition rate was largely independent of the operating parameters such as recycle ratio during oxy-fuel combustion. Also, fouling occurred more rapidly during oxy-fuel than during conventional air combustion. The impact was, however, small and the deposits were easy to remove.

Wall et al. [138,128] collected ash samples from the deposits in the radiative and convective sections of the IHI 1.2 MW test facility. SEM images showed no significant difference between samples from air and oxy-fuel combustion. The furnace deposits, however, contained significantly more sulphur compared to samples collected from air combustion. The deposition rates for the different combustion conditions were different. In the convective section (fouling) the coals tested generally showed increased fouling tendency during oxy-fuel combustion compared to air-firing. The slagging propensity of the different coals tested changed from being higher to less than that in air combustion.

The composition of the deposits from both the radiative and convective sections showed no difference between air and oxy-fuel conditions, except for the SO_3 content which was higher (0.65 (oxy) versus 0.2 (air) wt%) during oxy-fuel combustion for the coal with the highest sulphur content (0.88 wt%, dry). This particular coal does, at the same time, have the highest content of alkali and alkali earth metals in the ash prior to combustion. This could be the explanation to the increased sulphur retention, see Section 3.5.3.

A lower conversion of the iron species in the parent coal into oxides can increase the amount of iron melting into glass silicates and thus increase the slagging propensity of the coal. Untransformed FeO-FeS phase with an eutectic temperature of 940 °C will likewise increase the slagging propensity of the ash. This effect of reduced oxidation of iron-bearing species can be seen for relatively low char combustion temperatures and high CO concentrations inside the burning particles. However, no direct comparison between air- and oxy-firing at the same heat transfer rates with respect to slagging has been found. It is thus unknown, whether incompletely oxidized iron will induce a problem in a full-scale boiler.

Deposit sampling tests performed by Mönckert et al. [147] indicate that besides sulphation, carbonization of deposit surfaces occur. The most obvious reason is that the decomposition temperature of carbonates will increase due to the high partial pressure of carbon dioxide [4]. However, the implications of this observation is not clear.

The investigations reported till now indicate that the changes to depositions in an oxy-fuel plant compared to an air-fired unit will not be of essential significance to the plant operation.

3.6. Oxy-fuel combustion of biomass

Carbon capture and storage from combustion of biomass has the potential to reduce the CO_2 emission to below zero, i.e. to extract CO_2 from the atmosphere and possibly limit the anticipated global warming [84,157,180,211–214]. The abbreviation BECS is used to denote the concept of Biomass Energy for Carbon Capture and Sequestration [213–215]. In principle, all CCS technologies suggested for fossil fired power systems can be applied to systems utilizing biomass fuels [216].

This section contains a survey of the very limited amount of literature available on the use of biomass in oxy-fuel combustion. The main type of biomass investigated is wood. This is a natural consequence of its abundance compared to other types of biomass, such as straw and other annual plants, olive residues, or other dedicated energy crops. Additionally, the transport and feeding of wood is easier to perform than for herbaceous energy sources.

When utilizing biomass in oxy-fuel combustion it is important to consider whether there are any special issues regarding biomass compared to coal which could have a significant impact on the combustion process and related phenomena. Of particular importance will be the volatile matter content, the ash composition, i.e. the content of Cl and alkali, and the change in fuel particle size. At the same time, in order to conclude on specific aspects related to the change of combustion atmosphere when co-firing coal and biomass it is necessary to compare the reported results with the behaviour of these types of fuel blends in conventional combustion.

3.6.1. The combustion process

Arias et al. [180] have investigated the ignition behaviour of coal/biomass blends during oxy-fuel combustion and the effect of oxy-fuel conditions on burnout. Their experiments are performed in an electrically heated entrained-flow reactor (EFR) at about 500 °C for ignition tests and 1000 °C for combustion tests. Both fuels are ground and sieved to a particle size of 75–150 μm. Oxy-fuel combustion with 21, 30, and 35 vol% oxygen were compared with results obtained in air, see Fig. 46. As has previously been seen for pure coals, a delay in ignition (higher ignition temperature) is observed as the oxygen concentration in the oxy-fuel oxidizer is reduced. From these experiments the relative effect of oxygen concentration is nearly independent of the type of fuel.

In air there is a reduction in the ignition temperature when the bituminous coal is blended with the biomass, see the three most left-hand-side bars in the figure for each case. The effect is, however, much less pronounced in the case of oxy-fuel combustion regardless of the oxygen concentration. This can be attributed to the fact that even though the biomass has a high reactivity and a high volatile matter content the heating value is lower than for the coal. The heat released from the biomass during ignition is thus

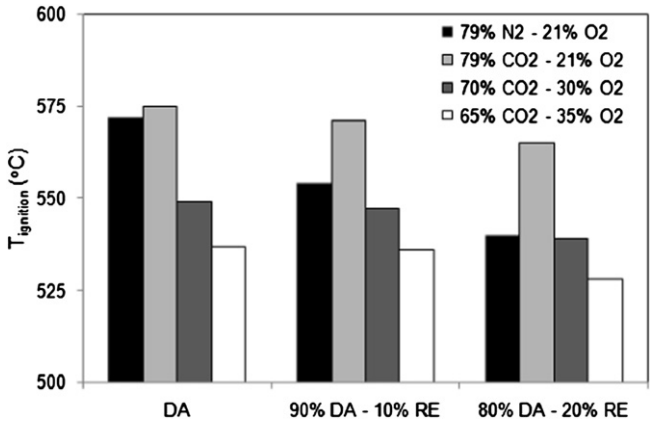

Fig. 46. Ignition temperatures of a high-volatile bituminous coal (DA) and blends of the coal and Eucalyptus (RE) in air combustion and oxy-fuel combustion with different O_2 concentrations at the inlet. The blending ratio is presumably given on a mass basis. Experiments are performed in an electrically heated entrained-flow reactor. Data taken from [180].

not substantial to enhance the heating of the coal particles and the ignition temperature is thus not increased significantly. As previously described, more heat is needed to increase the temperature of the surrounding gases and hence the coal particles in the case of oxy-fuel combustion than for combustion in air [180].

Results of burnout experiments for the same high-volatile coal and its blends with Eucalyptus are shown in Fig. 47. An obvious difference in burnout degree is seen for all three cases when changing the combustion atmosphere from air to CO_2-based. In oxy-fuel combustion with an air-like oxidizer composition the burnout degree decreases below that found in air. For oxygen concentrations of 30 and 35% the burnout increases above that found in air. However, the effect of blending biomass and coal is seen to have only little impact on the burnout, i.e. there is only a minor improvement by an increasing biomass content in the blend.

Because of the significantly higher volatile content in biomass compared to coal an improvement in the burnout degree of the fuel blends could be expected. However, reported data do not confirm this. Arias et al. [180] explain the lack of improvement in burnout for the blends in terms of the changes in oxygen and temperature

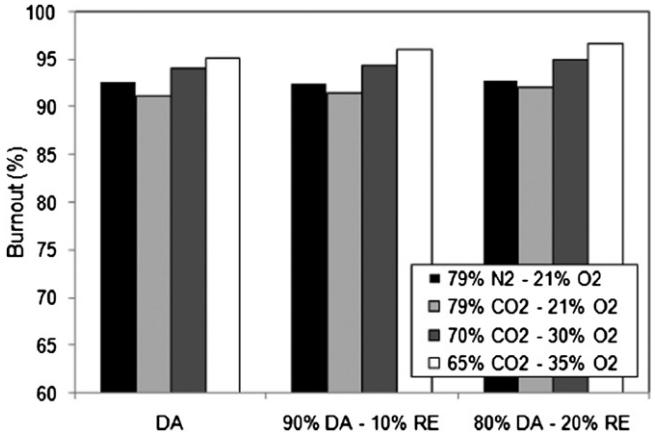

Fig. 47. Burnout of a high-volatile bituminous coal (DA) and blends of the coal and Eucalyptus (RE) at a stoichiometric value of 1.25. Experiments are performed in air and oxy-fuel atmospheres with different oxygen concentrations at the inlet of the entrained-flow reactor setup used. The blending ratio is presumably given on a mass basis. Data taken from [180].

profiles in the reactor caused by the introduction of the more reactive biomass fuel.

Characteristics of wood chip, rice husk, and forest residues chars obtained by pyrolysis in air and oxy-fuel atmospheres were investigated by Borrego et al. [217]. They saw that the char characteristics such as pore volume, morphology, optical texture, specific surface area, and reactivity showed no significant difference between air and oxy-fuel combustion. The authors thus concluded that the application of biomass in co-fired oxy-fuel boilers (coal/biomass) should not constitute any specific difficulties regarding the chars.

3.6.2. Emissions

In commercial-scale tests co-firing coal and biomass in air, large decreases and moderate increases are occasionally observed for the NO_x yields [218]. Tests by Robinson et al. [218] have shown that these changes most probably are caused by the biomass influencing fluid dynamics as well as temperature and stoichiometry profiles during the combustion. No fundamental synergistic chemical effects could be observed. The coals tested were bituminous whereas the biomass were red oak wood chips and switchgrass.

Fryda et al. [184] have found that the NO_x emission rate during oxy-fuel combustion can be decreased when coal (Russian) and biomass in the form of cocoa residues are co-fired in a lab-scale setup compared to tests with pure coal. Generally, using over-fire air (OFA) reduces the emission rate. The cocoa residues have a higher content of N compared to the pure coal (2.61 versus 0.87 wt%, dry basis) and thus has the fuel blend. The decrease in NO_x emission rate can thus be explained by the increased volatile content and the related, lower amount of fixed carbon in the blend compared to the pure coal.

Emissions of SO_x from oxy-fuel combustion of pure biomass or coal and biomass blends have not been reported in open literature.

3.6.3. Ash and corrosion

Robinson et al. [218] have investigated the ash deposition rates from both individual fuels and their blends (wood chips, coal, switchgrass, and wheat straw) during conventional combustion in air. They observed that the particle capture efficiency (the ash deposition rate normalized by the fuel ash content and the size of the deposition probe) was significantly larger for straw than for wood chips and coal in the order: wood chips < coal < switchgrass ≪ wheat straw. The order is closely related to the absolute amount of alkali in the fuels. Blending coal and biomass, especially straw, yield deposition rates which are lower than what would be expected based on the behaviour of the unblended fuels, see the upper part of Fig. 48. Especially in the case of co-firing coal and straw the particle capture efficiency is markedly reduced compared to the predicted value (about 10%). Sulphation of alkali chlorides released from the straw with sulphur from the coal is expected to account for part of the observed effect [218]. The main effect is due to incorporation of mainly potassium from the biomass into alumina-silicates in the coal ash followed by release of HCl, see (15).

$$(Al_2O_3)(SiO_2)_2 + 2KCl + H_2O \rightarrow (K_2O)(Al_2O_3)(SiO_2)_2 + 2HCl \quad (15)$$

This is a recognized method for reducing corrosion in biomass fired boilers.

In the bottom part of Fig. 48 the capture efficiency is calculated based on the amount of available alkali in the blend. It is clearly seen that this is a better measure of the slagging and fouling tendency of the fuel blends.

Studies of deposition and fouling in oxy-fuel combustion performed by Fryda et al. [184] have shown no significant change in

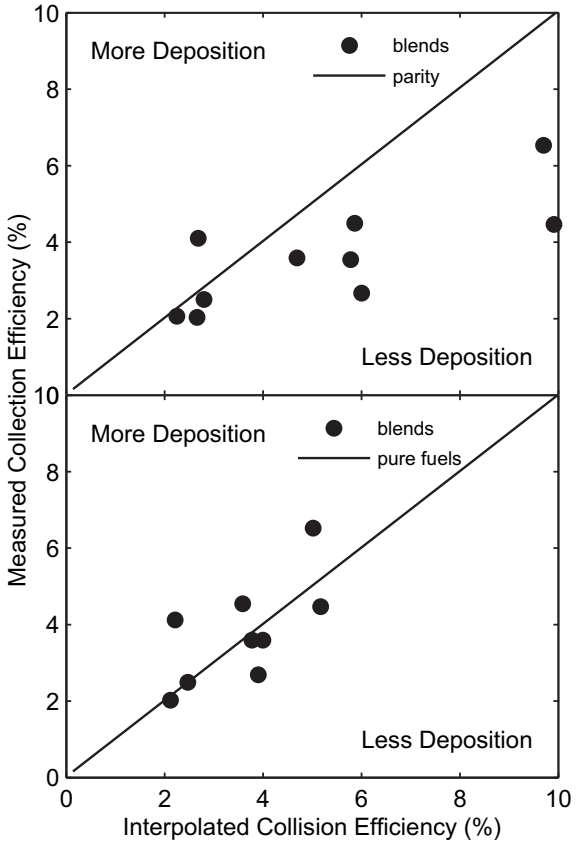

Fig. 48. Comparisons of measured and predicted particle capture efficiencies for different blends of coal and biomasses (wood chips, switchgrass, and wheat straw). Experiments are performed in a 30 kW down-fired, turbulent flow facility. Top: The predicted capture efficiencies are based on an interpolation between the two pure fuels and the fraction of the ash content originating from the coal. Bottom: The bias observed in the upper figure is removed by performing the interpolation based on the fuel-available alkali content rather than total ash. Data taken from [218].

deposition rate between pure coal and coal/biomass blends (cocoa residues and wood chips). The coal to biomass ratio in the blends is 80/20 on a mass basis. The coal/wood blends slightly increase the specific fouling factor, whereas blends with cocoa residues slightly decreases the fouling factor. This correlates well with the results obtained by Robinson et al. [218].

In relation to the aspects of corrosion and ash quality during co-combustion of coal and biomass at oxy-fuel conditions the sulphur and alkali contents of the parent fuels could induce both advantages and disadvantages. If the concentration of sulphur in the boiler during oxy-fuel combustion is enhanced there is a larger potential to convert alkali chlorides released from the biomass to sulphates before the flue gas meets the superheater banks and deposition occurs. The corrosion potential could thus be reduced. On the other hand, the higher alkali content in biomass ashes, and especially straw, will potentially increase the sulphur retention in the fly ash when co-firing with coal as described in Section 3.5.3.

3.7. Summary

Below is a short summary of the main findings presented in Section 3.

Research Groups: 26 research groups with different experimental equipment doing oxy-fuel combustion studies have been identified. The experimental setups range from 4.2 kW_{th} to 30 MW_{th} in size and include units both with and without flue gas recirculation.

Heat and Mass Transfer: The differences in thermo-chemical properties between CO_2 and N_2 cause changes in the heat and mass transfer rates within a boiler if CO_2 is substituted directly for N_2 in the oxidizer. In order to obtain an adiabatic flame temperature during combustion similar to that seen in air-firing the oxygen concentration in the oxidizer should be increased to 27–35 vol% depending on the type of fuel. Lower rank coals require lower oxygen concentations than higher rank coals.

CO_2 and H_2O are radiating gases whereas N_2 is not. The radiative heat transfer in oxy-fuel combustion is thus higher than in air combustion for the same flame temperature. In order to match the heat uptake profile in a retrofittet boiler the flame temperature should thus be kept lower than during air operation.

Combustion Process: Devolatilization and ignition of coal particles are affected by the change in oxidizer composition from air to oxy-fuel combustion. The rate of devolatilization is primarily determined by the surrounding gas temperature as the difference in thermal conductivity of N_2 and CO_2 is rather low. Particle ignition, on the other hand, is a strong function of both the transport properties of the gas phase surrounding the particles as well as the combustion heat release rate and the reactivity of the local fuel-oxidizer mixture. Ignition times comparable to those observed during air combustion can be obtained by increasing the oxidizer oxygen concentration to 27–35 vol% and thus the flame temperature. Burnout of volatiles and char are likewise affected by the high CO_2 and H_2O concentrations in the flame. Especially the lower diffusivity of both oxygen and small hydrocarbons in CO_2 compared to N_2 is an important factor. Generally, a slight improvement in char burnout is reported in the literature when the flame temperature matches that of air combustion. This improvement is assumed to be caused primarily by the higher oxygen partial pressure experienced by the burning particles. Gasification reactions and residence time differences are believed to be of minor influence.

Due to the high CO_2 concentration in the combustion environment high levels of CO are expected in the near-flame zone. There is thus an increased risk of CO corrosion in this zone. Because of the large oxygen partial pressure the CO is reported to oxidize before leaving the larger of the test furnaces yielding similar CO emission rates as for air combustion.

Emissions: NO_x emissions from oxy-fuel combustion is probably the single most investigated area of this technology. Due to the very low levels of molecular nitrogen a potential exists to reduce the emissions rate considerably compared to combustion in air through near-elimination of both thermal and prompt NO_x formation. Reductions by 70–80% have been reported. Different suggestions to the mechanisms responsible for the reduction have been proposed. However, it is generally accepted that reburning reactions play a major role. Experiments indicate that increasing the oxygen concentration and the oxygen excess yield higher emission rates. On the other hand, the use of oxidant staging, recycling of flue gas before drying, increasing the partial pressure of NO_x in the oxidant, increasing the oxygen purity, and limiting the air ingress into the boiler work to decrease the emission rate.

Sulphur oxides is the other major pollutant from coal-fired combustion. The emission of these oxides is not reduced to the same degree as NO_x. However, increased retention in ash due to the higher partial pressure of SO_2 in the boiler when flue gas is recirculated before the desulphurization unit has been reported. Increased risk of low-temperature corrosion by sulfuric acid and a higher acid dew point are some of the major concerns regarding sulphur in oxy-fuel combustion.

Limited work has been reported on the emission of trace elements from oxy-fuel combustion. The work performed has focused on Hg, Cd, As, and Se with Hg attracting the most attention.

No significant differences between air-firing and oxy-fuel combustion have been reported at this point.

Ash and Depositions: The transformations of coal mineral matter during combustion are affected by the temperature and the gas phase composition surrounding the coal particles. At low combustion temperature (for below 30% O_2 in CO_2) a shift in the size distribution of the sub-mircometer-sized fly ash toward smaller particles can be observed. Increasing the O_2 partial pressure provides a size distribution similar to that found in air combustion. The ash quality is crucial to its application in cement and concrete production. Significantly increased sulphur retention could cause problems in this respect.

The propensity for slagging and fouling in oxy-fuel combustion is likewise subject to research. At this point, the reported results suggest that only minor changes compared to air-firing will result from the change in the combustion environment.

BECS: Utilization of renewable biomass fuels such as wood, straw, and other energy crops in thermal power plants with carbon capture and storage is attracting increased attention. The combination of CO_2 neutral fuels with CCS opens a possibility of extracting CO_2 from the atmosphere. Until now, only few experiments on oxy-fuel combustion of biomasses have been reported. It is expected that further work on BECS will reveal comparable changes to the combustion fundamentals as is the case when biomass is introduced during combustion of coal in air.

4. Conclusions

The reduction of CO_2 emissions from power plants has become an increasing important topic in the discussions of how to prevent global warming arising from antropogenic CO_2 emissions. Three CCS (Carbon Capture and Storage) technologies have been suggested for medium term application which will reduce the emissions to near zero; Chemical absorption by amines (post-combustion capture), Integrated gasification combined cycle plants (pre-combustion capture), and oxy-fuel combustion capture. Of these, the post-combustion and oxy-fuel technologies can be applied as retrofit solutions to the existing fleet of pulverized-coal-fired power plants. Compared to post-combustion capture oxy-fuel combustion is less mature and thus requires comprehensive fundamental research as well as pilot and demonstration scale testing before commercial operation of an oxy-fuel power plant seems to be feasible. Currently, no full-scale oxy-fuel plants are in operation. The only announced large demonstration plant (250 MW_e) is planned to be put into operation in 2015 by Vattenfall. Commercial operation does thus not seem to be feasible before 2020.

The current literature review describes the available knowledge on the oxy-fuel technology. The focus has been on both the changes induced to an existing, conventional air-fired plant if retrofitted to oxy-fuel combustion and the research performed on the fundamental combustion characteristics including heat transfer effects, ignition and burnout, emissions, ash quality, and deposit build-up. Both coal and the application of CO_2 neutral fuels such as wood or other types of biomass are included in the review.

Retrofitting an existing pulverized-coal-fired power plant to oxy-fuel operation requires a number of new process units – an air separation facility to provide the combustion process with almost pure oxygen, ducts and fans for external recirculation of flue gas to the burners in order to control flame temperatures, and a CO_2 processing facility producing a near-pure CO_2 stream for storage. The retrofit to oxy-fuel operation will reduce the plant electrical efficiency by about 10 percent points depending on the initial efficiency. It is generally accepted that a 95% pure O_2 stream constitutes the optimum with respect to minimizing the combined expense for air separation and CO_2 cleaning. Leakage of air into the boiler necessitates removal of non-condensable species from the CO_2 stream prior to storage. The capture efficiency of an oxy-fuel power plant is thus expected to be around 90%. Two flue gas recycle streams are necessary. The primary stream is used for coal drying and transportation to the burners and should preferably be desulphurized and dry. Most process configuration suggestions avoid addition of O_2 to the primary stream. Instead, O_2 is added either to the secondary flue gas recycle stream or directly through special lances in the burners. The overall O_2 concentration at the inlet to the boiler should be between 27 and 35 vol% in order to yield comparable adiabatic flame temperatures and heat transfer profiles as seen for conventional combustion in air. The exact level depends on the type of coal and the boiler design. Even though CO_2 has significantly different thermo-chemical properties compared to N_2 increasing the O_2 concentration in oxy-fuel combustion yields similar devolatilization and ignition behaviour in the two environments. The burnout is reported to improve in oxy-fuel combustion. The emission rate of CO is reported to be similar in air and oxy-fuel combustion even though significantly increased CO levels are seen within the flame zone in the oxy-fuel environment. SO_2 emissions are likewise reported to be of similar magnitude regardless of flue gas composition. The NO_x emission is, however, significantly reduced during oxy-fuel combustion compared to air-firing due to a near-elimination of thermal NO formation and to reburning of NO_x passed through the burners with the recirculated flue gas. Reductions of the emission rate by 70–80% have been reported. Only minor changes to the deposit build-up are expected for oxy-fuel combustion compared to air-firing. However, the oxy-fuel environment is expected to lead to a significant increase in the SO_3 concentration within the boiler increasing the risk of both high and low-temperature corrosion as well as increased retention of sulphur in the fly ash.

A significant amount of new information on the oxy-fuel technology has been published since Wall and coworkers released their literature survey in 2005. At that time the following research needs were concluded to require the most attention in order to gain a deeper fundamental understanding of the oxy-fuel technology:

- Match of heat transfer characteristics in retrofitted boilers.
- The cost of electricity and the cost of CO_2 avoided.
- Combustion characteristics and emission levels (pilot plant scale).
- Requirements for gas cleaning - especially SO_2.

Based on the fact that no full-scale plants are in operation, the required large-scale investigations of heat transfer characteristics still remain. Additional work on both convective and radiative heat transfer in laboratory-scale reactors has however been conducted.

Several techno-economic assessments of the oxy-fuel technology exist and new are continuously being published. However, the estimated costs of electricity and CO_2 avoidance costs generally suffer from large uncertainties due to the lack of construction and operation experience from full-scale plants.

Few results regarding combustion characteristics and emission levels in pilot plant scale setups (>1 MW_{th}) have been published within the last five years. This area thus needs continued attention.

Suggestions to the purity requirements for CO_2 for sequestration and enhanced oil recovery have been published. No standards or legislative requirements have however been found. Clarification of the necessary extent of cleaning is very important to plant configuration and eventually the process economics.

Besides the topics discussed above, this review has revealed that a deeper understanding of the effect of a shift from air-blown combustion to oxy-fuel combustion on the following issues is necessary:

- Optimum oxygen excess and inlet oxygen concentration levels.
- Corrosion at both high and low temperatures.
- Ash quality, especially regarding the risk of enhanced sulphur retention.
- Operability, i.e. start-up and shut-down, dynamics during transients, the need for air-firing capability, etc.
- Models to predict NO_x and SO_3 formation.

The oxy-fuel combustion process is still in the developing phase and much research is still required in order to fully clarify the consequences of its implementation in power plants.

Acknowledgements

The work has been funded by Energinet.dk and The Danish Ministry of Science, Technology and Innovation (VTU) as well as the companies DONG Energy and Vattenfall. The help by Stine Hansen, Department of Chemical Engineering, Technical University of Denmark in producing the figures for this paper is greatly appreciated.

References

[1] International Energy Agency (IEA). World energy outlook 2007 – China and India insights. IEA Publications; 2007.
[2] International Energy Agency (IEA). World energy outlook 2008. IEA Publications; 2008.
[3] Kavouridis K, Koukouzas N. Coal and sustainable energy supply challenges and barriers. Energy Policy 2008;36(2):693–703.
[4] Buhre BJP, Elliott LK, Sheng CD, Gupta RP, Wall TF. Oxy-fuel combustion technology for coal-fired power generation. Prog Energy Combust Sci 2005;31(4):283–307.
[5] Wall TF. Combustion processes for carbon capture. Proc Combust Inst 2007;31(1):31–47.
[6] Solomon S, Qin D, Manning M, Chen Z, Marquis M, Averyt KB, et al., editors. IPCC, 2007: climate change 2007: the physical science basis. Contribution of working group I to the fourth assessment report of the intergovernmental panel on climate change. Cambridge, United Kingdom and New York, NY, USA: Cambridge University Press; 2007.
[7] Bachu S. CO_2 storage in geological media: role, means, status and barriers to deployment. Prog Energy Combust Sci 2008;34(2):254–73.
[8] Davison J. Performance and costs of power plants with capture and storage of CO_2. Energy 2007;32(7):1163–76.
[9] Tan Y, Thambimuthu KV, Douglas MA, Mortazavi R. Oxy-fuel combustion research at the CANMET Energy Technology Center. In: Proc 2003 5th Int Symp Coal Combust; 2003. p. 550–54.
[10] Jordal K, Anheden M, Yan J, Strömberg L. Oxyfuel combustion for coal-fired power generation with CO_2 capture – opportunities and challenges. In: The 7th International conference on greenhouse gas control technologies (GHGT-7). Vancouver, Canada; September 2004.
[11] Feron PHM, Hendriks CA. CO_2 capture process principles and costs. Oil Gas Sci Technol 2005;60(3):451–9.
[12] Tan R, Corragio G, Santos S. Oxy-coal combustion with flue gas recycle for the power generation industry – a literature review. Study report, IFRF Doc. No. G 23/y/1. Velsen Noord, The Netherlands: International Flame Research Foundation (IFRF); September 2005.
[13] Knudsen JN, Vilhelmsen P-J, Jensen JN, Biede O. First year operating experience with a 1 t/h CO_2 absorption – pilot plant at Esbjerg coal-fired power plant. VGB PowerTech 2007;87(3):57–61.
[14] Figueroa JD, Fout T, Plasynski S, McIlvried H, Srivastava RD. Advances in CO_2 capture technology – the U.S. department of energy's carbon sequestration program. Int J Greenhouse Gas Control 2008;2(1):9–20.
[15] Knauss KG, Johnson JW, Steefel CI, Nitao JJ. Evaluation of the impact of CO_2, aqueous fluid, and reservoir rock interactions on the geologic sequestration of CO_2, with special emphasis on economic implications. In: 1st national conference on carbon sequestration. NETL Publications; 2001.
[16] Varagani RK, Châtel-Pélage F, Pranda P, Rostam-Abadi M, Lu Y, Bose AC. Performance simulation and cost assessment of oxy-combustion process for CO_2 capture from coal-fired power plants. In: The fourth annual conference on carbon sequestration, May 2–5. Alexandria, VA; 2005.
[17] Gozalpour F, Ren SR, Tohidi B. CO_2 EOR and storage in oil reservoirs. Oil Gas Sci Technol 2005;60(3):537–46.
[18] Baes Jr CF, Beall SE, Lee DW, Marland G. The collection, disposal, and storage of carbon dioxide. In: Interactions of energy and climate, proceedings of an international workshop; 1980. p. 495–19.
[19] Grimston MC, Karakoussis V, Fouquet R, van der Vorst R, Pearson P, Leach M. The European and global potential of carbon dioxide sequestration in tackling climate change. Clim Policy 2001;1(2):155–71.
[20] Gunter WD, Wong S, Cheel DB, Sjostrom G. Large CO_2 Sinks: their role in the mitigation of greenhouse gases from an international, national (Canadian) and provincial (Alberta) perspective. Appl Energy 1998;61(4):209–27.
[21] Metz B, Davidson O, Swart R, Pan J, editors. IPCC, 2001: climate change 2001: mitigation. Contribution of working group III to the third assessment report of the intergovernmental panel on climate change (IPCC). Cambridge, United Kingdom and New York, NY, USA: Cambridge University Press; 2001.
[22] Davison J, Freund P, Smith A. Putting carbon back into the ground. Technology overview, the IEA greenhouse gas R&D programme; February 2001.
[23] Gibbins J, Chalmers H. Carbon capture and storage. Energy Policy 2008a;36(12):4317–22.
[24] Solomon S, Carpenter M, Flach TA. Intermediate storage of carbon dioxide in geological formations: a technical perspective. Int J Greenhouse Gas Control 2008;2(4):502–10.
[25] Bentham M, Kirby G. CO_2 storage in saline aquifers. Oil Gas Sci Technol 2005;60(3):559–67.
[26] Cailly B, Le Thiez P, Egermann P, Audibert A, Vidal-Gilbert S, Longaygue X. Geological storage of CO_2: a state-of-the-art of injection processes and technologies. Oil Gas Sci Technol 2005;60(3):517–25.
[27] Allam RJ, Spilsbury CG. A study of the extraction of CO_2 from the flue gas of a 500 MW pulverised coal fired boiler. Energy Convers Manage 1992;33(5–8):373–8.
[28] Abu-Khader MM. Recent progress in CO_2 capture/sequestration. A Review Energy Sources Part A Recovery Utilization Environ Effects 2006;28(14):1261–79.
[29] Fischedick M, Günster W, Fahlenkamp H, Meier H-J, Neumann F, Oeljeklaus G, et al. Separation in power plants – do retrofits make sense in existing plants? VGB PowerTech 2006;4:108–17 [in German].
[30] Pehnt M, Henkel J. Life cycle assessment of carbon dioxide capture and storage from lignite power plants. Int J Greenhouse Gas Control 2009;3(1):49–66.
[31] Sander MT, Mariz CL. The Fluor Daniel econamine FG process: Past experience and present day focus. Energy Convers Manage 1992;33(5–8):341–8.
[32] Reddy S, Scherffius J, Freguia S, Roberts C. Fluor's Econamine FG PlusSM technology – an enhanced amine-based CO_2 capture process. In: Proceedings of the second national conference on carbon sequestration. Alexandria, VA, USA: US Department of Energy National Technology Laboratory; May 2003.
[33] Yagi Y, Mimura T, Iijima M, Ishida K, Yoshiyama R, Kamino T. Improvements of carbon dioxide capture technology from flue gas. In: Greenhouse gas control technologies. Proceedings of the seventh international conference on greenhouse gas control technologies, 5–9 September 2004, Vancouver, Canada. Oxford, UK: Elsevier Ltd; 2005.
[34] Wegerich S, Witt A, Huizeling E, Rode H. Untersuchungen zur Nachrüstung einer CO_2-Abscheidetechnologie für das neue E.ON Kraftwerk Maasvlakte 3. In: 39. Kraftwerktechnisches Kolloquium. Dresden, Germany; October 11–12, 2007.
[35] Oexmann J, Kather A. Post-combustion CO_2-capture from coal-fired power plants – wet chemical absorption processes. VGB PowerTech 2009;89(1/2):92–103 [in German].
[36] Descamps C, Bouallou C, Kanniche M. Efficiency of an integrated gasification combined cycle (IGCC) power plant including CO_2 removal. Energy 2008;33(6):874–81.
[37] Kanniche M, Gros-Bonnivard R, Jaud P, Valle-Marcos J, Amann J-M, Bouallou C. Pre-combustion, post-combustion and oxy-combustion in thermal power plant for CO_2 capture. Appl Thermal Eng 2010;30(1):53–62.
[38] Okawa M, Kimura N, Kiga T, Takano S, Arai K, Kato M. Trial design for a CO_2 recovery power plant by burning pulverized coal in O_2/CO_2. Energy Convers Manage 1997;38:123–7.
[39] Altmann H, Stamatelopoulos G-N. Steps towards the minimisation of CO_2 emissions from coal-fired power plants. In: Conference and exhibition for the European power generation industry, POWER-GEN Europe 2005. Milan (Italy); June 28–30, 2005.
[40] Singh D, Croiset E, Douglas PL, Douglas MA. Techno-economic study of CO_2 capture from an existing coal-fired power plant: MEA scrubbing vs. O_2/CO_2 recycle combustion. Energy Convers Manage 2003;44(19):3073–91.
[41] Ewert M. The significance of power stations with CO_2 capture in planning future generation portfolio. VGB PowerTech 2005;85(10):36–40 [in German].
[42] Unknown. Chilling news for carbon capture [[carbon dioxide capture process]]. Mod Power Syst 2006;26(12):17–8.
[43] Xu B, Stobbs RA, White V, Wall RA, Gibbins J, Iijima M, et al. Future CO_2 capture technology options for the Canadian market. Technical Report Report No. COAL R309 BERR/Pub URN 07/1251. Doosan Babcock Energy Limited; March 2007.
[44] Wheeldon J, Booras G, Holt N. Post-combustion CO_2 capture from pulverized coal plants. In: 23rd Annual international Pittsburgh coal conference, PCC – coal-energy, environment and sustainable development; 2006.
[45] Notz R, Asprion N, Clausen I, Hasse H. Selection and pilot plant tests of new absorbents for post-combustion carbon dioxide capture. Chem Eng Res Des 2007;85(A4):510–5.
[46] Lee S, Maken S, Park J-W, Song H-J, Park JJ, Shim J-G, et al. A study on the carbon dioxide recovery from 2 ton-CO_2/day pilot plant at LNG based power plant. Fuel 2008;87(8–9):1734–9.
[47] Iea Ghg. Improvement in power generation with post-combustion capture of carbon dioxide. Report PH4/33, IEA greenhouse gas research and development programme; 2004.

[48] Williams TC, Shaddix CR, Schefer RW. Effect of syngas composition and CO_2-diluted oxygen on performance of a premixed swirl-stabilized combustor. Combust Sci Technol 2008;180(1):64–88.

[49] Damen K, van Troost M, Faaij A, Turkenburg W. A comparison of electricity and hydrogen production systems with CO_2 capture and storage. Part A: review and selection of promising conversion and capture technologies. Prog Energy Combust Sci 2006;32(2):215–46.

[50] Beér JM. High efficiency electric power generation: the environmental role. Prog Energy Combust Sci 2007;33(2):107–34.

[51] McDonald DK, Flynn TJ, DeVault DJ, Varagani R, Levesque S, Castor W. 30 MW_t clean environment development oxy-coal combustion test program. In: The 33rd international technical conference on coal utilization and fuel systems. Clearwater, Florida; 2008.

[52] Minchener AJ. Coal gasification for advanced power generation. Fuel 2005;84 (17):2222–35.

[53] Gericke B, Kuzmanovski P, Nassauer K. Conceptual solutions regarding the influence of the oxy-fuel-process on conventional power plants [Konzeptüberlegungen bezüglich der Auswirkungen des oxy-fuel-prozesses auf konventionelle Kraftwerksanlagen]. VGB PowerTech 2006;86(10):64–72 [in German].

[54] Chen C, Rubin ES. CO_2 control technology effects on IGCC plant performance and cost. Energy Policy 2009;37(3):915–24.

[55] Eide LI, Bailey DW. Precombustion decarbonisation processes. Oil Gas Sci Technol 2005;60(3):475–84.

[56] Lambertz J, Ewers J. Clean coal power – the response of power plant engineering to climate protection challenges. VGB PowerTech 2006;86(5):72–7 [in German].

[57] Gibbins J, Chalmers H. Preparing for global rollout: a 'developed country first' demonstration programme for rapid CCS deployment. Energy Policy 2008;36 (2):501–7.

[58] Horn FL, Steinberg M. Control of carbon dioxide emissions from a power plant (and use in enhanced oil recovery). Fuel 1982;61(5):415–22.

[59] Herzog H, Golomb D, Zemba S. Feasibility, modeling and economics of sequestering power plant CO_2 emissions in the deep ocean. Environ Prog 1991;10(1):64–74.

[60] Abraham BM, Asbury JG, Lynch EP, Teotia APS. Coal-oxygen process provides CO_2 for enhanced recovery. Oil Gas J 1982;80(11):68–70. 75.

[61] Nakayama S, Noguchi Y, Kiga T, Miyamae S, Maeda U, Kawai M, et al. Pulverized coal combustion in O_2/CO_2 mixtures on a power plant for CO_2 recovery. Energy Convers Manage 1992;33(5–8):379–86.

[62] Simmons M, Miracca I, Gerdes K. Oxyfuel technologies for CO_2 capture: a techno-economic overview. In: 7th international conference on greenhouse gas control technologies. Vancouver, Canada; September, 2004.

[63] Châtel-Pélage F, Varagani R, Pranda P, Perrin N, Farzan H, Vecci SJ, et al. Applications of oxygen for NO_x control and CO_2 capture in coal-fired power plants. Thermal Sci 2006;10(3):119–42.

[64] Anheden M, Andersson A, Bernstone C, Eriksson S, Yan J, Liljemark S, et-al. CO_2 quality requirement for a system with CO_2 capture, transport and storage. In: The 7th International Conference on greenhouse gas control technologies (GHGT7). Vancouver, Canada; September 5–9, 2004.

[65] Anheden M, Yan J, De Smedt G. Denitrogenation (or oxy-fuel concepts). Oil Gas Sci Technol 2005;60(3):485–95.

[66] Dillon DJ, Panesar RS, Wall RA, Allam RJ, White V, Gibbins J, et al. Oxy-combustion processes for CO_2 capture from advanced supercritical PF and NGCC power plant. In: 7th international conference on greenhouse gas control technologies. Vancouver, Canada; September, 2004.

[67] Dillon DJ, White V, Allam RJ, Wall RA, Gibbins J. Oxy Combustion Processes for CO_2 capture from power plant. Engineering Investigation Report, 2005/9, IEA Greenhouse Gas Research and Development Programme; June 2005.

[68] Kather A, Klostermann M, Hermsdorf C, Mieske K, Eggers R, Köpke D. Konzept für ein 600 MW_{el} Steinkohlekraftwerk mit CO_2-Abtrennung auf Basis des Oxyfuel-Prozesses. In: Kraftwerksbetrieb unter künftigen Rahmenbedingungen, 38. Kraftwerkstechnisches Kolloquium. Dresden, Germany; October 24–25, 2006.

[69] Rezvani S, Huang Y, McIlveen-Wright D, Hewitt N, Wang Y. Comparative assessment of sub-critical versus advanced super-critical oxyfuel fired pf boilers with CO_2 sequestration facilities. Fuel 2007;86(14):2134–43.

[70] Eide LI, Anheden M, Lyngfelt A, Abanades C, Younes M, Clodic D, et al. Novel capture processes. Oil Gas Sci Technol 2005;60(3):497–508.

[71] Hossain MM, de Lasa HI. Chemical-looping combustion (CLC) for inherent CO_2 separations–a review. Chem Eng Sci 2008;63(18):4433–51.

[72] Farley M. Developing oxyfuel capture as a retrofit technology. Mod Power Syst 2006;26(4):20–2.

[73] Aspelund A, Jordal K. A study of the interface between CO_2 capture and transport. In: The 8th International Conference on Greenhouse Gas Control Technologies (GHGT-8). Trondheim, Norway; 19–22 June, 2006.

[74] Aspelund A, Jordal K. Gas conditioning – the interface between CO_2 capture and transport. Int J Greenhouse Gas Control 2007;1(3):343–54.

[75] Sass BM, Farzan H, Prabhakar R, Gerst J, Sminchak J, Bhargava M, et al. Considerations for treating impurities in oxy-combustion flue gas prior to sequestration. Energy Procedia 2009;1(1):535–42.

[76] Anheden M, Rydberg S, Yan J. Consideration for removal of non-CO_2 components from CO_2 rich flue gas of oxy-fuel combustion. In 3rd workshop of the IEA GHG International oxy-combustion network. Yokohama, Japan; March 5–6, 2008.

[77] Lee CW, Miller CA. Understanding the potential environmental impacts of oxy-fuel combustion. In: 3rd Workshop of the IEA GHG international oxy-combustion network. Yokohama, Japan; March 5–6, 2008.

[78] Fout T. Oxy-COMBUSTION: research, development and systems analysis. In: 3rd Workshop of the IEA GHG international oxy-combustion network. Yokohama, Japan; March 5–6, 2008.

[79] Andersson K, Johnsson F, Strömberg L. Large scale CO_2 capture – applying the concept of O_2/CO_2 combustion to commercial process data. VGB PowerTech 2003;83(10):1–5.

[80] Andersson K, Johnsson F. Process evaluation of an 865 MWe lignite fired O_2/CO_2 power plant. Energy Convers Manage 2006;47(18–19):3487–98.

[81] Kakaras E, Koumanakos A, Doukelis A, Giannakopoulos D, Vorrias I. Simulation of a greenfield oxyfuel lignite-fired power plant. Energy Convers Manage 2007;48(11):2879–87.

[82] Hellfritsch S, Gilli PG, Jentsch N. Concept for a lignite-fired power plant based on the optimised oxyfuel process with CO_2 recovery. VGB PowerTech 2004;84(8):76–82.

[83] Zanganeh KE, Shafeen A. A novel process integration, optimization and design approach for large-scale implementation of oxy-fired coal power plants with CO_2 capture. Int J Greenhouse Gas Control 2007;1(1):47–54.

[84] Uddin SN, Barreto L. Biomass-fired cogeneration systems with CO_2 capture and storage. Renewable Energy 2007;32(6):1006–19.

[85] Li H, Yan J, Yan J, Anheden M. Impurity impacts on the purification process in oxy-fuel combustion based CO_2 capture and storage system. Appl Energy 2009;86(2):202–13.

[86] Payne R, Chen SL, Wolsky AM, Richter WF. CO_2 recovery via coal combustion in mixtures of oxygen and recycled flue gas. Combust Sci Technol 1989;67(1):1–16.

[87] Kimura N, Omata K, Kiga T, Takano S, Shikisima S. The characteristics of pulverized coal combustion in O_2/CO_2 mixtures for CO_2 recovery. Energy Convers Manage 1995;36(6–9):805–8.

[88] Woycenko DM, van de Kamp WL, Roberts PA. Combustion of pulverised coal in a mixture of oxygen and recycled flue gas. Summary of the APG research program, IFRF Doc. F98/Y/4. Ijmuiden, The Netherlands: International Flame Research Foundation (IFRF); October 1995.

[89] Tan Y, Douglas MA, Thambimuthu KV. CO_2 capture using oxygen enhanced combustion strategies for natural gas power plants. Fuel 2002;81(8): 1007–16.

[90] Andersson K, Normann F, Johnsson F, Leckner B. NO emission during oxy-fuel combustion of lignite. Ind Eng Chem Res 2008a;47(6):1835–45.

[91] Farzan H, McDonald DK, McCauley KJ, Varagani R, Prabhakar R, Periasamy C, et al. Oxy-coal combustion pilot. In: 3rd Workshop of the IEA GHG international oxy-combustion network. Yokohama, Japan; March 5–6, 2008.

[92] Strömberg L, Lindgren G, Jacoby H, Giering R, Anheden M, Burchhardt U, et al. Update on Vattenfall's 30 MWth oxyfuel pilot plant in Schwarze Pumpe. Energy Procedia 2009;1(1):581–9.

[93] Darde A, Prabhakar R, Tranier J-P, Perrin N. Air separation and flue gas compression and purification units for oxy-coal combustion systems. Energy Procedia 2009;1(1):527–34.

[94] Burchhardt U, Radunsky D. Erfahrungen aus der Planung und Genehmigung der Oxyfuel-Forschungsanlage von Vattenfall. In: 39. Kraftwerktechnisches Kolloquium. Dresden, Germany; October 11–12, 2007.

[95] Simpson AP, Simon AJ. Second law comparison of oxy-fuel combustion and post-combustion carbon dioxide separation. Energy Convers Manage 2007;48(11):3034–45.

[96] Hu Y, Naito S, Kobayashi N, Hasatani M. CO_2, NO_x and SO_2 emissions from the combustion of coal with high oxygen concentration gases. Fuel 2000;79 (15):1925–32.

[97] Croiset E, Thambimuthu KV. NO_x and SO_2 emissions from O_2/CO_2 recycle coal combustion. Fuel 2001;80(14):2117–21.

[98] White V, Torrente-Murciano L, Sturgeon D, Chadwick D. Purification of oxyfuel-derived CO_2. Energy Procedia 2009;1(1):399–406.

[99] Altmann H, Porsche T, Burchhardt U. Erfahrungen aus der Inbetriebnahme und dem Versuchsbetrieb der Oxyfuel-Forschungsanlage von Vattenfall. VGB PowerTech 2009;89(9):96–100.

[100] Smith AR, Klosek J. A review of air separation technologies and their integration with energy conversion processes. Fuel Processing Technol 2001;70 (2):115–34.

[101] Gonschorek S, Hellfritsch S, Weigl S, Gampe U. Entwicklungsstand des Oxyfuel-Prozesses für Braunkohlekraftwerke. In: Kraftwerkstechnisches Kolloquium, Zittau; 26–27 September, 2006.

[102] Vitalis B. Overview of oxy-combustion technology for utility coal-fired boilers. Advances in Materials Technology for Fossil Power Plants. In: Proceedings from the 5th International Conference; 2008. p. 968–81.

[103] Kather A, Klostermann M, Hermsdorf C, Mieske K, Eggers R, Köpke D. Steinkohlekraftwerk mit CO_2-Abtrennung auf Basis des Oxyfuel-Prozesses. In: 39. Kraftwerktechnisches Kolloquium. Dresden, Germany; October 11–12, 2007.

[104] European Standard. EN 450–1:2005 Fly ash for concrete. Definition, specifications and conformity criteria; 2005.

[105] Mauder R, Hugot A. Flugaschevermarktung in der Zukunft. VGB PowerTech 2008;88(11):62–6.

[106] Kluger F, Lysk S, Altmann H, Krohmer B, Stamatelopoulos G-N. 30 MW_{th} Oxyfuel-Pilotanlage – Untersuchungsschwerpunkte und Auslegung des Dampferzeugers. In: Kraftwerksbetrieb unter künftigen Rahmenbedingungen, 38. Kraftwerkstechnisches Kolloquium. Dresden, Germany; October 24–25, 2006.

[107] Toporov D, Förster M, Kneer R. How to burn pulverized coal in CO_2 atmosphere at low oxygen concentrations. VDI Berichte 1988;55–60:2007.
[108] Toporov D, Bocian P, Heil P, Kellermann A, Stadler H, Tschunko S, et al. Detailed investigation of a pulverized fuel swirl flame in CO_2/O_2 atmosphere. Combust Flame 2008;155(4):605–18.
[109] Nikzat H, Pak H, Fuse T, Hu Y, Ogyu K, Kobayashi N, et al. Characteristics of pulverized coal burner using a high-oxygen partial pressure. Chem Eng Res Des 2004;82(1):99–104.
[110] Hellfritsch S, Gonschorek S, Vilhelm R, Löser J, Klemm M, Weigl S, et al. Entwicklungsstand des Oxyfuel-Prozesses für Braunkohlekraftwerke. In Kraftwerksbetrieb unter künftigen Rahmenbedingungen, 38. In: Kraftwerkstechnisches Kolloquium. Dresden, Germany; October 24–25, 2006.
[111] Oryshchyn D, Gerdemann S, Armstrong J, Ochs T, Summers C. Oxy-firing flue-gas character and its effect on FGD – a process study for integrated pollutant removal. In: 23rd Annual international Pittsburgh coal conference, PCC – coal-energy, environment and sustainable development; 2006.
[112] EUROGYPSUM. Association of European gypsum industries. FGD Gypsum – quality criteria and analysis methods, www.eurogypsum.org; April 2005.
[113] Klostermann M. Efficiency Increase of the oxyfuel process by waste heat recovery considering the effects of flue gas treatment. In: 3rd workshop of the IEA GHG international oxy-combustion network. Yokohama, Japan; March 5–6, 2008.
[114] Suriyawong A, Hogan Jr CJ, Jiang J, Biswas P. Charged fraction and electrostatic collection of ultrafine and submicrometer particles formed during O_2–CO_2 coal combustion. Fuel 2008;87(6):673–82.
[115] Schnurrer S, Elliott L, Wall T, Liu Y. Influence of oxy-fuel environment on sulphur species in ash from pulverized coal combustion. In: Impacts of fuel quality on power production and the environment, September 29–October 3. Banff, Alberta, Canada: The Banff Centre; 2008.
[116] Khare SP, Wall TF, Farida AZ, Liu Y, Moghtaderi B, Gupta RP. Factors influencing the ignition of flames from air-fired swirl pf burners retrofitted to oxy-fuel. Fuel 2008;87(7):1042–9.
[117] Suriyawong A, Gamble M, Lee M-H, Axelbaum R, Biswas P. Submicrometer particle formation and mercury speciation under O_2–CO_2 coal combustion. Energy Fuels 2006;20(6):2357–63.
[118] Wang CS, Berry GF, Chang KC, Wolsky AM. Combustion of pulverized coal using waste carbon dioxide and oxygen. Combust Flame 1988;72(3):301–10.
[119] Nozaki T, Takano S-i, Kiga T, Omata K, Kimura N. Analysis of the flame formed during oxidation of pulverized coal by an O_2–CO_2 mixture. Energy 1997;22(2–3):199–205.
[120] Croiset E, Thambimuthu K, Palmer A. Coal combustion in O_2/CO_2 mixtures compared with air. Can J Chem Eng 2000;78(2):402–7.
[121] Liu H, Zailani R, Gibbs BM. Comparisons of pulverized coal combustion in air and in mixtures of O_2/CO_2. Fuel 2005;84(7–8):833–40.
[122] Tan Y, Croiset E, Douglas MA, Thambimuthu KV. Combustion characteristics of coal in a mixture of oxygen and recycled flue gas. Fuel 2006;85(4):507–12.
[123] Andersson K, Normann F, Johnsson F. Experiments and modeling on oxy-fuel combustion chemistry during lignite-firing. In: The 32nd international technical conference on coal utilization and fuel systems. Clearwater, Florida; 10–15 July2007.
[124] Mackrory AJ, Lokare S, Baxter LL, Tree DR. An investigation of nitrogen evolution in oxy-fuel combustion. In: The 32nd international technical conference on coal utilization and fuel systems, the power of coal. Clearwater, Florida; 10–15 June, 2007.
[125] Sheng C, Li Y. Experimental study of ash formation during pulverized coal combustion in O_2/CO_2 mixtures. Fuel 2008;87(7):1297–305.
[126] Molina A, Shaddix CR. Ignition and devolatilization of pulverized bituminous coal particles during oxygen/carbon dioxide coal combustion. Proc Combust Inst 2007;31(2):1905–12.
[127] Liu H, Okazaki K. Simultaneous easy CO_2 recovery and drastic reduction of SO_x and NO_x in O_2/CO_2 coal combustion with heat recirculation. Fuel 2003;82(11):1427–36.
[128] Wall T, Liu Y, Spero C, Elliott L, Khare S, Rathnam R, et al. An overview on oxyfuel coal combustion–State of the art research and technology development. Chem Eng Res Des 2009;87(8):1003–16.
[129] Bordenet B. Influence of novel cycle concepts on the high-temperature corrosion of power plants. Mater Corros 2008;59(5):361–6.
[130] Bordenet B, Kluger F. Thermodynamic modelling of the corrosive deposits in oxy-fuel fired boilers. Mater Sci Forum 2008;595–598(1):261–9.
[131] Kung SC, Tanzosh JM, Mcdonald DK. Fireside corrosion study using B&W clean environment development facility for oxy-coal combustion systems. Advances in materials technology for fossil power plants. In: Proceedings from the 5th International conference; 2008. p. 982–92.
[132] Abellán JPirón, Olszewski T, Penkalla HJ, Meier GH, Singheiser L, Quadakkers WJ. Scale formation mechanisms of martensitic steels in high CO_2/H_2O-containing gases simulating oxyfuel environments. Mater High Temp 2009;26(1):63–72.
[133] Rauscher K. Clean coal in the energy mix from tomorrow. VGB PowerTech 2005;85(9):70–2.
[134] Ritter R, Holling B, Altmann H, Biele M. Konzepte und Ausblick für eine CO_2-Anlage eines Oxyfuel-Kraftwerkes am Bespiel Schwarze Pumpe. In: 39. Kraftwerktechnisches Kolloquium. Dresden, Germany; October 11–12, 2007.
[135] McCauley KJ, Farzan H, Alexander KC, McDonald DK, Varagani R, Prabhakar R, et al. Commercialization of oxy-coal combustion: applying results of a large 30 MW_{th} pilot project. Energy Procedia 2009;1(1):439–46.
[136] Kiga T, Takano S, Kimura N, Omata K, Okawa M, Mori T, et al. Characteristics of pulverized-coal combustion in the system of oxygen/recycled flue gas combustion. Energy Convers Manage 1997;38:129–34.
[137] Watanabe S, Endo Y, Kiga T, Kimura N, Okawa M. Analysis of pulverized-coal flames in the system of oxygen/recycled flue gas combustion. Am Soc Mech Engineers, Environ Control Division Publ EC 1997;5:239–46.
[138] Wall TF, Elliott L, Khare S, Liu Y, Yamada T, Tamura M, et al. Ash impacts in oxy-fuel combustion. In: Proceedings: impacts of fuel quality on power production. Utah, USA; 2006.
[139] Wall TF. Performance of PF boilers retrofitted with oxy-coal combustion: understanding burnout, coal reactivity, burner operation, and furnace heat transfer. In: 3rd Workshop of the IEA GHG international oxy-combustion network. Yokohama, Japan; March 5–6, 2008.
[140] Goh B. 1 MW_{th} oxyfuel combustion test facility. "Recent developments in CCS" coal research forum – combustion division meeting 17th April 2007. Imperial College London; 2007.
[141] Goh B. Oxyfuel combustion pilot-scale testing. Oxyfuel combustion: opportunities and challenges–7th of May 2008. University of Leeds; 2008a.
[142] Goh B.E.ON UK's pilot scale oxyfuel combustion experiences: development, testing and modelling. In: 3rd workshop of the IEA GHG international oxy-combustion network. Yokohama, Japan; March 5–6, 2008.
[143] Dhungel B, Mönckert P, Maier J, Scheffknecht G. Investigation of oxy-coal combustion in semi-technical test facilities. In: 3rd international conference on clean coal technology. Italy, 2007.
[144] Maier J, Dhungel B, Mönckert P, Scheffknecht G. Combustion and emission behavior under oxyfuel conditions. In: 39. Kraftwerktechnisches Kolloquium. Dresden, Germany; October 11–12, 2007 [In German].
[145] Maier J, Dhungel B, Mönckert P, Kull R, Scheffknecht G. Impact of recycled gas species (SO_2, NO) on emission behaviour and fly ash quality during oxy-coal combustion. In: Proceedings of the 33rd international technical conference on coal utilization and fuel systems. Clearwater, Florida; June 1–5, 2008.
[146] Mönckert P, Reber D, Maier J, Scheffknecht G. Operation of a retrofitted 0.5 MW_{th} PF combustion facility under oxyfuel conditions–an experience report. In: The 32nd international technical conference on coal utilization and fuel systems, the power of coal. Clearwater, Florida; 10–15 June, 2007.
[147] Mönckert P, Dhungel B, Kull R, Maier J. Impact of combustion conditions on emission formation (SO_2, NO_x) and fly ash. In: 3rd workshop of the IEA GHG international oxy-combustion network. Yokohama, Japan; March 5–6, 2008.
[148] Scheffknecht G, Maier J. Firing issues related to the oxyfuel process. VGB PowerTech 2008;88(11):91–7.
[149] Zheng L, Furimsky E. Assessment of coal combustion in O_2 + CO_2 by equilibrium calculations. Fuel Processing Technol 2003;81(1):23–34.
[150] Chui EH, Douglas MA, Tan Y. Modeling of oxy-fuel combustion for a western Canadian sub-bituminous coal. Fuel 2003;82(10):1201–10.
[151] Chui EH, Majeski AJ, Douglas MA, Tan Y, Thambimuthu KV. Numerical investigation of oxy-coal combustion to evaluate burner and combustor design concepts. Energy 2004;29(9–10):1285–96.
[152] White V. Purification of oxyfuel-derived CO_2. In: 3rd workshop of the IEA GHG international oxy-combustion network. Yokohama, Japan; March 5–6, 2008.
[153] Andersson K, Johnsson F. Flame and radiation characteristics of gas-fired O_2/CO_2 combustion. Fuel 2007;86(5–6):656–68.
[154] Leiser S, Schnell U, Scheffknecht G. A kinetic homogeneous reaction model for oxy-fuel combustion. In: 9th conference on energy for a clean environment; 2007.
[155] Andersson K, Johansson R, Johnsson F, Leckner B. Radiation intensity of propane-fired oxy-fuel flames: implications for soot formation. Energy Fuels 2008b;22(3):1535–41.
[156] Normann F, Andersson K, Leckner B, Johnsson F. High-temperature reduction of nitrogen oxides in oxy-fuel combustion. Fuel 2008;87(17):3579–85.
[157] Valero A, Romeo LM, Díez LI, Pérez A. OXY-CO-FIRING: a negative CO_2 emission process. In: The 8th international conference on greenhouse gas control technologies (GHGT-8). Trondheim, Norway; 19–22 June, 2006.
[158] Okazaki K, Ando T. NO_x reduction mechanism in coal combustion with recycled CO_2. Energy 1997;22(2–3):207–15.
[159] Okazaki K. Technical consideration and challenges of oxy-pulverized coal combustion. In: 3rd workshop of the IEA GHG international oxy-combustion network. Yokohama, Japan; March 5–6, 2008.
[160] Hu YQ, Kobayashi N, Hasatani M. The reduction of recycled-NO_x in coal combustion with O_2/recycled flue gas under low recycling ratio. Fuel 2001;80(13):1851–5.
[161] Hu YQ, Kobayashi N, Hasatani M. Effects of coal properties on recycled-NO_x reduction in coal combustion with O_2/recycled flue gas. Energy Convers Manage 2003;44(14):2331–40.
[162] Liu H, Zailani R, Gibbs BM. Pulverized coal combustion in air and in O_2/CO_2 mixtures with NO_x recycle. Fuel 2005b;84(16):2109–15.
[163] Maier J, Dhungel B, Mönckert P, Scheffknecht G. Coal combustion and emission behaviour under oxy-fuel combustion. In: Proceedings of the 31st international technical conference on coal utilization and fuel systems. Clearwater, Florida; 21–26 May, 2006.
[164] Dhungel B, Maier J, Scheffknecht G. Emission behaviour during oxy-coal combustion in a 20 kW once through furnace. In: 9th conference on energy for a clean environment. Portugal; 2007.
[165] Al-Makhadmeh L, Maier J, Scheffknecht G. Coal pyrolysis and char combustion under oxy-fuel conditions. In: The 34th international technical conference on coal utilization and fuel systems. Clearwater, Florida; May 31–June 4, 2009.

[166] Murphy JJ, Shaddix CR. Combustion kinetics of coal chars in oxygen-enriched environments. Combust Flame 2006;144(4):710–29.
[167] Shaddix CR, Molina A. Effect of O_2 and High CO_2 concentrations on PC char burning rates during oxy-fuel combustion. In: The 33rd international technical conference on coal utilization and fuel systems, coal for the future. Clearwater, Florida; 1–5 June, 2008.
[168] Shaddix CR, Molina A. Particle imaging of ignition and devolatilization of pulverized coal during oxy-fuel combustion. Proc Combust Inst 2009;32 (2):2091–8.
[169] Shaddix CR, Molina A. Understanding the effects of O_2 and CO_2 on NO_x formation during oxy-coal combustion. In: 3rd Workshop of the IEA GHG international oxy-combustion network. Yokohama, Japan; March 5–6, 2008.
[170] Becher V, Goanta A, Gleis S, Spliethoff H. Controlled staging with non-stoichiometric burners for oxyfuel processes. In: The 32nd international technical conference on coal utilization and fuel systems, the power of coal. Clearwater, Florida; 10–15 June, 2007.
[171] Goanta A, Becher V, Bohn J-P, Gleis S, Spliethoff H. Controlled staging with non-stoichiometric burners for oxy-fuel processes–numerical validation. In: The 33rd international technical conference on coal utilization and fuel systems, coal for the future. Clearwater, Florida; 1–5 June, 2008.
[172] Glarborg P, Bentzen LLB. Chemical effects of a high CO_2 concentration in oxy-fuel combustion of methane. Energy Fuels 2008;22(1):291–6.
[173] Mendiara T, Glarborg P. Reburn chemistry in oxy-fuel combustion of methane. Energy Fuels 2009a;23(7):3565–72.
[174] Mendiara T, Glarborg P. Ammonia chemistry in oxy-fuel combustion of methane. Combust Flame 2009b;156:1937–49.
[175] Mackrory AJ, Tree DR. NO_x Destruction experiments and modeling in oxy-fuel combustion. In: The 33rd international technical conference on coal utilization and fuel systems, coal for the future. Clearwater, Florida; 1–5 June, 2008.
[176] Mackrory AJ, Tree DR. Predictions of NO_x in a laboratory pulverized coal combustor operating under air and oxy-fuel conditions. Combust Sci Technol 2009;181(11):1413–30.
[177] Heil P, Stadler H, Förster M, Kneer R. Flammlose Verbrennung in einer O_2/CO_2 Atmosphäre. In: 39. Kraftwerktechnisches Kolloquium. Dresden, Germany, October 11–12, 2007.
[178] Stadler H, Ristic D, Förster M, Schuster A, Kneer R, Scheffknecht G. NO_x-emissions from flameless coal combustion in air, Ar/O_2 and CO_2/O_2. Proc Combust Inst 2009;32(2):3131–8.
[179] Engels S. Developments in oxy-combustion technology for power plants with CCS. 1st Young Researchers Forum Organised by IEA Greenhouse Gas R&D Programme, Hamburg, Germany; December 8, 2006.
[180] Arias B, Pevida C, Rubiera F, Pis JJ. Effect of biomass blending on coal ignition and burnout during oxy-fuel combustion. Fuel 2008;87(12):2753–9.
[181] Bejarano PA, Levendis YA. Single-coal-particle combustion in O_2/N_2 and O_2/CO_2 environments. Combust Flame 2008;153(1–2):270–87.
[182] Sheng C, Li Y, Liu X, Yao H, Xu M. Ash particle formation during O_2/CO_2 combustion of pulverized coals. Fuel Processing Technol 2007a;88(11–12):1021–8.
[183] Sheng C, Lu Y, Gao X, Yao H. Fine ash formation during pulverized coal combustion–a comparison of O_2/CO_2 combustion versus air combustion. Energy Fuels 2007b;21(2):435–40.
[184] Fryda L, Cieplik MK, Jacobs JM, van de Kamp WL. Study of oxyfuel combustion of coal and biomass in a lab-scale pulverised fuel combustor. In: 16th European biomass conference and exhibition. Valencia, Spain; June 2–6, 2008.
[185] Spinti JP, Pershing DW. The fate of char-N at pulverized coal conditions. Combust Flame 2003;135(3):299–313.
[186] Zhang J, Eddings EG, Wendt JOL, Smith PJ. Model validation studies for pulverized coal jet ignition in O_2/CO_2 environments. In: 3rd workshop of the IEA GHG international oxy-combustion network. Yokohama, Japan; March 5–6, 2008.
[187] Naredi P, Pisupati SV. Comparison of char burnout and CO emissions from oxy-coal combustion with combustion in air: an experimental and numerical study. In: The 33rd international technical conference on coal utilization and fuel systems, coal for the future. Clearwater, Florida; 1–5 June, 2008.
[188] Andersson K, Johansson R, Hjartstam S, Johnsson F, Leckner B. Radiation intensity of lignite-fired oxy-fuel flames. Exp Thermal Fluid Sci 2008c;33(1):67–76.
[189] Huang X, Jiang X, Han X, Wang H. Combustion characteristics of Fine- and micro-pulverized coal in the mixture of O_2/CO_2. Energy Fuels 2008;22 (6):3756–62.
[190] Suda T, Masuko K, Sato J, Yamamoto A, Okazaki K. Effect of carbon dioxide on flame propagation of pulverized coal clouds in CO_2/O_2 combustion. Fuel 2007;86(12–13):2008–15.
[191] Stanmore BR, Visona SP. The Contribution to char burnout from gasification by H_2O and CO_2 during pulverized-coal flame combustion. Combust Flame 1998;113(1–2):274–6.
[192] Varhegyi G, Szabo P, Jakab E, Till F, Richard J-R. Mathematical modeling of char reactivity in $Ar–O_2$ and $CO_2–O_2$ mixtures. Energy Fuels 1996;10(6):1208–14.
[193] Borrego AG, Alvarez D. Comparison of chars obtained under oxy-fuel and conventional pulverized coal combustion atmospheres. Energy Fuels 2007;21(6):3171–9.
[194] Liu F, Guo H, Smallwood GJ. The chemical effect of CO_2 replacement of N_2 in air on the burning velocity of CH_4 and H_2 premixed flames. Combust Flame 2003;133(4):495–7.
[195] Liu F, Guo H, Smallwood GJ, Gülder Ö L. The chemical effects of carbon dioxide as an additive in an ethylene diffusion flame: implications for soot and NO_x formation. Combust Flame 2001;125(1–2):778–87.
[196] Masri AR, Dibble RW, Barlow RS. Chemical kinetic effects in nonpremixed flames of H_2/CO_2 fuel. Combust Flame 1992;91(3–4):285–309.
[197] Miller JA, Bowman CT. Mechanism and modeling of nitrogen chemistry in combustion. Prog Energy Combust Sci 1989;15:287–338.
[198] Johnsson JE. Formation and reduction of nitrogen oxides in fluidized-bed combustion. Fuel 1994;73:1398–415.
[199] Glarborg P, Jensen AD, Johnsson JE. Fuel nitrogen conversion in solid fuel fired systems. Prog Energy Combust Sci 2003;29(2):89–113.
[200] Turns SR. An introduction to combustion: concepts and applications. International Editions. McGraw-Hill; 2000.
[201] Normann F, Andersson K, Leckner B, Johnsson F. Emission control of nitrogen oxides in the oxy-fuel process. Prog Energy Combust Sci 2009;35 (5):385–97.
[202] Wendt JOL, Sternling CV, Matovich MA. Reduction of sulfur trioxide and nitrogen oxides by secondary fuel injection. Proc Combust Inst 1973;14(1):897–904.
[203] Levy JM, Chan LK, Sarofim AF, Beer JM. NO/char reactions at pulverized coal flame conditions. Proc Combust Inst 1981;18:111–20.
[204] Aarna I, Suuberg EM. A review of the kinetics of the nitric oxide-carbon reaction. Fuel 1997;76(6):475–91.
[205] Aarna I, Suuberg EM. The role of carbon monoxide in the NO-carbon reaction. Energy Fuels 1999;13(6):1145–53.
[206] López D, Calo J. The NO-carbon reaction: the influence of potassium and CO on reactivity and populations of oxygen surface complexes. Energy Fuels 2007;21(4):1872–7.
[207] Park D-C, Day SJ, Nelson PF. Nitrogen release during reaction of coal char with O_2, CO_2, and H_2O. Proc Combust Inst 2005;30(2):2169–75.
[208] Liu H, Katagiri S, Kaneko U, Okazaki K. Sulfation behavior of limestone under high CO_2 concentration in O_2/CO_2 coal combustion. Fuel 2000;79 (8):945–53.
[209] Liu H, Katagiri S, Okazaki K. Drastic SO_x removal and influences of various factors in O_2/CO_2 pulverized coal combustion system. Energy Fuels 2001b;15 (2):403–12.
[210] Krishnamoorthy G, Veranth JM. Computational modeling of CO/CO_2 ratio inside single char particles during pulverized coal combustion. Energy Fuels 2003;17(5):1367–71.
[211] Keith DW, Rhodes JS. Bury, burn or both: a two-for-one deal on biomass carbon and energy. Climatic Change 2002;54(3):375–7.
[212] Obersteiner M, Azar C, Kauppi P, Möllersten K, Moreira J, Nilsson S, et al. Managing climate risk. Science 2001;294(5543):786–7.
[213] Kraxner F, Nilsson S, Obersteiner M. Negative emissions from BioEnergy use, carbon capture and sequestration (BECS) – the case of biomass production by sustainable forest management from semi-natural temperate forests. Biomass Bioenergy 2003;24(4–5):285–96.
[214] Azar C, Lindgren K, Larson E, Mollersten K. Carbon capture and storage from fossil fuels and biomass – costs and potential role in stabilizing the atmosphere. Climatic Change 2006;74(1–3):47.
[215] Read P. Bioenergy with carbon storage – strengthening Kyoto through complementary action to address the threat of abrupt climate change. Renewable Energy Dev 2006;19(3):9–11.
[216] Rhodes JS, Keith DW. Biomass with capture: negative emissions within social and environmental constraints: an editorial comment. Climatic Change 2008;87(3–4):321–8.
[217] Borrego AG, Garavaglia L, Kalkreuth WD. Characteristics of high heating rate biomass chars prepared under N_2 and CO_2 atmospheres. Int J Coal Geol 2009;77(3–4):409–15.
[218] Robinson AL, Junker H, Buckley SG, Sclippa G, Baxter LL. Interactions between coal and biomass when cofiring. Proc Combust Inst 1998;27(1):1351–9.

Nomenclature

ASU: Air Separation Unit
BECS: Biomass Energy for Carbon Capture and Sequestration
CCS: Carbon Capture and Storage
EFR: Entrained-Flow Reactor
EOR: Enhanced Oil Recovery
ESP: Electrostatic Precipitator
FGD: Flue Gas Desulphurization
IGCC: Integrated Gasification Combined Cycle
ITM: Ion Transport Membrane (for air separation)
LCV/LHV: Low Calorific/Heating Value
RFG: Recirculated Flue Gas
SCR: Selective Catalytic Reduction

Research groups

ANL: Argonne National Laboratory
BYU: Brigham Young University (Utah, USA)
CANMET: Canada Centre for Mineral and Energy Technology
DTU: Technical University of Denmark
IFRF: International Flame Research Foundation
IHI: Ishikawajima-Harima Heavy Industries
IVD: Institute of Process Engineering and Power Plants Technology, University of Stuttgart
UU: University of Utah

OxyFuel Combustion of Coal and Biomass

Ph.D. Thesis

Maja Bøg Toftegaard

CHEC Research Centre
Department of Chemical Engineering
Technical University of Denmark

DONG Energy Power
Power Technology
Chemical Engineering

March 31, 2011

Preface and Acknowledgements

The work presented in this thesis has been conducted under the Industrial PhD programme supported by the Ministry of Science, Technology, and Innovation. The dissertation is submitted in accordance with the partial requirements for the Ph.D. degree at the Department of Chemical and Biochemical Engineering, Technical University of Denmark. The Ph.D. study was carried out in the period April 2007 to March 2011 in collaboration between DONG Energy Power, Chemical Engineering and the CHEC (Combustion and Harmful Emission Control) research centre at the Department of Chemical and Biochemical Engineering at the Technical University of Denmark. The work has been funded by DONG Energy and the Ministry of Science, Technology, and Innovation. The experimental work has likewise been partly funded by Energinet.dk through the PSO projects "PSO 7171 – Oxyfuel combustion for below zero CO_2 emissions" and "PSO 010069 – Advanced diagnostics on Oxy-fuel combustion processes". The project has been supervised by Professor Anker Degn Jensen, Professor Peter Glarborg, Associate Professor Peter Arendt Jensen, and Senior Engineer, Lic.Tech. Bo Sander (DONG Energy Power).

I wish to thank all my supervisors for their invaluable support and guidance throughout the project and for continuously challenging my ideas and results in order to improve the project. I am grateful to M.Sc. student Bjørn Maribo-Mogensen and Research Associate Professor Weigang Lin for their involvement in the experimental work. I would also like to thank the technical staff and the workshop at Department of Chemical and Biochemical Engineering, especially Thomas Wolfe, for helping me conquer a stubborn experimental setup.

My former and present colleagues at both the Technical University of Denmark and DONG energy all deserve my gratitude. Special thanks go to Rudolph Blum, Alice Jochumsen, and Ole Hede Larsen for believing in me, even at times when I did not, and to Ulrik Borg, the best office mate one could imagine.

Maja Bøg Toftegaard
Fredericia, March 2011

Summary

The power and heat producing sector is facing a continuously increasing demand to reduce its emissions of CO_2. Oxyfuel combustion combined with CO_2 storage is suggested as one of the possible, promising technologies which will enable the continuous use of the existing fleet of suspension-fired power plants burning coal or other fuels during the period of transition to renewable energy sources.

The oxyfuel combustion process introduces several changes to the power plant configuration. Most important, the main part of the flue gas is recirculated to the boiler and mixed with pure oxygen. The oxidant thus contains little or no nitrogen and a near-pure CO_2 stream can be produced by cooling the flue gas to remove water. The change to the oxidant composition compared to combustion in air will induce significant changes to the combustion process.

This Ph.D. thesis presents experimental investigations on the combustion of coal, biomass (straw), and blends of coal and straw in air and O_2/CO_2 mixtures. The experiments have been performed in semi-technical scale in a once-through 30 kW_{th} swirl-stabilized flame. The work has focused on improving the fundamental knowledge on oxyfuel combustion of coal and straw at conditions relevant to suspension-fired boilers by clarifying the effect of the change in combustion atmosphere on fuel burnout, flame temperatures, emissions of polluting species (NO, SO_2, and CO), fly ash quality, and deposit formation. This work is one of the first to investigate the important aspects of ash and deposit formation during co-firing of coal and biomass and combustion of pure biomass in oxyfuel atmospheres in semi-technical scale.

The presented work has lead to the identification of reference operating conditions which enables a direct comparison of combustion in air and oxyfuel atmospheres. Apart from slightly improved burnout and reduced emissions of NO during oxyfuel combustion these operating conditions yield similar combustion characteristics in both environments.

Co-firing coal and biomass or combustion of pure biomass in an oxyfuel power plant could yield a significant, additional CO_2 reduction, or even lead to below-zero emissions of CO_2 from power production. This work has shown that no significant changes occur to the fundamental combustion characteristics for straw when burned in the O_2/CO_2 atmosphere. Additionally, the combustion of a coal/straw blend with a straw share of 50 wt% has added valuable understan-

ding to the trends in ash and deposits chemistry for coal/straw co-firing.

Recirculation of untreated flue gas in oxyfuel plants will increase the in-boiler levels of NO and SO_2 significantly. Experiments with simulated recirculation of NO and SO_2 have provided insight into the mechanisms of the significant reduction in NO emission rates from the boiler and the increased uptake of sulphur in fly ash and deposits which were observed.

The single-largest penalty to the electrical efficiency and operating expenses of an oxyfuel power plant is the production of near-pure oxygen by cryogenic distillation. This thesis presents a possible strategy for reducing the oxygen demand and hence the penalty to the process. The strategy exploits the fact that the oxygen excess level during oxyfuel combustion is not directly linked to the flow of oxidant but can be adjusted independently. By increasing the concentration of oxygen in the oxidant, i.e. by reducing the flue gas recirculation ratio, it is possible to achieve similar burnout at lower oxygen excess levels. Further work on implications of this strategy are necessary in order to fully clarify its potential for improving the process economics of oxyfuel combustion.

Generally, no characteristics of the oxyfuel combustion process have been identified in this work which would be detrimental to its implementation as a carbon capture technology in full-scale power plants.

Resumé (Summary in Danish)

Kraftværkssektoren står overfor stadigt stigende krav til reduktion af dens CO_2-udledning. Oxyfuel forbrænding kombineret med CO_2-lagring er en af de mulige og lovende teknologier, som vil muliggøre en fortsat anvendelse af kul og andre brændsler i den eksisterende porteføljе af suspensionsfyrede kraftværker i overgangsperioden til vedvarende energi.

Ombygning af eksisterende kraftværker til oxyfuel forbrænding vil medføre adskillige ændringer i proceskonfigurationen. Vigtigst af disse er, at hovedparten af røggassen recirkuleres til kedlen hvor den blandes med ren ilt. Forbrændingsgassen indeholder derfor kun lidt eller intet nitrogen og en CO_2-strøm af høj renhed kan derfor produceres ved tørring af røggassen. Ændringen af forbrændingsgassens sammensætning i forhold til sammensætningen af luft vil medføre betydelige ændringer i forbrændingsprocessen.

Denne ph.d.-afhandling fremlægger eksperimentelle undersøgelser af forbrændingen af kul, biomasse (halm), og blandinger af kul og halm i luft og O_2/CO_2 blandinger. Forsøgene er udført i semi-teknisk skala i en 30 kW_{th} swirl-stabiliseret flamme. Arbejdet har fokuseret på at forøge den grundlæggende forståelse af oxyfuel forbrænding af kul og halm ved betingelser, som er relevante i forhold til suspensionsfyrede kedler, ved at klarlægge effekten af ændringen i forbrændingsatmosfæren på udbrænding, flammetemperaturer, emissioner af forurenende komponenter (NO, SO_2 og CO), flyveaskekvalitet og belægningsdannelse. Dette arbejde er et af de første til at undersøge de vigtige problemstillinger omkring aske- og belægningsdannelse under samfyring af kul og biomasse og ved forbrænding af ren biomasse i oxyfuel atmosfærer i semi-teknisk skala.

Det præsenterede arbejde har ført til identificeringen af reference driftsbetingelser som muliggør en direkte sammenligning af forbrænding i luft og oxyfuel atmosfærer. Bortset fra en fordelagtig, let forøget udbrænding og en reduceret NO-udledning ved oxyfuel forbrænding medfører disse driftsbetingelser ens karakteristika for forbrændingsprocessen i begge miljøer.

Samfyring af kul og biomasse eller forbrænding af ren biomasse i et oxyfuel kraftværk kan give en betydelig, ekstra reduktion af CO_2-udledningen eller endda føre til en negativ CO_2-udledning fra elproduktionen. Dette arbejde har vist at der ikke opstår nogen betydelige ændringer i de grundlæggende forbrændingsprocesser når halm afbrændes i O_2/CO_2-atmosfæren. Derudover har anvendelsen af

en kul/halm blanding med en halmandel på 50 wt% tilført værdifuld forståelse af tendenser i aske- og belægningskemi for samfyring af kul og halm.

Recirkulering af ubehandlet røggas i oxyfuel kraftværker vil øge niveauerne af NO og SO_2 i kedlen markant. Forsøg med simuleret recirkulering af NO og SO_2 har tilvejebragt indsigt i mekanismerne bag det observerede, betydelige fald i NO-emissionen fra kedlen og den forøgede indbinding af svovl i flyveaske og belægninger.

Den største, enkeltstående reduktion af elvirkningsgraden i et oxyfuel kraftværk i forhold til et konventionelt værk stammer fra produktionen af ilt ved kryogen destillation. Denne afhandling præsenterer en mulig strategi til reduktion af iltforbruget og dermed en forøgelse af den samlede elvirkningsgrad for processen. Strategien udnytter det faktum, at iltoverskuddet i oxyfuel forbrænding, i modsætning til forbrænding i luft, ikke længere er direkte knyttet til mængden af forbrændingsluft, men kan varieres uafhængigt. Ved at forøge koncentrationen af ilt i oxidanten, dvs. ved at mindske recirkulationsforholdet, er det muligt at opnå en sammenlignelig udbrændingsgrad ved lavere iltoverskud. For at klarlægge denne strategis potentiale i forhold til en forbedring af procesøkonomien for oxyfuel kraftværker er videre undersøgelser dog nødvendige.

Overordnet set har dette arbejde ikke identificeret nogle karakteristika ved oxyfuel forbrændingsprocessen, som vil gøre den uegnet til storskala implementering.

Contents

Chapter 1

Introduction

The world, and especially the developing countries such as China and India, is facing an increasing growth in the demand for electrical power [1, 2]. New power plants are thus being constructed at a considerable rate in order to keep up with this demand [1–3]. The majority of the recently constructed and planned power plants, on a world-wide basis, are coal fired [1, 2]. Coal is a cheaper and more abundant resource than other fossil fuels such as oil and natural gas while at the same time being a very safe and reliable fuel for power production [4, 5].

In the developed countries an increasing part of the energy consumption is being produced from renewable sources of energy; wind, biomass, solar, hydro power, etc. [1] The main purpose of the shift from a fossil fuel based production to renewable energy is to decrease the emission of greenhouse gases, primarily CO_2. Especially the emission of CO_2 from the combustion of fossil fuels has gained great focus in recent years in connection with the discussions of global warming. Since the beginning of the industrialization in the late part of the 18^{th} century the amount of CO_2 in the atmosphere has increased sharply from about 280 to 380 ppm, [6], see Figure 1.1 on the following page.

Table 1.1 lists the current and projected CO_2 emissions, in Gton carbon per year, from power generation (both electricity and heat) [1]. Both the emissions and the coal share of the emissions are seen to increase toward 2030 for the world as a whole. Even though the CO_2 emissions are seen to increase within Europe the percentage increase is much less pronounced than for the rest of the world and the coal share of the emissions is expected to decrease. Despite the fact

Table 1.1: Estimated CO_2 emissions from power generation (Gton C/year). The numbers in parenthesis indicate the percentage coal share of the emissions. Data taken from [1].

Region	2005	2015	2030
World	3.0 (72)	4.0 (74)	5.1 (74)
European Union	0.38 (70)	0.39 (66)	0.42 (61)

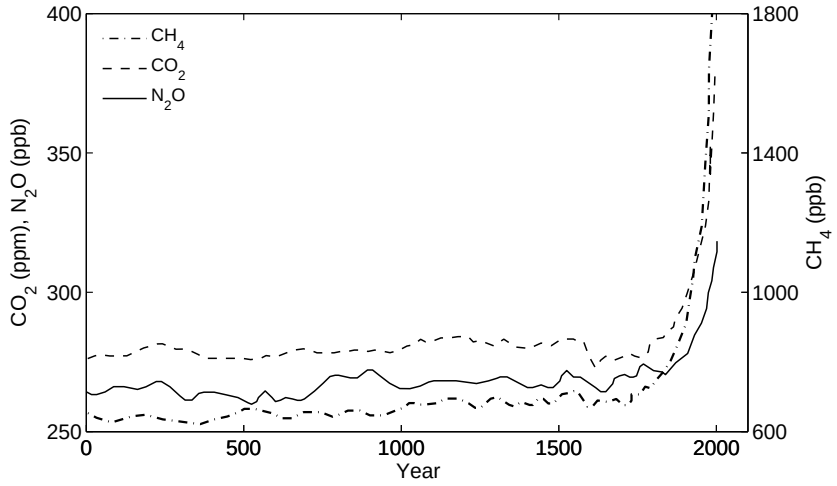

Figure 1.1: Development in the concentrations of important long-lived greenhouse gases in the atmosphere over the last 2,000 years. The increases in concentrations since about year 1750 are attributed to human activities in the industrial era. Reprinted from [6].

that the ultimate goal for most countries is to phase out all fossil fuels in heat and power production as well as in the transport sector, the share of renewable energy sources increases only slowly and the world will depend on fossil fuels for many years to come. A rapid move away from fossil fuels could result in great conflicts concerning water and land use between biomass for energy production, food production, and forestation [7] as well as in serious disruption to the global economy [8]. The latter is mainly caused by the long lifetime of the energy supply infrastructure. In the transitional period, technologies are sought which will enable the continuous usage of fossil fuels and at the same time eliminate the emission of CO_2.

1.1 Carbon Capture and Storage

Since power plants constitute large point sources of CO_2 emission the main focus is related to their operation. Currently, several possible technologies are being investigated which will enable the so called Carbon Capture and Storage (CCS) from power plants [5, 8–14]. Both researchers in universities and other research institutions, most manufacturers of boilers and other power plant related equipment, and many power companies are active. CCS will act as a complimentary technology to the ongoing work related to increasing fuel efficiency and the change toward fuels with lower fossil carbon content, e.g. natural gas and/or biomass. As indicated by the term CCS, the elimination of CO_2 emissions include two consecutive operations:

1. Capture of CO_2 from the power plant flue gas

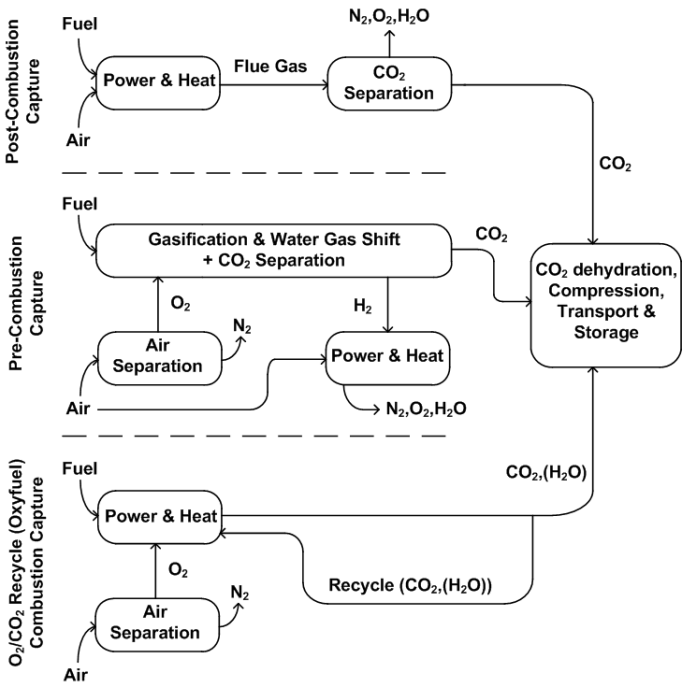

Figure 1.2: Possible, overall plant configurations for the three main categories of carbon capture technologies. Adopted from [10].

2. Storage of the CO_2 (incl. transport to storage site)

The identified technologies for carbon capture can be divided into four main categories [5, 11, 12, 15–19], described briefly below. Figure 1.2 shows the main operations concerned with the post-, pre-, and oxyfuel combustion technologies.

Post-combustion capture CO_2 is separated from the flue gas of conventional coal-fired power plants. The separation is typically performed via chemical absorption with monoethanolamine (MEA) [18, 20–24]. The demonstrated scale of operation is, however, significantly smaller than the typical size of power plants [23] and serious penalties to the plant efficiency, about 10-14 percent points, exist at the current state of development [5, 8, 12, 23, 25–31]. Retrofit to existing plants is considered relatively simple since the capture unit can be added downstream of the boiler and flue gas cleaning systems without significant changes to the original plant [8, 32]. There are, however, strict requirements for removal of SO_2 and NO_2 from the flue gas prior to the CO_2 capture since these compounds react irreversibly with the absorbent leading to its degradation. The chilled ammonia process also belongs in the category.

Pre-combustion capture Pre-combustion capture is typically used synonymously with Integrated Gasification Combined Cycle power plants with

CO_2 capture and termed IGCC-CCS. Coal gasification is applied to obtain syngas containing CO, CO_2, and H_2. The CO is transformed into CO_2 by the water-gas shift reaction and can then be separated from the remaining hydrogen-containing gas before the latter is combusted in a gas turbine. Some techno-economic calculations [11, 19, 33–35] show that IGCC has promising process economics and plant efficiency characteristics. However, high capital costs are associated with plant construction and IGCC plants are generally much more complicated systems than suspension fired boilers [36, 37] and retrofit is not a viable option for the latter [19, 36, 38, 39]. Only few electricity producing IGCC units exist [17, 34, 40–42], none of which are equipped with CCS. Only few IGCC plants exist and the demonstrated availability is significantly smaller than for the more matured, conventional pulverized coal-fired power plants (80-85 % vs. $\sim$96 %, respectively) [5, 19, 34, 37, 40, 43]. This is a consequence of the limited operating experience along with the highly integrated nature of the IGCC plants.

Oxyfuel combustion By near elimination of molecular nitrogen from the combustion medium the flue gas will consist mainly of CO_2 and water. The plant configuration typically suggested involves flue gas recirculation to the burners to control the flame temperature to within the acceptable limits of the boiler materials. Implementation of the oxyfuel combustion technology in existing pulverized coal-fired power plants will induce a larger change in the plant configuration when comparing to the post-combustion absorption process mentioned above. This is due to an introduction of several, new auxiliary processes. Several of the earlier techno-economic assessment studies indicate that oxyfuel combustion should be the most energy and cost efficient of the carbon capture technologies [9, 25, 27, 44–49]. The main disadvantage of the oxyfuel combustion technology is the need for almost pure oxygen. The available large-scale technology for air separation is based on cryogenic distillation which will impose a very large energy penalty on the plant [50]. The expected efficiency drop is about 7–11 percent points, or about 15–30 % of the generated electricity (net power output), depending on the initial plant efficiency [5, 8, 12, 15, 17, 27, 31, 44, 45, 51–54].

Emerging technologies Technologies such as membrane separation, chemical looping combustion, carbonation-calcination cycles, enzyme-based systems, ionic liquids, mineralization, etc. impose the possibility to drastically reduce the cost of electricity and the energy penalty concerned with carbon capture from power plants [14, 16, 55, 56]. However, these technologies have not been demonstrated at sufficient scales for industrialization.

The choice of technology will depend on several factors. First and foremost, the economy and the expected development in plant efficiency is of importance. The maturity, expected availability, operating flexibility, retrofit or green-plant built,

local circumstances, utilities preferences, etc. will likewise have to be taken into account. No general acceptance of superiority of one of the presented technologies over the others exist. Several techno-economic studies also indicate that with the current knowledge on the technologies no significant difference in cost within the limits of precision of the applied cost estimates can be determined between amine absorption capture, coal-based IGCC type capture, and oxyfuel combustion capture [5, 8, 39, 51, 52, 57, 58].

Because of the large changes induced in the power plant by the implementation of oxyfuel combustion, more research is needed to fully clarify the impacts of the introduction of this technology. Many laboratory scale investigations of the technology have been performed within the last two decades and it is generally accepted that it is possible to burn coal and natural gas in an O_2/CO_2 atmosphere. On the other hand, it is likewise recognized that much work still remains in obtaining sufficient insight into the effects on e.g. emissions, residual products such as fly ash, flue gas cleaning, heat transfer, etc.

1.2 Retrofitting Conventional Suspension-fired Power Plants for OxyFuel Combustion Carbon Capture

In open literature, oxyfuel combustion with recirculation of flue gas was proposed almost simultaneously by Horn and Steinberg [44] and Abraham et al. [46] in the early eighties. Abraham et al. proposed the process as a possible mean to produce large amounts of CO_2 for Enhanced Oil Recovery (EOR) whereas Horn and Steinberg had in mind the reduction of environmental impacts from the use of fossil fuels in energy generation. As such, the technology received renewed interest in the mid-90ties in connection with the re-emerging discussions of global warming caused by increased CO_2 levels in the atmosphere [12].

Oxy-combustion can in principle be applied to any type of fuel utilized for thermal power production. The research interests have mainly been focused on coal and natural gas since these are the most abundant fuels. Application of CCS through oxy-combustion of biomass or blends of coal and biomass will result in a possible mean of extracting CO_2 from the atmosphere and thereby possibly inverting the presumed anthropogenic caused changes to the climate [11, 18, 19].

Figure 1.3 on the next page provides a sketch of a coal-fired oxyfuel plant with indications of the major process steps and the necessary energy inputs and low-temperature-heat outputs new to the plant when retrofitting an existing coal-fired unit. The sketch covers the original state-of-the-art plant with boiler, coal mills, and flue gas cleaning equipment. The final processing of the CO_2 stream, i.e. the

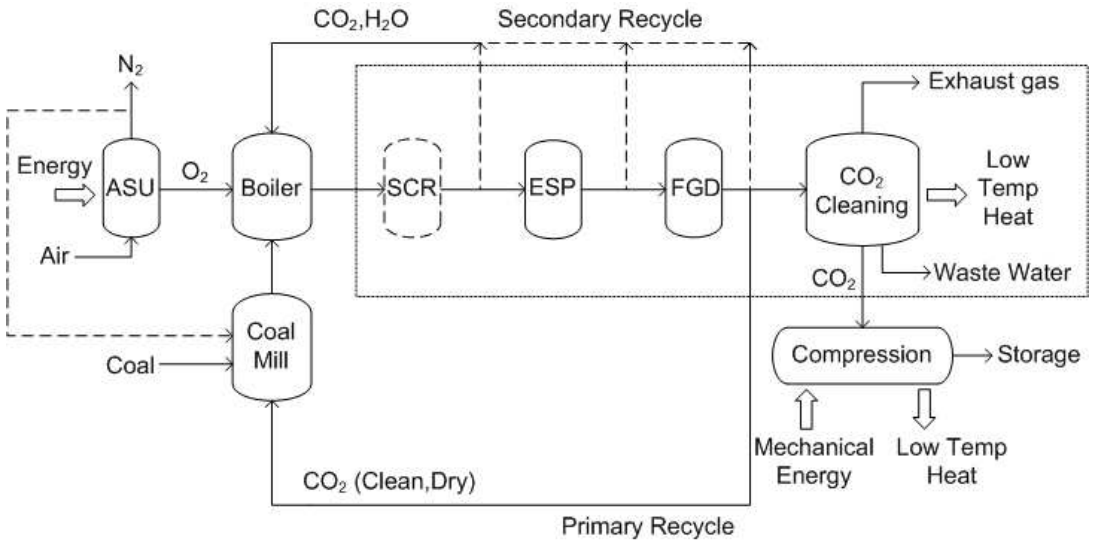

Figure 1.3: Possible configuration of an oxyfuel power plant. ASU: Air Separation Unit, SCR: Selective Catalytic Reduction reactor ($DeNO_x$), ESP: Electrostatic Precipitator, FGD: Flue Gas Desulphurization. Energy inputs and low-temperature heat outputs new to the plant in case of a retrofit are indicated.

removal of water and the non-condensible gases like O_2, N_2, Ar, etc. to meet the requirements regarding purity of the CO_2 stream, as well as the air separation unit (ASU) to provide the combustion process with almost pure oxygen, ducts and fans for external recirculation of flue gas to the burners in order to control flame temperatures, and the compression step for the CO_2 stream before it is transported to the storage site are new to the plant.

The review of the literature performed by this author [59] (Appendix A) has discussed the effects of retrofitting a suspension-fired power plant to oxyfuel operation and has shown that oxyfuel combustion of pulverized coal is technically and economically feasible for retrofitting of existing power plants. At the same time, oxyfuel combustion for CO_2 recovery and sequestration is a competitive power generation technology in relation to post-combustion capture with amines. However, a number of critical aspects regarding the technology have been identified, as listed below. These are the issues which should be investigated experimentally to ensure that the technology is in fact a useful alternative to post-combustion capture for retrofit of suspension-fired boilers.

- The cost and efficiency penalties associated with the technology are significant and should preferably be reduced. However, this is a common issue for the currently most developed CCS technologies.
- The significant risk of lowering the availability of the plant due to the introduction of the additional auxiliary equipment.

- The relatively low, permissible gradients for load change in the air separation unit compared to those for the thermal cycle could provide a problem with respect to operation of the plant in a system with a large amount of decentralized, non-constant electricity sources, e.g. wind mills. In Denmark, all central power plants are run with frequent changes in the load to adjust to the demand for electricity.
- The missing capability of current air separation units to run at low load without major penalties to the efficiency will require several oxygen plants running in parallel, as well as some sort of storage/buffer capacity. A storage capacity could partly solve some of the issues related to load changes, see above.
- The application of two purification steps, i.e. both the air separation unit and the pre-compression purification due to leakage of air into the flue gas ducts is one of the major disadvantages to the process. Post-combustion, in comparison, only needs the amine absorption step. The exact requirements for the final CO_2 quality are still to be determined and they will dictate the plant configuration with respect to the different purification units.
- The significant changes to the combustion process, including the potential effects on boiler heat uptake, fly ash quality, and fire-side corrosion likewise provide challenges.

Several of the above aspects are difficult to examine either theoretically or during small-scale tests. Only the operation of a larger-scale demonstration plant will provide the necessary information and experience.

The majority of issues regarding the combustion process are, on the other hand, possible to clarify in smaller scale experiments. Much work has already been done in this area including heat uptake and burner stability measurements as well as aspects regarding coal particle ignition, burnout, flame propagation, radiating properties of the flame, boiler efficiency, and changes in emission levels, see Section 1.3. However, several issues still require more insight in order to lay the ground for determining whether or not to apply oxyfuel combustion for carbon capture and storage in the future portfolio of power and heat producing plants.

1.3 OxyFuel vs Air-Firing – The Combustion Process

This section summarizes the knowledge found in open literature regarding oxyfuel combustion fundamentals and the relative variations when compared to conventional combustion in air. The chapter is build on the review paper "OxyFuel Combustion of Solid Fuels" [59] written by the author, see Appendix A.

1.3.1 Flame and Gas-Phase Temperatures

One of the key concerns when retrofitting conventional air-fired boilers to oxyfuel combustion is achieving similar temperature and heat uptake profiles in the radiative and convective sections of the boiler. The differences in thermo-chemical properties between CO_2 and N_2 causes changes in the heat and mass transfer rates within a boiler if CO_2 is substituted directly for N_2 in the oxidizer.

Data from pilot-scale experimental setups have shown that it is possible to match the temperature and heat uptake by increasing the inlet oxygen concentration during oxyfuel combustion to about 27-35 vol% compared to the 21 % found in air. The span covers the impact from fuel type and applied operating conditions, primarily the oxygen excess. High-rank fuels generally require an inlet concentration of oxygen in the upper end of the suggested interval while fuels of lower rank yield comparable tempeature profiles with lower oxygen inlet concentrations.

CO_2 and H_2O are radiating gases whereas N_2 is not. The radiative heat transfer in oxyfuel combustion is thus higher than in air combustion at the same flame temperature. In order to match the heat uptake profile in a retrofitted boiler the flame temperature should thus be kept lower than during air operation.

1.3.2 Ignition and Burnout

Devolatilization and ignition of coal particles are affected by the change in oxidizer composition from air to oxyfuel combustion. The rate of devolatilization is primarily determined by the surrounding gas temperature as the difference in thermal conductivity of N_2 and CO_2 is relatively small. Particle ignition, on the other hand, is a strong function of both the transport properties of the gas phase surrounding the particles as well as the combustion heat release rate and the reactivity of the local fuel-oxidizer mixture. Ignition times comparable to those observed during air combustion can be obtained by increasing the oxidizer oxygen concentration to 27-35 vol%, i.e. by achieving similar flame temperature to air-firing. Burnout of volatiles and char are likewise affected by the high CO_2 and H_2O concentrations in the flame. Especially the lower diffusivity of both oxygen and small hydrocarbons in CO_2 compared to N_2 is an important factor. Generally, an improvement in char burnout is reported in the literature when the oxyfuel combustion flame temperature matches that of air combustion. This improvement is assumed to be caused primarily by the higher oxygen partial pressure in the vicinity of the burning particles. Increased residence time of particles within the furnace due to a smaller flue gas volume would likewise contribute to an increase in the burnout efficiency for oxyfuel combustion compared to air-firing. Even though contribution of gasification by CO_2 and/or H_2O to the increased burnout is suggested several times in literature, it is questionable if this effect is of significant importance for the conversion of the fuel on the time scales relevant

to suspension-fired boilers.

CO levels in the flame zone are generally reported to increase significantly in oxyfuel combustion compared to air-firing. Even though the high CO_2 levels limits CO oxidation at high temperatures complete conversion is expected when excess oxygen is present during cool-down of the flue gas. CO emission rates similar to air combustion have been reported in literature for the larger of the test furnaces.

1.3.3 Formation of Gaseous Pollutants

The general conclusion in published literature is that the amount of NO_x emitted from an oxyfuel power plant can be reduced to somewhere between one-third and half of that from combustion in air. Sulphur oxides is the other major pollutant from coal-fired combustion. The emission of these oxides is, however, not reduced to the same degree as NO_x.

1.3.3.1 NO

The potential for reducing the NO_x emissions from a power plant considerably compared to air-firing has been one of the key drivers in oxyfuel combustion research, particularly in USA and thus, NO_x emissions from oxyfuel combustion is probably the single most investigated area of this technology.

Due to the very low levels of molecular nitrogen in the oxyfuel oxidant a potential exists to reduce the emissions rate considerably compared to combustion in air through near elimination of both thermal and prompt NO_x formation. The results reported in the literature generally show that combustion in air yields the highest NO_x emissions, oxyfuel combustion based on synthetic gas mixtures (CO_2 + O_2) yields lower emission rates at comparable conditions, whereas oxyfuel combustion with recirculation of flue gas yields the lowest emission rates. Reductions of up to 70–80 % have been reported for the latter. Different suggestions to the specific mechanisms responsible for the reduction have been proposed. However, it is generally accepted that reburning reactions play a major role. Experiments indicate that increasing the oxygen concentration and the oxygen excess yield higher emission rates. On the other hand, the use of oxidant staging, recycling of wet flue gas, increasing the partial pressure of NO_x in the oxidant, increasing the oxygen purity, and limiting the air ingress into the boiler works to decrease the emission rate.

Most of the reported experiments yield a decrease in the NO_x emission rate during oxyfuel combustion. However, some experiments show an increase which is suggested to be caused by the fact that the mechanism of Fuel-NO_x formation is very sensitive to the method with which oxygen and fuel is mixed in the flame. As oxyfuel burners are typically adopted from air-firing principles the resulting

fluid dynamics of the flame can be disadvantageous with respect to NO_x emissions even though the flames are stable.

1.3.3.2 SO_2

The substitution of N_2 by CO_2 in oxyfuel combustion does not affect the release of sulphur from the coal during combustion. However, the increased oxygen partial pressure necessary to maintain an appropriate flame temperature increases the formation rate of SO_3. During operation with a flue gas recycle without SO_2 removal the SO_2 and thus the SO_3 levels in the boiler and flue gas ducts increases significantly which will enhance the risk of sulphur-induced corrosion at both high and low temperatures. Increased risk of low-temperature corrosion by sulphuric acid condensation and a higher acid dew point are some of the major concerns regarding sulphur in oxyfuel combustion. High in-boiler concentrations of sulphur oxides can likewise increase retention of S in the fly ash. Increased retention will reduce the SO_2 emission rate but could at the same time yield problems with further utilization of the fly ash in cement and concrete production.

1.3.4 Ash and Deposit Formation

The transformations of coal mineral matter during combustion are affected by the temperature and the gas phase composition surrounding the coal particles. At low combustion temperature (for below 30 % O_2 in CO_2) a shift in the size distribution of the sub-mircometer sized fly ash towards smaller particles can be observed. Increasing the O_2 partial pressure to match the flame temperature of air combustion provides a size distribution similar to that found during air combustion. The ash quality is crucial to its application in cement and concrete production. Significantly increased sulphur retention could cause problems in this respect. The propensity for slagging and fouling in oxyfuel combustion is likewise subject to research. At this point, the reported results suggest that only minor changes compared to air-firing will result from the change in the combustion environment.

1.3.5 Co-Firing Coal and Biomass

Utilization of renewable biomass fuels such as wood, straw, and other energy crops in thermal power plants with carbon capture and storage is attracting increased attention. The combination of CO_2 neutral fuels with CCS opens up a possibility of extracting CO_2 from the atmosphere. Until now, only few experiments on oxyfuel combustion of biomasses have been reported in open literature. It is expected that further work on co-firing of biomass and coal in oxyfuel atmospheres will reveal comparable changes to the combustion fundamentals as is the case when biomass is introduced during combustion of coal in air. However, this area

of research is still relatively young when considering suspension-fired boilers and research on oxyfuel combustion of pulverized biomass could thus also be beneficial to the research within the conventional air-firing area.

1.4 Project Objectives

This PhD is aimed at improving the fundamental knowledge on oxyfuel combustion of coal and biomass (straw) at conditions relevant to suspension-fired boilers. The subjects specifically investigated cover:

- The general combustion characteristics of coal, straw and their blends (with 20 and 50 wt% straw) in an atmosphere of O_2/CO_2 with focus on the influence of excess oxygen and high CO_2 levels on burn-out
- Formation and emission of pollutants (CO, NO, and SO_2) as a function of excess oxygen, oxidant composition, and fuel
- The fate of N and S during simulation of flue gas recirculation without removal of NO and SO_2
- Ash and deposits characteristics – with emphasis on the chemical composition and the fate of potassium, sulphur, and chlorine during co-firing of biomass with coal
- The potential for reducing oxygen excess while maintaining high burnout

Comparison to representative reference data for combustion of coal, straw and their blends in air is performed. The objectives have been addressed by theoretical considerations and experiments in semi-technical scale. The following chapters contain the results of the work. The applied experimental setup and the methods used in the data treatment are presented in Chapter 2. Chapter 3 describes the observed differences in combustion fundamentals when changing the combustion atmosphere from N_2-based (air) to CO_2-based (oxyfuel) using pure coal as fuel. The impact on the combustion characteristics and the fly ash and deposit formation when pure biomass (straw) and blends of coal and biomass are combusted in air and oxyfuel atmospheres are discussed in Chapter 4. Chapter 5 is devoted the special topics related to the more specific process implications associated with oxyfuel combustion. The chapter is in two parts with the first part addressing the fate of N and S during simulation of flue gas recirculation without removal of NO and SO_2 for oxycoal combustion. The second part of Chapter 5 concerns potential improvements to the process economy for retrofitted power plants by means of reducing the oxygen demand. Chapters 6 and 7 summarize the work and point to more areas within the oxyfuel combustion technology which require further research.

Chapter 2

Experimental Methods

In the first part of this chapter, a short description of the experimental setup is given. A more thorough description is available in the design report for the setup [60]. The second part of this chapter provides overviews of the most important parts of the considerations regarding the operation of the experimental setup and the pre-treatment of the experimental data. The full description of the experimental considerations and calculation procedures is given in [61].

2.1 Description of the Experimental Setup

The 30 kW down-fired solid fuel combustor, shown in Figure 2.1 on the following page, has an inner diameter of 315 mm and a height of about 1.9 m. Table 2.1 on page 18 shows the design data for the setup. The combustion chamber is insulated with 80 mm two-layer refractory lining and cooled with room-temperature cooling air drawn through a void between the reactor shell and an outer insulation shell.

There are 8 measuring ports along the combustion chamber which can be used for e.g. thermocouples, gas sampling lines, deposit probe insertion, and other measuring probes. The ports are numbered 1 to 8, starting with 1 from the top. Fly ash is collected in the ash sampling system, see Figure 2.2 on page 15, which withdraws a portion of the flue gas through the bottom of the reactor. The sampling rate is between 60 and 150 L/min depending on the specific operating condition of the setup. Three fractions of ash are collected from the system designated "bottom", "cyclone", and "filter" ash. The results on fly ash composition, etc. will be from a mixture of those three fraction unless otherwise stated.

A loss-in-weight controlled twin-screw feeder (K-Tron K-ML-KT20-H-110L) feeds the pulverized solid fuel particles onto a vibrating table (Scan-Vibro) which acts as both a conveyor and for levelling out instabilities in the fuel flow from the feeder. From the vibrating table the fuel particles fall into the central, primary

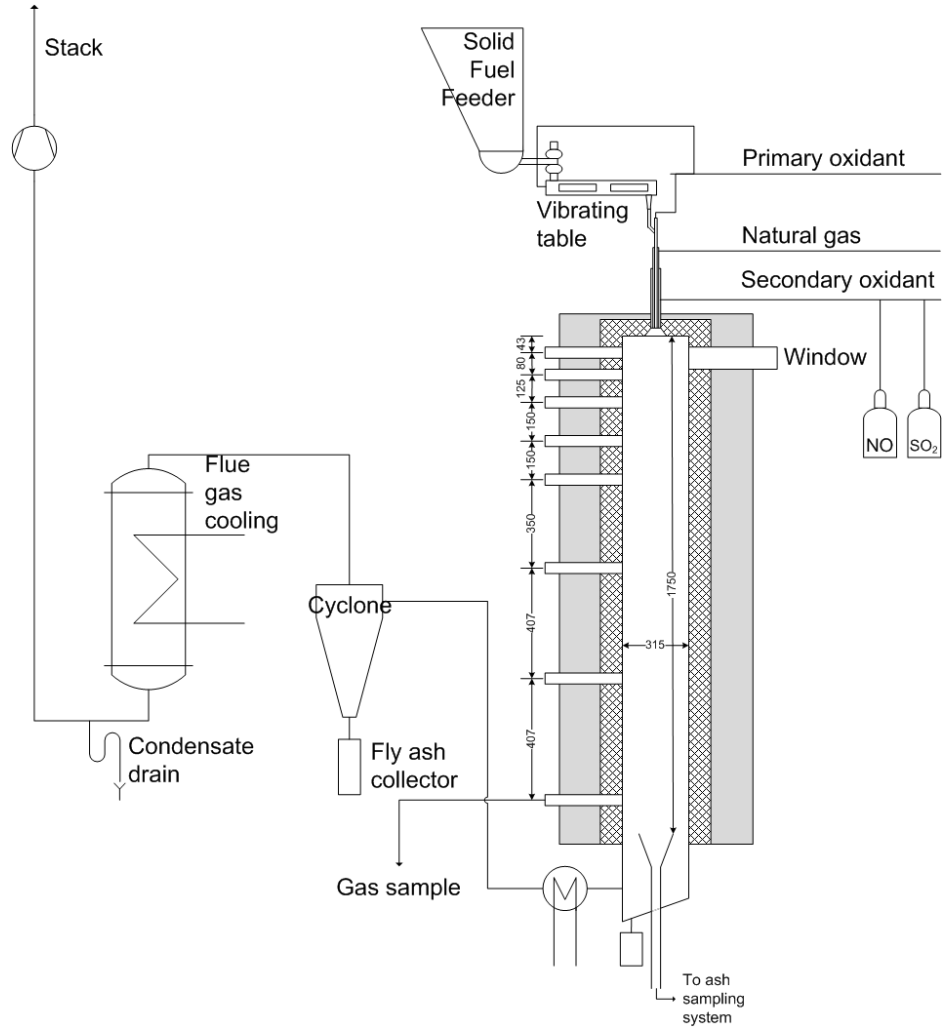

Figure 2.1: Schematic of the 30 kW swirl burner setup. All measures are in mm.

burner tube. A fraction of the primary oxidant is introduced in the back-end of the vibrating table to assist the feeding of fuel. The remaining, primary oxidant flow is fed directly into the central burner tube. The split between the two primary oxidant flows is adjusted during start-up of an experiment in order to achieve the best stability of the solid fuel feeding.

The burner is mounted on top of the combustion chamber as seen in Figure 2.3 on page 16. It consists of three tubes, two for primary and secondary oxidant and a separate natural gas inlet which is used during reactor heat-up and during the transition to the solid fuel flame. The secondary oxidant is introduced in the burner in two separate streams, an axial flow and a tangential flow. The latter is responsible for creating a swirling motion and the swirl number is adjusted by choosing the ratio between the axial and tangential flow. A detailed diagram of the burner is seen in Figure 2.4 on page 17.

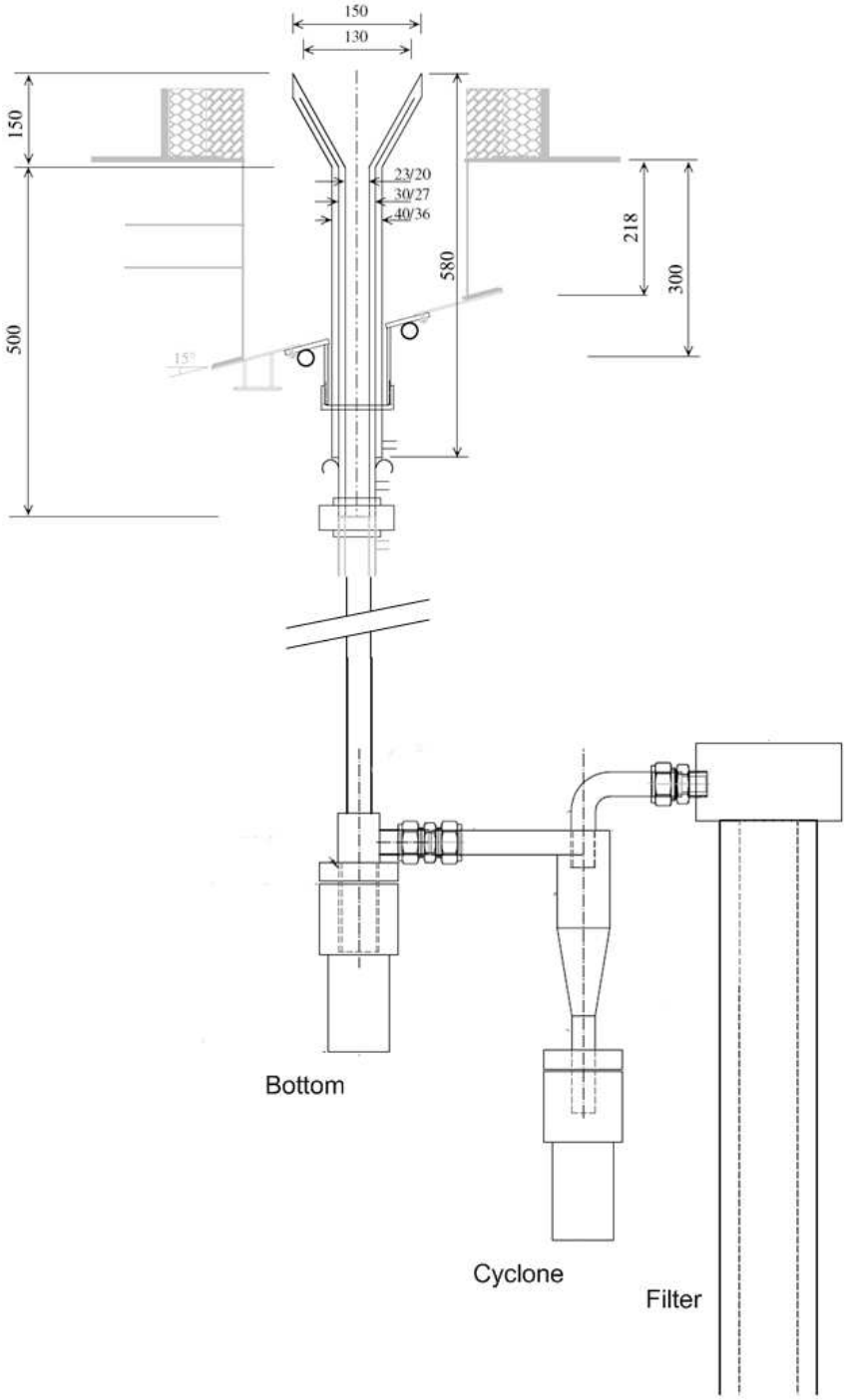

Figure 2.2: Sketch of the ash sampling system. The system consists of an about 2.5 m long vertical tube with a funnel, which is inserted through the bottom of the reactor. The vertical tube ends in a heated cup which collects the ash particles too big to follow the flue gas stream drawn through the cyclone and the filter. The cut-size of the fly ash sampling filter is 1 μm.

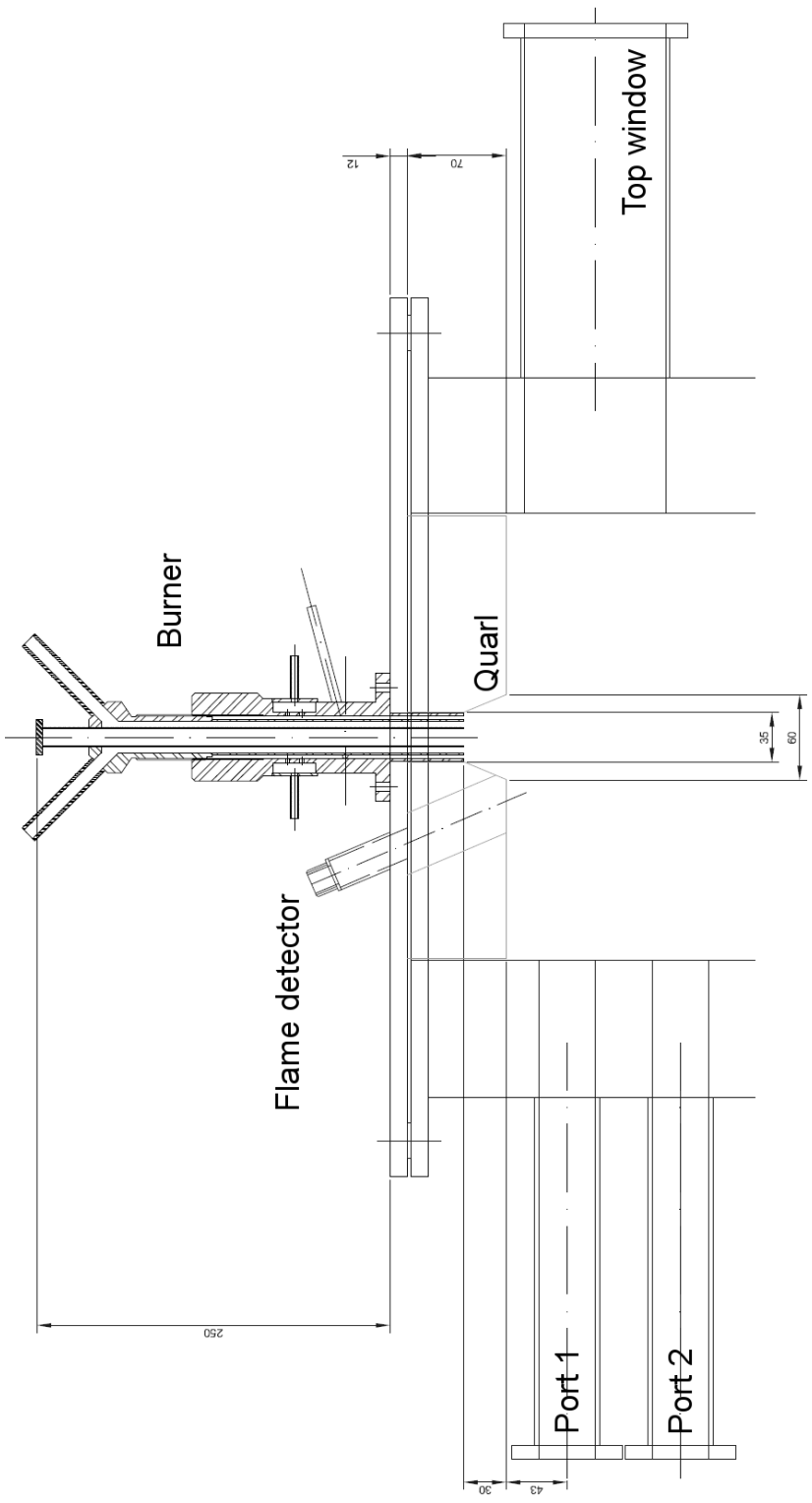

Figure 2.3: Detailed sketch of burner mounted in the top of the reactor chamber.

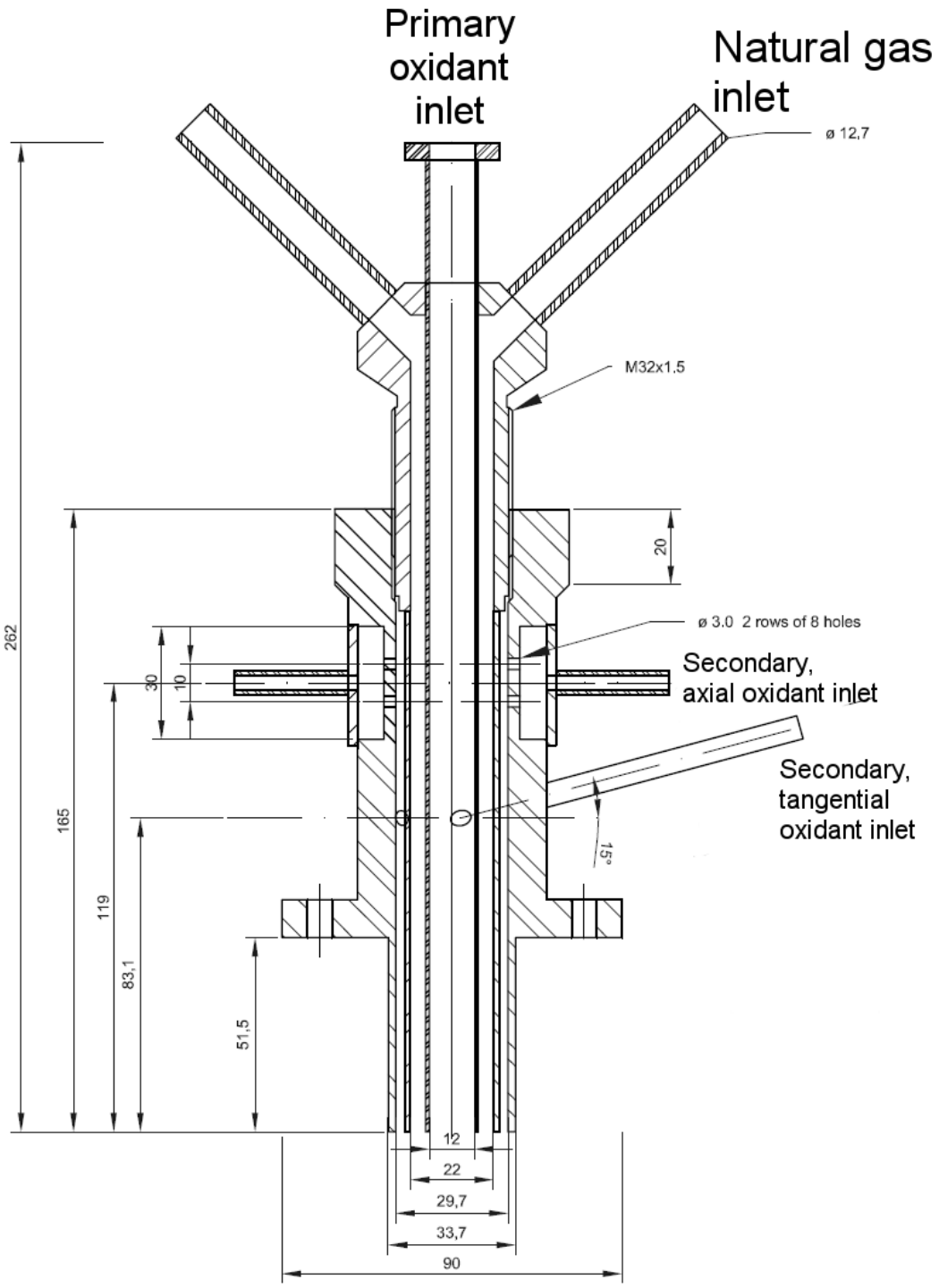

Figure 2.4: Detailed sketch of burner.

Table 2.1: Design data for experimental setup

Parameter	Value
Reactor inner diameter	315 mm
Reactor height, total	1.9 m
Port 1, distance from burner	43 mm
Port 2, distance from burner	123 mm
Port 3, distance from burner	248 mm
Port 4, distance from burner	398 mm
Port 5, distance from burner	548 mm
Port 6, distance from burner	898 mm
Port 7, distance from burner	1305 mm
Port 8, distance from burner	1712 mm
Ash sampling system, distance from burner	1.75 m
Sampling rate, ash sampling system	60–150 L/min
Flue gas sampling position	Port 8
Flue gas sampling rate	3 L/min
Deposit sampling position	Port 7
Temperature mapping, ports:	1-5, 7

For both air and oxyfuel experiments the primary oxidant flow is set at 20 vol% of the total oxidant flow at the reference conditions. This implies that the linear velocity of the primary oxidant leaving the burner will differ when the combustion atmosphere and/or the stoichiometry is changed. However, the swirl number is kept constant to obtain similar conditions for air and oxyfuel experiments.

The flow of oxidant is controlled by manual valves and adjusted according to readings from rotameters. A more accurate monitoring is performed by mass flow controllers in the oxidant mixing panel. The mass flow controllers are likewise responsible for correctly mixing the oxidant for oxyfuel experiments according to settings which are controlled in LABVIEW.

The combustor is heated by natural gas combustion over-night or for at least 14 hours before an experiment starts in order to achieve stable temperatures of the reactor lining. For oxyfuel combustion experiments the oxidant is switched to an O_2/CO_2 mixture before the solid fuel feeding is started. After a minimum of 1 hour with pure solid fuel combustion the combustion chamber temperature profile as well as the flue gas composition have stabilized and the measurements and sampling can be initiated. Depending on the scope of the test the measurements will proceed for about 2-6 hrs.

The reactor is a once-through type reactor and thus has no ducts for recirculating flue gas in oxyfuel operation. O_2/CO_2 mixtures are produced at chosen

molar ratios from gas bottles in the oxidant mixing panel. The primary and secondary oxidant flows are of the same composition. When adding NO and/or SO_2 to the oxidant in order to simulate recirculation of flue gas without prior gas cleaning (oxyfuel), these components are solely added to the secondary, tangential fraction of the oxidant. For air combustion the oxidant is supplied as pressurized air.

Flue gas samples are continuously drawn from the lowest measuring port (#8). The gas sample is filtered and dried before entering on-line gas analysers. Two analysers (Rosemount NGA 2000) are available, one which measures O_2, CO, and CO_2, and one which measures NO and SO_2. NO_2 has not been measured as it has been assumed that only negligible amounts leaves the reactor at the relatively low oxygen excess ratios and temperatures utilized [62]. For oxyfuel experiments with high oxygen concentration in the oxidizer (> 40 %), a measurable amount of NO_2 may be formed in the flame. However, it will most likely be destroyed before reaching the flue gas sampling position [62]. Different ranges are available for the individual gases on each analyser and the calibration is performed according to the expected flue gas composition. For oxyfuel experiments, CO_2, N_2, and O_2 are simultaneously measured on a MicroGC (Varian CP-4900) about every 2 minutes. The radial variation of the flue gas composition at port 8 was found to be relatively small during a test on a natural gas/air flame. Unless otherwise specifically noted, the flue gas sample is thus retrieved from within port 8 and not from the centre of the reactor in order to limit the dust loading on the flue gas particle filter.

2.2 Solid Fuel

2.2.1 Fuel Characterization

During the experiments two different fuels have been utilized, a bituminous coal from El Cerrejon, Colombia (COCERR), and pulverized straw pellets made from cereal straw (wheat and barley in a non-specified ratio). Fuel analysis have been performed by the laboratory at Ensted Power Station and the results are seen in Table 2.2 on the next page. The coal was delivered in 2007 from the OxyCoal-UK project in which DONG Energy participated and was ground at delivery. The straw was delivered as pellets from Køge Biopillefabrik in March 2010. The pellets were pulverized by Teknologisk Institut with a specification of 100 % being below 700 μm. The measured particle size distribution for the two fuels is shown in Figure 2.5 on page 21. The median particle sizes for the two fuels are given in Table 2.2.

The mean particle size of the straw is generally much smaller than usually utilized when co-firing straw at low weight fractions in suspension-fired boilers. However, when biomass constitute the major fraction of the fuel in suspension-

Table 2.2: Properties of El Cerrejon bituminous coal (Colombian) and Danish, pulverized, cereal straw pellets.

Fuel	**Coal**	**Straw**
KT Journal number	228-66	228-77
Heating value (MJ/kg, as received)		
LHV	27.09	16.40
Proximate analysis (wt%, as received)		
Moisture	5.03	5.10
Ash	9.62	4.40
Volatile	34.86	72.40
Fixed carbon (by difference)	50.49	18.10
Ultimate analysis (wt%, daf)		
C	80.70	48.62
H	5.41	6.41
N	1.69	0.49
S	0.726	0.094
Cl	0.016	0.419
O (by difference)	11.46	43.97
Ash forming elements composition (wt%, dry)		
Al	1.1	0.011
Ca	0.16	0.44
Fe	0.51	0.0076
K	0.18	1.00
Mg	0.14	0.054
Na	0.060	0.050
P	0.0078	0.062
Si	2.7	0.91
Ti	0.054	0.008
Bulk density (kg/m^3)	1000	450
Particle diameter, median/d_{50} (μm)	47	330

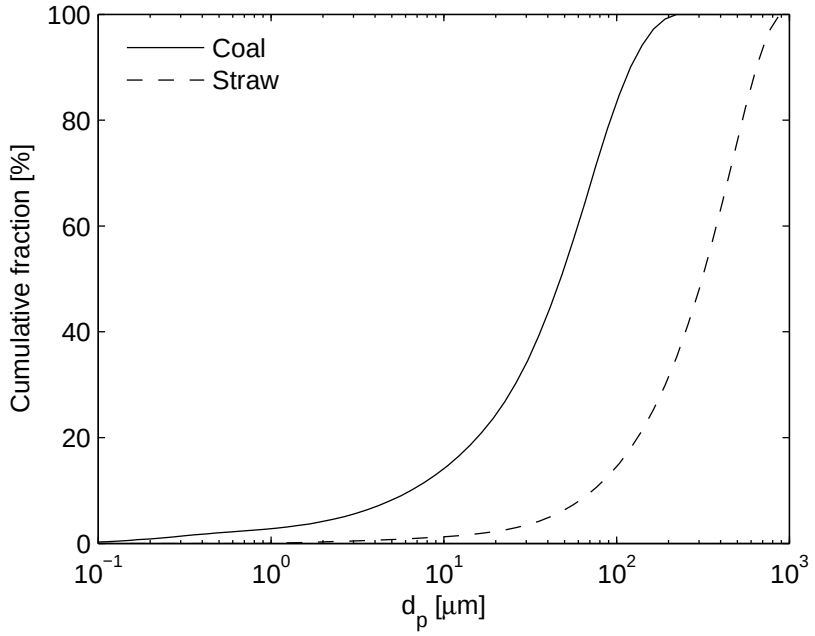

Figure 2.5: Cumulative particle size distributions for coal and straw. The distribution type is volumetric and is obtained from a Malvern laser diffraction particle size measurement.

fired boilers the particle size distribution is closer to the one used in the present experiments. The main reason is the need for the biomass to aid in flame stabilization. When co-firing straw up to about 20 wt%, coal acts to stabilize the flame and less strict demands regarding the particle size of the straw particles are necessary.

For experiments simulating co-firing of coal and straw two mixtures have been made by Teknologisk Institut. The mixtures have a 20 and 50 wt% content of straw. This corresponds to approximately 13 and 38 % straw on a thermal basis, respectively. The 20 wt% mixing ratio has been chosen based on the fact that it constitutes the maximum limit for the case where the fly ash is used for concrete [63]. The 50 wt% ratio is designed to give a relatively even distribution between datapoints and to aid in investigating the ability of coal to capture large amounts of potassium from biomass, which is important from a corrosion and $DeNO_x$ catalyst deactivation perspective.

The ratios of coal to straw in the blends were checked with TGA after arrival [61]. The average straw shares in each blend are seen in Table 2.3 on the next page. Note that the 50 wt% blend was delivered in two batches. The deviation from the specified straw share for the 50 wt% blends is taken into account in the data treatment.

Table 2.3: Overview of measured straw shares for fuel blends

Specified straw share	20 wt%	50 wt%, B1[a]	50 wt%, B2
Measured	20	52	46

[a] B1 = Batch 1, B2 = Batch 2

Table 2.4: Solid fuel feeder set points for applied fuels

Fuel	Feeding rate, SP [kg/hr]
Coal	3.99
20 wt% straw blend	4.33
50 wt% straw blend	5.0
Straw	6.6

2.2.2 Fuel Feeding Rates

For all experiments reported the solid fuel feeding system has been operated at a set point corresponding to a thermal load of 30 kW. Table 2.4 shows the set points of the feeding system for the different fuels which have been investigated.

The solid fuel feeding rate is logged as the feeder net weight signal in each data sampling point (usually each second). The actual feeding rate can thus theoretically be determined from the slope of the weight signal in each data point. Figure 2.6 on the next page shows an example of the net weight signal during straw combustion and illustrates the limited number of bits in the data sampling system causing the data points to be stair shaped with a step height corresponding to approximately 55 g.

Due to the nature of the data, one of two options for determining the fuel feeding rate can be chosen; (1) calculating an average feeding rate based on the data for the entire experiment, or (2) make an estimation based on a given number of data points before and after the data point (time) of interest.

The solid fuel feeding rate has been observed to yield both fast and slow fluctuations due to perturbations caused by e.g. step changes of the sub-pressure in the reactor and occasionally insufficient PID parameters in the control system of the feeder. A feeding rate based on (2) is thus likely to yield a better estimate of the instantaneous value provided the averaging time interval around the data point is of an appropriate size.

Figure 2.7 on the facing page shows the calculated fuel feeding rate during a limited time interval for an experiment with combustion of pure straw. The figure likewise shows the feeder set point, the average feeding rate for the entire period with solid fuel feeding, and the average feeding rate during the time interval

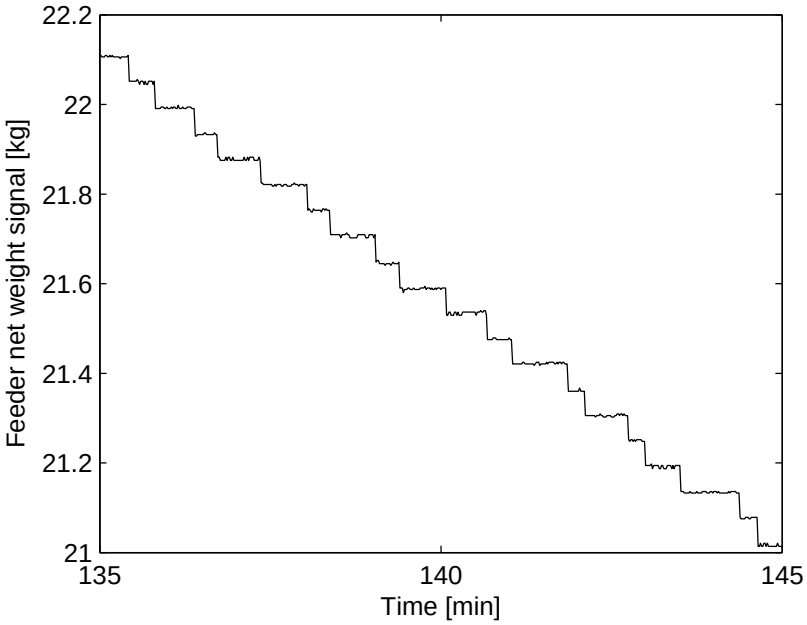

Figure 2.6: Example of weight signal from solid fuel feeder as a function of time for combustion of pure straw.

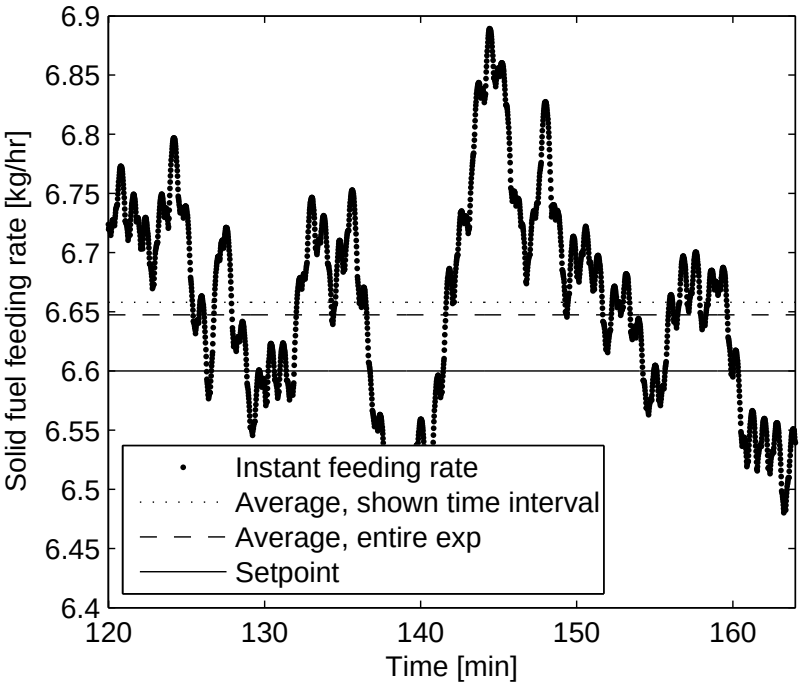

Figure 2.7: Calculated instantaneous and averaged solid fuel feeding rates for an experiment with combustion of pure straw.

shown in the figure. It is seen that the instantaneous feeding rate fluctuates on both a short and long time scale. A small deviation in feeding rate (~ 1 %) from the feeder set point is likewise observed, both for the selected time interval and for the entire experimental run.

In general, the average feeding rate is satisfactorily close to the set point. However, fluctuations occur which will have an impact on the combustion process. The instantaneous fuel feeding rate is thus used during the data treatment.

2.3 Experimental Considerations and Calculation Procedures

This section describes calculation procedures related to the evaluation of the collected experimental data and the considerations and assumptions made in that respect. The section also includes analysis procedures for the samples collected during the experiments. Additionally, examples of the determination of operating conditions based on the available measurements from the setup are given.

2.3.1 Data Structure

52 of the experimental runs performed on the swirl burner setup have been selected for data treatment. The sections below provide an introduction to the data collected during the individual experiments.

2.3.1.1 Numbering of Experiments

The experiments are numbered according to the following principle:

$$\text{Exp no.} = \text{XY\#\_E} \tag{2.1}$$

where X designates the fuel (S = straw, C = coal, M20 = 20% straw/coal blend, M50 = 50 % straw/coal blend), Y is the oxidant (A = air, O = oxyfuel), # is a running number for the specific combination of fuel and oxidant, and E indicates any additional data besides measurements of the exit flue gas composition (A = ash sampling, D = deposit sampling, T = temperature mapping with S-type thermocouple, M = Mapping with FTIR probe, L = oxygen excess different from the reference value of 5 vol% O_2 in dry flue gas, B = burner settings variation tests, S = SO_2 addition to oxidant, N = NO addition to oxidant). An example:

$$\text{Exp no.} = \text{SO05\_ADLT}$$

In the given example pure straw (S) has been combusted in O_2/CO_2 (O). The experiment is the fifth for that fuel/oxidant combination (05) and the stoichiometry was different from the reference conditions chosen (L). During the experiment fly ash (A) and a deposit sample (D) has been collected and a temperature profile was measured with a thermocouple (T).

2.3.1.2 Operating Parameters Overview

Table 2.5 on the next page provides an overview of the settings and variations of the key operating parameters applied during the experimental campaign. The table is divided according to the oxidant type and the four different fuels investigated. A further sub-division is made for oxyfuel combustion experiments with respect to the oxidant composition. More specific settings regarding individual oxidant flows and sampling rates can be seen in [61].

2.3.1.3 Raw Data

During experiments numerous data are logged. Most data are sampled automatically with LABVIEW; pressures, temperatures, gas concentrations, flows of NG and oxidizer, etc. For each experiment a data file is thus produced which contains the necessary data to characterize and analyse the experiment. The data have typically been logged with an interval of one second. Other data are logged manually or semi-automatically; flow rates of oxidizer to the individual registers of the burner, ash sampling velocity, as well as gas analysis results from the MicroGC.

Figure 2.8 on page 27 shows an example of the most important online data logged for an experiment with air as oxidant (M20A01_ADT). The specific experiment is for the 20 wt% straw/coal blend as fuel. During the experiment both fly ash and a deposit sample has been collected, and a temperature mapping has been performed. Time 0 corresponds to the initiation of the change from a NG flame to solid fuel feeding.

The flue gas composition is observed to fluctuate with a relatively high frequency. This is caused by formation of fuel agglomerates on the vibrating table which leads to instabilities in the fuel supply to the burner. From the CO_2 and O_2 data variations in the average fuel flow to the burner can likewise be observed as fluctuations with a significantly lower frequency. Deviations in the fuel flow from the set point are typically caused by disturbances of the reactor pressure which again influences the solid fuel feeding system.

From the NO and SO_2 data the approach to steady state for the solid fuel flame can be observed as a decrease and increase, respectively, in the concentrations over a period of approximately 90 minutes. Typically, this stabilization period is also associated with a change in the temperature at port 5. The reason is mainly that the NG flame is significantly shorter than the solid fuel flame and hence the temperature profile of the reactor will change, even though it was attempted to match the adiabatic temperature of the NG flame to the solid fuel flame. The approach to steady state has been observed to occur at different velocity for each experiment, depending primarily on the setting for the NG flame run prior to the experiment and the solid fuel, with coal stabilizing faster than pure straw, the coal flame being significantly shorter.

Table 2.5: Overview of operating parameter set points and their variations during the experimental campaign

	Load	Fuel flow	Inlet O_2	λ	Flue gas exit O_2	Oxidant flow	Swirl number	Inlet NO	Inlet SO_2
Air	[kW_{th}]	[kg/hr]	[vol%]	[-]	[vol%, dry]	[Nl/min]	[-]	[ppmv]	[ppmv]
Coal	30	3.99	-	1.1, 1.15, 1.25, 1.3	2, 2.8, 4.3, 5	525, 550, 595, 620	1.7, 1.8, 1.9, 2	-	-
Straw	30	6.6	-	1.3	5	600	1.8	-	-
20 wt% blend	30	4.33	-	1.3	5	620	1.8	-	-
50 wt% blend	30	5.0	-	1.3	5	615	1.8	-	-
Oxyfuel									
Coal	30	3.99	25	1.24	5	490	1.8	-	-
Coal	30	3.99	30	1.13	3.5	370	1.8	-	-
Coal	30	3.99	30	1.19	5	390	1.8	0, 500, 1300, 2000	0, 500, 1500, 3500
Coal	30	3.99	33.3	1.16	5	345	1.8	-	-
Coal	30	3.99	35	1.15	5	325	1.8	-	-
Straw	30	6.6	30	1.22	5	390	1.8	-	-
Straw	30	6.6	40	1.09	3	260	1.8	-	-
Straw	30	6.6	50	1.025, 1.05, 1.075, 1.09	1, 2, 3, 3.6	195, 200, 205, 208	1.7, 1.8, 1.9, 2	-	-
20 wt% blend	30	4.33	30	1.19	5	390	1.8	-	-
50 wt% blend	30	5.0	30	1.2	5	390	1.8	-	-

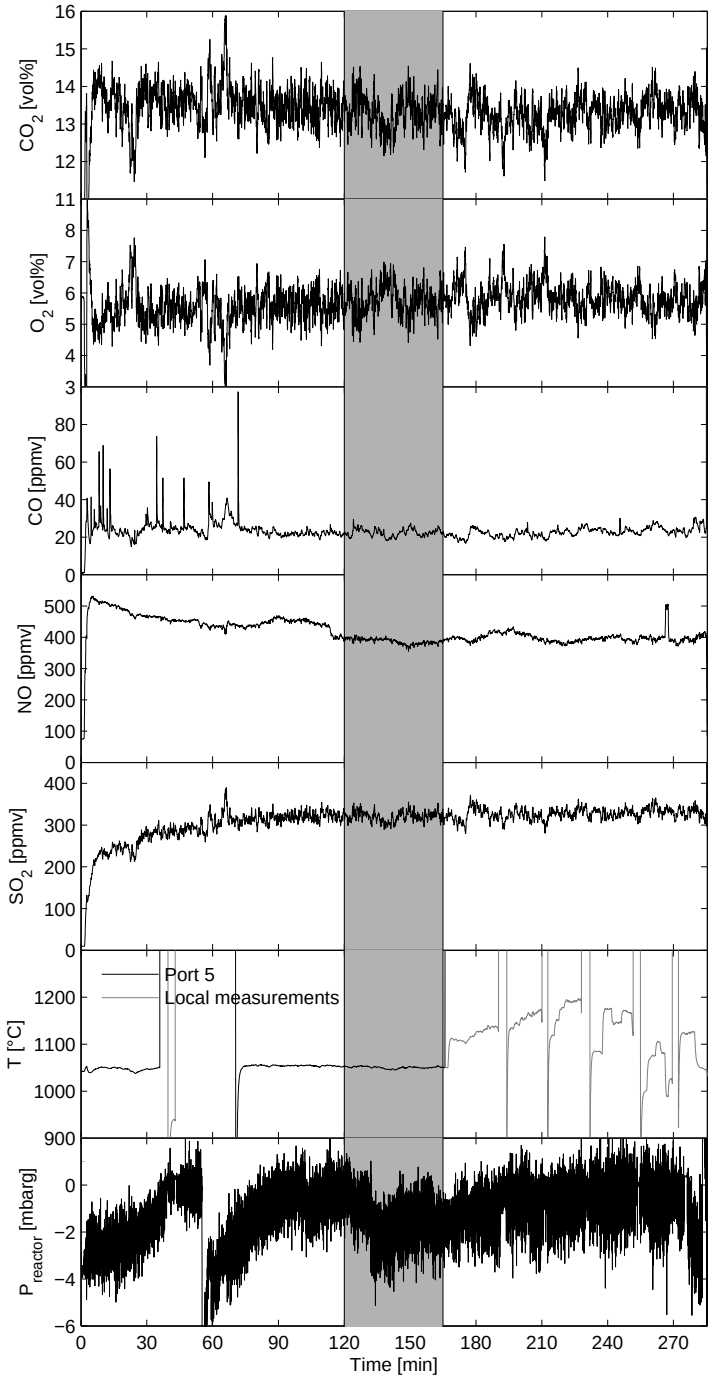

Figure 2.8: Concentrations of major flue gas components (CO_2, O_2, CO, NO, and SO_2) as function of time for experiment M20A01_ADT, as well as the pressure at the top of the reaction chamber, the reference temperature measured at the reactor wall at a vertical position about 55 cm from the burner (port 5), and the local temperature measurements conducted with the S-type thermocouple probe. The shaded area indicates the part of the data which are used during further data analysis.

The data within the time interval patched in grey are used for calculating mass balances, determining emission rates, conversion ratios of fuel-N and -S, etc. The time interval is preferably situated in a period where the reactor has reached steady state, has run stably, and without any measurement ports being opened to the surroundings in order to limit false air ingress.

Figure 2.9 on the next page shows the corresponding data for coal combustion at oxyfuel conditions (CO16_AL). Since the online gas analyser cannot measure CO_2 concentrations above 25 vol% it cannot be used for oxyfuel flue gas. Instead, the microGC is used to collect CO_2 data. The microGC measures O_2 and N_2 in addition to the CO_2 and these data are likewise shown. The sampling interval for the microGC measurements is significantly longer than the one second obtainable for the online analysers. Typically, the microGC provides data with a 1.5 to 2 minute interval.

Good correlation between the online and GC measurements of O_2 is observed. The N_2 measurements are seen to follow the trend of the reactor pressure. The N_2 present is a consequence of air leaking into the reactor system, with the ingress being a direct function of the sub-pressure in the reactor. The level of false air ingress is typically below 5 % of the total oxidant flow. Frequent CO peaks are registered compared to the example in Figure 2.8. This is caused by the fact that the stoichiometry for the oxyfuel example is lower and the sensitivity of the combustion process to fuel feeding instabilities thus has increased. The CO peaks in the time interval patched in grey are directly correlated to peaks in SO_2 which indicates feeding of excess fuel compared to the set point at distinct times.

An overview of all experiments can be found in the data collection [64]. For each experiment the objective is stated together with the basic operating parameters and a list of comments to the course of the experiment. For all experiments the flue gas, temperature, and pressure data are shown.

2.3.2 Sampling

In order to characterize the combustion process at the investigated operating conditions three types of samples are drawn from the setup; Flue gas, fly ash, and deposits. The following sections describe the sampling methods.

2.3.2.1 Flue Gas

Flue gas is continuously drawn from measurement port #8 (at a vertical position 1.7 m downstream of the burner within the furnace chamber) by the aid of a gas pump situated in a gas conditioning system. The flow rate is about 3 L/min. The gas conditioning system removes particles and moisture from the gas sample.

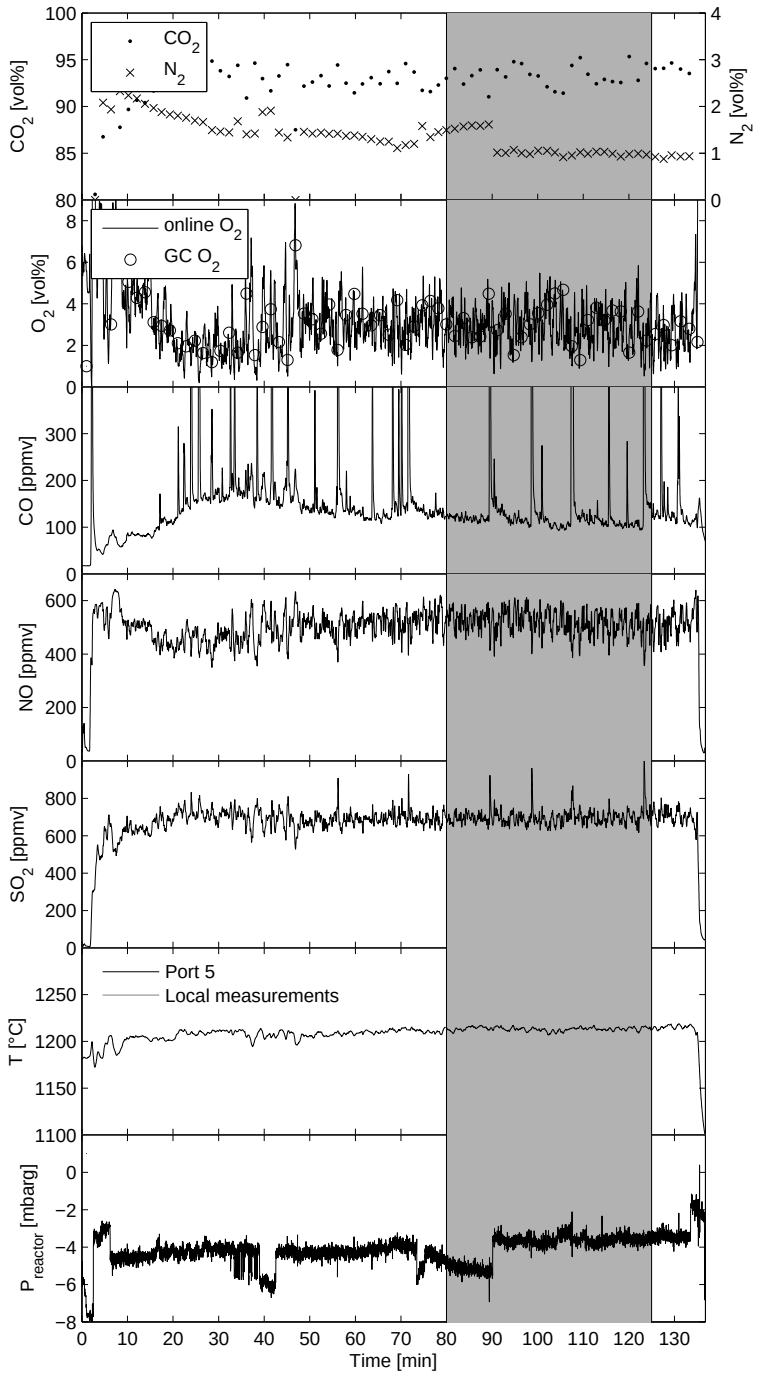

Figure 2.9: Concentrations of major flue gas components (CO_2, N_2, O_2, CO, NO, and SO_2) as function of time for experiment CO16_AL as well as the pressure at the top of the reaction chamber, and the reference temperature measured at the reactor wall at a vertical position about 55 cm from the burner (port 5). No local temperature measurements have been performed. The shaded area indicates the part of the data which are used during further data analysis.

Table 2.6: Uncertainties on flue gas species measurements dependent on measuring range and calibration gas

Gas species	Range UL[a]	Cal. gas	Uncertainty[b]
O_2	10 %	9.52 %	0.2 %
O_2	5 %	4.5–5.0 %	0.1 %
CO_2	25 %	18.8–19.3 %	0.5 %
CO	4000 ppm	3800 ppm	90 ppm
CO	1000 ppm[c]	100 ppm	10 ppm
NO	1500 ppm	900 ppm	20 ppm
SO_2	2500 ppm	2500 ppm	60 ppm
SO_2	1500 ppm	950 ppm	20 ppm
SO_2	500 ppm	460 ppm	10 ppm
O_2, μGC	10 %	0–9.52 %	< 0.2 %
N_2, μGC	100 %	0–99.95 %	< 0.2 %[d]
CO_2, μGC	100 %	0–99.95 %	< 1 %

[a] UL = upper limit

[b] Total uncertainty on measurement

[c] Lowest UL available for CO

[d] For measurements below 10 % N_2

Uncertainty on Flue Gas Composition from Continuous Gas Analysers The online gas analysers are calibrated prior to each experiment and adjusted if necessary. The gas species concentrations determined by the analysers are associated with an uncertainty. The uncertainty is the sum of the instrument uncertainty which is 1 % of the chosen measurement range and the uncertainty on the calibration gas composition (2 % on each species in the gas for all applied calibration gases). Table 2.6 provides an overview of the generel uncertainties on the flue gas measurements.

Evaluation of Flue Gas Data The raw flue gas measurements are used to determine several quantities with which the individual experiments are compared. It is difficult to compare experiments performed at different operating conditions based directly on the measured concentration of flue gas species. Instead, a parameter such as the emission rate (also denoted the specific emission) of NO, SO_2, and CO can be used. The emission rate corrects the NO, SO_2, and CO data for variations in stoichiometry, etc., and can be determined from Eq. (2.2).

$$\mathrm{E}_i = \frac{y_i \cdot F_{FG,\,dry} \cdot M_i}{\dot{m}_{SF} \cdot LHV} \qquad [\mathrm{mg/MJ}] \tag{2.2}$$

where y_i is the mole fraction of species i in the dry flue gas, $F_{FG,\,dry}$ is the dry flue gas flow [mole/s], M_i is the molar mass of species i [mg/mole], $\dot{m}_{SF}$ is the

mass flow rate of solid fuel [kg/s], and LHV is the lower heating vale of the fuel [MJ/kg].

With respect to NO and SO_2 another parameter used in the data analysis is the Fuel-N to NO or Fuel-S to SO_2 conversion ratio (CR). The conversion ratio is calculated from Eq. (2.3).

$$\mathrm{CR}_i = \frac{y_i \cdot F_{FG,\,dry} \cdot M_i}{x_{i,\,fuel} \cdot \dot{m}_{SF}} \qquad [\%] \tag{2.3}$$

$x_{i,\,fuel}$ is the mass fraction of N or S in the fuel.

2.3.2.2 Fly Ash

Fly ash is sampled through the bottom of the reactor. The sample probe is funnel shaped and the inlet to the probe has a diameter of 150 mm. The probe centreline is aligned with the reactor centre. The probe covers approximately 23 % of the cross sectional area of the reactor.

In order to sample fly ash with a size distribution comparative to the overall distribution in the flue gas, isokinetic sampling should be performed. During ash sampling the flow rate through the ash sampling system has been adjusted in order to reach near-isokinetic conditions under the assumption of a flat velocity profile. The assumption of a flat velocity profile is rather crude since the flow at the reactor outlet is laminar (Re $\approx$ 1000). However, due to the position of the sampling probe in the reactor bottom it has been assumed that the ash particle size distribution in the sample will not differ significantly from the overall distribution, even though ideal sampling is not performed. The construction of the ash sampling system, see [60], makes it very difficult to accurately control the flow rate through the probe as it is adjusted with a ball valve and according to readings of the sub-pressure at the sampling pump. The flow rate is calculated based on readings from a gas meter.

Ideally, the ash sampling system should collect 23 % of the ash species fed with the solid fuel. However, part of the ash is deposited within the reactor and the ash yield will thus be below 100 %. Ideal conditions also include a perfectly even distribution of the ash across the reactor cross-sectional area. Visual observation of the flames showed a tencency for larger particles to be concentrated around the burner/reactor centreline. This could lead to a biased size distribution with a relatively higher number of large particles. The yield of ash, Y_{ash}, is determined from (2.4).

$$Y_{\mathrm{ash}} = \frac{m_{\mathrm{ash,\,sampled}}}{m_{\mathrm{ash,\,sampled,\,theoretical}}} \tag{2.4}$$

Where $m_{\mathrm{ash,\,sampled,\,theoretical}}$ is determined according to (2.5):

$$m_{\mathrm{ash,\,sampled,\,theoretical}} = \dot{m}_{ash,\,SF} \cdot \Delta t_{ash} \cdot \frac{F_{ash\,sampling}}{F_{FG,\,dry}} \tag{2.5}$$

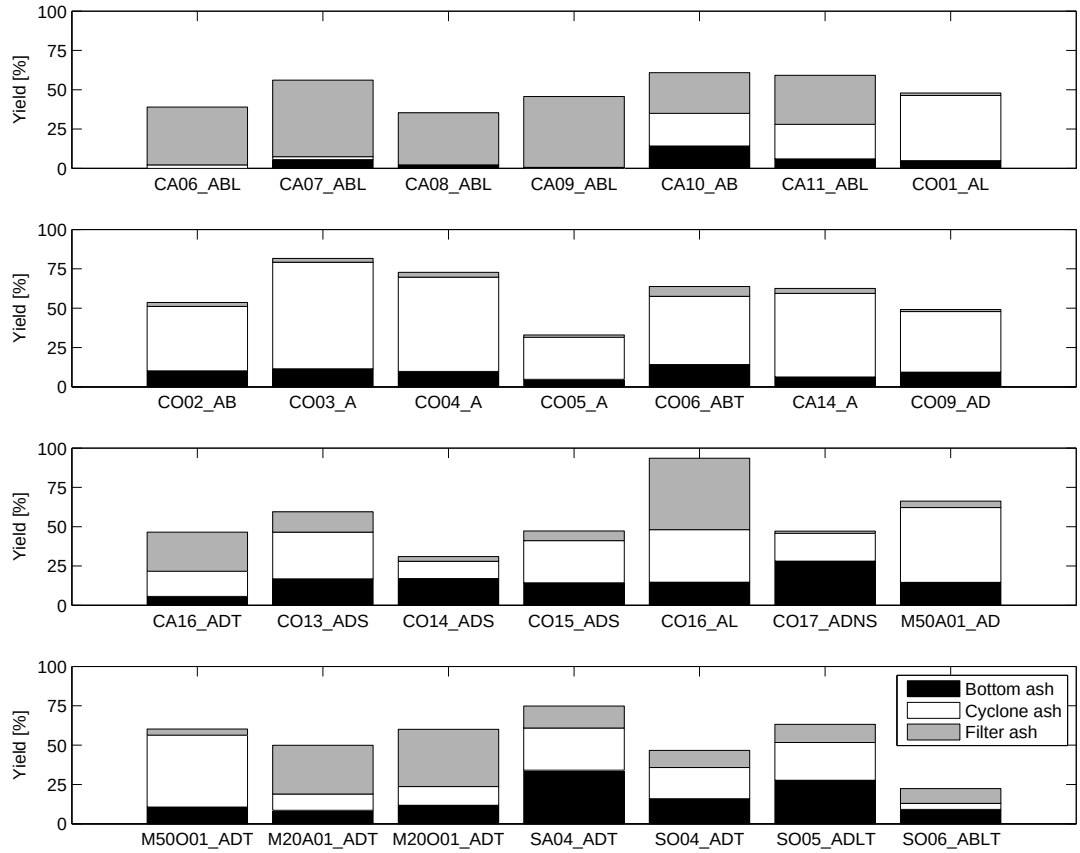

Figure 2.10: Ash yields for all experiments with ash sampling listed in chronological order. The yield is determined from the sampling flow-based method. The distribution of the total ash sample on the three fractions; bottom, cyclone, and filter ash, is given.

$\dot{m}_{ash,\,SF}$ is the mass flow of ash fed in with the solid fuel (SF), Δt_{ash} is the time with ash sampling, $F_{ash\,sampling}$ is the average flow rate through the ash sampling system and $F_{FG,\,dry}$ is the dry flue gas flow. $F_{FG,\,dry}$ is determined at ideal conditions, i.e. without false air ingress, see Appendix B, Eq. (B.7). The dry flue gas flow is used since the flow rate through the ash sampling system likewise has been measured when dry.

Figure 2.10 shows the obtained ash yields for all experiments with ash sampling. The total yield is divided on the three ash fractions collected from the sampling system. From the data it is seen that the ash yield for the majority of experiments is about 50 %. However, both significantly higher and lower yields have been obtained. The very low yields could have been caused by partly blockage of the ash sampling system, e.g. by deposits that have fallen into the probe. For experiments with very high yields there may be a risk that ash from a prior experiment has been transfered. However, this risk is small as the sampling system was cleaned after each run.

The distribution of ash between the three positions in the sampling system is seen to vary. There is a tendency for filter ash to be the primary fraction during coal/air experiments and for cyclone ash to be the primary fraction during coal/oxyfuel experiments. A possible explanation could be the lower flow rate through the sampling system (90 Nl/min versus 150 Nl/min, typically) for oxyfuel experiments. The lower flow rate provides a longer residence time in the cooled section of the probe. Combined with the higher concentration of H_2O in the oxyfuel flue gas (9 % versus 6 %) the ash particles may be more moist when reaching the cyclone leading to a higher collection efficiency. The split between the three fractions does not have an effect on the final results for the individual experiments. The same trend is not seen for the latter experiments with the other fuels. The relatively high bottom ash yields for straw experiments is caused by large char particles ($d_p = 0.5 - 1$ mm).

2.3.2.3 Deposits

A deposit probe, see Figure 2.11 on the following page, was used to collect samples from a fixed position in the reactor (port #7, 1.3 m from the burner). The probe has an outer diameter of 16 mm and an inserted length of 275 mm. The probe is inserted perpendicular to the flue gas flow. The deposit probe is cooled by pressurized air and the metal surface temperature is kept at an average about 500 ℃ by adjustment of the cooling air flow.

In connection with inserting the deposit probe the flue gas temperature at the reactor centre was measured with an S-type thermocouple. The measured temperature was generally in the range 900-950 ℃.

The deposit samples were collected by scraping off the deposit from the probe. The deposit was removed separately from the downstream and upstream parts of the probe in order to determine the mass of each fraction.

Based on the collected masses of deposit, m_{dep}, the deposit flux, N_{dep}, can be determined, see Eq. (2.6).

$$N_{dep} = \frac{m_{dep}}{A_{probe} \cdot \Delta t} \quad [\mathrm{g/m^2 \cdot hr}] \tag{2.6}$$

A_{probe} is the upstream or downstream area of the probe (half the surface area of the probe) and Δt is the time during which the deposit has been collected, typically 2 hr.

2.3.2.4 Analysis of Fly Ash and Deposit Samples

All fly ash samples have been analysed for their loss-on-ignition (LOI). LOI is used as a measure of the burnout efficiency of the fuel. LOI is determined from

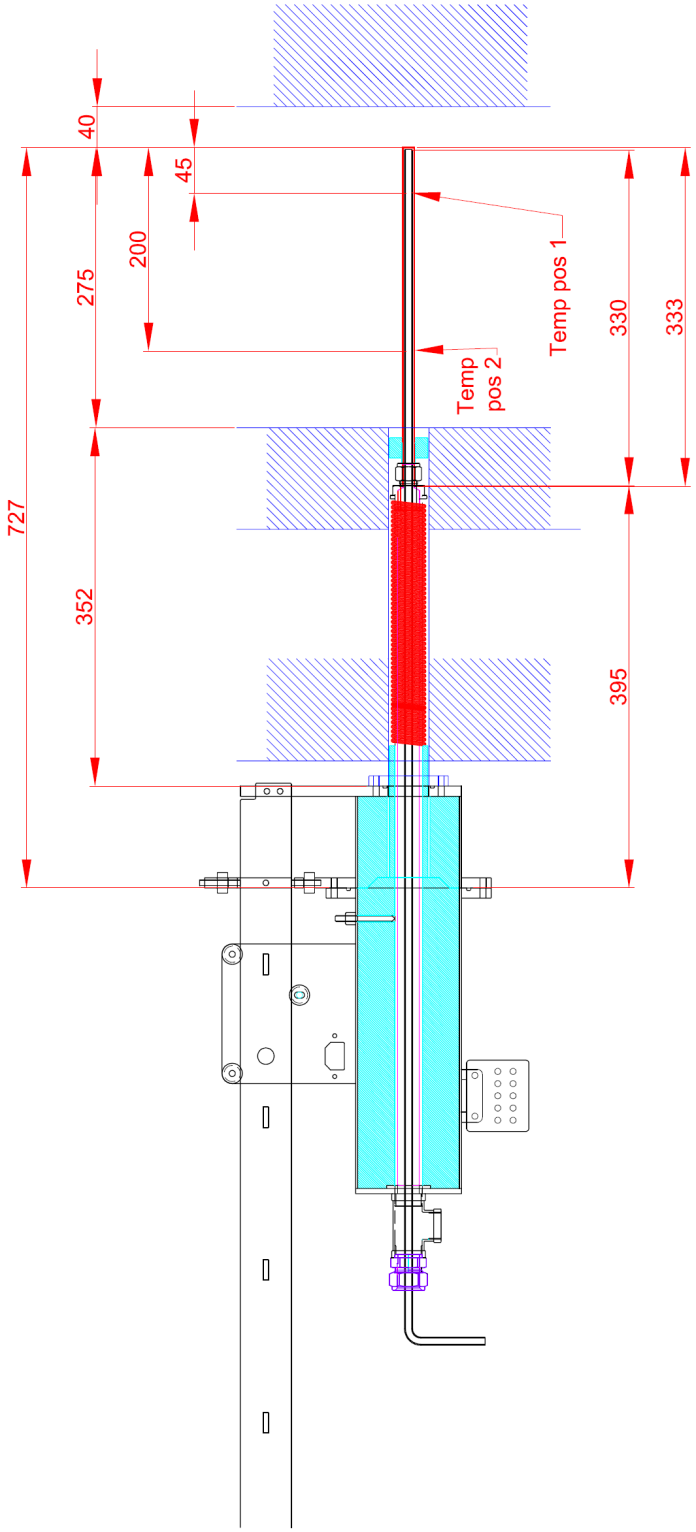

Figure 2.11: Sketch of deposit probe inserted in reactor

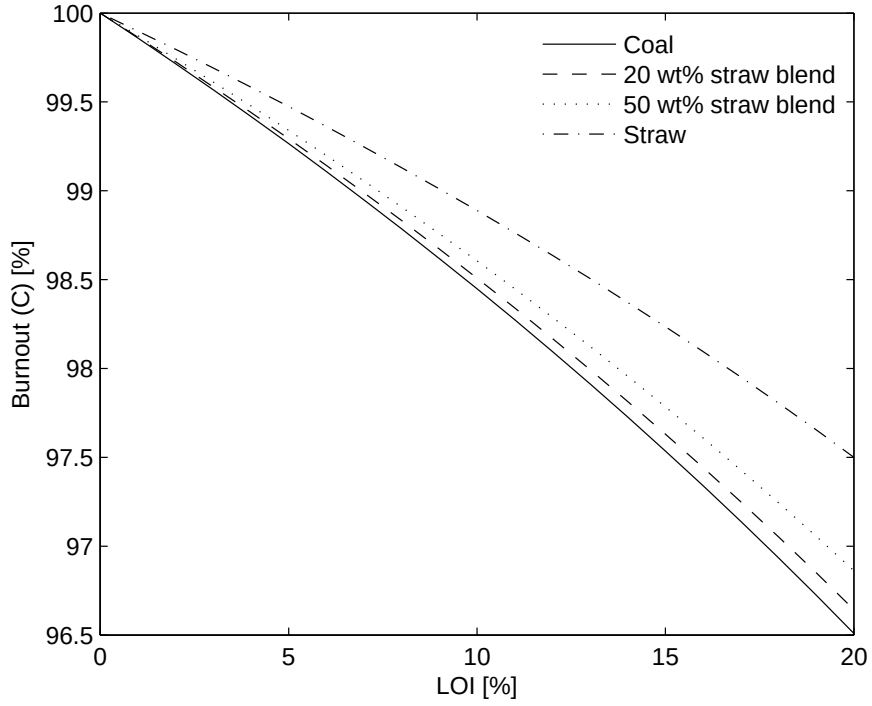

Figure 2.12: Correlation between measured LOI and carbon burnout for the four fuels investigated.

the mass loss observed when heating 1 g of dry ash sample to 550 ℃ in air for 2 hr or until constant mass, see (2.7).

$$\mathrm{LOI} = \frac{m_{dry} - m_{heated}}{m_{dry}} \tag{2.7}$$

Figure 2.12 shows the correlation between fuel burnout (on a carbon basis) and the LOI measured in fly ash. The data are produced under the assumption that all LOI consist of carbon. It is seen that an LOI of 5 % which is the maximum allowable value for fly ash used in concrete production [63] corresponds to about 99.5 % burnout. The increasing carbon burnout efficiency with increasing straw share of the fuel is caused by the relatively lower ash content in straw compared to coal.

Selected samples have been analysed for the carbon content of the ash at the laboratory at the DONG Energy Ensted Power Plant (ENV). A comparison of the carbon content and the measured LOI showed a significant deviation when the fuel contained straw, see Figure 2.13 on the following page. The difference between LOI and carbon content is believed to be caused by the presence of primarily H and O in straw char particles.

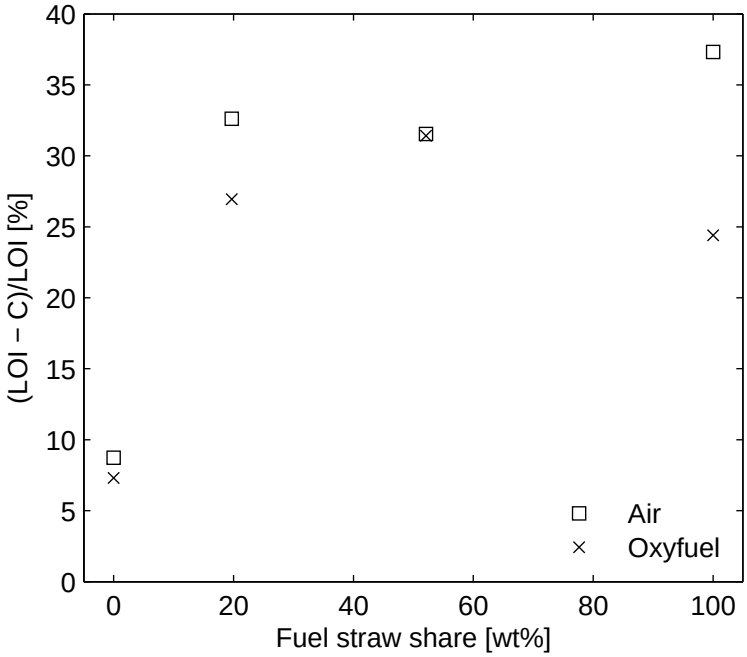

Figure 2.13: Difference between LOI and carbon content of fly ash as function of fuel straw share. Comparison of air and oxyfuel environments at the reference operating conditions.

In addition to analysis of the carbon content selected ash samples have been analysed with respect to their total S, Cl, and ash forming species content (Al, Si, Fe, K, Ca, Mg, Na, Ti, P). The content of water soluble K, Na, Mg, Ca, P, S, and Cl has likewise been determined. These analysis were also performed at ENV.

Deposit sampling was generally performed during a period of 2 hours in order to have sufficient sample for analysis. All collected deposits have been analysed with respect to their total content of S. Selected samples have likewise been analysed for the total Cl and ash forming species content (Al, Si, Fe, K, Ca, Mg, Na, Ti, P). The content of water soluble species (K, Na, Mg, Ca, P, S, and Cl) have been determined for all of the upstream samples. In some cases the sample mass collected from the downstream part of the probe was to small for an analysis of water soluble species to be performed.

2.3.2.5 Temperature Mapping

Temperature mappings with an S-type thermocouple have been performed for most fuel/oxidizer combinations. The measured temperature profiles for each experiment marked with a "T" are included in the data collection [64]. For some fuel/oxidizer combinations, especially coal experiments, several of the experimental runs include temperature measurements. An averaged data set is thus made

from the different experimental runs at similar operating conditions. For some of the earlier experiments, the temperature profile measurements were performed prior to the reactor reaching steady state temperature. This is especially relevant for ports 1 and 2 were the change from the NG flame to the solid fuel flame induces the greatest change to the fuel ignition and thus the temperature and radiation intensity. The averaged data sets are thus made without measurements performed less than 1.5 hour after the shift from the natural gas flame to the solid fuel flame.

Figure 2.14 on the next page shows the average, radial temperature profiles in the top five measurement ports in the reactor for combustion of the four different fuel blends in air. For experiments with no repetition of measurements, i.e. no error bars in the plot, it can be considered safe to assume that the uncertainty is of comparable size to the uncertainty for other fuel/oxidizer combinations in the same measurement point. The profiles are seen to be almost constant across the reactor in ports 3-5. A small temperature decrease is observed close to the reactor walls ($\pm$15.75 cm). In ports 1 and 2 a rather steep temperature gradient can be observed close to the reactor centre due to the flame front. The absence of the gradient for some fuels is due to insufficient resolution of the measurements.

The profiles in port 1 are only shown for one half of the reactor. The measurements performed at positive values of R are generally seen to be significantly higher than for the corresponding position at negative values of R. Figure 2.15 on page 39 shows the temperature measurements together with the concentrations of NO and CO in the exit flue gas during the time of temperature measurements. The increase in temperature is associated with a sharp increase in NO formation and a decrease in CO formation. The measured decrease in CO is less sharp due to a delayed effect in the online CO analyser making it unable to reproduce step changes in concentration from high to low values. The changes in temperature and emissions indicate a shift in flame properties from a low-NO_x flame to a high-NO_x flame. Figure 2.16 on page 39 shows pictures of the flame taken from the reactor bottom for each position of the thermocouple. A significant difference in flame shape can be observed. When inserted in front of the burner ($R > 0$) the thermocouple acts as a flame holder drawing the flame base closer to the burner creating a shorter and more intense flame producing more NO. Due to this phenomenon, all temperature measurements taken at positive values of R in port 1 have been omitted from the averaged temperature profiles.

It should be noted that the temperature profiles have been measured with shielded thermocouples (S-type shielded with ceramics). Hence, the temperature measurements are significantly influenced by the radiative heat flux within the reactor, primarily from the walls.

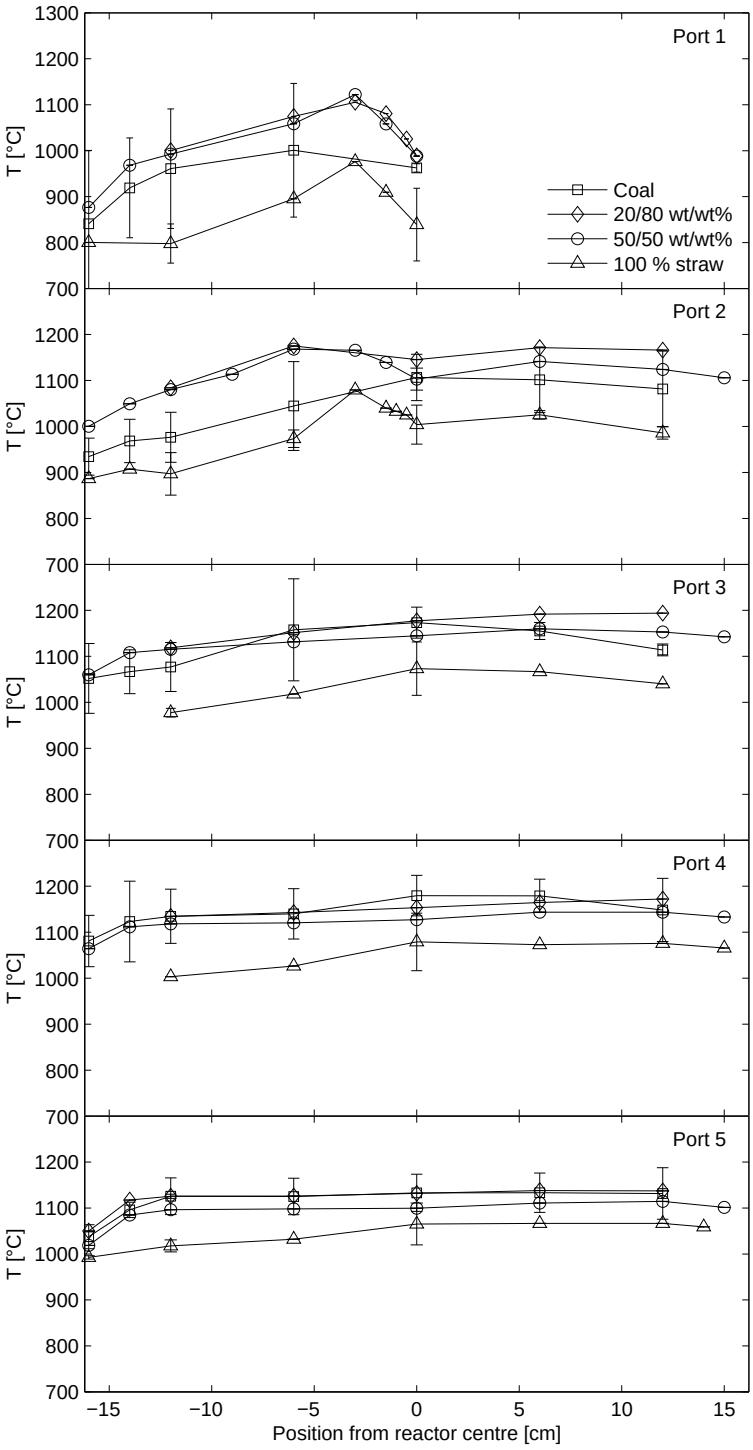

Figure 2.14: Temperature profiles measured with S-type thermocouple for the four different solid fuel mixtures combusted in air. Errorbars correspond to two times the standard deviation for repeated measurements.

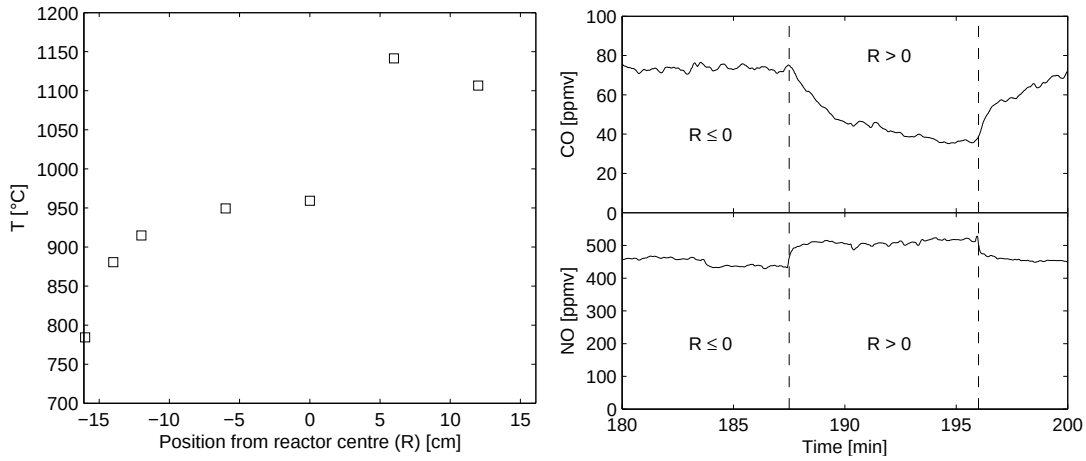

Figure 2.15: Left: Radial temperature profile in measurement port 1 for experiment CA15_T. Right: Shifts in NO and CO emissions depending on the radial position of the thermocouple tip during temperature measurements in measurement port 1. The thermocouple is moved across the reactor from negative to positive values of R.

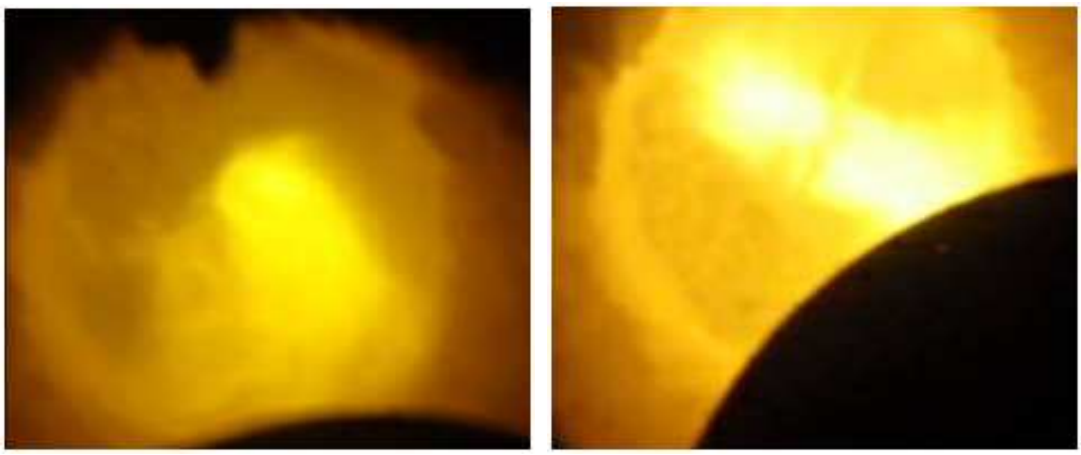

Figure 2.16: Left: Coal/air flame, thermocouple at $R < 0$. Right: Coal/air flame with thermocouple inserted across burner mouth, $R > 0$.

2.3.2.6 Advanced Diagnostics – Gas-Phase Temperature and Composition

In addition to the temperature mapping with shielded thermocouples and the analysis of the flue gas withdrawn from the bottom of the reactor, mapping of the reactor chamber through the top five measurement ports has been performed with a special, miniature fibre-optic FTIR (Fourier Transform Infra Red) probe. The probe was specially designed for this work and was applied for 5 reference experiments (coal/air, coal/oxyfuel, straw/oxyfuel, M50/air, and M50/oxyfuel). The probe enables measurements of local gas phase temperature and composition (CO_2, H_2O, and CO) in oxyfuel combustion whereas it is applicable for temperature measurements during air-firing. The principle of the gas temperature measurements is described in [65] and principles of the gas concentration measurements in [66], but a short outline of the FTIR system is provided in the following. A more detailed description of the system and the method of data treatment is provided in [67].

Visualization of the probe and its dimensions is given in Figure 2.17 on the facing page. When the FTIR probe is operated with the purpose of gas-phase concentration measurements the probe needs to operate with a beam stop as seen in Fig. 2.17. The beam stop is cooled by two 4 mm stainless steel tubes placed beside the probe with optics. The optical path length (field of view in Fig. 2.17) is 30 mm and the diameter of the probe with optics is only 10 mm. The small probe diameter ensures minimal disturbance of the flue gas within the setup and the relatively short path length ensures very localized measurements. A purged ceramic tube is mounted at the probe tip to reduce disturbances from particles in the flue gas and the cooled probe tip. Thermal light from the hot slab of gas between the ceramic tip and the beam stop is collected by a small 4 mm ZnSe lens focused on an IR-fibre connected to the FTIR-spectrometer. Gas-phase temperature measurements can be performed both with and without the presence of the beam stop. It is the emission signal from CO_2 that is used to determine the gas temperature and the signal needs to be strong enough for a temperature interpretation to take place. As the signal strength relates to the number of CO_2 molecules in the optic path, measurements in air are carried out without beam stop to ensure a longer path length, and therefore an increased number of CO_2 molecules. Determination of the gas-phase temperature is a necessary step in the determination of the gas-phase composition. Hence, it was not possible to use the probe for mapping the gas-phase composition during air combustion. Another consequence is that measurements in air are averages over a longer, however undetermined, distance than in oxyfuel flames.

The FTIR-spectrometer was mounted with a sensitive liquid nitrogen cooled InSb-detector sensitive in the range 1800 - 7000 cm^{-1}. Approximately 60 double-sided single scan spectra per minute could be obtained with a spectral resolution of 2 cm^{-1}. These spectra yielded time dependent concentration and gas-phase

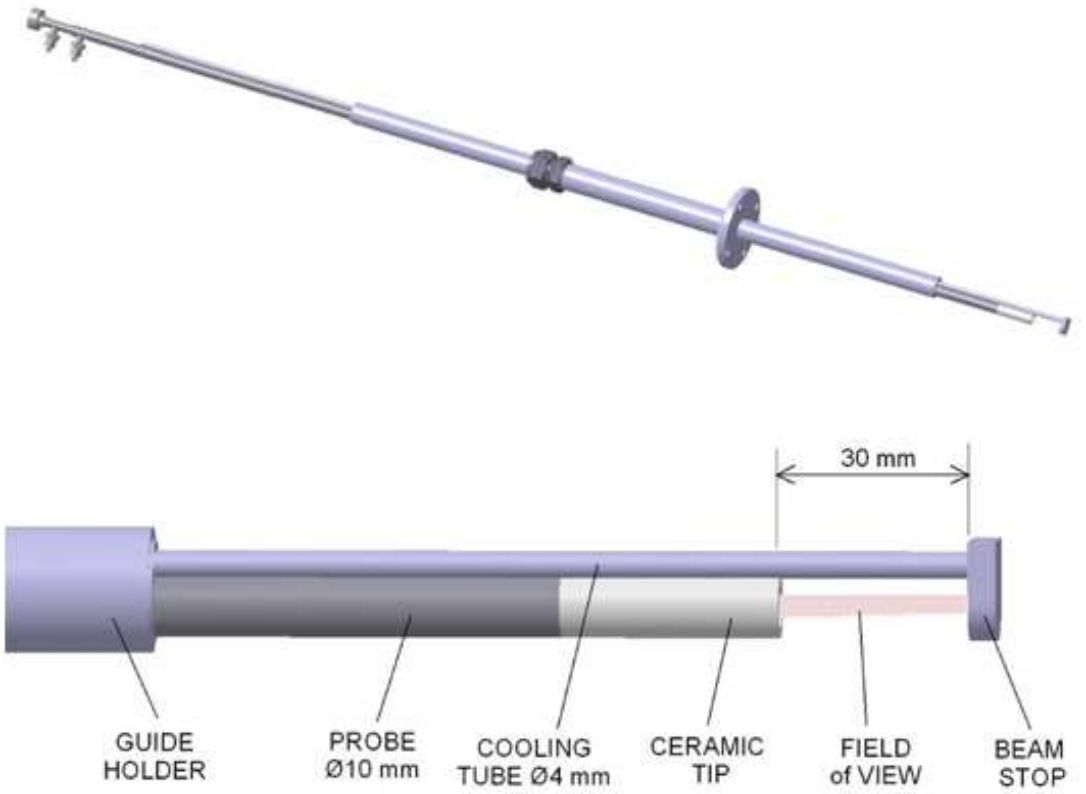

Figure 2.17: Top: The water-cooled fibre-optic probe for measurements of gas temperature and gas composition in the experimental setup. The FTIR-probe is inserted into a port holder with flange for leak tightness and easy handling during experiments. Bottom: Tip of the fibre-optic probe. Gas temperature and gas composition is measured along a 30 mm path between the beam stop and the front of the ceramic tip. Thermal light is collected with a 4 mm diameter ZnSe lens and focused on the end of a 550 μm IR-fibre placed in the 10 mm water-cooled probe.

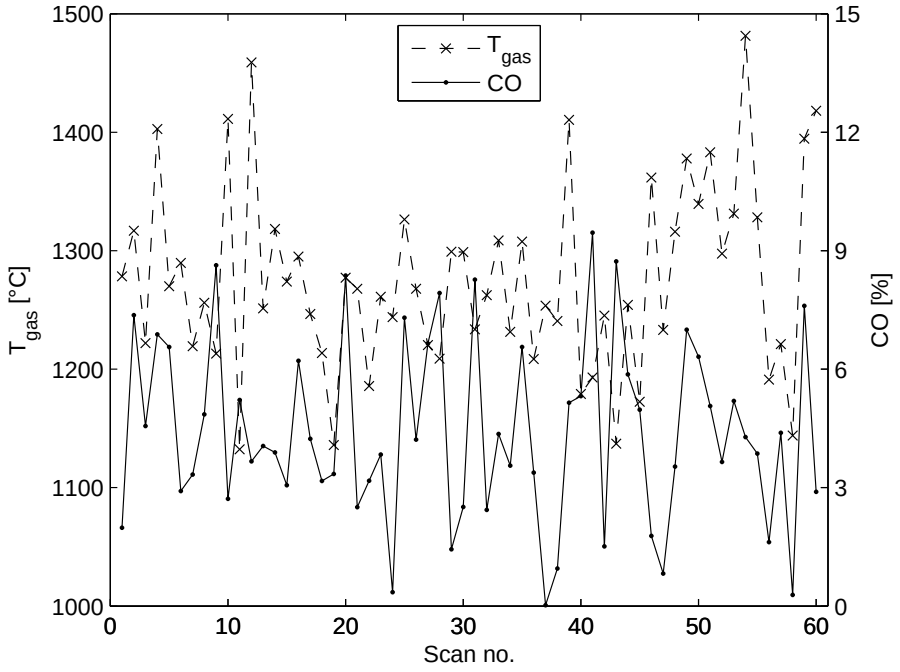

Figure 2.18: Time dependent gas-phase temperature and CO concentration data for the reactor centre position ($R = 0$) at port 3 for M50/oxyfuel combustion.

temperature profiles, from which average and standard deviation values of concentrations and temperatures could be determined. Figure 2.18 shows an example of the collected data. The high spectral resolution provides sufficiently well defined absorption peaks in the spectra allowing for determination of the gas species concentrations. A notebook PC has been used to control data acquisition and store data during experiments. The system was calibrated before and after experiments with a portable black body source with an uncertainty of $\pm 3\,^{\circ}\mathrm{C}$.

The FTIR technique is reliable though it cannot be stated as accurate for estimation of gas phase concentrations of H_2O, CO_2, and CO. The accuracy of the method is dependent on the similarity between the reference emission spectra of the gases and those obtained in the experiments as the transmittance intensity is not a linear function of concentration. Especially for H_2O a deviation existed. The unsteady flow phenomena encountered primarily in the upper two measurement ports induced large uncertainties on the measured gas species concentrations. Close to the fuel jet some of the measurements failed to yield physically sound results. The CO_2 and H_2O data are not shown in this thesis.

An investigation of the influence of the presence of the beam stop on the measured gas-phase temperatures showed a significant effect. Figure 2.19 on page 44 shows a comparison of the radial temperature profiles in ports 1-5 for the combustion of the 50 wt% straw blend for FTIR measurements both with and without the beam

stop and the measurements performed with the thermocouple. The figure illustrates the significant cooling effect of the beam stop. The difference is on average about 100-200 ℃. The cooling effect from the beam stop yields measurements comparable to the use of a traditional thermocouple. When operated without the beam stop the resolution of the temperature gradient observed in port 1 was weakened. This, on the other hand, illustrate the superiority of the fixed path length obtained during operation with the beam stop. On an overall level, it is concluded that the most accurate determination of the gas-phase temperature during oxyfuel combustion is obtained while the probe is operated without the beam stop. In this case the FTIR probe showed superior to traditional temperature measurements using a thermocouple in determining the gas-phase temperatures and providing a measure for the level of fluctuations due to mixing of fuel, oxidant, and hot flue gases. Generally, the fluctuations are observed to increase when the probe approaches the flame front which is located within the interval $R = [-6; 0]$ cm.

2.3.3 Combustion Conditions

The experiments have been operated at several different combustion conditions as shown in Table 2.5 on page 26. The investigated parameters for the four fuel types include:

Combustion oxidant type Air and O_2/CO_2 mixtures

Stoichiometry The theoretical oxygen concentration in the dry flue gas has been varied within the interval from 1 to 5 vol%. The applied stoichiometric oxygen excess ratios have accordingly been in the interval 1.025 to 1.3.

Oxidant O_2 concentration Only relevant for oxyfuel experiments. The values applied are: 25, 30, 33, 35, 40, and 50 %. Not all values have been used for all fuels.

Residence time This parameter has not been controlled but is a function of the oxidant type and stoichiometry due to the fixed length of the experimental setup. The calculated average residence times are ranging from 2.6 to 5.3 seconds.

Burner settings The influence of varying the burner swirl number, the linear velocity of the primary oxidant leaving the burner, etc. have been investigated in order to find operating conditions with a stable flame. The investigations were performed for coal/air combustion. No clear correlation between burner settings and flame properties were found for the range of investigated parameters [61].

The characterization of the combustion oxidant is described in Section 2.3.3.1 whereas considerations regarding residence time are provided in Section 2.3.3.2.

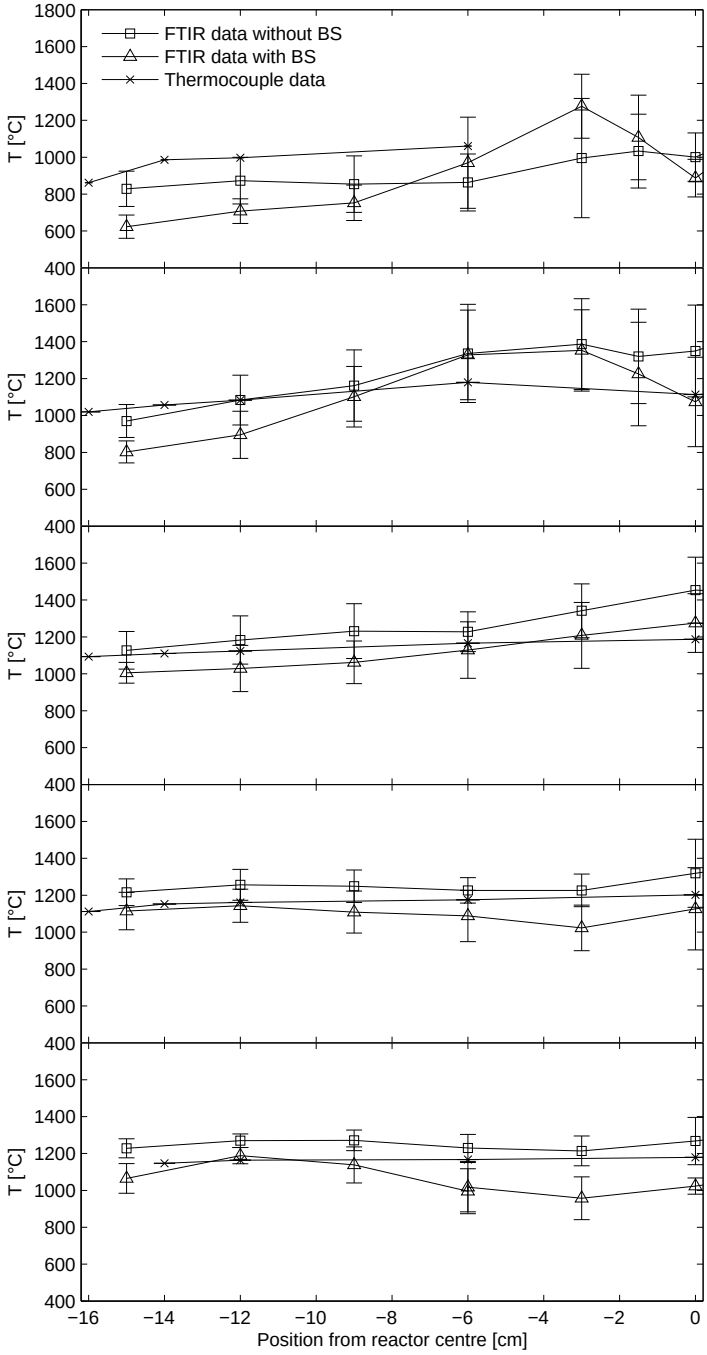

Figure 2.19: Comparison of temperature measurements in ports 1-5 for M50/oxyfuel combustion. FTIR data are taken with and without the beam stop (BS) mounted on the probe. Only measurements at negative radii are shown. Error bars on thermocouple data correspond to two times the standard deviation on repeated measurements. Error bars on FTIR data correspond to two times the standard deviation for the 60 scans and provide a measure of the level of fluctuations in the given measurement position.

2.3.3.1 Combustion Oxidant and Stoichiometry

When comparing air and oxyfuel combustion experiments it is important to consider which stoichiometric measure to use in order to match the combustion conditions. Three different measures for the combustion stoichiometry can be applied; the stoichiometric oxygen excess ratio, λ, the dry flue gas oxygen concentration, $y_{O_2}^{dry}$, and the wet flue gas oxygen concentration, $y_{O_2}^{wet}$ see Eqs. (B.5) and (B.9) in Appendix B.

It should be noted that the three stoichiometric parameters impacts the combustion process in different ways. The stoichiometric excess oxygen ratio provides information on the oxygen to fuel ratio within the flame whereas the flue gas O_2 concentration determines the conditions during fuel/char burnout. The wet flue gas oxygen concentration is the actual condition which the char particles experience during burnout, whereas the dry concentration is the parameter easiest to determine and thus would typically be the parameter from which a power plant is controlled. The distinction between the wet and dry oxygen concentration is relevant due to an about 50 % higher concentration of H_2O in the oxyfuel atmosphere compared to air in the case of a dry flue gas recycle. For a wet recycle, the difference will be larger. The difference is caused by the decreased flue gas flow leading to a higher relative difference between wet and dry O_2 for oxyfuel combustion than combustion in air.

Figure 2.20 on the following page shows a comparison of the stoichiometric oxygen excess ratio and the dry flue gas oxygen concentration for air and O_2/CO_2 atmospheres with different oxygen concentrations at the inlet. From the figure it is seen that a fuel particle burning at a given stoichiometric oxygen excess ratio in an oxyfuel atmosphere with higher than 21 % O_2 in the oxidant will experience a higher partial pressure of O_2 in the burnout stages of the combustion than for combustion in air.

Figure 2.21 on page 47 shows a comparison of the development in fly ash loss-on-ignition as function of the three different measures for the combustion stoichiometry for air and oxyfuel combustion experiments using coal as fuel. Only oxyfuel experiments performed with 30 % O_2 in the oxidant are shown. Due to the differences in the composition of the combustion atmosphere between air and oxyfuel combustion the data points for the two atmospheres are seen to move relative to each other when the independent variable is changed.

It is the partial pressure of O_2 rather than λ that influences the rate of combustion. For that reason it has been chosen to use the flue gas oxygen concentration as parameter when comparing air and oxyfuel combustion experiments and matching reference conditions. For simplicity, the concentration in the dry flue gas is chosen.

False Air Ingress Due to a safety demand of operating the experimental setup at sub-pressure ($P_{reac} \leq -2$ mbarg) a risk of false air entering the combustion

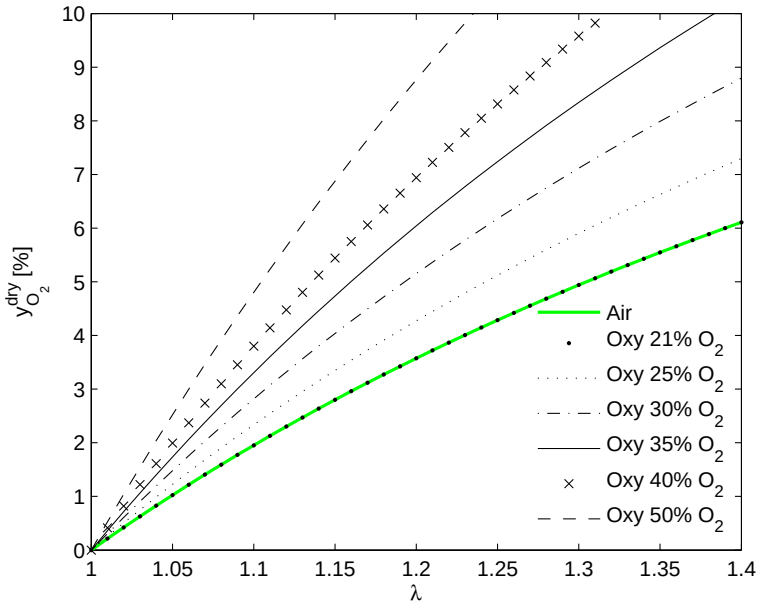

Figure 2.20: Comparison of the stoichiometric oxygen excess ratio, λ, and the concentration of O_2 in the dry flue gas for complete combustion of coal in air and O_2/CO_2 atmospheres with different oxygen concentrations at the inlet.

process is present. False air can enter the experimental setup in two ways:

- Into the gas sampling system – this amount of false air enters the gas sample at low temperature and can thus be considered a pure diluting agent without any effect on the combustion process. A test of the false air ingress into the gas conditioning system showed that the dilution factor for the gas sample is about 0.05–0.1 % of the sample flow of 3 L/min.

- Into the reactor – whether false air entering the reactor should be taken into account when determining stoichiometric values, etc., depends on its entering point and mixing with the remaining flue gas within the reactor. Two scenarios are relevant:

  - Near the burner – false air entering the reactor near the flame zone should be included in the calculations with the same significance as the oxidizing agent introduced through the burner. This will yield higher oxygen excess than can be determined theoretically from the fuel and oxidant flows.
  - Downstream of burner – false air entering very close to the sampling position can be regarded a pure diluting agent, since the residence time and temperature is low enough for the influence on the combustion process to be assumed insignificant. Additionally, it is unknown whether full mixing with the entire flue gas flow has been obtained.

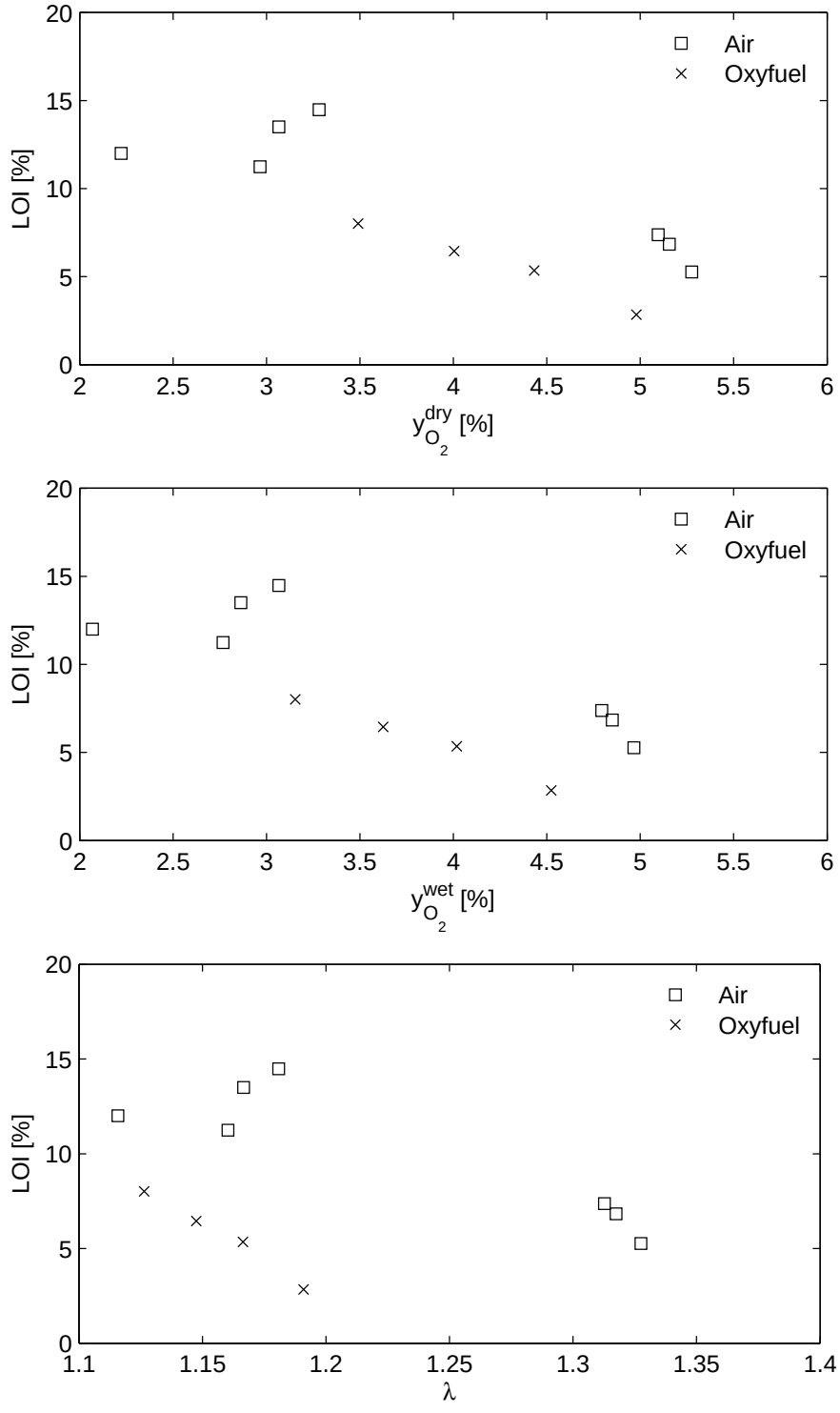

Figure 2.21: Comparison of loss-on-ignition (LOI) for coal combustion in air and 30% O_2/CO_2 at different stoichiometries with three different stoichiometric parameters acting as independent variable.

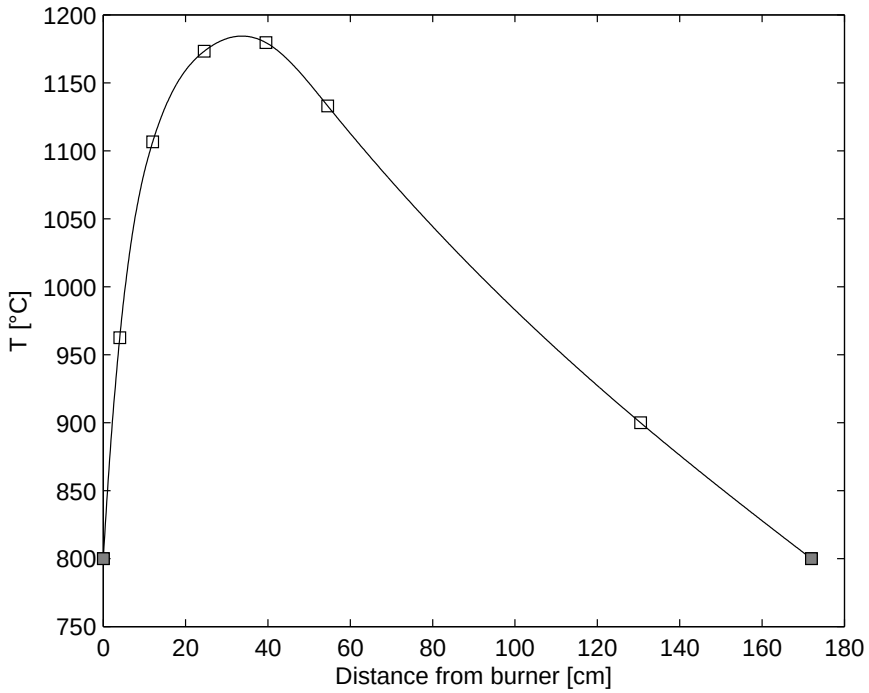

Figure 2.22: Temperature profile along reactor estimated from a cubic spline interpolation of the measured average temperatures in ports 1-5 and 7 and temperature estimates at the burner exit (L = 0) and ash sampling probe (L = 175 cm), closed symbols. Data are for coal/air combustion at the reference operating conditions and are measured with a thermocouple.

Different leak tests showed that the majority of the false air entering the reactor can be treated as a pure diluting agent [61]. The combustion stoichiometry is thus determined solely from the fuel and oxidant inlet flows.

2.3.3.2 Residence Time

An estimate of the average residence time of fuel particles in the reactor can be determined from a temperature profile and the theoretical total flue gas flow. The temperature in each position along the reactor is determined from a cubic spline interpolation of the average temperature profiles (reactor centre values) determined for each fuel/oxidizer combination with a thermocouple. Figure 2.22 shows an example of one of the estimated temperature profiles. The temperature immediately above the ash sampling probe has been assumed to be 100 ℃ below the value measured in port 7. The burner exit temperature has been selected in the range 700-850 ℃ depending on the fuel/oxidizer combination and the operating conditions. The value has generally been chosen in order to yield a smooth profile. The exact value has only a small effect on the calculated residence time.

Table 2.7: Average residence time for different oxidizers at selected flue gas oxygen levels.

Oxidizer	$y_{O_2}^{dry}$	τ [s]
Air	5	2.6-2.7
25 % O_2/CO_2	5	3.6
30 % O_2/CO_2	5	3.7-3.9
35 % O_2/CO_2	5	4.5
40 % O_2/CO_2	3	4.8
50 % O_2/CO_2	2	5.3

The residence time is calculated from Eq. (2.8).

$$\tau = \int \frac{dL}{u(L)} = \sum_i \frac{\Delta L_i}{u(L_i)} \tag{2.8}$$

where L is the total reactor length and $u(L)$ is the average linear velocity of the flue gas at a given position, L, in the reactor. The velocity profile and recirculation zones are not included in the calculation. In order to estimate the residence time, the reactor length is split into a number of volume elements within which the average temperature and linear gas velocity is determined, see (2.9).

$$u(L) = \frac{V_{FG}}{A_{reactor}} \cdot \frac{T(L)}{T_0} \tag{2.9}$$

V_{FG} is the volumetric flue gas flow [Nm^3/s], $A_{reactor}$ is the cross-sectional area of the reactor (constant), $T(L)$ is the flue gas temperature in position L, and T_0 is the reference temperature, 273.15 K. The flue gas is assumed to behave as an ideal gas.

Table 2.7 shows the residence times determined for each of the oxidizer compositions applied in the experiments. An increase of about 40-50 % in the average residence time of gas and particles in the reactor occurs when changing from air to oxyfuel combustion (30 % O_2) due to the lower flue gas flow. This will have an impact on the combustion process and the burnout efficiency in the two different combustion atmospheres.

2.4 Molar Balances

Molar balances for the elements C and S of the form

$$MB = \frac{X_{out}}{X_{in}} \tag{2.10}$$

have been set up. X_i are in units of [kmole/s]. Several levels of detail have been made for the balances with respect to the "out" term. Each new level build on the previous.

Level 1 Only flue gas measurements are taken into account, full burnout of the fuel is assumed. Calculated for both C and S.

Level 2 For experiments with ash sampling. It is assumed that all ash fed to the reactor end up as fly ash with the measured average carbon or sulphur content (if the C analysis does not exist the LOI value is used in determining the degree of burnout on a carbon basis and from that the C content of ash). C and S.

Level 3 For experiments with ash sampling. The amount of fly ash sampled compared to the theoretical amount is used to determine the split between ash ending up as fly ash and ash retained in the reactor as deposits. It is assumed that the fraction of ash retained in the reactor yields complete burnout. Only C.

Level 4 For experiments with ash and deposit sampling. The sulphur analysis on deposits is used to correct for the split between fly ash S and deposits S. Only S.

Level 1 can be calculated for each experiment performed, whereas levels 2-4 are only applicable to experiments with fly ash (and deposits) sampling. The equations for each individual level can be seen in Appendix C.

Balances for the remaining major elements in the combustion process; O, N, and H could likewise be set up. However, due to the design of the experimental setup and the analysis/data available these balances would be of a more theoretical interest. For instance, the N balance, which is highly relevant for oxyfuel experiments, would be heavily influenced by false air ingress into the reactor and would thus act more as a measure of this ingress than as a mass balance. For O and H, assumptions on the amount of water in the flue gas would be necessary and introduce a significant uncertainty on the results.

2.4.1 Carbon

The carbon balance is determined in each data point (time) and Figure 2.23 on the facing page shows an example of the development of the balance during the selected time interval for data analysis for an experiment with fly ash sampling. The balance is seen to fluctuate which is believed to be caused by the uncertainty on the fuel flow determination, see Section 2.2.2. Due to a high degree of burnout, no visual difference exist between the three levels. For the shown example, the data does not yield a 100 % fulfilment of the carbon balance. However, the

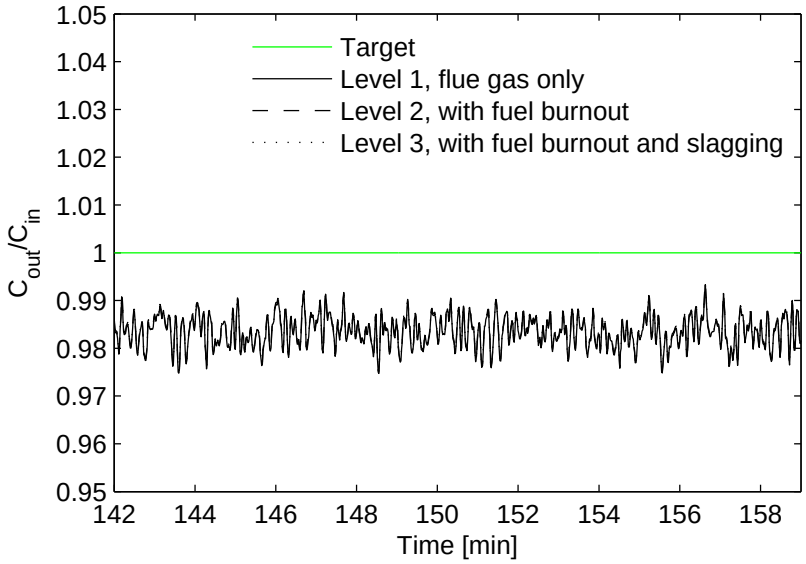

Figure 2.23: Carbon balance fulfilment as function of time for combustion of the fuel blend with 50 % straw in air (M50A01_AD).

error on the balance for the shown example is within 2 % and is considered very satisfactory.

Figure 2.24 on the next page shows the averaged carbon balance fulfilment for all air and oxyfuel experiments as function of the fuel composition. Only the highest level value is plotted for each individual experiment. For all air experiments the balance is seen to be satisfied to within an error of 3 %. This does not give cause to any remarks when taking the complexity of the experimental setup into account. However, the oxyfuel carbon balances show significantly larger errors, up to 15 %. As seen in Figure 2.25 on page 53 this is primarily a consequence of narrow time intervals chosen for data analysis. It is seen that the largest deviations occur for experiments with time intervals less than 10 minutes of length. Within these time intervals only few CO_2 measurements are available. In order to determine the carbon balance at each time, a linear interpolation is made between the data points from the GC. This approach is of course associated with a large degree of uncertainty the fewer the GC measurements within the time interval, as peak measurements will influence the results relatively much. In relation to the remaining data analysis the deviation seen here does not have an effect, as the GC measurements of CO_2 are not used to determine other parameters. It is thus considered safe to use all the experiments.

2.4.2 Sulphur

The sulphur balance is determined in each data point (time) and Figure 2.26 on page 54 shows an example of the development of the balance during the selected

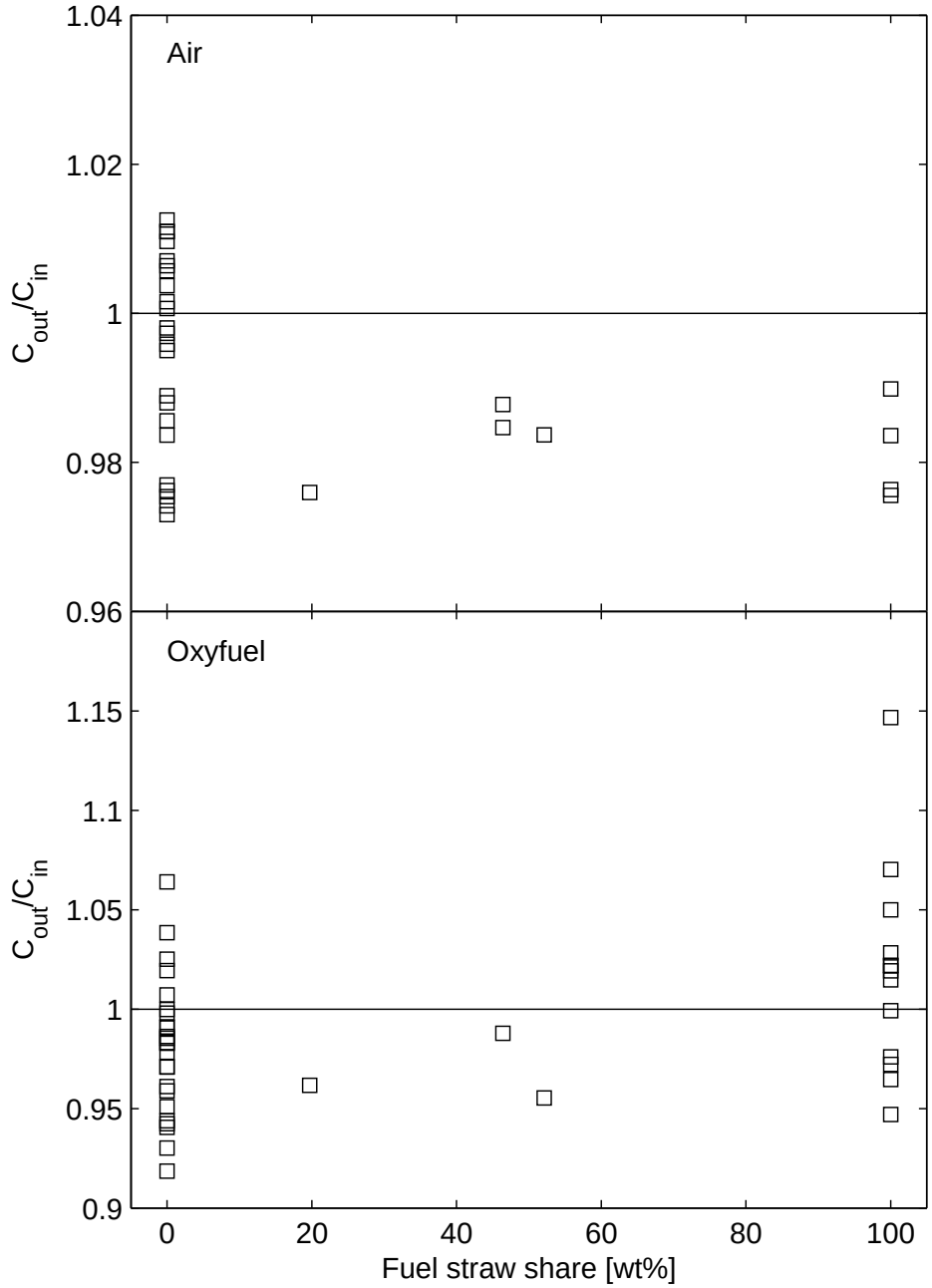

Figure 2.24: Carbon molar balance for air and oxyfuel experiments as function of the straw share of the fuel. Note that the scaling on the y-axis is different.

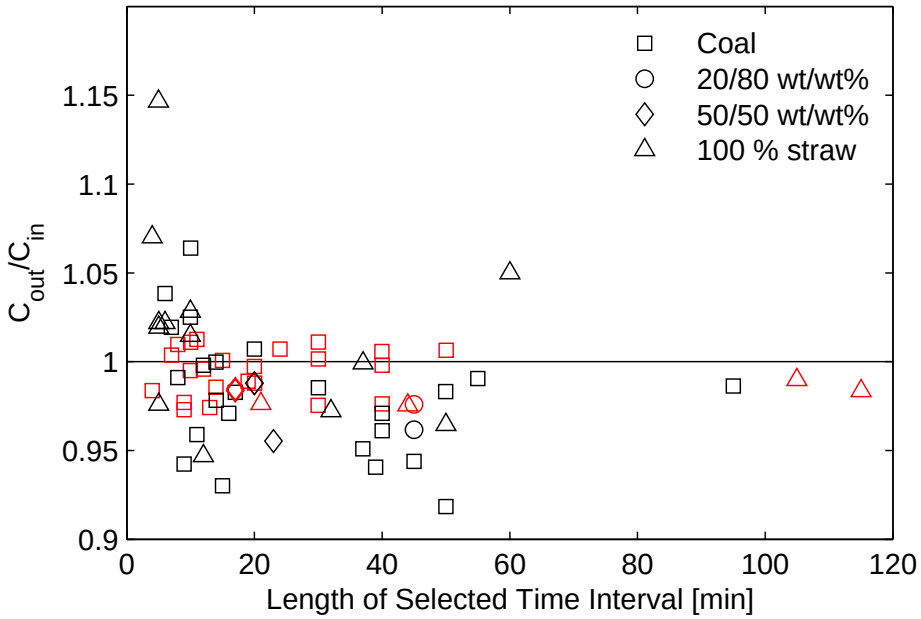

Figure 2.25: Carbon balance fulfilment (air: red symbols, oxyfuel: black symbols) as function of the length of the selected time interval for data treatment.

time interval for data analysis for the same experiment as discussed above. A similar fluctuating behaviour as for the carbon balances is seen. Still, the amplitude of the fluctuations is within reasonable levels. Advancing from the pure flue gas data approach (level 1) to accounting for sulphur in the fly ash (level 2) improves the overall balance with about 20 % points for the shown example. Taking the split between sulphur in fly ash and deposits into account (level 4) improves the fulfilment even further and the resulting overall error is less than 10 %. For the shown experiment the sulphur content in the fly ash is 0.8 wt% whereas it is 4.4 wt% in the deposit sample (upstream part). The relatively low error on the balance at level 4 indicates that the sulphur concentration in the upstream part of the deposit sample taken through port 7 is close to representative for all the deposits in the reactor chamber for the shown example. Taking sulphur retention in deposits into account has thus shown of considerable importance when determining sulphur balances.

Figure 2.27 on page 55 shows the averaged sulphur balance fulfilment for all air and oxyfuel experiments as function of the fuel composition. At level 1, a significant deviation exist between incoming and outgoing sulphur from the setup for all fuels. The deviation increases with increasing straw share of the fuel indicating the presence of increased amounts of alkali and alkali-earth species during combustion leading to sulphur retention in solid phases. As was shown for the example in Figure 2.26 on the next page, taking sulphur in the fly ash into account

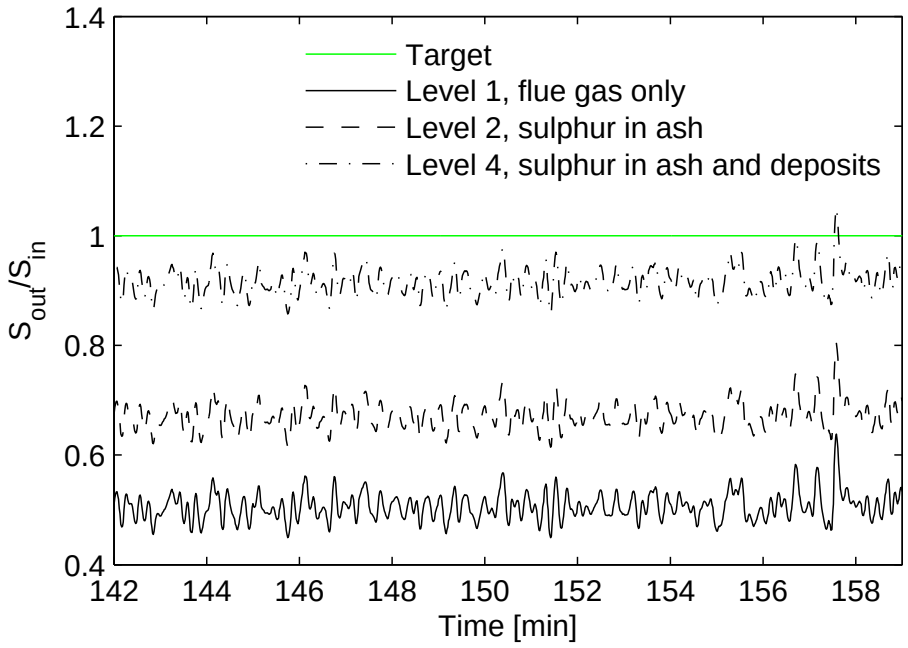

Figure 2.26: Sulphur balance fulfilment as function of time for combustion of the fuel blend with 50 % straw in air (M50A01_AD).

(level 2) improves the closure of the balance for all fuels. However, for the blends a significant error is still present, most pronounced for the high straw share. For pure straw combustion sulphur retention in ash can explain most of the sulphur missing at level 1. For all fuel/oxidizer combinations (except coal/air where the data are not available) accounting for sulphur in deposits (level 4) yields closures to within 10 %. Except for 100 % straw/oxyfuel the sulphur content of the deposit sample is higher than in the fly ash sample. For that particular experiment, level 2 overshoots and the inclusion of sulphur in the deposit thus improves the balance even though the trend in the data points is opposite to the remaining experiments. Based on the shown balances, the deposit samples can be considered representative for all the deposits within the reactor for all fuel/oxidizer combinations.

The significant retention of sulphur in deposits could explain the general problems which are encountered when performing sulphur mass balances on full-scale boilers [68]. The transient nature of sulphur retention in deposits (depends on fuel and operating conditions) induces great uncertainties on those investigations.

Besides sulphur in ash and deposits, the flue gas will contain minor amounts of SO_3. The SO_3 has not been measured and it is assumed that ignoring it only introduces a minor error on the sulphur balance. Furthermore, since the flue gas sample is dried by condensation before analysis a small amount of sulphur could be lost with the condensate due to dissolution of SO_2 and SO_3 and/or reaction

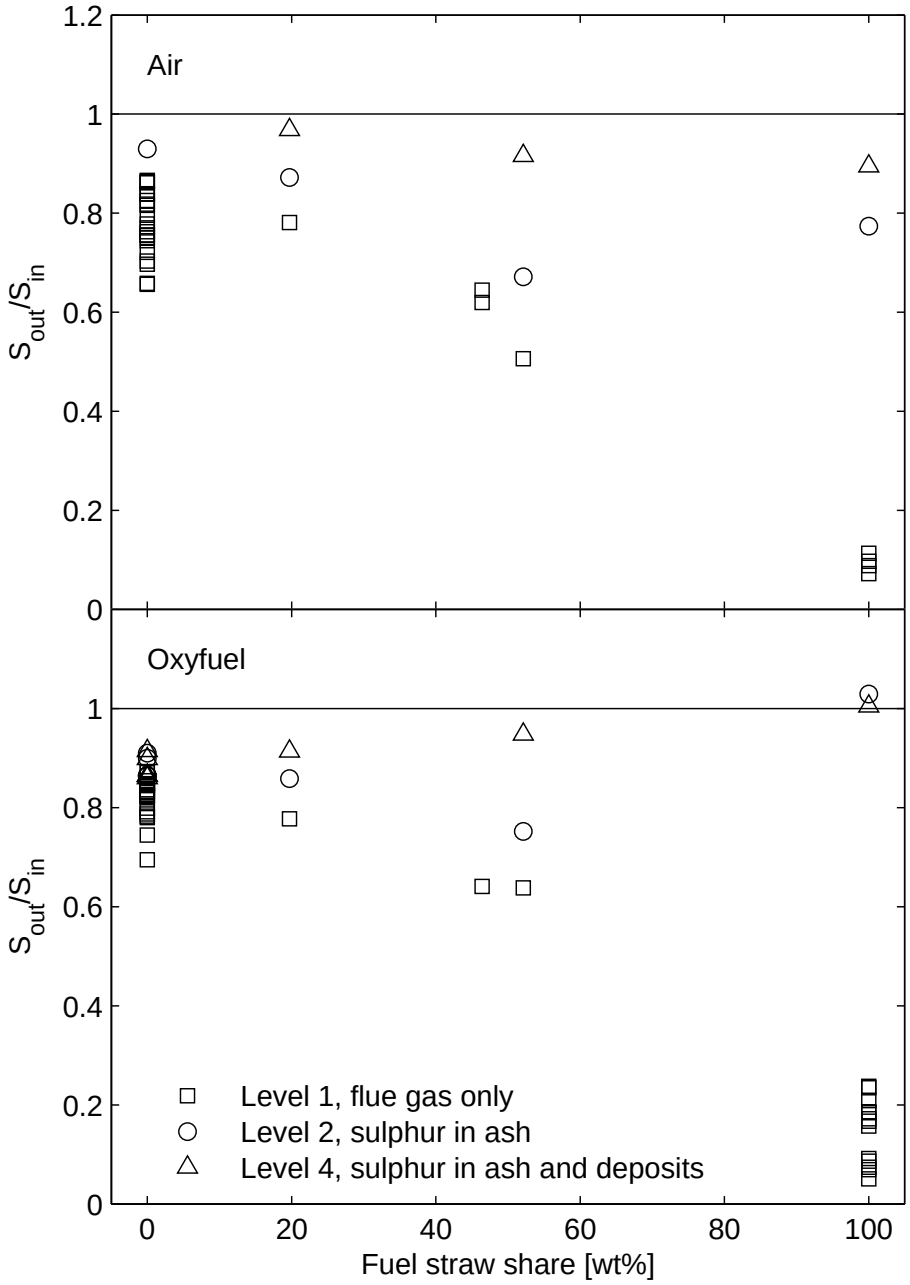

Figure 2.27: Sulphur molar balances for air and oxyfuel experiments as function of the straw share of the fuel.

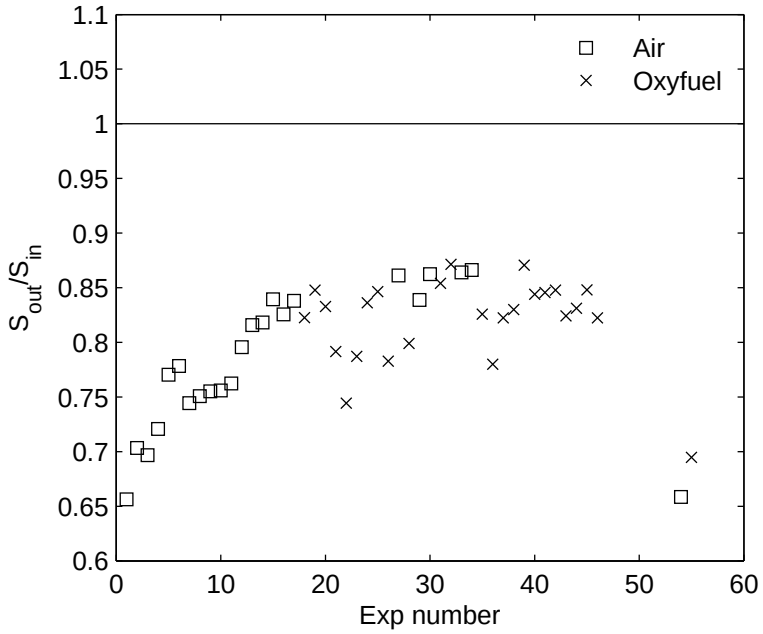

Figure 2.28: Sulphur balances at level 1 for coal combustion in air and O_2/CO_2 atmospheres as function of the experiment number (chronological order).

with ash. No quantification of the loss has been made. However, according to results reported by Fleig et al. [69] the sulphur lost with the condensate constitute no more than 0.5 % of the fuel-S forflue gas SO_2 concentrations comparable to this work.

For the pure coal a relatively large difference exists between the individual experiments. Figure 2.28 shows the sulphur balance fulfilment at level 1 in chronological order for the coal experiments. An increasing trend is seen during the first part of the first series of experiments (Exp number < 50). During this period several problems were encountered with the flue gas conditioning system and the poor degree of fulfilment is most likely due to reaction between moist ash in the sampling line and the SO_2 in the flue gas. The SO_2 data from these experiments are used with caution during the further data treatment. Additionally, a significant drop in the degree of fulfilment can be observed between the first experimental campaign (Exp number < 50) and the following campaign (Exp number > 50). During the execution of the latter two experiments problems with low suction capacity of the gas sampling pump were observed. This may have provided enough residence time for SO_2 from the flue gas to react with ash in the gas conditioning system. The SO_2 data for these experiments (CA17_M and CO18_M) are likewise used with caution during further data treatment.

Chapter 3

Air and OxyCoal Combustion Reference Cases

This chapter describes the experimental work related to the investigation of the differences in combustion fundamentals when changing the combustion atmosphere from N_2-based (air) to CO_2-based (oxyfuel). The analysis focuses on emissions, burnout, temperature profiles, deposit formation, and ash quality when using coal as fuel. Based on the investigations reference operating conditions are chosen for each type of combustion oxidant which allows a direct comparison of the oxidant types and yield combustion conditions which are relevant with respect to a comparison to full-scale power plants.

3.1 Determining Reference Conditions for Air Firing – Controlling Stoichiometry

The purpose of applying the swirl burner in the current experimental investigations is to simulate combustion in full-scale power plants. However, this is a challenge when performing experiments in down-scaled experimental setups.

The determination of the reference operating conditions for coal combustion in air, when the thermal load is fixed (30 kW), is thus limited to determining an appropriate oxygen excess level. In full-scale power plants an oxygen excess of about 15 %, corresponding to 3 % O_2 in the dry exit flue gas, is typically applied in order to achieve satisfying burnout of the fuel. The work related to choosing the reference operating conditions for coal combustion in air in the swirl burner has taken its starting point in these conditions.

3.1.1 Obtaining Burnout Comparable to Full-Scale Boilers

It can be difficult to obtain high burnout (low loss-on-ignition (LOI)) for solid fuels burned in small-scale experimental setups. However, in order for the results

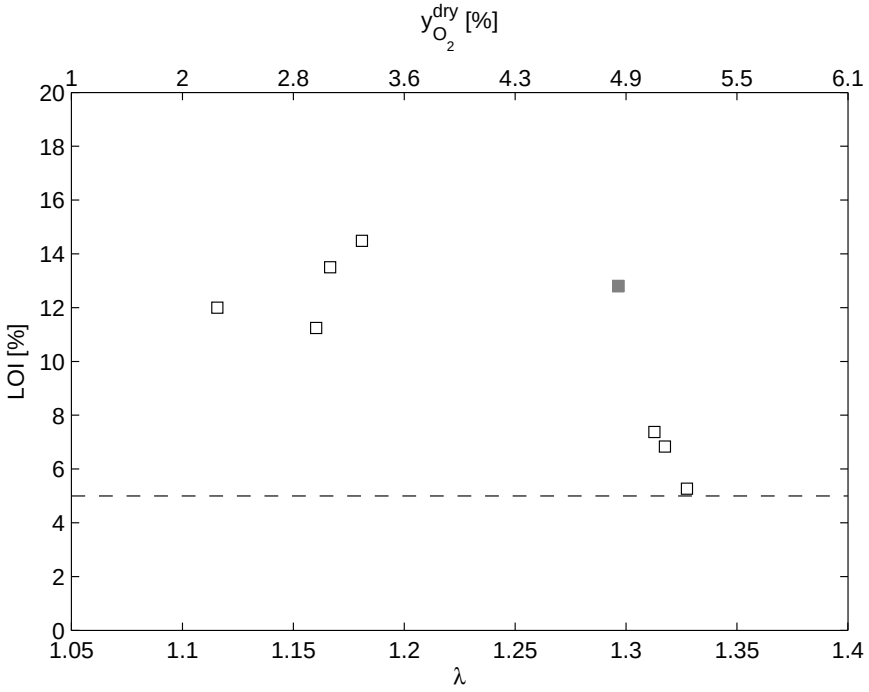

Figure 3.1: Loss-On-Ignition (LOI) for fly ash from coal/air combustion as function of the combustion stoichiometry given both as the stoichiometric oxygen excess ratio, λ, and the theoretical oxygen concentration in the dry flue gas, $y_{O_2}^{dry}$. The dashed line indicate the target LOI value of 5 % according to the maximum allowable LOI for fly ash used in concrete. Note that the two x-axes are not linearly dependent.

from small-scale experiments to be as applicable as possible to operation of full-scale plants a demand is that the burnout is comparable. In this project a target LOI value of 5 % for the ash fraction is therefore put up. This target value corresponds to the maximum allovable LOI for fly ash sold for concrete production [63].

Figure 3.1 shows the development in coal burnout for increasing oxygen excess. It is observed that due to the small scale of the experimental setup it is not possible to yield satisfying burnout at 15 % oxygen excess ($\lambda = 1.15$). Instead, between 30 and 35 % excess oxygen should be applied. The fixed length of the swirl burner setup causes the residence time to decrease with increasing oxygen excess, a factor which counteracts the improvement from increasing oxygen partial pressure in the burnout phase of combustion. For high oxygen excess ratios one might thus observe a decrease in burnout for the applied setup. It should be noted that the fact that an LOI of 5 % has been achieved is very satisfying and not something to take for granted for a setup of the current size.

The data point marked in grey is most probably an outlier as is discussed in Section 3.1.2.

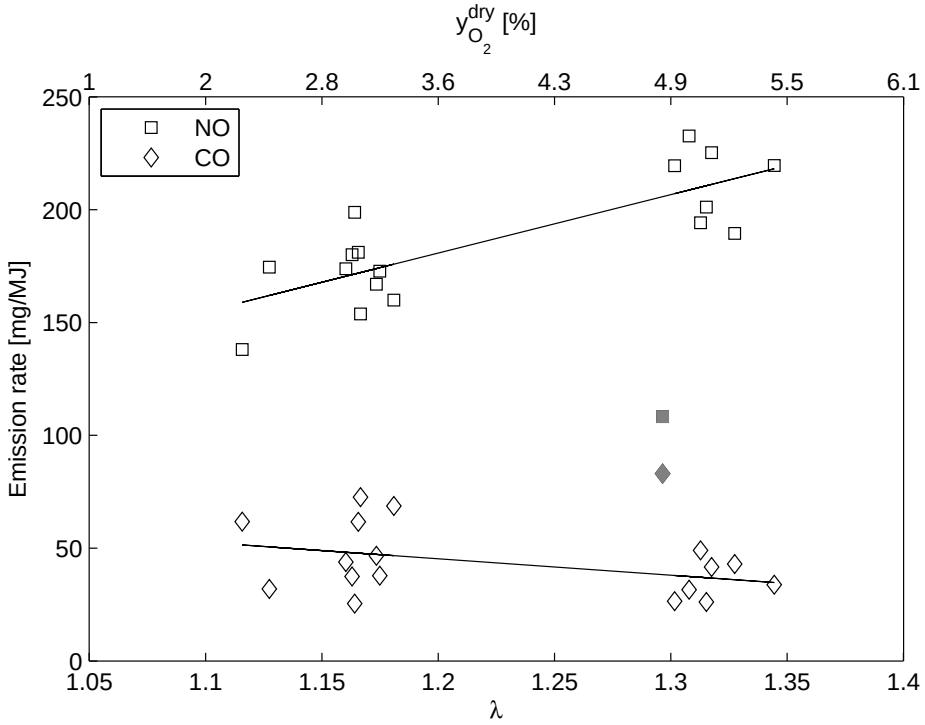

Figure 3.2: Emission rates of NO and CO for coal/air combustion as function of the combustion stoichiometry given both as the stoichiometric oxygen excess ratio, λ, and the theoretical oxygen concentration in the dry flue gas, $y_{O_2}^{dry}$. The full lines show the trends for the two data sets (open symbol data). Note that the two x-axes are not linearly dependent.

3.1.2 Effect of Excess Air on Pollutant Emission Rates

The NO and CO concentrations in the flue gas are typically a function of the oxygen excess. CO is related to the burnout and should thus decrease with increasing oxygen excess. NO formation is typically promoted by increasing oxygen excess [70] as is also seen in Figure 3.2. The observed NO emission rate is at the same level as in full-scale suspension-fired boilers.

SO_2 emissions (not shown) are independent of oxygen excess within the experimental uncertainty as long as the combustion is performed with excess oxygen. Almost all fuel bound sulphur is released to the gas phase as SO_2 when pure coal is combusted and the retention of S in ash and deposits is not strongly influenced by the oxygen excess.

The experiment at $\lambda = 1.29$ (grey points) falls outside the trend observed for the remaining experiments, as was also seen in Figure 3.1. Compared to the remaining data sets, this particular experiment is characterized by a significantly lower NO emission and a decreased burnout (high LOI and high CO) which are characteristic features of a low-NO_x flame. The most probable reason for this

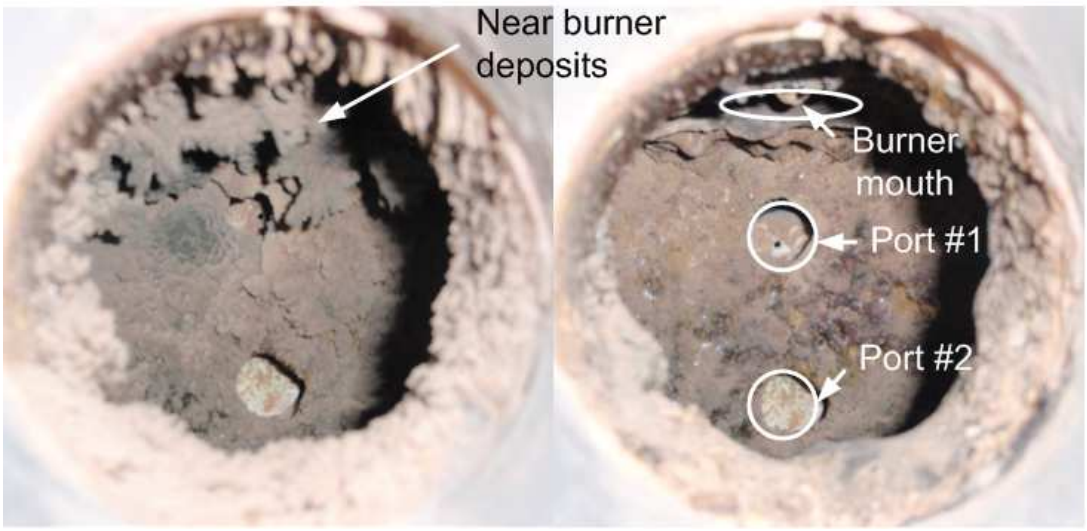

Figure 3.3: Left: Build-up of deposits around burner quarl (top centre) and on furnace walls observed through the top window of the experimental setup. Right: Inside of furnace after removal of deposits near burner.

shift in flame properties is build-up of deposits around the burner quarl during the experiment. This may lead to changes in the near burner fluid dynamics pattern at the flame base causing less O_2 to mix into the fuel. Generally, significant slagging was observed during the coal combustion experiments as seen in Figure 3.3. The deposits were removed between experiments.

Figures 3.4 and 3.5 show that the outlier (grey point) match the linear correlation between NO and CO emission rates as well as the linear correlation between the loss-on-ignition and the NO emission rate. This strongly indicates that it is solely the flame properties that have changed.

3.1.3 Reference Operating Conditions Chosen

In order to have a combustion process which best matches full-scale, a stoichiometric oxygen excess ratio of $\lambda = 1.3$ has been chosen as reference condition for combustion of coal in air. This excess oxygen ratio yields a theoretical concentration of O_2 in the dry exit flue gas of about 5 vol% and a loss-on-ignition for the fly ash which approaches the limit of 5 % set up for fly ash used for cement and concrete production. The reference operating conditions are summarized in Table 3.1.

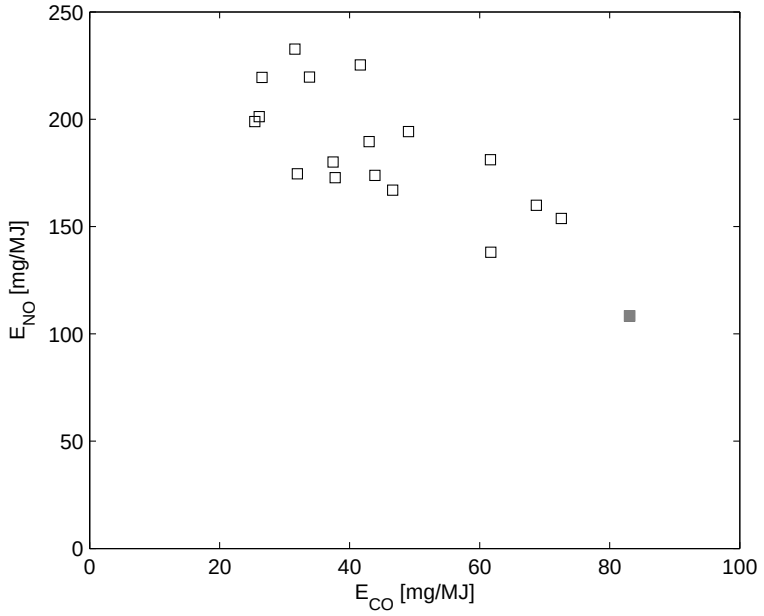

Figure 3.4: Correlation between NO and CO emission rates for coal combustion in air at a range of operating conditions (oxygen excess ratios).

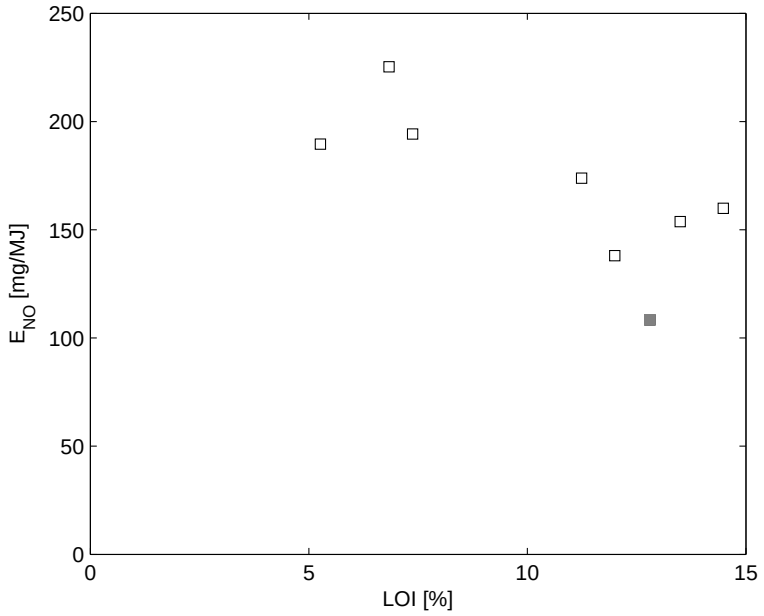

Figure 3.5: Correlation between obtained burnout of fuel, measured by the LOI of the fly ash, and the specific NO emission for coal/air combustion over a range of operating conditions (oxygen excess ratios)

Table 3.1: Operating parameters for coal combustion in air at the reference condition

Operating parameter	Unit	Value
Load	kW_{th}	30
Fuel flow	kg/hr	3.99
λ		1.3
Flue gas exit O_2	vol%	5
Oxidant flow	Nl/min	620
Swirl number		1.8

3.2 Determining Reference Conditions for Oxy-Coal Combustion

Four parameters can be applied as reference in the attempt of choosing the operating conditions for oxyfuel combustion which provides a match to air combustion; the three stoichiometric parameters, λ, $y_{O_2}^{wet}$, and $y_{O_2}^{dry}$, and the burnout of the fuel. As described in Section 2.3.3.1, the change from air to oxyfuel atmospheres induces a new correlation between the stoichiometric parameters. In the current work it has been chosen to use the oxygen excess during burnout measured in the dry exit flue gas, $y_{O_2}^{dry} = 5$ %, as a fix point between air and oxyfuel combustion. The results below thus focus on observing the effect on burnout and emissions when varying the oxygen concentration in the inlet gas and achieving comparable temperature profiles (measured with an S-type thermocouple).

3.2.1 Effect of Inlet Oxygen Concentration on Burnout and Emissions

Figures 3.6 and 3.7 show the effect of varying the inlet oxygen concentration on burnout and emissions. No significant difference in the LOI can be observed when maintaining constant O_2 concentration in the dry flue gas while changing the inlet oxygen concentration. The increased residence time associated with the increase in inlet oxygen concentration does not take effect either. The absence of an improved burnout could be caused by the fact that fuel feeding instabilities were present during these experiments possibly leading to periods with poor burnout regardless of the combined effect of the initially increased partial pressure of oxygen and the longer residence time.

From the emissions results the effect of the increasing availability of oxygen in the flame is observable. The average NO emission rate increases nearly 100 % when increasing the inlet oxygen concentration from 25 to 35 %. Due to the small variations in the stoichiometry between the individual experiments it is not possible to observe a significant trend in the CO emission. The data point marked

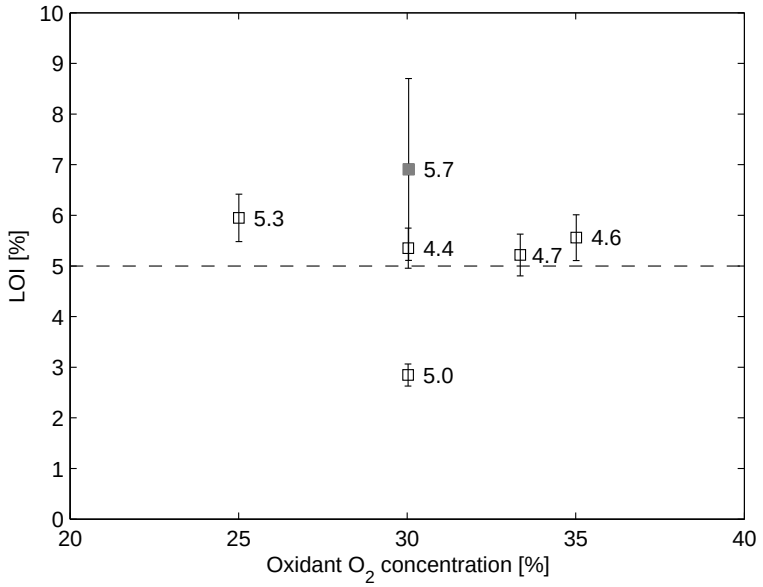

Figure 3.6: Loss-On-Ignition (LOI) for fly ash from coal/oxyfuel combustion as function of the concentration of O_2 in the O_2/CO_2 oxidant mixture. The numbers associated with each data point specifies the average oxygen concentration in the dry exit flue gas, $y_{O_2}^{dry}$ [%], as it was not possible to match the stoichiometry exactly for all experiments. Error bars correspond to two times the standard deviation on the LOI analysis.

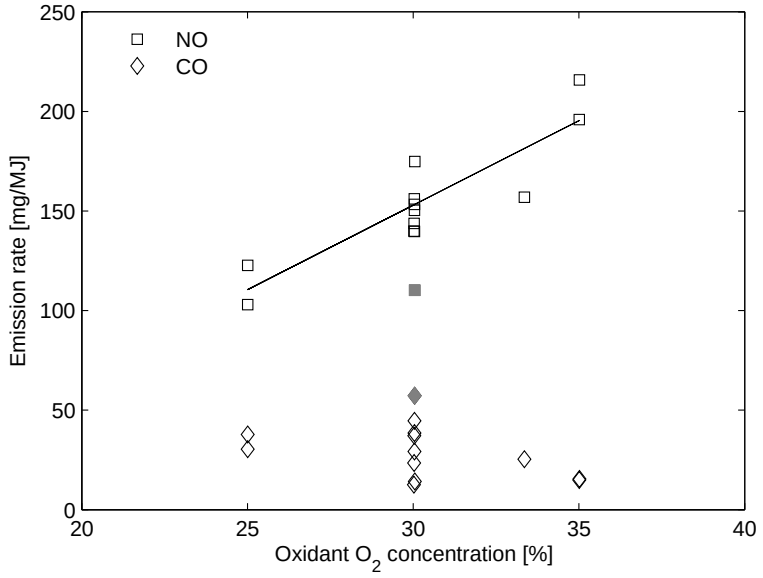

Figure 3.7: Emission rates of NO and CO from coal/oxyfuel combustion as function of the concentration of O_2 in the O_2/CO_2 oxidant mixture. The experiments have been carried out at flue gas oxygen concentrations in the interval $y_{O_2}^{dry} \in [4.2; 5.7]$ %. The line indicates the trend in the NO data (open symbols).

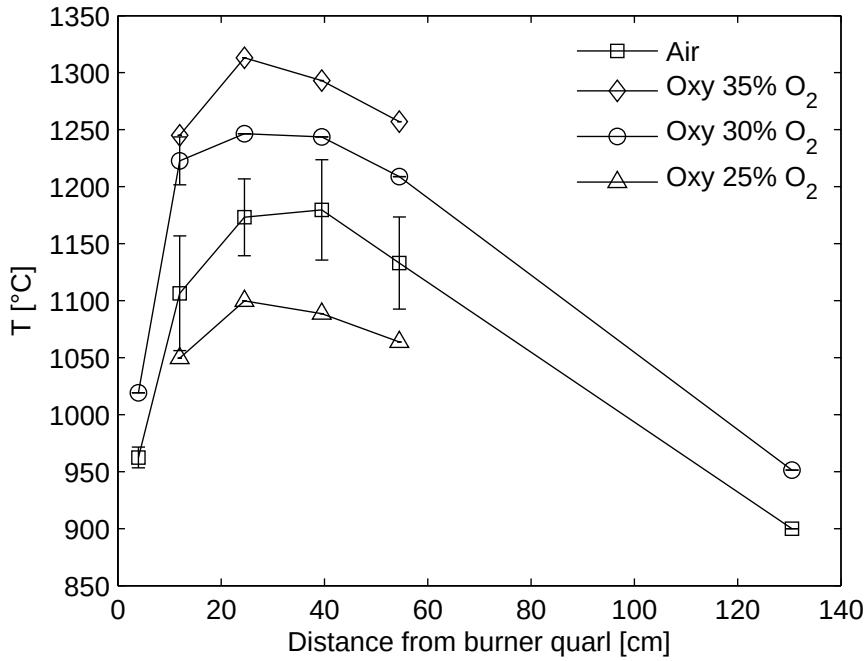

Figure 3.8: Reactor centre temperature profiles measured with S-type thermocouple for pure coal combustion in air and oxyfuel atmospheres with different inlet oxygen concentrations. The O_2 concentration in the exit flue gas has been kept at 5 % for all experiments. Error bars correspond to two times the standard deviation for repeated measurements.

in grey shows the same characteristics as the low-NO_x experiments described in relation to the air reference experiments. From the raw data a clear shift in NO emission was observed prior to ash sampling due to a change in the burner settings. For the remaining data treatment this experiment is considered an outlier.

3.2.2 Matching Air and OxyCoal Combustion Flame Temperatures

Centreline temperature profiles were measured for coal combustion in air and three different O_2/CO_2 atmospheres as seen in Figure 3.8. The temperature is observed to increase with increasing concentration of O_2 at the inlet. However, the peak temperature for the oxyfuel flames, observed at measurement port #3 (24.8 cm from the burner quarl), does not shift its vertical position as a consequence of the change in oxidant composition. For all oxidants a relatively high temperature is observed in the top of the reactor (close to the burner).

A comparison of the air reference temperature profile and the oxyfuel profiles indicates that an inlet oxygen concentration of 27-28 % would yield a match.

Table 3.2: Operating parameters for coal combustion in O_2/CO_2 at the reference condition

Operating parameter	Unit	Value
Load	kW_{th}	30
Fuel flow	kg/hr	3.99
Inlet O_2	vol%	30
λ		1.19
Flue gas exit O_2	vol%	5
Oxidant flow	Nl/min	390
Swirl number		1.8

3.2.3 OxyCoal Reference Operating Conditions Chosen

Based on the measured temperature profiles and fly ash quality it has been chosen to use 30 % O_2 as the reference inlet oxygen concentration. The higher temperatures observed at 30 % O_2 compared to 25 % O_2 at the inlet yields slightly improved burnout on average. Table 3.2 summarises the reference operating conditions.

3.3 Comparing Air and OxyCoal Reference Experiments

This section will investigate the differences in the combustion process between air and oxyfuel reference experiments. Due to the fact that it proved difficult to match the stoichiometry exactly to the defined reference condition, it has been chosen to consider experiments which have been run at an oxygen concentration in the dry exit flue gas between 4.5 and 5.5 % as reference cases.[1]

3.3.1 Changing Combustion Atmosphere – Effect on Combustion Fundamentals

FTIR mapping of the gas phase temperatures at the chosen reference conditions were performed in order to achieve a more accurate comparison than possible from the simple temperature measurements. Figure 3.9 on the following page shows the radial profiles determined with both the FTIR probe and the thermocouple in ports 2 and 4 (12.3 and 39.8 cm from the burner). Near the burner, only a small difference exist between the average temperatures measured for combustion

[1]The relevant experiments are named CA10_AB, CA12_T, CA13_T, CA14_A, CA15_T, CA16_ADT, CA17_M, CO09_AD, CO10_T, CO12, and CO18_M.

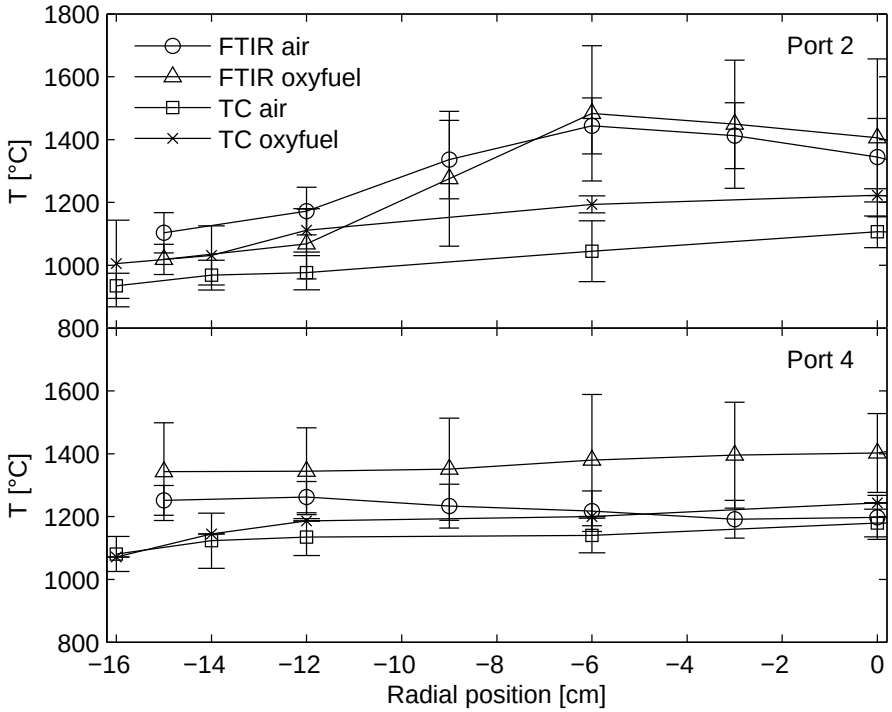

Figure 3.9: Comparison of radial FTIR gas-phase temperature profiles and profiles determined with an S-type thermocouple in selected measurement ports (2 and 4). Error bars on thermocouple data correspond to two times the standard deviation on repeated measurements. Error bars on FTIR data correspond to two times the standard deviation for the 60 scans and provide a measure of the level of fluctuations in the given measurement position.

Table 3.3: Average Loss-on-ignition (LOI [%]), emission rates for NO, SO_2, and CO (in [mg/MJ]), and the Fuel-N $\rightarrow$ NO (CR_N) and Fuel-S $\rightarrow$ SO_2 (CR_S) conversion ratios [%] at the air and oxyfuel reference conditions. The uncertainties correspond to two times the standard deviation on repeated experiments.

	LOI	NO	SO_2 [a]	CO	CR_N	CR_S
Air	6.5 ± 2.2	212 ± 33	389 ± 15	36 ± 18	19 ± 3	85 ± 3
Oxyfuel	2.8 [b]	152 ± 32	382 ± 44	20 ± 16	13 ± 3	84 ± 10

[a] The two experiments with advanced diagnostics mapping (CA17_M, CO18_M) have been omitted due to inconsistencies in SO_2 mass balances.

[b] Only one experiment is available, uncertainty is unknown.

in air and the reference oxyfuel atmosphere with the FTIR probe. Further down the reactor, the oxyfuel flue gas maintains a higher average temperature. This is most likely due to a combination of the higher heat capacity of CO_2 and the fixed amount of cooling air passing the outer surface of the reactor. Compared to the thermocouple data, significantly higher temperatures are observed near the burner when the true gas-phase temperature is measured (FTIR).

Table 3.3 provides a direct comparison of the air and oxyfuel reference experiments regarding burnout and emissions. For the burnout, only one oxyfuel experiment is available within the selected stoichiometric interval. The available experiment shows significantly better burnout than the air references. However, if the observed uncertainty for the air experiments is transferred to the oxyfuel data the difference can no longer be considered significant. It should be noted that the observed uncertainties (95 % confidence levels) become large when only few data points are available as is the case for the present investigation. Liu et al. [71] showed in their 20 kW once-through setup that the carbon-in-ash decreases from about 12.4 to 5.1 % for a UK bituminous coal when changing from air to 30% O_2/CO_2 as oxidant. They kept the stoichiometric oxygen excess ratio, $\lambda = 1.2$, constant for the two combustion atmospheres. This stoichiometric excess ratio corresponds to 3.6 and 5.2 % O_2 in the dry exit flue gas, respectively. Due to the lower level of O_2 during burnout in air compared to the oxyfuel atmosphere, the relative difference in burnout efficiency is larger for the experiments reported by Liu et al. [71] than for this work where the burnout conditions have been kept similar. However, their results are in godd agreement with the comparison shown in Figure 2.21 on page 47 for this work using λ as the independent variable.

Considering the emissions of CO and SO_2, no difference between the two combustion atmospheres can be determined. This is in agreement with observations from other once-through setups as reported by Liu et al. [71] and Croiset and coworkers [72, 73]. The conversion of Coal-S to SO_2 is slightly higher, 86-90 % for both atmospheres, in [71] than observed in this work. This could be a result of

the different Fuel-S contents (UK bit: 2.06 % compared to 0.62 % (COCERR)). With a lower sulphur content of the parent coal a comparably larger capacity for capture of sulphur exist in the fly ash if the amount of the different ash-forming species is similar. The Fuel-S to SO_2 conversion would thus be lower for the low-sulphur coal.

With respect to NO there is a tendency for decreasing emission rate when changing from air to oxyfuel combustion. On average, the NO formation during oxyfuel combustion of coal is reduced about 28 % compared to air-firing. Croiset and coworkers [72, 73] and Liu et al. [71] likewise reported a reduction in the NO emission compared to combustion in air in their once-through experiments. Liu et al. [71] showed that the Coal-N to NO conversion ratio was 27.6 % for air combustion and was reduced to about 80 % of that (22.6 %) for combustion in 30 % O_2/CO_2. The Fuel-N conversion ratio determined in this work is slightly lower for both air and oxyfuel combustion. This is most likely due to differences in the burner design and operating conditions. Four aspects regarding the combustion process could contribute to the reduced NO emission during oxyfuel combustion of the applied coal.

Reduced thermal NO formation The near elimination of N_2 from the oxyfuel oxidant will limit the formation of NO to Fuel-NO. In pulverized coal flames Fuel-NO typically accounts for about 80 % of the NO emission [70]. However, due to the high levels of NO formed from Fuel-N, temperatures in excess of 1900 °C should be obtained in order for thermal NO to contribute significantly to the NO emission from coal flames [70]. In this work flue gas temperatures up to 1700 °C were observed (Fig. 3.9). The difference in NO emission rates between air and oxyfuel combustion is thus not expected to be caused by reduced formation of thermal NO.

Smaller flue gas volume The smaller flue gas volume during oxyfuel combustion compared to combustion in air at comparable oxygen levels in the flue gas will reduce the dilution of the NO concentration within the furnace. A higher level of NO in the flue gas will increase the reaction rate for the 2. order reduction of NO with other nitrogen-containing species [70] thus leading to reduced NO emission.

Increased formation of CO in flame CO is known to promote the reduction of NO over char [70]. In-flame CO levels are reported to increase significantly during oxyfuel combustion compared to air-blown flames [59] and there is thus an increased potential for reduction of NO over char. CO levels of 5 % on average for oxyfuel combustion were measured about 12 cm from the burner (port 2) in this work, see Figure 4.8 on page 86.

Near burner fluid dynamics Depending on the obtained stoichiometry at the point of mixing of fuel and oxidant, NO emission rates can both increase

and decrease when changing from air to oxyfuel combustion. Mixing at reducing conditions will lead to an increase in the formation of NO whereas NO formation is inhibited at both stoichiometric and fuel-lean conditions. The presence of high CO_2 concentrations acts to increase the concentration of OH radicals under fuel-rich conditions thus promoting NO formation from volatile-N. When mixing occurs at conditions with oxygen excess, the reduced formation of NO is caused by a limitation of the O/H radical pool, particularly O, from the increased level of CO_2 [74, 75]. Since the burner applied in this work has been operated in high-NO_x mode, i.e. mixing of fuel and oxidant takes place at fuel-lean conditions, a decrease in NO formation compared to the air reference case should be expected.

The observed difference in the emission rate of NO from combustion in air and the reference oxyfuel atmosphere is most likely a consequence of a combination of the latter three effects. The relative importance of each mechanism is unknown.

3.3.2 Changing Combustion Atmosphere – Effect on Ash Quality and Deposit Formation

The particle size distribution for the fly ashes from air and oxyfuel combustion are shown in Figure 3.10 on the following page. Both distributions have the general, bimodal appearance with a peak between 0.1 and 1 μm and another around 10 μm. The small particles typically originate from aerosols and approximately 10-20 % (volume basis) of the fly ash particles have diameters below 1 μm. The larger particles stems from the residual ash particles formed during combustion. The reduced burnout during air combustion can explain the shoulder at 100 μm as the presence of residual carbon will increase the particle size of residual ash particles, see Figure 3.11 on the next page.

A full analysis with respect to the composition of the fly ash samples from experiments CA14_A and CO09_AD and the deposits from experiments CA16_ADT and CO09_AD have been obtained. Figure 3.12 on page 71 shows a comparison of the bulk composition of the fuel ash, fly ash, and deposits for the coal references. Except for S and Cl, the bulk composition of the fuel and fly ashes are similar. The main part of S and Cl is released to the flue gas as SO_2 and HCl. There is a slight tendency for the Si and Fe levels to increase in the deposits and the Al level to decrease. However, the difference to the ash fractions is small.

Even though the bulk composition of the fuel and fly ashes is similar, it is unknown whether there could be a difference in the types of minerals present in the two combustion atmospheres. An obvious question is if the significantly increased concentration of CO_2 in the furnace could lead to increased carbonate formation. Table 3.4 on page 71 shows the results from an analysis of the total carbon (organic and inorganic) and the total organic carbon (TOC) content of

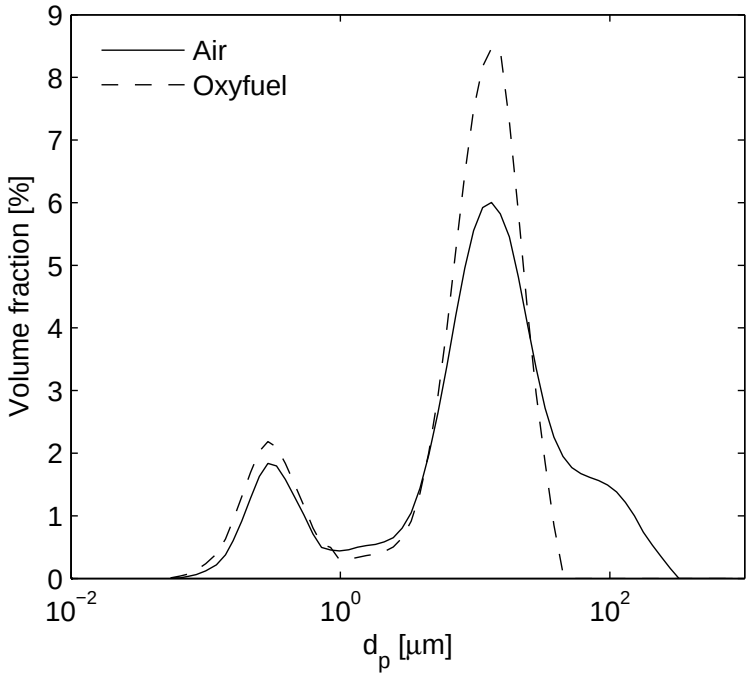

Figure 3.10: Comparison of ash size distributions for coal combustion in air and 30% O_2/CO_2 at the reference conditions. The ash is the combined cyclone and filter ash fractions from the ash sampling system. The distribution type is volumetric and is obtained from a Malvern laser diffraction particle size measurement.

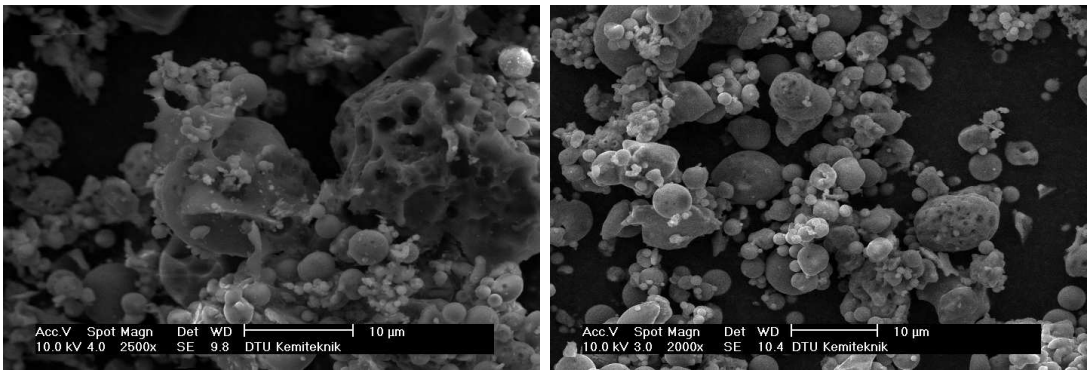

Figure 3.11: SEM images of fly ash. Left: coal combustion in air at $\lambda = 1.25$ ($y_{O_2}^{dry} = 4.4$ %); Right: coal combustion in 30 % O_2/CO_2 at $\lambda = 1.3$ ($y_{O_2}^{dry} = 7.3$ %). Even though the applied combustion conditions do not match the chosen reference values the influence on the size distribution of the fine ash particles is assumed to be negligeble.

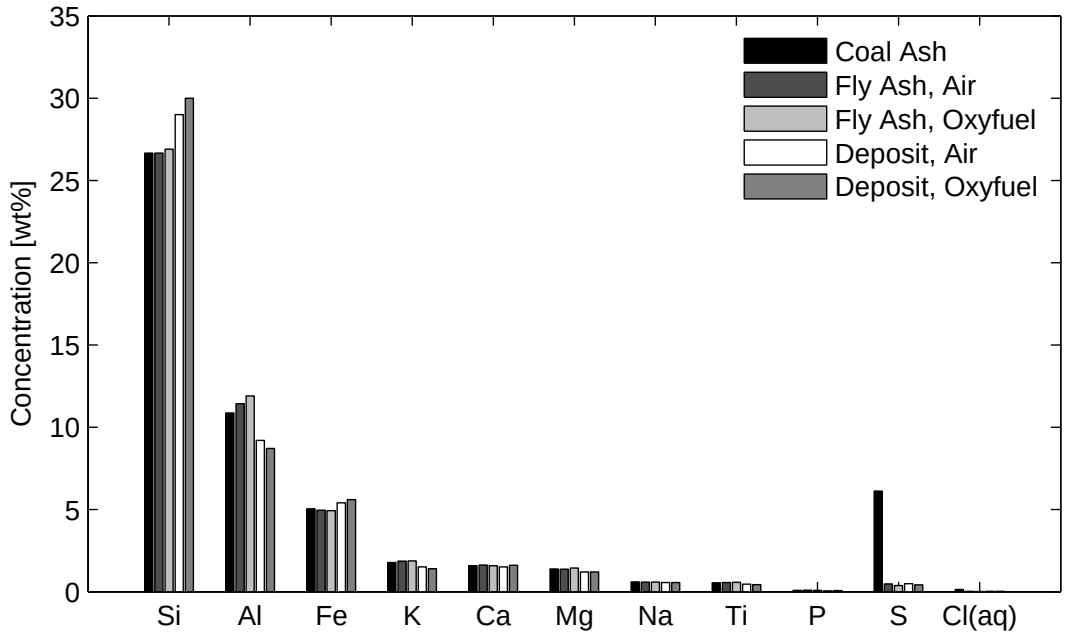

Figure 3.12: Comparison of fly ash and deposit compositions for coal combustion in air and 30% O_2/CO_2 at the reference conditions. The uncertainty is about 10 % on the individual values.

Table 3.4: Total carbon (C) and total organic carbon (TOC) contents of combined filter and cyclone ash fractions for air and oxyfuel coal references

	Air	Oxyfuel
C (total)	5.6 ± 0.5	2.6 ± 0.2
TOC	5.4 ± 0.3	2.4 ± 0.2

the air and oxyfuel ashes. The difference between the two values is a measure of the carbonate content of the ash. No difference can be observed between the two combustion oxidants and for the applied setup, oxyfuel combustion will thus not lead to increased carbonate formation in the fly ash. The appearance of the deposits from the two atmospheres is likewise similar as seen in Figure 3.13 on the following page. The upstream part of the deposits was loose and powdery, and easily removable from the deposit probe. The downstream part of the deposit could be identified as a condensed layer. The potential difference in the composition of upstream and downstream deposit fractions was not determined as the two fractions were mixed prior to analysis. However, the difference can be expected to be negligible.

Nothing in the data indicates that the change from air to O_2/CO_2 as oxidant will lead to significant differences in the mineralogy of the fly ash or deposits.

Figure 3.13: View of deposits from the side. The deposit probe has a diameter of 16 mm and the thickness of the upstream deposits is about 1 mm. Top: coal/air combustion; Bottom: coal/oxyfuel combustion. The upstream part of the probe faces upwards in the picture. Colour differences are a consequence of the picture recording.

Table 3.5: Average deposit fluxes as well as flue gas and deposit probe temperatures for air and oxyfuel coal references

Oxidant	Upstream [g/m^2·hr]	Downstream [g/m^2·hr]	Average [g/m^2·hr]	T_{probe} [°C]	T_{FG} [°C]
Air	107	11	59	500	900
Oxyfuel	75	3	39	500	950

The deposits were sampled during a period of about 2 hours. Based on the mass of deposits collected from the upstream and downstream halves of the probe the deposit flux for each atmosphere has been determined. Table 3.5 shows the results. The uncertainty on the fluxes to the downstream part of the probe are relatively large due to very small sample sizes. There is an indication that the deposit flux is smaller during oxyfuel combustion than in air. Due to very low flue gas velocities and small particle sizes the difference cannot be explained by variations in inertial impaction on the probe. Due to the fact that only one data set exist for each atmosphere, it is unknown whether the observed difference is within the experimental uncertainty. However, no obvious explanation to the difference exists.

3.4 Summary and Conclusions

Reference operating conditions for coal combustion in air and O_2/CO_2 at a thermal load of 30 kW have been defined. In order to yield experimental results comparable to full-scale boilers a target of a loss-on-ignition of maximum 5 % was set up for the fuel burnout efficiency. The target was reached for air-firing at a stoichiometric oxygen excess ratio of $\lambda = 1.3$ corresponding to 5 % O_2 in the burnout stages of combustion (measured in the dry exit flue gas).

The O_2 concentration in the char burnout stage (i.e. 5 vol%) were applied as the standard of reference during the work related to defining the reference operating parameters for oxyfuel combustion. Three different oxidant compositions (25, 30, and 35 % O_2 in CO_2) were investigated with respect to burnout efficiency, flame temperature profiles, and emissions. The investigations showed that a match of temperatures could be obtained with an inlet O_2 concentration between 25 and 30 %. An oxidant composition of 30 % O_2 in CO_2 was chosen as the reference case due to slightly improved burnout efficiency compared to 25 % O_2 in CO_2.

A comparison of the air and oxyfuel reference cases showed no significant differences between burnout efficiencies or emissions of CO and SO_2 even though there was a tendency for improved burnout. NO emissions from oxyfuel combustion was reduced approximately 28 % compared to combustion in air. The reduced NO emission is suggested to be a consequence of three effects; (1) higher NO levels in the flue gas promoting gas-phase reduction due to NO reacting with other nitrogen-containing species; (2) Increased reduction of NO over char due to significantly higher levels of CO in the flame zone; and (3) the application of a high-NO_x burner in combination with the alterations to the radical pool caused by the significantly increased concentration of CO_2. The composition of fly ash and deposits do not change with the change in combustion atmosphere. The deposit flux was, however, observed to be reduced about 30 % in oxyfuel compared to air combustion. No explanation was found for the difference in deposit flux. Good agreement between the results obtained in this work and results reported in open literature for comparable once-through reactors was observed.

Chapter 4

OxyFuel Combustion for Below-Zero CO_2 Emissions – Co-Firing Coal and Biomass

Co-firing coal with biomass is a relatively easy way of reducing CO_2 emissions from fossil fuel fired power plants. However, the biomass share of the fuel blend is typically kept low ($<$ 20 wt%) in order to ensure that residual products can be utilized, to prevent deactivation of SCR catalysts, and to reduce superheater corrosion risks. Oxyfuel combustion can be applied to biomass as well as coal and the use of CO_2 neutral fuels induces the potential of achieving an overall negative CO_2 emission from the power plant. The objective of this chapter is to illustrate the impact on the combustion characteristics including flame temperature, burnout, emissions, as well as fly ash and deposit characteristics when pure biomass (straw) and blends of coal and biomass are combusted in air and oxyfuel atmospheres. All experiments described in the following have been performed with equal thermal input (30 kW) and at the reference oxygen excess of 5 % in the dry flue gas. For oxyfuel experiments the inlet oxygen concentration is fixed at 30 %.

4.1 Flame Temperature – Effect of Fuel Change

Due to the differences in fuel characteristics between coal and straw, differences in ignition, flame shape, and temperature profiles are expected. The utilized straw has a significantly higher content of volatiles as well as a larger average particle size compared to the coal, see Table 2.2 on page 20. This section provides results from two different temperature measurement techniques; Thermocouple and FTIR; applied in the characterization of the effect of fuel change.

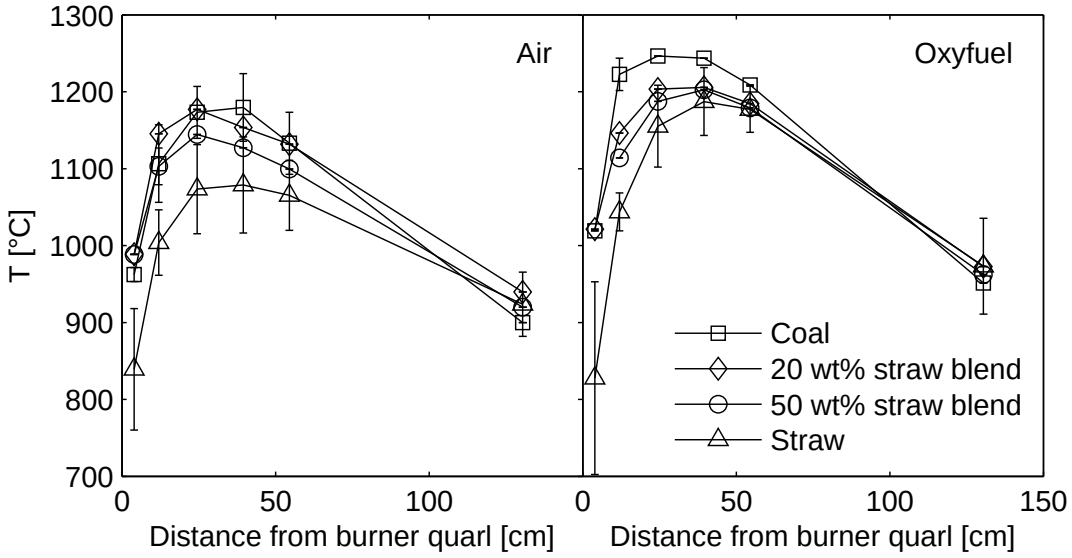

Figure 4.1: Reactor centreline temperature profiles measured with S-type thermocouple for co-firing experiments in air and in the oxyfuel atmosphere with 30 % O_2. Errorbars correspond to two times the standard deviation for repeated measurements.

4.1.1 Simple Flue Gas Temperature Measurements

Simple temperature measurements are performed with an S-type thermocouple as described in Section 2.3.2.5. Figure 4.1 shows reactor centre line profiles for the four investigated fuel blends for both air and 30 % O_2/CO_2 as oxidant. Figure 4.2 on the facing page shows a direct comparison of the temperature profiles for the pure fuels in the two combustion atmospheres. For both combustion atmospheres, near burner temperatures increase with increasing coal share of the fuel. The temperature difference between pure straw and the other three fuels when burned in air is significant and the presence of up to 50 wt% straw in the coal/straw blend does not significantly change the temperature profile compared to pure coal firing. The temperature profile for straw combustion in both atmospheres shows the characteristics of delayed ignition compared to the coal containing flames, i.e. a steeper temperature gradient in the first 3 measurement positions. Visual inspections of the flame proved this since a distinct, cold fuel jet was observable at port 1 with flame ignition initiating at port 2. For the remaining fuel blends ignition was observable at port 1. Peak flame temperatures are generally positioned between ports 3 and 4 (25 to 40 cm from the burner quarl). The peak flame temperature position for pure straw was likewise moved downstream from the burner relative to the remaining fuels.

The oxyfuel temperature profiles show similar peak flame temperature positions to the air profiles. However, in each specific position the temperature is generally higher than for air as oxidant as was also shown for pure coal in Section

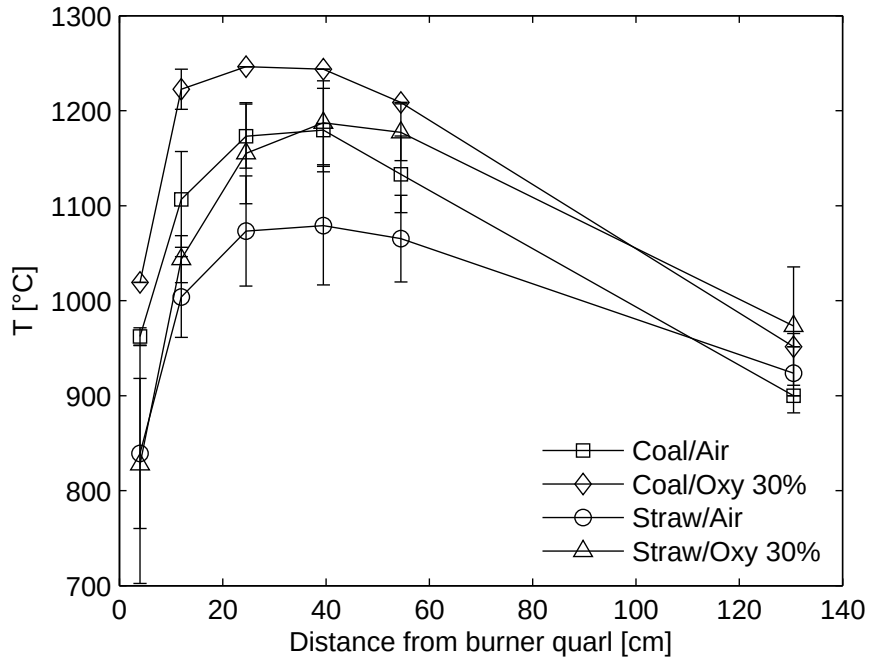

Figure 4.2: Comparison of reactor centre temperature profiles measured with S-type thermocouple for coal and straw combustion in air and the reference oxyfuel atmosphere. Error bars correspond to two times the standard deviation for repeated measurements.

3.2.2. The effect of changing combustion atmosphere is most pronounced for pure straw combustion where a temperature difference of more than 100 °C is measured in ports 4 and 5, see Fig. 4.2. Contrary to the case of air-firing, pure coal yields higher temperatures than blends. For the blends the straw content seems to have an insignificant effect on temperature. Compared to air combustion, less difference between coal-containing fuels and pure straw for the last three measurement points (ports 4, 5, and 7) exists in the oxyfuel case.

4.1.2 FTIR Measurements of Gas Phase Temperature

FTIR temperature mappings, see Section 2.3.2.6, have been performed for pure coal and the 50 wt% straw blend in air and 30 % O_2/CO_2 and for pure straw combustion in 30 % O_2/CO_2. However, during straw combustion only measurements with the beam stop were performed and for coal/oxyfuel combustion only ports 2 and 4 were mapped without the beam stop. Figure 4.3 on the next page compares the measured profiles for coal and the 50 wt% straw blend. A trend similar to the one observed from the simple temperature measurements with oxyfuel yielding higher centreline temperatures than combustion in air is seen. Also, the 50 wt% straw blend generally yields slightly lower temperatures than pure coal. For all fuels, peak temperatures reaching 1600-1700 °C are observed and the

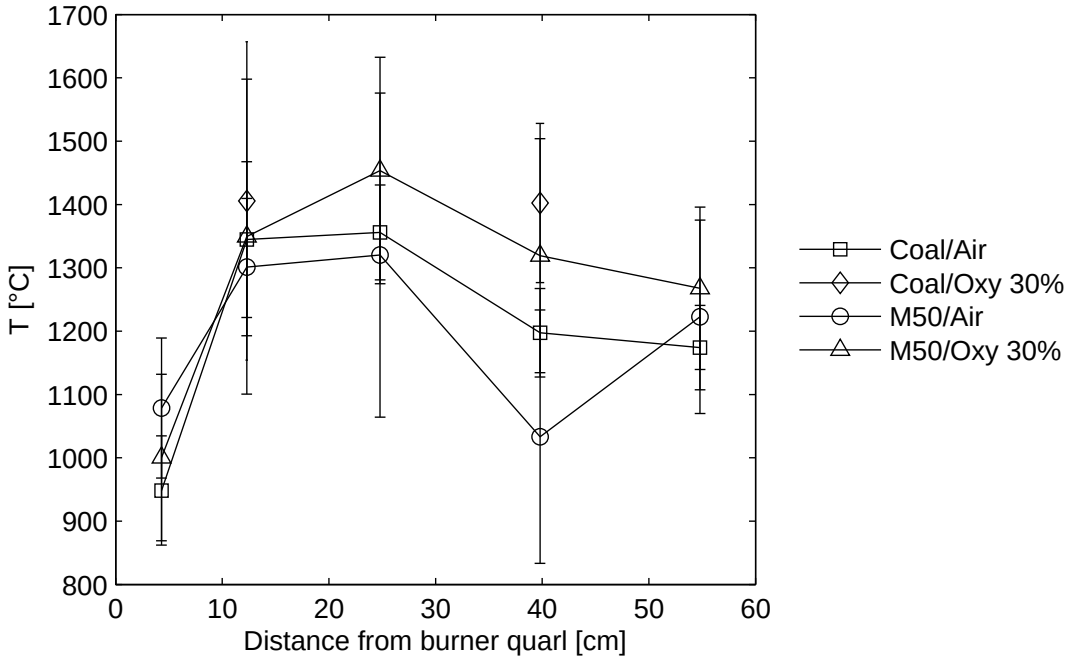

Figure 4.3: Comparison of reactor centre temperature profiles measured with the FTIR probe for combustion of coal and the 50 wt% straw blend in air and the reference oxyfuel atmosphere. Error bars correspond to two times the standard deviation for each time series and is a measure of the level of fluctuations in the given measurement position.

gas-phase temperatures are generally higher than what was observed from the thermocouple measurements which were not corrected for radiation. Since the furnace walls are cooled their radiative flux to the thermocouple will act to lower the measured temperature. The M50/air temperature shows an unexplainable drop at 40 cm from the burner. This is most likely due to either problems during the conversion of the obtained spectra to temperatures or errors during the measurement.

4.2 The Impact of Fuel Properties on Burnout

Co-firing coal with up to about 20 wt% straw is seen to improve the carbon burnout in full-scale plants [76]. Occasionally, unburned straw particles (from the nodes of the straw) can be observed in the fly ash. However, the overall burnout efficiency is not affected significantly by this.

Fly ash samples collected for combustion of the four investigated fuel blends in air and the reference oxyfuel atmosphere supports this trend, when the straw share does not exceed 20 wt%. Figure 4.4 on the following page shows the loss-on-ignition analysis results and the calculated carbon burnout efficiency for each condition as function of the fuel straw share. The carbon burnout efficiency (CB) is determined from (4.1).

$$\begin{aligned} \mathrm{CB} &= \frac{m_{C,\,fuel} - m_{C,\,ash}}{m_{C,\,fuel}} \\ \mathrm{CB} &= \frac{x_{C,\,fuel} - \frac{x_{C,\,ash}}{(1-x_{C,\,ash})}\, x_{ash,\,SF}}{x_{C,\,fuel}} \end{aligned} \tag{4.1}$$

where $m_{C,\,Fuel}$ is the amount of carbon fed with the fuel (kg/kg fuel) and $m_{C,\,ash}$ is the amount of carbon leaving the reactor with the fly ash (kg/kg fuel). It is assumed that all ash entering the reactor leaves as fly ash, i.e. deposition within the reactor is neglected. Since ash particles that are retained as deposits within the reactor are assumed to yield full burnout, see the discussion related to the carbon balance in Section 2.4.1, this assumption will lead to a conservative estimate of the burnout efficiency since the amount of carbon retained in fly ash is slightly overestimated. $x_{C,\,fuel}$ is the carbon content of the fuel given by the ultimate analysis. $x_{C,\,ash}$ is the measured carbon content of the fly ash sample and $x_{ash,\,SF}$ is the ash content of the fuel.

For both combustion atmospheres increasing the fuel straw share beyond 20 wt% leads to reduced burnout. The reduced burnout efficiency is mainly due to an increased amount of large straw and straw char particles being transported through the furnace with limited conversion of the fixed carbon content. Table 4.1 on page 81 illustrates the differences between the bottom ashes for the eight fuel/oxidant combinations investigated. From the pictures it is evident that

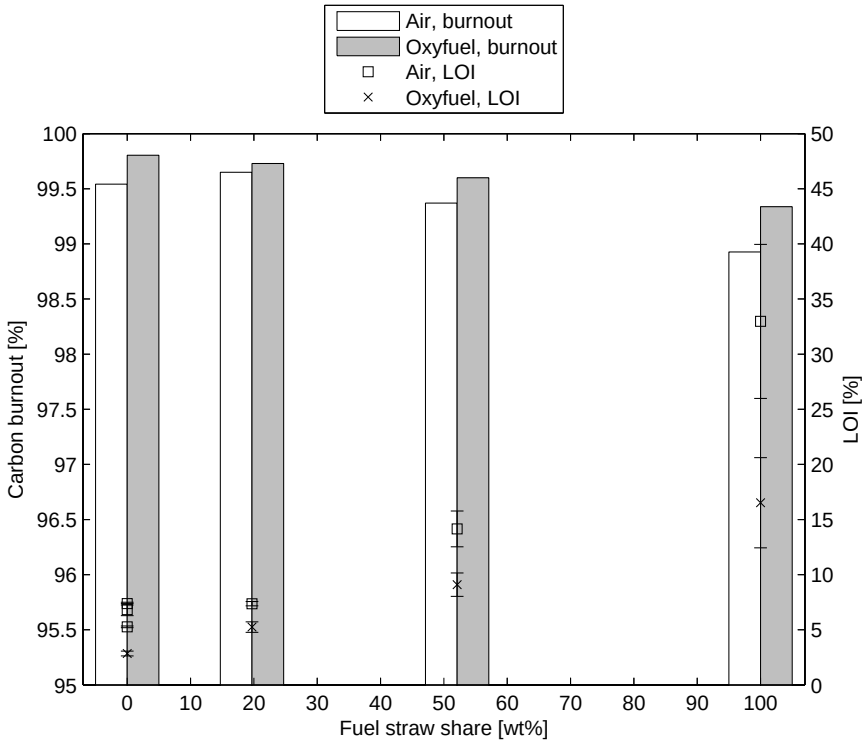

Figure 4.4: Calculated carbon burnout and loss-on-ignition analysis of fly ash as function of fuel straw share. Comparison of air and oxyfuel environments at the reference operating conditions. The error bars correspond to two standard deviations on the LOI analysis.

Table 4.1: Appearance of bottom ash samples collected from the setup. Top row: Air combustion experiments, bottom row: oxyfuel combustion experiments. Fuel straw share increases from left to right. Each picture has dimensions of approximately 20x20 mm.

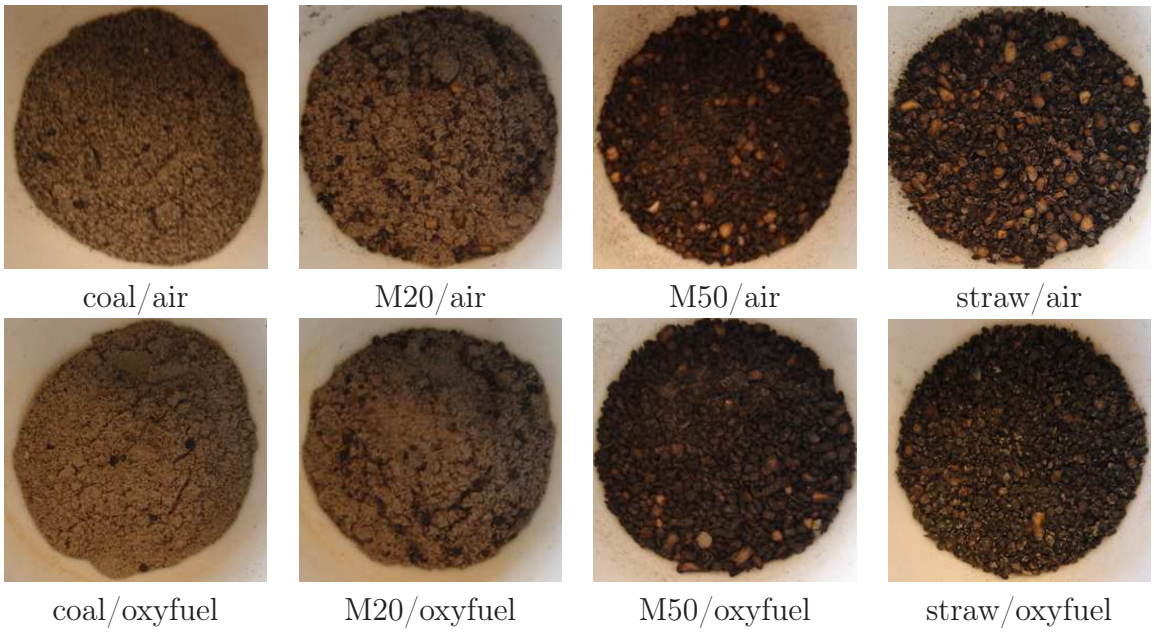

an increasing number of large straw particles ($d_p = 0.5 - 1$ mm) are transported through the furnace without being burned. Especially the increasing fraction of particles which still appear yellow and only have been blackened at the edges for the air experiments are contributing to the decreasing burnout efficiency and increasing LOI with increasing fuel straw share. Due to the lower fuel ash content of straw compared to coal (4.4 versus 9.6 %) the LOI values for the pure straw fly ashes appear very large even though the overall burnout is about 99 %. The increasing uncertainty in the values for increasing straw share is due to the high fraction of straw char particles in the bottom ash fraction making it increasingly difficult to extract a representative sample for analysis. The LOI value for straw/air is an average of 4 measurements (3 for the oxyfuel experiment).

The most likely explanation to the appearance of yellow particles is that they shoot directly through the flame without ignition. Visual inspection of the flame from the bottom of the reactor likewise revealed a significant portion of visible particles below the flame, see Figure 4.5 on the following page. Note that the pictures illustrate instantaneous flame shapes. Due to the swirling motion of the oxidant the fuel particles can be observed to burn in a rotating band down through the furnace and hence the flame is not axisymmetric.

Figure 4.6 on page 83 shows estimated heating profiles of straw particles of three characteristic sizes under the assumption that they do not ignite. The tem-

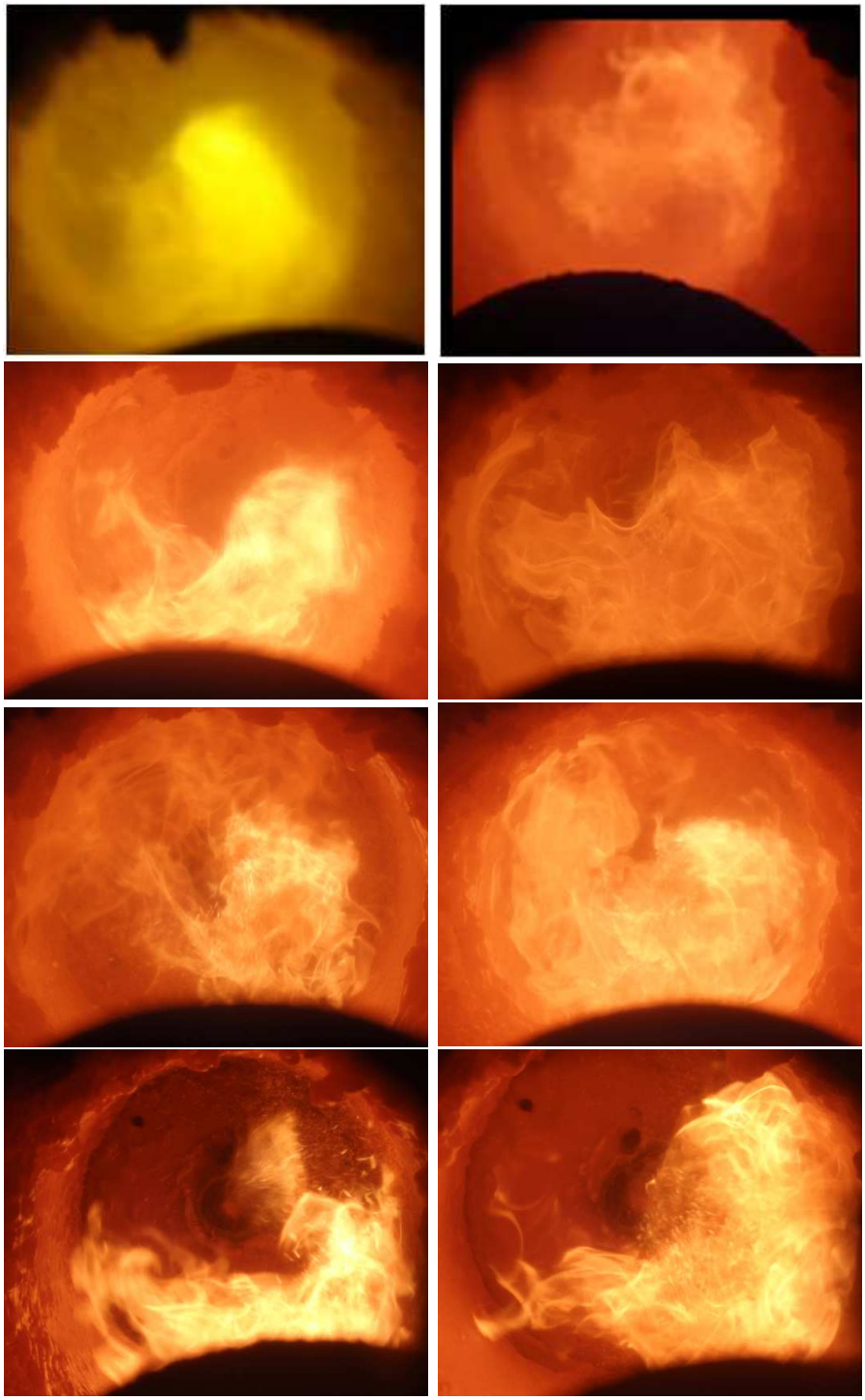

Figure 4.5: Appearance of flames recorded through the bottom of the reactor. Left column: Air combustion experiments, right column: oxyfuel combustion experiments. Top row: pure coal; second row: fuel straw share: 20 wt%; third row: fuel straw share: 50 wt%; bottom row: pure straw.

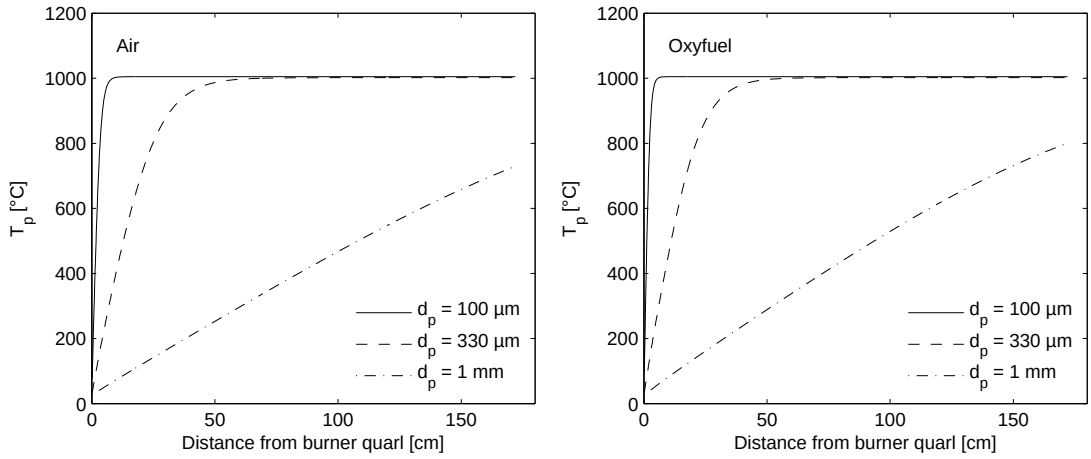

Figure 4.6: Heating profiles for straw particles of different size, assuming isothermal temperature gradient through particle and heating by both radiation and convection. Comparison of combustion in the reference air and oxyfuel atmospheres.

perature profiles are determined from combined radiative and convective heating of the particles by means of the energy balance shown in Eq. (4.2).

$$m_p C_{p,p} \frac{dT_p}{dt} = \pi d_p^2 \cdot \left(h \left(T_g - T_p \right) + \epsilon_p \sigma \left(T_w^4 - T_p^4 \right) \right) \tag{4.2}$$

Appendix D provides an overview of the parameters and the values applied.

The heating profiles show significant differences between the three particle sizes. Whereas the smaller particles reach temperatures of 1000 °C within the first 10 cm of the reactor, the largest particles are heated considerably slower. The slow heating of the 1 mm particles means that they reach the lower part of the furnace before being heated enough to ignite. In that position the partial pressure of oxygen surrounding the particles have dropped to about 5 vol%, further decreasing the ignitability of the particles. The result is that large straw particles leave the reactor with no or a very small degree of conversion as observed experimentally. Besides the effect of the size of the particles on the heating rate, their velocity relative to the flue gas will differ due to the difference in mass with increasing diameter. Table 4.2 on the following page shows average terminal velocities of the investigated particle sizes and their residence time within the furnace. The data further elucidate the problems encountered with large straw particles regarding burnout since the residence time is very limited. Due to the smaller flue gas flow during oxyfuel combustion the residence time is longer and hence the burnout should increase. The large increase in the terminal velocity of large particles compared to the smaller size fractions is especially a problem with respect to down-fired reactors as the one applied in this work. In full-scale boilers were the flue gas moves in the upward direction, the increased terminal velocity of large particles actually will increase their average residence time within the

Table 4.2: Terminal velocity, u_t, and average residence time, τ_p, of large straw particles in furnace

	Air		Oxyfuel	
d_p [μm]	u_t [m/s]	τ_p [s]	u_t [m/s]	τ_p [s]
100	0.05	2.42	0.05	3.25
330	0.59	1.38	0.61	1.58
1000	2.61	0.53	2.34	0.61

boiler compared to the smaller particles. For similar conditions, the burnout of large particles in full-scale boilers is thus expected to improve compared to what has been shown in this work.

The burnout efficiency is consistently higher during oxyfuel combustion than when using air as oxidant. The difference between the two atmospheres seems to increase with increasing fuel straw share. This indicates the relatively higher importance of the combined effect of the higher inlet O_2 concentration, increased maximum flue gas temperature, and increased residence time during oxyfuel combustion for the burnout of large straw char particles. Figure 4.7 on the next page shows the radial profiles of CO for the first 55 cm of the furnace (ports 1-5). The figure illustrates the change in flame length and width with the change in fuel composition. Downstream of the flame the CO is typically very low due to sufficient O_2 to oxidize CO to CO_2. However, near the flame front the concentration of CO can reach very high levels. For pure coal, the centreline concentration of CO (position 0 cm) drops to zero in port 5, whereas combustion of pure straw shows significant levels of CO (about 5% on average) at this distance from the burner. The flame length of pure straw is thus considerably larger than for pure coal elucidating the increasing importance of increased residence time on the burnout efficiency for increasing fuel straw share.

The exit flue gas CO emission as function of the fuel straw share is seen in Figure 4.8 on page 86. The figure shows a trend for pure straw experiments to yield increased CO emissions, the trend is however not consistent due to the large spread on the data. For several of the pure straw experiments the CO emission rate is observed to increase during the course of the experiment. The emission is also very sensitive towards external disturbances of the furnace, e.g. frequent changes to the pressure due to opening of measurement ports. From an overall perspective it is possible to obtain satisfactory low CO emissions for all fuel/oxidant combinations taking the relatively small size of the experimental setup into consideration.

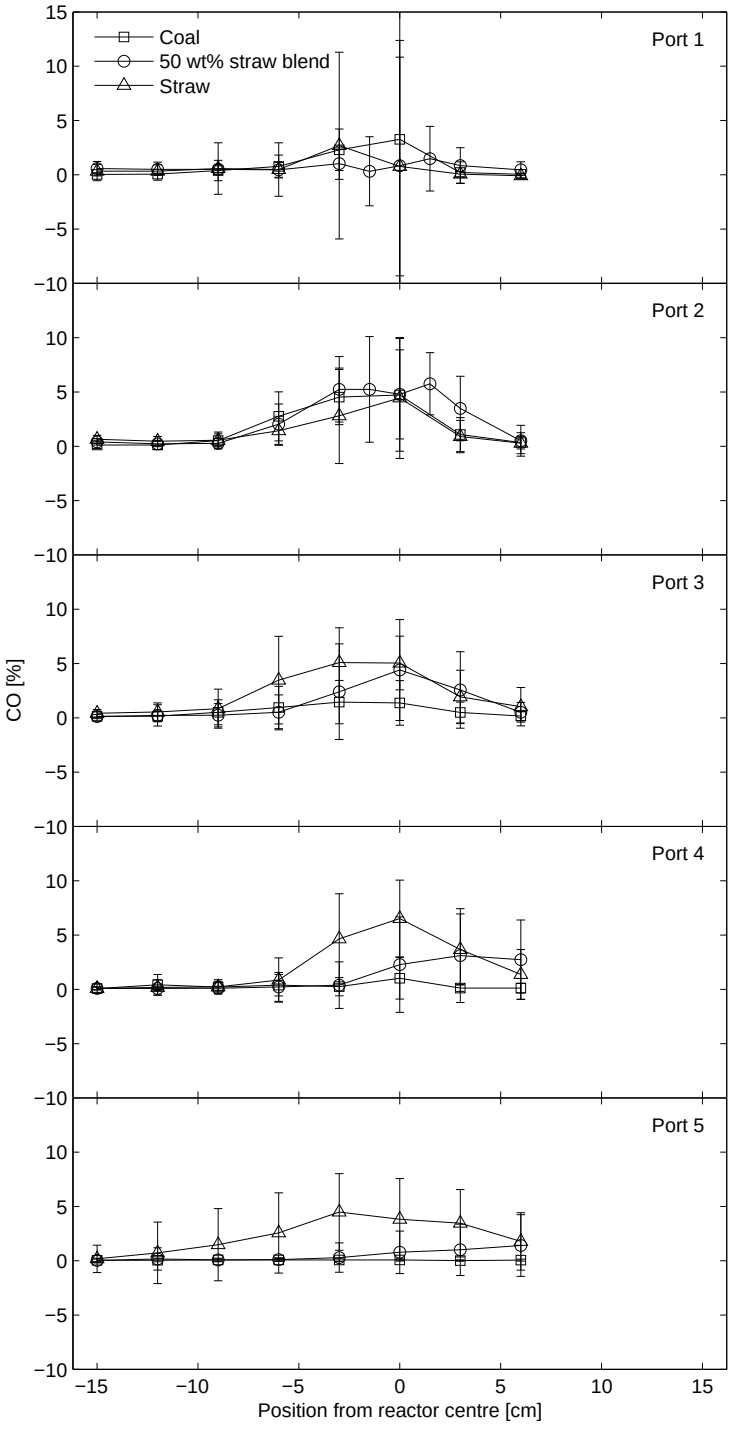

Figure 4.7: Radial profiles of CO concentrations for combustion of coal, straw and the 50 wt% straw blend in the reference oxyfuel atmosphere. The profiles are measured with the FTIR probe. Error bars correspond to two times the standard deviation on the 60 measurements in each position and is a measure of the level of fluctuations.

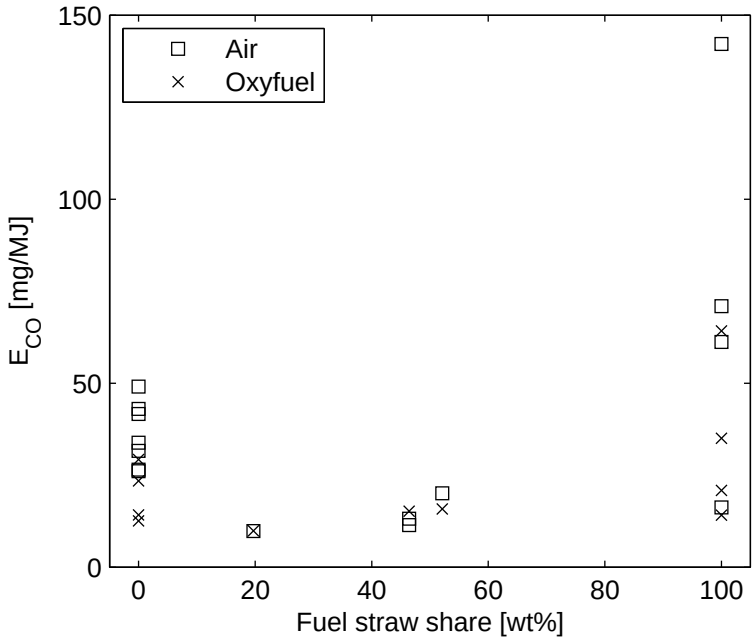

Figure 4.8: CO emission rates as function of fuel straw share. Comparison of air and oxyfuel environments at the reference operating conditions. The error bars correspond to two standard deviations on the LOI analysis.

4.3 Emission of NO and SO_2 for Varying Fuel Composition

Coal and straw contain significantly different amounts of N and S. Table 4.3 on the next page compares the values for the fuels used during the experimental investigations. The comparison is made both on a mass and an energy basis. Due to the fact that all experiments have been performed at constant thermal input to the reactor and thus varying fuel flows according to the difference in the heating value of coal and straw, the difference between the fuels is most precisely illustrated on an energy basis. Regardless of the reference basis, coal has the highest content of both elements. Especially with respect to sulphur the difference is marked. Based on the differences in fuel composition, the emissions of NO and SO_2 during combustion can be expected to differ.

4.3.1 NO Emissions

Figure 4.9 on the facing page shows the calculated emission rates of NO as a function of the fuel straw share for both air-firing and oxyfuel combustion. The figure also contains the trend lines for the data which show similar descending slopes. As observed for the coal reference experiments, the change from air com-

Table 4.3: Fuel-N and Fuel-S contents of the applied coal and straw on a mass and energy basis

	Coal	Straw
N [wt%, daf]	1.69	0.49
S [wt%, daf]	0.73	0.09
N [g/MJ, LHV]	0.53	0.27
S [g/MJ, LHV]	0.23	0.05

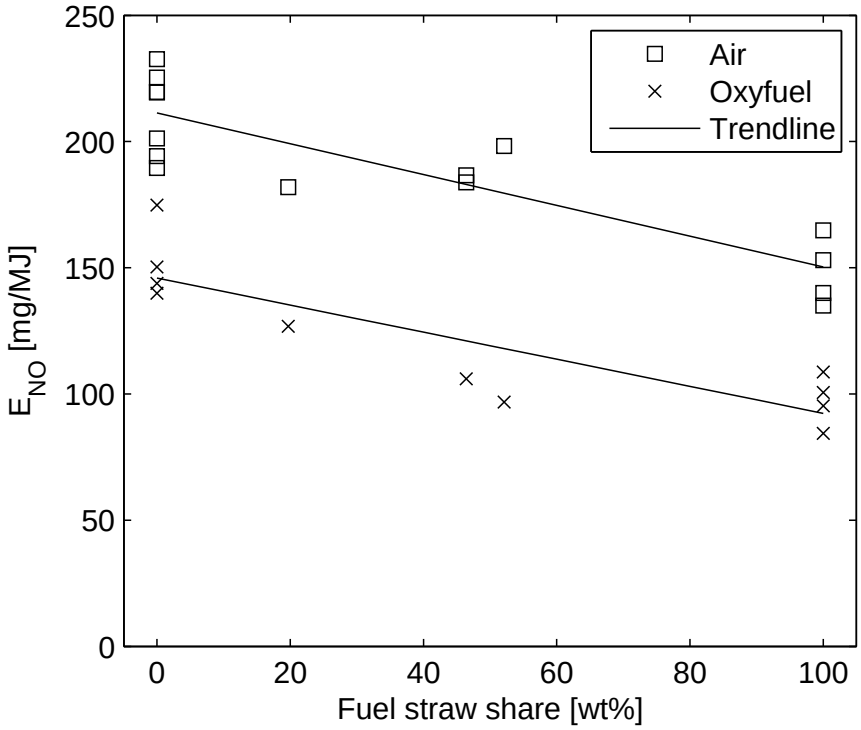

Figure 4.9: Emission rates of NO as a function of the weight based straw share of the fuel. Comparison of air and oxyfuel environments at the reference operating conditions.

Table 4.4: Average reduction of NO emission rate during oxyfuel combustion compared to air-firing

Fuel	Reduction [%]
Coal	28
20 wt% straw blend	30
50 wt% straw blend	47
Straw	34
Overall	35

bustion to oxyfuel combustion leads to reduced NO emission for all fuel blends investigated. Table 4.4 shows the average reductions for the individual fuels and the overall value determined as the average with equal weight to each fuel. The reduced NO emission is suggested to be a consequence of three effects; (1) higher NO levels in the flue gas promoting gas-phase reduction due to NO reacting with other nitrogen-containing species; (2) Increased reduction of NO over char due to significantly higher levels of CO in the flame zone; and (3) the application of a high-NO_x burner in combination with the alterations to the radical pool caused by the significantly increased concentration of CO_2. The tendency of decreasing NO emission rates with increasing fuel straw share has likewise been observed during full-scale experiments with up to 20 % co-firing of straw (thermal basis) in air [76, 77].

The difference in emission rates when changing from one fuel to another could be due to the decreasing Fuel-N content when changing from coal to straw and the trends thus include the fact that less N is available for conversion to NO. However, contrary to the full-scale results reported by Pedersen et al. [77], the conversion ratio of Fuel-N to NO increases with increasing straw share, i.e. decreasing fuel-N content, as seen in Figure 4.10 on the facing page. This difference is most likely due to the fact that the burners are dissimilar. The full-scale boiler operates with oxidant staging whereas the experimental setup is operated with the burner in high-NO_x mode. With low-NO_x burners it is exploited that volatile-N species are relatively easily reduced to N_2 compared to char-N which almost exclusively forms NO at the oxidizing conditions during burnout [70]. The ratio of volatile-N to char-N increases with increasing straw share explaining the reduction in the overall Fuel-N to NO conversion ratio with increasing straw share observed in full-scale. The high-NO_x burner, on the other hand, yields mixing of fuel and oxidant at oxidizing conditions. At these conditions, it is generally known [70] that a decreasing Fuel-N content will yield an increasing Fuel-N to NO conversion. The reaction between NO and N-containing, reducing species in the gas phase, e.g. NH_3, forming N_2 is a second order reaction and thus proceed at a higher rate with an increase in the concentrations of NO and/or NH_3 within the flame,

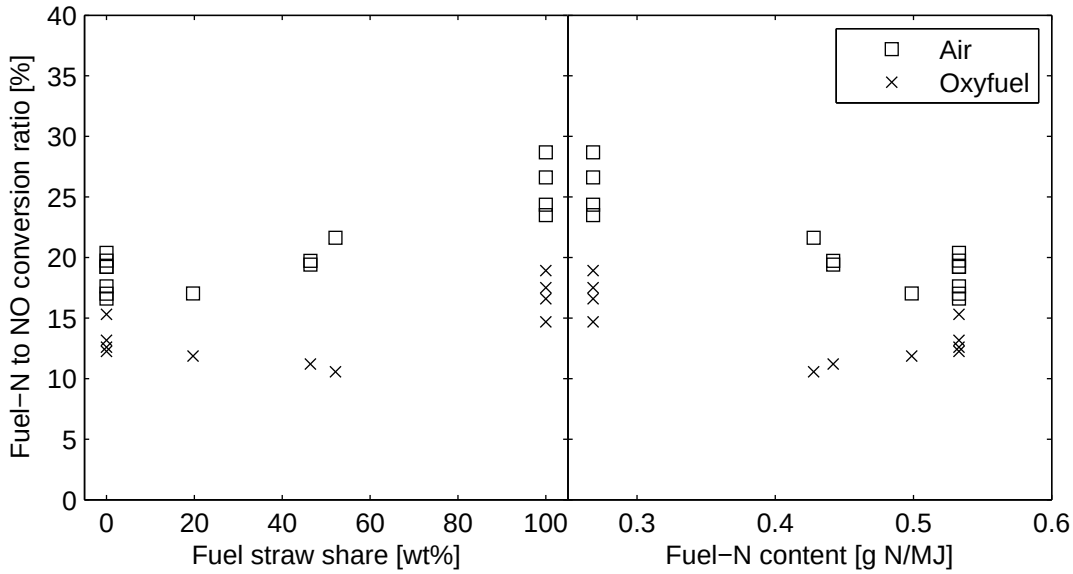

Figure 4.10: Fuel-N to NO conversion ratios as a function of the weight based straw share of the fuel (left) and the N content of the fuel based on heating value (right) - pure straw data to the left and coal data to the right. Comparison of air and oxyfuel environments at the reference operating conditions.

i.e. for increasing Fuel-N content. This shift in mechanisms leads to an overall increase in the Fuel-N to NO conversion ratio with increasing fuel straw share. Parameters such as flame temperature and the mixing of fuel and oxidant in the near-burner region which has an impact on e.g. the point of fuel ignition, and the release profile of Fuel-N which is dependent on the size of the individual fuel particles could also potentially influence the NO formation. The observed change in flame shape when varying the fuel composition will likewise have an impact on the formation of NO.

4.3.2 SO_2 Emissions

During combustion, essentially all organically bound sulphur and sulfides (mostly pyrite, FeS_2) are released to gas phase as SO_2 whereas sulfates are only released during char combustion [69]. Sulphur can also remain in residual ash without being released to gas phase. Depending on the characteristics of the residual ash, primarily the K/Si ratio, the SO_2 released to the gas phase can be captured in the ash as sulphate salts of alkali and alkali earth metals or be transported through the boiler in the gas phase due to lack of available alkali. Figure 4.11 on the next page provides a simplified description of the interaction between alkali and alkali earth metals (exemplified by potassium), gas phase SO_2, and silica-containing ash particles in the fuel. The figure shows that SO_2 competes with ash particles

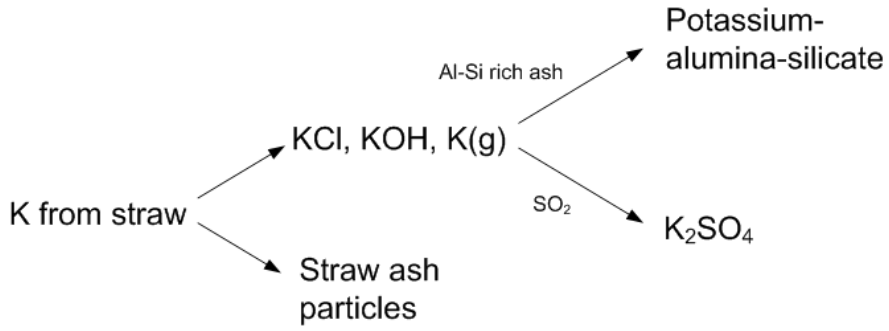

Figure 4.11: Simplified description of the mechanism for potassium transformation during combustion.

rich in Al and Si for potassium released to the gas phase. The emission rate of SO_2 is thus directly dependent on the amount of coal ash (Al-Si rich), the amount of S in the fuel (i.e. the SO_2 concentration during early stages of combustion), and the amount of potassium in the fuel (increases significantly with increasing straw share) [78].

The specific emission of SO_2 determined for the four fuel blends in the two reference combustion atmospheres is shown in Figure 4.12 on the facing page. The figure also contains the coinciding trend lines for the air and oxyfuel data and the theoretical emission rate for SO_2 determined under the assumption of full conversion of Fuel-S to SO_2, see (4.3).

$$E_{SO_2,\,theo} = \frac{\gamma \cdot M_{SO_2}}{LHV} \tag{4.3}$$

where γ is the molar content of S in the fuel [kmole/kg], M_{SO_2} is the molar mass of SO_2, and LHV is the lower heating value of the fuel. The theoretical line is not linear since both γ and LHV are linear functions (weighted averages) of the fuel straw share.

The measured emission rate of SO_2 shows a linearly decreasing trend with increasing fuel straw share. For all four fuel blends the measured emission lies below the theoretical curve emphasizing the retention of sulphur in solid phases, fly ash and deposits, within the system.

The ratio between the measured SO_2 emissions and the theoretical curve, i.e. the Fuel-S to SO_2 conversion ratio, is seen in Figure 4.13 on the next page. Contrary to Figure 4.12 on the facing page we can observe a non-linear trend with respect to the fuel straw share. However, when plotting the conversion ratio against the Fuel-S content on an energy basis (right-hand-side of Figure 4.13) a linear correlation is observed. Due to the different heating values of the applied coal and straw and the fact that the thermal input to the burner has been kept

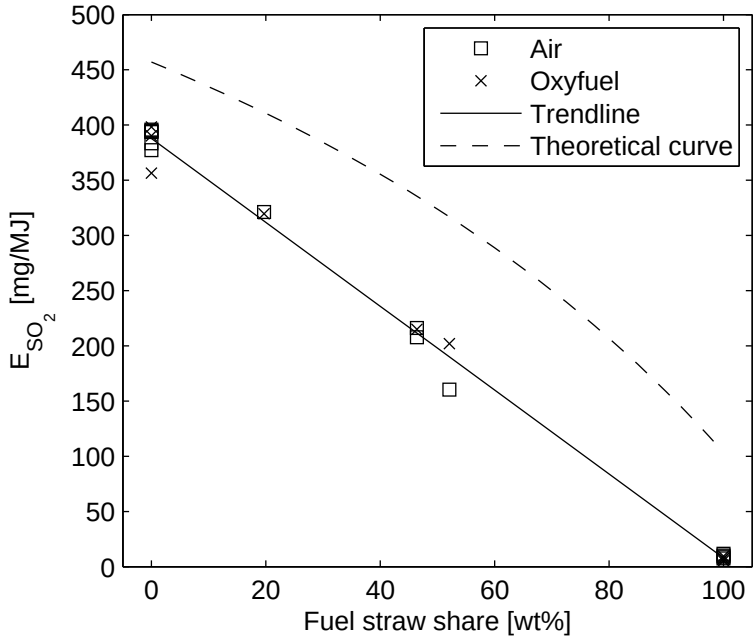

Figure 4.12: Emission rates of SO_2 as a function of the weight based straw share of the fuel. Comparison of air and oxyfuel environments at the reference operating conditions.

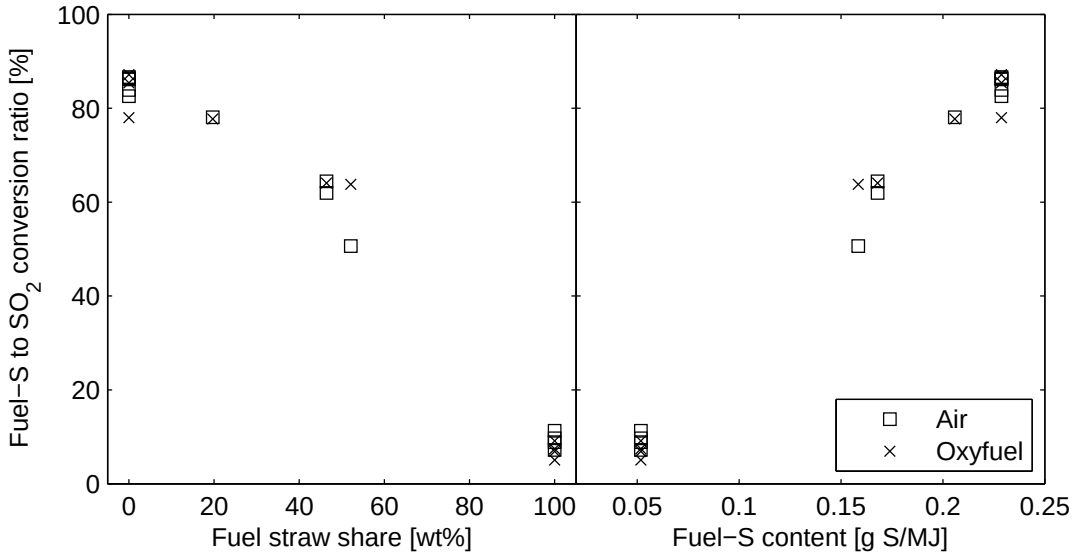

Figure 4.13: Fuel-S to SO_2 conversion ratios as a function of the weight based straw share of the fuel (left) and the S content of the fuel based on heating value (right) - pure straw data to the left and coal data to the right. Comparison of air and oxyfuel environments at the reference operating conditions.

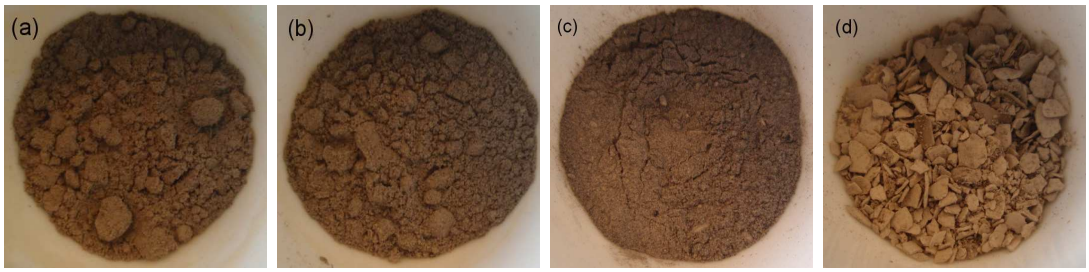

Figure 4.14: Appearance of ash samples collected from setup. (a) combined cyclone and filter ash samples from combustion of the 20 wt% straw blend. (b) combined cyclone and filter ash samples from combustion of the 50 wt% straw blend. (c) cyclone ash from combustion of pure straw. (d) filter ash from combustion of pure straw. Ash from combustion of pure coal resembles the samples for the coal-containing blends. Each picture has dimension of 20x20 mm.

constant irrespective of the fuel type a comparison on energy basis is more suited than the typically applied mass basis.

The variation in the Fuel-S to SO_2 conversion ratio with fuel composition is mainly due to differences in the composition of the fuel ash. The K/Si ratio in the fuel is a linear function of the fuel straw share. For pure coal and pure straw the ratios are 0.05 and 0.79, respectively. As expected from the mechanism in Figure 4.11, the SO_2 emission thus decreases with increasing fuel straw share both as a consequence of an increased K/Si ratio enabling formation of potassium sulphate and due to decreasing Fuel-S content. The mechanism is further investigated in relation to the treatment of the quality of fly ash in Section 4.4.

4.4 Ash and Deposits – Formation and Composition

The change in fuel characteristics when co-firing coal with increasing shares of straw will have an impact on the formation and composition of the produced fly ash and the deposits formed within the furnace.

4.4.1 Visual Appearance and Physical Properties of Fly Ash and Deposit Samples

The main part of the fly ash collected during the experiments is contained in the cyclone and filter ash fractions as was seen in Figure 2.10 on page 32. Figure 4.14 shows the appearance of these samples. The ash samples generally have a greyish-brown colour indicative of the high burnout efficiency in the experiments and resemble well ash collected in full-scale plants burning coal. The ashes from combustion of pure straw deviates from the remaining fuels in both colour and

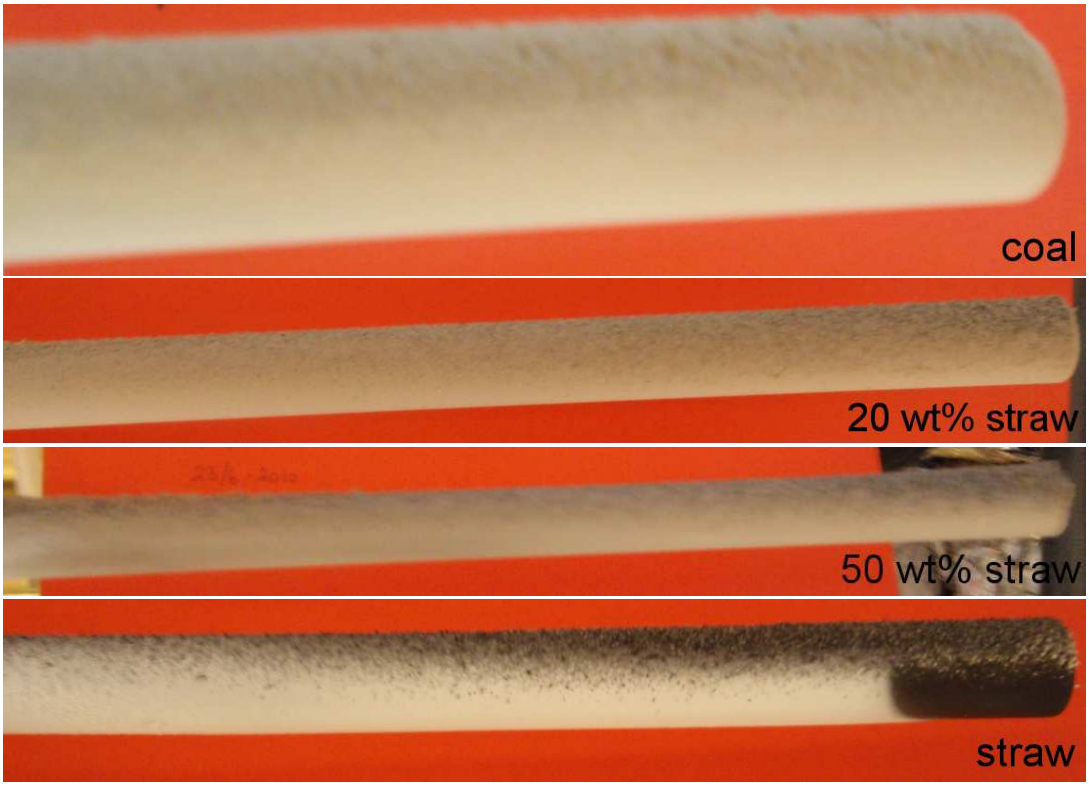

Figure 4.15: Side view of deposits. The deposit probe has a diameter of 16 mm. The top of the probe faces in the upstream direction,i.e. the flue gas flow is downwards in the pictures. Pictures have been recorded with different zoom.

morphology. The cyclone ash is more loose and flows easier than the combined ashes from combustion of the coal-containing fuels. It likewise has a stronger tendency to become static electric than the ashes from the coal-containing fuels. The filter ash, on the other hand, is very brittle and significantly lighter in colour. The filter ash is presumably formed from aerosols in the flue gas or from condensation of gas phase species on the filter cake due to the low temperature (about 100 ℃) at the filter.

Figure 4.15 illustrates the visual appearance of the deposits collected for each fuel. Only one example is shown for each fuel as the change in oxidant type did not influence the visual and physical appearance of the deposits. The colour of the deposit from pure coal combustion is light greyish-brown and the upstream part is very loose and powdery, and easy to remove from the probe. The downstream part is a thin, homogeneous layer which clearly consists of condensed matter. The deposits from combustion of the 20 and 50 wt% straw blends differ from the pure coal deposit only with respect to the thickness of the upstream layer. As seen from the picture of the 50 wt% straw blend, a thicker layer of

ash particles builds up at the ends of the probe in the upstream direction. The uneven distribution across the probe is most likely due the swirling motion of the flame moving ash particles from the centre of the reactor towards the walls. The flue gas temperature variation across the reactor at the deposit probe position in port 7 is assumed to be negligeble due to the flat profiles measured in port 5 for both oxidant types. The visual and physical appearance of the deposit from pure straw combustion deviates significantly from the remaining deposits shown in the figure. The downstream part is completely white which is indicative of a high content of salts. The upstream part is hard, almost completely sintered, and more difficult to remove from the probe than the remaining deposits which were all powdery. At the same time, the colour is darker than for the coal-containing fuel blends. The dark colour is typical for deposits containing SiO_2. As was the case for the 50 wt% straw blend the upstream deposit shows an unequal weight distribution across the probe with higher deposition towards the ends (reactor walls). The deposit thickness is however smaller for the pure straw case since the sintering acts to reduce the porosity of the deposit.

Based on the visual appearance of the deposits, co-firing up to 50 wt% straw should not induce problems with respect to the removal of deposits within full-scale boilers. However, firing of pure straw would most likely necessitate an increased frequency in soot-blowing.

4.4.2 Deposit Fluxes

Table 4.5 on the facing page compares the calculated deposit fluxes for each fuel/oxidant combination investigated. Contrary to the observation for the coal reference experiments in Section 3.3.2, oxyfuel combustion yields higher deposit fluxes than combustion in air for the straw-containing fuels. If the difference is larger than the experimental uncertainty, the most probable reason for the shift in the deposition propensity is a change in the sticking efficiency. Due to the presence of straw ash particles which generally have lower deformation temperatures than ash from pure coal combustion [79] the higher flue gas temperatures during oxyfuel combustion than during combustion in air for the same fuel will increase the stickiness of the deposit and ash particles.

A change in the fuel straw share for each of the combustion atmospheres induces no difference in the deposit flux for the blends, whereas pure straw combustion yields marked increases in deposition rates. This can also be attributed to the differences in the sticking probability with the change in the chemical composition of the ash particles. For coal-containing fuels the majority of the ash particles consist of alumina-silicates which have higher melting point temperatures than the K-silicates formed in pure straw ashes [80]. The salts which constitute a significant part of the straw ashes have even lower melting points than the silicate-containing compounds. A repetition of deposit sampling during oxyfuel combustion of pure straw have illustrated the effect of the flue gas tem-

Table 4.5: Average deposit fluxes as well as flue gas and deposit probe temperatures for combustion of coal, straw, and their blends in air and oxyfuel atmospheres for an exposure time of 2 hr.

Fuel	Oxidant	Upstream [g/m^2·hr]	Downstream [g/m^2·hr]	Average [g/m^2·hr]	T_{probe} [°C]	T_{FG} [°C]
Coal	Air	107	11	59	500	900
Coal	Oxy 30	75	3	39	500	950
20 wt% straw	Air	64	6	35	500	940
20 wt% straw	Oxy 30	90	2	46	500	970
50 wt% straw	Air	56	9	32	500	920
50 wt% straw	Oxy 30	89	4	46	500	960
Straw	Air	102	15	59	500	940
Straw[a]	Air	153	18	86	500	910
Straw	Oxy 30	194	12	103	500	950
Straw	Oxy 30	219	17	118	500	995

[a] 4.3 hr exposure time

perature. From the data in Table 4.5 it is seen that an increase in the flue gas temperature of about 50 °C yields a 10 % increase in deposit flux.

Prolonged exposure time (4.3 hr as opposed to 2 hr) also leads to an increase in the time-averaged flux for combustion of straw in air. This is due to the fact that the increasing thickness of the deposit leads to a higher surface temperature due to the insulating effect of the underlying deposit layer. The temperature increase at the surface consequently increases the sticking efficiency of the deposit. The deposition rate will thus increase over time.

Increased deposit formation has been observed in full-scale (MKS1) for co-firing of 10 % straw (energy basis). Some slagging problems were seen when 20 % straw was co-fired [81]. However, in another boiler (SSV4), no fouling problems were observed within the first two years of operation with co-firing up to 20 wt% straw with coal and soot-blowing was not increased. [76]

4.4.3 Chemical Composition of Fly Ash and Deposit Samples

In addition to the differences in physical properties of the ashes and deposits the chemical composition of the samples is of great importance with respect to characterizing the effect of fuel change. Figure 4.16 on the next page shows the variation in the ash forming elements for each fuel blend. The values for the 20 and 50 wt% straw shares are weighted averages of the compositions of the pure

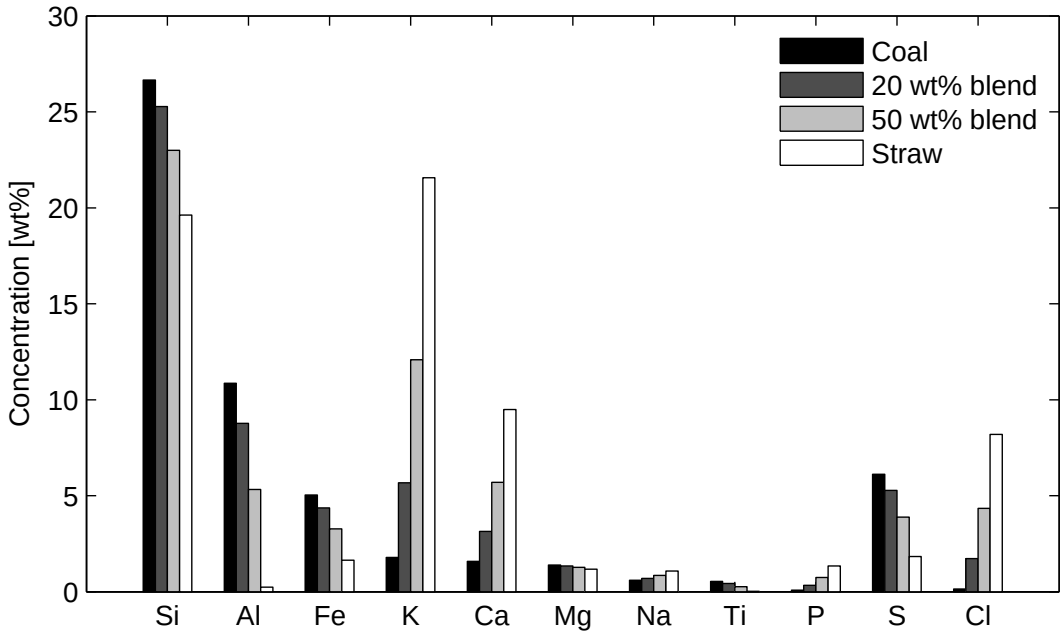

Figure 4.16: Comparison of calculated fuel ash compositions for the four different fuels. The concentrations are determined based on an analysis for the inorganic elements in the fuel sample. The values for the 20 and 50 wt% straw shares are weighted averages of the compositions of the pure fuels.

fuels. The most distinct differences are concerned with the Al, K, Ca, S, and Cl contents. These elements are important when considering the corrosion potential of the ashes and deposits. High concentrations of K, Cl, and S compared to Si and Al will increase the corrosion potential of the solid phase.

Figures 4.17 to 4.20 show the corresponding elemental analysis for the collected fly ash and deposit samples. Cl is shown as the result from the analysis of water soluble species, as this is the same as the total content. The analysis method for water soluble Cl has, however, a lower detection limit. For the pure coal experiments the deposit composition is from the analysis of the combined sample from the upstream and downstream parts of the deposit probe. For the remaining fuel/oxidizer combinations these two samples have been analysed separately.

As described in Section 3.3.2 the differences between fuel ash, fly ash, and deposits for pure coal combustion in both air and the reference oxyfuel atmosphere are insignificant. The high Fuel-S to SO_2 conversion ratio of about 85-90 % is the most striking for these data. In fact, for all of the investigated fuel blends, no significant differences between air-firing and oxyfuel combustion can be determined.

Adding 20 wt % straw to the fuel blend, see Figure 4.18, yields a similar low capture rate of S in the fly ash, see e.g. Figure 4.23 on page 104, but an increased

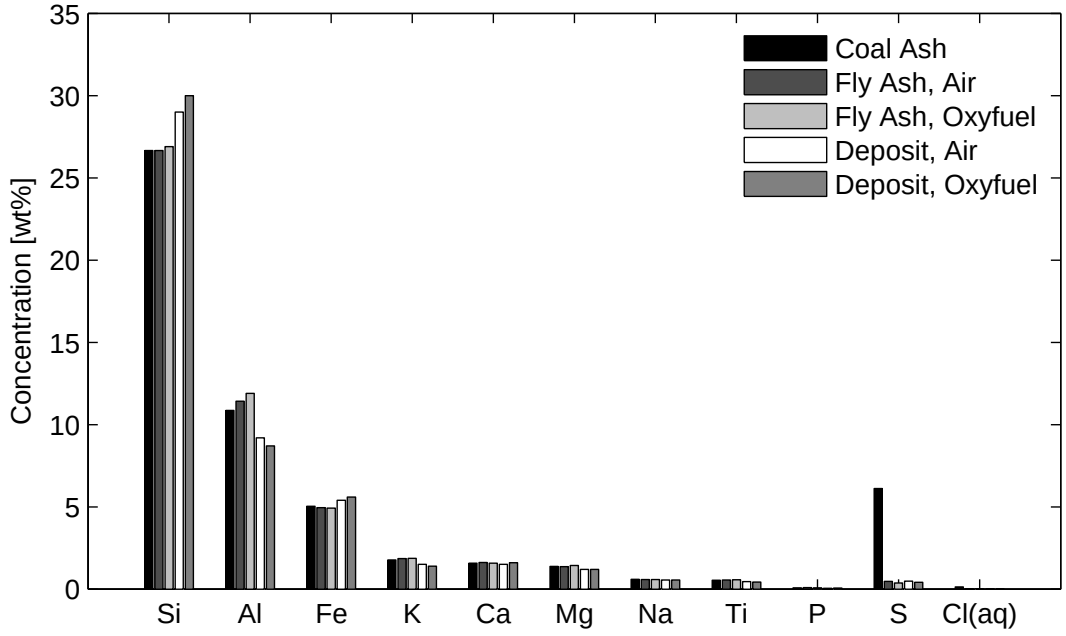

Figure 4.17: Comparison of fly ash and deposit compositions for coal combustion in air and 30% O_2/CO_2 at the reference conditions.

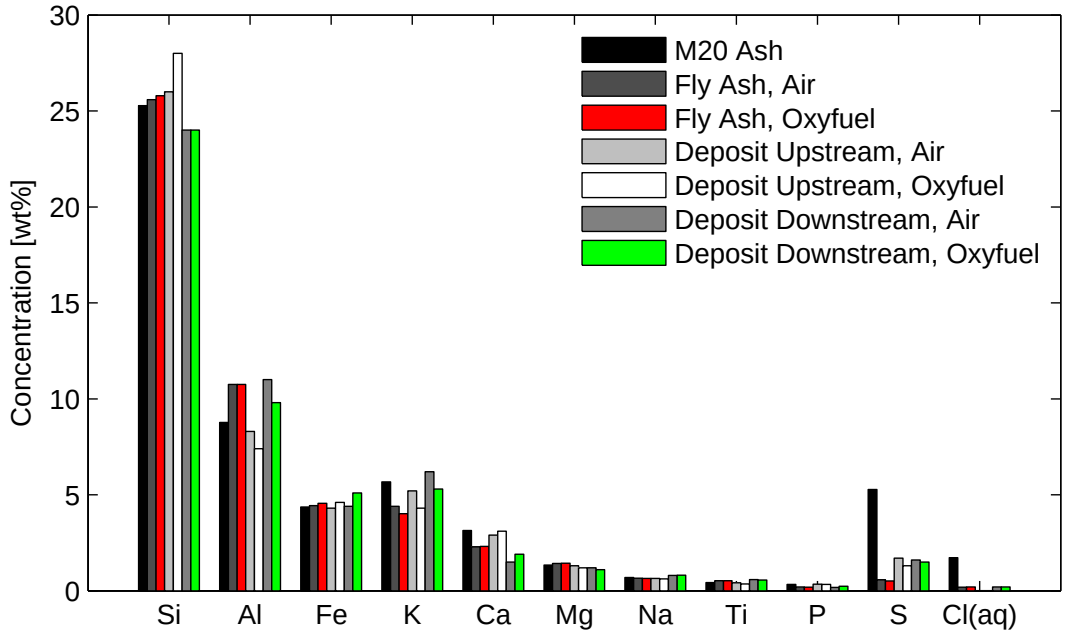

Figure 4.18: Comparison of fly ash and deposit compositions for combustion of the 20 wt % straw/coal blend in air and 30% O_2/CO_2 at the reference conditions.

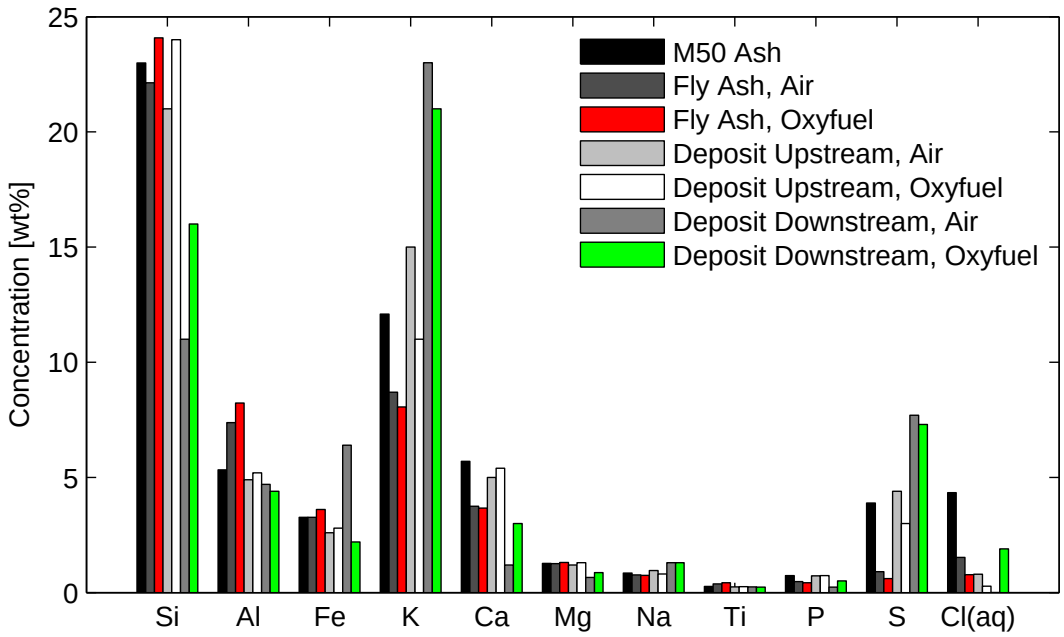

Figure 4.19: Comparison of fly ash and deposit compositions for combustion of the 50 wt % straw/coal blend in air and 30% O_2/CO_2 at the reference conditions. Cl data for the downstream deposit sample from combustion in air is not available. However, the level is expected to be similar to the corresponding oxyfuel sample.

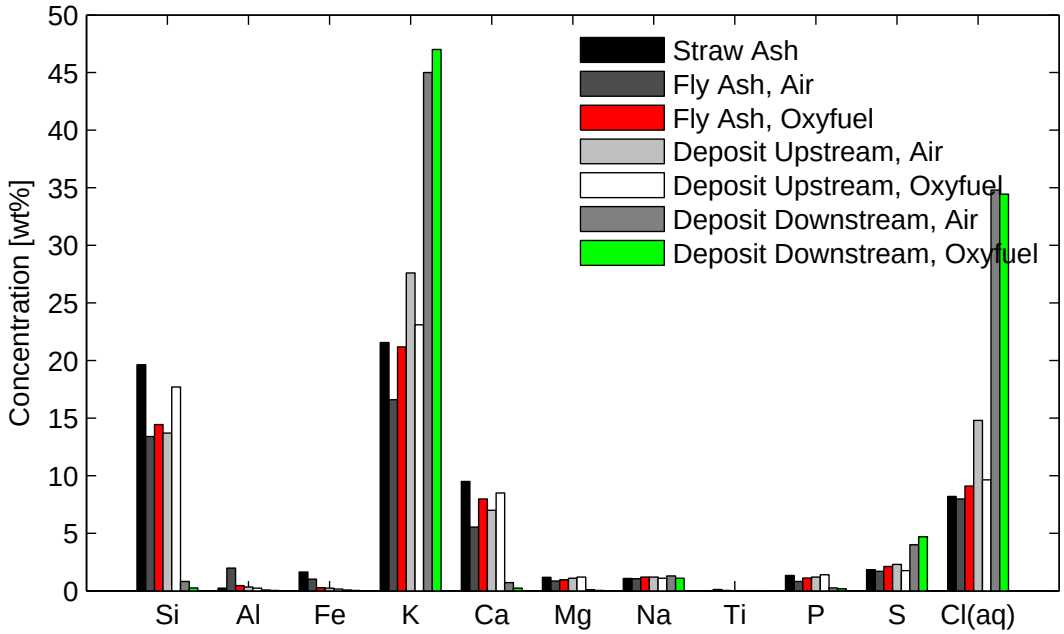

Figure 4.20: Comparison of fly ash and deposit compositions for straw combustion in air and 30% O_2/CO_2 at the reference conditions. Experiments SA04_ADT and SO04_ADT.

retention in the entire deposit even though the Fuel-S content has decreased. Since no Cl is present in the fly ash, it is unlikely that the increased S content in the deposit is due to on-site sulphation of KCl. Instead, capture of sulphur by Ca could explain the observation. Cl is absent in the deposits indicating that all K is bound in alumina-silicates or as K_2SO_4. The fuel-bound Cl is thus released to gas phase as HCl or Cl_2. K in the deposit is equally distributed between the upstream and downstream samples and at the same level as for the fly ash and the fuel indicating that all particles depositing on the probe have similar composition. The figure does not show the distribution between K bound in alumina-silicate compounds and K found in salts. This has a significant impact on the characteristics of the samples and will be treated later in this section. The higher concentration of Al in the downstream deposit samples compared to the upstream samples is not immediately explainable as this element is expected to mainly be associated with large residual ash particles. These particles would primarily deposit on the upstream part of the probe. The trend with higher concentration on the upstream part of the probe compared to the downstream part is seen for both Si and Ca which likewise are assumed to mainly be present in large ash particles due to their low volatility. However, the Si concentration in the downstream deposit is still very high indicating capture of residual ash particles on the downstream part of the probe due to recirculation zones.

The presence of 50 wt % straw in the fuel blend significantly alters the composition of the fly ash and deposit samples compared to the fuels with higher coal-share as seen in Figure 4.19. The ratio of K to Si (and Al) has increased significantly and especially the deposits show high retention of K, most pronounced in the downstream samples indicating condensation of K-rich salts, mostly sulphates which the correspondingly high S contents imply, but also chlorides unlike the case for the fuels with lower straw share. Condensation of Na-rich salts on the downstream side of the probe is likewise observed. Contrary to the observation for the previously described fuel, on-site sulphation of the deposit may have occured during the sampling period implied by the difference in both the S and Cl contents of the fly ash and deposit. In fact, even though the K content of the fly ash has increased the concentration of S in the fly ash is still low, indicating K being bound mainly in silicate compounds or as KCl. The Cl concentration in the fly ash and the deposit samples has increased compared to the 20 wt% straw blend samples (from about 0.1 to about 1 %). No analysis with respect to Cl exists for the downstream deposit sample for air combustion, however, the Cl concentration is assumed to be similar to the oxyfuel sample. As was seen for the 20 wt% straw blend the Al concentrations in both the upstream and downstream deposit samples are similar. However, the Si concentration in the downstream deposit samples is significantly lower than in the upstream samples which has the same Si content as the fly ash. A similar trend is seen for the distribution of Ca between the upstream and downstream of the deposit probe. The very high Fe concentration in the downstream deposit sample for the air experiment is most

likely due to contamination with Fe from the probe during sample collection. This contamination could have a minor impact on the measured concentrations of the remaining elements, however no changes to the conclusions would be made.

Combustion of pure straw leads to fly ash and deposits with a relatively high corrosion potential. Especially the downstream deposits consist almost solely of KCl, and K_2SO_4 in smaller amounts due to the very low Fuel-S content compared to the fuel blends containing coal, see Figure 4.20. Less on-site sulphation of the upstream deposit is likewise a result of the lower flue gas concentration of SO_2. No significant difference in the concentration of S in the fuel ash, fly ash and upstream deposits can be observed. The corresponding levels of Cl are likewise similar. The release of Cl to the gas phase is thus significantly reduced compared to combustion of coal-containing fuel blends, see also Figure 4.23 on page 104. The near absence of Al means that K-silicates with lower melting points than K-aluminium-silicates are formed. Additionally, Ca competes with K for the Si and thus increases the ratio of water soluble K to total K in fly ash and deposits [80].

In summary, increasing the straw share of a coal/straw blend will induce significant changes to the composition of fly ash and deposits. Most pronounced is the increasing corrosion potential of both ash and deposits due to significant increases in the K and Cl contents. Additionally, the on-site sulphation of deposits is likewise significantly affected by the fuel type. Figure 4.21 on the facing page illustrates these findings by directly comparing the concentrations of K, Cl, and S in deposits and fly ash for the investigated fuel/oxidizer combinations. The figure shows both the total contents of each element and the concentration of the elements in water soluble form. The total K and Cl contents are seen to be equally distributed between the fly ash and the upstream part of the deposit. Increased levels in the downstream part of the deposit compared to the upstream sample is likewise observed indicating that the downstream part of the deposit is mainly made up of aerosols. A comparison of the total and water soluble concentrations of K shows a tendency for the deposits to be enriched in K-containing salts when the fuel contains both straw and coal. This trend could be due to an over representation of KCl aerosols being deposited compared to the amount found in the fly ash. Subsequent on-site sulphation of KCl decreases the Cl concentration in the deposit and increases the concentration of S compared to the fly ash. The sulphur data confirms this as both blends show significantly increased concentrations in the deposits whereas both pure coal and pure straw yield an equal distribution between ash and deposit. A maximum in the sulphur retention in the deposit is seen at 50 wt % straw in the fuel blend due to the combined effect of high alkali and alkali earth metals present in the deposit from the straw and high levels of sulphur available from the coal. The trend is present both at the upstream and downstream of the deposit probe.

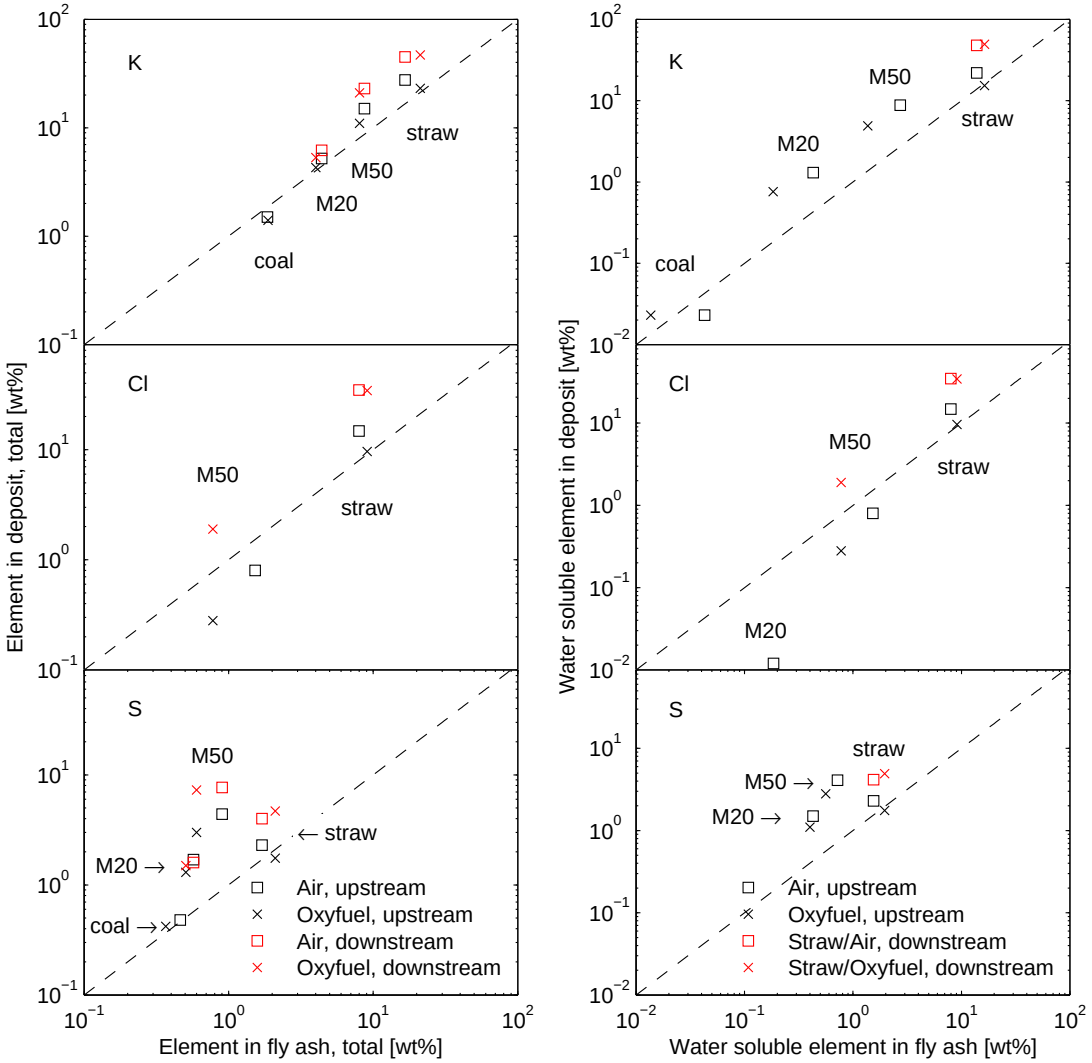

Figure 4.21: Comparison of K, Cl, and S in fly ash and deposits for the four fuel blends. Data shown for air and oxyfuel combustion at the reference operating conditions. Left: total contents, right: water soluble concentrations. The Cl data for the pure coal and 20 wt% straw blend which are below the detection limit are not shown. Water soluble K and S analysis does only exist for the downstream deposit samples for straw as fuel. Water soluble S has not been measured for the pure coal deposits but can be assumed to be equal to the total content.

The corrosive potential of fly ash and deposits is primarily determined by the presence of chlorides and sulphates of alkali and alkali earth metals. Figure 4.22 on the next page shows the concentrations of water soluble K, Ca, Cl, and S in the fly ash samples for each fuel/oxidant combination investigated. The concentration of water soluble K, Cl, and S in the ashes follows the trend from the total contents. With up to 20 wt% straw in the fuel blend only a small increase in salts in the ashes occurs. However, increasing the straw share above 20 wt% leads to significant increases in the alkali salt contents. This indicates surplus of primarily K from the straw compared to the alumina-silicates from the coal ash. The K is released to the gas phase due to the high temperatures in the flame and is thus available for condensation as sulphates or chlorides on ash particles or for reaction with alumina-silicates. Even though the total amount of Ca in the straw fuel and fly ashes is significantly higher than for coal ash the amount found in the fly ash in water soluble form is lower than for the experiments with coal-containing fuels. This could be a consequence of the limited solubility of $CaSO_4$ in water. However, a parallel analysis at a liquid-to-solid (LS) ratio of 50 instead of 100 yielded a higher concentration of Ca^{2+} in the solute and a value well below the solubility of $CaSO_4$ in water of about 2000 mg/L (600 mg Ca^{2+}/L) [82]. The results thus seem physically sound even with the solubility limitations occuring due to the presence of additional salts in the solution.

The requirements for fly ash used in concrete are less than 0.1 wt% Cl, less than 3 wt% S measured as SO_3, and less than 5 wt% total alkali [63]. For the fly ashes collected from the experiments it is seen that the requirement regarding Cl cannot be fulfilled unless for pure coal combustion. At 20 wt% straw in the fuel blend the Cl content in the fly ash is 0.2 wt%. The limits for total alkali (sum of K and Na) and sulphur are not exceeded for fuel straw shares up to 20 wt%. The relatively large capture efficiency of Cl in the swirl burner setup deviates significantly from full-scale boilers as discussed in Section 4.5.

Figure 4.23 on page 104 shows the retention in water soluble form of K, Ca, Cl, and S fed with the fuel in the fly ash. The retention shows similarly increasing trends for K, Cl, and S as did the absolute concentrations. Within the experimental uncertainty, full capture of both S and Cl is obtained by the fly ash obtained by combustion of pure straw. The lack of complete consistence between this figure and the Fuel-S to SO_2 conversion ratios shown in Figure 4.13 on page 91 is due to the small error on the mass balances. The K and S data confirms the competition between the capture of K in water insoluble alumina-silicates when coal ash is present and the increasing capture efficiency in water soluble sulphates (and chlorides) when the fuel straw share increases, as discussed in relation to Figure 4.11 on page 90.

Ca retention in water soluble form exhibits the opposite trend of the other elements in that almost none of the fuel-bound Ca is found in water soluble form in the fly ash for pure straw combustion whereas about 50 % of the Ca fed with the pure coal is retained in salts. The residual ash from straw combustion consists

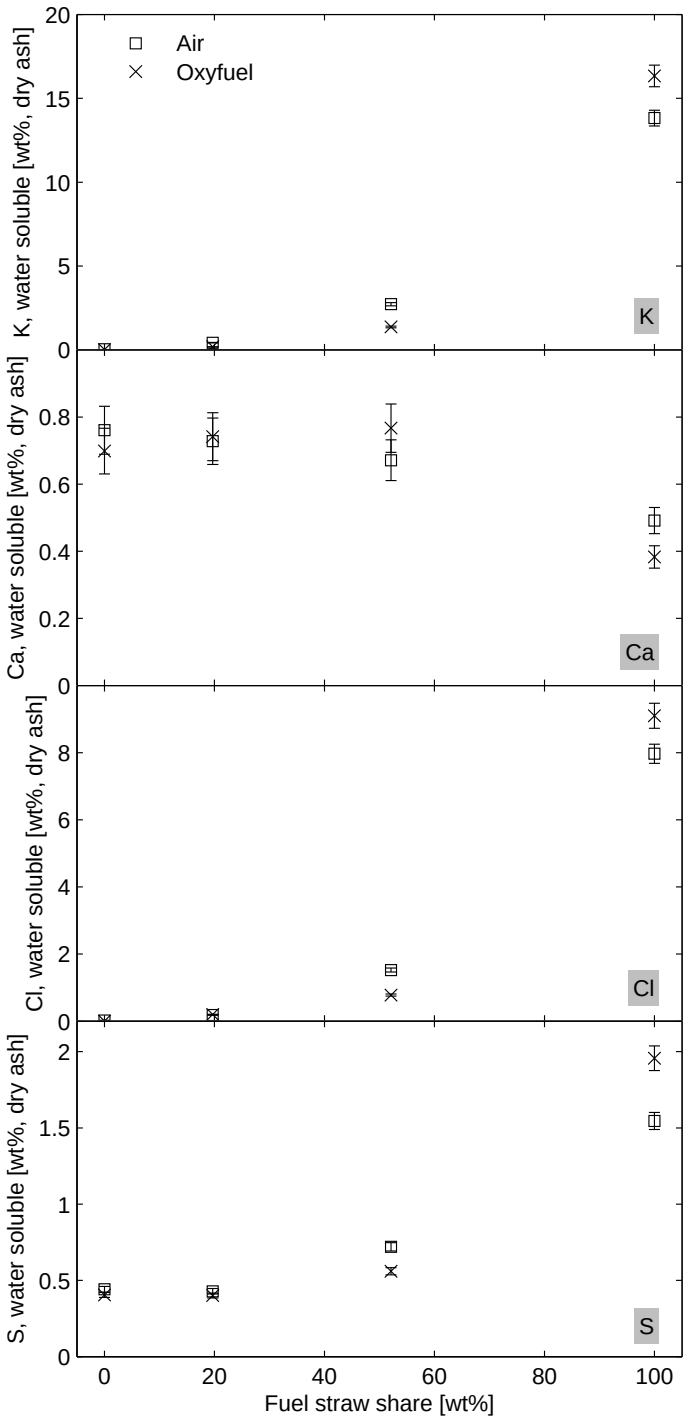

Figure 4.22: Concentration of water soluble K, Ca, Cl, and S in fly ash as a function of the weight based straw share of the fuel. Comparison of air and oxyfuel environments at the reference operating conditions. The error bars correspond to two times the standard deviation on the ash analysis. The analysis have been performed with liquid-to-solid ratios of 100.

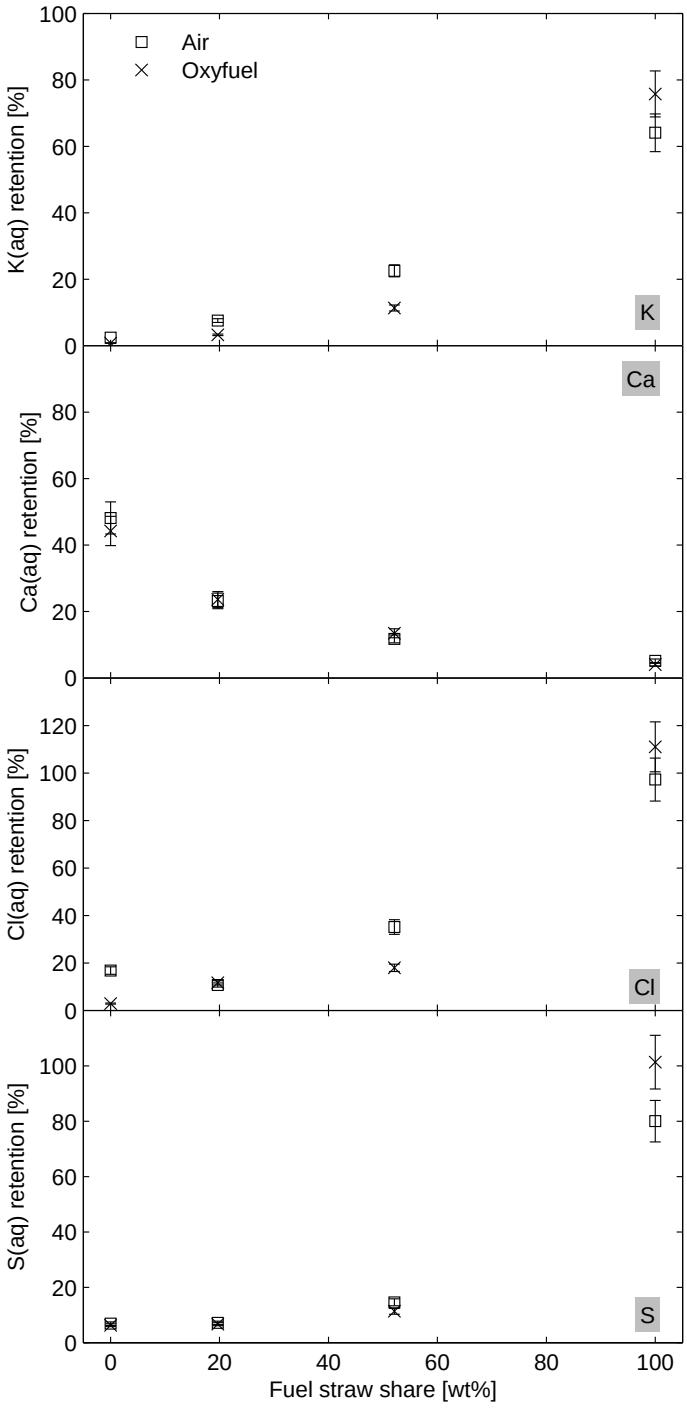

Figure 4.23: Capture of K, Ca, Cl, and S in water soluble form in fly ash as percentage of the amount of the element fed with the fuel and as a function of the weight based straw share of the fuel. Comparison of air and oxyfuel environments at the reference operating conditions. The error bars correspond to two times the standard deviation on the calculated value determined from the law of propagation of uncertainties.

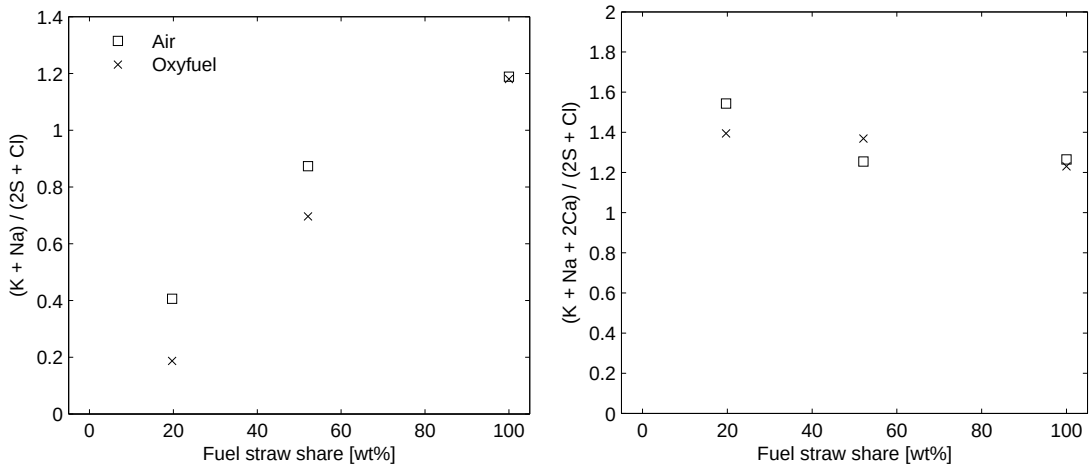

Figure 4.24: Stoichiometric ratio of water soluble alkali and alkali earth metals to sulphur and chloride in fly ashes as function of the fuel straw share.

primarily of Ca-Si compounds. As mentioned earlier, Ca competes with K for Si making the straw ash significantly less efficient for self-retention of gas-phase K in a water insoluble form compared to coal ash which has a higher Si and a lower Ca content. This is evident from the K data as between 60 and 80 % of the K fed with the straw is bound as salts in the ash, see Figure 4.23. The surplus of alkali metals in the straw ash (20 %) to form sulphate and chloride salts is seen in the left-hand-side of Figure 4.24. The figure shows that there is a deficit of water soluble alkali in the fly ash from combustion of the straw/coal blends to the amount of S and Cl. The right-hand-side of Figure 4.24 shows that the surplus of S and Cl is bound to alkali earth metals (represented by Ca).

4.5 Comparison to Full-Scale data

4.5.1 Comparable Fuels

Co-firing of straw and coal of the same type as utilized in the present work has been performed at the Studstrup power plant (SSV4) in Denmark as reported by Sander and Wieck-Hansen [78]. Fly ash was sampled from the flue gas duct upstream of the electrostatic precipitator and analysed for the content of water soluble elements (K, Na, Ca, Mg, Cl, P, and S). Between 0 and 20 wt% straw was fired and the boiler load was varied in the range 30-100 %. Figure 4.25 on the following page shows a comparison of the concentration and percentage retention of water soluble K and Cl in the ash samples and the data obtained in the present experiments. Due to the large influence of the weather conditions during the harvest season, the content of potassium and chlorine in straw varies significantly over the years. The potassium content of the straw used in this work

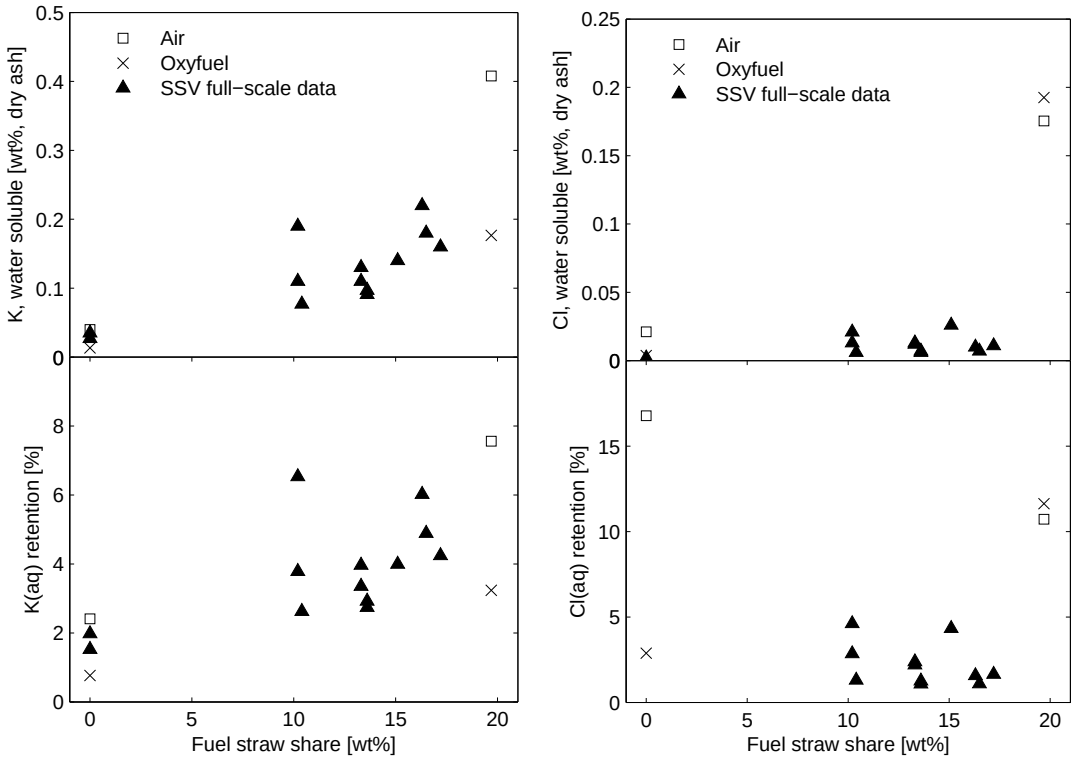

Figure 4.25: Concentration of water soluble K and Cl in fly ash and the percentage share of water soluble K and Cl in fly ash compared to K and Cl fed with the fuel as a function of the weight based straw share of the fuel. Comparison of air and oxyfuel environments at the reference operating conditions with full-scale data from Studstrup power plant (SSV) for comparable fuels (straw and Colombian coal (COCERR)).

Table 4.6: Characteristic fuel parameters and their importance in ash transformations during coal/straw co-firing

Fuel ash	Possible implication during ash transformation
K	Amount of K ending up in fly ash
K/Si	Availability of silicate and aluminosilicate to react with potassium salts
K/(S+Si)	Availability of silicate and aluminosilicate to react with potassium salts, and the extent of potassium sulphation
S/Cl	The fraction of potassium in form of K_2SO_4 and KCl

is about 2/3 of the amount in the full-scale experiments (1 wt% and 1.5 wt%, respectively). Despite this difference, a good agreement between the full-scale and semi-technical scale data is observed with respect to the K content. The swirl burner air data generally yields higher levels of water soluble K than full-scale and the oxyfuel data are situated in the lower range of the full-scale data. This could suggest that the lower flame and flue gas temperatures obtained in the swirl burner during air-firing compared to full-scale flames reduces the reactions between K in the gas phase and Al-Si compounds in the ash particles. Better agreement is thus seen for oxyfuel combustion due to the higher temperatures obtained here. The retention of Cl in the fly ash from the full-scale boiler is relatively low compared to the fly ash obtained in the present work. This supports the assumption of decreased retention of potassium in alumina-silicates in the small-scale setup. Another explanation to the discrepancy could be differences in the degree of sulphation of the fly ash. The following section provides a more general comparison of the fly ashes obtained in the present work to full-scale experiments with co-firing of coal and biomass (primarily straw).

4.5.2 General Comparison of Fly Ash Quality to Full-Scale Co-Firing Experiments with Air as Oxidant

Zheng et al. [80] made a detailed study of the transformation of ash during co-firing of coal and straw. The study included lab-scale combustion experiments in an entrained-flow reactor and a literature review of full-scale experiments primarily performed on Danish power plants. The study considered the interaction effects occurring between coal and straw ashes and the resulting effect on the fly ash. Zheng et al. [80] identified a number of characteristic fuel parameters which can be used to predict the quality of the fly ash. The parameters and their importance during ash transformations are given in Table 4.6.

Figure 4.26 on the following page shows the linear dependence between potassium in the fuel and the total amount of potassium in the fly ash for both the data shown in [80] for bituminous coals and from this work. A relatively good

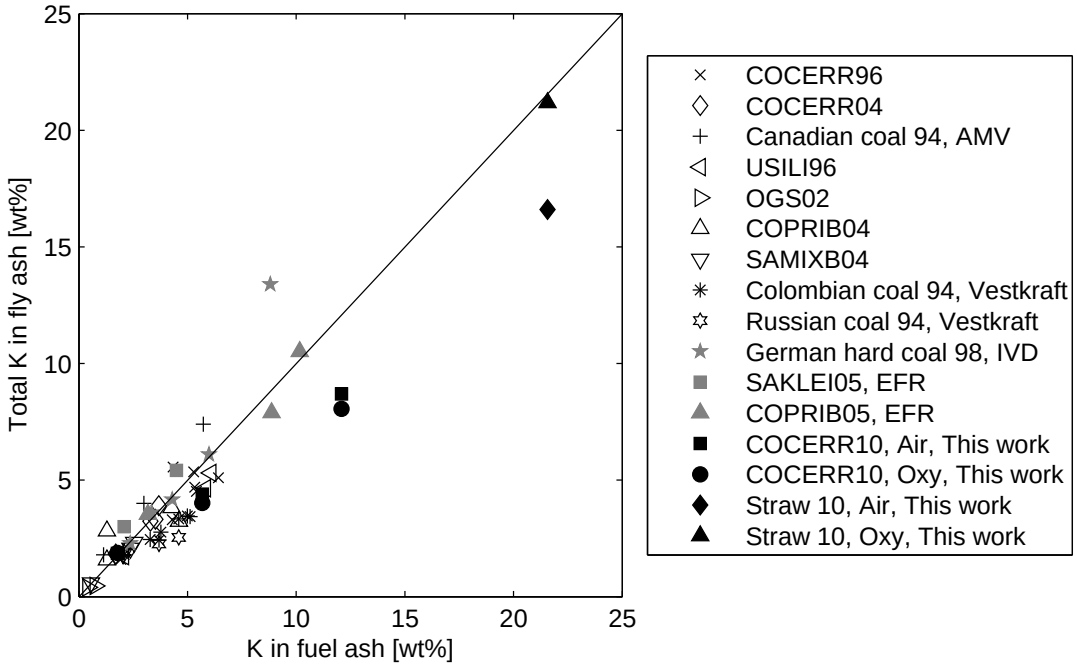

Figure 4.26: Total K in fly ashes as function of the K content of the fuel ash. Open symbols: literature data from [80]; closed, grey symbols: semi-technical and entrained flow reactor (EFR) data from [80]; closed, black symbols: semi-technical scale data from this work.

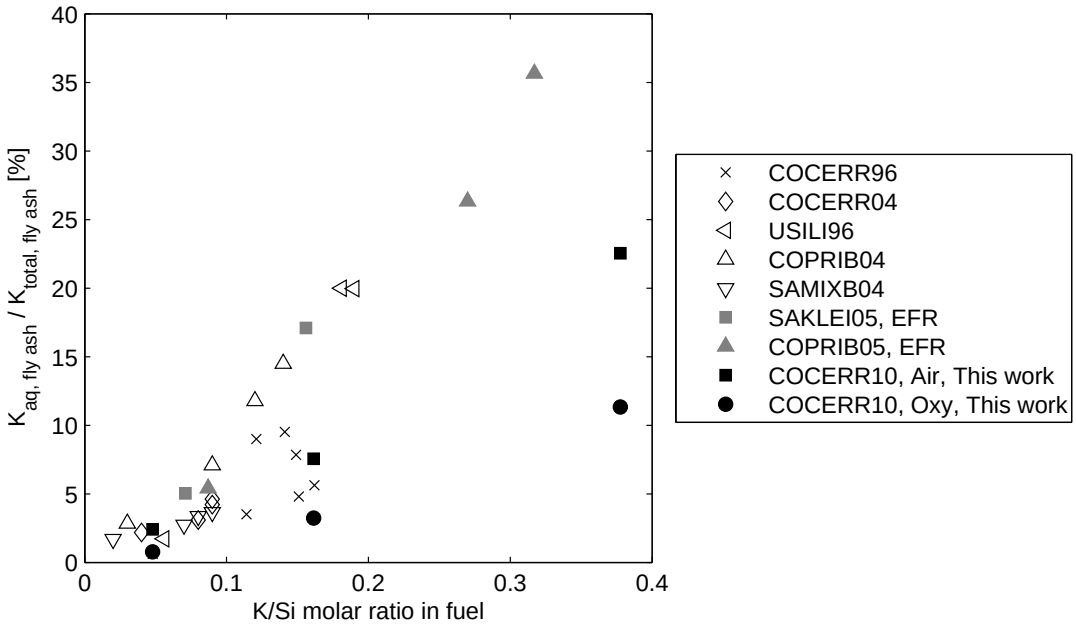

Figure 4.27: Percentage share of water soluble K in fly ash to total K in fly ash as a function of the K/Si ratio of the fuel for coal/straw co-firing. Open symbols: literature data from [80]; closed, grey symbols: Entrained flow reactor (EFR) data from [80]; closed, black symbols: semi-technical scale data from this work.

agreement with the full-scale data is observed for this work with up to 20 wt% straw in the fuel blend. Co-firing with high straw shares (increasing K in fuel ash) and combustion of pure straw tend to decrease the relative conversion of Fuel-K to fly ash potassium (this work). This deviation supports the increased level of total K in deposits compared to fly ash for the 50 wt% straw blend (air and oxyfuel) and the pure straw (air) shown in Figure 4.21 on page 101. For high fuel straw shares K is generally retained to a larger degree in deposits than in fly ash in the semi-technical scale setup. The observed split between fly ash and in-furnace deposits in the experimental setup of about 50:50 yields enough deposits to support this explanation.

The availability of silicate and aluminosilicate to react with potassium salts (K/Si molar ratio in fuel) has a significant effect on the amount of water soluble potassium found in the fly ash as seen in Figure 4.27. The retention of potassium in water soluble salts increases with increasing K/Si ratio, i.e. decreasing Si availability. A comparison of both the data from this work and the entrained flow reactor experiments show very good agreement to the full-scale trends for similar coals (COCERR and COPRIB). The best agreement for the data from this work is seen for the air-firing experiments whereas the oxyfuel combustion experiments, even though they are close to the full-scale data, generally yield lower levels of water soluble K than the trend suggests. The difference between

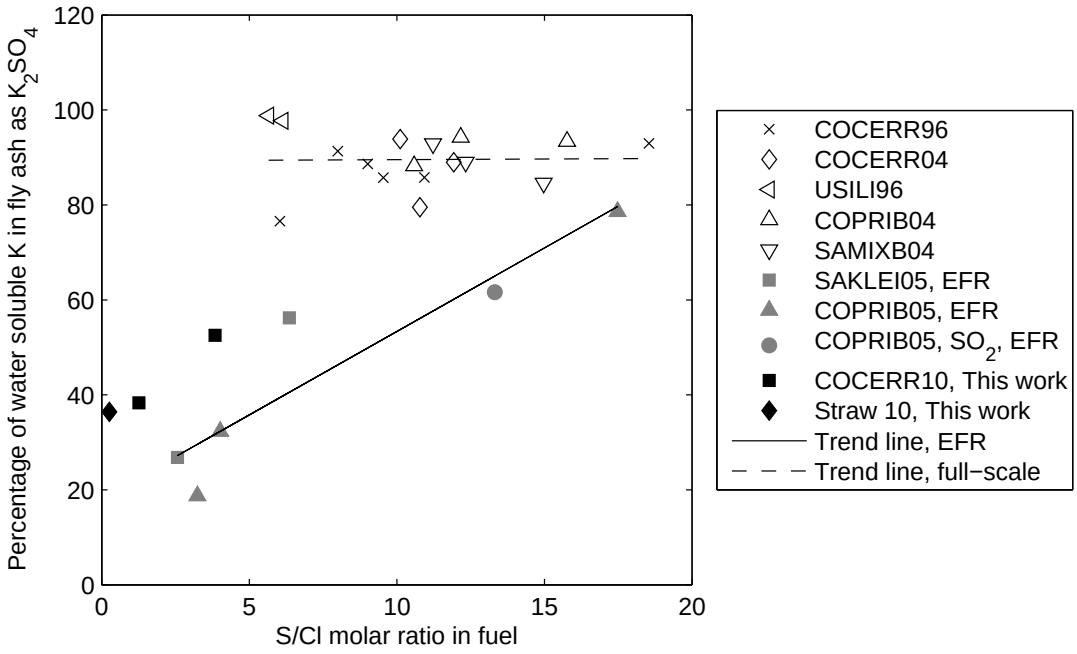

Figure 4.28: Percentage share of water soluble K in fly ash that appears as K_2SO_4 as a function of the S/Cl ratio of the fuel. Open symbols: literature data from [80]; closed, grey symbols: Entrained flow reactor (EFR) data from [80]; closed, black symbols: semi-technical scale data from this work. Pure coal data from this work have been omitted.

the air and oxyfuel combustion data is suggested to be caused by the increased, average residence time and increased flame and flue gas temperatures during oxy-fuel combustion possibly leading to an increased capture of K in alumina-silicates, thus decreasing the amount of water soluble K.

The water soluble potassium found in the fly ash is suggested to exist in the form of KCl and K_2SO_4. Under the assumption that all Cl found in the fly ash exist as KCl, the amount of potassium found as K_2SO_4 can be determined from (4.4).

$$K_{aq,\,K_2SO_4} = 1 - \frac{x_{Cl_{aq},\,ash} \cdot M_K}{x_{K_{aq},\,ash} \cdot M_{Cl}} \tag{4.4}$$

where $x_{Cl_{aq},\,ash}$ and $x_{K_{aq},\,ash}$ are the mass fractions of water soluble Cl and K in the fly ash, and M_i are the corresponding molar weights. The fraction of the Cl being bound to Na in the fly ash is neglected.

Figures 4.28 and 4.29 show the observed difference between full-scale ashes and those obtained in the lab-scale and semi-technical scale experimental setups with respect to the sulphation of chlorides in the fly ash. Whereas the fraction of water soluble K in fly ash from full-scale boilers appears independent of the S/Cl molar ratio in the fuel, both the lab-scale and semi-technical scale experiments yield

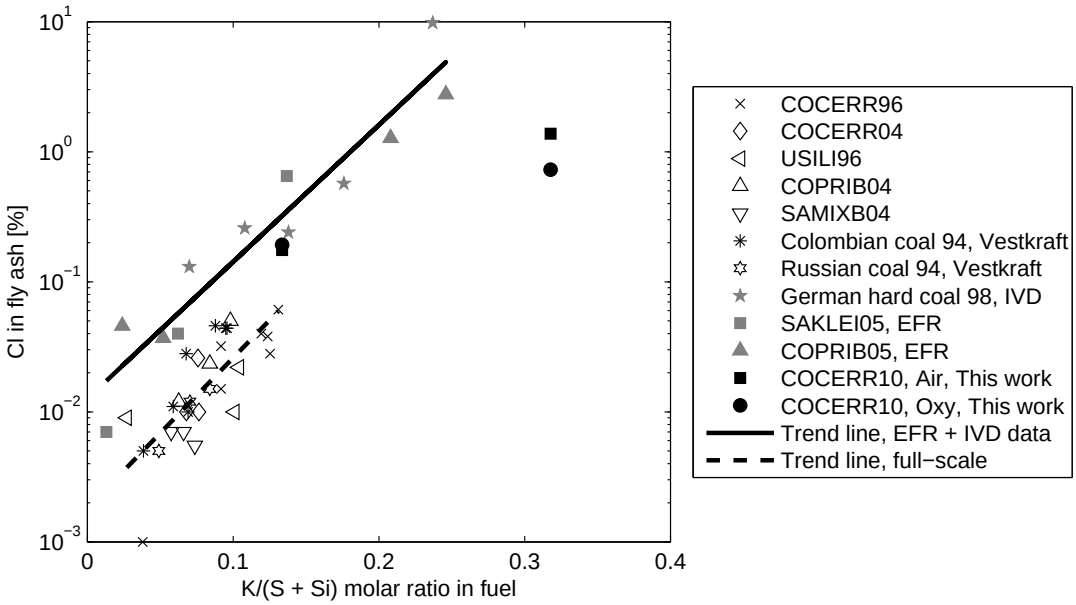

Figure 4.29: Percentage share of water soluble Cl in fly ash as a function of the K/(S + Si) ratio of the fuel. Open symbols: literature data from [80]; closed, grey symbols: semi-technical and entrained flow reactor (EFR) data from [80]; closed, black symbols: semi-technical scale data from this work. Only data for the straw/coal blends are shown for this work.

increasing sulphation propensity with increasing surplus of sulphur compared to Cl. The share of K_2SO_4 is higher for the experiments in this work than for the lab-scale setup probably due to a longer residence time in the temperature window where sulphation occurs (about 900 °C). For all of the investigated, straw-containing fuels in this work the degree of sulphation is lower than in full-scale. However, the data sets do not overlap with respect to the S/Cl ratio. A possibility exists, that for very low S/Cl ratios (high straw share) there would be a drop-off in the percentage of K occurring as K_2SO_4 due to the increased surplus of Cl in full-scale boilers as well. It is however unknown, if the full-scale fly ashes would resemble the data obtained in this work. Figure 4.29 confirms that the chloride retention in the fly ash is higher for the small-scale setups than for full-scale boilers, i.e. a larger percentage of the water soluble K could be expected to be bound in KCl. However, for the experiments with co-firing 50 wt% straw in this work (K/(S + Si) $\sim$ 0.32) the chloride content of the fly ash is closer to the trendline for the full-scale experiments (if extrapolated) than to the other lab-scale data. The reason for this is unknown.

4.6 Summary and Conclusions

Combustion of coal/straw blends with straw shares of 0, 20, 50, and 100 % was carried out at the reference air and oxyfuel conditions. The effect of the variation of the fuel composition was investigated with respect to flame temperatures, burnout efficiency, emissions, fly ash characteristics, and deposit formation.

It was shown that increasing fuel straw share yields decreasing flame and flue gas temperatures and increasing flame length. The most pronounced difference occurred with the change from the 50 wt% coal/straw blend to pure straw combustion.

Increasing the fuel straw share likewise had a significant impact on the fuel carbon burnout efficiency. For pure coal a burnout efficiency in air of 99.5 % was obtained while it dropped to 98.9 % for pure straw. Oxyfuel combustion consistently yielded higher burnout efficiencies than in air (99.3-99.8 %) and the difference to the data obtained in air increased with increasing fuel straw share. This is suggested to be a consequence of the relatively higher importance of the combined effect of higher inlet O_2 concentration, increased maximum flue gas temperature, and increased residence time when large straw particles ($d_p = 0.5-1$ mm) are fed to the reactor.

The observation made for pure coal with a change from air to oxyfuel combustion leading to a reduction in the emission of NO of about 30 % and to no difference with respect to SO_2 was also obtained for straw-containing fuels. However, the emission rates of both NO and SO_2 decrease with increasing fuel straw share. The slope is similar for both combustion atmospheres. The decrease is a consequence of the lower amount of Fuel-N and Fuel-S in straw compared to coal. An investigation of the Fuel-N to NO conversion ratio showed that a larger percentage of the Straw-N was converted to NO compared to coal. This is due to the fact that internal, gas-phase reduction of NO to N_2, proceeds via a 2nd order reaction whose reaction rate decreases relatively more than the 1st order oxidation of reduced N-species to NO with decreasing concentration of N-species in the gas-phase, i.e. decreasing Fuel-N. The Fuel-S to SO_2 conversion ratio for combustion of pure straw is essentially zero whereas it is above 80 % for combustion of pure coal. The difference is caused by the competing reactions between Al-Si containing ash particles and SO_2 for the potassium present in the parent fuel. At high K/Si ratios (straw), most SO_2 released to the gas phase is captured in sulphate salts.

The chemical composition of the collected fly ash samples was highly dependent on the fuel straw share. Significantly increased corrosion potential was observed for pure straw combustion compared to combustion of coal and the 20 wt% straw/coal blend. Due to the relatively low content of Si compared to K in the straw almost full capture of S and Cl as potassium salts in the ash was observed. A tendency for increased capture of water soluble K and S was found in deposits compared to the fly ash, further increasing the corrosion potential for the

straw-containing fuels. The deposition propensity likewise increases significantly when pure straw is burned compared to pure coal and the applied coal/straw blends. The deposit also became more sintered and difficult to remove.

A comparison of the fly ash data from this work to data from full-scale boilers co-firing coal and straw showed good agreement with respect to the capture of potassium in water soluble form in the fly ash. However, deviations were observed with respect to the degree of sulphation of the fly ash with full-scale plants achieving higher amount of K_2SO_4 in the fly ash than the semi-technical setups applied in this work and reported in literature.

Chapter 5

Special Topics

This chapter presents results regarding the combustion fundamentals for pure fuels (coal or straw) related to two different areas of the oxyfuel power plant process. The first part of the chapter treats the results related to the fate of N and S during simulated recirculation of flue gas prior to flue gas cleaning. The second part of the chapter describes results obtained during an investigation regarding the potential for improvement of the process economy of a retrofitted oxyfuel power plant by reducing the overall level of excess oxygen.

5.1 Sulphur and Nitrogen Chemistry in OxyCoal Combustion with Simulated Recirculated Flue Gas

The flue gas cleaning strategy for an oxyfuel power plant will have a significant impact on the level of pollutants such as NO and SO_2 within the boiler. If the recirculated flue gas is taken downstream of the $DeNO_x$ and desulphurization units the composition of the flue gas within the boiler would resemble what has been measured in the once-through experiments presented in Chapters 3 and 4. However, if flue gas is recirculated to the boiler prior to desulphurization and without NO_x removal accumulation of NO and SO_2 will occur in the flue gas. This section investigates the impact of the most often suggested process design of an oxyfuel power plant with recirculation of flue gas to the boiler prior to desulpurization and without NO_x removal on the nitrogen and sulphur species, i.e. emissions of NO and SO_2, as well as the impact on the ash and deposits quality. The experiments are performed using pure coal as fuel and at the reference operating conditions determined in Chapter 3.

5.1.1 Specific Experimental Methods and Considerations

The experimental setup applied in this work is a once-through setup and does thus not enable a physical recirculation of flue gas in its current configuration. Instead, NO and SO_2 can be added to the secondary, tangential oxidant flow in varying amounts. During the experiments the SO_2 and NO concentrations in the total oxidant flow have been varied in the range 0–3500 ppm and 0–2000 ppm, respectively. The operation of the experimental setup corresponds to recirculation of dry flue gas since no steam is added to the oxidant.

5.1.1.1 Addition of NO and SO_2 to Oxidant

During experiments with NO and/or SO_2 addition to the secondary tangential oxidant the flow of each species is set according to simultaneous measurements of the species concentration in the oxidant flow. Based on the measurements the overall concentration of the species, y_i^{ox}, in the entire oxidant flow can be determined from (5.1).

$$y_i^{ox} = \frac{y_i^{tan} F_{ox}^{tan}}{F_{ox}} \tag{5.1}$$

y_i^{tan} is the mole fraction of species i in the tangential flow, F_{ox}^{tan}, and F_{ox} is the total flow rate of oxidant.

5.1.1.2 Flue Gas Dilution

During the experiment with high concentrations of NO and/or SO_2 in the oxidant (CO17_ADNS with 2000 ppm NO and 3500 ppm SO_2) it was necessary to dilute the flue gas prior to analysis. The largest available upper limit on the measurement range on the online gas analysers for the two gases were 2500 ppm. The dilution was performed with an injector-type dilution panel. The diluting gas was pure N_2. Figure 5.1 on the next page shows the measured flue gas concentrations during the experiment. In order to correct the raw data the dilution ratio should be known. The dilution ratio could not be set directly at the dilution panel and is thus determined from the measurements on the oxidant which has a known composition. These measurements are located prior to the shaded areas in Figure 5.1. Neglecting the added species, the oxidant consists of 30 % O_2 and 70 % CO_2. From the measurements of O_2 and CO_2 in the oxidant the dilution ratio (DR) can be determined:

$$\mathrm{DR}_{\mathrm{O_2}} = \frac{0.30}{y_{\mathrm{O_2}}^{\mathrm{diluted}}} = 11.6 \pm 0.3 \tag{5.2}$$

$$\mathrm{DR}_{\mathrm{CO_2}} = \frac{0.70}{y_{\mathrm{CO_2}}^{\mathrm{diluted}}} = 12.3 \pm 0.2 \tag{5.3}$$

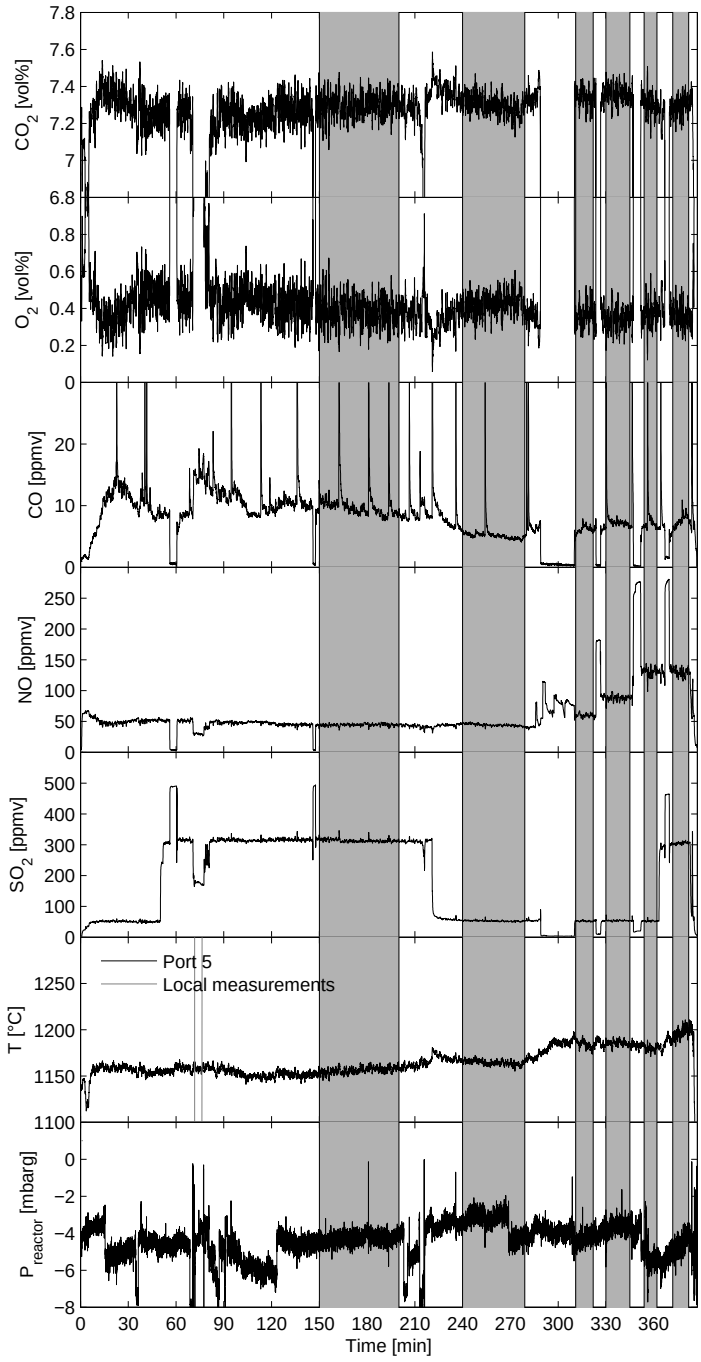

Figure 5.1: Diluted concentrations of major flue gas components (CO_2, O_2, CO, NO, and SO_2) as function of time for experiment CO17_ADNS, as well as the pressure at the top of the reaction chamber, the reference temperature measured at the reactor wall at a vertical position about 55 cm from the burner (port 5), and the local temperature measurements conducted with the S-type thermocouple probe. The shaded areas indicate the part of the data which are used during further data analysis.

The uncertainties on the determined ratios are due to fluctuating concentrations of the individual species during the measurement periods. The flue gas emision data are corrected by multiplying with the mean of the determined dilution ratios (DR = 12.0). It should be noted that the uncertainty on the measurements is increased significantly due to the dilution.

5.1.2 Simulated Recirculation of NO in Semi-Technical Scale

A large fraction of NO introduced with the recirculated flue gas to the furnace through the burner during oxyfuel combustion will be reduced to N_2 due to re-burning reactions [59]. A high gas phase concentration of NO during combustion could also reduce the percentage conversion of Fuel-N to NO. The relevant reactions are shown below. HCN is used as synonym for reduced N-species in the gas phase.

$$\mathrm{NO} + \mathrm{HCN} \rightleftharpoons \mathrm{N_2} + \ldots \tag{5.4}$$

$$\mathrm{HCN} + \mathrm{O_2} \rightleftharpoons \mathrm{NO} + \ldots \tag{5.5}$$

The split between gas-phase NO being reduced and Fuel-N not forming NO is unknown.

Figure 5.2 on the facing page compares the actual inlet NO concentrations used in the individual experiments with the measured exit flue gas concentration of NO corrected for the dilution by false air ingress. Three levels of NO in the oxidant have been tested; 550, 1300, and 2000 ppmv. With 2000 ppm NO in the oxidant the effect of a simultaneous high concentration of SO_2 (3500 ppmv) was also investigated. In the interval 0–1300 ppmv NO in the oxidant the concentration of NO in the flue gas increases linearly. Above 1300 ppmv NO in the oxidant a larger fraction of the NO doped to the oxidant appears to go unconverted through the furnace. The addition of 3500 ppmv SO_2 to the oxidant decreases the exit flue gas NO level when all other conditions are kept constant. This is in accordance with results reported in literature [83] which indicate that the presence of high levels of SO_2 may enhance the rate of consumption of NO in the gas phase. The formation of significant levels of radicals like SO, SH, and S at high temperature acts to reduce NO present in the gas phase [83].

Figure 5.3 on the next page shows the apparent conversion of NO introduced with the oxidant to N_2 under the assumption that the Fuel-N to NO conversion rate does not change compared to the case with no NO in the oxidant. The reduction, η_{NO}, is determined from Eq. (5.6).

$$\eta_{NO} = \frac{n_{NO,in} + n_{NO,0} - n_{NO,FG}}{n_{NO,in}} \tag{5.6}$$

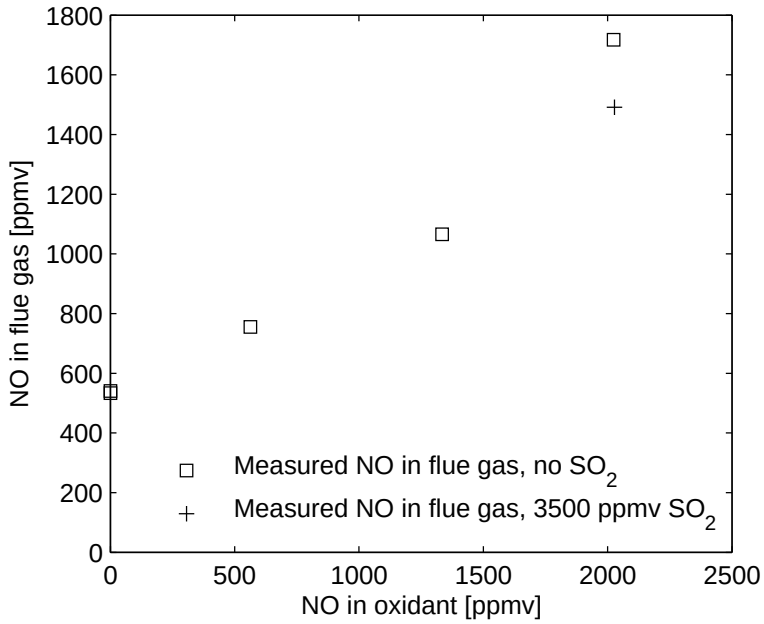

Figure 5.2: Comparison of the concentration of doped NO in the oxidant and the NO concentration measured in the resulting flue gas.

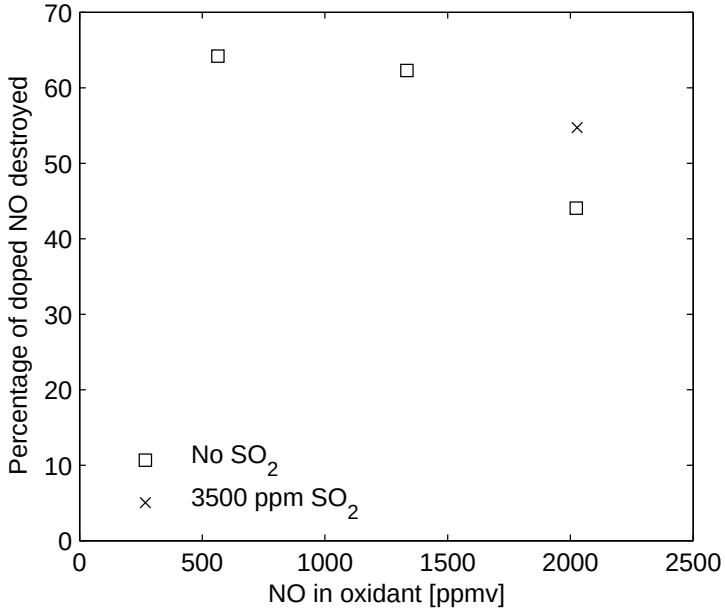

Figure 5.3: Apparent reduction of NO recirculated through the burner shown as the fraction of the NO in the oxidant which has been destroyed as a function of the concentration in the oxidant.

where $n_{NO,in}$ is the amount of NO introduced with the oxidant [mole/s], $n_{NO,0}$ is the amount of NO formed from Fuel-N when no NO is doped to the oxidant, and $n_{NO,FG}$ is the amount of NO in the flue gas.

The conversion efficiency decreases with increasing gas-phase NO concentration. For an inlet NO concentration of 550 and 1300 ppm about 62-65 % of the NO is reduced to N_2. These results are in good agreement with results presented by Liu et al. [84] from a comparable setup which yields reduction efficiencies between 68 and 82 % for an inlet NO concentration of about 500 ppmv. Liu et al. observed that the reduction efficiency increases with decreasing coal reactivity, i.e. decreasing burnout. This is most likely due to the increased amount of char present during combustion which reduces NO through the reactions:

$$\mathrm{NO + C} \rightarrow 0.5\,\mathrm{N_2 + CO} \tag{5.7}$$

$$\mathrm{NO + CO} \rightarrow 0.5\,\mathrm{N_2 + CO_2} \tag{5.8}$$

For a burnout efficiency similar to the one obtained in this work ($>$ 99 %) and with similar stoichiometric oxygen excess (1.2 versus 1.19 for this work) the NO reduction efficiency obtained in [84] was 68-70 %. The reported results by Liu et al. [84] likewise show only a marginal decrease in the reduction efficiency with an increase in the inlet NO concentration from 500 ppmv to 1000 ppmv when the NO is introduced with the secondary oxidant flow like in this work.

Increasing the inlet NO concentration from 1300 to 2000 ppmv yields a decrease in the reduction efficiency. These results are in contrast to the general observation that increased NO levels in the flame yields increased reduction of NO to N_2 [70] due to the fact that reactions of the type shown in (5.4) have second-order rate expressions. The results shown here indicate that the NO reduction potential of the flame is approaching its capacity when the NO concentration increases above a certain level. It is possible that, instead of NO, the concentration of reduced N-species becomes the limiting reactant since the applied burner is operated in high-NO_x mode.

The simultaneous presence of 3500 ppmv SO_2 and 2000 ppmv NO in the oxidant yields a 10 % point increase in the reduction efficiency of NO, from 44 to 54 %, compared to the case with only NO present in the oxidant flow.

The variation of the inlet NO concentration independently of the main oxidant composition is only relevant in a once-through reactor. For a setup with actual recirculation of the flue gas the inlet NO concentration at steady state operation will be determined by the chosen recirculation ratio, i.e. the inlet O_2 concentration at the burner. Figure 5.4 on the facing page illustrates the flows and the main gas species present in each flow for oxyfuel combustion with recirculation and without false air ingress. The part of the system positioned within the dashed square corresponds to a once-through setup as the one used in this work.

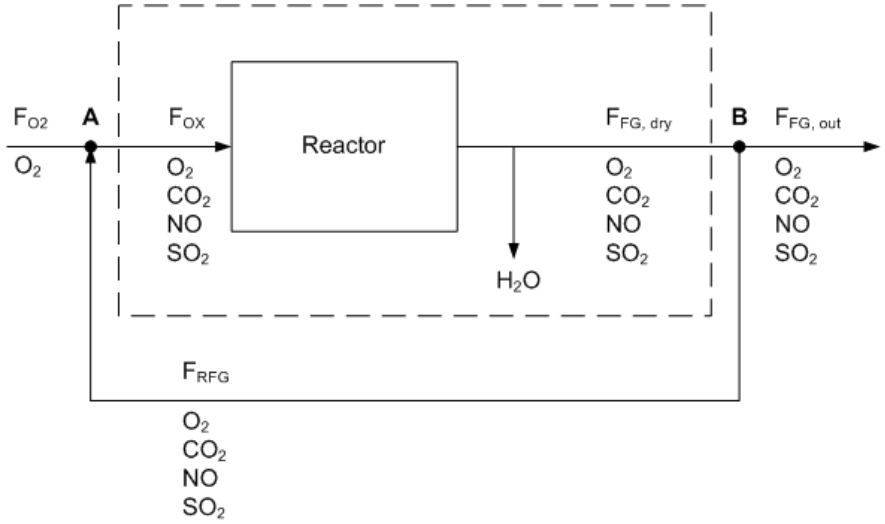

Figure 5.4: Flow diagram for an oxyfuel combustion reactor with recirculation of flue gas indicating the gas species present in each subflow. The part of the system situated within the dashed square corresponds to a once-through reactor.

Based on the measured NO concentration in the flue gas ($F_{FG,\,dry}$) for varying inlet NO concentrations it is possible to calculate the steady state concentration of NO at the reactor inlet if flue gas recirculation was performed. A comparison of the calculated inlet concentration and the actual concentration of NO doped to the oxidant will enable a determination of the inlet NO concentration at steady state during recirculation. The mole fraction of NO at the inlet, $y^{calc}_{NO,\,in}$, can be determined from (5.9).

$$y^{calc}_{NO,\,in} = \frac{y^{RFG}_{NO} \cdot F_{RFG}}{F_{ox}} \tag{5.9}$$

where y^{RFG}_{NO} is the mole fraction of NO in the recirculated flue gas, F_{RFG} is the flow of dry, recirculated flue gas, and F_{ox} is the total amount of oxidizer sent to the burner. The concentration of NO in the recirculated flue gas corresponds to the concentration in the entire flue gas flow leaving the reactor and is determined from the measured concentration, y^{dry}_{NO}, by Eq. (5.10).

$$y^{RFG}_{NO} = \frac{y^{dry}_{NO} \cdot F_{FG,\,dry,\,FA}}{F_{FG,\,dry}} \tag{5.10}$$

The measured concentration, y^{dry}_{NO}, is corrected for the flue gas dilution occurring due to the ingress of false air (FA) into the experimental setup.

The ratio between the recirculated flue gas flow and the total oxidant flow is determined from the mass balances in (5.11) and (5.12).

Overall balance for oxidant mixing point (point **A**):

$$F_{O2} + F_{RFG} = F_{ox} \tag{5.11}$$

F_{O2} is the flow of oxygen from the air separation unit (ASU). For simplicity it is assumed to be 100 % pure O_2.

O_2 balance at oxidant mixing point (point **A**):

$$F_{O2} + y_{O_2}^{dry} \cdot F_{RFG} = y_{O_2}^{ox} \cdot F_{ox} \tag{5.12}$$

The concentration of O_2 in the recirculated flue gas, $y_{o_2}^{dry}$, is about 5 % for the actual experiments and the oxidant inlet O_2 concentration, $y_{O_2}^{ox}$, is 30 %. The recirculation rate of flue gas, RR see (5.13), is about 70 %.

$$RR = \frac{F_{RFG}}{F_{FG,\,dry}} \tag{5.13}$$

The calculated mole fraction of NO in the oxidant for a setup with flue gas recirculation, based on known quantities, can thus be determined from:

$$y_{NO,\,in}^{calc} = \frac{y_{NO}^{dry} \cdot F_{FG,\,dry,\,FA} \left(1 - y_{O_2}^{ox}\right)}{F_{FG,\,dry} \left(1 - y_{O_2}^{dry}\right)} \tag{5.14}$$

Figure 5.5 on the next page compares the calculated inlet values based on the measured flue gas concentration with the actual inlet NO concentrations used in the individual experiments. The figure also shows the measured exit flue gas concentrations from Fig. 5.2. For low, doped inlet NO concentrations ($<$ 550 ppmv) the calculated inlet concentration is higher than the actually applied level, whereas for inlet concentrations above 550 ppmv the calculated levels are below the actual levels. This implies that the inlet NO concentration at steady state if flue gas recirculation was established would be around 550 ppmv, i.e. where the line with a slope of 1 (dashed line) crosses the trend line through the data points. The concentration of NO in the dry exit flue gas at steady state would thus be about 750 ppmv corresponding to an emission rate of 203 mg/MJ at the furnace exit ($F_{FG,\,dry}$) and 50 mg/MJ in the flue gas ($F_{FG,\,out}$) transported to the chimney (or other downstream processes). Compared to the once-through experiments with no addition of NO to the oxidant which have a NO emission rate of about 150 mg/MJ the recirculation of flue gas induces a reduction of the NO emission of about 67 %. An overall NO emission rate of 50 mg/MJ correspond well to the lower range of levels reported in literature for pilot scale and semi-technical scale experimental facilities with flue gas recirculation [59].

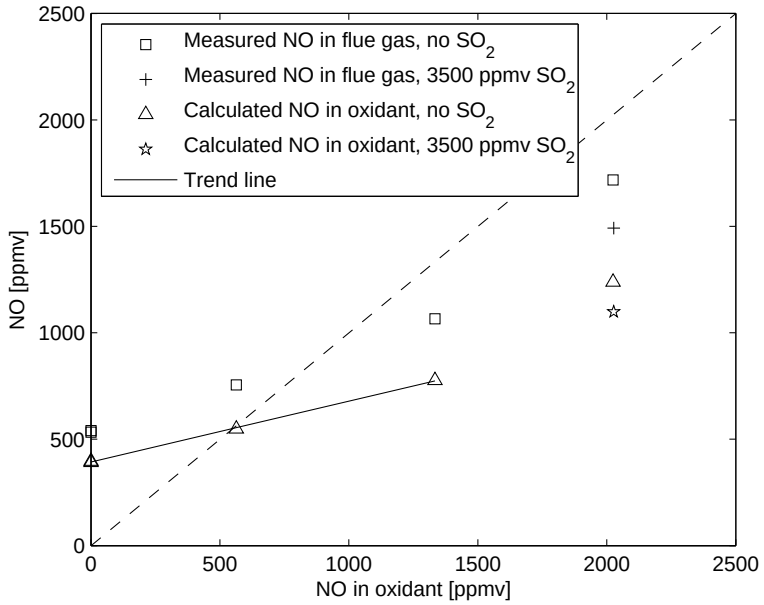

Figure 5.5: Comparison of the concentration of doped NO in the oxidant and the calculated concentration in the oxidant if flue gas with an NO concentration equal to the one measured in the resulting flue gas was recirculated to the burner.

5.1.3 Simulated Recirculation of SO_2 in Semi-Technical Scale

Unlike NO, SO_2 introduced through the burner in oxyfuel combustion will not be subject to reburning reactions. Instead, a significantly increased concentration of SO_2 within the furnace would be the result of accumulation due to the recirculation of SO_2-containing flue gas [59]. Generally, the reported SO_2 levels in flue gas from experimental setups with flue gas recirculation is lower than anticipated. This decrease is typically associated with increased retention of sulphur in fly ash and deposits and absorption in the flue gas condensate. This section investigates the impacts of increased in-furnace SO_2 concentrations on the flue gas SO_2 concentration and the retention of sulphur in ash and deposits. The concentration of doped SO_2 in the oxidant has been varied from 0 to 3500 ppmv. At 3500 ppmv the effect of a simultaneous high concentration of NO (2000 ppmv) was investigated.

5.1.3.1 Sulphur Retention in Ash and Deposits

The amount of sulphur doped to the oxidant which is removed from the gas phase during combustion is expected to mainly be captured by fly ash and deposits. An increase in the concentration of SO_3 is also expected since about 0.1-1 % of the SO_2 is oxidized to SO_3 in the flue gas [69]. However, the increase in the SO_3 concentration in the flue gas with increasing in-furnace SO_2 levels is

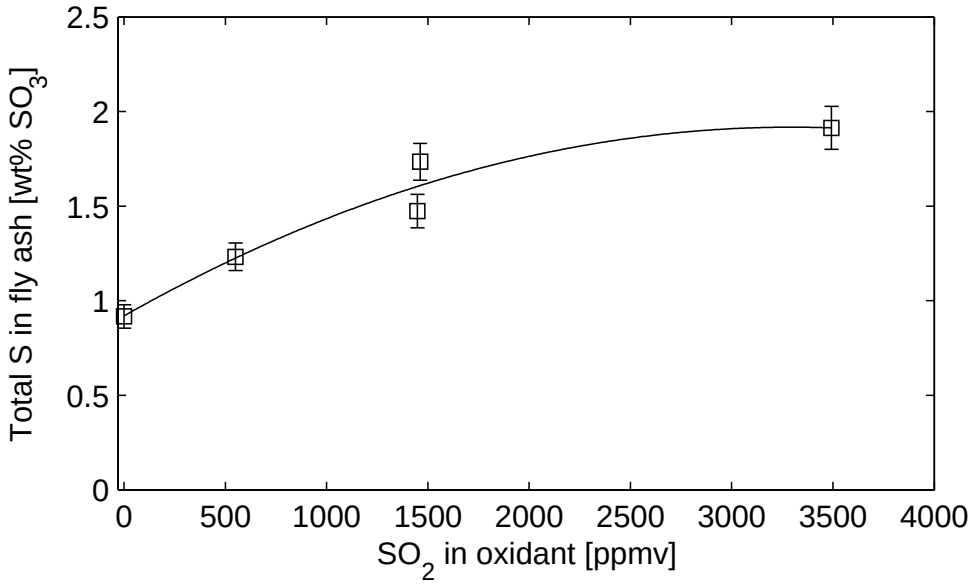

Figure 5.6: Relation between the total amount of sulphur captured in fly ash, measured as SO_3, and the concentration of SO_2 in the oxidant. Error bars correspond to two times the standard deviation in the analysis. The data have been fitted with a second order polynomial trend line.

insignificant with respect to the overall mass balance for sulphur in the system. Figure 5.6 shows the increasing retention of sulphur in the fly ash with increasing SO_2 concentration in the oxidant. Increasing the oxidant SO_2 concentration from 0 ppmv to 3500 ppmv yields an about 100 % increase in the sulphur content of the fly ash. The data corresponds well with the findings by Fleig et al. [69], that a high in-furnace SO_2 concentration in oxyfuel combustion with FGR favours sulphation and stabilises the sulphates formed. The non-linear trend in the fly ash sulphur content indicates the approach to the capacity of the ash to capture sulphur. Figure 5.7 on the next page shows the ratio of water soluble alkali and alkali earth metals to sulphur in the ash. A stoichiometric ratio is reached at approximately 1500 ppmv SO_2 in the oxidant and it can thus be anticipated that a further increase in the flue gas concentration of SO_2 beyond 3500 ppmv would not yield a significant increase in the sulphur content of the fly ash.

One of the critical aspects regarding the implementation of the oxyfuel combustion technology in power plants is the quality of the fly ash. In order to observe to the criteria of maximum 3 wt% S in fly ash (measured as SO_3) for utilisation of fly ash in concrete [63] it has been a question whether flue gas recirculation prior to desulphurization was possible. The data in Figure 5.6 shows that the quality criteria can be met with a considerable safety margin for the coal used in this work. The coal has a relatively low sulphur content (0.62 wt%, as received) and for coals with higher sulphur contents the significant increase in

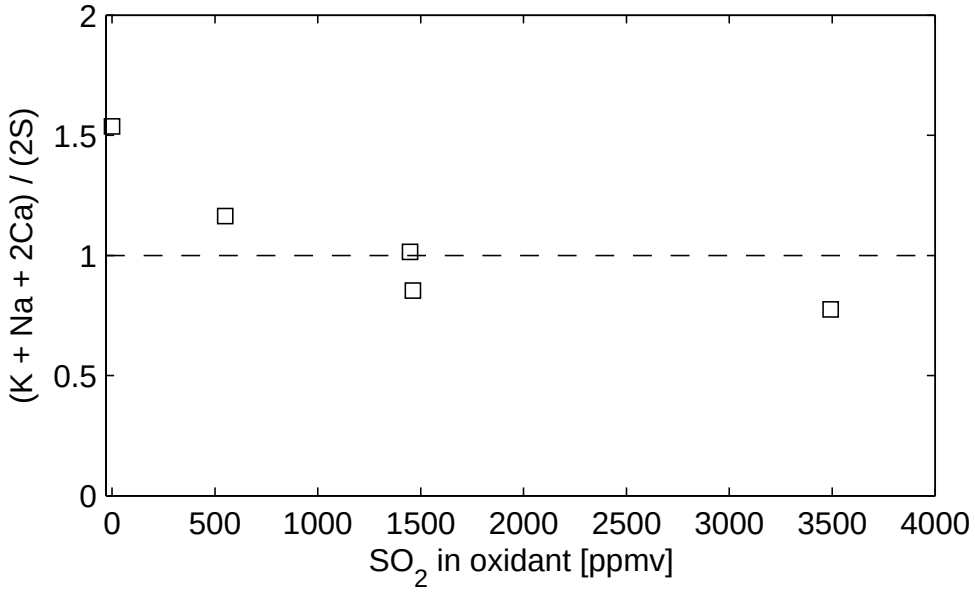

Figure 5.7: Stoichiometric ratio of water soluble alkali and alkali earth metals to sulphur in fly ash samples as function of the concentration of SO_2 in the oxidant.

the sulphur retention by the fly ash with increasing in-furnace SO_2 levels could pose a problem with respect to its utilization.

The three fly ash fractions; bottom, cyclone, and filter ashes, see Section 2.3.2.2, were analysed separately. The analysis indicated that sulphur is captured preferentially in the smaller particles, as the S content of the ash fractions increases in the order: Bottom ash $<$ Cyclone ash $<$ Filter ash for all experiments. This corresponds well with formation of sulphate-rich aerosols which mainly will end up in the filter ash fraction.

Table 5.1 on the following page shows the measured sulphur concentrations in the collected deposits and the calculated deposit fluxes. Similarly to the fly ash, the sulphur content of the deposits is observed to increase with increasing level of SO_2 in the flue gas. Except for one experimental run, the increase is linearly correlated to the fly ash sulphur content, as seen in Figure 5.8 on the next page. The data point that falls outside the trend of equal sulphur content in fly ash and deposit has an exposure time which is only about half as long (1.3 hr) as for the other experiments (2 hr). The most plausible cause to the deviation from the trend is the reduced sampling time and the relatively low yield of fly ash, 30 versus typically 50 %, see Figure 2.10 on page 32, which induces a significant uncertainty on the result.

Table 5.1: Average deposit fluxes as well as flue gas and deposit probe temperatures for exposure times of 1-2 hr and total S content in deposit for combustion of coal in the reference oxyfuel atmosphere with doping of SO_2 to the oxidant.

Inlet SO_2 [ppmv]	Exposure time [hr]	Up-stream	Down-stream	Average	T_{probe} [°C]	T_{FG} [°C]	S_{tot} [wt%]
0	2.3	75	3	39	500	950	0.42
550	2.0	62	8	35	500	-	0.50
1460	1.3	64	5	34	500	-	0.50
1450	2.0	74	8	41	500	880	0.51
3500	2.2	67	10	38	500	810	0.68

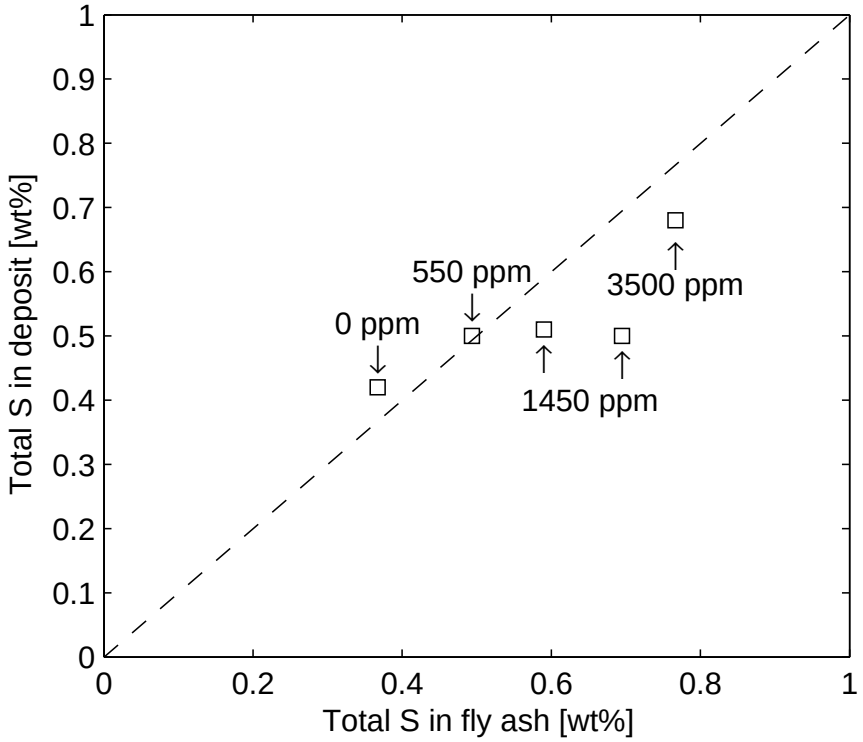

Figure 5.8: Comparison of the total sulphur content of related fly ash and deposit samples. The oxidant SO_2 concentration is stated for each data point.

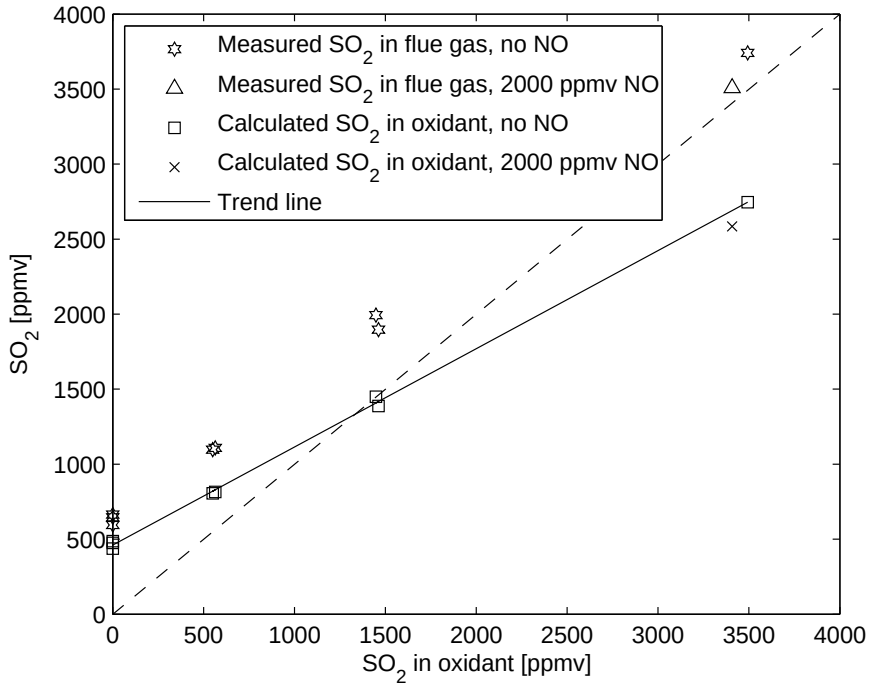

Figure 5.9: Comparison of the concentration of doped SO_2 in the oxidant and the calculated concentration in the oxidant if flue gas with a SO_2 concentration equal to the one measured in the resulting flue gas was recirculated to the burner. The experiments have been performed both with and without simultaneous addition of NO to the oxidant.

5.1.3.2 Impact of Increased Furnace SO_2 Level on the SO_2 Emission

Figure 5.9 shows the relationships between the doped inlet concentration of SO_2 and the flue gas SO_2 concentration as well as the calculated SO_2 concentration in the oxidant if flue gas recirculation was performed. A linearly increasing trend is seen for the calculated oxidant concentrations. The steady state inlet concentration if the experimental setup was equipped with flue gas recirculation would be about 1500 ppmv and the flue gas concentration would be about 1950 ppmv at the reference operating conditions. Compared to the experiments without SO_2 addition to the oxidant the in-furnace SO_2 concentration thus increases with a factor of 3 (from 645 ppmv). The exit furnace emission rate of SO_2 would be 1130 mg/MJ which corresponds to about 280 mg/MJ after the point of flue gas recirculation. Compared to the once-through experiments which have an SO_2 emission rate of about 390 mg/MJ the recirculation of flue gas induces an overall reduction of the SO_2 emission of about 28 %. An overall SO_2 emission rate of 280 mg/MJ correspond well to results reported in literature for combustion of coals with similar sulphur contents combusted in pilot scale and semi-technical scale experimental facilities with flue gas recirculation [72, 73]. At high burnout efficiencies the SO_2 emission rate is determined only by the sulphur content of

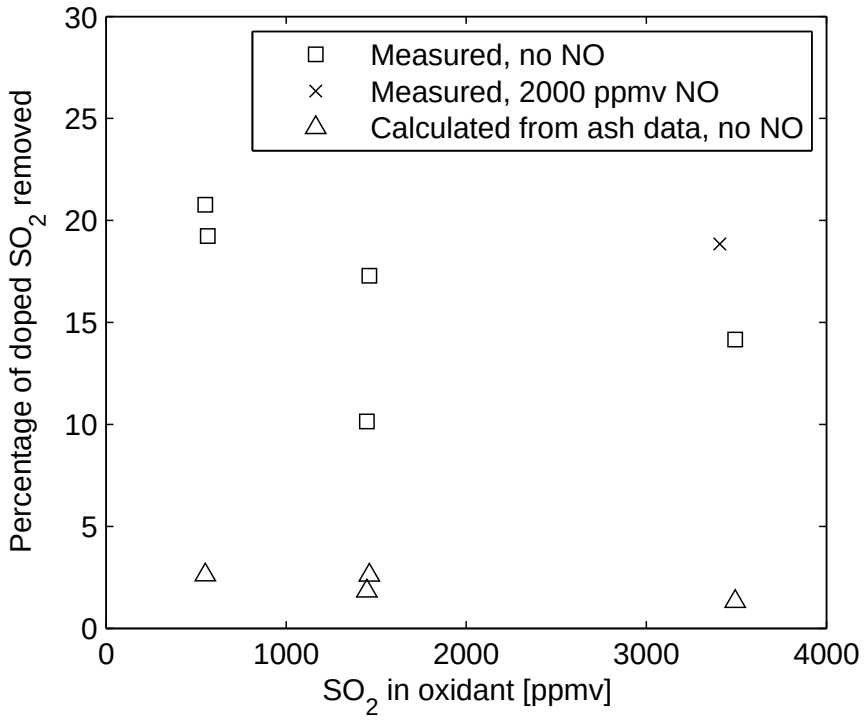

Figure 5.10: Apparent removal from the gas phase of SO_2 introduced through the burner as a function of the concentration in the oxidant. The experiments have been performed both with and without simultaneous addition of NO to the oxidant. The figure shows both removal efficiencies based on the measured flue gas concentration of SO_2 and based on the amount of sulphur measured in the fly ash samples.

the coal.

The presence of 2000 ppmv NO does not seem to have a significant effect on the gas phase sulphur chemistry.

Figure 5.10 shows the percentage of the doped SO_2 which has been removed from the gas phase during the combustion. The removal has been determined according to the procedure described in Section 5.1.2. The observed reduction is between 10 and 20 % and tends to decrease with increasing in-furnace SO_2 level. The decrease indicates the approach to the capacity limit for sulphur retention in fly ash and deposits when the in-furnace SO_2 concentration becomes very large. The removal of SO_2 from the gas phase during combustion is significantly smaller than for NO which is a consequence of the different removal mechanisms – capture by solid phases versus gas phase reactions. An explanation to the large difference between the points at 1500 ppmv SO_2 in the oxidant has not been found.

A comparison of the flue gas and fly ash samples shows that the removal efficiency which can be determined based on the measured sulphur levels in the

fly ash correlates poorly to the values based on the flue gas measurements with respect to the absolute values, see Fig. 5.10. The trend of decreasing removal efficiency with increasing in-furnace SO_2 level is, however, the same. This deviation is indicative of a significant source of error on the flue gas SO_2 measurements. A loss of SO_2 occurs in the flue gas sampling system prior to analysis, either due to absorption in the condensate or by reaction with moist ash. Alternatively, the SO_2 levels in the oxidant have been overestimated.

5.1.4 Summary and Conclusions

Dry flue gas recirculation for an oxyfuel combustion system without removal of NO and SO_2 has been simulated in the once-through experimental setup used in this work. NO and SO_2 levels of 0-2000 ppmv and 0-3500 ppmv, respectively, have been applied during combustion of pure coal.

The investigation showed that the steady state NO concentration in the oxidant would be around 550 ppmv if flue gas gas was recirculated. This implies that about 65 % of the NO in the recirculated flue gas is reduced to N_2 during combustion. The NO emission rate is likewise reduced to about 1/3 (50 mg/MJ) of the level for once-through operation which corresponds well to results reported in literature for experimental facilities with actual flue gas recirculation.

Simultaneous presence of NO and high levels of SO_2 leads to an increased reduction of NO formed in the gas phase. At 2000 ppmv NO in the inlet addition of 3500 ppmv SO_2 increases the reduction efficiency of NO with 10 % points.

The simulated recirculation of SO_2 showed that the in-furnace SO_2 level increases with a factor of 3 due to accumulation and the fact that only 10-20 % of the SO_2 is removed from the gas phase during combustion. At steady state the inlet SO_2 level would be about 1500 ppmv and the flue gas concentration about 1950 ppmv for the coal applied in this work. Unlike NO which is reduced due to reburning reactions, SO_2 is removed mainly due to capture by fly ash and deposits. The data showed an increasing capture with increasing flue gas SO_2 level and at steady state the amount of sulphur in the fly ash would increase about 60 % compared to the case with no SO_2 in the oxidant. However, due to the fact that a coal with a relatively low sulphur content (0.62 wt%, as received) has been applied, the requirement of a maximum content of 3 wt% SO_3 in the fly ash can be met with significant safety margen.

The capture of sulphur by fly ash and deposits is seen to be similar and the increase in the in-furnace SO_2 level was not observed to have an effect on the rate of formation of deposits.

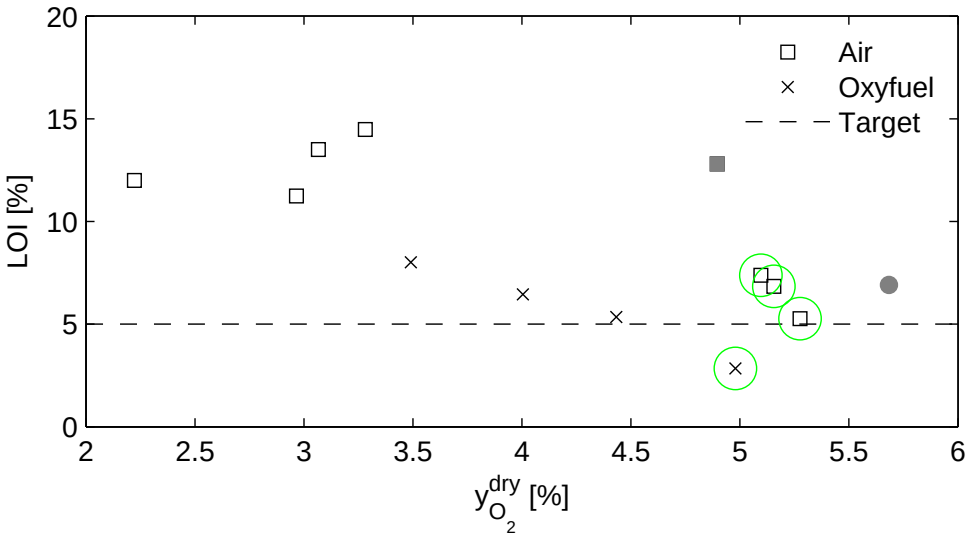

Figure 5.11: Comparison of loss-on-ignition (LOI) for coal combustion in air and 30% O_2/CO_2 at different flue gas oxygen levels. Data points marked with green circles are the experiments with realized operating conditions corresponding to the chosen reference parameters (CA10, CA14, CA16, and CO09). The air experiment marked in grey and the oxyfuel experiment marked with a grey circle fall outside the trend for the remaining experiments according to the discussion in Sections 3.1.2 and 3.2.1.

5.2 Improving Process Economics

The major penalty to the oxyfuel combustion process economy is at present the high operating expenses associated with cryogenic oxygen production [59]. This section provides results for both coal and straw combustion showing that there is a potential for reducing oxygen excess in oxyfuel combustion compared to conventional air-firing and hence improve process economics. The analysis is made under the assumption that a conventional air-blown power plant is retrofitted to oxyfuel combustion and that a design criteria is that the exit flue gas oxygen concentration is kept at the same level as in the original plant. A key issue in relation to the reduction of oxygen excess is that the change is not made at expense of the quality of the combustion process, i.e. giving rise to increased emissions or reduced burnout.

5.2.1 Comparing Air and OxyCoal Burnout and Emission Rates as Function of Oxygen Excess

Figure 5.11 shows a comparison of the development in fly ash loss-on-ignition as function of the combustion stoichiometry for air and 30 % O_2/CO_2 experiments. The general trend in the data is that the burnout efficiency for comparable flue

gas oxygen levels is higher during oxyfuel combustion than in air for a plant of a given size. It is thus possible to decrease the oxygen excess level to some degree in an oxyfuel power plant compared to the corresponding plant using air as oxidant without compromising fuel burnout. A potential requirement is that the residence time in the retrofitted oxyfuel plant is increased relative to the air conditions with the same factor of about 1.5 as has been the case for the experiments displayed here.

Figure 5.12 on the following page shows comparisons of the NO, SO_2, and CO emission rates for air and oxyfuel combustion as function of the oxygen concentration in the dry exit flue gas. Based on the available data, reducing the oxygen excess does not induce significant changes to the emission rates of the polluting species and no limitations should be put up for the reduction in oxygen excess.

For the experimental setup, a reduction from about 5 % to about 4.5 % O_2 in the dry flue gas is possible without compromising fuel burnout (LOI = 5 %). Under the assumption that the same relative reduction of the oxygen excess can be applied at a full-scale power plant, the associated decrease in the oxygen demand for the power plant can be estimated from (5.15).

$$\begin{aligned} \mathrm{O}_{2,\,\mathrm{saved}} &= \frac{\mathrm{F}_{\mathrm{O}_2,\,\mathrm{Oxy\ 30/5}} - \mathrm{F}_{\mathrm{O}_2,\,\mathrm{Oxy\ 30/4.5}}}{\mathrm{F}_{\mathrm{O}_2,\,\mathrm{Oxy\ 30/5}}} \\ &= \frac{\lambda_{30/5} - \lambda_{30/4.5}}{\lambda_{30/5}} \\ &= \frac{1.19 - 1.17}{1.19} = \mathbf{2}\ \% \end{aligned} \tag{5.15}$$

where $F_{O_2,\,Oxy\ XX/YY}$ is the required oxygen flow to the boiler for an oxidant with XX % O_2 (remaining CO_2) and an oxygen excess corresponding to YY % O_2 in the dry flue gas.

Even though the saving may seem insignificant, it may induce a marked reduction of the operating expenses for an oxyfuel power plant. The potential for reducing the oxygen excess in full-scale is very dependent on the possibility of achieving good mixing of oxidant and fuel within the boiler.

5.2.2 Taking Advantage of the Extra Degree of Freedom in OxyStraw Combustion

For the coal experiments discussed above the concentration of oxygen at the burner inlet was fixed. However, oxyfuel combustion has the advantage over air-firing that the oxygen excess and inlet oxygen concentration are no longer dependent variables. This section describes an investigation which exploits the

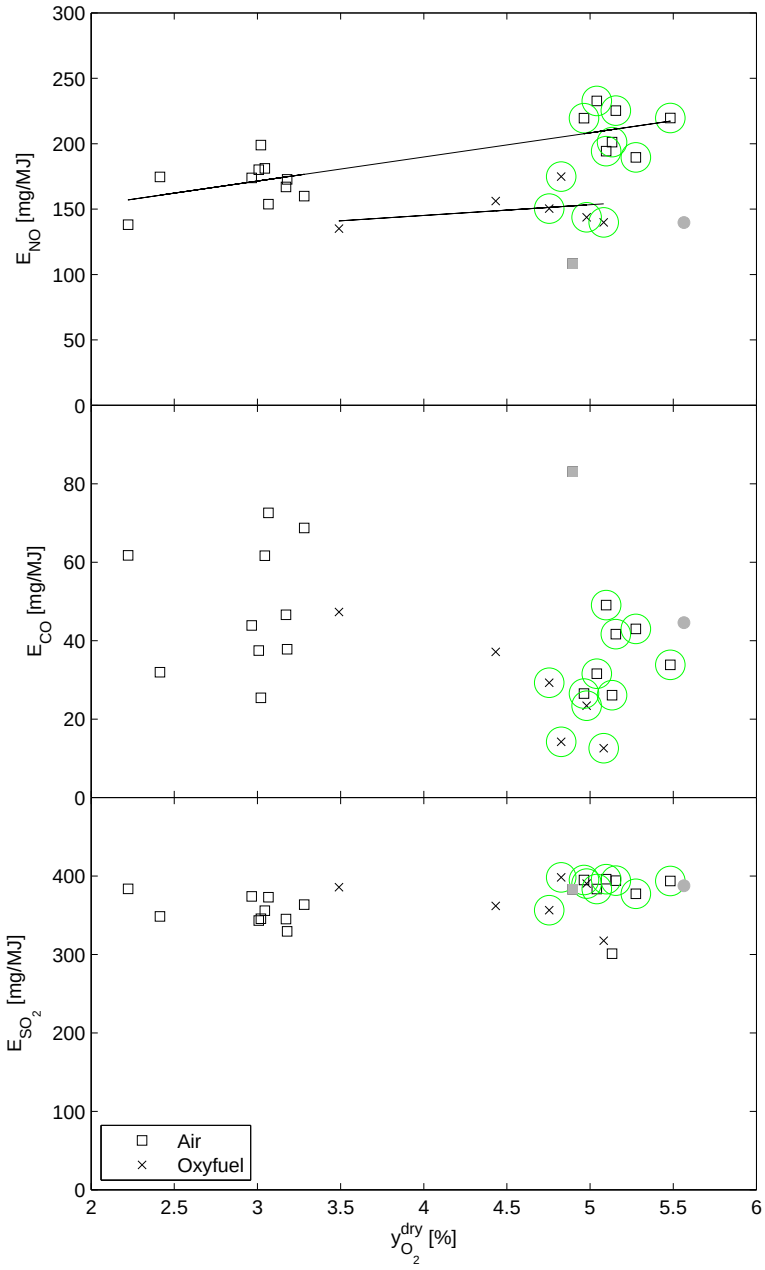

Figure 5.12: Comparison of the emission rate of NO, CO, and SO_2 for coal combustion in air and 30% O_2/CO_2 at different stoichiometries. Data points marked with green circles are the experiments with realized operating conditions corresponding to the chosen reference parameters (CA10, CA12-17, CO09, CO10, CO12, and CO18). CA17 and CO18 have been omitted in the SO_2 plot according to the discussion in Section 2.4.2. The air experiment marked in grey and the oxyfuel experiment marked with a grey circle fall outside the trend for the remaining experiments according to the discussion in Sections 3.1.2 and 3.2.1. These points have been omitted in the determination of trend lines.

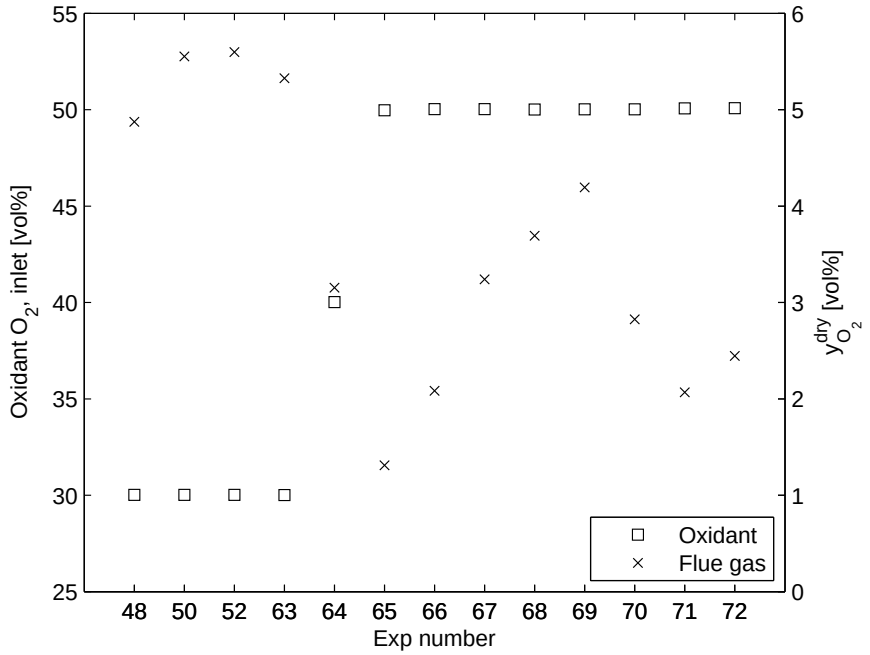

Figure 5.13: Related values of oxidant O_2 concentration and theoretical O_2 concentration in the dry exit flue gas as function of the experiment number (chronological order).

effect of increasing inlet oxygen concentration while simultaneously reducing the flue gas oxygen level. The investigation is performed with pure straw as fuel. The choice of straw over coal is made with the aim of investigating the savings potential for the most difficult fuel where large particles causes challenges during burnout.

Figure 5.13 provides an overview of the combustion conditions for the series of experiments in the investigation. Only experiments 63, 64, and 72 includes fly ash sampling while the remaining experiments are used solely for evaluation of emissions.

The development in fly ash loss-on-ignition when changing combustion conditions is seen in Figure 5.14 on the following page. The oxidant and stoichiometry is given as e.g. Oxy 40/3 meaning that the oxygen concentration at the inlet is 40 % and the corresponding concentration in the dry flue gas is 3 %. The change from air-firing to oxyfuel combustion yields a significant improvement in burnout for all combustion conditions. For all oxyfuel experiments no change in the burnout efficiency is observed with the change in conditions. The decreasing trend in the uncertainty on the measurements with increasing inlet O_2 concentration is a consequence of decreasing occurrence of char particles in the bottom ash fraction.

Changing the oxyfuel combustion conditions from a 30 % O_2/CO_2 oxidant mix-

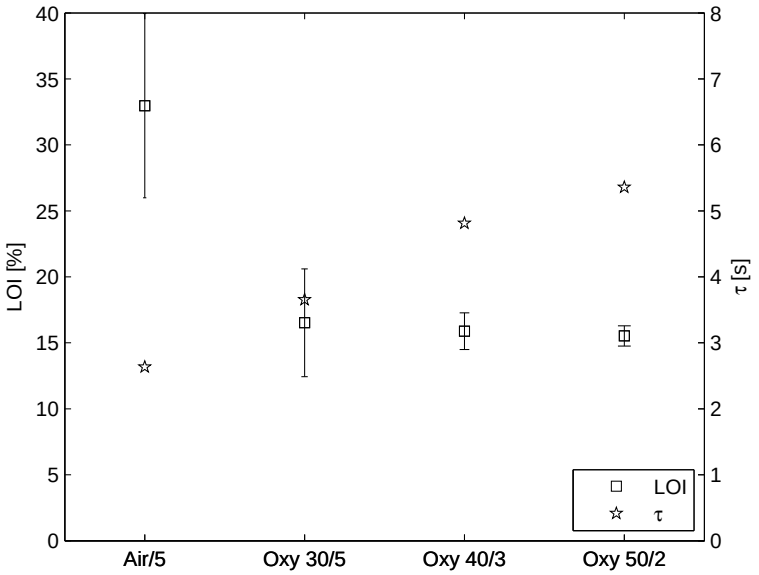

Figure 5.14: Comparison of loss-on-ignition (LOI) and average gas and particle residence time for straw combustion in air and oxyfuel atmospheres with varying oxidant compositions and stoichiometries. Error bars correspond to two times the uncertainty on the LOI analysis.

ture with an oxygen excess corresponding to 5 % O_2 in the dry flue gas to a 50 % O_2/CO_2 oxidant mixture with an oxygen excess corresponding to 2.4 % O_2 in the dry flue gas would yield an approximately 13 % decrease in the required oxygen demand, as shown below.

$$\begin{aligned} O_{2,\,\text{saved}} &= \frac{F_{O_2,\,\text{Oxy }30/5} - F_{O_2,\,\text{Oxy }50/2}}{F_{O_2,\,\text{Oxy }30/5}} \\ &= \frac{\lambda_{30/5} - \lambda_{50/2}}{\lambda_{30/5}} \\ &= \frac{1.21 - 1.05}{1.21} = \mathbf{13}\ \% \end{aligned} \tag{5.16}$$

Compared to the coal case described previously which had a potential of a 2 % reduction in oxygen production demand, the 13 % reduction in oxygen demand shown here implies a great potential in favour of the oxyfuel technology.

5.2.2.1 Implications of Major Changes to OxyFuel Combustion Conditions

The change of the operating conditions described above has a number of implications on the combustion process. First of all, the increase in the initial oxygen concentration in the reactor yields a smaller flue gas volume flow and

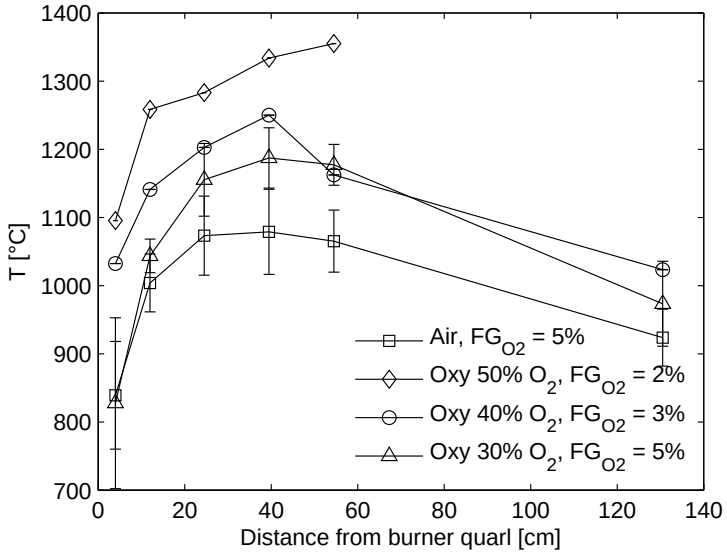

Figure 5.15: Reactor centre temperature profiles measured with S-type thermocouple for pure straw combustion in air and oxyfuel atmospheres with different inlet oxygen concentrations and stoichiometry. Errorbars correspond to two times the standard deviation for repeated measurements.

hence an increased residence time for the fuel particles within the reactor as seen in Figure 5.14 on the preceding page. The increase in residence time is one of the important factors necessary for keeping a satisfying burnout efficiency even though the oxygen excess is decreased.

The increasing oxygen partial pressure in the flame zone has a significant impact on the flue gas temperature in the furnace. Figure 5.15 shows reactor centre temperature profiles for the investigated combustion conditions. A flame temperature difference of about 300 °C is observable between air combustion and combustion in 50 % O_2/CO_2. This temperature increase will aid the fuel conversion rate but at the same time, it is a critical parameter with respect to full-scale boilers. Significantly increased temperatures in the radiative section of the boiler could lead to problems with the boiler walls as these are not capable of withstanding these higher temperatures without tube failures. Protection of the boiler materials could prove necessary, e.g. by recirculating cold flue gas close to the walls. This protection strategy would decrease the overall residence time in the boiler and could thus reduce the burnout efficiency.

The effect of varying oxidant composition and stoichiometry on emissions is shown in Figure 5.16 on the next page. The change from air combustion to combustion in a 30 % O_2/CO_2 oxidant leads to a decrease in NO emission. Increasing the oxygen concentration at the inlet from 30 to 40 % and decreasing oxygen excess yields a further decrease of the NO emission without any change to CO or SO_2

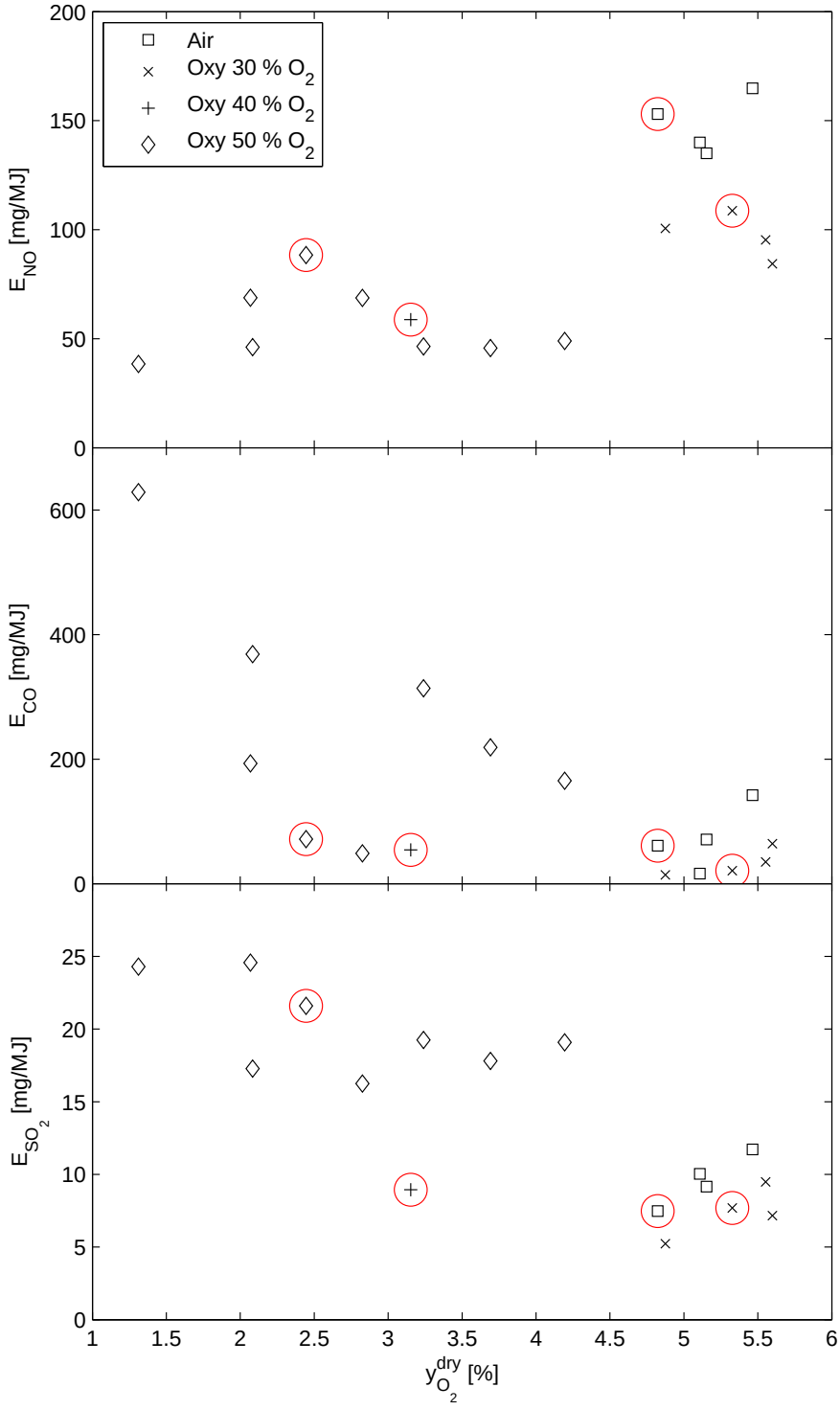

Figure 5.16: Comparison of the emission rate of NO, CO, and SO_2 for straw combustion in air and oxyfuel atmospheres with varying oxidant compositions and stoichiometries. The points marked with red circles are the experiments with fly ash sampling.

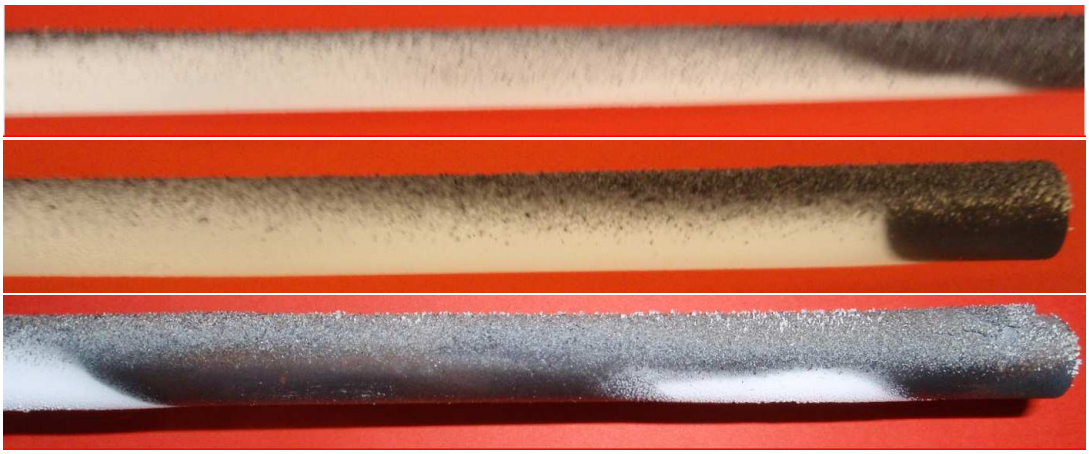

Figure 5.17: Sideview of deposits. The deposit probe has a diameter of 16 mm. Top: Straw combustion in air; Middle: Straw combustion in 30 % O_2/CO_2; Bottom: Straw combustion in 40 % O_2/CO_2. Colour differences are a consequence of the picture recording.

emissions. The experiments performed with 50 % O_2 at the inlet show no clear trend in NO and CO emissions. This is a consequence of necessary changes to the individual burner flow settings (increasing ratio of primary oxidant to total oxidant and decreasing secondary axial flow) in order to stabilize the flame. The high CO emissions cover high frequencies of CO peaks due to instabilities in the transport of the solid fuel through the burner. Increasing the primary oxidant flow lead to less frequent CO peaks due to more smooth fuel feeding. The fly ash was sampled at conditions with low CO emission but increased NO emission compared to the combustion with 40 % O_2 at the inlet. However, the NO emission does not exceed the value for the reference state with 30 % O_2 at the inlet. There seems to be a higher SO_2 emission for the experiments with 50 % O_2 at the inlet but all levels are very low and in reality within the measurement uncertainty.

Besides fly ash, a deposit sample was collected for all but the Oxy 50/2 conditions. The visual appearance of the deposits is seen in Figure 5.17. For all conditions the deposit on the upstream part of the probe is dominated by residual ash particles reaching the surface and sticking to the thin, soft layer of condensed salts build up following the insertion of the probe in the reactor. For the air and Oxy 30/5 deposits a large fraction of the upstream deposit is white. This is not the case for the Oxy 40/3 conditions which is assumed to be a consequence of the higher flue gas temperature. For all combustion conditions the upstream part of the deposit is highly sintered and increasingly difficult to remove as the oxygen concentration was increased. Condensation of salts on the downstream part of the probe is seen to be almost equally distributed along the probe for the air and Oxy 30/5 conditions whereas for the Oxy 40/3 conditions areas without

Table 5.2: Average deposit fluxes as well as flue gas and deposit probe temperatures for straw combustion in air and oxyfuel atmospheres for an exposure time of 2 hr.

Oxidant	Upstream [g/m^2·hr]	Downstream [g/m^2·hr]	Average [g/m^2·hr]	T_{probe} [℃]	T_{FG} [℃]
Air	102	15	59	500	940
Oxy 30/5[a]	206 ± 35	14 ± 7	110 ± 21	500	970 ± 30
Oxy 40/3	295	16	156	500	1025

[a] Average ± two standard deviations for two repetitions (exp SO02 and SO04)

condensation is observed. The absence of condensed salts in the latter case is most likely due to differences in the flue gas flow conditions around the probe since the temperature difference across the probe is small.

Table 5.2 shows the calculated deposit fluxes based on the collected samples. A significant increase in the average fluxes are seen with each change in combustion conditions. Part of the explanation to the increase is the increase in flue gas temperature at the deposit sampling position, T_{FG}. From air combustion to Oxy 30/5 the temperature increases about 30 ℃ and a further increase of about 60 ℃ is again seen with the change to Oxy 40/3. The increase in gas phase temperature will increase the stickiness of the ash particles and hence increase the deposition on the upstream part of the probe. Within the experimental uncertainty, no change to the downstream deposit flux (condensation) can be observed.

5.2.3 Summary and Conclusions

The potential for improving the process economy of an oxyfuel power plant by reducing the overall level of excess oxygen for combustion has been investigated. The investigation covered experiments with pure coal and pure straw combustion in air and oxyfuel atmospheres with varying oxidant composition and oxygen excess level.

For the case of matching flame temperature between air and oxyfuel atmospheres (30 % O_2/CO_2) it has been shown with coal as fuel that similar burnout to the air reference can be achieved in the swirl burner setup during oxyfuel combustion with lower oxygen excess level. A potential decrease in oxygen demand of 2 % was determined for these conditions and no problems regarding pollutants emissions were observed.

Advantage was taken of the fact that the oxidant oxygen concentration and the oxygen excess level can be fixed independently during oxyfuel combustion during a series of experiments with pure straw as fuel. The inlet oxygen concentration was increased in two steps from 30 % to 40 and 50 % and the oxygen excess level was decreased from 5 % in the dry flue gas to 3 and 2.4 %. Loss-on-ignition analysis on fly ash samples showed that comparable burnout was obtained for

all three combustion conditions and the potential decrease in oxygen demand for the combustion process was about 13 % for the swirl burner setup. Compared to the coal experiments, significant differences to the combustion fundamentals were observed for this strategy. Flame temperatures and, as a results of higher temperature, deposit fluxes increased significantly with increasing inlet oxygen concentration. Both aspects could impose challenges to full-scale oxyfuel power plants and further investigations are needed in order to determine whether this would be ditrimental to this strategy for reducing the process operating costs. The emission rates of NO, SO_2, and CO did not change with the change in combustion conditions. However, it is questionable if significant thermal NO_x formation could be avoided in a full-scale plant with a considerably larger degree of false air ingress to the high-temperature zones for the case of the very high inlet oxygen concentration.

Chapter 6

Conclusions

The results reported in this thesis cover five important aspects with respect to the operation of a power plant, both the conventional air-blown type and oxyfuel combustion plants; (1) Combustion fundamentals, including in-furnace temperature profiles and burnout; (2) Emissions of polluting species (NO, SO_2, and CO); (3) Quality of residual products, here only fly ash is considered; (4) Slagging and fouling, focusing on the deposit formation propensities and deposit composition for different fuels at different operating conditions; (5) Process economics, targeting the area of an oxyfuel power plant with the largest potential of reducing operating expenses – the oxygen demand.

The above areas have been investigated experimentally in a once-through, 30 kW_{th} semi-technical scale setup which simulates combustion in suspension-fired boilers. Four different fuels have been applied; a pulverized, bituminous Colombian coal; pulverized, Danish cereal straw pellets; and two coal/straw blends with straw shares of 20 and 50 wt%. The fuels have been burned in air and synthetic O_2/CO_2 mixtures simulating recirculation of dry flue gas in an oxyfuel power plant.

Combustion Fundamentals

A match of flue gas temperature profiles and burnout efficiency was obtained for combustion of the bituminous coal in air and an 30 % O_2/CO_2 mixture at an oxygen level of 5 % in the dry, exit flue gas. At these conditions the burnout efficiency was sufficiently high (> 99.5 %) in order for the fly ash to be comparable to fly ash from full-scale power plants.

Co-firing coal with straw and combustion of pure straw yields significant changes to the combustion conditions compared to the case with pure coal as fuel. For very high straw shares (> 50 %) the flue gas temperature decreases significantly due to delayed ignition and hence, the flame length increases significantly, as observed from in-flame CO measurements. The occurence of large straw particles (originating from straw nodes) travelling almost unconverted through

the experimental setup leads to a decrease in burnout efficiency, from 99.5 to 98.9 % for combustion in air and from 99.8 to 99.3 % during oxyfuel combustion. This corresponds to changes in fly ash carbon contents from 5.0 wt% (coal/air) to 20.7 wt% (straw/air) and from 2.6 wt% (coal/oxyfuel) to 12.5 wt% (straw/oxyfuel).

In-flame peak CO levels of 10 vol% have been measured during oxyfuel combustion of coal, straw and a coal/straw blend with a straw share of 50 wt%.

Emissions

Whereas no significant change to the CO and SO_2 emissions are associated with the change in combustion atmosphere, the emission rate of NO was reduced 35 % on average during oxyfuel combustion compared to the conventional air-firing. Three mechanisms were suggested to explain this reduction; increased internal NO reduction due to reduced dilution of NO in the gas phase, increased reduction of NO over char promoted by high CO levels in the flame, and the influence of high concentrations of CO_2 on the radical pool promoting reduction of NO when fuel and oxidant are mixed at oxidizing conditions.

Also, the change in fuel type affects the emission rates of NO and SO_2. For a given combustion atmosphere increasing the straw share of the fuel reduces both NO and SO_2 emission rates. For NO this is in accordance with the decreasing Fuel-N content with increasing fuel straw share. At the same time, the Fuel-N to NO conversion ratio increases with decreasing Fuel-N content due to the lower reduction of NO in the gas phase from other gaseous N-containing species. The relative difference in the NO emission between air and oxyfuel combustion increases with increasing fuel straw share which is a further benefit of oxyfuel combustion. The reduced emission of SO_2 with increasing fuel straw share is a consequence of a higher availability of water soluble potassium in fly ash and deposits capable of capturing SO_2 from the gas phase.

The effect of the plant configuration, i.e. the position of the withdrawal of flue gas for recirculation downstream of the boiler, on the emission of NO and SO_2 was investigated for combustion of pure coal. Recirculation of untreated flue gas was simulated by doping NO and SO_2 to the oxidant in different amounts. The results showed that about 75 % reduction of the NO emission rate compared to air-firing could be obtained while the presence of high levels of SO_2 within the boiler will increase the capture of sulphur (SO_3) in the fly ash and deposits by up to 100 %. Even so, less than 5 % of the recirculated SO_2 is removed from the gas-phase due to capture by solid phases.

Fly Ash Quality and Deposit Formation

One of the main concerns regarding the oxyfuel combustion technology is the risk of compromising the fly ash quality with respect to its applicability as an additive in concrete production. In this respect, the most often suggested plant

configuration with recirculation of flue gas prior to desulphurization induces a risk of increasing the amount of sulphur in the fly ash above the permissible level of 3 wt% SO_3. The results obtained in this work show that simulating a recirculation of SO_2 to the boiler yielded an increase of about 60 % in the amount of sulphur captured in the fly ash from combustion of coal. The applied coal has a relatively low sulphur content (0.62 wt%, as received) and even with the increased retention (1.6 wt% SO_3 in the fly ash), the requirements could be met with considerable margin.

Co-firing of coal with straw has significant effects on the fly ash quality. Compared to the applied coal the straw has a markedly different content of K, Ca, Al, S, and Cl. A considerable increase in the corrosion potential is observed due to formation of water soluble alkali and alkali earth sulphates and chlorides in the ash with increasing straw share above 20 wt%.

A comparison of the fly ash data from this work to data from full-scale boilers co-firing coal and straw showed good agreement with respect to the capture of potassium in water soluble form in the fly ash. However, deviations were observed with respect to the degree of sulphation of the fly ash with full-scale plants achieving a higher amount of K_2SO_4 in the fly ash than the semi-technical setups applied in this work and reported in literature.

Similar deposition propensities have been found for co-firing coal with 20 to 50 wt% straw in each combustion atmosphere. However, significantly increased flux to the deposit probe was observed for combustion of pure straw. The deposit also became more sintered and difficult to remove. The change from combustion in air to oxyfuel combustion increased the deposition rate, most likely due to higher flue gas temperatures at the sampling position. High in-furnace levels of SO_2 during oxyfuel combustion lead to increased sulphation of coal deposits.

Process Economics

The production of near-pure oxygen for oxyfuel power plants constitutes the single-largest penalty to the operating expenses. An investigation was made which showed that it is possible to reduce the excess oxygen level during combustion, and hence the operating costs, by increasing the concentration of oxygen at the burners. For example, the oxygen excess could be reduced to 2.4 % in the exit flue gas at an inlet O_2 concentration of 50 vol% while obtaining a burnout of 99.6 % during pure straw combustion. The change to the oxidant composition therefore did not compromise the fuel burnout and further did not increase the emission rates of NO and SO_2. It did, however, induce significant changes to the in-furnace temperature profile, i.e. higher near-burner temperatures, and increased the rate of deposition of ash on cooled surfaces. Further investigations are needed in order to determine the potential of this strategy for reducing the operating expenses for the oxyfuel process.

Implications for OxyFuel Combustion

An incentive to the execution of this work was to investigate whether any show-stoppers regarding the oxyfuel combustion technology could be identified. A number of critical aspects were found from which the potential changes to the combustion conditions have been investigated experimentally. The main concerns were associated with the risk of increased fire-side corrosion and the risk of a reduction in fly ash quality.

The results from this work has not brought forth any disqualifying characteristics of the oxyfuel combustion process rendering it unsuited for implementation as carbon capture technology in suspension-fired power plants. On the contrary, increased burnout and lower NO emission rates were observed during oxyfuel combustion.

Chapter 7

Suggestions for Further Work

This work has shown that it is indeed possible to achieve similar combustion conditions with air and an O_2/CO_2 mixture as oxidant. In order to further investigate the applicability of the oxyfuel combustion technology in large scale for carbon capture the following areas are of interest:

- The effect on burnout efficiency when solid fuels burned in the oxyfuel atmosphere are subject to similar residence times within the furnace as found during air-firing. This will be of interest in relation to design of green-field plants where a reduced boiler size typically is suggested.
- More detailed studies on the sulphur chemistry:
  - Closure of the sulphur mass balance during recirculation of high levels of SO_2. Closure of sulphur balances is typically very difficult and further work could be performed in order to understand the deviations observed in this work.
  - The effect of changes to the fuel (coal) ash composition with respect to the capture of sulphur by fly ash and deposits. Fly ash from combustion of coals with high alkali and sulphur contents could potentially exceed the limit for sulphur regarding its applicability in concrete if flue gas is recirculated to the boiler prior to desulphurization. From an economic perspective, it is rather important that the change from air-firing to oxyfuel combustion does not impose a limitation to the choice of fuel, i.e. coal type.
  - The impact of wet versus dry flue gas recycling on the sulphur uptake in fly ash and deposits.
- Even though the NO_x chemistry of oxyfuel combustion has been intensively studied the specific mechanisms responsible for the differences observed between combustion in air and oxyfuel atmospheres and their relative importance have not been completely established.

- The observed differences in deposition propensity for the two combustion atmospheres are worth further analysis since slagging and fouling are of great importance to the operation of full-scale boilers.

- Due to the ongoing efforts to replace coal with biomass in power plants more research into all of the areas investigated in this work should be further elucidated. Especially co-firing at high straw shares (> 50 wt%) in suspension-fired boilers is relatively unexplored and the results obtained in this work have shown interesting trends regarding ash and deposits chemistry.

- The initial work on a potential improvement of the process economy of an oxyfuel power plant by reducing the demand for oxygen shown in this work needs further investigations, amongst others on the consequence to the boiler heat uptake, deposit formation, emission levels, etc. The investigations should aid in the determination of whether this strategy should be pursued further.

- The flame mappings – temperature and gas phase composition measurements – conducted during this work are well suited for validation of e.g. Computational Fluid Dynamics (CFD) models of the oxyfuel combustion process. A validated model is an important tool in the design process for plant retrofits or new-builds.

Bibliography

[1] Energy Agency (IEA) International. *World Energy Outlook 2007 – China and India Insights*. IEA Publications, 2007.

[2] Energy Agency (IEA) International. *World Energy Outlook 2008*. IEA Publications, 2008.

[3] K Kavouridis and N Koukouzas. Coal and sustainable energy supply challenges and barriers. *Energy Policy*, 36(2):693–703, 2008.

[4] BJP Buhre, LK Elliott, CD Sheng, RP Gupta, and TF Wall. Oxy-fuel combustion technology for coal-fired power generation. *Prog Energy Combust Sci*, 31(4):283–307, 2005.

[5] TF Wall. Combustion processes for carbon capture. *Proc Combust Inst*, 31 (1):31–47, 2007.

[6] S Solomon, D Qin, M Manning, Z Chen, M Marquis, KB Averyt, M Tignor, and HL Miller, editors. *IPCC, 2007: Climate Change 2007: The Physical Science Basis. Contribution of Working Group I to the Fourth Assessment Report of the Intergovernmental Panel on Climate Change*. Cambridge University Press, Cambridge, United Kingdom and New York, NY, USA, 2007.

[7] S Bachu. CO_2 storage in geological media: Role, means, status and barriers to deployment. *Prog Energy Combust Sci*, 34(2):254–73, 2008.

[8] J Davison. Performance and costs of power plants with capture and storage of CO_2. *Energy*, 32(7):1163–76, 2007.

[9] Y Tan, KV Thambimuthu, MA Douglas, and R Mortazavi. Oxy-fuel combustion research at the CANMET Energy Technology Center. *Proc 2003 5th Int Symp Coal Combust*, pages 550–4, 2003.

[10] K Jordal, M Anheden, J Yan, and L Strömberg. Oxyfuel combustion for coal-fired power generation with CO_2 capture – opportunities and challenges. *The 7th International Conference on Greenhouse Gas Control Technologies (GHGT-7). Vancouver, Canada, September*, 2004.

[11] PHM Feron and CA Hendriks. CO_2 capture process principles and costs. *Oil Gas Sci Technol*, 60(3):451–9, 2005.

[12] R Tan, G Corragio, and S Santos. Oxy-Coal Combustion with Flue Gas Recycle for the Power Generation Industry – A Literature Review. Study Report, IFRF Doc. No. G 23/y/1, International Flame Research Foundation (IFRF), Velsen Noord, The Netherlands, September 2005.

[13] JN Knudsen, P-J Vilhelmsen, JN Jensen, and O Biede. First year operating experience with a 1 t/h CO_2 absorption – pilot plant at Esbjerg coal-fired power plant. *VGB Powertech*, 87(3):57–61, 2007.

[14] JD Figueroa, T Fout, S Plasynski, H McIlvried, and RD Srivastava. Advances in CO_2 capture technology – The U.S. Department of Energy's Carbon Sequestration Program. *Int J Greenhouse Gas Control*, 2(1):9–20, 2008.

[15] RJ Allam and CG Spilsbury. A study of the extraction of CO_2 from the flue gas of a 500 MW pulverised coal fired boiler. *Energy Convers Manage*, 33 (5-8):373–8, 1992.

[16] MM Abu-Khader. Recent Progress in CO_2 Capture/Sequestration: A Review. *Energy Sources, Part A: Recovery, Utilization, and Environmental Effects*, 28(14):1261–79, 2006.

[17] M Fischedick, W Günster, H Fahlenkamp, H-J Meier, F Neumann, G Oeljeklaus, H Rode, A Schimkat, J Beigel, and D Schüwer. Separation in Power Plants – Do Retrofits Make Sense in Existing Plants? *VGB PowerTech*, 4: 108–17, 2006. In German.

[18] J Gibbins and H Chalmers. Carbon capture and storage. *Energy Policy*, 36 (12):4317–22, 2008.

[19] M Pehnt and J Henkel. Life cycle assessment of carbon dioxide capture and storage from lignite power plants. *Int J Greenhouse Gas Control*, 3(1):49–66, 2009.

[20] MT Sander and CL Mariz. The Fluor Daniel econamine FG process: Past experience and present day focus. *Energy Convers Manage*, 33(5-8):341–8, 1992.

[21] S Reddy, J Scherffius, S Freguia, and C Roberts. Fluor's Econamine FG Plus^{SM} technology – an enhanced amine-based CO_2 capture process. In *Proceedings of the second national conference on carbon sequestration*, Alexandria, VA, USA, May 2003. US Department of Energy National Technology Laboratory.

[22] Y Yagi, T Mimura, M Iijima, K Ishida, R Yoshiyama, and T Kamino. Improvements of carbon dioxide capture technology from flue gas. In *Greenhouse gas control technologies. Proceedings of the seventh international conference on greenhouse gas control technologies, 5–9 September 2004*, Vancouver, Canada, 2005. Oxford, UK: Elsevier Ltd.

[23] S Wegerich, A Witt, E Huizeling, and H Rode. Untersuchungen zur Nachrüstung einer CO_2-Abscheidetechnologie für das neue E.ON Kraftwerk Maasvlakte 3. In *39. Kraftwerktechnisches Kolloquium, October 11-12, 2007, Dresden, Germany*, 2007.

[24] J Oexmann and A Kather. Post-Combustion CO_2-Capture from Coal-fired Power Plants – Wet Chemical Absorption Processes. *VGB PowerTech*, 89 (1/2):92–103, 2009. In German.

[25] M Okawa, N Kimura, T Kiga, S Takano, K Arai, and M Kato. Trial design for a CO_2 recovery power plant by burning pulverized coal in O_2/CO_2. *Energy Convers Manage*, 38:123–7, 1997.

[26] H Altmann and G-N Stamatelopoulos. Steps towards the Minimisation of CO_2 Emissions from Coal-Fired Power Plants. *Conference and Exhibition for the European Power Generation Industry, POWER-GEN Europe 2005, Milan (Italy), June 28-30*, 2005.

[27] RK Varagani, F Châtel-Pélage, P Pranda, M Rostam-Abadi, Y Lu, and AC Bose. Performance Simulation and Cost Assessment of Oxy-Combustion Process for CO_2 Capture from Coal-Fired Power Plants. *The Fourth Annual Conference on Carbon Sequestration, May 2-5. Alexandria, VA*, 2005.

[28] D Singh, E Croiset, PL Douglas, and MA Douglas. Techno-economic study of CO_2 capture from an existing coal-fired power plant: MEA scrubbing vs. O_2/CO_2 recycle combustion. *Energy Convers Manage*, 44(19):3073–91, 2003.

[29] M Ewert. The Significance of Power Stations with CO_2 Capture in Planning Future Generation Portfolio. *VGB PowerTech*, 85(10):36–40, 2005. In German.

[30] Unknown. Chilling news for carbon capture [carbon dioxide capture process]. *Modern Power Systems*, 26(12):17–18, 2006.

[31] B Xu, RA Stobbs, V White, RA Wall, J Gibbins, M Iijima, and A MacKenzie. Future CO_2 Capture Technology Options for the Canadian Market. Technical Report Report No. COAL R309 BERR/Pub URN 07/1251, Doosan Babcock Energy Limited, March 2007.

[32] R Notz, N Asprion, I Clausen, and H Hasse. Selection and pilot plant tests of new absorbents for post-combustion carbon dioxide capture. *Chem Eng Research Design*, 85(A4):510–15, 2007.

[33] K Damen, M van Troost, A Faaij, and W Turkenburg. A comparison of electricity and hydrogen production systems with CO_2 capture and storage. Part A: Review and selection of promising conversion and capture technologies. *Prog Energy Combust Sci*, 32(2):215–46, 2006.

[34] JM Beér. High efficiency electric power generation: The environmental role. *Prog Energy Combust Sci*, 33(2):107–34, 2007.

[35] C Descamps, C Bouallou, and M Kanniche. Efficiency of an Integrated Gasification Combined Cycle (IGCC) power plant including CO_2 removal. *Energy*, 33(6):874–81, 2008.

[36] DK McDonald, TJ Flynn, DJ DeVault, R Varagani, S Levesque, and W Castor. 30 MW_t Clean Environment Development Oxy-Coal Combustion Test Program. *The 33rd International Technical Conference on Coal Utilization and Fuel Systems, Clearwater, Florida*, 2008.

[37] M Kanniche, R Gros-Bonnivard, P Jaud, J Valle-Marcos, J-M Amann, and C Bouallou. Pre-combustion, post-combustion and oxy-combustion in thermal power plant for CO_2 capture. *Appl Thermal Eng*, 30(1):53–62, 2010.

[38] J Lambertz and J Ewers. Clean Coal Power – The response of power plant engineering to climate protection challenges. *VGB PowerTech*, 86(5):72–7, 2006. In German.

[39] J Gibbins and H Chalmers. Preparing for global rollout: A 'developed country first' demonstration programme for rapid CCS deployment. *Energy Policy*, 36(2):501–7, 2008.

[40] AJ Minchener. Coal gasification for advanced power generation. *Fuel*, 84 (17):2222–35, 2005.

[41] B Gericke, P Kuzmanovski, and K Nassauer. Conceptual Solutions Regarding the Influence of the Oxy-Fuel-Process on Conventional Power Plants (Konzeptüberlegungen bezüglich der Auswirkungen des Oxy-Fuel-Prozesses auf konventionelle Kraftwerksanlagen). *VGB PowerTech*, 86(10):64–72, 2006. In German.

[42] C Chen and ES Rubin. CO_2 control technology effects on IGCC plant performance and cost. *Energy Policy*, 37(3):915–24, 2009.

[43] LI Eide and DW Bailey. Precombustion Decarbonisation Processes. *Oil Gas Sci Technol*, 60(3):475–84, 2005.

[44] FL Horn and M Steinberg. Control of carbon dioxide emissions from a power plant (and use in enhanced oil recovery). *Fuel*, 61(5):415–22, 1982.

[45] H Herzog, D Golomb, and S Zemba. Feasibility, modeling and economics of sequestering power plant CO_2 emissions in the deep ocean. *Environmental Prog*, 10(1):64–74, 1991.

[46] BM Abraham, JG Asbury, EP Lynch, and APS Teotia. Coal-oxygen process provides CO_2 for enhanced recovery. *Oil Gas J*, 80(11):68–70, 75, 1982.

[47] S Nakayama, Y Noguchi, T Kiga, S Miyamae, U Maeda, M Kawai, T Tanaka, K Koyata, and H Makino. Pulverized coal combustion in O_2/CO_2 mixtures on a power plant for CO_2 recovery. *Energy Convers Manage*, 33(5-8):379–86, 1992.

[48] M Simmons, I Miracca, and K Gerdes. Oxyfuel Technologies for CO_2 Capture: A Techno-Economic Overview. *7th International Conference on Greenhouse Gas Control Technologies. Vancouver, Canada, September*, 2004.

[49] F Châtel-Pélage, R Varagani, P Pranda, N Perrin, H Farzan, SJ Vecci, Y Lu, S Chen, M Rostam-Abadi, and AC Bose. Applications of Oxygen for NO_x Control and CO_2 Capture in Coal-Fired Power Plants. *Thermal Sci*, 10(3): 119–42, 2006.

[50] M Anheden, J Yan, and G De Smedt. Denitrogenation (or Oxyfuel Concepts). *Oil Gas Sci Technol*, 60(3):485–95, 2005.

[51] DJ Dillon, RS Panesar, RA Wall, RJ Allam, V White, J Gibbins, and MR Haines. Oxy-Combustion Processes for CO_2 Capture from Advanced Supercritical PF and NGCC Power Plant. *7th International Conference on Greenhouse Gas Control Technologies. Vancouver, Canada, September*, 2004.

[52] DJ Dillon, V White, RJ Allam, RA Wall, and J Gibbins. Oxy Combustion Processes for CO_2 Capture from Power Plant. Engineering Investigation Report, 2005/9, IEA Greenhouse Gas Research and Development Programme, June 2005.

[53] A Kather, M Klostermann, C Hermsdorf, K Mieske, R Eggers, and D Köpke. Konzept für ein 600 MW_{el} Steinkohlekraftwerk mit CO_2-Abtrennung auf Basis des Oxyfuel-Prozesses. In *Kraftwerksbetrieb unter künftigen Rahmenbedingungen, 38. Kraftwerkstechnisches Kolloquium, October 24-25, 2006, Dresden, Germany*, 2006.

[54] S Rezvani, Y Huang, D McIlveen-Wright, N Hewitt, and Y Wang. Comparative assessment of sub-critical versus advanced super-critical oxyfuel fired PF boilers with CO_2 sequestration facilities. *Fuel*, 86(14):2134–43, 2007.

[55] LI Eide, M Anheden, A Lyngfelt, C Abanades, M Younes, D Clodic, AA Bill, PHM Feron, A Rojey, and F Giroudiere. Novel Capture Processes. *Oil Gas Sci Technol*, 60(3):497–508, 2005.

[56] MM Hossain and HI de Lasa. Chemical-looping combustion (CLC) for inherent CO_2 separations–a review. *Chem Eng Sci*, 63(18):4433–51, 2008.

[57] J Davison, P Freund, and A Smith. Putting Carbon Back into the Ground. Technology overview, The IEA Greenhouse Gas R&D Programme, February 2001.

[58] M Farley. Developing oxyfuel capture as a retrofit technology. *Modern Power Systems*, 26(4):20–2, 2006.

[59] MB Toftegaard, J Brix, PA Jensen, P Glarborg, and AD Jensen. Oxy-fuel combustion of solid fuels. *Prog Energy Combust Sci*, 36(5):581–625, 2010.

[60] MB Toftegaard. 045-8 Swirl Burner: Experimental Setup for Air and Oxy-fuel Combustion of Coal and Biomass – Design, Construction, and Commissioning. CHEC Report, 2011.

[61] MB Toftegaard. Introducing Biomass in Carbon Capture Power Plants: Coal and Biomass Combustion in Air and OxyFuel Atmospheres – Experimental Investigations in a Swirl Burner. CHEC Report, R003, 2011.

[62] JA Miller and CT Bowman. Mechanism and modeling of nitrogen chemistry in combustion. *Prog Energy Combust Sci*, 15(4):287–338, 1989.

[63] European Standard. EN 450-1:2005 Fly ash for concrete. Definition, specifications and conformity criteria, 2005.

[64] MB Toftegaard. Data Collection: Coal and Biomass Combustion in Air and OxyFuel Atmospheres – Experimental Investigations in a Swirl Burner. CHEC Report, 2011.

[65] S Clausen. Local measurement of gas temperature with an infrared fibre-optic probe. *Measurement Sci Technol*, 7(6):888–96, 1996.

[66] J Bak and S Clausen. FTIR emission spectroscopy methods and procedures for real time quantitative gas analysis in industrial environments. *Measurement Sci Technol*, 13(2):150–6, 2002.

[67] J Brix, MB Toftegaard, S Clausen, and AD Jensen. Advanced Diagnostics in Oxy-Fuel Combustion Processes – The Use of IR- and FTIR in Pilot- and Laboratory-Scale Reactors. Final Report, PSO project 010069, 2011.

[68] Bo Sander. DONG Energy. Personal Communication, 2010.

[69] D Fleig, K Andersson, F Johnsson, and B Leckner. Conversion of Sulfur during Pulverized Oxy-coal Combustion. *Energy Fuels*, 25(2):647–55, 2011.

[70] P Glarborg, AD Jensen, and JE Johnsson. Fuel nitrogen conversion in solid fuel fired systems. *Prog Energy Combust Sci*, 29(2):89–113, 2003.

[71] H Liu, R Zailani, and BM Gibbs. Comparisons of pulverized coal combustion in air and in mixtures of O_2/CO_2. *Fuel*, 84(7-8):833–40, 2005.

[72] E Croiset, K Thambimuthu, and A Palmer. Coal combustion in O_2/CO_2 mixtures compared with air. *Canadian J Chem Eng*, 78(2):402–7, 2000.

[73] E Croiset and KV Thambimuthu. NO_x and SO_2 emissions from O_2/CO_2 recycle coal combustion. *Fuel*, 80(14):2117–21, 2001.

[74] T Mendiara and P Glarborg. Ammonia chemistry in oxy-fuel combustion of methane. *Combust Flame*, 156:1937–49, 2009.

[75] T Mendiara and P Glarborg. Reburn Chemistry in Oxy-fuel Combustion of Methane. *Energy Fuels*, 23(7):3565–72, 2009.

[76] P Overgaard, B Sander, H Junker, K Friborg, and OH Larsen. Two Years' Operational Experience and Further Development of Full-Scale Co-Firing of Straw. In *2nd World Conference and Exhibition on Biomass for Energy, Industry and Climate Protection, Rome, Italy*, 2004.

[77] LS Pedersen, HP Nielsen, S Kiil, LA Hansen, K Dam-Johansen, F Kildsig, J Christensen, and P Jespersen. Full-scale co-firing of straw and coal. *Fuel*, 75(13):1584–90, 1996.

[78] B Sander and K Wieck-Hansen. Full-Scale Investigations on Alkali Chemistry and Ash Utilisation by Co-Firing of Straw. In *14th European Biomass Conference, Paris, France*, pages 1131–34, 2005.

[79] LA Hansen. *Melting and Sintering of Ashes*. PhD thesis, Department of Chemical Engineering, Technical University of Denmark, 1998.

[80] Y Zheng, PA Jensen, AD Jensen, B Sander, and H Junker. Ash transformation during co-firing coal and straw. *Fuel*, 86(7):1008–20, 2007.

[81] M Montgomery and OH Larsen. Field test corrosion experiments in Denmark with biomass fuels. Part 2: Co-firing of straw and coal. *Materials Corrosion*, 53(3):185–94, 2002.

[82] DR Lide (editor-in chief). *Handbook of Chemistry and Physics*. CRC Press, 85th edition, 2004-2005.

[83] P Glarborg. Hidden interactions – Trace species governing combustion and emissions. *Proc Combust Inst*, 31(1):77–98, 2007.

[84] H Liu, R Zailani, and BM Gibbs. Pulverized coal combustion in air and in O_2/CO_2 mixtures with NO_x recycle. *Fuel*, 84(16):2109–15, 2005.

[85] A Jensen. Heating and devolatilization of coal particles. note, Department of Chemical Engineering, Technical University of Denmark, 1997.

Appendix A

OxyFuel combustion of solid fuels (Review Paper)

Appendix B

Stoichiometric Calculations

B.1 Ideal Conditions

Complete combustion of a solid fuel with a molar composition, $C_\alpha H_\beta S_\gamma N_\delta O_\phi \cdot (H_2O)_\mu$, is given by (B.1).

$$\begin{aligned} C_\alpha H_\beta S_\gamma N_\delta O_\phi \cdot (H_2O)_\mu \quad + \quad & \left(\alpha + \frac{\beta}{4} + \gamma + \frac{\delta}{2} - \frac{\phi}{2}\right) O_2 \\ \rightarrow \quad & \alpha\, CO_2 + \left(\frac{\beta}{2} + \mu\right) H_2O + \gamma\, SO_2 + \delta\, NO \end{aligned} \tag{B.1}$$

where the stoichiometric coefficients, α, β, etc., are determined from the ultimate and proximate analysis of the fuel by:

$$\text{coefficient} = \frac{x_i}{M_i} \tag{B.2}$$

x_i is the mass fraction of C, H, S, N, O, or H_2O in the fuel and M_i is the molar mass of that component. The coefficient has units of moles/kg fuel.

The minimum amount of oxidizer needed for complete combustion is given by:

$$N_{OX,\,min} = \frac{N_{O_2,\,min}}{y^{ox}_{O_2}} = \frac{\alpha + \frac{\beta}{4} + \gamma + \frac{\delta}{2} - \frac{\phi}{2}}{y^{ox}_{O_2}} \tag{B.3}$$

where $y^{ox}_{O_2}$ is the molar fraction of O_2 in the oxidizer (air or an O_2/CO_2 mixture).

The corresponding, minimum amount of flue gas produced is given by:

$$N_{FG,\,min} = N_{OX,\,min} + \frac{\beta}{4} + \mu + \frac{\delta}{2} + \frac{\phi}{2} \tag{B.4}$$

Since the reported experiments have been conducted with different types of oxidizer, the excess ratio, λ, is defined as the oxygen excess ratio for simplicity:

$$\lambda = \frac{N_{O_2}}{N_{O_2,\,min}} \tag{B.5}$$

It should be noted that the value of λ will be equal to e.g. the value computed based on the total and minimum air amounts for air experiments.

The amount of flue gas on a wet (total) and dry basis can be determined from:

$$N_{\mathrm{FG}} = N_{\mathrm{FG,\,min}} + (\lambda - 1) N_{\mathrm{OX,\,min}} \tag{B.6}$$

$$N_{\mathrm{FG,\,dry}} = \lambda N_{\mathrm{OX,\,min}} - \frac{\beta}{4} + \frac{\delta}{2} + \frac{\phi}{2} \tag{B.7}$$

For the calculations performed in the present work it is assumed that the pressurized air used as oxidizer is dry, no correction of the oxidant flow is thus necessary. Likewise for the oxyfuel combustion experiments, only dry flue gas recirculation has been simulated.

The molar fractions of the different, major flue gas components in wet and dry flue gas are given by:

$$y_{\mathrm{CO_2}} = \frac{\alpha}{N_{\mathrm{FG}}} \quad ; \quad y_{\mathrm{CO_2}}^{\mathrm{dry}} = \frac{\alpha}{N_{\mathrm{FG,\,dry}}} \tag{B.8}$$

$$y_{\mathrm{O_2}} = \frac{(\lambda - 1)\, N_{\mathrm{OX,\,min}} \cdot y_{\mathrm{O_2}}^{\mathrm{ox}}}{N_{\mathrm{FG}}} \quad ; \quad y_{\mathrm{O_2}}^{\mathrm{dry}} = \frac{(\lambda - 1)\, N_{\mathrm{OX,\,min}} \cdot y_{\mathrm{O_2}}^{\mathrm{ox}}}{N_{\mathrm{FG,\,dry}}} \tag{B.9}$$

$$y_{\mathrm{SO_2}} = \frac{\gamma}{N_{\mathrm{FG}}} \quad ; \quad y_{\mathrm{SO_2}}^{\mathrm{dry}} = \frac{\gamma}{N_{\mathrm{FG,\,dry}}} \tag{B.10}$$

$$y_{\mathrm{NO}} = \frac{\delta}{N_{\mathrm{FG}}} \quad ; \quad y_{\mathrm{NO}}^{\mathrm{dry}} = \frac{\delta}{N_{\mathrm{FG,\,dry}}} \tag{B.11}$$

$$y_{\mathrm{H_2O}} = \frac{\frac{\beta}{2} + \mu}{N_{\mathrm{FG}}} \quad ; \quad y_{\mathrm{H_2O}}^{\mathrm{dry}} = 0 \tag{B.12}$$

B.2 Incomplete Combustion and False Air Ingress

The expressions in Section B.1 are for the ideal case with complete combustion of the solid fuel and a leak tight reactor system. For the actual experiments, the solid fuel yield incomplete combustion and false air is drawn into the reactor due to the operation at sub-atmospheric pressure.

Including the false air (FA) ingress, for full burnout, leads to:

$$N_{\mathrm{FG,\,FA}} = N_{\mathrm{FG,\,min}} + (\lambda - 1) N_{\mathrm{OX,\,min}} + N_{\mathrm{FA}} \tag{B.13}$$

$$N_{\mathrm{FG,\,dry,\,FA}} = \lambda N_{\mathrm{OX,\,min}} - \frac{\beta}{4} + \frac{\delta}{2} + \frac{\phi}{2} + N_{\mathrm{FA}} \tag{B.14}$$

The concentrations of CO_2, SO_2, NO, and H_2O are calculated equivalently to equations (B.8), and (B.10)–(B.12). The concentration of O_2 in the flue gas will increase compared to the ideal conditions due to the O_2 content of the false air. For oxyfuel experiments the N_2 content of the flue gas will likewise increase and will be a direct indicator of the level of false air ingress, under the assumption that all Fuel-N is converted to NO, see (B.1), and no thermal NO is formed.

$$y_{O_2}^{FA} = \frac{(\lambda - 1)\, N_{OX,\,min} \cdot y_{O_2}^{ox} + N_{FA} \cdot y_{O_2}^{air}}{N_{FG}} \tag{B.15}$$

$$y_{O_2}^{dry,\,FA} = \frac{(\lambda - 1)\, N_{OX,\,min} \cdot y_{O_2}^{ox} + N_{FA} \cdot y_{O_2}^{air}}{N_{FG,\,dry}} \tag{B.16}$$

$$y_{N_2,\,oxy}^{FA} = \frac{N_{FA} \cdot y_{N_2}^{air}}{N_{FG}} \tag{B.17}$$

$$y_{N_2,\,oxy}^{dry,\,FA} = \frac{N_{FA} \cdot y_{N_2}^{air}}{N_{FG,\,dry}} \tag{B.18}$$

The amount of dry flue gas which is used in the molar balances for C and S can be determined from the measured concentration of O_2 (and N_2) in the dry flue gas sample. Combining Eqs. (B.14) and (B.16) provides an expression for determining the amount of false air leaking into the reactor, see (B.19). Inserting (B.19) in (B.14) yields a method for calculating the total amount of flue gas from the reactor, see (B.20).

$$N_{FA} = \frac{y_{O_2}^{dry,\,FA} \cdot N_{FG,\,dry} - y_{O_2}^{ox}\,(\lambda - 1)\, N_{OX,\,min}}{\left(y_{O_2}^{air} - y_{O_2}^{dry,\,FA}\right)} \tag{B.19}$$

$$N_{FG,\,dry,\,FA} = \frac{y_{O_2}^{air}\left(\lambda N_{OX,\,min} - \frac{\beta}{4} + \frac{\delta}{2} + \frac{\phi}{2}\right) - y_{O_2}^{ox}\,(\lambda - 1)\, N_{OX,\,min}}{\left(y_{O_2}^{air} - y_{O_2}^{dry,\,FA}\right)} \tag{B.20}$$

For air as oxidant this simplifies to:

$$N_{FG,\,dry,\,FA} = \frac{y_{O_2}^{air}\left(N_{OX,\,min} - \frac{\beta}{4} + \frac{\delta}{2} + \frac{\phi}{2}\right)}{\left(y_{O_2}^{air} - y_{O_2}^{dry,\,FA}\right)} \tag{B.21}$$

With N_2 as base:

$$N_{FA} = \frac{y_{N_2,\,oxy}^{dry,\,FA}\left(\lambda N_{OX,\,min} - \frac{\beta}{4} + \frac{\delta}{2} + \frac{\phi}{2}\right)}{\left(y_{N_2}^{air} - y_{N_2,\,oxy}^{dry,\,FA}\right)} \tag{B.22}$$

$$N_{FG,\,dry,\,FA} = \frac{y_{N_2}^{air}}{y_{N_2}^{air} - y_{N_2,\,oxy}^{dry,\,FA}} \tag{B.23}$$

If assuming that the combustible fraction of the fuel left in the fly ash consists solely of C, the amount of flue gas will not change due to incomplete combustion, since C and O_2 react in the ratio 1:1. However, the amount of false air determined from the measured oxygen concentration is a function of the fuel burnout. This correction has not been taken into account due to the high degree of burnout observed during the experiments.

Appendix C

Mass Balances

The sections below contain the equations used in determining the C and S balances for the individual experiments.

C.1 Carbon

The incoming carbon originates potentially from both the solid fuel (SF) and the oxidant flow (OX), see (C.1).

$$\begin{aligned} C_{in} &= C_{OX} + C_{SF} \\ C_{in} &= y_{CO_2,OX} \cdot F_{OX} + \alpha \cdot \dot{m}_{SF} \end{aligned} \tag{C.1}$$

where $y_{CO_2,OX}$ is the molar fraction of CO_2 in the oxidizer (assumed 0 for air) and F_{OX} is the molar flow rate of oxidizer. α is the fuel carbon content (moles/kg fuel), see Appendix B, and $\dot{m}_{SF}$ is the mass flow rate of solid fuel.

During oxyfuel experiments the amount of CO_2 fed with the oxidizer constitute most of the C in the system. However, the C fed with the solid fuel amounts to between 19 and 48 % depending on the fuel, the stoichiometry, and the O_2 concentration in the oxidizer. It is thus still relevant to determine the carbon balance.

The equations for the three levels on the "out" term are seen in Eqs. (C.2), (C.3), and (C.5).

Level 1

$$C_{out} = (y_{CO} + y_{CO_2}) \cdot F_{FG,dry,FA} \tag{C.2}$$

y_X are the measured concentrations of CO and CO_2 in the dry flue gas sample. $F_{FG,dry,FA}$ is the dry flue gas flow. No measurement of the true flue gas flow exist and thus the flue gas flow is determined from the measured oxygen concentration

in the dry flue gas. The determination of $F_{FG,dry,FA}$ takes false air ingress and incomplete combustion into account, see Appendix B, Section B.2.

Level 2

$$\begin{aligned} C_{out} &= (y_{CO} + y_{CO_2}) \cdot F_{FG,dry,FA} + \dot{n}_{C\ with\ ash} \\ C_{out} &= (y_{CO} + y_{CO_2}) \cdot F_{FG,dry,FA} + \frac{\dot{m}_{C\ with\ ash}}{M_C} \\ C_{out} &= (y_{CO} + y_{CO_2}) \cdot F_{FG,dry,FA} + \frac{x_{C,ash}}{M_C(1 - x_{C,ash})} \cdot \dot{m}_{ash,SF} \\ C_{out} &= (y_{CO} + y_{CO_2}) \cdot F_{FG,dry,FA} + \frac{x_{C,ash} \cdot x_{ash,SF}}{M_C(1 - x_{C,ash})} \cdot \dot{m}_{SF} \end{aligned} \tag{C.3}$$

$\dot{n}_{C\ with\ ash}$ and $\dot{m}_{C\ with\ ash}$ are the moles and mass of carbon bound in the fly ash, respectively. M_C is the molar mass of carbon. $x_{C,ash}$ is the measured mass fraction of C in the dry fly ash sample. The fraction $x/(1-x)$ is introduced in order to account for the fact that $x_{C,ash}$ is given from Eq. (C.4). $\dot{m}_{ash,SF}$ is the mass flow of ash fed in with the SF. $x_{ash,SF}$ is the mass fraction of ash in the SF (from the proximate analysis), and $\dot{m}_{SF}$ is the mass flow of SF to the burner.

$$x_{C,ash} = \frac{m_{C\ in\ fly\ ash}}{m_{ash\ species\ in\ fly\ ash} + m_{C\ in\ fly\ ash}} \tag{C.4}$$

Level 3

$$\begin{aligned} C_{out} &= (y_{CO} + y_{CO_2}) \cdot F_{FG,dry,FA} + \frac{x_{C,ash} \cdot x_{ash,SF}}{M_C(1 - x_{C,ash})} \cdot \dot{m}_{SF} \cdot Y_{ash} \\ C_{out} &= (y_{CO} + y_{CO_2}) \cdot F_{FG,dry,FA} + \frac{x_{C,ash}}{M_C} \frac{m_{fly\ ash}}{\Delta t_{ash}} \frac{F_{FG,dry}}{F_{sampling}} \end{aligned} \tag{C.5}$$

Y_{ash} is the yield of fly ash calculated based on the realized sampling flow through the ash sampling system, see Section 2.3.2.2. $m_{fly\ ash}$ is the total amount of fly ash sampled over the time interval Δt_{ash}. $F_{FG,dry}$ is the theoretical flue gas flow, disregarding false air ingress and $F_{sampling}$ is the flow rate through the ash sampling system. An average value is used for the latter.

C.2 Sulphur

Sulphur is introduced with the solid fuel and potentially with the oxidizer. The latter is the case for the oxyfuel experiments with simulated recirculation of SO_2 containing flue gas.

$$S_{in} = y_{SO_2,OX} \cdot F_{OX} + \gamma \cdot \dot{m}_{SF} \tag{C.6}$$

where $y_{SO_2,\,OX}$ is the molar fraction of CO_2 in the oxidizer (0 for all air experiments) and F_{OX} is the molar flow rate of oxidizer. γ is the fuel sulphur content (moles/kg fuel), see Appendix B, and $\dot{m}_{SF}$ is the mass flow rate of solid fuel.

During coal/oxyfuel experiments with SO_2 addition to the oxidant the amount of SO_2 fed with the oxidizer constitute most of the S in the system. However, the S fed with the coal amounts to between 17 and 57 % depending on the SO_2 concentration in the oxidizer. It is thus still relevant to determine the sulphur balance for these experiments.

The equations for the three levels on the "out" term are seen in Eqs. (C.7), (C.8), and (C.9).

Level 1

$$S_{out} = y_{SO_2} \cdot F_{FG,\,dry,\,FA} \tag{C.7}$$

y_{SO_2} is the measured concentration of SO_2 in the dry flue gas sample. $F_{FG,\,dry,\,FA}$ is the dry flue gas flow. No measurement of the true flue gas flow exist and thus the flue gas flow is determined from the measured oxygen concentration in the dry flue gas. The determination of $F_{FG,\,dry,\,FA}$ takes false air ingress and incomplete combustion into account, see Appendix B, Section B.2.

Level 2

$$\begin{aligned}
S_{out} &= y_{SO_2} \cdot F_{FG,\,dry,\,FA} + \dot{n}_{S\ with\ ash} \\
S_{out} &= y_{SO_2} \cdot F_{FG,\,dry,\,FA} + \frac{\dot{m}_{S\ with\ ash}}{M_S} \\
S_{out} &= y_{SO_2} \cdot F_{FG,\,dry,\,FA} + \frac{x_{S,\,ash}}{M_S(1 - x_{C,\,ash})} \cdot \dot{m}_{ash,\,SF} \\
S_{out} &= y_{SO_2} \cdot F_{FG,\,dry,\,FA} + \frac{x_{S,\,ash} \cdot x_{ash,\,SF}}{M_S(1 - x_{C,\,ash})} \cdot \dot{m}_{SF}
\end{aligned} \tag{C.8}$$

$\dot{n}_{S\ with\ ash}$ and $\dot{m}_{S\ with\ ash}$ are the moles and mass of sulphur bound in the fly ash, respectively. M_S is the molar mass of sulphur. $x_{S,\,ash}$ and $x_{C,\,ash}$ are the measured mass fractions of S and C in the dry fly ash sample, respectively. $x_{S,\,ash}$ is assumed to be defined equally to Eq. (C.4). $\dot{m}_{ash,\,SF}$ is the mass flow of ash fed in with the SF. $x_{ash,\,SF}$ is the mass fraction of ash in the SF (from the proximate analysis), and $\dot{m}_{SF}$ is the mass flow of SF to the burner.

Level 4

$$
\begin{aligned}
S_{out} &= y_{SO_2} \cdot F_{FG,dry,FA} + \dot{n}_{S\ in\ fly\ ash} + \dot{n}_{S\ in\ deposits} \\
S_{out} &= y_{SO_2} \cdot F_{FG,dry,FA} + \frac{x_{S,ash}}{M_S} \cdot \dot{m}_{fly\ ash} + \frac{x_{S,dep}}{M_S} \cdot \dot{m}_{deposits} \\
S_{out} &= y_{SO_2} \cdot F_{FG,dry,FA} + \frac{x_{S,ash}}{M_S} \cdot \dot{m}_{fly\ ash} + \ldots \\
&\quad \frac{x_{S,dep}}{M_S} \cdot (\dot{m}_{ash,SF} - \dot{m}_{ash,sampled}) \\
S_{out} &= y_{SO_2} \cdot F_{FG,dry,FA} + \frac{x_{S,ash}}{M_S} \cdot \dot{m}_{fly\ ash} + \ldots \\
&\quad \frac{x_{S,dep}}{M_S} \cdot (x_{ash,SF} \cdot \dot{m}_{SF} \cdot (1 - Y_{ash})) \\
S_{out} &= y_{SO_2} \cdot F_{FG,dry,FA} + \frac{x_{S,ash}}{M_S} \cdot \frac{m_{fly\ ash}}{\Delta t_{ash}} \cdot \frac{F_{FG,dry}}{F_{ash\,sampling}} + \ldots \\
&\quad \frac{x_{S,dep}}{M_S} \cdot (x_{ash,SF} \cdot \dot{m}_{SF} \cdot (1 - Y_{ash}))
\end{aligned} \tag{C.9}
$$

$\dot{n}_{S\ in\ fly\ ash}$ is the amount of sulphur bound in the sampled fly ash. $\dot{n}_{S\ in\ deposits}$ and $\dot{m}_{S\ in\ deposits}$ are the moles and mass of sulphur in deposits, respectively. $\dot{m}_{fly\ ash}$ is the mass flow rate of the entire fly ash flow, including unburnt carbon. $x_{S,dep}$ is the mass fraction of sulphur in deposits. The value used in the calculations is from the upstream part of the sampled deposits as this is assumed to represent the best estimate of the average concentration of sulphur in all deposits in the reactor. $\dot{m}_{deposits}$ is the mass flow rate at which deposits are build up in the reactor and this is assumed to constitute the amount of ash fed to the reactor which does not end up as fly ash, i.e.$(1 - Y_{ash})$. $\dot{m}_{ash,sampled}$ is the mass flow rate of ash species sampled from the setup. $m_{fly\ ash}$ is the total amount of fly ash sampled over the time interval Δt_{ash}. $F_{FG,dry}$ is the theoretical flue gas flow, disregarding false air ingress and $F_{ash\,sampling}$ is the flow rate through the ash sampling system. An average value is used for the latter.

Appendix D

Heating of Large Straw Particles

Heating of large particles ($d_p > 100\ \mu$m) occurs by both radiation and convection. The relative importance of convection decreases with increasing particle size [85].

The energy balance for a particle subject to heating by radiation and convection is seen in (D.1). Regardless of the size of the particle, it has been assumed isothermal.

$$m_p C_{p,p} \frac{dT_p}{dt} = \pi d_p^2 \cdot \left(h \left(T_g - T_p \right) + \epsilon_p \sigma \left(T_w^4 - T_p^4 \right) \right) \tag{D.1}$$

Parameter	Description	Value
m_p	particle mass	Eq. (D.2)
$C_{p,p}$	specific heat of the particle	1000 [J/kg-K]
T_p	instantaneous particle temperature	$T_{p,0} = 298$ K
t	time	
d_p	particle diameter, fixed	100, 330, and 1000 μm
h	heat transfer coefficient	Eq. (D.3)
T_g	flue gas temperature	from T-profile
ϵ_p	particle emissivity	0.85 (black body)
σ	Stefan-Boltzmann constant	$5.67051 \cdot 10^{-8}$ [W/m^2·K^4]
T_w	wall temperature	1000 °C, assumed constant
ρ_p	particle density	500 [kg/m^3]
Nu	Nusselt number	Eq. (D.4)
λ_g	thermal conductivity of gas	0.09 [W/m·K]
m	constant	0.6 (single phase flow)
Re	Reynolds number for particle	Eq. (D.5)
Pr	Prandtl number	1
ρ_g	density of flue gas	$f(T_g)$, about 0.3 [kg/m^3]
u_t	relative velocity of particle to flue gas	Eq. (D.6) or (D.7)
μ_g	viscosity of flue gas	$5 \cdot 10^{-5}$ [kg/m·s]
g	gravitational constant	9.81 [m/s^2]

$$m_p = \frac{\pi}{6}\, d_p^3\, \rho_p \tag{D.2}$$

$$h = \frac{Nu\ \lambda_g}{d_p} \tag{D.3}$$

$$Nu = 2 + m\, Re^{1/2} Pr^{1/3} \tag{D.4}$$

$$Re_p = \frac{\rho_g u_t d_p}{\mu_g} \tag{D.5}$$

$$u_t = \frac{g\, d_p^2\, (\rho_p - \rho_g)}{18\, \mu_g} \quad ;\ Re_p < 2 \tag{D.6}$$

$$u_t = 0.153 \left(\frac{g\, (\rho_p - \rho_g)\, d_p^{1.6}}{\mu_g^{0.6}\ \rho_g^{0.4}} \right)^{0.714} \quad ;\ 2 < Re_p < 400 \tag{D.7}$$

The terminal velocity, relative velocity of particle to flue gas, of the particles are found in an iterative procedure using Equations (D.5) to (D.7).

Fuel 89 (2010) 3373–3380

Contents lists available at ScienceDirect

Fuel

journal homepage: www.elsevier.com/locate/fuel

Coal devolatilization and char conversion under suspension fired conditions in O_2/N_2 and O_2/CO_2 atmospheres

Jacob Brix, Peter Arendt Jensen, Anker Degn Jensen *

Department of Chemical and Biochemical Engineering, Building 229 Søltofts Plads, 2800 Kgs. Lyngby, Denmark

ARTICLE INFO

Article history:
Received 23 December 2009
Received in revised form 8 March 2010
Accepted 9 March 2010
Available online 20 March 2010

Keywords:
Oxy-fuel
Devolatilization
Combustion
Char

ABSTRACT

The aim of the present investigation is to examine differences between O_2/N_2 and O_2/CO_2 atmospheres during devolatilization and char conversion of a bituminous coal at conditions covering temperatures between 1173 K and 1673 K and inlet oxygen concentrations between 5 and 28 vol.%. The experiments have been carried out in an electrically heated entrained flow reactor that is designed to simulate the conditions in a suspension fired boiler. Coal devolatilized in N_2 and CO_2 atmospheres provided similar results regarding char morphology, char N_2-BET surface area and volatile yield. This strongly indicates that a shift from air to oxy-fuel combustion does not influence the devolatilization process significantly. Char combustion experiments yielded similar char conversion profiles when N_2 was replaced with CO_2 under conditions where combustion was primarily controlled by chemical kinetics. When char was burned at 1573 K and 1673 K a faster conversion was found in N_2 suggesting that the lower molecular diffusion coefficient of O_2 in CO_2 lowers the char conversion rate when external mass transfer influences combustion. The reaction of char with CO_2 was not observed to have an influence on char conversion rates at the applied experimental conditions.

1. Introduction

It is a growing concern that anthropogenic CO_2 emission to the atmosphere causes the planets temperature to raise. This concern has initiated extensive research programs to pursue alternative energy sources that can meet the increasing demands in both industrialized and developing countries without emitting CO_2 as fossil fuel based power plants are large emission sources. Today fossil fuels accounts for approximately 85% [1,2] of the energy production world wide and it is therefore not likely that new technologies, which is not presently mature, can substitute fossil fuels, such as coal, in the short to midterm future [3]. To overcome the challenges the power industry, which is today relaying on conventional coal combustion, must find alternative technologies that allow for the continued use of coal, a fuel which is abundant, relatively cheap and steady in supply.

An interesting alternative to traditional air-blown combustion is the oxy-fuel combustion process. In oxy-fuel combustion, oxygen is separated from air before it enters the boiler and mixed with recycled flue gas to obtain a plant exit stream of almost pure CO_2 [3]. This CO_2 stream can subsequently be stored in suitable geological formations such as depleted oil and gas reservoirs or saline aquifers [2].

Many technical aspects still need to be clarified for oxy-fuel combustion to be industrialized. Fundamental knowledge of the oxy-fuel combustion process is therefore of importance. This knowledge must include an understanding of coal devolatilization and char conversion in a CO_2 rich gas since these processes influence heat release characteristics, fuel burn out and the need for oxygen, all of which have important economic implications for the process.

Rathnam et al. [4] examined the reactivity of four pulverized coals in the size range 69–90 μm. They conducted experiments in a drop tube furnace (DTF) at 1673 K under single particle conditions using oxygen concentrations between 3% and 21% in N_2 and 5% and 30% in CO_2. From their experiments they found 4–24% higher apparent volatile yields in CO_2 compared to N_2 although the standard deviations of the data indicated possible overlaps between N_2 and CO_2 yields for three of the four coals studied. The authors attributed the higher volatile yield in CO_2 to gasification. That the presence of CO_2 increases the volatile yield compared to N_2 was also found by Al-Makhadmeh et al. [5] from entrained flow reactor (EFR) pyrolysis tests. Using a bituminous coal they found an increase in volatile yield of approximately 16% when N_2 was replaced with CO_2 at 1423 K. This contradicts the findings of Borrego and Alvarez [6] that devolatilized high and low volatile bituminous coal particles in the size range 36–75 μm using a DTF operated at 1573 K. They found a decrease in volatile yield of 62% and 32% for the low volatile and high volatile coal, respectively, when N_2

* Corresponding author. Tel.: +45 45 25 28 41; fax: +45 45 88 22 58.
E-mail address: aj@kt.dtu.dk (A.D. Jensen).

0016-2361/$ - see front matter © 2010 Elsevier Ltd. All rights reserved.
doi:10.1016/j.fuel.2010.03.019

was replaced with CO_2. These decreases in volatile yield are surprisingly high and could be caused by the high amount of cold gas (1/3 of the total gas volume) used for particle transport during their experiments. Since CO_2 has a higher thermal capacity than N_2 the large amount of cold gas could lower the particle heating rate in CO_2 causing the lower volatile yields.

To examine the difference in volatile yield closer Rathnam et al. [4] conducted thermogravimetric analysis (TGA) pyrolysis on one of their coals in pure N_2 and CO_2, using a heating rate of 25 K/min. They found very similar weight loss curves at temperatures below 1030 K. At this temperature the weight loss in CO_2 started to accelerate compared to N_2 indicating an effect of char gasification by CO_2. This effect of CO_2 was also found by Li et al. [7] in their TGA pyrolysis experiment using pulverized bituminous coal at similar temperatures and heating rates of 10, 20 and 30 K/min. That CO_2 gasification can take place during pyrolysis have also been found by other investigators [8,9]. Due to the long residence time and low heating rate of the coal in a TGA direct comparison with DTF and EFR experiments, where devolatilization is completed in a time scale of less than a second, should however be made with caution, especially if these experiments are carried out in an oxidizing atmosphere. Rathnam et al. [4] also compared coal burnout in O_2/N_2 and O_2/CO_2 at varying oxygen concentrations using their DTF. Here a tendency of higher overall coal conversions (1–3 wt.%) in O_2/CO_2 was found for two of the four coals with most pronounced differences at low oxygen concentrations. Chars produced in their DTF and combusted in a TGA, using a heating rate of 25 K/min, showed an increased reactivity in CO_2 compared to N_2 at temperatures above 1100 K and an oxygen concentration of 2%. At oxygen concentrations above 2% the TGA experiments showed no difference in reactivity as char burnout was accomplished at lower temperatures where the effect of CO_2 gasification does not impact on char consumption. In the TGA experiments of Várhegyi et al. [10], which were carried out by burning bituminous coal in oxygen concentrations ranging between 5 and 100 vol.% in Ar or CO_2, the effect of CO_2 gasification was also found to be negligible due to the low gasification rate compared to the char oxidation rate.

Bejarano and Levendis [11] conducted single particle combustion experiments in both O_2/N_2 and O_2/CO_2 using a bituminous coal, a lignite coal and a synthetic char in a laminar DTF with fixed temperatures of 1400 K and 1600 K. Using a three-color pyrometer they were able to measure the temperature of the burning particles. The particle size fractions of the coal used in their experiments were 45–53 μm, 75–90 μm and 150–180 μm whereas the synthetic char had a diameter of 43 μm. When burning 45–53 μm bituminous coal particles at a reactor temperature of 1400 K a particle temperature drop at 50% burnout, of approximately 150–200 K, was observed for oxygen concentrations in the range 20–80 vol.% when N_2 was replaced with CO_2. In this range of oxygen concentrations the particle temperature increased approximately from 1800 K to 2620 K in O_2/CO_2 and from 2000 K to 2800 K in O_2/N_2. Burnout times at identical oxygen concentrations were found to be 44–80% longer in O_2/CO_2 compared to O_2/N_2 depending on the oxygen concentration. The authors argued that the combustion was taking place in Zone II by comparing calculated diffusion-limited burnout times with experimental data. Their conclusion is however sensitive to factors such as particle swelling, development of char morphology during devolatilization and choice of combustion model. If a shrinking sphere model is applied to calculate burnout times in Zone III the relative difference in burnout times is a measure of the relative difference in oxygen diffusivity in the particle boundary layer. For the experiments just mentioned the burnout times in 20% O_2/80% CO_2 and 40% O_2/60% CO_2 is approximately 44% and 46% higher than in the corresponding N_2 based atmospheres. The diffusion coefficient of O_2 in N_2, as calculated by Chapman–Enskog's equation [12], using average temperatures between the particles and the bulk gas, is however, 42% and 40% higher than in CO_2. This could imply that the experimental data of Bejarano and Levendis [11] is obtained closer to Zone III than anticipated by the authors, which is most clearly seen at the lower oxygen concentrations where the largest differences in conversion rates exist. When experiments were carried out using lignite lower differences in particle temperatures were found between N_2 and CO_2 based atmospheres (~100 K) compared to combustion of bituminous coal. Burnout times for lignite were found to be lower than for bituminous coal with smaller differences (~3 ms) between O_2/N_2 and O_2/CO_2 environments. Bejarano and Levendis [11] attributed this behavior to a higher reactivity and a lower fixed carbon content of lignite. In addition, low rank coals tend to form network chars whereas medium rank coals have a tendency to form cenospheric chars [13]. It is therefore likely that a more pronounced effect from CO_2 gasification on char conversion will be present during combustion of a low rank coal where CO_2 can react on the pore surface of the char when the reaction with oxygen is controlled partly or completely by external mass transfer.

Molina and Shaddix [14] carried out experiments in a laminar EFR under single particle conditions using bituminous coal particles in the size range 106–125 μm. Using a Charged-Coupled Device (CCD) camera they obtained luminous profiles of particles burning in both O_2/N_2 and O_2/CO_2 mixtures from which the time where devolatilization begins and the time where volatile ignition takes place could be deduced based on a large number of repeated experiments. Ignition time in 21% O_2/79% CO_2 was approximately 11% (~3 ms) longer than in the equivalent N_2 mixture at the same gas temperature. For 30% O_2 the increase in ignition time was reduced to approximately 8% (~2 ms). The authors explained these observations with the increased thermal capacity ($\rho_p \cdot C_p$) and lower diffusivity of gaseous components in CO_2 compared to N_2. These factors cause a delayed ignition and a slower consumption of volatiles through an increased heat uptake by the gas and a lower reactant mixing rate during devolatilization. No visual differences were found in devolatilization time neither between carrier gases or oxygen concentrations, which the authors explained with similar particle heating curves.

The short review above presents data from several researchers. Conclusions based on the comparison of their data are however difficult as differences in particle temperature histories, coal composition, and equipment limitations such as gas mixing, strongly influences the results. It is therefore apparent that there is a continued need for broad consistent data sets that can promote the understanding of coal conversion in oxy-fuel combustion.

The present investigation aims at clarifying differences in consumption rates when bituminous coal is devolatilized and burned in O_2/N_2 and O_2/CO_2 mixtures. To base discussions on data obtained from combustion in both Zone I, Zone II and Zone III experiments have been carried out covering a wide range of both temperatures and oxygen concentrations. As the aim of this study has been char conversion rate at constant oxygen concentrations no focus has been on stoichiometries other than to ensure sufficient amounts of oxygen in the reactor.

2. Experimental

2.1. Equipment

The experiments were carried out using an entrained flow reactor shown in Fig. 1. The reaction zone is cylindrical with a length of 2 m and a diameter of 0.08 m and it is heated by seven electrical heating elements. The maximum temperature of these heating

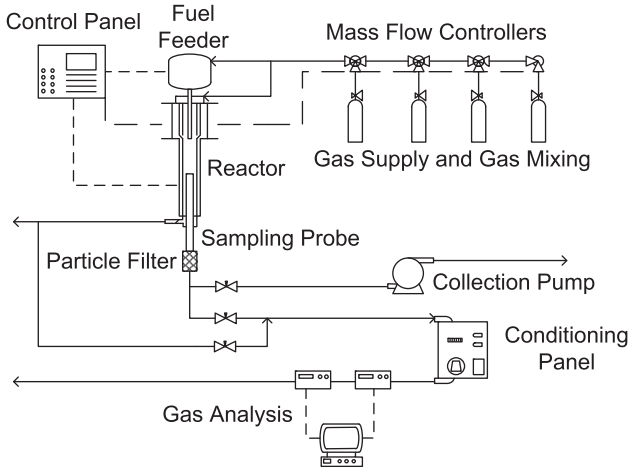

Fig. 1. Experimental setup. Solid lines indicate tubes and dashed lines indicate wires for control and data logging. All streams leaving the setup is sent to a central ventilation system.

elements is 1773 K. On top of the reactor a 0.8 m long gas preheater, consisting of two electrical heating elements, preheats the secondary gas stream to a prescribed temperature. Coal particles are fed to the reactor from a dosing system consisting of a silo and a screw feeder connected to a vibration transporter. This transporter is connected to a water cooled feeding probe going through the center of the gas preheater. The actual feed rate is controlled by the weight of the silo and screw feeder. The feeding equipment is contained in an airtight chamber so that the primary gas used for pneumatic particle transport to the reactor can be controlled accurately. This primary gas was either N_2 or CO_2 except when experiments were carried out in air.

Sampling of particles at different residence times is done using a water cooled sampling probe that can be used over the entire reaction zone. The top of the probe is shaped like a funnel and has a diameter of 0.034 m. At the bottom of the probe a filter separates gas and particles. The gas suction through the probe is performed alternately depending on whether the purpose of suction is particle collection or gas analysis. Both gas analysis and char sampling were performed at each sampling position. The oxygen concentration measured at the sampling position is the local concentration after volatile consumption and initial char oxidation. CO and CO_2 concentrations were detected by an IR-analyzer and a paramagnetic analyzer were used for analysis of O_2. All streams leaving the setup are sent to a central flue gas ventilation system.

The analysis gas is sent through a conditioning panel where it is cleaned for remaining dust and particles and any water vapor is removed. Very small amounts of water vapor were present in the gas due to a low fuel feed rate. All mass flow controllers, heating elements and the fuel feeder can be controlled from a central panel and all measurements from the gas analyzers are stored by a computer using LabVIEW software. When experiments were carried out in 21 vol.% O_2 in N_2, air was used directly from a compressor. All other gaseous environments were created by mixing bottled gases.

2.2. Devolatilization

Devolatilization experiments were carried out at the temperatures shown in Table 1. Table 1 also show residence times and the carrier gas used at each temperature. The residence times, τ_{dev}, are found by extrapolation of char conversion profiles at each temperature to a residence time where the char conversion is zero indicating that particle heating and devolatilization is completed.

Table 1
Devolatilization temperatures used in the experiments. CO_2/N_2 indicates that devolatilization have been carried out separately in both gases. $\tau_{sampling}$ is the reactor residence time where char sampling took place as defined by Eq. (1). τ_{dev} is the residence time where particle heating and devolatilization is completed.

T (K)	1173	1273	1373	1473	1573	1673
Gas	CO_2	CO_2	CO_2	CO_2	CO_2/N_2	CO_2/N_2
$\tau_{sampling}$ (s)	0.47	0.39	0.25	0.22	0.16	0.15
τ_{dev} (s)	0.297	0.221	0.209	0.196	0.182	0.15

When treating char conversion profiles this residence time is subtracted from the particle sampling time in order to get a time scale where only heterogeneous char conversion is taking place. The residence times at the sampling positions, $\tau_{sampling}$, are calculated assuming a laminar flow profile, which is integrated with the radius of the sampling probe as the upper radial boundary condition. The result is shown in Eq. (1). The mean gas velocity in the reactor, v_{mean}, has been close to 1 m s^{-1} in all experiments, both during devolatilization and char combustion. $L_{sampling}$, $R_{reactor}$ and R_{probe} are the traversed reactor length, reactor diameter, reactor radius and sampling probe radius, respectively.

$$\tau_{sampling} = \frac{R_{reactor}^2 \cdot L_{sampling}}{v_{mean} \cdot (2 \cdot R_{reactor}^2 - R_{probe}^2)} \quad (1)$$

Because tar was clogging the sampling probe and central flue gas ventilation systems it was necessary to add oxygen to the secondary gas stream to crack/partially burn the tar molecules released during devolatilization. A stoichiometric ratio of three (corresponding to 5–6 vol.% O_2) was found to remove the tar without promoting heterogeneous char consumption. That the degree of heterogeneous char consumption was negligible, due to low residence times and mixing limitations at the reactor entrance, was confirmed by sampling also at a position slightly further downstream in the reaction zone for selected experiments, which showed similar weight losses. The position in the reactor, $L_{sampling}$, used as sampling point was a few centimeters below the location with the highest measured CO concentration.

Devolatilization was mainly carried out using CO_2 as carrier gas. At 1573 K and 1673 K experiments were also carried out in N_2 to see any effects of carrier gas. The amount of remaining char combustibles was found using ash tracing in a muffle furnace at 1088 K for 2.5 h in air. The volatile content was subsequently found by the mass balance shown in (2), which assumes that no ash leaves the particles during devolatilization.

$$\alpha_v = 1 - m_{so}\frac{\alpha_A}{m_A} - \alpha_m \quad (2)$$

In (2) α_A, α_m and α_v are the weight fractions of coal ash, coal moisture and coal volatiles, respectively. m_{so} and m_A are the masses of sampled char and of ash measured after burn-off in the muffle furnace.

2.3. Combustion

Combustion studies were carried out at the same temperatures as shown in Table 1. Both N_2 and CO_2 were used as carrier gas with inlet oxygen concentrations between 5 and 28 vol.%. These concentrations correspond to stoichiometric ratios between 2 and 15 at a coal feed rate of 50 g h^{-1}, which was used in all experiments. A total of 31 char conversion profiles were obtained from the experiments of which only representative samples are shown in this paper. Char was sampled at reactor residence times from about 0 to 1 s. Reynolds numbers for the gas were between 400 and 1100 depending on reactor conditions meaning that the gas flow profile was laminar. A laminar flow profile along with a carefully

controlled sampling volume flow allow for a precise determination of particle residence times using Eq. (1). To calculate char conversion at each sampling point Eqs. (3) and (4) are constructed from mass balances using the same assumption as for Eq. (2).

$$\alpha_A^* = \frac{\alpha_A}{1-\alpha_v-\alpha_m} \tag{3}$$

$$X = \frac{m_A(1-\alpha_A^*)-\alpha_A^* m_c}{m_A(1-\alpha_A^*)} \tag{4}$$

α_A^*, m_c and X are the initial weight fraction of ash in the char after devolatilization, the mass of remaining combustibles in a char sample and dimensionless char conversion, respectively. The definition in Eq. (4) allows for accurate comparison of char conversion rates across a wide temperature interval as the increase in volatile yield when the temperature increases is accounted for.

2.4. Fuel

The coal is a South American bituminous coal (El Cerrejón) sieved to the size range 90–106 μm. The composition of the unsieved coal is given in Table 2 in the column "Original". Ash tracing was used on the sieved coal and the ash content of the applied size fraction was 5.9 wt.%. Ash tracing was also done on a smaller particle size fraction and this confirmed that the ash was concentrated in the small particles. In all calculations the original values in Table 2 have therefore been corrected for ash content assuming that the same fractional correction applies to all coal constituents. The actual composition of the size range 90–106 μm can be seen in the column "Corrected". Correction of the volatile yield has not been attempted as this is determined by experiments at each experimental temperature. The heating values has not been corrected either as this information is not used here.

Even though sieving was used to obtain a narrow particle size fraction of 90–106 μm laser diffraction measurements using a Malvern Mastersizer with ethanol as solvent revealed the particle size distribution (PSD) shown in Fig. 2.

That the PSD has a long tail towards small particle sizes is most likely caused by small particles adhering to each other or to the larger particles when placed in the sieves, a problem which has also been reported by Ballester and Jiménez [15]. The mass based mean diameters of the PSD's for unsieved and sieved coal particles are 56.8 μm and 75.8 μm, respectively.

3. Results

3.1. Repeatability

To test the repeatability of the char conversions several experiments have been carried out twice. These experiments show a pooled standard deviation of 3.3% though individual sets of experiments showed uncertainty up to 12%.

Table 2
Proximate and ultimate analysis of the coal used for experiments. In the column "Corrected" the original data has been corrected for ash content the particle size fraction 90–106 μm.

Proximate analysis		Original	Corrected
Upper heating value	MJ/kg ar	28.19	28.19
Effective heating value	MJ/kg ar	27.09	27.09
Moisture	wt.% ar	5.0	5.2
Ash	wt.% ar	9.6	5.9
Volatiles	wt.% ar	34.9	34.9
Ultimate analysis			
Carbon	wt.% ar	68.9	71.73
Hydrogen	wt.% ar	4.61	4.8
Oxygen (diff.)	wt.% ar	9.82	10.23
Nitrogen	wt.% ar	1.44	1.5
Sulfur	wt.% ar	0.62	0.64

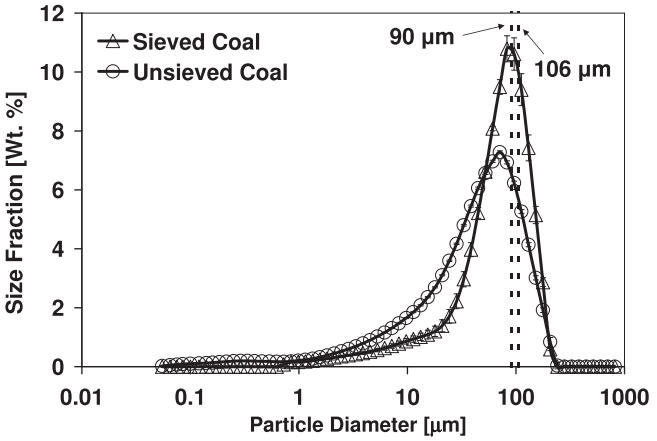

Fig. 2. Particle size distributions of sieved and unsieved coal.

Fig. 3 shows three sets of repeated experiments performed at 1373 K in CO_2. Both char and gas sampling were done at each residence time so all char conversions has a corresponding measured oxygen concentration. The oxygen concentrations given in the captions in this paper are the average oxygen concentration of each experiment.

3.2. Devolatilization

The results obtained from devolatilization experiments are shown in Fig. 4. It may seem suspicious that the volatile content drops at the temperatures 1573 K and 1673 K compared to at 1473 K. That it does so for both temperatures in N_2 and CO_2 suggest that the drop is not due to experimental inaccuracy. The explanation for this drop is found in two factors, namely the low residence time used for sampling and that Eq. (2) is sensitive towards inaccuracies in ash content determination. Sampling at low residence time at the high temperatures was done to avoid heterogeneous char conversion caused by the presence of oxygen. The sensitivity of Eq. (2) towards inaccuracies in ash content means that ash evaporation could affect the calculated volatile content. Because of the lower volatile content found at 1573 K and 1673 K the value found at 1473 K will be used in (3) and (4) for all three temperatures.

Fig. 4 shows that at 1173 K the volatile yield found using the EFR is slightly lower than that found by proximate analysis. This

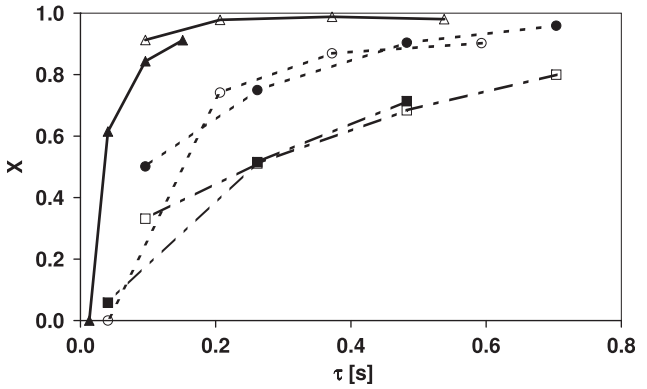

Fig. 3. Char conversion profiles obtained in CO_2 at 1373 K (●, 6.1 vol.% O_2; ○, 5.9 vol.% O_2, ▲, 19.0 vol.% O_2; △, 18.2 vol.% O_2; □, 3.6 vol.% O_2; ■, 4.6 vol.% O_2). Oxygen concentrations are the averages of the local concentrations measured in each experiment. $\lambda \sim 2.4$–10.2.

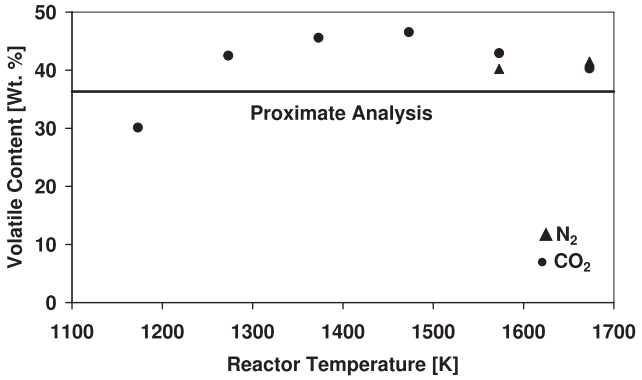

Fig. 4. Volatile content found at the experimental temperatures.

is expected as the residence time in the EFR is much lower than that used in proximate analysis, which limits the influence of secondary pyrolysis. The fact that char has been sampled under identical conditions at 1573 K and 1673 K in N_2 and CO_2 suggest that no pronounced effect of CO_2 on volatile yield exists at these conditions. This is not in agreement with neither Rathnam et al. [4] and Al-Makhadmeh et al. [5] nor Borrego and Alvarez [6]. Al-Makhadmeh et al. [5] and Rathnam et al. [4] used sampling residence times of 1 s (1423 K) and 0.62 s (1673 K) and found the volatile yield in CO_2 to increase 16% and 4–24%, depending on the coal type. The reactor used by Al-Makhadmeh et al. [5] was electrically heated with a cold entrainment gas that only made up 4% of the total gas volume. The heat source and ratio of cold to hot gas is not stated explicitly by Rathnam et al. [4]. Borrego and Alvarez [6] used a residence time of 0.3 s (1573 K) and found a decrease in volatile yield of 62% and 32% in CO_2, depending on the coal type. As discussed earlier the large differences could be influences by the high amount of cold entrainment gas used by the authors. Authors that find an increased volatile yield in CO_2 often contribute this to gasification of the fuel. Though this appears to be a natural conclusion and a likely cause, the low residence times needed for devolatilization at high temperatures (>1500 K) and the fact that a volatile cloud is expected to form around the particles [14], thereby limiting the access of the CO_2 to the particle surface, makes it prudent to examine other possibilities. The conditions used during experiments will inevitably affect the results wherefore factors such as mixing between cold and hot gas streams, particle heating rate and total particle residence times must be included when data is compared. The cold fuel carrier gases used in the present investigation made up approximately 18 vol.% of the total gas volume at 1573 K and 1673 K and the sampling residence times are much lower than in any of the referred investigations. Under these conditions no difference was found between devolatilization in N_2 and CO_2. In suspension fired boiler operation, where heating and devolatilization is completed in a time scale of 150–200 ms it is therefore questionable if CO_2 gasification will make a significant contribution to fuel conversion during devolatilization of low to medium reactive coals.

3.2.1. Char morphology

Fig. 5 shows scanning electron microscopy (SEM) images of chars obtained from devolatilization at 1673 K in N_2 and CO_2 and reveal no visual differences.

N_2-BET analysis of the chars in Fig. 5 showed surface areas of 270 and 280 $m^2\,g^{-1}$ for char devolatilized in N_2 and CO_2, respectively, further suggesting that no significant differences exists. This is not in agreement with the N_2-BET results of Borrego and Alvarez [6] who found an increased surface area of as much as several hundred percent, depending on the coal, when chars were prepared in CO_2 compared to N_2. Al-Makhadmeh et al. [5] finds both a decreased and an increased surface area also of as much as several hundred percent, depending on the coal, when CO_2 is used to prepare the char compared to N_2. Care should however be taken when comparing measured surface areas of chars prepared in different reactors from different coals. Factors such as heating rate, coal composition, residence time and temperature are known to cause variations [13] and the residence time and temperature are especially important factors if CO_2 gasification shall contribute to a

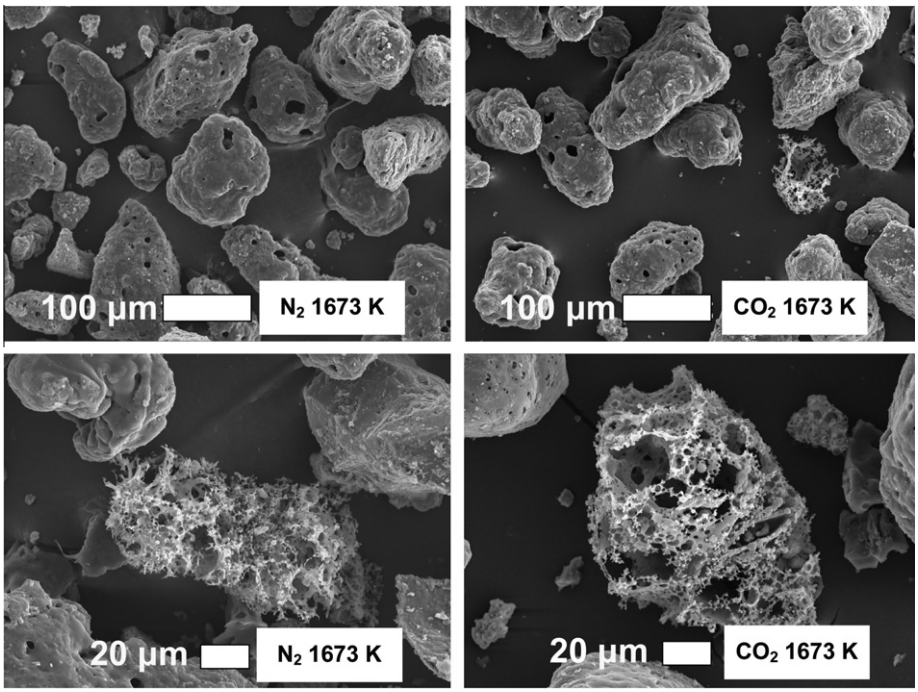

Fig. 5. SEM images of chars obtained at 1673 K in N_2 and CO_2.

higher specific surface. As a further example of this Borrego and Alvarez [6] finds no significant differences in CO_2-BET surface areas between char prepared in N_2 and CO_2 whereas Rathnam et al. [4] reports increases of 10–43% when chars are prepared in CO_2 compared to N_2.

The PSD's of chars prepared in CO_2 were found to change with the temperature as shown in Fig. 6. The peak of the PSD is shifted from 82.6 μm for sieved coal to 96.2 μm at 1273 K and 112.1 μm at 1473 K and 1673 K. The corresponding weight based mean diameters are 75.8 μm, 90.4 μm, 105.6 μm and 113.7 μm.

That the peaks of the PSD's in Fig. 6 shifts towards higher values is a clear sign of swelling, which is expected behavior for a bituminous coal [13]. Fitting the weight based mean diameters to a second order polynomium yield Eq. (5) that describes the temperature dependent swelling ratio of the particles in the interval 1173–1673 K.

$$SR = -1.375 \times 10^{-6} \cdot T^2 + 4.826 \times 10^{-3} \cdot T - 2.725 \quad (5)$$

It can also be seen from Fig. 6 that the amount of fines decreases as the temperature is raised. This is partly due to swelling but as fragmentation is also known to take place [13,16], producing fines,

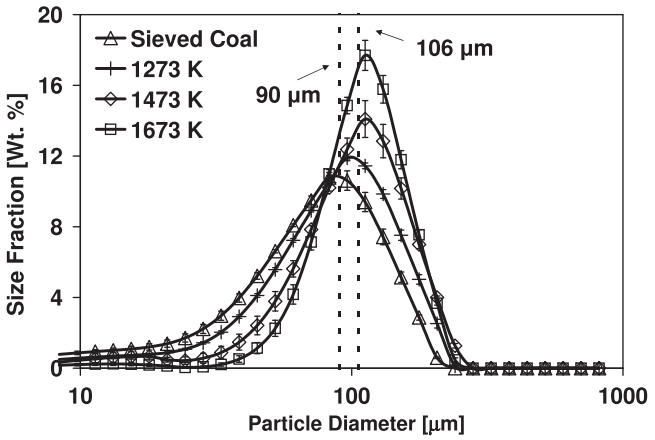

Fig. 6. Particle size distributions of sieved coal and chars obtained in CO_2 at 1273 K, 1473 K and 1673 K.

some char oxidation has been taking place. The contribution of the fines to the overall weight of char is however relatively low with approximately 7 wt.% under 10 μm so if a slight consumption has been taking place it is not enough to cause large deviations in the determined volatile content in Fig. 4. Fig. 7 show SEM images of the particles corresponding to the PSD's shown in Fig. 6 supporting that the amount of fines decrease with increasing temperature and that swelling is taking place.

3.3. Char combustion

The dependence of oxygen concentration on char conversion rate was found in both N_2 and CO_2 based atmospheres by plotting char conversion against oxygen concentration at fixed residence times. This can be seen in Fig. 8 using results obtained at 1373 K.

Fig. 8 shows that there is no conspicuous difference in the influence of oxygen concentration on char conversion whether combustion is taking place in N_2 or CO_2 based atmospheres. Results obtained at 1173 K and 1273 K confirms this conclusion. That there is no apparent change in the dependence of oxygen concentration on char conversion indicates that the kinetic parameters governing char consumption is not changed when N_2 is replaced with CO_2 under similar conditions. In Fig. 9 conversion profiles, obtained at 1173 K and approximately 27.8 vol.% O_2, supports the conclusion based on Fig. 8. In Fig. 10 char conversion profiles obtained at 1373 K and approximately 6.1 vol.% O_2, which is expected to cause the combustion to take place in Zone II, does not show apparent differences in conversion rate either.

In Figs. 9 and 10 the dashed conversion profiles are calculated for a shrinking particle burning in Zone III using Eq. (6) and the residence time $\tau(\tau_{sampling} - \tau_{dev})$. Eq. (5) is used to calculate the actual mean particle radius, R_0, from the mass mean diameter of the sieved coal. The bulk oxygen partial pressure, P_b, is found from the average of the measured local concentrations. Values of particle density and molar mass, ρ_p and M_p, are set to 1000 kg m^{-3} and 12 g mol^{-1} as approximate values for a graphite particle with a porosity of 50%. The binary diffusion coefficient, D_m, is found at the reactor temperature, T_b, using Chapman–Enskog's equation [12]. Calculations show initially a lower conversion rate than found from experiments. This stresses the uncertainty inherent in this

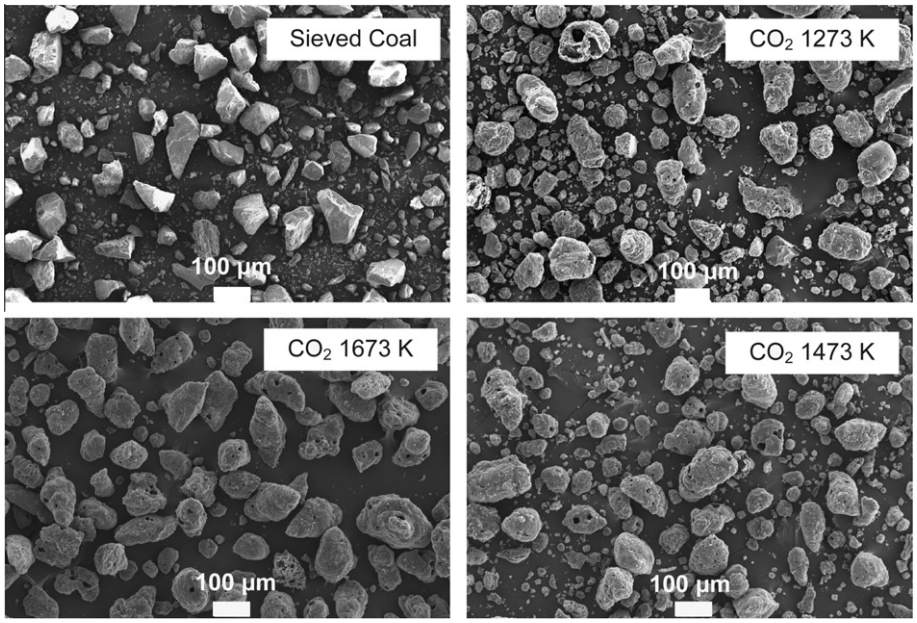

Fig. 7. SEM images of the PSD's shown in Fig. 6.

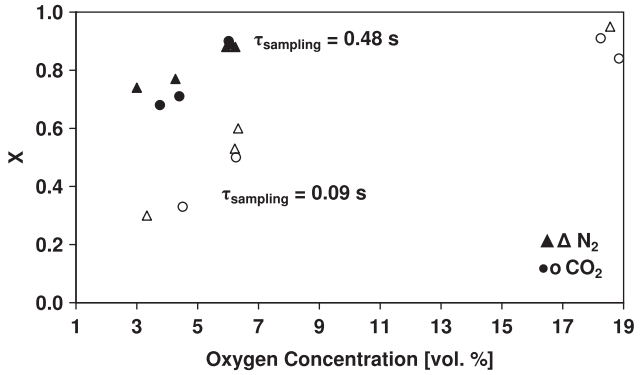

Fig. 8. Char conversions vs. oxygen concentrations at 1373 K for two different sampling residence times. $\lambda \sim 2.4$–10.2.

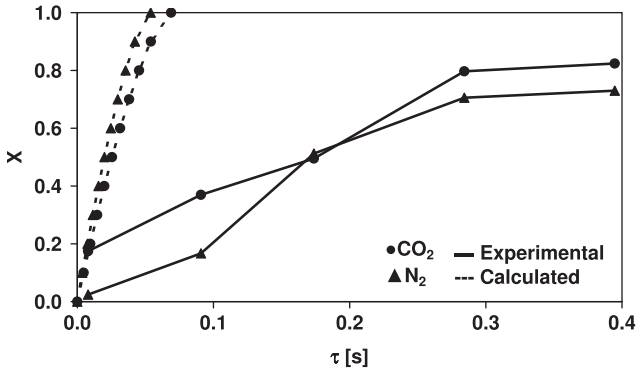

Fig. 9. Char conversion profiles obtained at 1173 K. The calculated profiles are found for a shrinking sphere in Zone III using Eq. (6) (●, 27.9 vol.% O_2; ▲, 27.7 vol.% O_2). Oxygen concentrations are the averages of the local concentrations measured in each experiment. $\lambda \sim 15$.

method of determining experimental combustion regimes as the calculated conversion profiles are restricted to one representative particle size whereas Figs. 5–7 show that several particle sizes and different morphologies are in fact present. That the experimental conversion profiles initially increases steeper than the calculated is most likely caused by rapid conversion of the smaller particle sizes, a phenomenon that is not captured by the calculations.

$$\tau = \frac{1}{2} \cdot \left(\frac{R \cdot T_b \cdot \rho_p \cdot R_0^2}{2 \cdot D_m \cdot P_b \cdot M_p} \right) \cdot \left(1 - (1 - X)^{\left(\frac{2}{3}\right)} \right) \quad (6)$$

The possible effect of CO_2 gasification on char conversion is often discussed in the oxy-fuel literature [4–7,10] In neither Fig. 9 or Fig. 10 this effect has been ascertainable but the temperatures have also been quite low and the oxygen excess quite high for this reaction to contribute significantly to the overall char conversion rate. In order to provoke an effect of CO_2 gasification, experiments have also been carried out at higher temperatures and lower oxygen concentrations. Fig. 11 show conversion profiles obtained at 1573 K and 1673 K in oxygen concentrations between 3.1 and 3.7 vol.%. At these conditions the effect of CO_2 gasification would be expected to appear if important for practical boiler operation.

It can be seen from Fig. 11 that the conversion rates in N_2 generally are higher than in CO_2, which is likely caused by an approximately 28% lower diffusion coefficient of O_2 in CO_2 at these temperatures. The results strongly imply that CO_2 gasification does not have a practical effect on overall char conversion under suspension fired conditions for the investigated coal. In Fig. 11 the conversion profile found in CO_2 at 1573 K crosses that found at 1673 K. The initial trend of the profiles obtained in N_2 is the same but the profile at 1573 K breaks off in the last two data points. That conversion takes place faster at 1573 K than at 1673 K seem contradictive at first. The conversion profile in Fig. 11, calculated using Eq. (6), does however imply that char consumption is taking place in Zone III meaning that even small differences in bulk oxygen concentrations and particle swelling has a significant influence. Fig. 12 show conversion profiles calculated using Eq. (6) and the experimental conditions in Fig. 11.

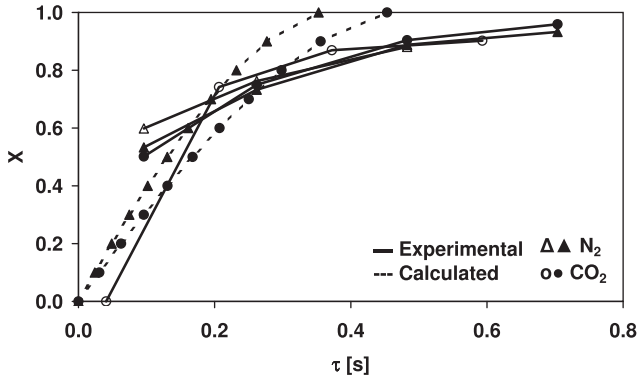

Fig. 10. Char conversion profiles obtained at 1373 K. The calculated profiles are found for a shrinking sphere in Zone III using Eq. (6) (▲, 6.2 vol.% O_2; △, 6.3 vol.% O_2; ●, 6.1 vol.% O_2; ○, 5.9 vol.% O_2). Oxygen concentrations are the averages of the local concentrations measured in each experiment. $\lambda \sim 4.1$.

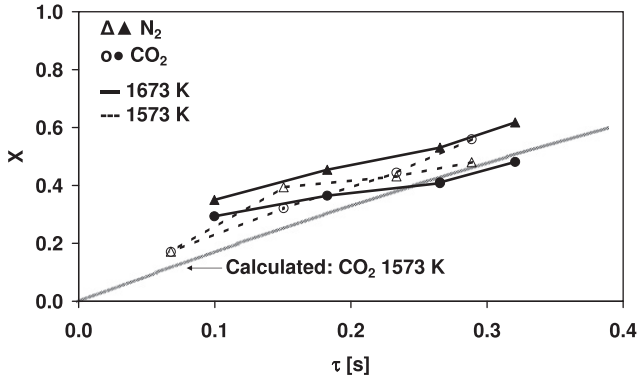

Fig. 11. Char conversion profiles obtained at 1673 K and 1573 K. The calculated profile is found for a shrinking sphere in Zone III using Eq. (6) (▲, 3.1 vol.% O_2; △, 3.4 vol.% O_2, ● 3.2 vol.% O_2; ○, 3.7 vol.% O_2). Oxygen concentrations are the averages of the local concentrations measured in each experiment. $\lambda \sim 2$.

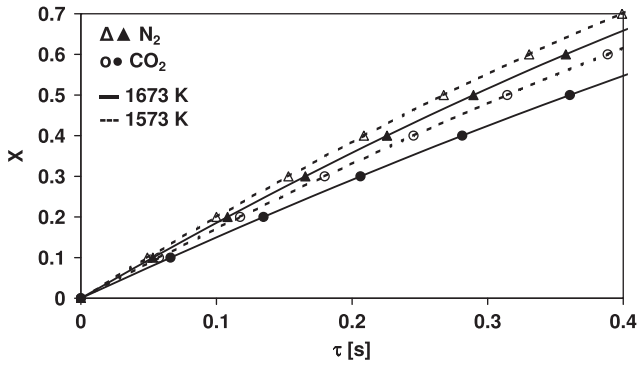

Fig. 12. Calculated char conversion profiles for a shrinking sphere in Zone III using Eq. (6).

That conversion rates in Fig. 12 are faster at the lower temperature illustrates the importance of the increased particle size at 1673 K, caused by an increase in swelling ratio, and the slightly higher experimental oxygen concentrations at 1573 K. These two factors outweigh the increase in O_2 diffusion coefficient from 1573 K to 1673 K and results in a faster char conversion rate at 1573 K.

4. Conclusion

Devolatilization and combustion of a bituminous coal have been studied in both N_2 and CO_2 based atmospheres under suspension fired conditions. Results have been obtained in the temperature range 1173–1673 K using inlet oxygen concentrations of 5–28 vol.% and sampling residence times up to approximately 1 s. No noticeable differences have been found in volatile yield between N_2 and CO_2 based environments and SEM images and N_2-BET surface areas of char obtained at 1673 K also show no differences between N_2 and CO_2 based atmospheres. This indicates that char properties are not influenced by the gas atmosphere for the investigated bituminous coal. The differences observed in the literature are believed to be caused by differences in particle temperature histories and long residence times, which can induce CO_2 gasification of reactive coals. With respect to char conversion, the data show no indication of char gasification by CO_2 and the rate of char conversion is identical at temperatures up to 1373 K in O_2/N_2 and O_2/CO_2 atmospheres. Experiments at 1573 K and 1673 K and low oxygen concentrations between 3.1 and 3.7 vol.% have however shown that the lower molecular diffusion coefficient of O_2 in CO_2 compared to N_2 becomes important when reaction is taking place under the influence of external mass transfer limitations leading to slower burnout in O_2/CO_2. Comparison of experimental char conversion profiles and profiles calculated for a shrinking sphere have shown the importance of considering the entire PSD and char morphology when modeling char oxidation.

Acknowledgement

The research leading to these results has received funding from the European Community's Research Fund for Coal and Steel (RFCS) under contract no. RFCR-CT-2006-00007, project FRIENDLY COAL, and is also sponsored by the Danish Agency for Science, Technology and Innovation. The support and funding from these entities are greatly valued.

References

[1] Davison J. Performance and costs of power plants with capture and storage of CO_2. Energy 2007;32:1163–6.
[2] Figueroa JD, Fout T, Plasynski S, McIlvried H, Srivastava RD. Advances in CO_2 capture technology – the US department of energy's carbon sequestration program. Int J Greenhouse Gas Control 2008;2:9.
[3] Buhre BJP, Elliot LK, Sheng CD, Gupta RP, Wall TF. Oxy-fuel combustion technology for coal-fired power generation. Prog Energy Combust Sci. 2005;31:283–7.
[4] Rathnam RK, Elliot LK, Wall TF, Liu Y, Moghtaderi B. Differences in reactivity of pulverized coal in air (O_2/N_2) and oxy-fuel (O_2/CO_2) conditions. Fuel Process Technol 2009;90:797–802.
[5] Al-Makhadmeh L, Maier J, Scheffknecht G. Coal pyrolysis and char combustion under oxy-fuel conditions. In: 34th international technical conference on coal utilization and fuel systems. Clearwater Florida; 2009.
[6] Borrego AG, Alvarez D. Comparison of chars obtained under oxy-fuel and conventional pulverized coal combustion atmospheres. Energy Fuels 2007;21:3171–9.
[7] Li Q, Zhao C, Chen X, Wu W, Li Y. Comparison of pulverized coal combustion in air and in O_2/CO_2 mixtures by thermo-gravimetric analysis. J Anal Appl Pyrolysis 2009;85:521–8.
[8] Duan L, Zhao C, Zhou W, Qu C, Chen X. Investigation on coal pyrolysis in CO_2 atmosphere. Energy Fuels 2009;23:3826.
[9] Jamil K, Hayashi J-i, Li C-Z. Pyrolysis of Victorian brown coal and gasification of nascent char in CO_2 atmosphere in a wire-mesh reactor. Fuel 2004;83:833–43.
[10] Várhegyi G, Szabó P, Jakab E, Till F. Mathematical modeling of char reactivity in Ar-O_2 and CO_2–O_2 mixtures. Energy Fuels 1996;10:1208–14.
[11] Bejarano PA, Levendis YA. Single-coal-particle combustion in O_2/N_2 and O_2/CO_2 environments. Combust Flame 2008;153:270–7.
[12] Bird RB, Stewart WE, Lightfoot EN. Transport phenomena. 2nd ed. John Wiley and Sons, Inc.; 2002.
[13] Yu J, Lucas JA, Wall TF. Formation of the structure of chars during devolatilization of pulverized coal and its thermoproperties. Prog Energy Combust Sci 2007;33:135.
[14] Molina A, Shaddix CR. Ignition and devolatilization of pulverized bituminous coal particles during oxygen/carbon dioxide combustion. Proc Combust Inst 2007;31:1905–12.
[15] Ballester J, Jiménez S. Kinetic parameters for the oxidation of pulverized coal as measured from drop tube tests. Combust Flame 2005;142:210–2.
[16] Chen W-H, Du S-W, Yang T-H. Volatile release and particle formation characteristics of injected pulverized coal in blast furnaces. Energy Convers Manage 2007;48:2025–33.

Coal Char Reactivity: A Thermogravimetric Study on Chars Obtained in O_2/N_2 and O_2/CO_2 in an Entrained Flow Reactor Under Suspension Fired Conditions and in a TGA.

Jacob Brix, Morten Storgaard Petersen, Jesper Banke Grossmann, Peter Glarborg, Peter Arendt Jensen, Anker Degn Jensen*

Department of Chemical and Biochemical Engineering, Building 229 Søltofts Plads, 2800 Kgs. Lyngby, Denmark
**Corresponding Author: e-mail: aj@kt.dtu.dk, Fax: +45 45 88 22 58, Phone: +45 45 25 28 41*

Abstract

Intrinsic kinetics for combustion and gasification of coal char has been studied by TermoGravimetric Analysis (TGA) in O_2/N_2 and O_2/CO_2 at 5 vol. % O_2 and in CO_2/N_2 at 80 vol. % CO_2. Chars were prepared in situ in the TGA in N_2 or in an Entrained Flow Reactor (EFR) in either O_2/N_2 or O_2/CO_2 under suspension fired conditions. Experiments did not reveal a change in char combustion reactivity with O_2 when N_2 was replaced with CO_2 during char formation and combustion. Gasification was seen in the TGA at temperatures above app. 1100 K in an O_2 free environment but in the presence of O_2 char consumption was completed below 1000 K. A gradual deactivation of chars produced in the EFR at progressively increasing temperatures was observed in the TGA. Combustion reactivity profiles of chars partly combusted in the EFR at high O_2 concentrations showed two distinct peaks indicating phases of different reactivity. This is attributed to high particle peak temperatures in the EFR that cause a molten/deactivated phase to form. An Arrhenius expression including both deactivation and activation energy is presented for both combustion and gasification.

Keywords: Oxy-fuel, Combustion, TGA, EFR, Char, Kinetics

1. Introduction

In the global political and scientific communities, it is a growing concern that anthropogenic CO_2 emissions seem to cause increasing temperatures on earth. As a result research programs to pursue alternative energy production technologies are initiated all over the world, many of which are focusing on the emission of CO_2 from fossil fuel combustion. Today fossil fuels account for approximately 85 % [1,2] of the power and heat production world wide wherefore new technologies, not presently mature, are unlikely to substitute fossil fuels such as coal the next several decades [3]. To accommodate this, power plants today relaying on conventional coal combustion are under strain to reduce their emissions through technological innovation.

A new technology that could prove able to reduce power plants CO_2 emissions markedly is the oxy-fuel combustion process. In oxy-fuel combustion, O_2 is separated from air before the boiler and mixed with recycled flue gas to obtain a plant exit stream of almost pure CO_2 [3,4]. This CO_2 stream can subsequently be stored in suitable geological formations such as depleted oil and gas reservoirs or saline aquifers [2,4].

Being an emerging technology many technical aspects still need to be clarified if oxy-fuel combustion is to be industrialized. A key aspect for industrialization is the clarification of coal and char combustion characteristics, and a question often raised is whether CO_2 gasification may contribute to char conversion or changes in char reactivity. To address these issues, experimental methods for reliable kinetic measurements must be established as the feature of CO_2 as a reactant that can influence devolatilization and char conversion is highly dependent on operating conditions. Furthermore, char formation and deactivation in O_2/N_2 and O_2/CO_2 must also be elucidated.

Li *et al.* [5] investigated pulverized bituminous coal pyrolysis and combustion in N_2 and CO_2 based atmospheres. They used a TGA at heating rates of 10, 20 and 30 K min^{-1}, a maximum temperature of 1273 K and particle sizes in the ranges < 48 μm, 48 – 74 μm and 74 – 90 μm. For their combustion experiments they used O_2 concentrations of 21, 30, 40 and 80 vol. % in CO_2 or air. From pyrolysis experiments Li *et al.* [5] saw an effect of CO_2 gasification at temperatures above 1073 K that resulted in a faster sample mass loss than in N_2. The quantitative effect of CO_2 gasification was small, however, and the overall pyrolysis mass loss rate was lower than 2.5 wt. % min^{-1} even at 1273 K. This is

consistent with results of Várhegyi *et al.* [6] and Rathnam *et al.* [7] who also saw a small quantitative effect of gasification above 1030 - 1073 K at similar conditions. Duan *et al.* [8] conducted TGA pyrolysis with a bituminous coal (< 100 μm) using either N_2 or CO_2 and heating rates of 10, 30, 50 or 70 K min^{-1}. Peak temperatures of 973 K, 1073 K, 1173 K or 1273 K were reached in their experiments. When N_2 was replaced with CO_2, Duan *et al.* [8] saw increases in weight loss of as much as 8 wt. % at 1273 K and gasification was initiated already at 753 K. This initiation temperature is much lower than found by Li *et al.* [5], Várhegyi *et al.* [6] and Rathnam *et al.* [7] and could indicate that the char used by Duan *et al.* [8] was particularly reactive. Even though CO_2 gasification was observed by Li *et al.* [5], Várhegyi *et al.* [6], Rathnam *et al.* [7] and Duan *et al.* [8], their results can not be transferred directly to industrial conditions as residence times used by the authors were from 10 min. and up whereas industrial scale pyrolysis is finished in a few hundred milliseconds.

In the presence of O_2 Li *et al.* [5] found an app. 7 % lower conversion rate in O_2/CO_2 than in O_2/N_2 at 21 vol. % O_2, which they attributed to a characteristic difference between N_2 and CO_2 based combustion. Further analysis of their results by the present authors yields activation energies in the range 20 – 50 kJ mol^{-1}, however; well below the values typically reported in the literature for char combustion under kinetic control. This implies that the difference encountered by Li *et al.* [5] arise from mass transfer limitations in their TGA. Using a char obtained from Drop Tube Furnace (DTF) pyrolysis of a low rank coal at 1673 K in N_2 Li *et al.* [9] also found that mass transfer influenced their TGA reactivity measurements resulting in activation energies of 82.46 kJ mol^{-1} and 74.66 kJ mol^{-1} in O_2/CO_2 and O_2/N_2 respectively.

Várhegyi *et al.* [6] conducted TGA experiments at O_2 concentrations between 5 and 100 vol. % using either Ar or CO_2 as balance gas under careful control of the combustion regime to ensure a kinetically controlled reaction. Using two different bituminous coals and a lignite coal Várhegyi *et al.* [6] did not find an effect of CO_2 when O_2 was present at heating rates of 10, 20 and 50 K min^{-1} to a maximum temperature of 1223 K. Similar experiments by Liu [10] and Rathnam *et al.* [7] support the conclusion of Várhegyi *et al.* [6]. In O_2/CO_2 Liu [10] found an activation energy of 127.8 kJ mol^{-1} for bituminous char and 138.0 kJ mol^{-1} for anthracitic char, both of which are consistent with literature

findings in O_2/N_2 [11]. Rathnam *et al.* [7] used a bituminous char pyrolized in a DTF at 1673 K in N_2, similar to the work of Li *et al.* [9], whereas Liu [10] prepared his chars at the same conditions as proximate analysis. Even though results of Li *et al.* [5], Li *et al.* [9], Várhegyi *et al.* [6], Liu [10] and Rathnam *et al.* [7] do not suggest that gasification is influencing intrinsic kinetics, it is not possible from their experiments to foresee a potential effect at suspension fired conditions as only Rathnam *et al.* [7] and Li *et al.* [9] prepared their chars in high temperature setups and both in N_2.

Zolin *et al.* [11] investigated the reliability of kinetic measurements by comparing TGA reactivities of a suite of coals, ranking from subbituminous to low volatile bituminous, with reactivities found from EFR experiments. Their TGA experiments were carried out isothermally in the temperature interval 723 – 923 K at 20 vol. % O_2 using in situ pyrolysis at 1173 K in N_2 to prepare chars from 90 – 105 μm coal samples. EFR reference experiments were carried out at 6 and 12 vol. % O_2 with coal particles in the size range 106 – 125 μm and combustion temperatures of approximately 1673 K. For most of the coals tested a good consistency in the trend of relative reactivities found in the TGA and EFR was seen, even though the absolute reactivity for individual coals deviated between the two setups. Zolin *et al.* [11] found that for some of the coals the reactivity dropped significantly when shifting the TGA with the EFR compared to the behavior of the other coals. This was explained by the authors with a high content of inertinite compared to vitrinite in these coals, causing a more severe deactivation at EFR conditions. The reactivity measured from TGA experiments were generally significantly higher than that measured from EFR experiments, witnessing of significant thermal deactivation of the char in the EFR. Zolin et al. [11] also saw deviations in reactivity between the TGA and EFR experiments caused by the catalytic effect of mineral matter in the TGA. The work of Zolin *et al.* [11] illustrates the inherent uncertainty that exists when kinetic parameters derived from TGA experiments where both pyrolysis and char oxidation is performed at low temperatures and heating rates are used at suspension fired conditions; a conclusion that is supported by the similar work of Manquais *et al.* [12] and from measurements of ignition temperatures in similar setups by Faúndez *et al.* [13].

The short review above shows that there is a need for a consistent TGA analysis of char reactivity in O_2/CO_2 and O_2/N_2 combustion at high temperatures. This paper presents a

reactivity study carried out on char formed in a TGA and in an EFR at suspension fired conditions in N_2 and CO_2 based atmospheres. From reactivity profiles consistent kinetic expressions for combustion and gasification are derived that allows extrapolation to temperatures of relevance in industrial boilers.

2. Experimental

All experiments presented here have been carried out in a thermogravimetric analyzer of the type Netzsch STA 449 F1 where gaseous atmospheres have been created by mixing bottled gases. Samples were placed in alumina crucibles and positioned automatically on a highly sensitive balance located in a chamber that was purged with 20 ml min^{-1} of N_2. This N_2 made up 20 vol. % of the total flow in all experiments. The weight of the sample and the crucible temperature were recorded continuously as reaction progressed. Temperature programs dictating heating rates and maximum temperatures were specified for the Netzsch STA 449 F1 and for each program a calibration curve was made to ensure that possible fluctuations caused by the TGA did not influence the experimental measurements. By repetition of experiments the deviation in weight losses was found to be less than 1 %.

Three different types of experiments have been carried out. The first type of experiments, with particles of El Cerrejón coal sieved into the size ranges 63 – 90, 90 – 106 and 150 - 180 μm, were done to establish experimental conditions where mass transfer limitations did not influence the combustion rate and to investigate at what temperature CO_2 gasification could be expected to influence the sample consumption rate. The ultimate and proximate analysis of the unsieved coal is shown in **Fejl! Henvisningskilde ikke fundet.**. The coal particles in all of these experiments were pyrolized in situ using N_2 and heating rates between 5 and 20 K min^{-1} to a maximum temperature of 1273 K. After pyrolysis the samples were allowed to cool to a temperature of 473 K at what point a heating rate of 5 or 10 K min^{-1} were used for non-isothermal char combustion at 5 vol. % O_2 in N_2 or CO_2. The maximum temperature of char combustion was 1373 K in all experiments and to evaluate the influence of sample mass on combustion regime samples of 2, 5 and 10 mg were used.

Table 1 Proximate and ultimate analysis of the coal used for experiments.

Proximate Analysis		**Value**
Upper heating value	MJ/kg ar	28.19
Effective heating value	MJ/kg ar	27.09
Moisture	Wt. % ar	5.0
Ash	Wt. % ar	9.6
Volatiles	Wt. % ar	34.9
Ultimate Analysis		
Carbon	Wt. % ar	68.9
Hydrogen	Wt. % ar	4.61
Oxygen (diff.)	Wt. % ar	9.82
Nitrogen	Wt. % ar	1.44
Sulfur	Wt. % ar	0.62

The second type of experiments were conducted using chars obtained from devolatilization and combustion of 90 – 106 μm El Cerrejón coal particles in an EFR designed to simulate suspension firing. The combustion experiments in the EFR were carried out isothermally at reactor temperatures of 1173 - 1673 K using inlet O_2 concentrations between 5 - 28 vol. % in either N_2 or CO_2. Devolatilization experiments were carried out in the same temperature interval in N_2 or CO_2 with app. 5 vol. % O_2 to overcome problems with tar clogging the sampling lines and ventilation. The EFR experiments are described in detail elsewhere [14]. Based on experience from the first type of TGA experiments a heating rate of 5 K min^{-1} were used to reach a maximum temperature of 1123 K and sample masses between 1.2 and 1.5 mg were combusted in 5 vol. % O_2 in either N_2 or CO_2 to ensure that the process took place in zone I.

The third type of experiment was carried out using the same char as in the second type of experiments, the same heating rate and the same sample masses. However the gas atmosphere consisted of 80 vol. % CO_2 and 20 vol. % N_2 and the peak temperature was 1473 K.

In the following, the reactivity, listed in the figures as $\frac{d(X)}{dt}$, is defined by (**1**) where m_0 is the initial mass of char (dry and ash-free) and m is the mass of char at time t (dry and ash-free).

$$\frac{d(X)}{dt} = -\frac{1}{m_0} \cdot \frac{d(m)}{dt} \qquad (1)$$

3. Results

3.1 The Role of Gasification

The effect of CO_2 gasification on char conversion was discussed in the introduction and for reliable conclusions to be drawn with respect to char oxidation by O_2 it is important to evaluate this effect in the present experiments. Figure 1 show the effect of gasification in the presence and absence of O_2.

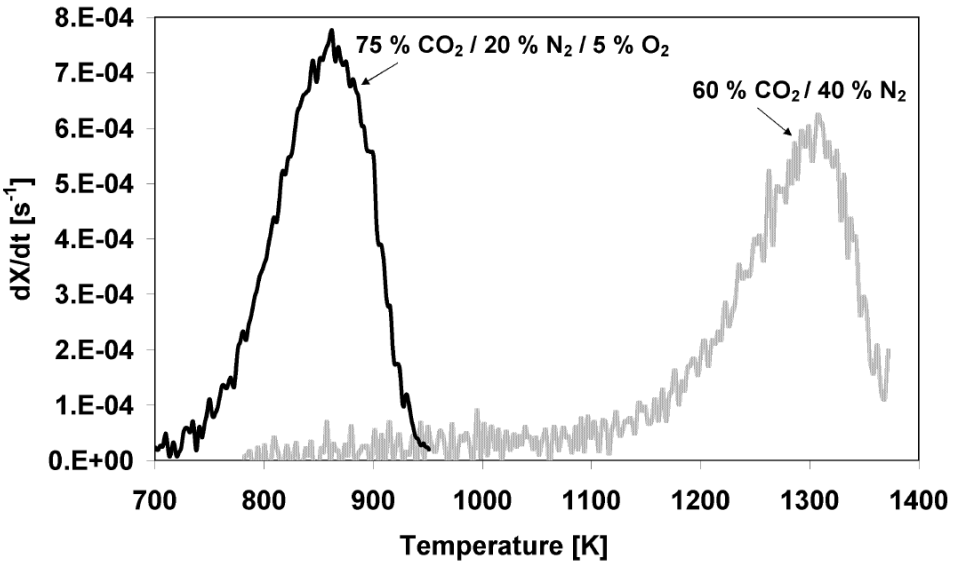

Figure 1 Reactivity of 63 – 90 μm coal particles pyrolized in N_2 using a heating rate of 20 K min^{-1} to a maximum temperature of 1273 K after which combustion/gasification is taking place from 473 K – 1373 K at a TGA heating rate 5 K min^{-1}. Sample masses were 5 mg.

The figure show an effect of CO_2 gasification at temperatures above approximately 1100 K, which is consistent with the results of Li *et al.* [5], Várhegyi *et al.* [6] and Rathnam *et*

al. [7]. This effect is however also seen to be negligible when O_2 is added to the system as the temperature window of char conversion is lowered significantly. This is consistent with the observations of Várhegyi *et al.* [6] and Rathnam *et al.* [7]. The same conclusion can be drawn from figure 2 that show reactivities of char obtained by devolatilization in the EFR at 1673 K in N_2. As all the combustion experiments in this study is carried out at 5 vol. % O_2 where no differences are seen to exist when either N_2 or CO_2 is used as carrier gas the remaining of the combustion experiments presented here have been carried out in O_2/N_2.

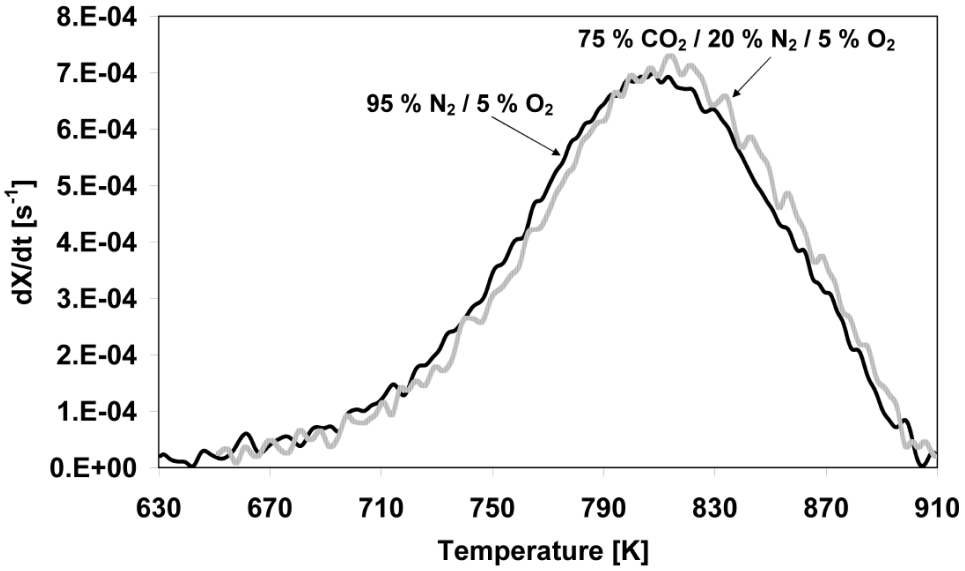

Figure 2 Combustion reactivity of EFR char obtained from devolatilization at 1673 K in N_2. A TGA heating rate of 5 K min^{-1} has been used to reach a maximum temperature of 1123 K. Sample masses were within 1.3 – 1.4 mg.

3.2 Combustion Reactivity of EFR Chars

When experiments to investigate char conversion are carried out under conditions resembling those found in a suspension fired boiler the influence of mass transfer phenomena make direct conclusions on intrinsic combustion reactivities difficult. To evaluate changes in intrinsic combustion reactivity when N_2 is replaced with CO_2 at suspension fired conditions a series of TGA experiments have been conducted on chars sampled in the EFR.

Figure 3 shows combustion TGA reactivity profiles of chars obtained by devolatilization at 1573 K and 1673 K in N_2 or CO_2 in the EFR. It is seen from the figure that the switch of carrier gas from N_2 to CO_2 at the high temperatures where the chars were formed does not cause a significant change in combustion reactivity. The small differences in combustion reactivity between N_2 and CO_2 chars observed in figure 3 is within the experimental repeatability of the EFR as discussed in [14] and particle to particle variations in the small sample masses used in the TGA.

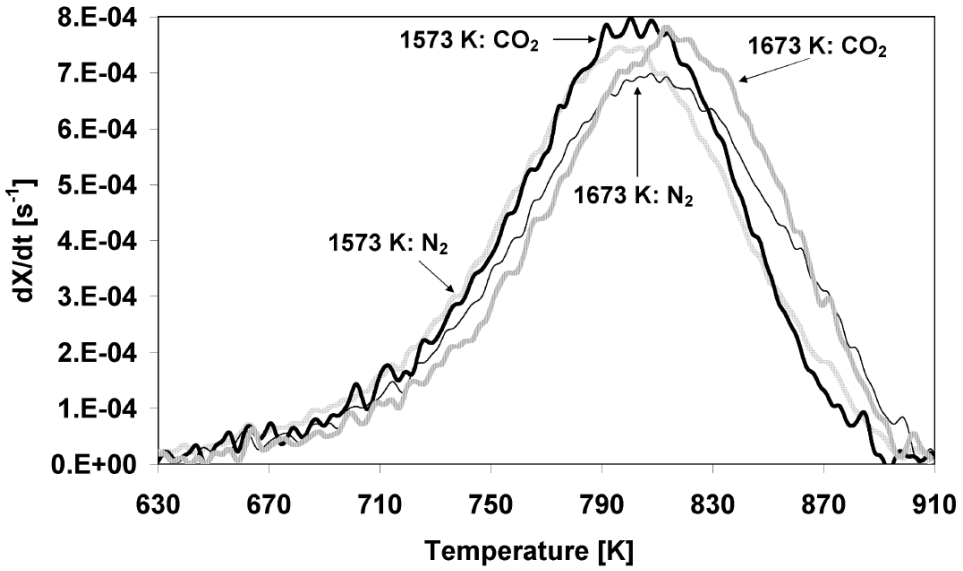

Figure 3 Combustion reactivity of EFR char obtained from devolatilization at 1573 K and 1673 K in N_2 and CO_2. A TGA heating rate of 5 K min^{-1} has been used to reach a maximum temperature of 1123 K in 5 vol. % O_2 and 95 vol. % N_2. Sample masses were within 1.2 – 1.5 mg.

The findings from figure 3 are consistent with related work [14,15] and they support conclusions that physical properties such as densities and heat capacities of N_2 and CO_2 [16] and their influence on flame propagation speed [17] are more likely to account for changes in ignition between O_2/CO_2 and O_2/N_2 atmospheres rather than the ability of CO_2 to react with the coal/char particles. However it is also important to stress that different ignition and combustion characteristics in O_2/CO_2 and O_2/N_2 are found for coals of different ranks [18].

In figure 4 and figure 5 the development of intrinsic combustion reactivity is followed as conversion is progressing in the EFR. Figure 4 shows combustion reactivity profiles of

char devolatilized at 1673 K and char partly combusted at 1673 K and 3.1 – 3.2 vol. % O_2 (measured at the sampling positions) in N_2 and CO_2 based atmospheres. The degree of char conversion in the EFR is listed for each of the profiles in figure 4. It is seen from these values that the char conversions are 21 and 29 % higher in O_2/N_2 relative to O_2/CO_2.

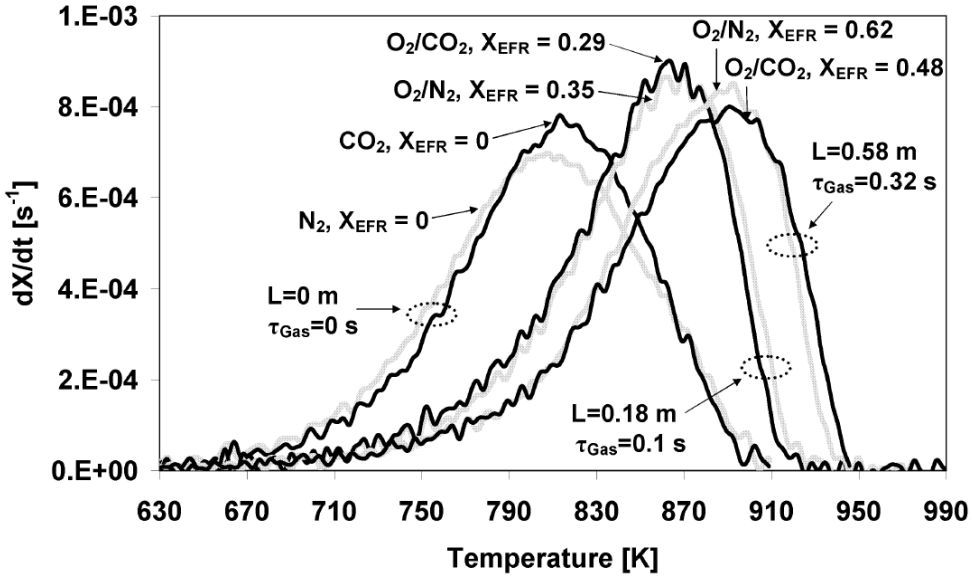

Figure 4 Combustion reactivity of EFR char obtained from devolatilization at 1673 K in N_2 and CO_2 and from combustion at 1673 K in 3.1 – 3.2 vol. % O_2 in N_2 or CO_2. A TGA heating rate of 5 K min^{-1} has been used to reach a maximum temperature of 1123 K in 5 vol. % O_2 and 95 vol. % N_2. Sample masses were within 1.2 – 1.5 mg.

This indicates that combustion in the EFR takes place in zone III as the diffusion coefficient of O_2 in N_2 is approximately 22 % higher than in CO_2 at 1673 K. Despite of the differences in char conversions there are no differences in combustion reactivity of chars sampled at the same position in the EFR. A clear char deactivation is seen however as the EFR residence time is increasing since the profiles are moving to higher temperatures.

Figure 5 shows combustion reactivity profiles of char devolatilized at 1173 K in CO_2 and char partly combusted at 1173 K and 27.7 – 27.9 vol. % O_2 (measured at the sampling positions) in N_2 and CO_2 based atmospheres. It is seen from the figure that the combustion reactivity of devolatilized char (X = 0) and that of char sampled shortly after

devolatilization (X = 0.17, X = 0.02) show a single peak whereas a second peak at around 900 K starts to appear at X = 0.50 and X = 0.51. At the highest degrees of conversion the char clearly consists of two constituents of different reactivity.

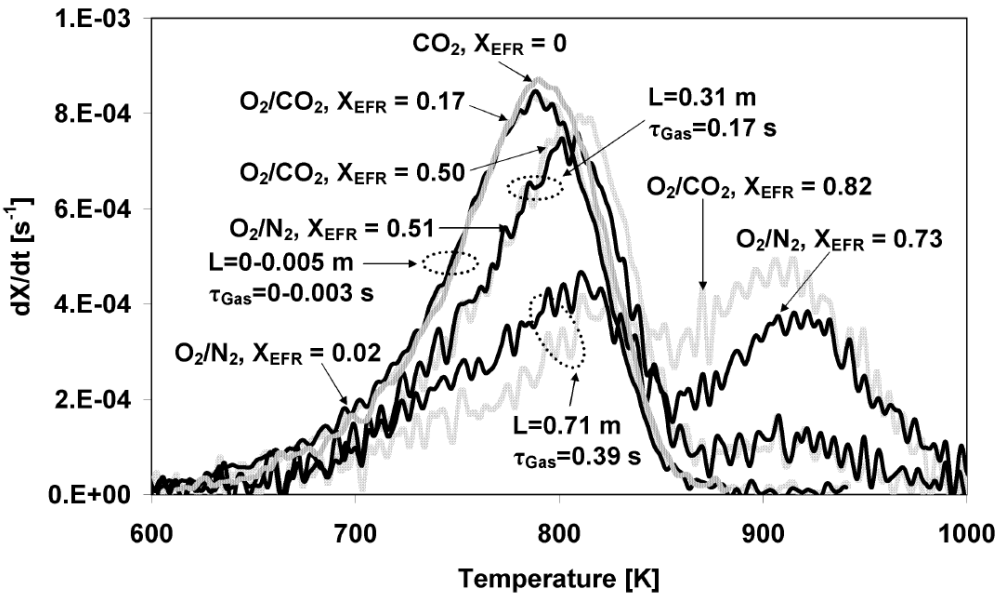

Figure 5 Combustion reactivity of EFR char obtained from devolatilization at 1173 K in CO_2 and by combustion at 1173 K in 27.7 – 27.9 vol. % O_2 in N_2 or CO_2. A TGA heating rate of 5 K min^{-1} has been used to reach a maximum temperature of 1123 K in 5 vol. % O_2 and 95 vol. % N_2. Sample masses were within 1.2 – 1.5 mg.

Zhang et al. [19] reported similar observations, which they attributed to the existence of a mineral cluster phase formed by a melt of inorganic components and trapped volatiles arising from a fierce devolatilization. That such a phase could be formed is supported by complementary work from the present authors [15]. Here it was found from modeling of single particle combustion that high particle peak temperatures (~ 1773 K) were reached shortly after heterogeneous ignition suggesting the existence of a second devolatilization. According to the model some particles reached their peak temperature at heating rates as high as 20000 K s^{-1}. Scanning Electron Microscopy (SEM) images also showed intact particles at high overall degrees of char conversion [15]. In figure 5 the development of a second phase is seen to proceed identically in O_2/N_2 and O_2/CO_2 with a peak temperature that is unchanged as char conversion in the EFR progress.

3.3 Kinetics of EFR Char Combustion and Gasification

An important feature of the thermogravimetric analyzer is its capability to combust well defined sample masses in the absence of mass transfer limitations. For this reason it is often used to extract intrinsic kinetic parameters for combustion and gasification of coal and char.

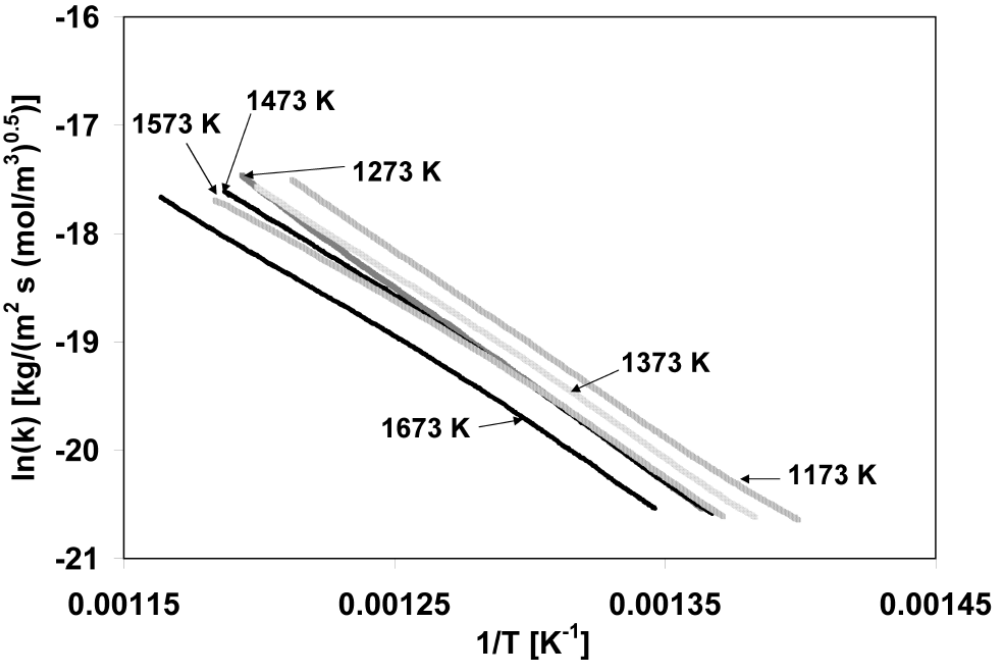

Figure 6 Arrhenius plots of combustion rate constants for char obtained by devolatilization in the EFR in CO_2.

Figure 6 and figure 7 shows Arrhenius plots for combustion and gasification of EFR chars obtained by devolatilization in CO_2 respectively. Due to a limited amount of char only three Arrhenius plots are shown in figure 7 for gasification by CO_2. Reaction rates covering char consumption between 10 % and 90 % conversion in the TGA are represented in both figures. The rate constants have been found from equation (2) with a specific char surface area, S_0, of 240 m^2 g^{-1} found from BET measurements [15]. The concentration of O_2 or CO_2, C, are found using the temperature measurements at each data point.

$$k = \frac{d(X)}{dt} \cdot (1 - X)^{-1} \cdot S_0^{-1} \cdot \left(C^n\right)^{-1} \tag{2}$$

The kinetic parameters found from the TGA data have been used in modeling work at the conditions of the EFR [15] and a decision must therefore be made when determining the reaction orders n as these are known to vary between temperatures. For combustion intrinsic reaction orders between 0.5 – 1 have been reported for the temperature interval used in the TGA [20] while intrinsic reaction orders between 0 – 1, though with the majority being 0, have been reported at the temperature interval used in the EFR [21]. To make the kinetic parameters as consistent as possible when they are found at low temperatures but used at high temperatures a reaction order of 0.5 has been chosen for use in equation (2). For gasification, intrinsic reaction orders found in the literature varies around 0.5 [22,23] and this value of reaction order has therefore been chosen for use in equation (2).

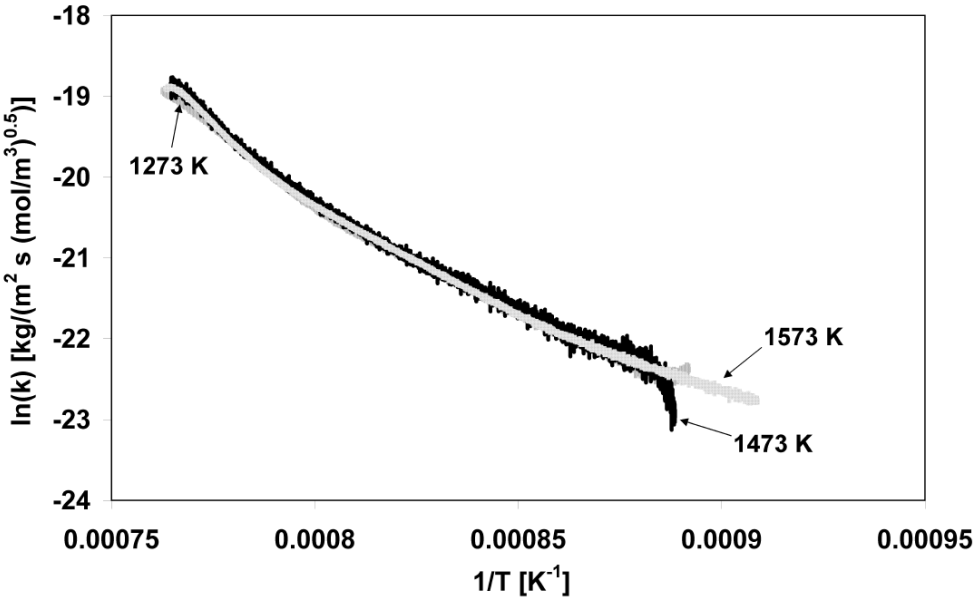

Figure 7 Arrhenius plots of gasification rate constants for char obtained by devolatilization in the EFR in CO_2.

Linear regression on the data in figure 6 and figure 7 yields the activation energies, E_A, and the pre-exponential factors, A_0, shown in table 1 and table 2.

Table 1 Activation energies and pre-exponential factors found from linear regression on the combustion data in figure 6. Also shown in the table are average combustion temperatures and standardized pre-exponential factors defined by (3).

T_{EFR} [K]	E_A [kJ mol^{-1}]	A_0 [kg m^{-2} s^{-1} (mol m^{-3})$^{-0.5}$]	T_{Avg} [K]	k_0 [kg m^{-2} s^{-1} (mol m^{-3})$^{-0.5}$]
1173 K	141.5	22.3	769	12
1273 K	148.6	46.5	785	8.5
1373 K	138.1	10.8	778	9.8
1473 K	138.0	8.6	786	8
1573 K	130.0	2.3	787	7.7
1673 K	128.9	1.5	801	5.4
Avg.	137.5 +/- 7.4			

Table 2 Activation energies and pre-exponential factors found from linear regression on the gasification data in figure 7. Also shown in the table are average combustion temperatures and standardized pre-exponential factors defined by (3).

T_{EFR} [K]	E_A [kJ mol^{-1}]	A_0 [kg m^{-2} s^{-1} (mol m^{-3})$^{-0.5}$]	T_{Avg} [K]	k_0 [kg m^{-2} s^{-1} (mol m^{-3})$^{-0.5}$]
1273 K	232.5	8.3	1216	7.0547
1473 K	238.5	15.9	1216	7.4273
1573 K	221.5	3	1205	7.5026
Avg.	230.8 +/- 8.6			7.3282 +/- 0.2398

For combustion similar activation energies are obtained for chars formed at each of the devolatilization temperatures used in the EFR but there are variations in the pre-exponential factors. As char consumption between X = 0.1 – 0.9 is taking place in a narrow temperature window of 110 – 130 K an average combustion temperature, listed in table 1, is used to define a standardized reactivity of the individual chars. Using equation (3) a new pre-exponential factor, k_0, is then defined for each char using the average activation energy of all chars. These standardized pre-exponential factors are also listed

in table 1 and they are seen to show a more consistent trend of decrease as the devolatilization temperature at which the chars were formed increases.

$$k_0 = A_0 \cdot \exp\left(\frac{1}{R \cdot T_{Avg}} \cdot \left(E_{A,Avg} - E_A \right) \right) \qquad (3)$$

The trend in the standardized pre-exponential factors in table 1 is a measure of deactivation caused by the increasing char formation temperatures. Figure 8 shows the Arrhenius plot of the standardized pre-exponential factors found by equation (3) from which linear regression yields a deactivation energy, E_D, of 20.5 kJ mol^{-1} and a pre-exponential factor, k_0^*, of 1.4359 kg m^{-2} s^{-1} (mol m^{-3})$^{-0.5}$.

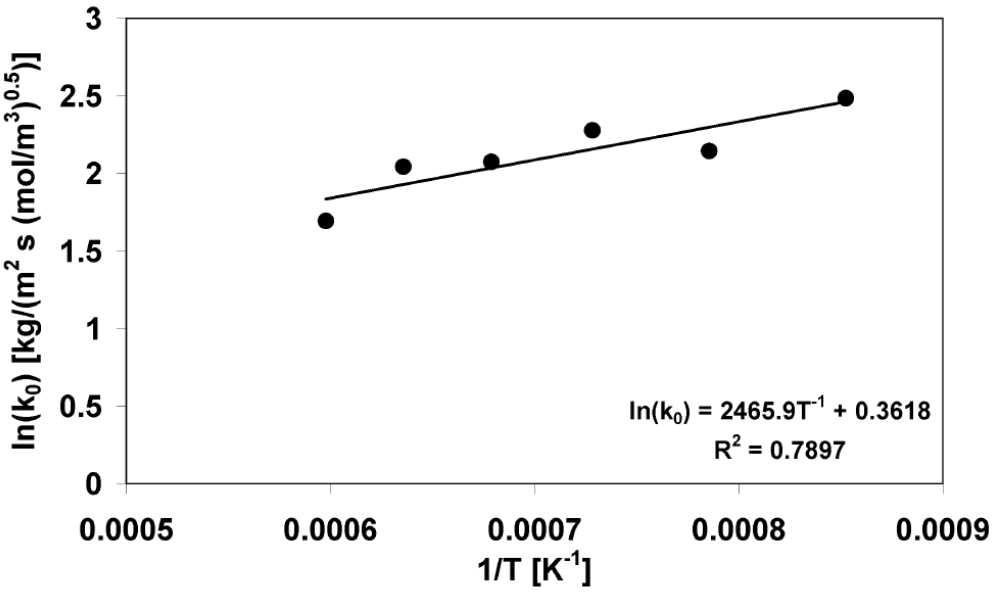

Figure 8 Arrhenius plot of the standardized pre-exponential factors in table 1.

In table 2 and from figure 7 it is seen that similar activation energies are found for gasification of each of the chars but that pre-exponential factors are fluctuating, similar to what was found for combustion. The standardized pre-exponential factors in table 2, found from equation (3), do not however show any trend towards deactivation. Rather

they are nearly constant implying a deactivation energy of 0 kJ mol^{-1} and an average standardized pre-exponential factor of 7.3282 kg m^{-2} s^{-1} $(mol\ m^{-3})^{-0.5}$.

From the kinetic analysis of combustion and gasification above, a general Arrhenius expression that includes thermal deactivation as well as the traditional activation exponential can be defined as in equation (4). When equation (4) is used T^* is the highest temperature a particle has reached at any degree of conversion, which assumes a rapid deactivation to a pseudo steady value at any given T^*. For gasification the deactivation part in equation (4) will cancel and the expression will reduce to a normal Arrhenius expression.

$$k = k_0^* \cdot \exp\left(\frac{E_D}{R \cdot T^*}\right) \cdot \exp\left(\frac{-E_A}{R \cdot T}\right) \qquad (4)$$

The rate constant in (4) has been used successfully for both combustion and gasification to describe the EFR experiments in a parallel work by the authors [15].

4. Conclusion

Combustion and gasification of char has been studied in a ThermoGravimetric Analyzer (TGA). Chars were prepared from in situ pyrolysis in the TGA using N_2 and from devolatilization and combustion in O_2/N_2 and O_2/CO_2 in an Entrained Flow Reactor (EFR) under suspension fired conditions. From experiments on TGA chars in CO_2/N_2 and $O_2/CO_2/N_2$ it was found that the influence of CO_2 gasification during combustion in the TGA was negligible in the temperature window where the chars were converted.

Combustion reactivity profiles of EFR chars did not reveal any differences between chars obtained by devolatilization in N_2 and CO_2. The development of two char constituents with different reactivity was seen when combustion in the EFR was taking place at high O_2 concentrations of about 28 vol. %. This is attributed to high particle peak temperatures that cause a highly deactivated phase, composed of organic as well as inorganic components, to form in some particles.

Intrinsic kinetics in terms of Arrhenius parameters for combustion and gasification were obtained from reactivity profiles of char formed at temperatures between 1173 K and 1673 K in the EFR. For combustion it was found that significant char deactivation was taking place in the EFR as the reactor temperature increased and the kinetic expression for combustion therefore includes a deactivation term. Surprisingly, deactivation with respect to CO_2 gasification was not observed for the same chars wherefore this reaction is described adequately by a traditional Arrhenius expression.

The results presented here confirm that TGA experiments can be a useful tool for the examination of chars obtained at industrially relevant conditions as the TGA allows for pure zone I operation and for elucidation of reactivity distributions within the same particle sample, seen as multiple peaks in the reactivity profile.

Acknowledgement

The research leading to these results has received funding from the European Community's Research Fund for Coal and Steel (RFCS) under contract n° RFCR-CT-2006-00007, project FRIENDLYCOAL, and is also sponsored by the Danish Agency for Science, Technology and Innovation and Energinet.dk. The support and funding from these entities are greatly valued.

References

[1] Davison J. Performance and costs of power plants with capture and storage of CO_2. Energy 2007;32:1163-6.

[2] Figueroa JD, Fout T, Plasynski S, McIlvried H, Srivastava RD. Advances in CO_2 capture technology-The U.S. department of energy's carbon sequestration program. Int J Greenhouse Gas Control 2008;2:9-0

[3] Buhre BJP, Elliot LK, Sheng CD, Gupta RP, Wall TF. Oxy-fuel combustion technology for coal-fired power generation. Prog Energy Combust Sci. 2005;31:283-7

[4] Toftegaard MB, Brix J, Jensen PA, Glarborg P, Jensen AD. Oxy-fuel combustion of solid fuels. Prog Energ Combust 2010;36:581-5

[5] Li Q, Zhao C, Chen X, Wu W, Li Y. Comparison of pulverized coal combustion in air and in O_2/CO_2 mixtures by thermo-gravimetric analysis. J. Anal. Appl. Pyrolysis 2009;85:521-8

[6] Várhegyi G, Szabó P, Jakab E, Till F, Richard J-R. Mathematical modeling of char reactivity in Ar-O_2 and CO_2-O_2 mixtures. Energy Fuels 1996;10:1208-4

[7] Rathnam RK, Elliott LK, Wall TF, Liu Y, Moghtaderi B. Differences in reactivity of pulverized coal in air (O_2/N_2) and oxy-fuel (O_2/CO_2) conditions. Fuel Process. Technol. 2009;90:797-2

[8] Duan L, Zhao C, Zhou W, Qu C, Chen X. Investigation on coal pyrolysis in CO_2 atmosphere. Energy Fuels 2009;23:3826-0

[9] Li X, Rathnam RK, Yu J, Wang Q, Wall T, Meesri C. Pyrolysis and combustion characteristics of an Indonesian low-rank coal under O_2/N_2 and O_2/CO_2 conditions. Energy Fuels 2010;24:160-4

[10] Liu H. Combustion of coal chars in O_2/CO_2 and O_2/N_2 mixtures: A comparative study with non-isothermal thermogravimetric analyzer (TGA) tests. Energy Fuels 2009;23:4278-5

[11] Zolin A, Jensen A, Pedersen LS, Dam-Johansen K, Tørslev P. A comparison of coal char reactivity determined from thermogravimetric and laminar flow reactor experiments. Energy Fuels 1998;12:268-6

[12] Manquais KL, Snape C, McRobbie I, Barker J, Pellegrini V. Comparison of the combustion reactivity of TGA and drop tube furnace chars from a bituminous coal. Energy Fuels 2009;23:4269-7

[13] Faúndez J, Arenillas A, Rubiera F, García X, Gordon AL, Pis JJ. Ignition behavior of different rank coals in an entrained flow reactor. Fuel 2005;23:2172-7

[14] Brix J, Jensen PA, Jensen AD. Coal devolatilization and char conversion under suspension fired conditions in O_2/N_2 and O_2/CO_2 atmospheres. Fuel 2010;89:3373-0

[15] Brix J et al. Modeling Char Conversion under Suspension Fired Conditions in O_2/N_2 and O_2/CO_2 Atmospheres. Article in progress

[16] Molina A, Shaddix CR. Ignition and devolatilization of pulverized bituminous coal particles during oxygen/carbon dioxide coal combustion. Proc Combust Inst 2007;31:1905-2

[17] Suda T, Masuko K, Sato J, Yamamoto A, Okazaki K. Effect of carbon dioxide on flame propagation of pulverized coal clouds in CO_2/O_2 combustion. Fuel 2007;86:2008-5

[18] Bejarano PA, Levendis YA. Single-coal-particle combustion in O_2/N_2 and O_2/CO_2 environments. Combust Flame 2008;153:270-7

[19] Zhang H, Pu W-X, Ha S, Li Y, Sun M. The influence of included minerals on the intrinsic reactivity of chars prepared at 900 ^{o}C in a drop tube furnace and a muffle furnace. Fuel 2009;88:2303 – 0

[20] Hurt RH, Haynes BS. On the origin of power-law kinetics in carbon oxidation. Proc Combust Inst 2005;30:2161-8

[21] Hurt RH, Calo JM. Semi-global intrinsic kinetics for char combustion modeling. Combust Flame 2001;125:1138-9

[22] Kajatani S, Hara S, Matsuda H. Gasification rate analysis of coal char with a pressurized drop tube furnace. Fuel 2002;81:539-6

[23] Liu H, Luo C, Toyota M, Uemiya S, Kojima T. Kinetics of CO_2/char gasification at elevated temperatures. Part II: Clarification of mechanism through modeling and char characterization. Fuel Process. Technol. 2006;87:769-4

Fuel 90 (2011) 2224–2239

Contents lists available at ScienceDirect

Fuel

journal homepage: www.elsevier.com/locate/fuel

Modeling char conversion under suspension fired conditions in O_2/N_2 and O_2/CO_2 atmospheres

Jacob Brix, Peter Arendt Jensen, Anker Degn Jensen *

Department of Chemical and Biochemical Engineering, Building 229, Søltofts Plads, 2800 Kgs. Lyngby, Denmark

ARTICLE INFO

Article history:
Received 7 October 2010
Received in revised form 5 January 2011
Accepted 10 January 2011
Available online 25 January 2011

Keywords:
Oxy-fuel
Combustion
Char
Modeling

ABSTRACT

The aim of this investigation has been to model combustion under suspension fired conditions in O_2/N_2 and O_2/CO_2 mixtures. Experiments used for model validation have been carried out in an electrically heated Entrained Flow Reactor (EFR) at temperatures between 1173 K and 1673 K with inlet O_2 concentrations between 5 and 28 vol.%. The COal COmbustion MOdel, COCOMO, includes the three char morphologies: cenospheric char, network char and dense char each divided between six discrete particle sizes. Both combustion and gasification with CO_2 are accounted for and reaction rates include thermal char deactivation, which was found to be important for combustion at high reactor temperatures and high O_2 concentrations. COCOMO show in general good agreement with experimental char conversion profiles at conditions covering zone I–III. From the experimental profiles no effect of CO_2 gasification on char conversion has been found. COCOMO does however suggest that CO_2 gasification in oxy-fuel combustion at low O_2 concentrations can account for as much as 70% of the overall char consumption rate during combustion in zone III.

1. Introduction

There is an increasing global focus on the anthropogenic CO_2 emission to the atmosphere due to its claimed effect on the earth's climate. This focus has caused fossil fuelled power plants to explore technologies that will allow them to keep using fossil fuels, such as coal, as a feedstock while reducing CO_2 emissions markedly. One technology is oxy-fuel combustion in which near pure O_2 is mixed with recycled flue gas at the entrance to the boiler, thereby creating a plant exit stream of almost pure CO_2 [1]. This CO_2 stream can subsequently be sent to storage in geological formations such as saline aquifers or depleted oil and gas fields [2].

An important part of the scale up process of the oxy-fuel technology is clarifying differences in char conversion rates between this technology and conventional air-blown combustion. As it is the time required for char conversion that determines the size of a boiler and its heat release profile it is also important that predictive modeling tools are developed.

There exist many attempts to model char combustion in the literature [3–10]. Many of the models are very detailed in their description of char morphology, particle size, fragmentation, ash inhibition, thermal char deactivation and film layer mass transport of O_2, which also means that their outcome is depending on a wide range of parameters that are often related to specific experimental conditions and equipment. A more detailed model does however in general do a better job in predicting the combustion process than simple global models.

In their Char Burnout Kinetic (CBK) model Hurt et al. [4] described the oxidation of coal char and thereby estimated the fly ash carbon content. The model includes thermal annealing, statistical kinetics and char densities as well as ash inhibition. The ability of the model to predict a decrease in conversion rate at high degrees of conversion ($X > 90\%$), where many other models fail, were mostly due to the inclusion of ash inhibition. The effect of ash inhibition or ash retention on the conversion rate were also investigated by Murphy and Shaddix [5] using a shrinking sphere approach. They showed that low or even negative apparent Arrhenius reaction orders could be expected at the late stages of char combustion ($X > 70\%$). Murphy and Shaddix [5] did not find that ash retention caused a decrease in char conversion rate at conversions below approximately 90%. On the contrary the lower carbon density caused by the retention of ash caused slightly higher conversion rates in the earlier stages of combustion than did predictions without ash retention.

In the development of the CBK model Hurt et al. [11] examined the effect of coal heterogeneity and found that a distribution of pre-exponential Arrhenius factors, accounting for the heterogeneity of a Particle Size Distribution (PSD), improved burnout predictions especially during zone I combustion, where no mass transport limitations exist and conversion rate is

* Corresponding author. Tel.: +45 45 25 28 41; fax: +45 45 88 22 58.
E-mail address: aj@kt.dtu.dk (A.D. Jensen).

0016-2361/$ - see front matter © 2011 Elsevier Ltd. All rights reserved.
doi:10.1016/j.fuel.2011.01.021

Symbols

A	area (m^2) or pre-exponential Arrhenius factor ($kg\,m^{-2}\,s^{-1}(mol\,m^{-3})^{-0.5}$)
a	polynomial coefficient (K^{-2}) or ( )
b	polynomial coefficient (K^{-1})
C	heat capacity ($J\,kg\,K^{-1}$) or ($J\,mol^{-1}\,K^{-1}$) or concentration ($mol\,m^{-3}$)
c	polynomial coefficient (K^2)
D	diffusion coefficient ($m^2\,s^{-1}$) or diameter (m)
d	char pore- or particle diameter (m)
E	activation- or deactivation energy ($J\,mol^{-1}$)
EF	Einstein function
$\bar{e}$	char emissivity
F	gaseous flow rate ($mol\,s^{-1}$)
g	gravity ($m\,s^{-2}$)
H	enthalpy ($J\,mol^{-1}$) or ($J\,kg^{-1}$)
ΔH	reaction enthalpy ($J\,mol^{-1}$) or ($J\,kg^{-1}$)
h	heat transfer coefficient ($W\,m^{-2}\,K^{-1}$)
k	rate constant ($kg\,m^{-2}\,s^{-1}(mol\,m^{-3})^{-0.5}$) or mass transfer coefficient ($m\,s^{-1}$)
L	reactor length (m)
M	molar mass ($kg\,mol^{-1}$) or ($g\,mol^{-1}$)
m	mass (kg)
N	number quantity or particle concentration (m^{-3})
n	reaction order
P	pressure (Pa), (Bar) or (atm)
Pr	Prandtl's number
Q	convective heat transfer ($W\,m^{-3}$) or heating value ($J\,kg^{-1}$)
R	radius (m) or gas constant ($J\,mol^{-1}\,K^{-1}$) or ($J\,kg^{-1}\,K^{-1}$)
Re	Reynolds number
r	reaction rate ($mol\,m^{-3}\,s^{-1}$) or (s^{-1})
S	specific surface area ($m^2\,kg^{-1}$)
Sc	Schmidt's number
T	temperature (K)
V	volume (m^3)
VM	volatile fraction
W	initial weight percent of particle size k
w	molar fraction of a char constituents (*daf*)
X	char conversion
x	molar fraction
z	oxidizer to fuel ratio
α	initial weight fraction of a char morphology
δ	cenosphere wall thickness (μm) or cenosphere wall thickness divided by cenosphere radius
ε	char porosity
ε/κ	Lennard-Jones parameter (K)
ς	stoichiometric coefficient
η	internal particle effectiveness factor
Θ	initial weight fraction of a particle size
θ	Einstein temperature (K)
Λ	stoichiometric coefficient of heterogeneous reaction
λ	thermal conductivity ($W\,m^{-1}\,K^{-1}$)
μ	viscosity (Pa s)
ν	linear velocity ($m\,s^{-1}$)
ρ	skeletal density (unless indexed by superscript a) ($kg\,m^{-3}$)
σ_{SB}	Stefan–Boltzmann constant ($W\,m^{-2}\,K^{-4}$)
σ	Lennard-Jones parameter (Å)
$\overline{\tau}$	tortuosity
ϕ	thiele modulus
Ψ	particle sphericity
Ω	collisional integral

Subscripts

A	activation
a	stoichiometric coefficient of carbon in char
b	stoichiometric coefficient of hydrogen in char
C	cenospheric char
c	mass transfer coefficient
D	deactivation or dense char
d	stoichiometric coefficient of nitrogen in char
daf	dry and ash free basis
e	stoichiometric coefficient of sulfur in char
F	funnel of sampling probe
G	index of all gaseous species
f	gas film layer property
H	index of all homogeneous reactions
h	index of gaseous component
I	cenosphere cavity radius
i	index of homogeneous reaction
j	index of gaseous component
K	Knudsen diffusivity
k	index of initial particle size
LHV	lower heating value
l	index of char morphology
m	relating property to mass
mix	property of N_2, CO_2 and O_2 mixture
N	network char
p	particle property or constant pressure gas property
pore	pore property
R	reactor property
r	index of gaseous reactant
s	particle slip velocity
T	total amount
u	stoichiometric coefficient of ash in char
Wall	wall of a particle
w	reactor wall property
y	stoichiometric coefficient of oxygen in char
0	initial property

Superscripts

a	apparent density
B	bulk gas property
n	reaction order
S	particle surface property
$*$	effective diffusivity
^	mean gas flow
•	dimensionless property
x	based on mass
∼	flow in time

determined only by chemical kinetics, and in the case of broad PSD's. The estimation of kinetic parameters is often a cause for concern in modeling. It has been found that the intrinsic reactivity of bituminous char decreases as the particle temperature and heating rate during pyrolysis increases. This is due to an increased graphitization of the char leading to more basal planes that have a lower content of active carbon sites [12]. The effect of thermal deactivation along with an exact determination of intrinsic kinetic parameters, obtained in zone I, needs to be accounted for in trustworthy kinetic expressions that are to be used for combustion across zone I–III where mass transfer limitations on reactants gradually cause concentration gradients to form in the particles as the effective concentrations on their surfaces approach zero.

An important feature of many detailed combustion models is the presence of char of different morphologies. Cloke et al. [6] conducted Drop Tube Furnace (DTF) experiments at 1573 K, 1423 K and 1273 K using pulverized coal in the size range 106–125 μm at 5% O_2. The coal was first devolatilized at the different temperatures using 1% O_2. Through digital images, taken under a microscope and analyzed by a computer, they divided the chars into three categories: cenospheric char, network char and mixed char, the latter category being predominately dense. Similar char classifications are suggested by other researchers [7,13,14]. The char size distribution was described by Cloke et al. [6] using eight discrete intervals covering particles between 0 and 150 μm. With char morphology as input in the CBK model they found relatively good agreement between simulations and experimental results, though with a tendency of under prediction by the model. This under prediction was attributed to an over estimation of ash inhibition in the beginning of the process, i.e. the opposite of what was found by Murphy and Shaddix [5]. This contradiction witness of the sensitivity of detailed models to inputs such as ash/char porosities, pore sizes, turtoisities and the way in which phenomena such as ash inhibition are described. In a later paper Cloke et al. [7] conducted similar experiments at 1573 K using 15 different coals. The chars were classified from image analysis both as individual coals and as a collected standardized set of input data covering all coals. Results of predicted char burnout showed reasonable agreement with experimental results when both types of char classification were used as model input, suggesting that a generalized morphological description of char can enhance the accuracy of model prediction without the need for specific experimental measurements.

Experimental char conversion data obtained under oxy-fuel combustion at high temperatures have been published by several authors [15–19] and low temperature data are also available in the literature [17,20–22]. Data obtained at high temperatures at conditions that are encountered in industrial boilers are contradictory regarding the effect of CO_2 gasification. In addition the effect of CO_2 gasification suggested by some TGA investigations appear more likely to be caused by the long residence times and low O_2 concentrations used in the experiments.

In the present investigation char consumption from reaction with both O_2 and CO_2 is included in a detailed single particle combustion model as an attempt to elucidate under what conditions CO_2 gasification can be expected to contribute to fuel conversion. Model predictions are compared with an extensive data set covering suspension fired O_2/N_2 and O_2/CO_2 combustion under a wide range of conditions. Conclusions are hereafter drawn from particle conversion rates, temperature histories and optical appearances determined by Scanning Electron Microscopy (SEM).

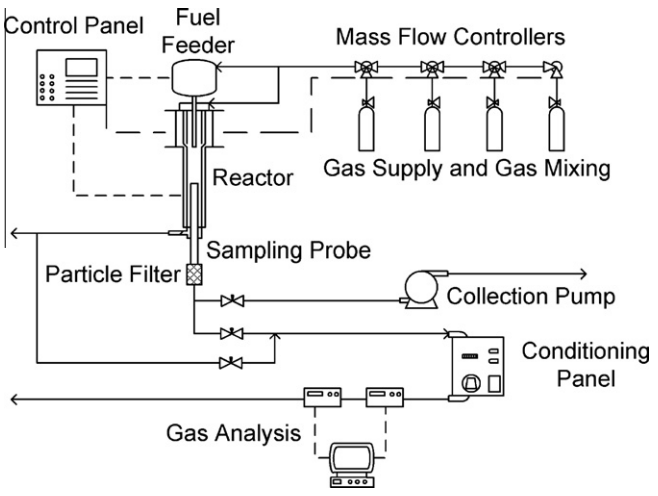

Fig. 1. Experimental setup. Solid lines indicate tubes and dashed lines indicate wires for control and data logging. All streams leaving the setup is sent to a central ventilation system.

2. Experimental

The experiments were carried out in an electrically heated EFR and are previously described in the literature [15]. All data on char conversion presented in this text is taken directly from this reference. The reactor is cylindrical and measures 2 m in length, 0.08 m in diameter and is shown schematically in Fig. 1 along with its utilities. The reaction zone is heated by seven electrical heating elements and can reach temperatures up to 1773 K. On top of the reactor a 0.8 m long gas preheater, consisting of two heating elements, preheats the secondary gas stream to a prescribed temperature. Coal is fed to the reactor at a constant rate of 50 g h^{-1} using a dosing system consisting of a silo and a screw feeder connected to a vibration transporter. Coal injection into the top of the reaction zone is done through a water cooled probe that goes through the center of the gas preheater.

During experiments char has been sampled at different reactor positions using a water cooled sampling probe with an outer radius of 0.017 m. The sampling end of this probe is shaped as a funnel. Sampling has been done iso-kinetically with an average gas velocity of 1.81 m s^{-1} in all the experiments. Through the probe, gas sampling for analysis for CO, CO_2 and O_2 has also been done at each sampling point. Except when experiments were carried out in air all gaseous environments used in the experiments were created by mixing bottled gases.

Experiments were carried out in the temperature interval 1173–1673 K with increments of 100 K. Inlet O_2 concentrations were in the range 5–28 vol.%, corresponding to stoichiometric ratios between 2 and 15, with either N_2 or CO_2 as carrier gas. O_2 concentrations given in this paper are however lower, as these are measured after complete devolatilization and are the concentrations experienced by the burning char particles. During experiments the aim has been to obtain char conversion profiles at near constant O_2 concentrations, in order to use them for model validation. The only consideration towards stoichiometry has therefore been to ensure sufficient amounts of O_2.

At each of the experimental temperatures a devolatilization experiment was also carried out in order to correct char conversion for volatile weight loss. Due to problems with tar clogging the probe the devolatilization experiments were carried out at approximately 5 vol.% O_2 corresponding to a stoichiometric ratio of approximately 3. This did however not affect coal mass losses

Table 1
Proximate and ultimate analysis of the coal used for experiments. In the column "Corrected" the original data has been corrected for the ash content of the particle size fraction 90–106 μm.

Proximate analysis	Original	Corrected
Upper heating value (MJ/kg ar)	28.19	28.19
Effective heating value (MJ/kg ar)	27.09	27.09
Moisture (Wt.% ar)	5.0	5.2
Ash (Wt.% ar)	9.6	5.9
Volatiles (Wt.% ar)	34.9	34.9
Ultimate analysis		
Carbon (Wt.% ar)	68.9	71.73
Hydrogen (Wt.% ar)	4.61	4.8
Oxygen (diff.) (Wt.% ar)	9.82	10.23
Nitrogen (Wt.% ar)	1.44	1.5
Sulfur (Wt.% ar)	0.62	0.64

[15] and the presence of O_2 during devolatilization was not found to affect char reactivity [23].

El Cerrejón coal sieved to the size range 90–106 μm has been used in all the experiments. Ash tracing on the sieved coal fraction revealed an ash content of 5.9 wt.%, which is lower than that of proximate analysis on the unsieved coal. The proximate and ultimate analysis of the coal in Table 1 is therefore shown both as received from the lab and corrected for ash content using the same fractional correction factor for all coal constituents.

3. Model development

3.1. Classification of char morphology and size

Both char morphology and its influence on conversion rates has been investigated by several authors [6,7,14,24–31]. Bailey et al. [25] and Shu and Xu [24] developed detailed char classification systems based on microscopy [24,25] and measurements of specific surface area and pore volume [24] and Yu et al. [14] reviewed the literature providing a thorough discussion on the classification of char. Common for these detailed classification systems is that they are difficult to apply when predicting the behavior of a practical system. In order to apply char morphology in predictive models each morphological group needs to be quantified and described with respect to porosity, density, size, geometry, specific surface area and abundance. Because of this, generalized morphologies as suggested by Cloke et al. [6], Wu et al. [7], Ma and Mitchell [13] and Yu et al. [14] are often used in modeling to lower the requirement for input parameters. Common for the latter authors is that they divide the char into a cenospheric fraction, a network/mixed fraction and a solid/dense fraction. The generalized morphologies used by the authors are shown in Table 2 along with key characteristics used to define each group.

Besides the characteristic parameters provided in Table 2 knowledge on pore size/pore size distribution, distribution of char between the categories, specific surface area, densities, char composition and PSD are important to know in modeling but the table clearly shows the challenges encountered when constructing a detailed combustion model founded on a description of char morphology. There is a general agreement that a highly porous, nearly spherical, cenospheric char is present. When dealing with network chars more disagreement can be found between the authors in Table 2. Yu et al. [14] assumes quite porous chars of varying geometry. Wu et al. [7] and Ma and Mitchell [13] are in relative agreement on porosity and to some extent on wall thickness but Ma and Mitchell [13] assume more spherical chars than does Wu et al. [7]. Cloke et al. [6] defines network chars with a broad range of porosities but with wall thicknesses well in line with those of Wu et al. [7]. Also for dense/solid chars is there disagreement among the authors, especially with respect to porosities.

In this study char particles have been investigated by SEM as a mean to establish a qualitative description of the morphologies present.

Fig. 2A and B shows SEM images of char sampled at two different positions in the reactor at 1173 K in 27.9 vol.% O_2 in CO_2. At 37% conversion the three morphologies of Table 2 are all seen to be present. Even at 80% conversion there are still particles present of distinctively different morphologies where some have surfaces with low macro porosity and some is almost fully consumed. Fig. 2C and D shows SEM images of char obtained from devolatilization at 1673 K in N_2. Here both network and dense chars can be seen but the presence of char that does not fall easily into one category is seen in picture C. The network/cenosphere char in this picture has regions with large cavities and thin walls, characteristic of cenospheres, but it also has regions with a pore system resembling that of network chars. The inclusion of such a char into a practical morphological system must be based on judgment of its average wall thickness.

In Table 2 the sphericity found for char particles belonging to different morphological categories varies between the authors. Fig. 3 shows SEM images of sieved coal and char formed at three different devolatilization temperatures. From the figure it can be seen that swelling is taking place at all three devolatilization temperatures thereby producing oval chars with a smooth surface whereas the raw coal particles are clearly fragments created mechanically from the milling of larger lumps.

The structural changes taking place during the transformation from coal to char in Fig. 3 is due to the metaplast formed during devolatilization that allows more spherical particles to evolve from the high internal particle pressures caused by the release and entrapment of volatiles [14,33]. Markings from the release of volatile bubbles can be seen on the surfaces of the chars in Figs. 2 and 3 where it has resulted in the formation of craters. Fig. 3 also shows that even though the particles were sieved prior to experiments there still seems to be a fraction of small particles. This fraction seems to increase when devolatilization is carried out at 1273 K but its presence then appears to decrease as the devolatilization temperature increases. This is an indication of a decreased particle fragmentation rate compared to small particle conversion rate as the temperature goes up. Fragmentation of the sampled particles during SEM preparation and storage can however not be ruled out as a source of uncertainty and swelling may also play a role. Even if a slight consumption of fines, due to the presence of O_2 in the devolatilization experiments, has been taking place it will not affect the volatile weight losses significantly as the fines only makes up a few percent of the total mass. Regarding the shape of the particles after devolatilization, Fig. 3 suggests that sphericities

Table 2
Char morphology categories found in the literature and the characteristics used to define them.

	Cloke et al. [6]	Wu et al. [7]	Ma and Mitchell [13]	Yu et al. [14]
Cenospheric char				
ε	>71.48%	>68%	>70%	>80%
δ_{Wall}	<4.63 μm	55% under 3 μm	<10 μm (thin)	<5 μm
Ψ	N/A	$\Psi \sim 0.65–0.73$	$\Psi > 0.85$	Spherical
Network char				
ε	38.83–84.92%	47–69%	40–60%	>50%
δ_{Wall}	4.13–6.89 μm	8–48% under 3 μm	>10 μm (medium)	Variable
Ψ	N/A	$\Psi \sim 0.47–0.82$	$\Psi > 0.8$	Variable
Dense/solid char				
ε	<12.51%	3–33%	<40%	~50%
δ_{Wall}	~13.01 μm	9–41% under 3 μm	>10 μm (thick)	>5 μm
Ψ	N/A	$\Psi \sim 0.67–0.68$	$\Psi < 0.7$	Variable

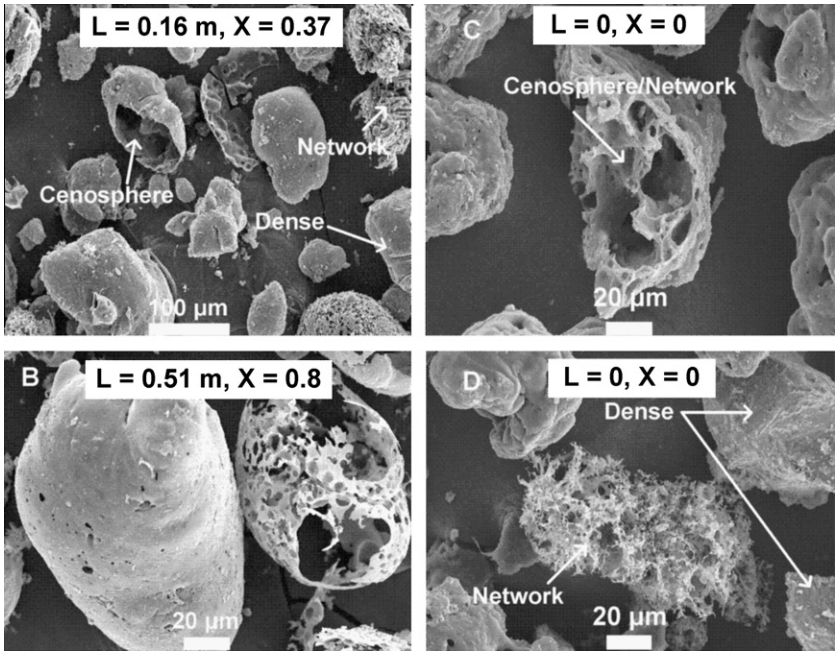

Fig. 2. (A and B) SEM images of chars obtained at 1173 K in CO_2 with an O_2 concentration of 27.9 vol.%. The O_2 concentration is the average of the local concentrations at each sampling position. $\lambda \sim 15$. (C and D) SEM images obtained from devolatilization at 1673 K in N_2.

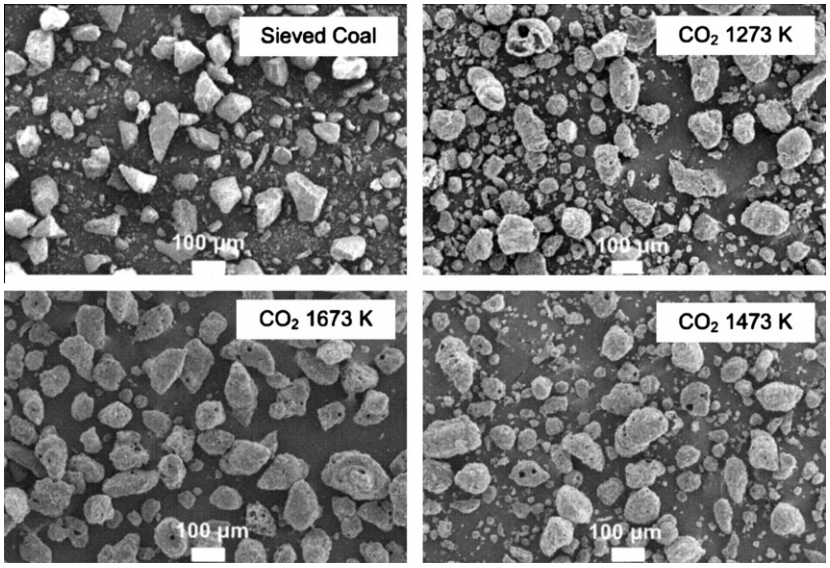

Fig. 3. SEM images of sieved coal and chars obtained by devolatilization in CO_2 at 1273 K, 1473 K and 1673 K.

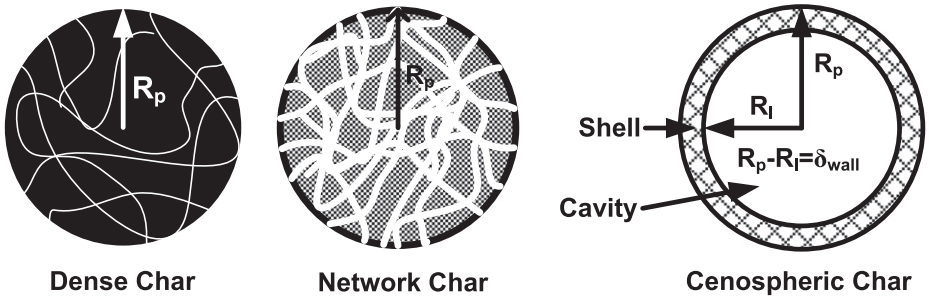

Fig. 4. Schematics of char morphologies used to derive particle mass balances.

are varying though with a tendency that supports the higher values of Table 2.

Based on the discussion above the chars in this study will be assumed perfect spheres falling into the three morphologies: cenospheric chars, network chars and dense chars as presented schematically in Fig. 4.

In [15] a correlation describing the char swelling ratio as a function of temperature was presented from PSD's of the char samples shown in Fig. 3. From these PSD's temperature dependent weight percents of six discrete particle sizes: 11.5 μm, 44.3 μm, 73.7 μm, 104.5 μm, 140 μm, 190.1 μm have been described by (1), which is valid in the temperature interval 1173–1673 K. The temperature is that of the gas.

$$W(R_{p0,k}) = a_k \cdot T^2 + b_k \cdot T + c_k \tag{1}$$

Constants used in (1) for the six particle sizes are presented in Table 3.

The behavior of each particle size reflects the overall swelling described in [15]. The two smallest sizes decrease as the reactor temperature is increased whereas the remaining four particle sizes increase.

3.2. Model equations and solution procedure

A COal COmbustion MOdel, COCOMO, has been implemented as a FORTRAN 77 code that calls on the CHEMKIN II [32] subroutine library for calculations of species enthalpies and stoichiometric coefficients in homogenous reactions, homogeneous reaction rates and bulk gas heat capacities used in the gas phase energy balance. The homogenous reaction mechanism encompasses 185 chemical species and 1173 reactions [34] although in the present simulations only CO oxidation to CO_2 is relevant. The heterogeneous reactions taking place in COCOMO are (R1) and (R2). The stoichiometric coefficients of (R1) are: $\Lambda_{1,k,l} = a/z_{k,l} + b/4 + d/2 - y/2 + e$, $\Lambda_{2,k,l} = (2/z_{k,l} - 1)a$, $\Lambda_{3,k,l} = 2(1 - 1/z_{k,l})a$, $\Lambda_4 = b/2$, $\Lambda_5 = e$, $\Lambda_6 = d$, $\Lambda_7 = u$. The fuel to oxidizer ratio, accounting for the production of CO_2 relative to CO, is found as suggested by Norman et al. [35]: $z_{k,l} = (5000 \cdot \exp(-6249/T_{p,k,l}) + 2)/(2500 \cdot \exp(-6249/T_{p,k,l}) + 2)$. The stoichiometric coefficients of (R2) are: $\Lambda_8 = a - y$, $\Lambda_9 = 2a - y$, $\Lambda_{10} = b/2 - e$, $\Lambda_{11} = e$, $\Lambda_{12} = d/2$.

$$C_aH_bO_yN_dS_eA_u + \Lambda_{1,k,l}O_2 \rightarrow \Lambda_{2,k,l}CO_2 + \Lambda_{3,k,l}CO + \Lambda_4H_2O + \Lambda_5SO_2 + \Lambda_6NO + \Lambda_7A \tag{R1}$$

$$C_aH_bO_yN_dS_eA_u + \Lambda_8CO_2 \rightarrow \Lambda_9CO + \Lambda_{10}H_2 + \Lambda_{11}H_2S + \Lambda_{12}N_2 + \Lambda_7A \tag{R2}$$

In the present investigation the char is assumed only to consist of carbon and ash, specified as silicon dioxide. The possibility to include H, O, N and S in the char is included to increase the applicability of COCOMO in future investigations of NO_x and SO_x emissions.

In Sections 3.2.1–3.2.3 only the mass- and energy balances of COCOMO are presented. Auxiliary equations are found in Appendix A and a derivation of the mass balances is given in Appendix B.

Table 3
Constants used in (1).

Particle Size/Constant	a (K^{-2})	b (K^{-1})	c
W (11.5 μm)	-6.25×10^{-6}	3.1625×10^{-3}	13.902444
W (44.3 μm)	2.625×10^{-5}	-1.095825×10^{-1}	114.05964
W (73.7 μm)	2.125×10^{-5}	-7.38525×10^{-2}	86.277991
W (104.5 μm)	3.625×10^{-5}	-8.35425×10^{-2}	70.905426
W (140 μm)	-1.25×10^{-5}	6.2325×10^{-2}	−41.683113
W (190.1 μm)	-6.5×10^{-5}	2.0149×10^{-1}	−143.46238

3.2.1. Solid mass balances

There exist different classical approaches when heterogeneous gas–solid reactions are to be described mathematically [36–42]. The Grain Model (GRM), developed by Szekely and coworkers [39–41], considers the particles to be made from numerous small grains. Yagi and Kunii [42] presented the Unreacted Shrinking Core Model (USCM) where the gas–solid reaction is considered to take place on a well defined front between an ash layer and a solid core. Wen [36] also treated the USCM and discussed cases where the front between the ash layer and the core was not well defined or where reaction occurred homogeneously throughout the solid phase. Both the approaches of Wen [36] and Szekely and coworkers [39–41] are termed as Progressive or Volumetric Reaction Models (PRM's, VRM's). The surface area available for reaction in VRM's is also subject to modeling efforts though it is given by the grain packing in the GRM. An often used description of surface area development, especially when dealing with gasification, is the Random Pore Model (RPM) developed by Bhatia and Perlmutter [37,38]. This model takes pore expansion and fusion during reaction into account through the inclusion of a characteristic pore structural parameter and a logarithmic dependence on solid conversion. In processes where pore structural variation does not play an important role during reaction the char surface area is normally considered proportional to the mass of solid.

From TGA experiments [23] it was found that the conversion rates of char sampled in the EFR at all experimental temperatures are adequately described by a VRM. In the present model the char burning rate is modeled as taking place on both the particles interior and exterior surface while char consumption is modeled as a shrinking spherical particle where the ash formed during reaction breaks of. The burning rate expression is therefore similar to that used for a porous catalyst while the accompanying char consumption takes place by radial shrinkage of the particle with no formation of an ash layer. This entails shrinking particles of constant particle density which ease calculations considerably. In the derivation of the particle mass balances both internal and external surface area is included, which yields a conversion rate for a cenospheric char described for each gaseous reactant by (2) and for all gaseous reactants by (3). The conversion rates for network and dense chars are described by the same equations when $\delta_0 = 1$. The first term in (2) describes the reaction rate in the interior of the particle while the second term accounts for the reaction rate at its exterior surface.

$$\frac{dX_{k,l,r}}{dL} = \frac{k_{k,l,r} \cdot (C_r^S)_{k,l}^{n_r}}{v_{s,k,l} + v_g} \cdot \left(S_0 \cdot (1 - X_{k,l}) \cdot \eta_{k,l,r} + \frac{3 \cdot (1 - X_k \cdot (1 - (1 - \delta_0)^3))^{(\frac{2}{3})}}{\rho_p \cdot R_{p0,k} \cdot (1 - (1 - \delta_0)^3)} \right) \tag{2}$$

$$\frac{dX_{k,l}}{dL} = \sum_r \frac{dX_{k,l,r}}{dL} \tag{3}$$

The effectiveness factor, $\eta_{k,l,r}$, is included in (2) to account for internal mass transfer resistance in the char particles. When mass transfer limitations cause internal concentration gradients of reactants to form inside the particles the effectiveness factor will gradually decrease from one to account for the internal surface area not accessible for reaction. In (2) the surface concentrations of the reactants are found from mass balances across the laminar gas film layer surrounding the particles as shown in (4).

$$k_{c,k,l,r} \cdot A_{p,k,l} \cdot (C_r^B - (C_r^S)_{k,l}) = \frac{\Lambda_{k,l,r} \cdot m_{p0,k,l}}{M_p} \cdot \frac{dX_{k,l,r}}{dL} \cdot (v_{s,k,l} + v_g) \tag{4}$$

The solution of (3) yields the conversion of a particle size belonging to one of the three morphologies. To calculate the total conversion of a morphological group or of all char (5) and (6) are used.

$$X_l = 1 - \sum_k (1 - X_{k,l}) \cdot \Theta_k \quad (5)$$

$$X_T = 1 - \sum_l (1 - X_l) \cdot \alpha_l \quad (6)$$

3.2.2. Solid energy balance

The energy balance for a burning char particle is given by (7). The energy balance takes into account convective heat transfer between the gas and particle, radiation between the particle and reactor wall and the heat generated by the oxidation and gasification of the particle. These are the general terms included in modeling studies [3,6,8,10,18].

$$\frac{dT_{p,k,l}}{dL} = \frac{-m_{p0,k,l} \cdot (v_{s,k,l} + v_g) \cdot \sum_r \frac{dX_{k,l,r}}{dL} \cdot \Delta H_{k,l,r} + A_{p,k,l} \cdot (h_{p,k,l} \cdot (T_g - T_{p,k,l}) + \bar{e} \cdot \sigma_{SB} \cdot (T_w^4 - T_{p,k,l}^4))}{(v_{s,k,l} + v_g) \cdot m_{p,k,l} \cdot C_{p,k,l}} \quad (7)$$

The particle energy balance in (7) does not include radiation between particles of different sizes and morphologies due to the low coal feed rate used during the experiments.

3.2.3. Gas phase mass and energy balances

To account for changes in the gas temperature the energy balance in (8) is set up. This energy balance includes the heat generated by homogeneous reactions along with convective heat transfer with the particles and reactor wall. The mass balance in (9) accounts for both heterogeneous and homogeneous contributions.

$$\frac{dT_g}{dL} = A_R \cdot \left(\frac{\sum_{i=1}^{N_H} r_i \cdot (-\Delta H_i) + a_w \cdot h_w \cdot (T_w - T_g) + \sum_l \sum_k Q_{k,l}}{\sum_{j=1}^{N_G} F_j \cdot C_{p,j}} \right) \quad (8)$$

$$\frac{dF_j}{dL} = A_R \cdot \left(\sum_{i=1}^{N_H} \zeta_{j,i} \cdot r_i + \sum_r \sum_l \sum_k N_{k,l} \cdot \zeta_{j,k,l,r} \cdot r_{k,l,r} \right) \quad (9)$$

Even though the experiments presented in this study are carried out at conditions where the molar gas flow, its composition and its temperature are nearly constant the gas phase mass- and energy balance in (8) and (9) are included to enhance model accuracy and general applicability. In the present simulations the only significant gas phase reaction is CO oxidation and simulated gas temperatures are less than 30 K higher than the reactor wall at all times. In (8) the convective heat transfer between gas and particles is found as $Q_{k,l} = N_{k,l} \cdot h_{p,k,l} \cdot A_{p,k,l} \cdot (T_{p,k,l} - T_g)$. The reactor surface area pr. reactor volume, a_w, is found as $4 \cdot D_R^{-1}$.

3.3. Model input parameters

The model presented in (2)–(9) requires a range of input parameters, which are given in Table 4 for the simulations presented here. Skeletal density, porosity and abundance of morphologies are found for El Cerrejón chars by the respective authors. The density is found by correcting the apparent value taken from Zolin et al. [43] with the porosity obtained from Cloke et al. [6]. Char porosities and morphology abundances of Cloke et al. [6] are found by DTF experiments at 1423 K, which is the average temperature used during the EFR experiments presented here. Cloke et al. [6] did not find strong effects of temperature on either porosity or abundance in the interval 1273–1573 K. The values of tortuosity and char emissivity are used in combustion modeling by Charpenay et al. [44] and Mon and Amundson [45]. Weight fractions of discrete particle sizes are found from (1) and are assumed the same for all three morphologies.

The value of the specific surface area is found as an average from N_2-BET measurements on the chars in Fig. 3, which yielded the specific surface areas: N_2-BET(1273 K) = 243 $m^2\,g^{-1}$, N_2-BET(1473 K) = 200 $m^2\,g^{-1}$ and N_2-BET(1673 K) = 280 $m^2\,g^{-1}$. The specific surface area is used for simulations in both N_2 and CO_2 [15].

$$k_{k,l,r} = A_{0,r} \cdot \exp\left(\frac{E_{D,r}}{R \cdot T_{p,d,k,l}}\right) \cdot \exp\left(\frac{-E_{A,r}}{R \cdot T_{p,k,l}}\right) \quad (10)$$

The rate constants used in (2) are found from the extended Arrhenius expression in (10) [23]. The expression includes a pre-exponential factor, $A_{0,r}$, which has a value of 1.4359 kg $m^{-2}\,s^{-1}$ (mol m^{-3})$^{-0.5}$ when used for O_2 and a value of 7.3282 kg $m^{-2}\,s^{-1}$ (mol m^{-3})$^{-0.5}$ when used for CO_2. The deactivation energy, $E_{D,r}$, is 20.5 kJ mol^{-1} for O_2 and 0 kJ mol^{-1} for CO_2 and an activation energy of 137.5 kJ mol^{-1} and 230.8 kJ mol^{-1} is used for O_2 and CO_2 respectively. It should be noted that a deactivation energy of 0 kJ mol^{-1} for CO_2 means that the gasification rate is not affected by thermal char deactivation though this is the case for the combustion rate. While this may strike as odd the kinetic data is a result of detailed data treatment on TGA reactivity profiles obtained with authentic EFR chars [23]. The deactivation temperature, $T_{p,d,k,l}$, is the highest temperature a particle has experienced at a given position in the reactor and is used assuming that the level of deactivation quickly adjusts to the experienced temperatures.

4. Comparison between model and experiments

Comparison between COCOMO and experimental profiles can be seen in Figs. 5–10 where data are collected for each experimental temperature. Simulated profiles found for O_2/CO_2 combustion are shown both with and without the contribution from CO_2 gasification in Figs. 9 and 10. It is only at these high temperature conditions that a detectable contribution from CO_2 gasification to overall char conversion is seen. In the remaining figures throughout the text CO_2 gasification is included in the simulations though it does not influence char conversion. In the following the ability of the model to predict the experimental data will be commented. The discussion of Figs. 5 and 6 will however be postponed as it prepares the ground for the detailed discussion of the data that will follow later in the text.

Table 4
Input parameters used in the simulations.

Parameter	ρ_p [43]	S_0	τ [44]	ε_N [6]	ε_D [6]	δ_0
Value	1453 (kg m^{-3})	240 ($m^2\,g^{-1}$)	2	38%	19%	0.05
Parameter	α_C [6]	α_N [6]	α_D [6]	$\bar{e}$ [44]	d_{pore}	$n_{O_2} = n_{CO_2}$
Value	0.2	0.71	0.09	0.93	1 μm	0.5

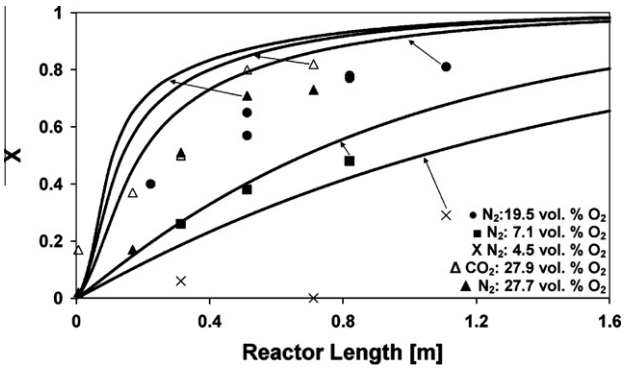

Fig. 5. COCOMO profiles and experimental profiles obtained at 1173 K in N_2 and CO_2. The O_2 concentrations are the averages of the local concentrations at each sampling position. $\lambda \sim 2.7–15.2$.

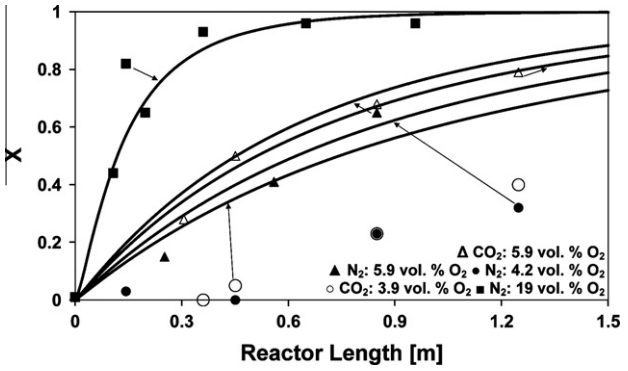

Fig. 6. COCOMO profiles and experimental profiles obtained at 1273 K in N_2 and CO_2. The O_2 concentrations are the averages of the local concentrations at each sampling position. $\lambda \sim 2.5–10.5$.

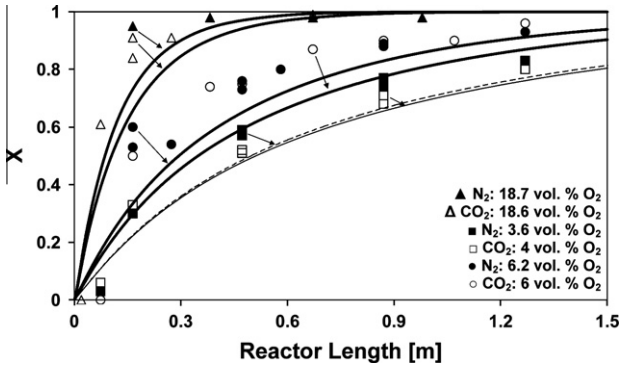

Fig. 7. COCOMO profiles and experimental profiles obtained at 1373 K in N_2 and CO_2. The O_2 concentrations are the averages of the local concentrations at each sampling position. $\lambda \sim 2.3–9.8$.

Figs. 7–10 show in general a reasonable agreement between simulations and experimental data at all O_2 concentrations in both N_2 and CO_2. A tendency of under prediction by the model in Figs. 7 and 8 and a slight over prediction in Figs. 9 and 10 can however be seen, which are most likely caused by small variations in the abundance of morphologies and physical properties such as size and porosity. Fig. 8 also shows the conversion profiles for each of the morphologies making up the total conversion profile. It can be seen from Fig. 8 that the presence of cenospheres, that predominantly burn in zone I, is very important for the steepness of the profile wherefore an increased cenosphere formation or an increase in

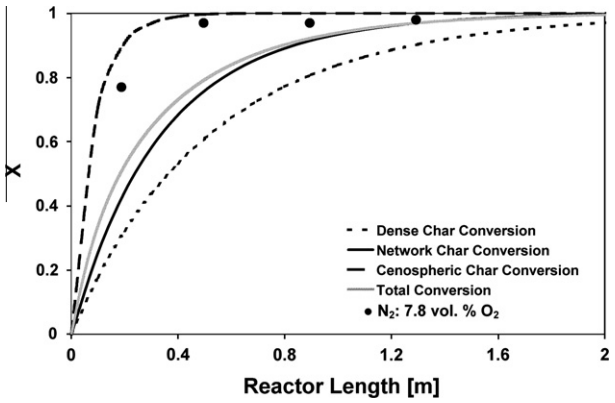

Fig. 8. COCOMO profile and experimental profile obtained at 1473 K in N_2. The O_2 concentration is the average of the local concentrations at each sampling position. $\lambda \sim 3.7$. Also shown are COCOMO conversion profiles of each of the three morphologies.

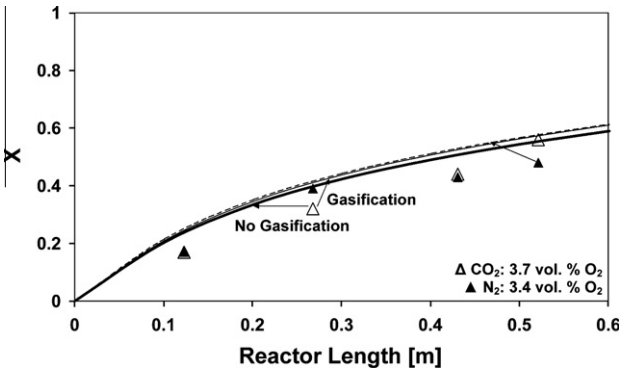

Fig. 9. COCOMO profiles and experimental profiles obtained at 1573 K in N_2 and CO_2. The thin dashed line is the simulation in O_2/N_2 and the thin unbroken line is the simulation in O_2/CO_2 with gasification included. The O_2 concentrations are the averages of the local concentrations at each sampling position. $\lambda \sim 2$.

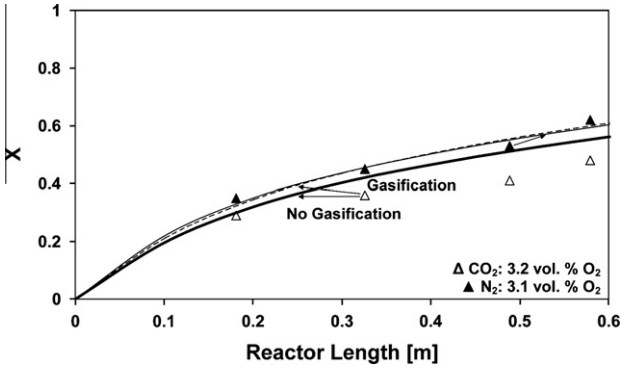

Fig. 10. COCOMO profiles and experimental profiles obtained at 1673 K in N_2 and CO_2. The thin dashed line is the simulation in O_2/CO_2 with gasification included and the thin unbroken line is the simulation in O_2/N_2. The O_2 concentrations are the averages of the local concentrations at each sampling position. $\lambda \sim 1.9$.

porosity will increase the initial char conversion rate. Besides morphology, variations in particle size are also influencing the conversion rate. Fig. 11 shows conversion profiles and effectiveness factors for network chars of three different sizes belonging to the overall network conversion profile in Fig. 8. From Fig. 11 it is seen that the smallest particle size is rapidly converted in zone I. For a medium sized particle conversion is slower and takes place from

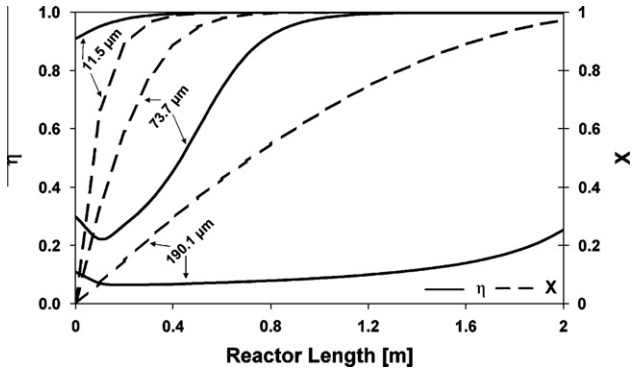

Fig. 11. COCOMO conversion profiles and effectiveness factors for network particles at 1473 K and 7.8 vol.% O_2 in N_2. The O_2 concentration is the average of the local concentrations at each sampling position. $\lambda \sim 3.7$.

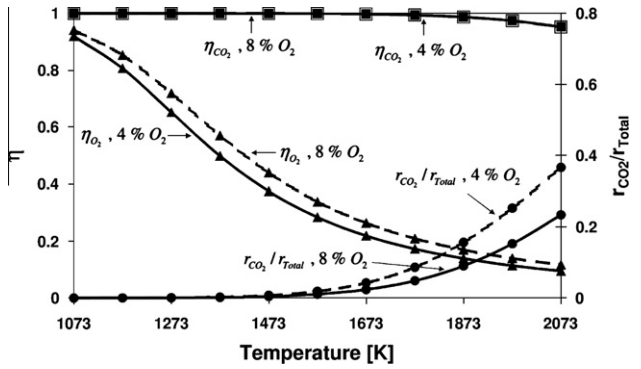

Fig. 12. CO_2 gasification rate relative to overall char conversion rate and internal particle effectiveness factors at 4 and 8 vol.% O_2 and different particle temperatures. Network char, $T_g = T_p$, $\lambda = 1.05$, $d_p = 44.3$ µm, $v_s = 0$.

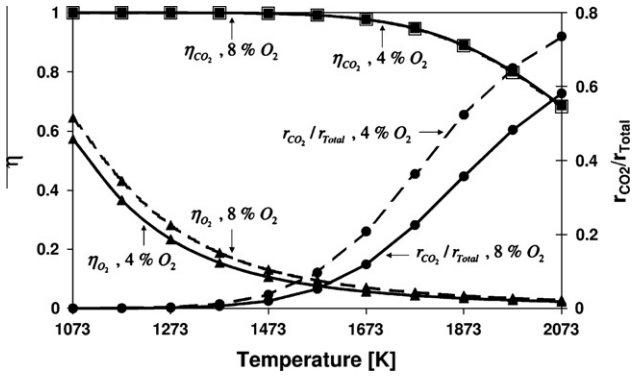

Fig. 13. CO_2 gasification rate relative to overall char conversion rate and internal particle effectiveness factors at 4 and 8 vol.% O_2 and different particle temperatures. Network char, $T_g = T_p$, $\lambda = 1.05$, $d_p = 140$ µm, $v_s = 0$.

near zone III to zone I throughout its consumption. The largest particle size present in the simulation is burning under almost complete external mass transfer control during the entire process. The strong influence of internal and external mass transfer control for the medium to large particles means that a faster overall char conversion would be achieved if a larger fraction of small particles is present, e.g. as a result of fragmentation.

In Figs. 9 and 10 COCOMO predicts an observable influence of CO_2 gasification on char conversion. In Fig. 9 this influence does not markedly change the conversion rate in O_2/CO_2, which is close to that in O_2/N_2, and in reasonable agreement with experimental data. In Fig. 10 the effect is more pronounced and does not tally with the experimental profiles. According to the experimental profiles in Fig. 10 the conversion rate in O_2/N_2 is significantly higher than in O_2/CO_2, suggesting an effect of O_2 diffusivity, which is approximately 22% lower in CO_2 at these conditions. The simulated profiles show however that the conversion rates in O_2/N_2 and O_2/CO_2 are similar and that the conversion rate in O_2/CO_2 outpaces that in O_2/N_2 at conversions higher than approximately 50%. The reason for the inconsistency between model and experiments can be found as a continuation of the discussion of Figs. 8 and 11 that illustrated the importance of variations in PSD and morphology abundances. Figs. 12 and 13 show the calculated importance of CO_2 gasification for a small (44.3 µm) and large (140 µm) network particle respectively. In both figures a decrease in bulk O_2 concentration from 8 vol.% to 4 vol.% cause a more significant contribution from CO_2 gasification as expected. Furthermore, as the particle temperature goes up CO_2 gasification becomes increasingly important. The reason for this behavior can be deduced from the internal effectiveness factors of O_2. At the higher temperatures the reaction with O_2 approaches zone III wherefore only moderate increases in consumption rate are gained as the temperature continues to increase. At these temperatures CO_2 gasification is taking place in zone I or zone II resulting in a fast increase in consumption rate as the temperature increase.

The crucial importance of O_2 combustion zone and zone III conversion rate (particle size and bulk O_2 concentration) illustrated in Figs. 12 and 13 means that even small variations in PSD, char porosity and abundance of morphologies between simulations and experiments can cause inconsistencies in overall char conversion rate as found in Fig. 10. Figs. 9, 10, 12 and 13 do however show that CO_2 gasification can play a role when combustion is taking place in zone III. The discussion of the importance of CO_2 gasification, as indicated by the model, is however with the specific kinetic parameters used in the simulations [23]. These are based on TGA experiments at much lower temperatures causing significant extrapolation of the kinetics to the conditions used in the simulations. Though qualitatively unambiguous it must therefore be said that changes in kinetic rates can change the quantitative importance of CO_2 gasification at the conditions used in the preceding figures.

The differences between model predictions and experimental results in Figs. 5 and 6 are most significant for the lowest and highest O_2 concentrations. For a concentration of 4.5 vol.% O_2 in N_2 in Fig. 5 and for concentrations of 4.2 vol.% O_2 and 3.9 vol.% O_2 in N_2 and CO_2 in Fig. 6 the reaction appears delayed compared to the remaining experimental profiles. All three profiles were obtained at conditions similar to those used for the devolatilization experiments where an O_2 concentration of approximately 5 vol.% was used in order to overcome problems with tar clogging the sampling probe and reactor ventilation system. During sampling of devolatilized char it was reassured that no significant heterogeneous conversion took place that could result in misleading values of volatile weight loss. This was done by sampling at reactor positions downstream of the actual sampling point and comparing char ash contents. From this it was found that no significant heterogeneous conversion took place, which indicates a delay between the end of devolatilization and onset of heterogeneous ignition under these conditions. This is not captured by the model in Figs. 5 and 6 wherefore a significant absolute error exists between model and experiments though the slope of the experimental conversion profiles are predicted quite accurately once reaction begins.

In Fig. 5 the model over predicts the conversion rate at high O_2 concentrations though it captures the abrupt char deactivation that takes place at 70–80% conversion. In Fig. 14 SEM images of char sampled at three different degrees of conversion at 1173 K and 27.9 vol.% O_2 (left panel) and 1673 K and 3.2 vol.% O_2 both in CO_2 (right panel) both shows that a fraction of non-reactive

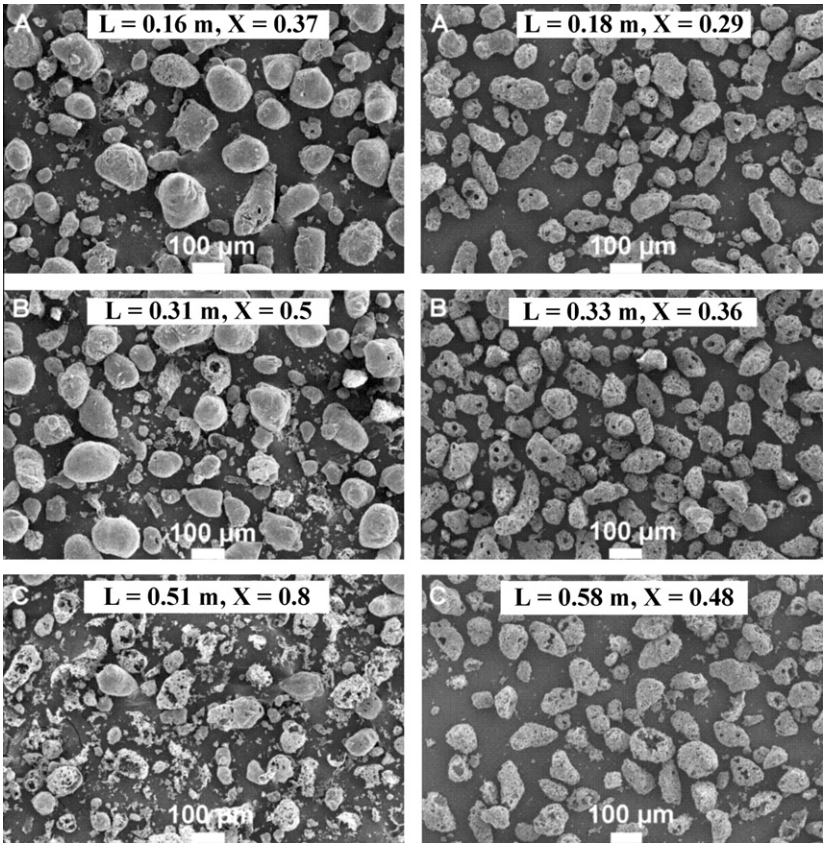

Fig. 14. SEM images at three different degrees of conversion in CO_2. Left: T = 1173 K, 27.9 vol.% O_2. $\lambda \sim 15.2$. Right: T = 1673 K, 3.2 vol.% O_2. $\lambda \sim 1.9$.

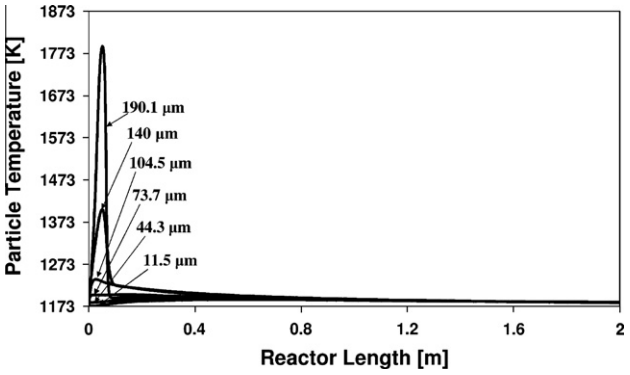

Fig. 15. COCOMO temperature profiles for cenospheric char at 1173 K and 27.9 vol.% O_2 in CO_2. The O_2 concentration is the average of the local concentrations at each sampling position. $\lambda \sim 15.2$.

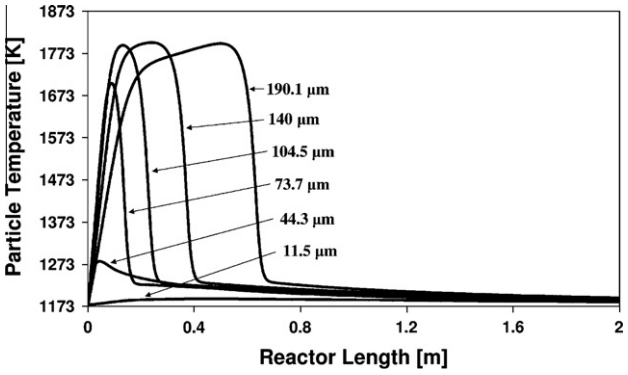

Fig. 16. COCOMO temperature profiles for network char at 1173 K and 27.9 vol.% O_2 in CO_2. The O_2 concentration is the average of the local concentrations at each sampling position. $\lambda \sim 15.2$.

chars remain at 1173 K even at high overall degrees of conversion.

The behavior observed in Fig. 14 can be discussed on the basis of simulations. The deactivated particles at 1173 K of Fig. 14 are quite large and they appear to be present throughout the process. Figs. 15–17 show the particle temperature profiles at 1173 K and 27.9 vol.% O_2 in CO_2 for cenospheres, network chars and dense chars respectively. From these figures it is seen that very high particle temperatures (1700–1800 K) are reached shortly after ignition for 190.1 μm cenospheres, 73.7 μm, 104.5 μm, 140 μm and 190.1 μm network chars and 104.5 μm, 140 μm and 190.1 μm dense chars. These high temperatures will result in a second devolatilization and a distinct deactivation. For 190.1 μm cenospheres and 73.7 μm network chars, heating rates of approximately 20,000 K s^{-1} and 12,000 K s^{-1} are reached, which will facilitate an intense second devolatilization. Zhang et al. [46] found that when the three factors: high mineral content, high volatile content and high heating rate was met combustion was inhibited by the formation of an inactive mineral cluster phase. Zhang et al. [46] suggested that this phase is formed when liquid/volatile organic fractions are absorbed on the minerals thereby significantly reducing the void fraction in the particle, increasing the order in its structure and hence lowering its reactivity. The phase showed up as a second peak on TGA reactivity profiles in the work of Zhang et al. [46]. TGA measurements on the char sampled at 1173 K and 27.9 vol.% O_2 in CO_2 indeed also showed two distinct peaks in the reactivity profile [23] indicating that a separate highly inactive phase is present. This is not accounted for in COCOMO where

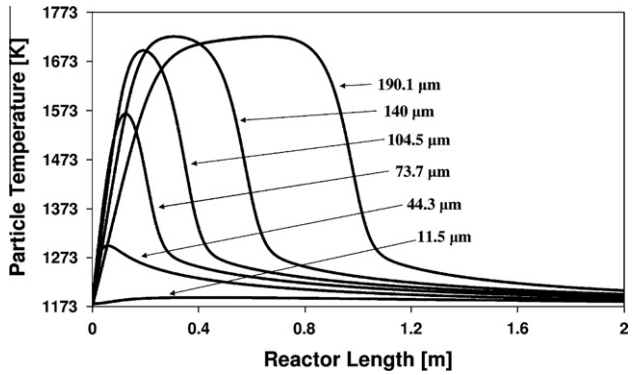

Fig. 17. COCOMO temperature profiles for dense char at 1173 K and 27.9 vol.% O_2 in CO_2. The O_2 concentration is the average of the local concentrations at each sampling position. $\lambda \sim 15.2$.

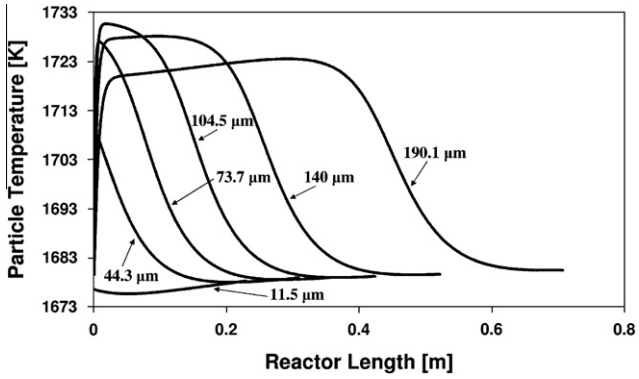

Fig. 18. COCOMO temperature profiles for cenospheric char at 1673 K and 3.2 vol.% O_2 in CO_2. The O_2 concentration is the average of the local concentrations at each sampling position. $\lambda \sim 1.9$.

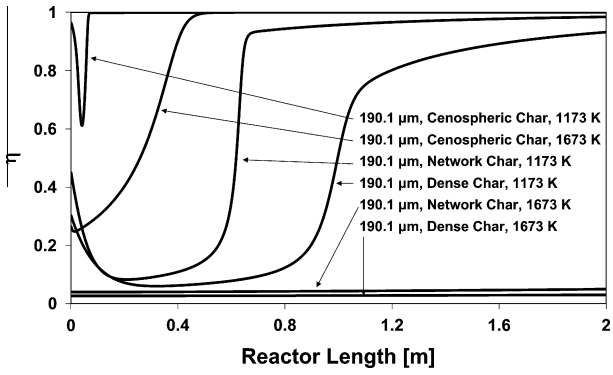

Fig. 19. COCOMO effectiveness factor profiles at 1173 K, 27.9 vol.% O_2 in CO_2 and $\lambda \sim 15.2$ and at 1673 K, 3.2 vol.% O_2 in CO_2 with $\lambda \sim 1.9$ for 190.1 µm particles. The O_2 concentration is the average of the local concentrations at each sampling position.

char deactivates homogeneously and it therefore causes over predictions by the model when high particle temperatures are reached at high heating rates. The strong effect of particle temperature history on char conversion is made clear in Fig. 14 where SEM images of char conversions at 1173 K in 27.9 vol.% O_2 and at 1673 K and 3.2 vol.% O_2 in CO_2 are compared. Where the particles at 1173 K undergo substantial morphological changes due to the intense ignition, the particles at 1673 K seem to burn uniformly throughout the process. This is due to uniform particle temperatures illustrated for cenospheres by Fig. 18 where it is seen that the highest

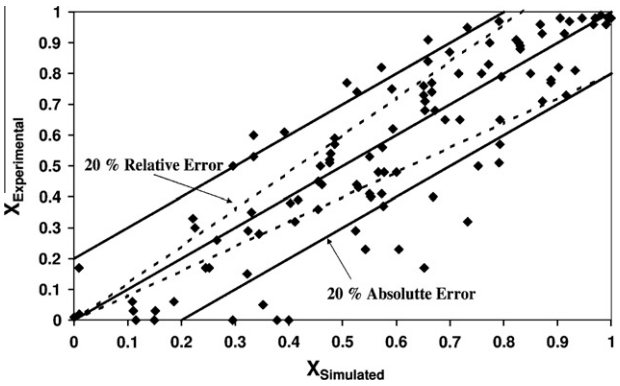

Fig. 20. Comparison between COCOMO and experimental data.

temperature difference between gas and particle is reached by 104.5 µm particles and is less than 60 K. This is the highest temperature difference between gas and particle for any particle size and morphology at 1673 K and 3.2 vol.% O_2 in CO_2. The cause of the differences in temperature histories of especially the larger particles between the two experiments are illustrated by the internal effectiveness factors in Fig. 19. In Fig. 19 it is seen that at a reactor temperature of 1173 K the combustion process starts in zone II for network and dense chars and in zone I for cenospheres. Since the devolatilization has taken place at 1173 K thermal deactivation of the particles have only been moderate at the onset of ignition and the high O_2 concentration enables efficient mass transfer across the gas film layer. This allows the particles to reach high peak temperatures before a combination of thermal char deactivation and external mass transfer limitations slows down the reaction rate. Fig. 19 also shows that when ignition takes place at 1673 K cenospheres burn in zone II and dense and network chars burns in zone III where the low O_2 concentration hinders effective mass transfer across the gas film layer. Furthermore Fig. 13 shows a more pronounced effect of CO_2 gasification at 1673 K and low O_2 concentration, which also drives down the particle temperatures. It is however not the main reason for the uniform temperature profiles in Fig. 18.

Fig. 20 compares the collected experimental data points from Figs. 5–10 with model predictions, in total 108 data points. The data in Fig. 20 covers both combustion in zone I, zone II and zone III.

It can be seen from Fig. 20 that the largest deviations between model and experiments come from over predictions by the model at experimental conversions below 40%. The reasons for these deviations were discussed above in connection with the profiles of Figs. 5 and 6. Besides these data points Fig. 20 shows a reasonable consistency between model and experiments both in the dynamic part of the combustion at low char conversion and in the final burnout phase at high char conversion where much of the char is significantly deactivated.

5. Conclusions

A combustion model encompassing dense, network and cenospheric char each distributed between six discrete particle sizes have been compared to experimental char conversion profiles obtained in O_2/CO_2 and O_2/N_2 mixtures under suspension fired conditions. The model applies kinetic parameters for char oxidation and CO_2 gasification obtained from TGA experiments with char formed at the experimental temperatures under suspension fired conditions. The expressions for the rate constants include the effect of thermal char deactivation only on the reaction with O_2, since no

deactivation was observed with CO_2. The kinetic expression for O_2 combustion has proven to work satisfactorily under a wide range of suspension fired conditions while that for CO_2 gasification show a slight over prediction at high temperatures.

In the temperature interval 1173–1673 K reasonable consistency was found between experiments and simulations at inlet O_2 concentrations between 5 and 28 vol.%. At high O_2 concentrations and low reactor temperatures simulations showed that the larger particles of all three morphologies reached high over temperatures of up to 500–600 K shortly after ignition causing additional heating with rates as high as 20,000 K/s for 190.1 μm cenospheres. SEM images of partly combusted char, sampled at these conditions showed large unreacted particles even at high overall degrees of conversion. It is suggested that these particles are formed during the intense heating from interactions between products of a secondary devolatilization and particle mineral matter though it is also possible that mineral matter itself affects char reactivity by ash layer inhibition. Due to the fraction of highly deactivated particles significant absolute deviation exists between model and experiment at low reactor temperature and high O_2 concentration as thermal char deactivation is modeled as homogeneous. When both reactor temperature and O_2 concentrations were low a delay between the end of devolatilization and onset of particle ignition also caused deviations.

From experimental profiles obtained in a range of operating conditions, covering zone I–III, no evidence suggesting an effect of CO_2 gasification on char conversion has been found. In fact the only indication of an effect of CO_2 on char conversion rate is seen in zone III where the lower diffusion coefficient of O_2 in CO_2 appears to slow down the reaction rate compared to O_2/N_2. Modeling does however suggest that CO_2 gasification can contribute to char consumption when the O_2 concentration is low, the particle temperature high and combustion is taking place in zone III, especially for large particles. It is however questionable whether this effect will be of importance for industrial applications as the combinations of large particles, low O_2 concentrations and high particle temperatures are difficult to find in a specific position of a boiler. For particularly reactive coals, such as lignite coal, the window where CO_2 gasification is important could be wider, also encompassing common industrial conditions but further studies are needed on this topic.

Acknowledgement

The research leading to these results has received funding from the European Community's Research Fund for Coal and Steel (RFCS) under Contract No. RFCR-CT-2006-00007, Project FRIENDLYCOAL, and is also sponsored by the Danish Agency for Science, Technology and Innovation and from Energinet.dk under Project PSO-7171. The support and funding from these entities are greatly valued.

Appendix A. Auxiliary equations

To simplify the calculations of physical properties of the gas, not carried out by CHEMKIN II [32], it is assumed that only three gaseous species, N_2, O_2 and CO_2, are present in sufficient amounts during the experiments to influence the properties of the gas phase. Where multi component properties, indexed *mix*, are used calculations are based on bulk gas composition.

A.1. Equations relating to particle geometries and mass

An expression for the development of particle radius for a cenospheric char is given by (A1) and for dense chars and network chars by (A2).

$$R_{p,k} = R_{p0,k}(1 - X_k \cdot (1 - (1 - \delta_0)^3))^{(\frac{1}{3})} \tag{A1}$$

$$R_{p,k,l} = R_{p0,k,l} \cdot (1 - X_{k,l})^{(\frac{1}{3})} \tag{A2}$$

Geometric surface areas and volumes of the particles can be calculated immediately from (A1) and (A2). When the volume is used to calculate particle mass and effectiveness factor (A1) can however not be applied directly as it does not take the cavity of a cenosphere into account. The expression for the volume of a cenosphere occupied by a continuous char matrix is given by (A3).

$$V_{p,m,k} = \frac{4}{3} \cdot \pi \cdot R_{p0,k}^3 \cdot (1 - (1 - \delta_0)^3) \cdot (1 - X_k) \tag{A3}$$

The apparent densities of the three char morphologies can be found from (A4)–(A6) where the skeletal density, ρ_p, is assumed to be the same for all particle sizes and morphologies.

$$\rho_{p,N}^a = (1 - \varepsilon_N) \cdot \rho_p \tag{A4}$$

$$\rho_{p,C,k}^a = \frac{(1 - (1 - \delta_0)^3) \cdot (1 - \varepsilon_N) \cdot \rho_p \cdot (1 - X_k)}{(1 - X_k \cdot (1 - (1 - \delta_0)^3))} \tag{A5}$$

$$\rho_{p,D}^a = (1 - \varepsilon_D) \cdot \rho_p \tag{A6}$$

When the apparent density of cenospheric char is used to calculate the effectiveness factor and particle mass based on (A3), (A4) is applied instead of (A5) as these calculations are based on particle volume occupied by a continuous matrix.

A.2. Effectiveness factors and diffusion coefficients

Because the char oxidation rate is *n*th order in O_2 concentration a generalized Thiele modulus, expressed in (A7), is used to calculate the effectiveness factors, $\eta_{k,l,r}$ [47]. The volume of the particle and the apparent density refers to the fraction of particle occupied by a continuous matrix.

$$\phi_{k,l,r} = \frac{V_{p,k,l}}{A_{p,k,l}} \cdot \sqrt{\frac{n_r + 1}{2} \cdot \frac{k_{k,l,r} \cdot (C_r^S)_{k,l}^{n_r - 1} \cdot \rho_{p,k,l}^a \cdot S_0}{M_p \cdot D_{k,l,r}^*}} \tag{A7}$$

The value of the effectiveness factor is found using (A8), which is an approximation to the classical expression for a sphere [47], for all char morphologies.

$$\eta_{k,l,r} = \frac{1}{\sqrt{1 + \phi_{k,l,r}^2}} \tag{A8}$$

The effective diffusion coefficients of O_2 and CO_2 through the pore system of the char matrix, $D_{k,l,r}^*$, are found from (A9) [47].

$$D_{k,l,r}^* = \frac{\varepsilon_l}{\tau} \cdot \left(\frac{1}{D_{K,k,l,r}} + \frac{1}{D_{mix,k,l,r}} \right)^{-1} \tag{A9}$$

The Knudsen diffusion coefficient in (A9) is found from (A10) [47].

$$D_{K,k,l,r} = \frac{d_{pore}}{3} \cdot \left(\frac{8 \cdot R \cdot T_{p,k,l}}{\pi \cdot M_r} \right)^{0.5} \tag{A10}$$

The molar diffusion coefficient of the reactant is calculated from (A11) [47]. This equation is a simplification of Stefan-Maxwell's equation known as Wilke's equation and is derived for the diffusion of a key component through a stagnant mixture.

$$D_{mix,k,l,r} = \frac{1 - x_r}{\sum_{j \neq r}^{j} \frac{x_j}{D_{k,l,j,r}}} \tag{A11}$$

The bimolecular diffusion coefficients, $D_{k,l,j,r}$, used in (A11) are calculated by Chapman–Enskog's relation, (A12) [48], which includes the collision integral, $\Omega_{k,l,j,r}$, to account for intermolecular forces. The molar unit used here is (g mol^{-1}).

$$D_{k,l,j,r} = 1.8583 \cdot 10^{-7} \cdot \sqrt{T_{p,k,l}^3 \cdot \left(\frac{1}{M_j} + \frac{1}{M_r}\right)} \cdot \frac{1}{P_{atm} \cdot \sigma_{j,r}^2 \cdot \Omega_{k,l,j,r}} \tag{A12}$$

$$\Omega_{k,l,j,r} = \frac{1.06036}{\left(\frac{\kappa \cdot T_{p,k,l}}{\varepsilon}\right)_{j,r}^{0.1561}} + \frac{0.193}{\exp\left(0.47635 \cdot \left(\frac{\kappa \cdot T_{p,k,l}}{\varepsilon}\right)_{j,r}\right)} + \frac{1.03587}{\exp\left(1.52996 \cdot \left(\frac{\kappa \cdot T_{p,k,l}}{\varepsilon}\right)_{j,r}\right)} + \frac{1.76474}{\exp\left(3.89411 \cdot \left(\frac{\kappa \cdot T_{p,k,l}}{\varepsilon}\right)_{j,r}\right)} \tag{A13}$$

A.3. Equations relating to heat and mass transfer

The convective heat transfer coefficient between gas and particles are described by (A14), which is valid for forced convection around a sphere submerged in a fluid [48].

$$h_{p,k,l} = \left(2 + 0.60 \cdot \mathrm{Re}_{p,k,l}^{\frac{1}{2}} \cdot \mathrm{Pr}_{p,k,l}^{\frac{1}{3}}\right) \cdot \left(\frac{\lambda_{mix,f,k,l}}{d_{p,k,l}}\right) \tag{A14}$$

The particle Reynolds and Prandtl numbers are defined by (A15) and (A16) where the subscript f indicates that the physical properties of the gas are found at an average temperature between the particle and the bulk gas.

$$\mathrm{Re}_{p,k,l} = \frac{d_{p,k,l} \cdot v_{s,k,l} \cdot \rho_{mix,f,k,l}}{\mu_{mix,f,k,l}} \tag{A15}$$

$$\mathrm{Pr}_{p,k,l} = \frac{C_{p,mix,f,k,l} \cdot \mu_{mix,f,k,l}}{\lambda_{mix,f,k,l}} \tag{A16}$$

The heat transfer between the gas and reactor wall is taking place by forced convection in the laminar regime ($\mathrm{Re}_g < 4000$). The wall heat transfer coefficient, h_w, is described by (A17) that applies for heat transfer in a circular tube [49].

$$h_w = 1.62 \cdot \mathrm{Re}_g^{\frac{1}{3}} \cdot \mathrm{Pr}_g^{\frac{1}{3}} \cdot \left(\frac{D_R}{L_R}\right)^{\frac{1}{3}} \cdot \left(\frac{\lambda_{mix}}{D_R}\right) \tag{A17}$$

In order to increase the applicability of the model (A18) is also included to account for heat transfer between the gas and reactor wall in case of turbulent gas flow ($\mathrm{Re}_g > 4000$) [49]. As it is the case for (A17), (A18) applies for heat transfer in a circular tube.

$$h_w = \left(0.023 \cdot \mathrm{Re}_g^{\frac{4}{5}} \cdot \mathrm{Pr}_g^{\frac{1}{3}}\right) \cdot \left(\frac{\lambda_{mix}}{D_R}\right) \tag{A18}$$

The Reynolds and Prandtl numbers of the gas are defined by (A19) and (A20) where the absence of the subscript f indicates that the physical properties of the gas are found at the bulk gas temperature.

$$\mathrm{Re}_g = \frac{D_R \cdot \hat{v}_g \cdot \rho_{mix}}{\mu_{mix}} \tag{A19}$$

$$\mathrm{Pr}_g = \frac{C_{p,mix} \cdot \mu_{mix}}{\lambda_{mix}} \tag{A20}$$

It should be noted that there exists a transitional interval, $\mathrm{Re}_g \sim 2000$–4000, where the flow is shifting gradually from laminar to turbulent. The bulk gas Reynolds numbers during the experiments have however been between 400 and 1100 wherefore (A17) has been used in all the simulations presented here.

In (A14)–(A20) heat capacities, viscosities and thermal conductivities of the gas are depending on temperature, which is also indicated by the subscripts on the Reynolds and Prandtl number. In addition these properties also depend on the composition of the gas. The pure component viscosities of N_2, CO_2 and O_2 are found from (A21), which originates from gas kinetic theory and includes the collision integral, Ω_j (A22), to account for intermolecular forces [48]. The molar weight M_j is in the unit (g mol^{-1}).

$$\mu_j = 2.6693 \cdot 10^{-6} \cdot \frac{\sqrt{M_j \cdot T}}{\sigma_j^2 \cdot \Omega_j} \tag{A21}$$

$$\Omega_j = \frac{1.16145}{\left(\frac{\kappa \cdot T}{\varepsilon}\right)_j^{0.14874}} + \frac{0.52487}{\exp\left(0.77320\left(\frac{\kappa \cdot T}{\varepsilon}\right)_j\right)} + \frac{2.16178}{\exp\left(2.43787\left(\frac{\kappa \cdot T}{\varepsilon}\right)_j\right)} \tag{A22}$$

In (A21) and (A22) the temperature T is not indexed as this can be either the bulk gas or a film layer temperature. When used for film layer calculations the indexes k and l are used to account for particle size and morphology.

Using the pure component viscosity in (A21) the Eucken equation (A23) [48] and the Eucken correlation (A24) [50] are used to find thermal conductivities of the pure components. The Eucken equation is used for N_2 and O_2 and the Eucken correlation is used for CO_2 as this was found to give the best fits with available data of thermal conductivities.

$$\lambda_j = \left(C_{p,j} + \frac{5}{4} \cdot \frac{R}{M_j}\right) \cdot \mu_j \tag{A23}$$

$$\lambda_j = \left(C_{p,j} - R \cdot \left(1 - \frac{9}{4 \cdot M_j}\right)\right) \cdot \mu_j \tag{A24}$$

From the pure component properties the thermal conductivity and viscosity of the mixture are found from (A25) [51].

$$\mu_{mix}/\lambda_{mix} = \sum_j \frac{\mu_j/\lambda_j}{1 + \frac{1}{x_j} \cdot \sum_{h \neq j}^{h} x_h \cdot \Gamma_{j,h}} \tag{A25}$$

$$\Gamma_{j,h} = \frac{1}{\sqrt{8}} \cdot \left(1 + \frac{M_j}{M_h}\right)^{-\frac{1}{2}} \cdot \left(1 + \left(\frac{\mu_j/\lambda_j}{\mu_h/\lambda_h}\right)^{\frac{1}{2}} \cdot \left(\frac{M_h}{M_j}\right)^{\frac{1}{4}}\right)^2 \tag{A26}$$

The pure component heat capacities, necessary to calculate the Prandtl numbers and thermal conductivities are described by a second order polynomial given in (A27) [52].

$$C_{p,j} = a_j + b_j \cdot T + c_j \cdot T^{-2} \tag{A27}$$

Values used in (A27) for the three gases are shown in Table A1 [52].

As it was the case with (A21) and (A22) the temperature in (A27) is not indexed as this can be either a particle film layer or bulk gas temperature. The heat capacity of the gas mixture is found from (A28).

$$C_{p,mix} = \sum_j x_j \cdot C_{p,j} \tag{A28}$$

Similar to (A28) the mixture density is found from (A29) where the temperature also can by either that of a particle film layer or the bulk gas.

$$\rho_{mix} = \frac{P \cdot \sum_j x_j \cdot M_j}{R \cdot T} \tag{A29}$$

The mass transfer coefficient of the gas film layer, $k_{c,k,l,r}$, is found from (A30) [48], which applies for a sphere experiencing forced convection in a fluid.

Table A1
Constants used in (A27) [52].

Component/constant	a (J K^{-1} kg^{-1})	b (J K^{-2} kg^{-1})	c (J K kg^{-1})
N_2	1020.71	$1342.86 \cdot 10^{-4}$	$-1785.71 \cdot 10^3$
CO_2	1004.55	$1997.73 \cdot 10^{-4}$	$-1959.09 \cdot 10^4$
O_2	936.25	$1306.25 \cdot 10^{-4}$	$-5218.75 \cdot 10^3$

$$k_{c,k,l,r} = \left(2 + 0.60 \cdot \mathrm{Re}_{p,k,l}^{\frac{1}{2}} \cdot Sc_{p,k,l,r}^{\frac{1}{3}}\right) \cdot \left(\frac{D_{mix,f,k,l,r}}{d_{p,k,l}}\right) \tag{A30}$$

The particle Reynolds and Schmidt's number is defined by (A15) and (A31).

$$Sc_{p,k,l,r} = \frac{\mu_{mix,f,k,l}}{\rho_{mix,f,k,l} \cdot D_{mix,f,k,l,r}} \tag{A31}$$

The molar diffusion coefficient of the reactant, $D_{mix,f,k,l,r}$, is found from (A11) using the film layer temperature to calculate bimolecular diffusion coefficients in (A12) and (A13).

A.4. Particle slip velocity, heat capacity, enthalpy and concentration

The slip velocity of a particle is used in both the mass and energy balances in Section 3.2 and to calculate the Reynolds number of a particle in (A15). The particle slip velocity is found in (A32)–(A34) as suggested by Haider and Levenspiel [53].

$$v_{s,k,l} = \frac{v_{s,k,l}^{\bullet}}{\left(\frac{\rho_{mix,f,k,l}^2}{g \cdot \mu_{mix,f,k,l} \cdot (\rho_{p,k,l}^a - \rho_{mix,f,k,l})}\right)^{\frac{1}{3}}} \tag{A32}$$

$$v_{s,k,l}^{\bullet} = \left(\frac{1}{\frac{10.8323}{(d_{p,k,l}^{\bullet})^{1.6486}} + \frac{0.626029}{(d_{p,k,l}^{\bullet})^{0.41215}}}\right)^{1.21315} \tag{A33}$$

$$d_{p,k,l}^{\bullet} = d_{p,k,l} \cdot \left(\frac{g \cdot \rho_{mix,f,k,l} \cdot (\rho_{p,k,l}^a - \rho_{mix,f,k,l})}{\mu_{mix,f,k,l}^2}\right)^{\frac{1}{3}} \tag{A34}$$

In (A32) and (A34) values of film layer viscosity is found from (A25), film layer density is found from (A29) and apparent particle densities are found from (A4)–(A6).

In the solid energy balances it is necessary to describe the solid heat capacity as a function of particle temperature. This relationship is described by Coimbra and Queiroz [54] in (A35)–(A38). In (A36) the characteristic Einstein temperature, θ_1, which is a measure of the energy in atomic vibrations, has a constant value of 380 K.

$$R^x = R \cdot \left(\sum_{j=0}^{N} \frac{w_j}{M_j}\right) \tag{A35}$$

$$EF_{i,k,l} = \left(\frac{\theta_i}{T_{p,k,l}}\right)^2 \cdot \frac{\exp\left(\frac{\theta_i}{T_{p,k,l}}\right)}{\left(\exp\left(\frac{\theta_i}{T_{p,k,l}}\right) - 1\right)^2} \tag{A36}$$

$$\theta_2 = \frac{Q_{LHV}}{R^x} \cdot \left(\frac{9 - 4.973 \cdot (1 - VM_{daf})}{100}\right) \tag{A37}$$

$$C_{p,k,l} = 3 \cdot R^x \cdot \left(\frac{EF_{1,k,l}}{3} + \frac{2 \cdot EF_{2,k,l}}{3}\right) \tag{A38}$$

In (A37) the volatile content is zero in all of the simulations as the equation is used on devolatilized char. The lower heating value, Q_{LHV}, is 32.75 MJ kg^{-1} corresponding to the oxidation of one kg carbon to carbon dioxide at standard conditions.

The solid enthalpy, used to calculate the particle heat of reaction, will be approximated as that of graphite [34].

$$H_{p,k,l} = 2.286 \cdot T_{p,k,l} - 1099.5 \tag{A39}$$

The concentration of a particle fraction defined by size and morphology will change down the reactor as the slip velocity of that fraction will decrease during its consumption. The concentration of a particle fraction defined by size and morphology is given by (A40).

$$N_{l,k} = \frac{\tilde{m}_{Char} \cdot \alpha_l \cdot \Theta_k}{V_{p0,k} \cdot \rho_{p0,l}^a \cdot (v_{s,k,l} + v_g) \cdot A_R} \tag{A40}$$

A.5. Gas velocities

The linear velocity of the section of the laminar gas front where particles are sampled during experiments is given by (A41). The average linear gas velocity in the reactor is calculated as (A42).

$$v_g = \frac{\hat{v}_g \cdot (2 \cdot R_R^2 - R_F^2)}{R_R^2} \tag{A41}$$

$$\hat{v}_g = \frac{F_T \cdot R \cdot T_g}{A_R \cdot P} \tag{A42}$$

Appendix B. Derivation of particle mass balances

The particle mass balances for cenospheres, network chars and dense chars are derived in the following. All mass balances include reaction on both exterior and interior surfaces but consumption is taking place after a shrinking sphere model. To describe the development of interior surface the volumetric reaction model is used for all char morphologies.

B.1. Cenospheric char

The mass balance for a cenospheric char particle is based on continuous char matrix and its derivation proceeds as shown below.

$$\begin{aligned}\frac{dm_{p,k,r}}{dt} &= -(m_{p,k} \cdot S_k \cdot k_{k,r} \cdot (C_r^S)_k^{n_r} \cdot \eta_{k,r} + A_{p,k} \cdot k_{k,r} \cdot (C_r^S)_k^{n_r}) \\ &\Rightarrow \frac{d\frac{4}{3} \cdot \pi \cdot \rho_p \cdot (R_{p,k}^3 - R_{p,k,I}^3)_r}{dt} = -\left(\frac{4}{3} \cdot \pi \cdot (R_{p,k}^3 - R_{p,k,I}^3) \cdot \rho_p \cdot S_k \right. \\ &\left. \cdot k_{k,r} \cdot (C_r^S)_k^{n_r} \cdot \eta_{k,r} + 4 \cdot \pi \cdot R_{p,k}^2 \cdot k_{k,r} \cdot (C_r^S)_k^{n_r}\right) \Rightarrow \frac{d(R_{p,k}^3 - R_{p,k,I}^3)_r}{dt} \\ &= -\left((R_{p,k}^3 - R_{p,k,I}^3) \cdot S_k \cdot k_{k,r} \cdot (C_r^S)_k^{n_r} \cdot \eta_{k,r} + \frac{3 \cdot R_{p,k}^2}{\rho_p} \cdot k_{k,r} \cdot (C_r^S)_k^{n_r}\right)\end{aligned} \tag{B1}$$

Before continuing the derivation the differential in (B1) must be redefined using particle conversion. This redefinition is shown in the following equation:

$$\begin{aligned}X_k &= \frac{m_{p0,k} - m_{p,k}}{m_{p0,k}} \Rightarrow X_k = 1 - \frac{\frac{4}{3} \cdot \pi \cdot (R_{p,k}^3 - R_{p,k,I}^3) \cdot \rho_{p,N}^a}{\frac{4}{3} \cdot \pi \cdot (R_{p0,k}^3 - R_{p,k,I}^3) \cdot \rho_{p,N}^a} \Rightarrow X_k \\ &= 1 - \frac{(R_{p,k}^3 - R_{p,k,I}^3)}{(R_{p0,k}^3 - R_{p,k,I}^3)} \Rightarrow (R_{p,k}^3 - R_{p,k,I}^3) = (R_{p0,k}^3 - R_{p,k,I}^3) \cdot (1 - X_k)\end{aligned} \tag{B2}$$

Substituting (B2) into (B1) yields (B3), the last intermediate expression before the final formulation of the mass balance is achieved.

$$\frac{dX_{k,r}}{dt} = k_{k,r} \cdot (C_r^S)_k^{n_r} \cdot \left((1 - X_k) \cdot S_0 \cdot \eta_{k,r} + \frac{3 \cdot R_{p,k}^2}{\rho_p \cdot (R_{p0,k}^3 - R_{p,k,I}^3)}\right) \tag{B3}$$

In order to express the radius in (B3) as a function of char conversion the derivation below is made from (B2). The definition $\delta_0 = (R_{p0,k} - R_{p,k,I})/R_{p0,k}$ is utilized in the derivation.

$$\begin{aligned}(R_{p,k}^3 - R_{p,k,I}^3) &= (R_{p0,k}^3 - R_{p,k,I}^3) \cdot (1 - X_k) \Rightarrow R_{p,k} \\ &= ((R_{p0,k}^3 - R_{p,k,I}^3) \cdot (1 - X_k) + R_{p,k,I}^3)^{(\frac{1}{3})} \Rightarrow R_{p,k} \\ &= (R_{p0,k}^3 - R_{p0,k}^3 \cdot X_k + R_{p,k,I}^3 \cdot X_k)^{(\frac{1}{3})} \Rightarrow R_{p,k} \\ &= (R_{p0,k}^3 \cdot (1 - X_k) + R_{p0,k}^3 \cdot (1 - \delta_0)^3 \cdot X_k)^{(\frac{1}{3})} \\ &\Rightarrow R_{p,k} = R_{p0,k}(1 - X_k \cdot (1 - (1 - \delta_0)^3))^{(\frac{1}{3})}\end{aligned} \tag{B4}$$

Substituting (B4) into (B3) and using the definition of δ_0 the final form of the cenospheric mass balance is (2).

$$\frac{dX_{k,r}}{dL} = \frac{k_{k,r}\cdot (C_r^S)_k^{n_r}}{v_{s,k}+v_g} \cdot \left(S_0\cdot(1-X_k)\cdot\eta_{k,r} + \frac{3\cdot(1-X_k\cdot(1-(1-\delta_0)^3))^{\left(\frac{2}{3}\right)}}{\rho_p\cdot R_{p0,k}\cdot(1-(1-\delta_0)^3)} \right) \quad (2)$$

B.2. Network chars and dense chars

The derivation of the mass balance for a network char and a dense char is identical and proceeds as follows.

$$\begin{aligned} \frac{dm_{p,k,l,r}}{dt} &= -(m_{p,k,l}\cdot S_{k,l}\cdot k_{k,l,r}\cdot (C_r^S)_{k,l}^{n_r}\cdot\eta_{k,l,r} + A_{p,k,l}\cdot k_{k,l,r}\cdot (C_r^S)_{k,l}^{n_r}) \\ &\Rightarrow \frac{d\frac{4}{3}\cdot\pi\cdot\rho_p\cdot R_{p,k,l,r}^3}{dt} = -\left(\frac{4}{3}\cdot\pi\cdot R_{p,k,l}^3\cdot\rho_p\cdot S_{k,l}\cdot k_{k,l,r}\cdot (C_r^S)_{k,l}^{n_r}\right. \\ &\left.\cdot\eta_{k,l,r} + 4\cdot\pi\cdot R_{p,k,l}^2\cdot k_{k,l,r}\cdot (C_r^S)_{k,l}^{n_r}\right) \Rightarrow \frac{dR_{p,k,l,r}^3}{dt} \\ &= -\left(R_{p,k,l}^3\cdot S_{k,l}\cdot k_{k,l,r}\cdot (C_r^S)_{k,l}^{n_r}\cdot\eta_{k,l,r} + \frac{3\cdot R_{p,k,l}^2}{\rho_p}\cdot k_{k,l,r}\cdot (C_r^S)_{k,l}^{n_r}\right) \end{aligned} \quad (B5)$$

Before the derivation can continue the differential in (B5) must be redefined using char conversion to express the particle radius. This definition is shown in the following equation:

$$R_{p,k,l} = R_{p0,k,l}\cdot(1-X_{k,l})^{\left(\frac{1}{3}\right)} \quad (B6)$$

Substituting (B6) into (B5) yields the final form of the network- and dense char mass balances, shown in (B7). It can be seen that (B7) is identical to (2) when $\delta_0 = 1$.

$$\begin{aligned} \frac{dX_{k,l,r}}{dt} &= k_{k,l,r}\cdot(C_r^S)_{k,l}^{n_r}\cdot\left(\frac{R_{p,k,l}^3}{R_{p0,k,l}^3}\cdot S_{k,l}\cdot\eta_{k,l,r} + \frac{3\cdot R_{p,k,l}^2}{R_{p0,k,l}^3\cdot\rho_p}\right) \\ &\Rightarrow \frac{dX_{k,l,r}}{dL} = \frac{k_{k,l,r}\cdot(C_r^S)_{k,l}^{n_r}}{v_{s,k,l}+v_g}\cdot\left(S_0\cdot(1-X_{k,l})\cdot\eta_{k,l,r} + \frac{3\cdot(1-X_{k,l})^{\left(\frac{2}{3}\right)}}{\rho_p\cdot R_{p0,k,l}}\right) \end{aligned} \quad (B7)$$

References

[1] Buhre BJP, Elliot LK, Sheng CD, Gupta RP, Wall TF. Oxy-fuel combustion technology for coal-fired power generation. Prog Energy Combust Sci 2005;31:283–307.

[2] Figueroa JD, Fout T, Plasynski S, McIlvried H, Srivastava RD. Advances in CO_2 capture technology – The US Department of Energy's carbon sequestration program. Int J Greenhouse Gas Control 2008;2:9–20.

[3] Murphy JJ, Shaddix CR. Combustion kinetics of coal chars in oxygen-enriched environments. Combust Flame 2006;144:710–29.

[4] Hurt R, Sun J-K, Lunden M. A kinetic model of carbon burnout in pulverized coal combustion. Combust Flame 1998;113:181–97.

[5] Murphy JJ, Shaddix CR. Effect of reactivity loss on apparent reaction order of burning char particles. Combust Flame 2010;157:535–9.

[6] Cloke M, Wu T, Barranco R, Lester E. Char characterisation and its application in a coal burnout model. Fuel 2003;82:1989–2000.

[7] Wu T, Lester E, Cloke M. A burnout prediction model based around char morphology. Energy Fuels 2006;20:1175–83.

[8] Ballester J, Jiménez S. Kinetic parameters for the oxidation of pulverized coal as measured from drop tube tests. Combust Flame 2005;142:210–22.

[9] Jiménez S, Ballester J. Study of the evolution of particle size distributions and it effects on the oxidation of pulverized coal. Combust Flame 2007;151:482–94.

[10] Mitchell RE, Ma L, Kim BJ. On the burning behavior of pulverized coal chars. Combust Flame 2007;151:426–36.

[11] Hurt RH, Lunden MM, Brehob EG, Maloney DJ. Statistical kinetics for pulverized coal combustion. In: 26th Symposium (international) on combustion; 1996. p. 3169–77.

[12] Gale TK, Bartholomew CH, Fletcher TH. Effects of pyrolysis heating rate on intrinsic reactivities of coal char. Energy Fuels 1996;10:766–75.

[13] Ma L, Mitchell R. Modeling char oxidation behavior under zone II burning conditions at elevated pressures. Combust Flame 2009;156:37–50.

[14] Yu J, Lucas JA, Wall TF. Formation of the structure of chars during devolatilization of pulverized coal and its thermoproperties: a review. Prog Energy Combust Sci 2007;33:135–70.

[15] Brix J, Jensen PA, Jensen AD. Coal devolatilization and char conversion under suspension fired conditions in O_2/N_2 and O_2/CO_2 atmospheres. Fuel 2010;89:3373–80.

[16] Bejarano PA, Levendis YA. Single-coal-particle combustion in O_2/N_2 and O_2/CO_2 environments. Combust Flame 2008;153:270–87.

[17] Rathnam RK, Elliot LK, Wall TF, Liu Y, Moghtaderi B. Differences in reactivity of pulverized coal in air (O_2/N_2) and oxy-fuel (O_2/CO_2) conditions. Fuel Process Technol 2009;90:797–802.

[18] Molina A, Shaddix CR. Ignition and devolatilization of pulverized bituminous coal particles during oxygen/carbon dioxide coal combustion. Proc Combust Inst 2007;31:1905–12.

[19] Shaddix CR, Molina A. Particle imaging of ignition and devolatilization of pulverized coal during oxy-fuel combustion. Proc Combust Inst 2009;32:2091–8.

[20] Li Q, Zhao C, Chen X, Wu W, Li Y. Comparison of pulverized coal combustion in air and in O_2/CO_2 mixtures by thermo-gravimetric analysis. J Anal Appl Pyrolysis 2009;85:521–8.

[21] Várhegyi G, Szabó P, Jakab E, Till F. Mathematical modeling of char reactivity in Ar–O_2 and CO_2–O2 mixtures. Energy Fuels 1996;10:1208–14.

[22] Liu H. Combustion of coal char in O_2/CO_2 and O_2/N_2 mixtures: a comparative study with non-isothermal thermogravimetric analyzer (TGA) tests. Energy Fuels 2009;23:4278–85.

[23] J. Brix, PhD thesis, Department of Chemical and Biochemical Engineering, Technical University of Denmark, 2011, To be submitted.

[24] Shu X, Xu X. Study on morphology of chars from coal pyrolysis. Energy Fuels 2001;15:1347–53.

[25] Bailey JG, Tate A, Diessel CFK, Wall TF. A char morphology system with applications to coal combustion. Fuel 1990;69:225–39.

[26] Tsai C-Y, Scaroni AW. Reactivity of bituminous coal chars during the initial stage of pulverized-coal combustion. Fuel 1987;66:1400–6.

[27] Tsai C-Y, Scaroni AW. The structural changes of bituminous coal particles during the initial stages of pulverized-coal combustion. Fuel 1987;66:200–6.

[28] Gao H, Murata S, Nomura M, Ishigaki M, Qu M, Tokuda M. Experimental observation and image analysis for evaluation of swelling and fluidity of single coal particles heated with CO_2 laser. Energy Fuels 1997;11:730–8.

[29] Gao H, Murata S, Nomura M, Ishigaki M, Tokuda M. Preliminary surface structure transition of coal particles during prepyrolysis with CO_2 laser. Energy Fuels 1996;10:1227–34.

[30] Gale TK, Bartholomew CH, Fletcher TH. Decreases in the swelling and porosity of bituminous coals during devolatilization at high heating rates. Combust Flame 1995;100:94–100.

[31] Fletcher TH. Swelling properties of coal chars during rapid pyrolysis and combustion. Fuel 1993;72:1485–95.

[32] Kee RJ, Rupley FM, Miller JA. CHEMKIN II: a FORTRAN chemical kinetics package for the analysis of gas-phase chemical kinetics, report no. SAND 89-8009, Sandia National Laboratories; 1989.

[33] Oh MS, Peters WA, Howard JB. An experimental and modeling study of softening coal pyrolysis. AIChE J 1989;35:775–92.

[34] Brix J. A model for entrained flow reactor gasification of solid fuels for syngas production, MSc thesis, Department of Chemical and Biochemical Engineering, CHEC Research Center, Technical University of Denmark, 2007.

[35] Norman J, Pourkashanin M, Williams A. Modeling the formation and emission of environmentally unfriendly coal species in some gasification processes. Fuel 1997;76:1201–16.

[36] Wen CY. Noncatalytic heterogeneous solid fluid reaction models. Ind Eng Chem 1968;9:34–54.

[37] Bhatia SK, Perlmutter DD. A random pore model for fluid–solid reactions: I. Isothermal, kinetic control. AIChE J 1980;26:379–86.

[38] Bhatia SK, Perlmutter DD. A random pore model for fluid–solid reactions: II. Diffusion and transport effects. AIChE J 1981;27:247–54.

[39] Szekely J, Evans JW. A structural model for gas–solid reactions with a moving boundary. Chem Eng Sci 1970;25:1091–107.

[40] Szekely J, Evans JW. A structural model for gas–solid reactions with a moving boundary – II. Chem Eng Sci 1971;26:1901–13.

[41] Sohn HY, Szekely J. A structural model for gas–solid reactions with a moving boundary – III. A general dimensionless representation of the irreversible reaction between a porous solid and a reactant gas. Chem Eng Sci 1972;27:763–78.

[42] Yagi S, Kunii D. Studies on combustion of carbon particles in flames and fluidized beds. In: Fifth symposium (international) on combustion; 1955. p. 231–44.

[43] Zolin A, Jensen A, Pedersen LS, Dam-Johansen K. A comparison of coal char reactivity determined from thermogravimetric and laminar flow reactor experiments. Energy Fuels 1998;12:268–76.

[44] Charpenay S, Serio MA, Solomon PR. The prediction of coal char reactivity under combustion conditions. In: Twenty-fourth symposium (international) on combustion; 1992. p. 1189–97.

[45] Mon E, Amundson NR. Diffusion and reaction in a stagnant boundary layer about a carbon particle. 2. An extension. Ind Eng Chem Fundam 1978;17:313–21.

[46] Zhang H, Pu W-X, Ha S, Li Y, Sun M. The influence of included minerals on the intrinsic reactivity of char prepared at 900 °C in a drop tube furnace and a muffle furnace. Fuel 2009;88:2303–10.

[47] Froment GF, Bischoff KB. Chemical reactor analysis and design. 2nd ed. John Wiley & Sons, Inc.; 1990.
[48] Bird RB, Stewart WE, Lightfoot EN. Transport phenomena. 2nd ed. John Wiley & Sons, Inc.; 2002.
[49] Griskey RG. Transport phenomena and unit operations – a combined approach. 1st ed. John Wiley & Sons, Inc.; 2002.
[50] Gosse J. The thermal conductivity of pure polyatomic gasses at moderate pressure. Int J Heat Mass Transfer 1992;35:599–604.
[51] Wilke CR. A viscosity equation for gas mixtures. J Chem Phys 1950;18:517–9.
[52] Laidler KJ, Meiser JH, Sanctuary BC. Physical chemistry. 4th ed. Houghton Mifflin; 2002.
[53] Haider A, Levenspiel O. Drag coefficient and terminal velocity of spherical and nonspherical particles. Powder Technol 1989;58:63–70.
[54] Coimbra CFM, Queiroz M. Evaluation of a dimensionless group number to determine second-Einstein temperatures in a heat capacity model for all coal ranks. Combust Flame 1995;101:209–20.

I&EC research
Industrial & Engineering Chemistry Research

ARTICLE

pubs.acs.org/IECR

Performance of a Wet Flue Gas Desulfurization Pilot Plant under Oxy-Fuel Conditions

Brian B. Hansen,[†] Folmer Fogh,[‡] Niels Ole Knudsen,[§] and Søren Kiil*[,†]

[†]Department of Chemical and Biochemical Engineering, Technical University of Denmark, Building 229, DK-2800 Kongens Lyngby, Denmark

[‡]Dong Energy A/S, Kraftværksvej 53, DK-7000 Fredericia, Denmark

[§]Vattenfall A/S, Nordjyllandsværket, Nefovej 50, DK-9310 Vodskov, Denmark

ABSTRACT: Oxy-fuel firing is a promising technology that should enable the capture and storage of anthropogenic CO_2 emissions from large stationary sources such as power plants and heavy industry. However, this new technology has a high energy demand for air separation and CO_2 compression and storage. Unresolved issues, such as determination of the optimal recycle location of flue gas, the flue gas cleaning steps required (SO_2, NO_x, and particles), and the impact of an oxy-fuel flue gas on the cleaning steps, also persist. The aim of this work was to study the performance of the wet flue gas desulfurization (FGD) process under operating conditions corresponding to oxy-fuel firing. The most important output parameters were the overall degree of desulfurization and the residual limestone concentration in the gypsum slurry. Pilot-scale experiments quantified that the introduction of a flue gas with 90 vol % CO_2, at a holding tank pH 5.4, reduced the limestone dissolution rate significantly and thereby increased the residual, particulate limestone concentration in the gypsum slurry from 3.2 to 5.0 g/L slurry relative to a base-case (air-firing) experiment with a flue gas CO_2 concentration around 7 vol %. In the same experiment, due to the higher residual limestone concentration, the degree of desulfurization increased from 91 to 94%. The addition of 10 mM adipic acid to the slurry was not sufficient to return the increased concentration of residual limestone to the base-case level, but an additional increase in desulfurization degree, from 94 to 97%, was obtained. Using a holding tank pH 5.0 (no adipic acid) returned both parameters to the levels observed in the base-case experiment.

1. INTRODUCTION

Combustion of fossil fuels, such as coal and oil, results in flue gases containing mainly N_2, CO_2, O_2, and H_2O, but with traces of pollutants such as NO_x, SO_2, and particles. In modern power plants, NO_x, SO_2, and particles are efficiently removed using selective catalytic reduction, wet flue gas desulfurization, and electrostatic precipitators. CO_2, on the other hand, is released in large amounts to the atmosphere. Increased public and political attention to the world's anthropogenic (i.e., caused by human activity) CO_2 emissions and the potential influence of these on the global climate has stimulated research in alternative energy sources, novel technologies, and adaptations of technologies currently in use. Technical solutions for CO_2 capture and subsequent storage in geological formations have received significant attention.[1,2] Three different main approaches for CO_2 capture exist as discussed in detail by Buhre et al.[1] and Toftegaard et al.:[2] precombustion capture, postcombustion capture, and oxy-fuel combustion. In oxy-fuel combustion, as opposed to conventional air-firing, the fuel is burned in a mixture of O_2 (from an air separation process) and recirculated CO_2 and water. After other pollutants (SO_2, NO_x, and particles) and water have been removed, the concentrated CO_2 flue gas can be compressed to liquid CO_2 and stored in geological formations.

In this work, the effect of oxy-fuel combustion on limestone-based wet flue gas desulfurization (FGD) is investigated using a pilot-scale wet FGD plant. The wet scrubber constituted the vast majority (>85%) of FGD capacity installed at power plants worldwide in 1999[3] and it is still the dominant FGD technology today, which makes it the most relevant FGD technology to study. To achieve the goal of capture and storage of CO_2, with as low concentrations of impurities as possible, and thereby reach close to zero CO_2 emissions from fossil fuel combusting power plants, a continued highly efficient operation of the wet FGD process, as well as other flue gas cleaning processes, is an important requirement. However, no previous studies of wet FGD performance under oxy-fuel conditions have been found in the literature.

2. THE OXY-FUEL PROCESS AND WET FGD

The oxy-fuel combustion process takes place in a gas phase consisting of CO_2, H_2O, and O_2. The N_2 has been removed from the "combustion air", by an air separation process. To avoid excessive flame temperatures, flue gas will be recycled to the burners. The concentrated CO_2 gas phase can be compressed into liquid CO_2 and stored in geological formations. Different potential locations of the recycle stream exist, and this choice may influence the flue gas flow rate, the flue gas composition, and the overall performance of the power plant.[1,2,4]The high CO_2 concentration in the flue gas may influence the operation of the boiler, steam cycle, and any flue gas cleaning technologies, which are still needed to clean and dewater the flue gas to obtain a liquid CO_2 product suitable for transport and storage in geological formations.[4−6] A combined SO_2 and NO_x removal during CO_2

Received: November 2, 2010
Accepted: March 4, 2011
Revised: March 4, 2011

dx.doi.org/10.1021/ie1022173 | *Ind. Eng. Chem. Res.* XXXX, XXX, 000–000

Table 1. Overview of Experiments Performed and Operating Conditions Selected (Concentrations Expressed on Wet Basis)

experiment	flue gas flow rate ($Nm^3 \cdot h^{-1}$)	SO_2 (ppm(v))	CO_2[a] (%)	H_2O[b] (%)	O_2 (%)	N_2 (%)	T_{slurry} (°C)
base-case, pH 5.4	17.9	970	~7	9.8	6.8	76.3	45.6
oxy-fuel, pH 5.4	19.0	940	88.2	9.2	0.5	2.0	44.2
oxy-fuel, pH 5.4 (10 mM adipic acid)[c]	19.1	940	87.4	9.0	0.7	2.8	43.8
oxy-fuel, pH 5	18.9	1030	91.3	8.6	0.0	0.0	42.9
oxy-fuel, pH 5, low flow	3.9	4480[d]	87.7	9.3	0.5	2.0	44.4
oxy-fuel, pH 5, low flow, high temperature	4.1	4240[d]	84.2	14.4	0.2	0.8	53.3

[a] Estimated based on O_2, N_2, and water content (except for base case, pH 5.4). [b] H_2O content at saturation estimated based on temperature and Antoine parameters from Gubkov et al.[17] [c] For 10 mM in feed tank, corresponding to 5.5 mM in holding tank.[18] [d] SO_2 measured at Q = 19 Nm^3/h and subsequently recalculated to the concentration at Q = 4 Nm^3/h.

compression and liquefaction (reactions with water forming H_2SO_4 and HNO_3) is currently being researched in a bench-scale setup (4 and 1 L reactors in series and a flue gas flow rate of 1−5 L/min).[7,8] This novel process is relevant, but it may face some challenges in terms of scale-up and the fact that no cleaning of the recycle stream upstream will take place. This can lead to potential system/boiler corrosion, slagging, and fouling due to the pollutants accumulating in the recycle stream.[2] Operation of traditional flue gas cleaning technologies at oxy-fuel conditions may prove highly relevant when a dry and noncorrosive recycle stream is necessary and for the potential retrofitting of existing units.

One such flue gas cleaning process is the widely used wet flue gas desulfurization process, in which the SO_2 and other acidic compounds (SO_3, HCl, and HF) formed during combustion are removed by absorption using a limestone slurry. The slurry leaving the absorber is collected in a holding tank, where the SO_2 absorbed reacts with dissolved limestone and oxidation air injected, forming gypsum of a commercial grade. The overall wet FGD reaction can be expressed as[3,9]

$$CaCO_3(s) + SO_2(g) + 2H_2O(l) + 1/2O_2(g) \rightarrow CaSO_4 \cdot 2H_2O(s) + CO_2(g) \quad (1)$$

The mass transfer rate of SO_2, and thereby the degree of desulfurization, can be influenced by both a gas and a liquid film resistance.[9] The ratio of gas to liquid film resistance is determined by the SO_2 concentration in the flue gas, the liquid to gas ratio (L/G), the contacting pattern, the reactant used, and the potential use of organic buffers in the slurry. The simultaneous absorption of HCl may also influence the SO_2 absorption through a reduced absorber pH, and in the case of accumulation in the slurry the limestone dissolution rate may decrease due to a lower driving force ($[Ca^{2+}]_s - [Ca^{2+}]_b$)[9,10]

The differences in operating conditions of an oxy-fuel power plant, compared to conventional air-firing, may influence the overall performance of a wet FGD plant in a number of ways:

1. reduced limestone dissolution rate
2. increased wet FGD operating temperature
3. external oxidation
4. flue gas flow rate

Reduced Limestone Dissolution Rate. Dissolution of limestone in acidic media in contact with a flue gas can be written as

$$CaCO_3(s) \rightleftarrows Ca^{2+} + CO_3^{2-} \quad (2)$$

$$H^+ + CO_3^{2-} \rightleftarrows HCO_3^- \quad (3)$$

$$HCO_3^- + H^+ \rightleftarrows CO_2(aq) + H_2O(l) \quad (4)$$

$$CO_2(aq) \rightleftarrows CO_2(g) \quad (5)$$

Other species present in the wet FGD slurry, such as HSO_3^-, Cl^-, SO_2, and SO_4^{2-}, also influence the rate of dissolution,[9] but this aspect is not so important for this discussion on how CO_2 influences the rate. Below a bulk phase pH value of about 5.2−5.5 (the exact value depends on temperature), an increased CO_2 absorption from a CO_2-rich gas (relative to an inert N_2 gas) enhances the rate of limestone dissolution in a $CaCl_2$ solution.[11−13] This is because H^+ ions, which increase the dissolution rate, are formed in the kinetically controlled reaction 4 that takes place in the boundary layer around the limestone particles.[13] Therefore, CO_2(aq) indirectly helps in transporting H^+ toward the limestone surface. The simultaneous formation of HCO_3^- does not inhibit the rate of dissolution of limestone because the equilibrium 3 is shifted to the right at these pH values (i.e., the concentration of CO_3^{2-} is kept low and thereby does not have a significant influence on the equilibrium 2). However, above a bulk phase pH value of 5.2−5.5, a high CO_2 content in the gas phase (80−90 vol %) increases the liquid phase concentration of HCO_3^-, via reactions 4 and 5, and due to the higher values of bulk phase pH, the equilibrium 3 is now shifted more to the left, whereby the bulk phase concentration of CO_3^{2-} increases. This also leads to a higher concentration of CO_3^{2-} at the particle surface and causes a drastic reduction in limestone dissolution rate via equilibrium 2 as verified experimentally by Allers et al.[11,12] and Chan et al.[13] To clarify, the driving force for the rate of limestone dissolution is the Ca^{2+} concentration difference between the limestone surface and the bulk phase ($[Ca^{2+}]_s - [Ca^{2+}]_b$),[9] and because the bulk phase concentration of Ca^{2+} is constant, due to the large background concentration of $CaCl_2$, it is the surface concentration of Ca^{2+} that is decreased at oxy-fuel conditions and pH values higher than about 5.2−5.5. At the particle surface, the solubility product of $CaCO_3$, equilibrium 2, must be fulfilled,[9] and when the concentration of CO_3^{2-} increases, the concentration of Ca^{2+} must decrease.

Increased Wet FGD Operating Temperature. A wet flue gas recycle will increase the water content in the gas phase, and a content of 30 vol % water or more may be obtained depending on coal quality, moisture content, and recycle ratio.[14] This will limit the evaporation taking place in the wet FGD plant, leading to a higher operating temperature. The SO_2 solubility in aqueous solution decreases with increasing temperatures, and the effect could therefore be a lower degree of desulfurization at a higher operating temperature.[15]

dx.doi.org/10.1021/ie1022173 |Ind. Eng. Chem. Res. XXXX, XXX, 000–000

External Oxidation. Pure oxygen, or an external oxidation tank, may replace the conventional air injection, used to ensure oxidation of HSO_3^- to SO_4^{2-}, to minimize the concentration of N_2 in the CO_2 stream to be compressed.[14] External oxidation has previously been used in some of the first wet FGD configurations, but these plant configurations suffered from scaling, plugging, and lower degrees of desulfurization than plants using in situ oxidation.[16]

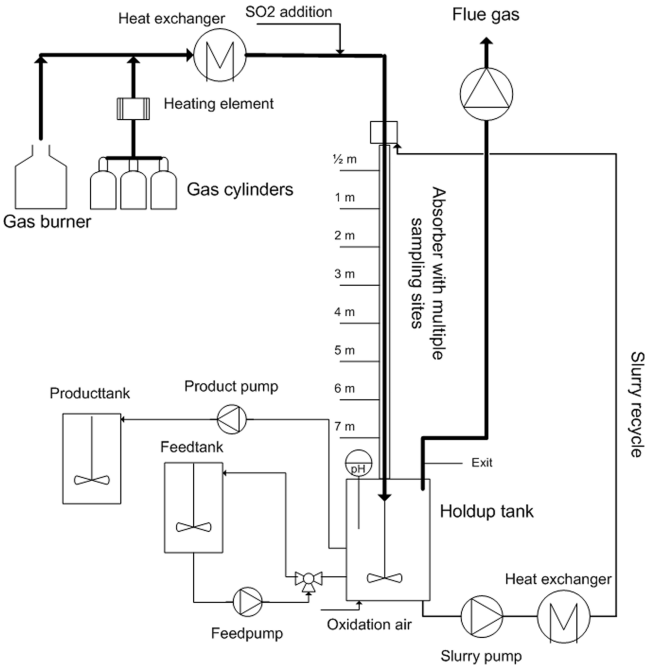

Figure 1. Outline of wet FGD pilot plant used in the experiments. The absorber is based on the falling film principle and gas and liquid flow cocurrently.

Flue Gas Flow Rate. Power plants will most likely be expected to be able to operate in both air-firing (start-up and shutdown) and oxy-fuel firing modes.[2] This will generate considerable variations in the flue gas flow rate, thereby affecting the plant performance in terms of for instance pressure drop and gas/liquid contact pattern.

Due to the high ionic strength in the slurry (high $CaCl_2$ concentration), the increased concentration of carbonate species is not expected to influence the solubility of acidic gases (SO_2 and CO_2) in the wet FGD slurry.

3. STRATEGY OF INVESTIGATION

The present investigation of the wet FGD performance under oxy-fuel conditions is based on a series of pilot-scale experiments. The pilot plant enables a high degree of control of the experimental conditions such as the flue gas flow rate, the gas phase composition (SO_2 and CO_2), and slurry pH. The conditions of the experiments performed, shown in Table 1, have been chosen to simulate the potential flue gas compositions obtained by various locations of the flue gas recycle in both new and retrofitted plants. The CO_2 concentration in the base-case experiment is somewhat lower than what may be experienced for full-scale air-fired coal combustion. However, based on the results obtained for oxy-fuel conditions in this work, this difference in CO_2 concentration is not expected to influence the results to any

Table 2. Residual Limestone Concentration in the Gypsum Slurry, Reactant Feed Rate, Holding Tank pH, and Overall Degree of Desulfurization for the Six Experiments[a]

	holding tank pH		total degree of desulfurization (±0.01)	
experiment	set point	average measured	measured	Frandsen et al.[20]
base-case, pH 5.4	5.4	5.58	0.91	–
base-case, pH 5.5	5.5	–	–	0.83[b]
base-case, pH 5.5 (adipic acid)	5.5	–	–	0.92[b]
oxy-fuel, pH 5.4	5.4	5.43	0.94	–
oxy-fuel (adipic acid)	5.4	5.43	0.97	–
oxy-fuel, pH 5.0	5.0	5.17	0.92	–
oxy-fuel, pH 5.0, low flow	5.0	5.17	0.99	–
oxy-fuel, pH 5.0 low flow, T = 53 °C	5.0	5.18	0.99	–

	residual limestone			
experiment	measured g/L slurry	measured[c] (wt %)	Frandsen et al.[20] (wt %)	slurry feed rate, 7.1 wt % $CaCO_3$ (kg/h)
base-case, pH 5.4	3.2 (±0.4)	2.1 (±0.2)	–	1.1
base-case, pH 5.5	–	–	4.6 (±0.2)	–
base-case, pH 5.5 (adipic acid)	–	–	2.2 (±0.2)	–
oxy-fuel, pH 5.4	5.0 (±0.6)	3.5 (±0.4)	–	1.6
oxy-fuel (adipic acid)	5.2 (±0.1)	3.3 (±0.1)	–	1.2
oxy-fuel, pH 5.0	2.3 (±0.1)	3.0 (±0.1)	–	1.1
oxy-fuel, pH 5.0, low flow	1.9 (±0.1)	2.3 (±0.1)	–	1.1
oxy-fuel, pH 5.0 low flow, T = 53 °C	1.7 (±0.1)	2.4 (±0.0)	–	1.1

[a] The standard deviation, stated in parentheses, has been obtained from the analysis of two separate samples retrieved at the same point in time. The total degree of desulfurization was measured in the stack (see Figure 1). [b] Degree of desulfurization in stack after 5 m absorber. Note that all other results are from a 7 m absorber. [c] Based on dry solids.

dx.doi.org/10.1021/ie1022173 |*Ind. Eng. Chem. Res.* XXXX, XXX, 000–000

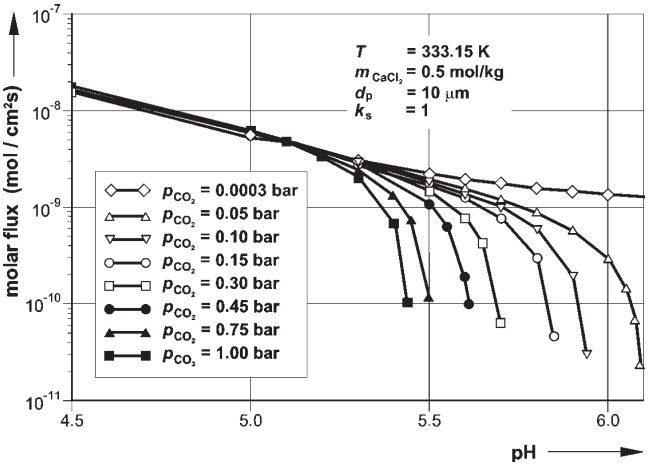

Figure 2. Simulated dissolution rate of limestone particles with a diameter of 10 μm. Simulations are based on the model by Allers et al.[11] (Reproduced with permission from ref 11. Copyright 2003, Wiley-VCH Verlag GmbH & Co. KGaA.)

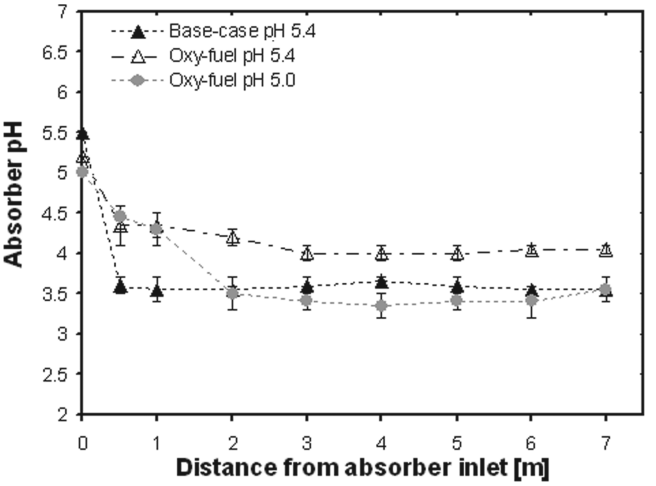

Figure 3. Absorber pH as a function of distance from the absorber inlet in the pilot plant for air-firing (pH 5.4) and oxy-fuel experiments (pH 5.0 and 5.4). See Figure 1 for plant details. The error bars shown for each condition provide the lowest and highest measured pH values within a 2 min sampling interval. Legend refers to the pH set point in the holding tank (corresponding to the absorber inlet). Experimental conditions are provided in Table 1.

significant extent. The impact of the new operating conditions on important wet FGD process parameters, in particular the desulfurization degree and the concentration of residual limestone, in the slurry has been followed. To enable a comparison of experiments with different solid concentrations, the concentration of residual limestone in the slurry as opposed to residual limestone in the gypsum is used.

4. EXPERIMENTAL SETUP AND PROCEDURE

Description of Setup. The wet FGD pilot plant, outlined in Figure 1, simulates a single vertical channel in a full-scale cocurrent flow wet FGD grid absorber.[15] The setup enables a detailed study of the processes taking place within a wet FGD plant, and the results obtained will be of relevance to other wet FGD absorber designs because the same overall chemical and physical processes take place. Due to differences in mass transfer rates and specific contact areas at different configurations, differences may exist when specific plant data are compared. The flue gas, to which pure SO_2 is subsequently added, can either be generated by a 110 kW natural gas burner (90% CH_4, 6% C_2H_6, and 2% C_3H_8), supplied from a CO_2 gas cylinder battery, or a combination of the two. The flue gas is brought into contact with limestone slurry in the absorber, a 7 m PVC pipe (inner diameter of 3.3 cm) with multiple sampling sites, and is subsequently led to the stack (i.e., no flue gas recycle). The slurry is collected in a holding tank, inner diameter of 0.4 m, where air injection (15−18 L/min), reactant addition (for maintaining a constant holding tank pH), and slurry removal (for maintaining a constant slurry level) take place. From the holding tank the slurry is recycled to the absorber, ensuring a liquid/gas ratio of ~16 L of slurry/m^3 of flue gas (base-case experiment with air-firing). Additional details concerning the pilot plant can be found in previous publications,[9,15] but it should be noted here that the absorber length has been increased from 5 to 7 m since the original publications, to obtain higher degrees of desulfurization.

Experimental Procedure. The experimental series was initiated by 4 days desulfurization of a 1000 ppm(v) SO_2 (on dry basis) flue gas stream using a feed stream containing 7.1 wt % Faxe Bryozo limestone ($d_{50} \sim 5$ μm)[19] and 2.2 wt % Cl^- (25 g/L). A Cl^- concentration of 25 g/L is typical for Danish wet FGD plants with forced oxidation followed by a wastewater treatment plant.[20] This 4 day operation allowed the system to approach steady state operation in terms of gypsum content, concentration of residual limestone, and degree of desulfurization. The different operating conditions in Table 1 were then introduced and operation continued until a constant limestone consumption rate was obtained (usually within a few hours). For experiments with dry CO_2 from gas cylinders, additional distilled water was introduced to the holding tank to compensate for the evaporation taking place in the top of the absorber (approximately 1.5 L of water/h). The limestone consumption rate, and thereby the desulfurization operation, stabilized within a few hours and the SO_2 absorber profile (Rosemount NGA 2000 gas analyzer), pH absorber profile (Sentron 1001 pH measurement), and residual limestone concentration (Netsch STA/TGA 449; 10 K/min heating in N_2) could be obtained. No significant SO_2 loss in the condensate water, removed before the SO_2 gas analyzer, was observed; an overall sulfur mass balance was used for verification. Subsequently, the next set of experimental conditions was established and the procedure was repeated until the final experiment where adipic acid was introduced into the holding and feed tanks.

5. RESULTS AND DISCUSSION

The experimental work includes one wet FGD experiment with air-firing and five with oxy-fuel firing at operational conditions of industrial relevance. Details of the experiments are given in Tables 1 and 2. It can be seen in Table 2 that the average pH deviates somewhat from the set point. This is due to the stepwise limestone addition at the set point, after which the pH increases slightly as the limestone dissolves.

Residual Limestone Concentration. The limestone slurry added to the holding tank dissolves in both absorber and holding tank and stabilizes the slurry holding tank pH near the set point.

dx.doi.org/10.1021/ie1022173 |*Ind. Eng. Chem. Res.* XXXX, XXX, 000–000

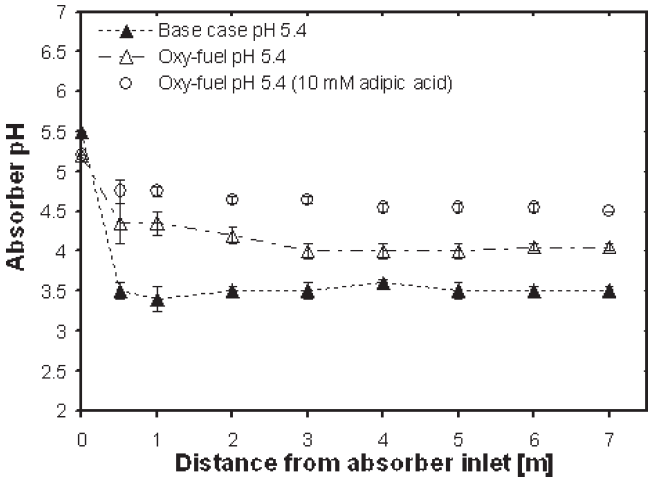

Figure 4. Absorber pH as a function of distance from the absorber inlet in the pilot plant for air-firing (pH 5.4) and oxy-fuel experiments with and without adipic acid (pH 5.4). See Figure 1 for plant details. The error bars shown for each condition provide the lowest and highest measured pH values within a 2 min sampling interval. Legend refers to the pH set in the holding tank (corresponding to the absorber inlet). Experimental conditions are provided in Table 1.

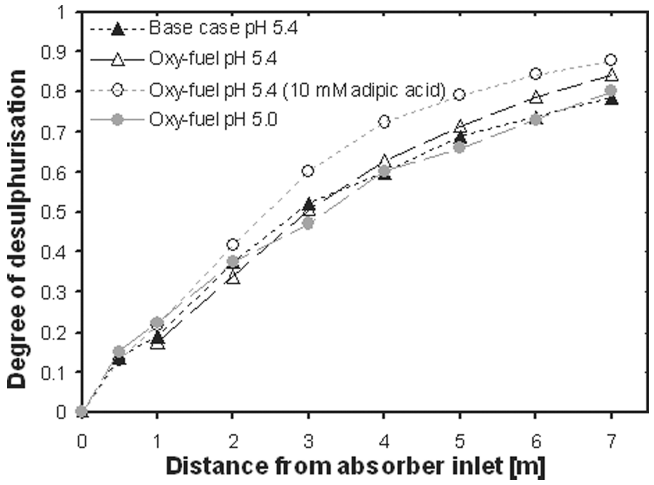

Figure 5. Degree of desulfurization (±0.01) as a function of distance from absorber inlet in the pilot plant for air-firing (pH 5.4) and oxy-fuel experiments with and without adipic acid (pH 5.0 and 5.4). See Figure 1 for plant details. Experimental conditions are provided in Table 1.

Table 2 shows the residual limestone concentration in the slurry obtained in the experiments performed. Wet FGD pilot plant operation at pH 5.4 yielded significantly different results for air-firing (base case) and oxy-fuel firing, with the latter causing elevated levels of residual limestone (from 3.2 to 5.0 g/L slurry). The limestone dissolution rate is reduced at oxy-fuel conditions and pH above 5.2−5.5, because of increased levels of $CO_2(aq)$, HCO_3^-, and CO_3^{2-}, originating from $CO_2(g)$ absorbed. The oxy-fuel experiment performed at pH 5.0 gave a residual limestone concentration and desulfurization degree very similar to the base-case air-firing experiment. This corresponds well with the expected decreased HCO_3^- and CO_3^{2-} concentrations at pH 5.0 compared to the oxy-fuel experiment with pH 5.4. The HCO_3^- and CO_3^{2-} concentrations will decrease as the pH value moves away from the pK_a of $CO_2(aq)$ (6.29),[21] as described by eq 4. The addition of 10 mM adipic acid to the slurry was also expected to improve the performance at pH 5.4 during oxy-fuel firing, due to the buffering effect of the additive, as seen in the air-firing experiments by Frandsen et al.[20] (Table 2). However, the concentration of residual limestone could not be distinguished from the corresponding experiment without adipic acid addition again suggesting that the concentrations of HCO_3^-, CO_3^{2-}, and $CO_2(aq)$ are very important for the rate of dissolution of limestone. The drastic reduction in limestone dissolution rate above pH 5.2−5.5 in the presence of high levels of CO_2,[11,12] as illustrated in Figure 2, makes the concentration of residual limestone highly sensitive to the operating pH and any uncertainties of this parameter. This provides a possible explanation to the similar concentration of residual limestone in the two experiments. Due to the increased SO_2 concentration, the two experiments with a reduced oxy-fuel flue gas flow rate were performed at the same total SO_2 load as the other experiments. The residual limestone concentration of those two experiments was somewhat lower than the corresponding experiment with a high oxy-fuel flue gas flow rate, but the desulfurization degree was also higher.

Absorber pH. Figures 3 and 4 show the development in absorber pH as a function of distance measured from the absorber inlet. As the recycled slurry from the holding tank enters the absorber, it is brought into contact with the SO_2 flue gas (cocurrent flow) and a steep decrease in pH can be observed as SO_2 is absorbed. As the flue gas moves down through the absorber, the pH will begin to stabilize as less SO_2 is absorbed from the flue gas and the limestone dissolution rate increases at lower values of pH. A similar development in absorber pH can be seen in the base-case experiment and the oxy-fuel pH 5.0 experiment, for which a comparable concentration of residual limestone will be available to stabilize the pH in the absorber. However, the elevated residual limestone concentration in the oxy-fuel pH 5.4 experiment enables a higher absorber pH compared to the base-case experiment. Finally, the buffering effect of adipic acid and the high concentration of residual limestone yield an almost constant pH (4.5−5.0) through the absorber. A higher flue gas O_2 concentration in the oxy-fuel experiments would enhance HSO_3^- oxidation in the absorber, thereby forming H^+ ions and potentially lowering pH. However, previous pilot plant work has shown that oxidation in the absorber has little effect on the SO_2 removal.[15]

Degree of Desulfurization. The combination of high inlet SO_2 and an only slightly acidic slurry pH enables a high degree of desulfurization in the initial part of the cocurrent absorber. Figures 5 and 6 illustrate the degree of desulfurization measured as a function of distance from the absorber inlet. No degree of desulfurization could be determined in the initial part of the absorber (until 2 m position) during the low flow rate experiments because the SO_2 concentration exceeded the range of the analyzer. Some desulfurization also takes place in the holding tank, from about 6% in the low flow experiments to about 12% in the experiments with higher flow rates.

The higher limestone concentration in the oxy-fuel pH 5.4 experiment also enables a higher absorber pH, and thereby degree of desulfurization, compared to the base-case experiment. This effect is, however, only pronounced beyond 3 m of absorber length, possibly due to the flow of evaporating water into the dry CO_2 flue gas and thereby in the opposite direction of the SO_2 to be absorbed. The development in the degree of desulfurization

dx.doi.org/10.1021/ie1022173 |*Ind. Eng. Chem. Res.* XXXX, XXX, 000–000

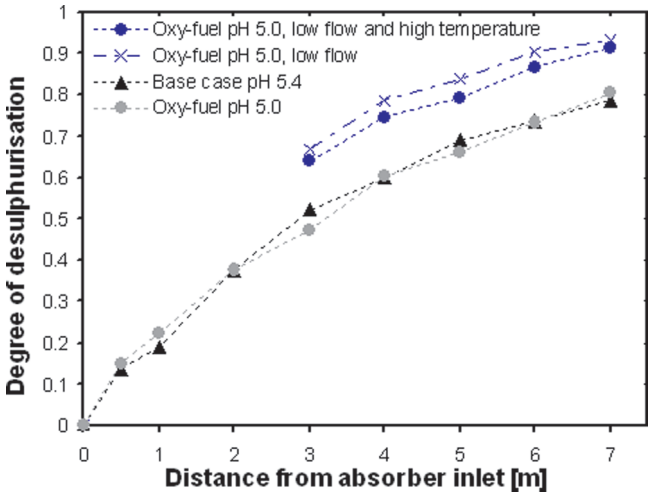

Figure 6. Degree of desulfurization (±0.01) as a function of distance from absorber inlet in the pilot plant for air-firing (pH 5.4) and oxy-fuel experiments with decreased flue gas flow rates (pH 5.0). See Figure 1 for plant details. Experimental conditions are provided in Table 1.

for the base-case experiment and the oxy-fuel pH 5.0 experiment are very similar, as could be expected based on the comparable residual limestone concentration and absorber pH. The buffering effect of adipic acid and the high concentration of residual limestone yields an almost constant pH 4.5−5.0 through the absorber and thereby an excellent SO_2 capture. The prolonged flue gas residence time (i.e., increased liquid/gas ratio) of the two experiments with low flue gas flow rates yielded very high total desulfurization degrees, making a distinction between the two experiments (44.4 vs 53.3 °C) impossible. However, the SO_2 removal down through the absorber indicates a decreased performance at elevated temperatures, possibly due to the lower solubility of SO_2 in the liquid phase.[15]

6. CONCLUSIONS

A systematic pilot-scale investigation of wet flue gas desulfurization performance under oxy-fuel conditions has demonstrated that a change from air-firing to oxy-fuel firing can result in increased levels of residual limestone in the gypsum product and thereby higher degrees of desulfurization at slurry pH 5.4. However, wet FGD oxy-fuel operation at slurry pH 5.0 returns the process performance to what was obtained for air-firing at pH 5.4. A lower slurry pH would likely increase the limestone dissolution rate further, but also reduce the SO_2 absorption/desulfurization degree.[20]

The buffering properties of a 10 mM adipic acid solution caused an increased pH in the absorber and thereby a higher degree of desulfurization, but no effect on the residual limestone concentration could be seen at pH 5.4 in the presence of an oxy-fuel flue gas stream. This is most likely due to the highly sensitive limestone dissolution rate above pH 5.2−5.5 in the presence of high levels of CO_2,[11−13] but it needs to be verified by detailed modeling of the wet FGD pilot plant at oxy-fuel conditions.

Apart from the changes described above for the wet FGD operation, other initiatives such as external oxidation or a reduced oxidation air flow, or measures to increase the desulfurization degree, may prove necessary to obtain a CO_2 product of a purity suitable for transport and storage. This may also influence the wet FGD plant performance in terms of concentration of residual limestone, degree of desulfurization, and quality of the gypsum obtained.

AUTHOR INFORMATION

Corresponding Author

*Tel.: +45 45252827. Fax: +45 45882258. E-mail: sk@kt.dtu.dk.

ACKNOWLEDGMENT

The authors wish to thank technician Anders Tiedje for technical assistance. Financial support by DONG Energy A/S and Vattenfall A/S (Contract Nos. 1-00550 and V3-203) is gratefully acknowledged.

NOMENCLATURE

d_{50} = volumetric mean particle diameter (μm)
d_p = particle diameter (μm)
k_s = empirical correction factor
m = molality (mol kg^{-1})
p = partial pressure (bar)
pK_a = acid dissociation constant
Q = flow rate (Nm^3·h^{-1})
T = temperature (°C or K)

Subscript

b = bulk phase
s = at the surface of limestone particle

REFERENCES

(1) Buhre, B. J. P.; Elliott, L. K.; Sheng, C. D.; Gupta, R. P.; Wall, T. F. Oxy-fuel combustion technology for coal-fired power generation. *Prog. Energy Combust. Sci.* **2005**, *31* (4), 283–307.

(2) Toftegaard, M. B.; Brix, J.; Jensen, P. A.; Glarborg, P.; Jensen, A. D. Oxy-fuel combustion of solid fuels. *Prog. Energy Combust. Sci.* **2010**, *36* (5), 581–625.

(3) Soud, H. N. *Developments in FGD*; IEA Coal Research: London, 2000.

(4) Tigges, K. D.; Klauke, F.; Bergins, C.; Busekrus, K.; Niesbach, J.; Ehmann, M.; Wu, S.; Walchuk, O.; Kukoski, A. *Oxyfuel Combustion Retrofits for Existing Power Stations—Bringing "Capture Ready" to Reality*; Hitachi Power Europe Gmbh: Duisburg, Germany, Hitachi Power Systems America Ltd.: Basking Ridge, NJ, USA, 2008.

(5) Gonschorek, S.; Hellfritsch, S.; Weigl, S.; Gampe, U. Entwicklungsstand des Oxyfuel-Prozesses für Braunkohlekraftwerke. Presented at the Kraftwerkschemisches Kolloquium, Zittau, Germany, September 2006.

(6) Doctor, R. D.; Molburg, J. C. High-sulfur Coal Desulfurization for Oxyfuels. Presented at the 7th Annual Conference on Carbon Capture & Sequestration, Pittsburgh, PA, USA, May 2008.

(7) White, V.; Torrente-Murciano, L.; Sturgeon, D.; Chadwick, D. Purification of Oxyfuel-Derived CO_2. *Energy Procedia* **2009**, *1* (1), 399–406.

(8) White, V.; Torrente-Murciano, L.; Sturgeon, D.; Chadwick, D. Purification of Oxyfuel-Derived CO_2. *Int. J. Greenhouse Gas Control* **2010**, *4*, 137–142.

(9) Kiil, S.; Michelsen, M. L.; Dam-Johansen, K. Experimental investigation and modelling of a wet flue gas desulfurization pilot plant. *Ind. Eng. Chem. Res.* **1998**, *37*, 2792–2806.

(10) Kiil, S; Nygaard, H.; Johnsson, J. Simulation studies of the influence of HCl absorption on the performance of a wet flue gas desulphurisation pilot plant. *Chem. Eng. Sci.* **2002**, *57* (3), 347–354.

(11) Allers, T.; Luckas, M.; Schmidt, K. G. Modelling and Measurement of the Dissolution Rate of Solid Particles in Aqueous Suspensions —Part I: Modelling. *Chem. Eng. Technol.* **2003**, *26* (11), 1131–1136.

(12) Allers, T.; Luckas, M.; Schmidt, K. G. Modelling and Measurement of the Dissolution Rate of Solid Particles in Aqueous Suspensions —Part II: Experimental Results and Validation. *Chem. Eng. Technol.* **2003**, *26* (12), 1225–1229.

(13) Chan, P.; Rochelle, G. T. Limestone Dissolution: Effect of pH, CO_2 and Buffers Modeled by Mass Transfer. *ACS Symp. Ser.* **1982**, *188*, 75–97.

(14) Jinying, Y.; Faber, R.; Jacoby, J.; Anheden, M.; Giering, R.; Schmidt, T.; Ross, G.; Stark, F.; Kosel, D. Flue-gas Cleaning Processes for CO_2 Capture from Oxyfuel Combustion—Experience of FGD and FGC at 30 MWth Oxyfuel Combustion Pilot. Presented at the 1st IEA Oxyfuel Combustion Conference, Cottbus, Germany, September 2009.

(15) Kiil, S. Experiments and Theoretical Investigations of Wet Flue Gas Desulphurization. Ph.D. Thesis, Department of Chemical Engineering, Technical University of Denmark, Lyngby, Denmark, 1998.

(16) Takeshita, M.; Soud, H. *FGD Performance and Experience on Coal-fired Plants*; IEA Coal Research: London, 1993.

(17) Gubkov, A. N.; Fermor, N. A.; Smirnov, N. I. Vapor Pressure of Mono-Poly Systems. *Zh. Prikl. Khim.* **1964**, *37*, 2204–2210. Obtained though NIST Chemistry Webbook (http://webbook.nist.gov).

(18) Buchardt, C. N.; Johnsson, J. E.; Kiil, S. Experimental investigation of the degradation rate of adipic acid in wet flue gas desulphurisation plants. *Fuel* **2006**, *85* (5−6), 725–735.

(19) Kiil, B.; Johnsson, J. E.; Dam-Johansen, K. D. Modelling of Limestone Dissolution in Wet FGD Systems: The Importance of an Accurate Particle Size Distribution. *PowerPlant Chem.* **1999**, *1* (5), 26–30.

(20) Frandsen, J. B. W.; Kiil, S.; Johnsson, J. E. Optimisation of a wet FGD pilot plant using fine limestone and organic acids. *Chem. Eng. Sci.* **2001**, *56*, 3275–3287.

(21) Brewer, L. *Thermodynamic Values for Desulfurization Processes*; Hudson, J., Rochelle, G. T., Eds.; ACS Symposium Series 188; American Chemical Society: Washington, DC, 1982.

SCR catalyst performance under oxyfuel conditions

Research Report

Putluru Siva Sankar Reddy

Jan Erik Johnsson

Rolf Ringborg

Anker Degn Jensen

CHEC Research centre

Department of Chemical and Biochemical Engineering

Technical University of Denmark

Contents

SCR catalyst performance under oxyfuel conditions

1. Abstract

The oxyfuel combustion process differs from air combustion in several ways like high concentrations of CO_2 and water in the flue as well as increased levels of SO_2/SO_3 if recirculation is before the desulfurization plant. Furthermore, the use of pure oxygen in the combustion process is costly, and so lowering of the combustion stoichiometry is attractive from an economic point of view. This, however, will lead to low oxygen concentrations in the flue gas and possibly increased CO levels.

In this part of the project an introductory experimental investigation has looked into some of the influences that oxyfuel combustion has on SCR performance: Influence of CO_2 as carrier gas, influence of low oxygen concentration and the ability of the SCR catalyst to act as an oxidation catalyst for CO. It was found that the SCR activity was slightly lower (10-15 %) in CO_2 rich flue gases as compared to conventional air combustion flue gas. The difference may be explained by a lower diffusion coefficient of NO and NH_3 in CO_2 compared to N_2 which becomes evident at high temperature where diffusion limitations play a role. The lower activity at low temperature may possibly be explained by adsorption of CO_2 to active sites. Regarding the influence of oxygen concentration in the flue gas it was found that if the oxygen concentration was above about 5000 ppmv (0.5 vol.%) the reaction was not influenced by the oxygen concentration. At lower concentrations, however, the reaction rate decreased fast with decreasing oxygen concentration. Finally it was found that SCR catalysts are not able to catalyze CO oxidation. Overall it may be concluded from the performed studies that the tested effects of oxy-fuel flue gases do not constitute a problem to the SCR reaction.

2. Introduction

Energy consumption continues to increase globally. As a resulting consequence, the emission of CO_2 will also continue to grow every year if the technology or the type of fuel is not being changed. Countries will continue to make legislations to lower the emission of CO_2, NO_X and SO_X, but a demand for possible zero-emission technology ascends. The proposed technology of oxy-fuel combustion [1], utilizing the underground as a deposition site for CO_2 will not prove to be a long term solution, but only delay the pollution of the environment until new technology is found. Vattenfall states in a press release that its vision is to be climate neutral in the year 2050. A pilot plant, recently build (in Sept. 2008), is used for research and demonstration of oxy-fuel combustion, carbon capture and storage (CCS), a possible place for deposition was found at Northern Jutland in Denmark. Investigations of the geological conditions have started and Vattenfall wants to have the first CCS plant in Europe running at the location in 2013 [2].

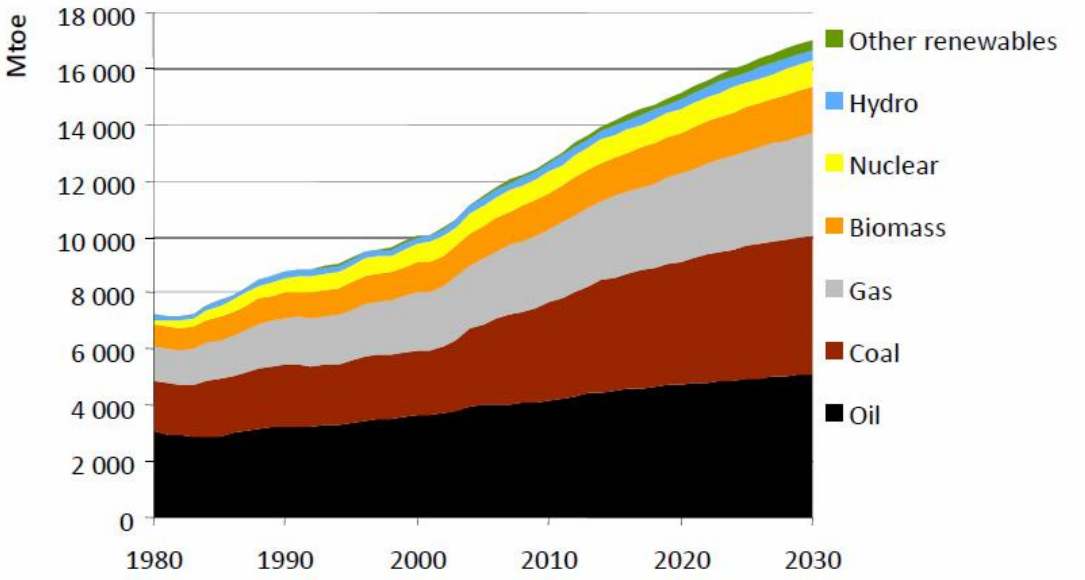

Fig. 1: Million tons oil equivalent vs. decades [3].

A report published by the Chinese government shows the energy consumption trend within the country with a vast rate of economical growth [4]. It is expected that from 2008 to 2030 an increase in energy demand will be 45% (Fig. 1) with over a third of the increase being coal fired energy. China and India will account for more than half of the incremental energy demand. By opening a new coal fired power plant every week, that request was made possible. Even though the efficiency of the new power plants is very good [5], the vast amount still proves to be a heavy pollutant.

With coal being stable both in cost and supply, proven coal reserves are estimated to last 133 years [6]. The research for replacement of this energy source is very time-demanding. Therefore the need to make the power plants even more efficient and less polluting is now more important than ever. The acknowledgement of the environmental problem by many governments stimulates change and makes the public more conscious about the environment which will then lead to a higher prioritization of the funding for research. But still the foresight for new technology e. g. fusion power plants such as ITER is at least 50 years away [7].

Oxy-fuel technology still utilizes the combustion of pulverized coal. During combustion, the nitrogen in the fuel is oxidized and NO_X is formed. NO_X is considered to be health damaging, contributing to acid rain and damaging the environment with N-pollution. Consequently strong legislation is contributed to avoid the emission of this gas. It is therefore needed to clean the flue gas of NO_X by using a selective catalytic reduction (SCR) reactor. The research concerning the combination of SCR and oxy-fuel is yet to be done. This report will try to describe the changes under oxy-fuel conditions.

2.1 Oxyfuel technology

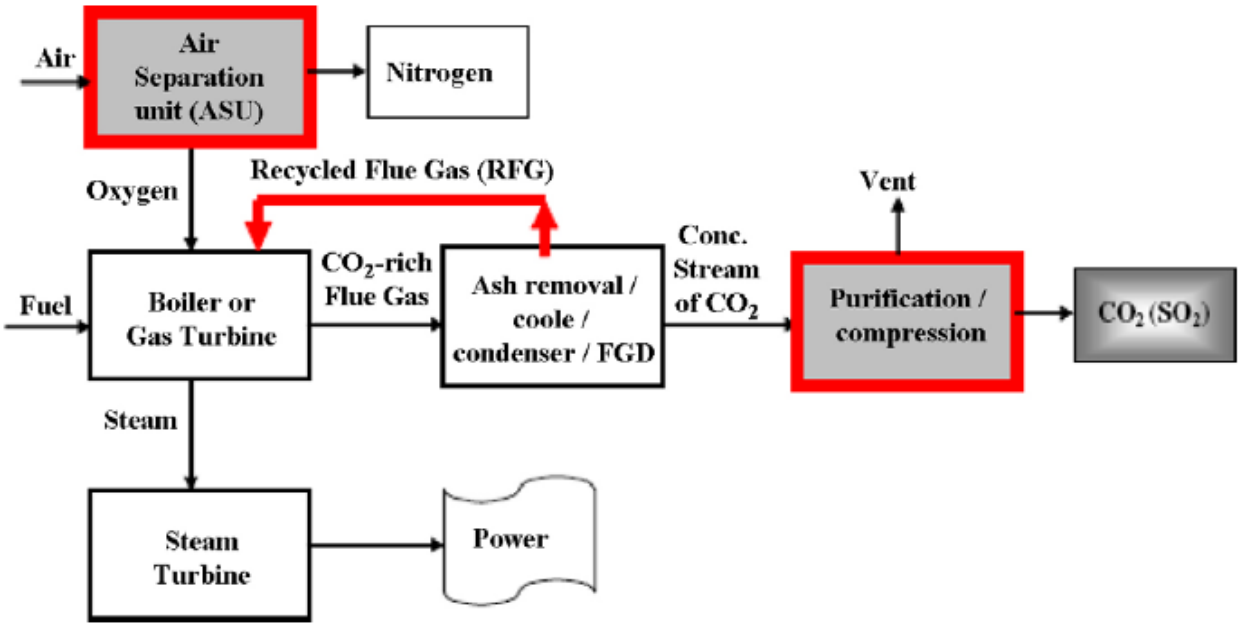

Fig. 2: Flow sheet of oxyfuel technology for power generation with CO_2 capture and storage, showing the additional unit operations in bold [8].

When Vattenfall states that they want to be climate neutral by the year of 2050, it is not possible without the oxy-fuel power plant. In the process of looking into zero emission, CO_2 sequestration and oxy-fuel combustion is introduced. Conventional coal-fired boilers, i.e., currently being used in power industry, use air for combustion in which the nitrogen from the air (approximately 79% by volume) dilutes the CO_2 concentration in the flue gas. During oxyfuel combustion, a combination of oxygen (typically of greater than 95% purity) and recycled flue gas is used for combustion of the fuel. A gas consisting mainly of CO_2 and water is generated with a concentration of CO_2 ready for sequestration. The recycled flue gas is used to control flame temperature and make up the volume of the missing N_2 to ensure there is enough gas to carry the heat through the boiler. A general flow sheet is shown in Fig. 2. CO_2 capture and storage by the current technically viable options post-combustion capture, pre-combustion capture and oxyfuel

combustion will impose a 7–10% efficiency penalty on the power generation process. The major contributors to this efficiency penalty are oxygen production and CO_2 compression.

From pilot-scale and laboratory scale experimental studies, oxyfuel combustion has been found to differ from air combustion in several ways, including reduced flame temperature, delayed flame ignition, reduced NO_x and SO_x emissions.

Many of these effects can be explained by differences in gas properties between CO_2 and N_2, the main diluting gases in oxyfuel and air respectively [8, 9]. CO_2 has different properties from N_2 which influence both heat transfer and combustion reaction kinetics:

- Density: The molecular weight of CO_2 is 44, compared to 28 for N_2, thus the density of the flue gas is higher in oxyfuel combustion.
- Heat capacity: The heat capacity of CO_2 is higher than N_2.
- Diffusivity: The oxygen diffusion rate in CO_2 is 0.8 times that in N_2 and that of NO in CO_2 is 0.85 times that in N_2. Over all the gases diffusivity is decreased in oxyfuel condition.
- Radioactive properties of the furnace gases: Oxyfuel combustion has higher CO_2 and H_2O levels, both having high emitting power.
- Changes in oxygen proportion and volume of the inlet gas

The following list identifies differences for oxy-firing compared to air-firing

- To attain a similar adiabatic flame temperature (AFT) the O_2 proportion of the gases passing through the burners is higher, typically 30%, than that for air (of 21%), necessitating that about 60% of the flue gas is recycled.
- The high proportions of CO_2 and H_2O in the furnace gases result in higher gas emissivities, so that similar radioactive heat transfer for a boiler retrofitted to oxyfuel will be attained when the O_2 proportion of the gases passing through the burner is less than the 30% required for the same AFT.

- The volume of gases flowing through the furnace is reduced by which the extent is dependent on the flue gas recycle ratio, and the volume of flue gas emitted from power plant is reduced by about 80%.
- Typically, when air-firing coal, 20% excess air is used. Oxyfuel requires a percent excess O_2 (defined as the O_2 supplied in excess of that required for stoichiometric combustion of the coal supply) to achieve a similar O_2 fraction in the flue gas as air-firing, in the range of 3–5%.
- Due to the recycling of flue gases to the furnace, species (including corrosive sulphur gases) have higher concentrations than in air-firing, if these species are not removed prior to recycle.
- As oxyfuel combustion combined with sequestration must provide power to several significant unit operations, such as flue gas compression, that are not required in a conventional plant without sequestration, oxyfuel combustion/sequestration is less efficient per unit of energy produced.

2.2 Conventional SCR mechanisms on vanadium catalyst

Numerous studies have been published related to catalytic activity, reaction mechanism, effects of vanadia loading, effects of active phase composition, and other pertinent topics; these have been summarized in several recent reviews [10, 11]. Despite the number of works concerning the development of active catalysts for SCR, a lack of knowledge about the mechanism of the process exists.

SCR reactor is used for $DeNO_x$ of the flue gas from a boiler. Ammonia is added to the flue gas and is then reacting with nitrogen oxide and oxygen over the catalyst, reducing NO to molecular nitrogen. The following overall reactions take place.

$$4NO + 4NH_3 + O_2 \rightarrow 4N_2 + 6H_2O \qquad (1)$$

There are two popular mechanisms in the literature namely Eley-Rideal and Topsøe.

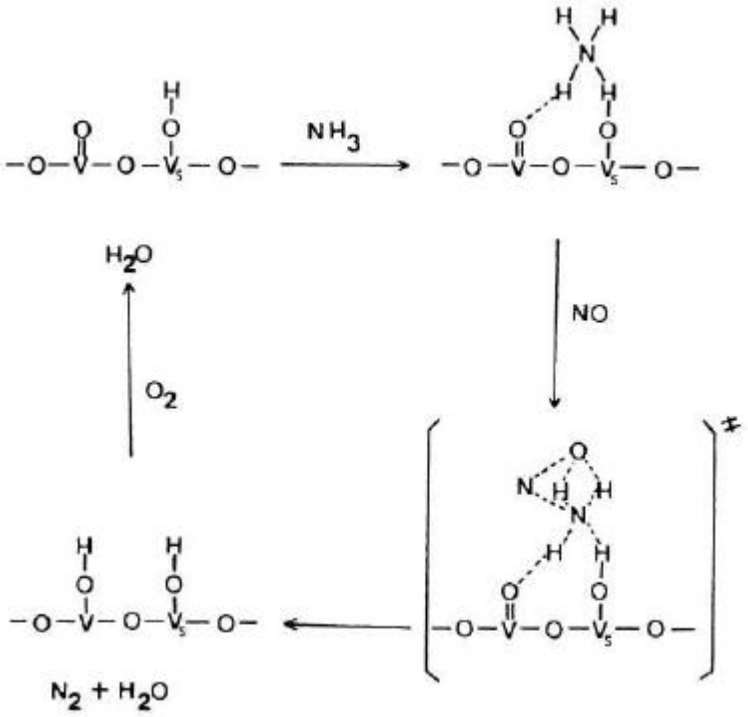

Fig. 3: Eley-Rideal mechanism of the NO-NH_3 reaction on vanadium oxide proposed by Inomata et al. [10].

In 1979 Inomata et al. proposed a mechanism for the SCR reaction on vanadium oxides. The authors suggested that the reaction proceeds by an Eley-Rideal mechanism, in which NO reacts directly from the gas phase with an absorbed ammonium ion throughout an H-bonded 'activated complex', shown in Fig.3 [10]. Inspite of the electronic structure, the interactions of the intermediate and the movements of electrons have not been specified; the mechanism in Fig. 3 is still very popular.

Based on in situ on-line FTIR studies under steady-state conditions, Topsøe et al. [11-17] proposed the mechanistic scheme shown in Fig. 4. Herein it was suggested that both the Eley-Rideal and Langmuir-Hinshelwood are possible mechanisms, but that NO more likely reacts as a weakly adsorbed species. They considered that vanadia-titania catalysts exhibit two separate catalytic functions, i.e. acid and redox functions, in a dual-mechanistic fashion. Turco et al. [16] also agree with this scheme. Although the overall reaction not has been equalized (i.e. all components reacts in the stoichiometry of 1 to 1), it gives a good idea of the possible reaction mechanism.

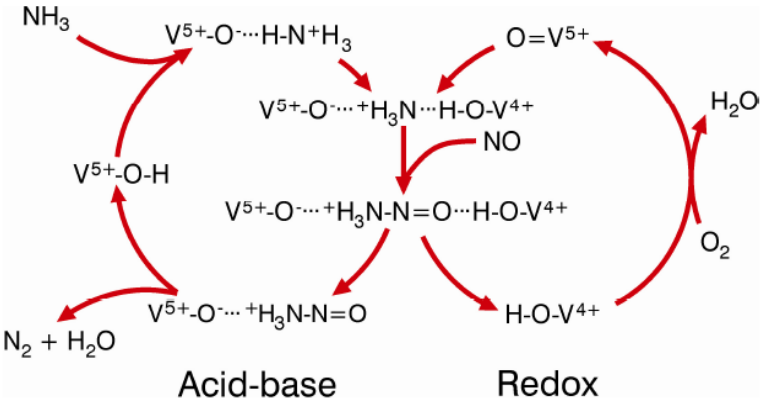

Fig. 4: The acid-redox catalytic cycle of the SCR reaction over the vanadia-titania catalyst in the presence of oxygen, proposed by Topsøe [11].

The key and rate-determining step in this mechanism is assumed to be the activated adsorption of ammonia on the V^{5+}-OH Brøndsted acid site, which reduces a nearby V^{5+}=O redox site to V^{4+}. This activated intermediate V^{4+}–OH, is very reactive toward gaseous NO, leading to the products, N_2 and H_2O, which desorb from the surface.

Dumesic et al. [12, 17] proposed the following simplified reaction scheme to describe the NO conversion and the ammonia slip behavior for vanadia/titania catalysts under industrial SCR conditions

$NH_3 + M \quad \Longleftrightarrow \quad M\text{-}NH_3$ (fast) (2)

$M\text{-}NH_3 + S \quad \Longleftrightarrow \quad S\text{-}NH_3 + M$ (slow) (3)

$NO + S\text{-}NH_3 \quad \Longleftrightarrow \quad$ Products + S (slow) (4)

Where M represents an ammonia adsorption site and S represents a reactive site on which ammonia is activated. These three steps (2)-(4) are some of the steps in the catalytic cycle proposed by Topsøe in Fig. 4. Combining the reaction scheme with the Fig. 4, it is seen that M in the steps (2) and (3) are V^{5+}-OH and the S sites in the steps (3) and (4) can be identified as V^{5+}=O surface groups.

So far no exclusive reaction mechanism is found for the SCR reaction over vanadia on titania catalysts which can explain all experimental observations. The Eley-Rideal mechanism, however, is favored by many investigators. Finally, it is concluded that the SCR reaction is most favorable on polymeric vanadate species with more Brønsted acid sites such as vanadium hydroxyl groups (V-OH).

2.3 SCR under oxyfuel conditions

Oxyfuel technology concept is well known and its influence on harmful effluent gases is not known much. The studies of oxy-fuel has separated into two pathways, one studying the generation of the purest CO_2 gas for sequestration and one wanting to reduce the cost of pollutant emission, with emphasis on NO_x. Both are depicting primary measures and neither of these will be looked at very thoroughly, since the focus of this assignment lies upon the changes in the SCR reactor when running under oxy-fuel conditions. Configured this way, oxy-fuel combustion involves very high CO_2 concentrations. The implications of the high CO_2 levels are not yet fully appreciated, but it is likely that they induce changes in the performance of SCR catalyst. However,

it will still be necessary to verify the performance of SCR unit, which is the typical choice for large power plants, if the NO_x reduction obtained during the oxy-fuel combustion, is not adequate. An increase in the CO_2 concentration above the catalyst is not considered to have an effect on performance. The possibly increased levels of both SO_2 and SO_3 in the flue gas do, however, impose a risk for reduced performance. SO_3 in the flue gas is known to form sticky and corrosive ammonium bisulfate when NH_3 is added [18]. Increasing the SO_3 level will likewise increase the dew-point temperature for ammonium bisulfate. If the SCR operating temperature falls below the dew point, especially during low load operation, severe clogging of the catalyst must be expected. Additionally, the catalyst acts as an oxidizer and will convert part of the SO_2 content of the flue gas to SO_3 increasing the risk of ammonium bisulfate formation [18].

It is generally assumed that approximately 10–40 % of the total NO_x formed from pulverized coal combustion in air is due to thermal NOx and about 60– 90 % is derived from fuel-N while the prompt-NO_x mechanism is negligible, depending on the quantity of fuel-bound nitrogen species. The low level of molecular nitrogen in oxy-fuel combustion will suppress the formation of thermal and prompt NO_x and hence potentially lower the overall NO_x emission rate. The general conclusion in published literature is that the amount of NO_x emitted from an oxy-fuel plant can be reduced to somewhere between one-third and half of that from combustion in air [9, 19-37].

However, the application of higher than 21 % oxygen concentration to obtain adequate flame temperatures could result in an enhancement of fuel NO_x formation [38]. The potential of reducing the NO_x emissions from a power plant considerably compared to air-firing [9, 39] has been one of the key drivers in oxy-fuel combustion research in particular in USA [40] and thus, NO_x chemistry has been one of the most heavily investigated areas within the oxy-fuel combustion technology.

2.4 Mechanism for the Reduced levels of NO_x during Oxyfuel Combustion

Okazaki and Ando [41] exploited the different sub-mechanisms responsible for NO_x reduction in oxy-fuel combustion. Besides the near elimination of thermal and prompt NO_x formation due to a very low concentration of N_2 in the oxidizer they detected the following three main effects:

1. Reduction of NO_x on char surfaces due to reaction with CO. CO levels increases because of the high CO_2 concentration, oxygen concentrations above 21 % act to increase the concentration of CO and other combustion products due to less dilution.
2. Reduction of recycled NO_x through reactions with fuel-N.
3. Reburning effects; A further decrease in NO_x formation can occur from the interactions between recycled NO_x and hydrocarbon radicals (volatiles) released from the coal particles in the early flame zone

Of the three effects, Okazaki and Ando concluded that the reburning of recycled NO_x is the dominant mechanism in reducing NO_x emissions and that it accounts for 50–80 % of the decrease. The first effect was found to have significance below 10 % and the second amounted to 10–50 %. The effect of all three mechanisms will increase with increasing equivalence ratio and thus will the overall NO_x reduction efficiency [42].

Tree and coworkers [43, 44] suggest additional mechanisms to account for reduction of NO_x emissions from oxy-fuel combustion:

4. At high temperatures and with CO present, nitrogen in the char can be released directly as N_2 without forming NO.
5. For staged combustion, the time for NO_x formation is shorter. The period of time where O_2 is present is reduced due to higher temperature in the early flame zone and hence a more rapid consumption of volatiles will occur.

6. The ratio between NO and reduced N-species formed from volatile-N could be altered by the presence of high CO_2 (CO) concentrations.

In continued work in the BYU group the following possible reasons, in addition to the above mechanisms, for reduced NO_x emission in oxy-fuel combustion are proposed [28, 36]:

7. Less secondary oxidizer entrainment into the burner's recirculation zone due to a more detached flame, i.e. reduced oxygen availability and limited initial NO formation.
8. High NO concentrations. The NO destruction rate is first order with respect to NO in fuel-rich zone.
9. Temperature increase in fuel-rich zone will increase the rate of NO destruction. At higher temperatures the conversion of volatile-N proceeds faster toward N_2 than NO.
10. Reduced NO formation from char since more fuel-N is released with the volatiles.
11. Indirect effects through changes in reaction rates (combustion) and temperatures from the enhanced importance of gasification reactions.

Their overall conclusion is that faster NO destruction in oxy-fuel combustion appears to be at least partially due to the higher CO and NO concentrations.

2.5 SO_2 and SO_3 formation in oxyfuel conditions

Sulphur emissions and the effect on ash properties and boiler tube corrosion in oxy-fuel combustion from significantly increased levels of gas-phase-S in the boiler have obtained increasing attention in the recent years. There have been contradictory observations on the SO_2 emissions from oxy-fuel combustion. Some researchers experimentally show a decrease when comparing to combustion in air [22, 37] whereas others on the basis of either experiments [18, 27] or equilibrium calculations [30] report no differences.

Kiga et al. [37] reports oxy-fuel experiments performed in the IHI 1.2 MWth combustion facility with recirculation of dry flue gas. The investigations show that the conversion of the coal sulphur content, measured as the amount of S in the outlet divided by the amount going in with the coal, decreased markedly in oxy-fuel combustion compared to air-firing operation.

It has been found that oxy-fuel combustion can decrease the SO_2 emissions compared to that in air combustion [24, 23]. Croiset and Thambimuthu observed that the conversion of coal sulphur to SO_2 decreased from 91% for the air case to about 64% during oxy-fuel combustion. The reason they suggested is that high SO_3 concentrations in the flue gas during oxy-fuel combustion can result in sulphur retention by ash or deposits in the furnace. SO_2 concentration from oxy-fuel combustion is known to be higher than that from air combustion due to flue gas recirculation [26].

Contrary to experimental observations, thermodynamic modeling has suggested that SOx emissions would be unaffected during oxy-fuel combustion, being governed only by oxygen concentration [30]. As thermodynamic calculations assume equilibrium is established, the conflicting results of these studies suggest that the formation of SOx in either oxy-fuel combustion or air combustion has not reached equilibrium and is governed by rate limitations.

Similarly the SO_2 in the flue gas (in ppm) of the pilot-scale experiments was directly proportional to the fuel sulphur content in both oxyfuel and air combustion, but it was three times greater in oxyfuel combustion compared to air combustion and the concentration did not change significantly with increasing recycle ratio. The total mass (mg/MJ) of sulphur emitted during oxyfuel combustion was two-thirds of the total sulphur in the flue gas of air combustion, and a very small additional decrease in mass of sulphur was observed when the recycle of flue gas through the furnace was increased. The SO_3 concentration is approximately two and a half (2.5) to three (3.0) times higher in oxyfuel combustion than in air combustion. In general the fly ash produced during oxyfuel combustion contained slightly more sulphur and the furnace deposits contained

significantly more sulphur compared to air combustion samples. This is consistent with the higher SO_2 and SO_3 concentration levels measured. The mass balance of the coal ash could not be closed as a significant proportion of the ash was not accounted for in the experiment. It appears that ash was depositing throughout the furnace, or lost in ducts, which contained a significant proportion of the coal sulphur. Deposition of sulphurous species due to elevated gas phase SO_3 concentrations in oxyfuel combustion is expected to increase the amount of furnace corrosion experienced. The acid dew point was shown to be increased under oxyfuel combustion conditions further increasing the potential corrosion during operation, which may result in the need for desulphurisation of the flue gas or limit oxyfuel combustion to low sulphur coals.

Overall there is a decrease in sulphur emission levels under oxyfuel condition. Due to flue gas recirculation to accommodate rich CO_2 atmosphere in the furnace SO_2 concentration from oxy-fuel combustion is known to be higher than that from air combustion and its influence on SCR is not know.

2.6 Oxygen requirement for oxyfuel combustion

It is important to note that excess oxygen for oxy-fuel combustion carries a much greater penalty than in the air-firing case and that the power consumption in the ASU is directly proportional to the oxygen excess number [45]. A reduction in the oxygen excess would thus benefit both the ASU and CO_2 compression train power demands [45, 46]. In modern power plants the air excess is typically 15 % (λ = 1.15) [47]. The excess is predominantly determined by the uncertainty in the coal mass flow to each burner. By introducing more efficient monitoring of the coal flow to each burner and thus more control of the oxidizer flow for the same it should be possible to reduce the required oxygen excess during oxy-fuel combustion to no more than 10 % [48].

Simpson and Simon [45] have computed the impact of equivalence ratio as a measure of oxygen excess for both an air-fired base case as well as for post- combustion and oxy-fuel combustion on the second law efficiency. The opposite responses for the post-combustion and oxy-fuel combustion processes which means that oxy-fuel combustion becomes the more attractive capture technology as the oxygen excess decreases. The use of coal instead of a gaseous fuel would lower the value of the equivalence ratio where oxy-fuel systems become more favorable with respect to efficiency than post-combustion systems.

Process calculations performed and cited by Khare et al. [49] have shown that it is possible to yield the same radioactive heat transfer in oxy-fuel combustion as in air combustion with 27 % O_2 in the combustion medium and a excess oxygen level of only 3.5 % compared to 20 % for air. The oxygen level in the wet flue gas is 3.3 % for both cases. Through the above reports it is more essential to run the plant under less excess oxygen and its influence on SCR performance should be tested as well.

2.7 CO emissions in oxyfuel conditions

CO_2 at high partial pressure and high temperature can dissociate into CO and O_2 through the strongly endothermic reaction, (Equation. 5), [50].

$$CO_2 = CO + O_2 \qquad (5)$$

In the flame zone in oxy-fuel combustion both of the above conditions are present. However, among researchers there is a difference in opinion on whether it is the thermal dissociation, [36], or the gasification reactions, [30], that plays the dominant role in the significant increase in CO concentration in the flame compared to air-firing.

Reaction of CO_2 with different radicals, e.g. H and CH_2, will likewise contribute to enhance the concentration of CO in the flame zone [50]. Whether the emission of CO from oxyfuel

combustion is larger than from air-firing is subject to investigation. Because of its large toxicity it is important that oxyfuel combustion does not lead to an increased CO emission. Wang et al. [51] report no significant difference in the CO concentration levels both within the latter part of the flame zone and in the exhaust from the burner for both air and oxy-fuel combustion experiments with comparable flame temperatures. A five time increase in the CO level within the flame was however expected based on a modeling study. Lower CO concentration in the flame zone was observed for the oxy-fuel experiment with an air-like composition of the oxidant even though it was expected to be slightly larger than for air combustion. All experiments yielded full burnout of CO before the exhaust.

Experiments performed by IFRF [22] show significantly increased CO levels within the flame zone. Still, the combustion of CO has completed before the furnace exit and no significant CO emission is observed. Similar results were obtained by Liu et al. [27], even when the excess oxygen level is slightly higher for the oxy-fuel test. Changing the oxygen concentration from 30 to 21 % increased the CO emission from 34 to 200 ppmv, due to delayed ignition and lower peak temperature.

Experiments performed by Glarborg and Bentzen [50] and Mendiara [52] indicate that the high levels of CO_2 in oxy-fuel combustion prevent complete oxidation of fuel (CO) to CO_2 at high temperatures even when excess oxygen is present. However, the effect is most pronounced at fuel-rich or stoichiometric conditions. There is no indication that high CO_2 levels influence CO oxidation at low temperatures when oxygen is in excess and hence there should be no increased risk of high CO emissions from a gas fired oxy-fuel plant if mixing of fuel and oxidant is adequate. Over all there is a possible increase in CO levels during oxyfuel combustion and should be oxidized further to follow the emission regulations.

3. Experimental

The following section will describe the experimental setup and explain some of the initial observations. All the gas flasks were placed in the laboratory where the experiments were conducted. The toxic ammonia gas bottle was put in a ventilated cabinet to prevent any slips into the laboratory. The gasses were then led by Teflon tubes to the setup. As seen in Fig. 5, the amount of gas led to the reactor was controlled by MFCs (mass flow controllers). Afterwards the gas was checked by a bubble flow meter. The flow of every gas line was checked individually and by knowing the concentration of the base gases it was possible to calculate an expected concentration.

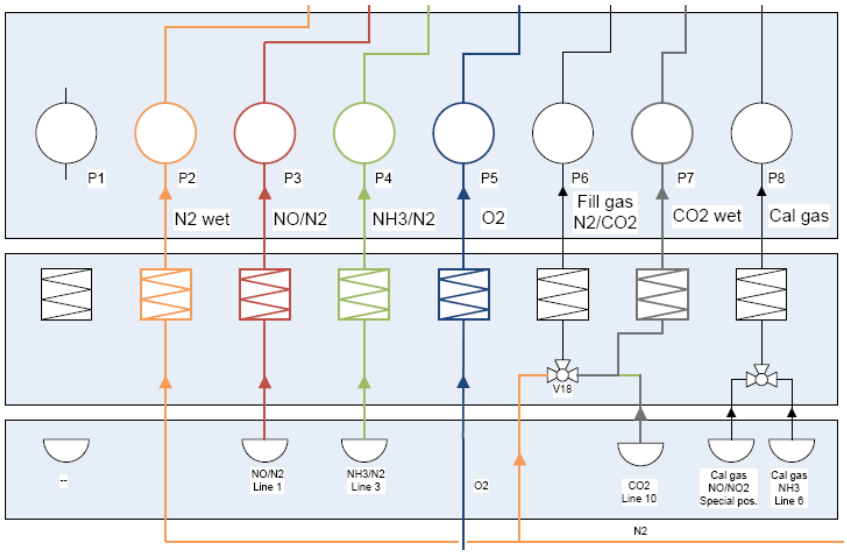

Fig. 5: Gas connection to the experimental setup.

As shown in Fig. 6 the valve setup was built in order to make it easy to switch to exactly the composition and the pathway wanted. Ammonia, represented by the green line, was led to the main and secondary entry and the carrier gases were connected to the same lines with three-way valves. From the valve board, the gas was led to the reactor, as showed in Fig. 7. By letting part of the carrier gas enter the evaporator, it was possible to add water to the gas stream. By controlling the temperature and assuming that the gas would be saturated with water vapor, it was

therefore possible to control the amount of water added. From the Antoine equation, the saturated partial pressure of water, $p^*_{H_2O}$, is calculated by (Equation. 6).

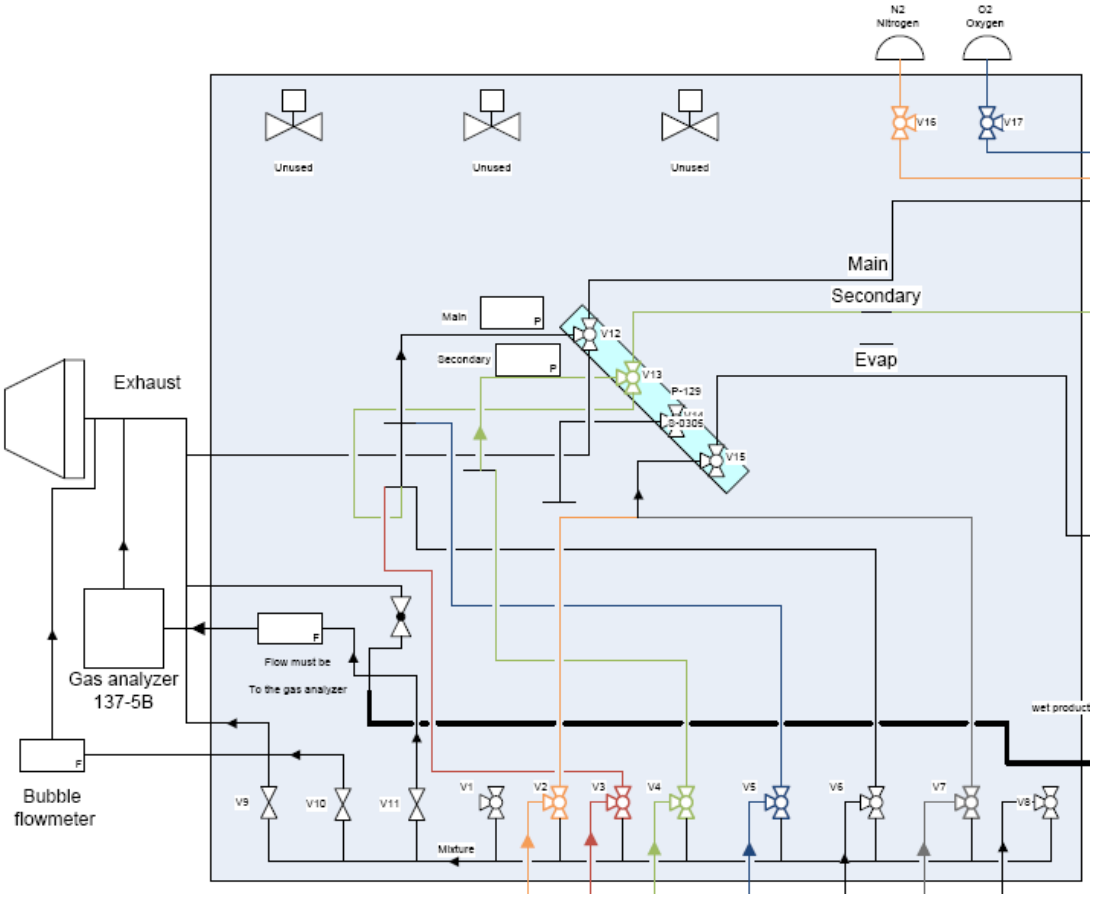

Fig. 6: Valve setup, the bold black line is traced, NH_3 (green), NO (red), O_2 (blue), N_2 (orange), CO_2 (gray).

$$\log(p^*_{H_2O}) = 5.1962 - \frac{1730}{T + 273.5} \qquad (6)$$

The relative humidity is given by $\phi = \frac{p_{H_2O}}{p^*_{H_2O}}$ where ϕ is the relative humidity and p_{H_2O} is the partial pressure of water. By calculating the partial pressure of wet nitrogen and dividing it by the total pressure it is possible to get the volume fraction of water, $y = \frac{p_{H_2O}}{P}$.

In order to avoid condensation, the gas line from the evaporator was traced. The gas enters the reactor in the bottom of the oven and is then led through the outer tube into the inner tube where catalyst was placed, seen in Fig. 8. The gas then exits the reactor and is led to the analyzer through a traced tube.

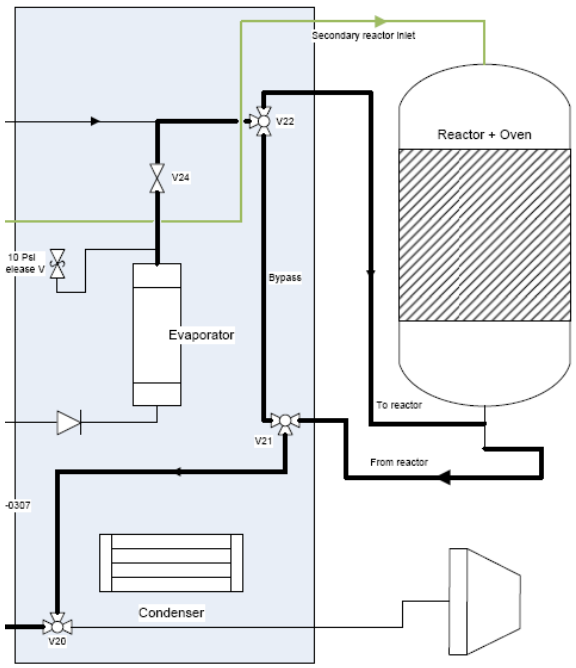

Fig.7: Reactor setup, the bold black line is traced. NH_3 (green).

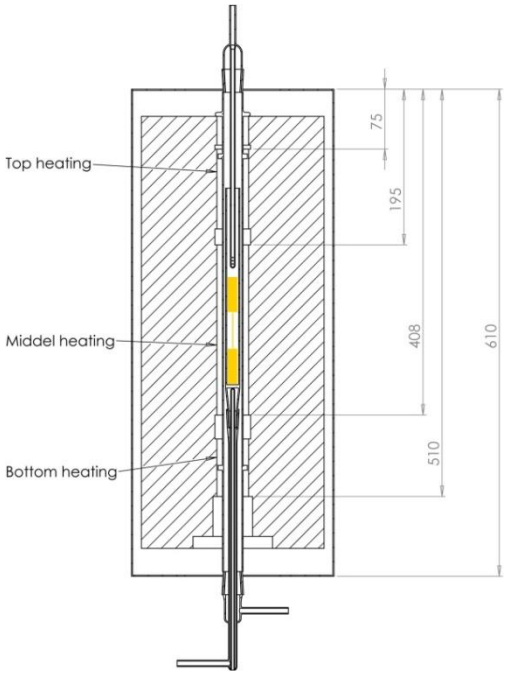

Fig. 8: Reactor with catalyst packing.

3.1 Catalyst composition

Vanadium based catalyst plates were supplied by Haldor Topsoe. The composition of the catalyst mass base is approx. 1.2% V_2O_5, 7% WO_3 and the rest TiO_2 (anatase) and fiber. Fiber material consists primarily of SiO_2 and also alumina and calcium to a lesser extent. The dimensions of the catalyst plates are 1.7 x 1.7 cm^2 Weight approx. 0.3 grams.

3.2 SCR activity measurements

The SCR activity measurements were carried out at atmospheric pressure in a fixed-bed quartz reactor loaded with 200 mg of fractionized (180-300 μm) catalyst powder sample or 1.7 x 1.7 cm^2 catalyst plate sample. The reactant gas composition was adjusted to 415 ppm NO, 500 ppm NH_3, 5% O_2, 2.3% H_2O and balance N_2 (92.6%) for conventional SCR conditions. A gas composition of 415 ppm NO, 500 ppm NH_3, 5% O_2, 2.3% H_2O, N_2 (7.6%) and balance CO_2 (85%) for oxyfuel conditions. The total flow rate was maintained at 3 l/min (ambient conditions). During the experiments the temperature was increased stepwise from 200 to 400 ^oC while the NO and NH_3 concentrations were continuously monitored by ABB gas analyzer. The principle behind the appliance is based on the gas to absorb light in the range between 200 and 600 nm. Analysis area is for NH_3 and NO_2 at 0-500 ppm and for NO from 0-1000 ppm. One should expect an uncertainty in the measurement of less than ± 1%. The catalytic activity is represented as the first-order rate constant ($m^3/kg{\cdot}s$), since the SCR reaction is known to be first-order with respect to NO under stoichiometric NH_3 conditions. The first-order rate constants were obtained from the conversion of NO as:

$$k' \cdot \tau = \ln(1 - x) \qquad (7)$$

4. Results and Discussion

4.1 Diffusivity

It is interesting to see if the changes contributed to the change of carrier gas can be explained by the differences in bulk diffusion. The following will calculate theoretical values for the bulk diffusion rate. When conducting the experiments, a gas which contains multiple species will make up a gas mixture that resembles the flue gas from an oxy-fuel power plant. By assuming that the mixture can be expressed as a binary gas, that is composed of NO and the carrier gas, it is possible to calculate a diffusion coefficient. This is theoretically calculated with the method described by Bird et al. [53]

Table 1: Data from Bird *et al.* [53].

	NO	CO_2	N_2
ε/k	119.	190.0	99.8
Sigma	3.470	3.996	3.667
Molar weight	30.006	44.010	28.013

Boltzmann's constant being $k = 1{,}3806504 \cdot 10^{-23}\ {}^{m^2 \cdot kg}/_{s^{-2} \cdot K}$

$$\frac{k \cdot T}{\varepsilon_{12}} = \frac{k \cdot T}{\sqrt{\varepsilon_1 \varepsilon_2}} \quad (8) \qquad \sigma_{12,1} = \frac{\sigma_{NO} + \sigma_{N_2}}{2} \quad (9)$$

By calculation of (8) and insertion into (10) and sigma is calculated for the specific gas composition by (9), the values are then substituted into the formula for calculating diffusion in bulk flow.

$$\Omega_{g,m} = \frac{1.06036}{\left(\frac{\kappa T}{\varepsilon_{12}}\right)} + \frac{0.193}{\exp\left(0.47635 \cdot \left(\frac{\kappa T}{\varepsilon_{12}}\right)\right)} + \frac{1.03587}{\exp\left(1.52996\left(\frac{\kappa T}{\varepsilon_{12}}\right)\right)} + \frac{1.76475}{\exp\left(3.89411 \cdot \left(\frac{\kappa T}{\varepsilon_{12}}\right)\right)} \quad (10)$$

$$D_{12}P = 0001858\sqrt{T \cdot \left(\frac{1}{M_g} + \frac{1}{M_m}\right)} \frac{1}{P \cdot \sigma_{12}^2 \cdot \Omega_{g,m}} \quad (11)$$

Table 2: Theoretically calculated bulk diffusivity.

Temperature	D_{NO,N_2}	D_{NO,CO_2}	Difference
$[°C]$	$\left[\frac{m^2}{s}\right]\cdot 10^{-5}$	$\left[\frac{m^2}{s}\right]\cdot 10^{-5}$	$[\%]$
200	4.65	4.03	13.3
250	5.36	4.71	12.1
300	6.25	5.63	9.96
350	7.20	6.51	9.59
400	8.20	7.43	9.38

Table 2 shows values which fit the spectrum given by Levenspiel et al. [54]. It also shows diffusivity coefficients of NO in CO_2 and N_2 with respect to different temperatures, and It can be seen that the diffusion coefficient of NO in N_2 is 13.3% to 9.38% larger compared to that of NO in CO_2.

4.2 Comparison of SCR Activity

Fig. 9 shows that activity of the catalytic plate is lower in the CO_2 environment compared to the N_2. At low temperatures the difference in activity was more and gradually it is coming closer as the reaction temperature is increased. The figure also shows how the catalyst is influenced by mass transfer limitations at higher temperatures, T>300 ^{o}C. It is also noted that the slope is larger in the CO_2 environment. Rate constant values are shown in Table 3 along with the difference over the temperature range 200-400 ^{o}C. Overall there is a 7-18% decrease in activity in CO_2 environment as compared to N_2.

Such a decrease in SCR activity can be divided into two ways:

1. Physical effects
2. Chemical effects

Under physical effects it seems there is a direct correlation is seen between activity and bulk diffusion. They follow similar characteristic features of temperature dependency and overall decrease in values of SCR activity and diffusion as well. It has been shown that the difference of bulk diffusion was around 10% which agrees well with the loss of activity at high temperature where the reaction on the plates is severely influenced by diffusion limitations. The influence of CO_2 seems even higher at low temperature where diffusion limitations play a minor role. This could indicate that CO_2 also has a chemical effect, for example adsorption at the active sites. At higher temperature the CO_2 desorbs and only the effect of diffusion remains.

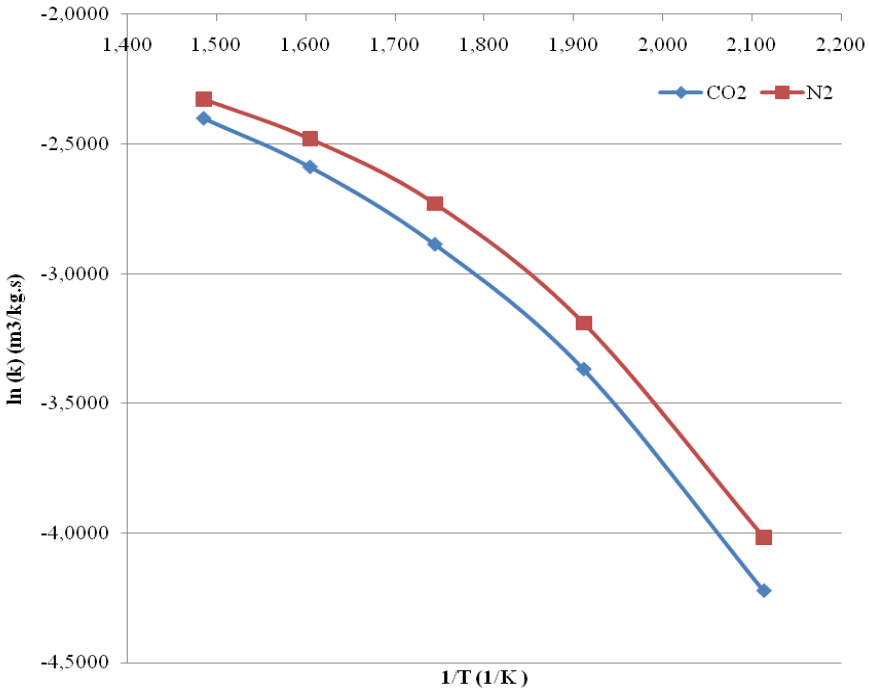

Fig. 9: Arrhenius plot for plate catalysts with dimensions 1.7 x 1.7 cm, temperatures ranging from 200 to 400 °C, total flow 3 L/min.

Table 3: Rate constant values in N_2 and CO_2 environment over plate catalysts.

Temperature	Rate constant (k_{N2})	Rate constant (k_{CO2})	Difference
$[°C]$	$m^3/kg.s$	$m^3/kg.s$	[%]
200	0.0180	0.0146	18.5
250	0.0411	0.0344	16.2
300	0.0652	0.0557	14.6
350	0.0837	0.0750	10.3
400	0.0975	0.0905	7.2

To test this further, additional experiments were made with powdered catalyst where diffusion limitations were absent. The results are shown in figure 10. It can be seen that at high temperature there is no difference between CO_2 and N_2 while the difference remains at low temperature. These observations support the picture described above, i.e. a chemical effect of CO_2 at low temperature (adsorption on active sites) and a slower diffusion of NO/NH_3 in CO_2 which becomes evident a high temperature where the reaction is diffusion limited.

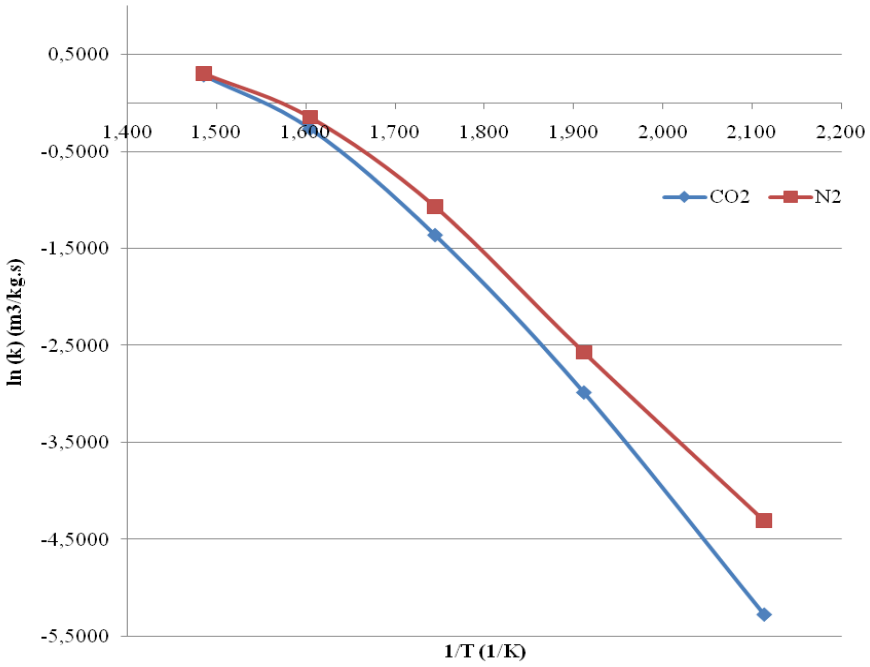

Fig. 10: Arrhenius plot of powder catalysts (0.1845 gm), temperatures ranging from 200 to 400 °C, total flow 3 L/min.

4.3 Investigation of oxygen dependency in CO_2 environment

A description of oxygen influence in the catalytic reaction should be developed. Therefore, a series of experiments has been conducted. This is very important as it is desired to run with very low oxygen concentrations on oxy-fuel power plants. First experiments were performed with plates and with varying oxygen concentration, from 2 to 5%. Very little difference was observed. It was therefore decided to run experiments with powder and much less oxygen concentrations to obtain the true difference at intrinsic kinetics of the catalyst. The oxygen concentration would now range from 0 ppm to 5000 ppm. The experimental results can be seen in Fig. 11.

It is observed that the activation energy is rather constant but the overall rate constant is decreased by lowering the oxygen concentration (Table 5). It can be concluded that there is a correlation between the oxygen concentration and the rate constant. A significant decrease in activity is seen when the oxygen concentration is lowered to zero but the reaction still continues even though it is not at a high rate.

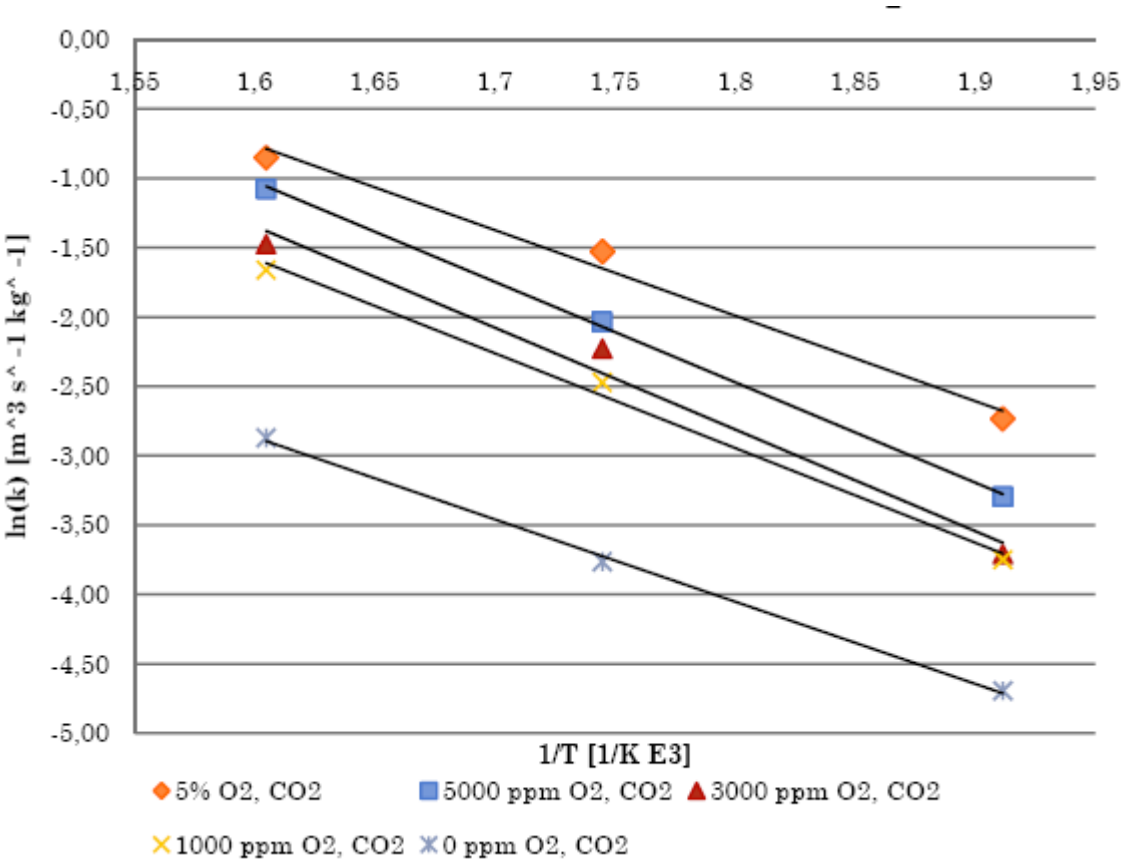

Fig. 11: Activity measurement of powder catalyst at 250-350 °C, 380 ppm NO, excess NH_3, total flow of 3 L/min, catalyst material 0.1234 g. between 82-92 % (vol) CO_2.

Table 5: Activation energies for the different concentration of oxygen.

Oxygen concentration	Slope	Activation energy (*KJ/mol*)
5 $\cdot 10^4$ ppm	-6.17	51.3
5000 ppm	-7.23	60.1
3000 ppm	-7.33	61.0
1000 pmm	-6.82	56.7
0	-5.93	49.3

It is proposed that the oxygen dependency is connected with the rate constant by (12) and (13), it should be noted that these terms are only apparent at low oxygen concentrations:

$$k_{obs} = k \cdot \Theta_{O_2} \quad (12) \qquad \Theta_{O_2} = \frac{K_{1,O_2} p_{O_2}}{1 + K_{2,O_2} p_{O_2} + K_{NO} p_{NO}} \qquad k_{obs} = k \cdot C_{O_2}^n \quad (13)$$

Equation (12) proposes that oxygen is adsorbed to reoxidize the catalyst. Θ_{O_2} describes the coverage of oxygen. The reason for NO to be in the coverage term of oxygen as a competing factor is that it can also reoxidize the catalyst. This will not happen very frequently, as earlier described; NO is only lightly adsorbed on the surface. In the conducted experiments the concentration of NO was very low, on that background the term of oxygen coverage is reduced to equation (14).

$$\Theta_{O_2} = \frac{K_{1,O_2} p_{O_2}}{1 + K_{2,O_2} p_{O_2}} \quad (14)$$

Equation (13) states that the rate constant is dependent on the oxygen concentration by some order. Both cases will be discussed in the following. By plotting the observed rate vs. the partial pressure of oxygen (Fig. 12), it is possible to fit the expression to the data by the least squares method.

Table 6: 2 Adsorptions coefficients found from fitting to the experimental work

	250 C	300 C	350 C
K_{1,O_2}	$1.22 \cdot 10^{-4}$	$5.88 \cdot 10^{-4}$	$1.53 \cdot 10^{-3}$
K_{2,O_2}	$1.67 \cdot 10^{-3}$	$2.51 \cdot 10^{-3}$	$3.37 \cdot 10^{-3}$

It is seen from Table 6 that the adsorption coefficients has a temperature dependency, which is found by making an Arrhenius plot (Fig. 13).

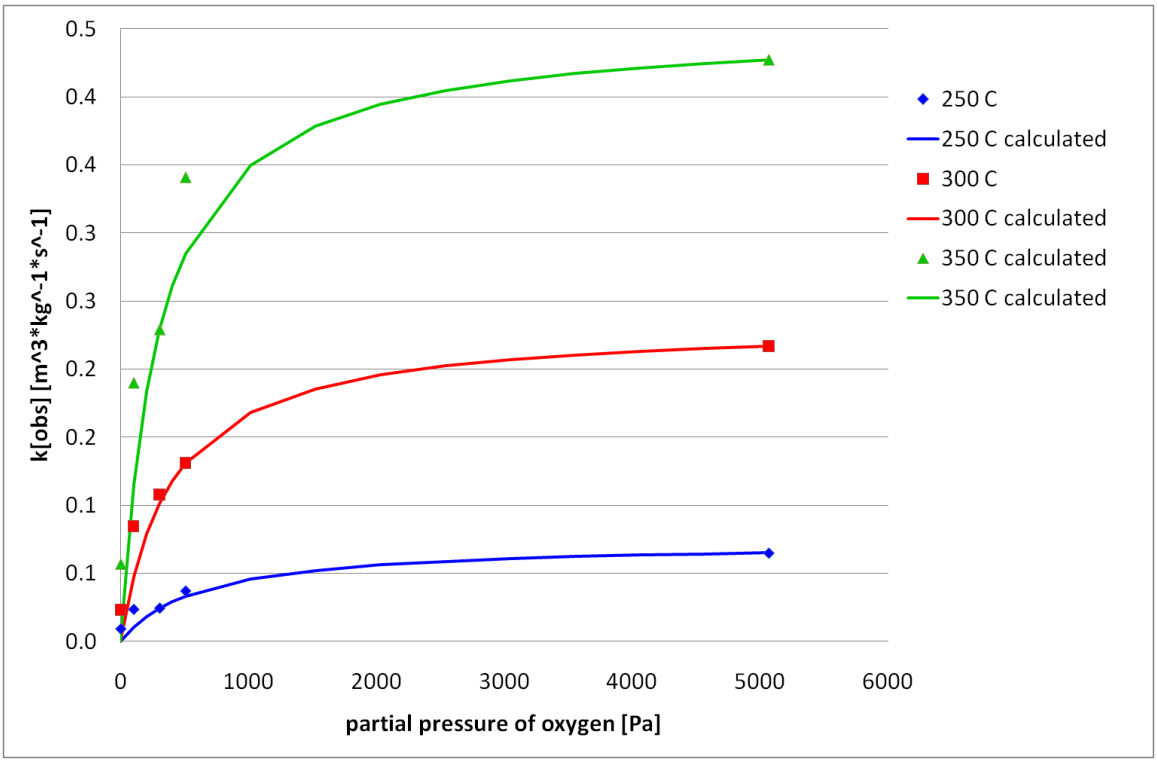

Fig. 12: k[obs] vs. partial pressure of oxygen and model of how the oxygen influences the activity.

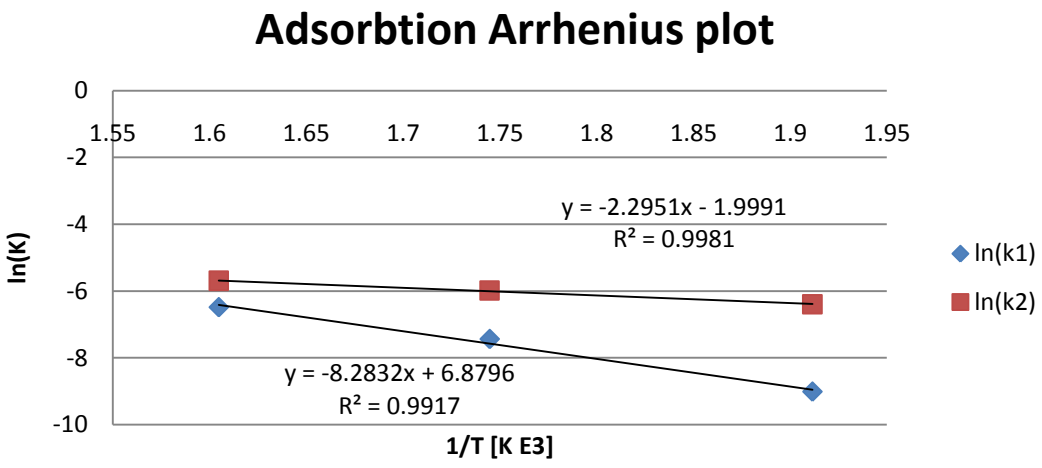

Fig. 13: Arrhenius plot of the adsorption coefficients.

The adsorption coefficients can now be expressed by eqn. (15) and (16).

$$K_{1,O_2} = e^{\frac{-8.2832}{T}\cdot 10^3 + 6.8796} \quad (15) \qquad K_{2,O_2} = e^{\frac{-2.2951}{T}\cdot 10^3 + 1.9991} \quad (16)$$

A very good regression was made with a high squared R value. It is now possible to determine at which oxygen concentration maximum activity is obtained. As earlier assumed, it can be seen that the activity becomes independent of oxygen at concentrations higher than 5%. By taking the logarithm of eqn. (13) a linear correlation for finding n is achieved as

$$\ln\left(k_{obs}\right) = \ln\left(k\right)\cdot n \cdot \ln\left(C_{O_2}\right) \quad (17)$$

The power of which the oxygen concentration influences the rate constant can be found and it is done by plotting (17), see Fig. 14.

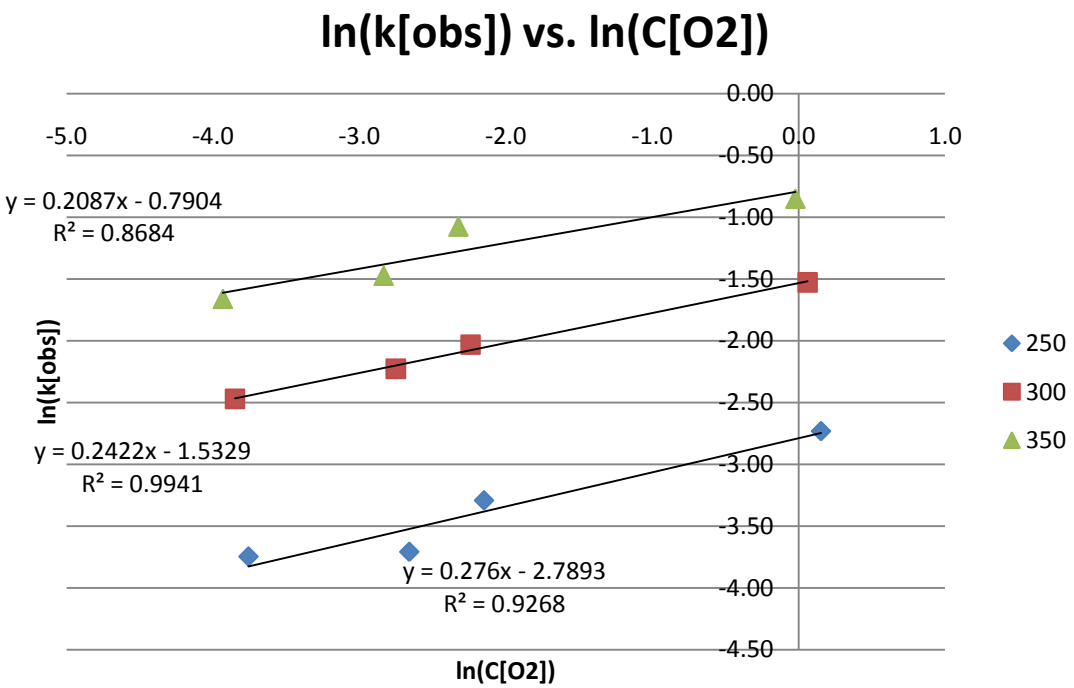

Fig. 14: shows a plot of eqn.(16).

The value of the slope equals n. n changes from 0.21 to 0.28 and by plotting the slope vs. the temperature, one can see the temperature dependency of the slope *n*, Fig. 15. Now, an expression can be set up which describes oxygen's influence on the reaction rate, see eqn. (16).

$$-r_A = k \cdot C_{NO} \cdot C_{O_2}^{\,0.00067 \cdot T - 0.14343} \qquad (18)$$

The term should only be used in areas where the concentration is below $5 \cdot 10^4$ ppm oxygen and temperatures below 350 ^{o}C. It can be observed that in both expressions the influence of oxygen becomes more apparent at higher temperatures.

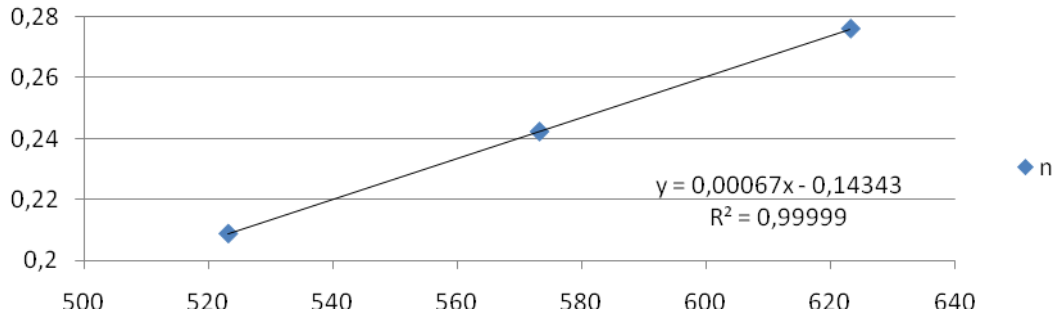

Fig. 15: A plot of n vs. temperature.

4.4 CO oxidation ability of SCR catalyst

It is know that under oxyfuel conditions CO_2 contains approximately 90% of the volume. CO_2 at high partial pressure and high flame temperatures can dissociate into CO and O_2 as given in Equation (5). This dissociated CO may not be directly released into the exhaust since it is one of the potential harmful effluents and should be converted into CO_2. SCR catalysts are also know to be good oxidation catalysts as well [56] and it would be useful if the SCR catalyst could carry out the oxidation of CO.

CO oxidation measurements were carried out at atmospheric pressure in a fixed-bed quartz reactor loaded with 200 mg of fractionized (180-300 µm) catalyst powder sample or 1.7 x 1.7 cm^2 catalyst plate sample. The reactant gas composition was adjusted to 500 ppm CO, 500 ppm CO_2, 5% O_2, 2.3% H_2O and balance N_2 (92.6%) used. The total flow rate was maintained at 3 l/min (ambient conditions). During the experiments the temperature was increased stepwise from 200 to 400 ^oC while the CO, CO_2 and O_2 concentrations were continuously monitored by ABB gas analyzer.

The SCR catalyst did not show any CO oxidation ability both in powder and plate catalyst experiments with in this experimental conditions. Ruszel et al. also observed similar type of results and finally concluded that vanadium is has got very poor oxidation ability and with a promoter like Au can accelerate the CO oxidation reaction [57]. Ruszel et al. observed a maximum CO conversion of 10% at 300 ^oC with a very low space velocity 3600 h^{-1} and in the present experimental conditions space velocities are very high and should be tested in this range only since CO oxidation is a possible parallel reaction along with SCR.

4.5 SCR in the presence of SO_x

In the present investigation no such measurements are done and it is known that in conventional SCR unit with few ppm levels of SO_x can accelerate the reaction. Under Oxyfuel conditions with the recycled stream of CO_2 the concentration of SO_x gases increases and the catalyst should with stand comparatively high concentration levels of SO_x.

5. Conclusions

Three aspects of the different flue gas composition of oxy-fuel combustion compared to normal air-combustion on the operation of the selective catalytic reduction of NO_x have been investigated: The influence of a high CO_2 concentration, the influence of a low O_2 concentration as would be beneficial from a process economic point of view and finally the possibility of using the SCR catalyst as an oxidation catalyst for a potentially increased CO level in the flue gas.

It was found that the activity of the typical industrial V_2O_5-WO_3/TiO_2 SCR catalyst is about 10 % lower when the carrier gas is CO_2 corresponding to oxyfuel conditions compared to when the carrier gas is N_2. At high temperature the difference is due to increased diffusion limitations of the reacting species, NO and NH_3, in CO_2 compared to N_2, while at low temperature the lower activity is speculated to be due to adsorption of CO_2 on the catalyst active sites. The catalyst activity is optimal when the oxygen concentration is above about 5000 ppmv, but below this level the rate decreases fast with decreasing oxygen concentration. Finally, it was found that the catalyst is inactive for CO oxidation.

Overall, the performed investigations do not indicate any problems for the SCR process in oxy-fuel flue gases.

6. References

[1] U. Gampe, S. Hellfritsch, S. Gonschorek. Oxyfuel technology for fossil fuel-fired power plants with carbon sequestration – technical and economic feasibility, Chair of power plant technology, Dresden University of Technology.

[2] http://www.vattenfall.dk/www/vf_dk/vf_dk/916035vores/917127forsk/917145null/index.jsp.

[3] http://www.iea.org/Textbase/speech/2008/Birol_WEO2008_PressConf.pdf.

[4] http://politiken.dk/udland/article234404.ece.

[5] http://ing.dk/artikel/98615-kina-vil-overhale-usa-med-renere-kulkraft.

[6] http://www.worldcoal.org/assets_cm/files/PDF/coalfacts08.pdf.

[7] http://www.iter.org/a/index_nav_2.htm.

[8] W. Terry, L. Yinghui, S. Chris, E. Liza, K. Sameer , R. Renu , Z. Farida, M. Behdad, B. Bart, S. Changdong, G. Raj, Y. Toshihiko, M. Keiji, Y. Jianglong. An overview on oxyfuel coal combustion—State of the art research and technology development. Chemical engineering research and design 87: 1003, 2 0 0 9.

[9] B. J. P. Buhre, L.K. Elliot, C.D. Sheng, R.P. Gupta, T.F. Wall. Oxy-fuel combustion technology for coal-fired power generation, Progress in Energy and Combustion Science 31: 283, 2005.

[10] G. Busca, L. Lietti, G.DRamis, F. Berti. Chemical and mechanistic aspects of the selective catalytic reduction of NOx by ammonia over oxide catalysts: A review, Appl. Catal. B, 18: 1, 1998.

[11] N. Topsøe. "Infrared spectroscopic investigations of enviromental denox and hydrotreating catalysts," 1998. Doctoral Thesis.

[12] N. Topsøe, H. Topsøe, J.A. Dumesic. Vanadia/Titania Catalysts for Selective Catalytic Reduction (SCR) of Nitric-Oxide by Ammonia: I. Combined Temperature-Programmed *in-Situ* FTIR and On-line Mass-Spectroscopy Studies, J. Catal., 151: 226, 1995.

[13] N.Y. Topsøe. Characterization of the nature of surface sites on vanadia-titania catalysts by FTIR, J. Catal., 128: 499, 1991.

[14]. N.Y. Topsøe, H. Topsøe. Combined in-situ FTIR and on-line activity studies: applications to vanadia-titania DeNox catalyst, Catal. Today, 9: 77, 1991.

[15] N. Topsøe, H. Topsøe, J.A. Dumesic. Vanadia-Titania Catalysts for Selective Catalytic Reduction of Nitric-Oxide by Ammonia : I.I. Studies of Active Sites and Formulation of Catalytic Cycles, J. Catal., 151: 241, 1995.

[16] V.Tufano, M. Turco. Kinetic modelling of nitric oxide reduction over a high-surface area V_2O_5-TiO_2 catalyst, Appl. Catal. B, 2: 9, 1993.

[17] J.A. Dumesic, N. Topsøe, H. Topsøe, Y. Chen, T. Slabiak. Kinetics of Selective Catalytic Reduction of Nitric Oxide by Ammonia over Vanadia/Titania, J. Catal.163: 409, 1996.

[18] M. Klostermann. Efficiency Increase of the Oxyfuel Process by Waste Heat Recovery Considering the Effects of Flue Gas Treatment. 3rd Workshop of the IEA GHG International Oxy-Combustion Network, Yokohama, Japan, March 5-6, 2008.

[19] F. Châtel-Pélage, R. Varagani, P. Pranda, N. Perrin, H. Farzan, S.J. Vecci, Y. Lu, S. Chen, M. Rostam-Abadi, and A.C. Bose. Applications of Oxygen for NOx Control and CO_2 Capture in Coal-Fired Power Plants. Thermal Science, 10(3):119–142, 2006.

[20] R. Payne, S.L. Chen, A.M. Wolsky, and W.F. Richter. CO_2 Recovery via Coal Combustion in Mixtures of Oxygen and Recycled Flue Gas. Combustion Science and Technology, 67(1):1–16, 1989.

[21] N. Kimura, K. Omata, T. Kiga, S. Takano, and S. Shikisima. The char- acteristics of pulverized coal combustion in O_2/CO_2 mixtures for CO_2 recovery. Energy Conversion and Management, 36(6-9):805–808, 1995.

[22] D.M. Woycenko, W.L. van de Kamp, and P.A. Roberts. Combustion of Pulverised Coal in a Mixture of Oxygen and Recycled Flue Gas. Summary of the APG Research Program, IFRF Doc. F98/Y/4, International Flame Research Foundation (IFRF), Ijmuiden, The Netherlands, October 1995.

[23] Y. Hu, S. Naito, N. Kobayashi, and M. Hasatani. CO_2, NOx and SO_2 emissions from the combustion of coal with high oxygen concentration gases. Fuel, 79(15):1925–1932, 2000.

[24] E. Croiset and K.V. Thambimuthu. NOx and SO_2 emissions from O_2/CO_2 recycle coal combustion. Fuel, 80(14):2117–2121, 2001.

[25] T. Nozaki, S.-i. Takano, T. Kiga, K. Omata, and N. Kimura. Analysis of the flame formed during oxidation of pulverized coal by an O_2-CO_2 mixture. Energy, 22(2-3):199–205, 1997.

[26] E. Croiset, K. Thambimuthu, and A. Palmer. Coal combustion in O_2/CO_2 mixtures compared with air. Canadian Journal of Chemical Engineering, 78(2):402–407, 2000.

[27] H. Liu, R. Zailani, and B.M. Gibbs. Comparisons of pulverized coal com- bustion in air and in mixtures of O_2/CO_2. Fuel, 84(7-8):833–840, 2005.

[28] A.J. Mackrory, S. Lokare, L.L. Baxter, and D.R. Tree. An Investigation of Nitrogen Evolution in Oxy-fuel Combustion. The 32nd International Technical Conference on Coal Utilization and Fuel Systems, The Power of Coal, 10-15 June, Clearwater, Florida, 2007.

[29] H. Liu and K. Okazaki. Simultaneous easy CO_2 recovery and drastic reduc- tion of SOx and NOx in O_2/CO_2 coal combustion with heat recirculation. Fuel, 82(11):1427–1436, 2003.

[30] L. Zheng and E. Furimsky. Assessment of coal combustion in O_2+CO_2 by equilibrium calculations. Fuel Processing Technology, 81(1):23–34, 2003.

[31] E.H. Chui, M.A. Douglas, and Y. Tan. Modeling of oxy-fuel combustion for a western Canadian sub-bituminous coal. Fuel, 82(10):1201–1210, 2003.

[32] E.H. Chui, A.J. Majeski, M.A. Douglas, Y. Tan, and K.V. Thambimuthu. Numerical investigation of oxy-coal combustion to evaluate burner and combustor design concepts. Energy, 29(9-10):1285–1296, 2004.

[33] Y.Q. Hu, N. Kobayashi, and M. Hasatani. The reduction of recycled-NOx in coal combustion with O_2/recycled flue gas under low recycling ratio. Fuel, 80(13):1851–1855, 2001.

[34] Y.Q. Hu, N. Kobayashi, and M. Hasatani. Effects of coal properties on recycled-NOx reduction in coal combustion with O_2/recycled flue gas. Energy Conversion and Management, 44(14):2331–2340, 2003.

[35] H. Liu, R. Zailani, and B.M. Gibbs. Pulverized coal combustion in air and in O_2/CO_2 mixtures with NOx recycle. Fuel, 84(16):2109–2115, 2005.

[36] A.J. Mackrory and D.R. Tree. NOx Destruction Experiments and Modeling in Oxy-Fuel Combustion. The 33rd International Technical Conference on Coal Utilization and Fuel Systems, Coal for the Future, 1-5 June, Clearwater, Florida, 2008.

[37] T. Kiga, S. Takano, N. Kimura, K. Omata, M. Okawa, T. Mori, and M. Kato. Characteristics of pulverized-coal combustion in the system of oxygen/recycled flue gas combustion. Energy Conversion and Management, 38:S129–S134, 1997.

[38] Y. Tan, E. Croiset, M.A. Douglas, and K.V. Thambimuthu. Combustion characteristics of coal in a mixture of oxygen and recycled flue gas. Fuel, 85(4):507–512, 2006.

[39] S.R. Turns. An Introduction to Combustion : Concepts and Applications. McGraw-Hill International Editions, 2000.

[40] T.F. Wall. Combustion processes for carbon capture. Proceedings of the Combustion Institute, 31 I:31–47, 2007.

[41] K. Okazaki and T. Ando. NOx reduction mechanism in coal combustion with recycled CO_2. Energy, 22(2-3):207–215, 1997.

[42] Y.Q. Hu, N. Kobayashi, and M. Hasatani. Effects of coal properties on recycled-NOx reduction in coal combustion with O_2/recycled flue gas. Energy Conversion and Management, 44(14):2331–2340, 2003.

[43] D.R. Tree. Multi-Pollutant Controls by OxyCombustion – A Mechanistic Investigation of Nitrogen Evolution and Corrosion with OxyCombustion. Project Description, Internal Report, Brigham Young University, November 2004.

[44] D.R. Tree, T. Fletcher, L. Baxter, S. Lokare, A. Mackrory, and R. Shurtz. A Mechanistic Investigation of Nitrogen Evolution and Corrosion with OxyCombustion. Status Report, DOE Award Number: DE-FG26- 05NT42530, Brigham Young University, January 2007.

[45] A.P. Simpson and A.J. Simon. Second law comparison of oxy-fuel combustion and post-combustion carbon dioxide separation. Energy Conversion and Management, 48(11):3034–45, 2007.

[46] D.J. Dillon, R.S. Panesar, R.A. Wall, R.J. Allam, V. White, J. Gibbins, and M.R. Haines. Oxy-Combustion Processes for CO_2 Capture from Advanced Supercritical PF and NGCC Power Plant. 7th International Conference on Greenhouse Gas Control Technologies. Vancouver, Canada,September, 2004.

[47] A. Kather, M. Klostermann, C. Hermsdorf, K. Mieske, R. Eggers, and D. Köpke. Steinkohlekraftwerk mit CO_2-Abtrennung auf Basis des Oxyfuel-Prozesses. In 39. Kraftwerktechnisches Kolloquium, October 11- 12, 2007, Dresden, Germany, 2007. In German.

[48] A. Kather, M. Klostermann, C. Hermsdorf, K. Mieske, R. Eggers, and D. Köpke. Konzept für ein 600 MWel Steinkohlekraftwerk mit CO_2-Abtrennung auf Basis des Oxyfuel-Prozesses. In Kraftwerksbetrieb unter künftigen Rahmenbedingungen, 38. Kraftwerkstechnisches Kolloquium, October 24-25, 2006, Dresden, Germany, 2006. In German.

[49] S.P. Khare, T.F. Wall, A.Z. Farida, Y. Liu, B. Moghtaderi, and R.P. Gupta. Factors influencing the ignition of flames from air-fired swirl pf burners retrofitted to oxy-fuel. Fuel, 87(7):1042–1049, 2008.

[50] P. Glarborg and L.L.B. Bentzen. Chemical Effects of a High CO_2 Concentration in Oxy-Fuel Combustion of Methane. Energy & Fuels, 22(1): 291–296, 2008.

[51] C.S. Wang, G.F. Berry, K.C. Chang, and A.M. Wolsky. Combustion of pulverized coal using waste carbon dioxide and oxygen. Combustion and Flame, 72(3):301–310, 1988.

[52] T. Mendiara. Experimental study of methane oxy-fuel combustion in the presence of NH_3 or NO in a flow reactor. Status Report, Technical University of Denmark, Department of Chemical Engineering, March 2008.

[53] R.B. Bird, W.E. Stewart, E.N. Lightfoot, Transport phenomena, 2nd ed. 2002, John Wiley & sons.

[54] O. Levenspiel, The Chemical Reactor Omnibook. 4th. Ed. 1993.

[55] A.B.roduit, A. Wokaun, Baiker, ind. Eng. Chem. Res. 1998, 37, 4577-4590.

[56] S. Brandenberger, O. Kröcher, A. Tissler, R. Althoff, Catalysis Reviews 50 (2008) 492.

[57] M. Ruszel, B. Grzybowska, M. Ga¸ sior, K. Samson, I. Gressel, J. Stoch, Catalysis Today 99 (2005) 151.

Literature survey:
Potential corrosion problems in oxyfuel environments

Melanie Montgomery
DTU Mekanik/Vattenfall/Dong Energy

Part of PSO 7171
21st December 2008

Contents

1. Introduction

This report seeks to give a realistic assessment of the possible corrosion problems that could be encountered during the process of oxyfuel firing and capturing of CO_2. This report was funded by PSO 7171 project in collaboration with CHEC, DONG Energy and Vattenfall. Although this is not an exhaustive list of problems, it highlights what now could be considered as problematic areas. Bordenet[1] describes the challenges and maps out the unanswered questions with respect to high temperature corrosion in oxyfuel combustion plants and CO_2 capture.

In oxyfuel firing, fuel combustion occurs with oxygen such that the resulting flue gas will be mainly CO_2 and H_2O. In addition there maybe recirculation of the about 2/3 of the flue gas, thus any trace elements in the flue gas will with time build up in concentration. This could be important with respect to the amount of sulphur within the flue gas. The higher content of CO_2 in the flue gas will make it more cost effective to recapture CO_2 after combustion.

DONG Energy will model the possible consequences for a retrofit of Studstrupværket and it is especially in this context that an assessment of material selection is required. The steam temperature will not be changed from its current status of 540°C however the flue gas composition changes due to oxyfuel firing. It is assumed that the temperatures of metallic components are similar to their present data, i.e. there is no increase in heat flux, however this may not be the case as the higher CO_2 and H_2O concentration may result in higher radiative heat fluxes.

2. Gas composition from oxyfuel firing

To assess the corrosivity within the boiler in oxy-fuel combustion, it is important to compare the flue gas composition of conventional firing and oxy-fuel firing. It has been estimated that a coal with 1% S will due to flue gas recycling be the same as using a 3.5% S coal in a conventional boiler[2]. CANMET[3,4] has conducted trials with lignite and bituminous coal and revealed the typical gas compositions with air firing and oxyfuel firing with different types of coal (Table 1).

Table 1: Flue gas compositions cited from reference 3.

	O_2 %	CO_2 %	CO ppm	SO_2 ppm	NO ppm
Bituminous + air	2.0	17	51	615	583
Lignite + air	3.3	17	1	277	771
Lignite + oxyfuel and recirculation of flue gas	2.7	92	14	785	555

As is expected the CO_2 levels increase, however the oxygen levels are similar. The sulphur levels are very dependant on coal type as shown in Table 1. Bituminous coal + air has similar sulphur dioxide levels to lignite in oxyfuel with recirculation. However it is clear that oxyfuel with recirculation increases the CO_2, CO and SO_2 content: the gases are measured on a dry basis in Table 1. Khare et al[5] estimated an increase in H_2O composition by 6 wt.% with oxyfuel. Ochs et al[6] compared the flue

gas composition of products leaving the boiler in vol. fraction including H_2O, and this indicates a fourfold H_2O concentration increase.

Table 2: Concentrations in flue gas (cited from Ochs et al[6]).

Vol. fraction	Flow (lb/hr)	CO_2	O_2	N_2	H_2O	SO_2	Ar
Combustion supported by air	3,539,738	0.1368	0.0350	0.7345	0.0829	0.0020	0.0088
Combustion supported by O2 with recycled flue gas	4,154,215	0.6085	0.0350	0.0206	0.3269	0.0090	0.0000

Bordenet[1] has found that the difference between gas compositions based on combustion of Lausitz coal as pulverized fuel is as in Table 3.

Table 3: Concentrations in flue gas according to Bordenet[1].

Vol %	CO_2	O_2	N_2	H_2O	SO_2	Ar
Combustion supported by air	15.3	2.5	71.3	10.0	0.13	0.8
Combustion supported by O2	58.9	1.9	4.8	31.8	0.49	2.1

J. Yan[7] has also calculated gas compositions given in Table 4. This is a worst case scenario with flue gas recirculation.

Table 4: Flue gas composition based on calculations[7]

Mass %	CO_2	O_2	N_2	H_2O	SO_2
Air-firing	22.5	2.6	66.50	6.0	0.26
Oxy firing	72.3	1.7	3.3	16.1	0.85

To summarise, based on measurements in laboratory burner rigs and theoretical calculations, it is clear that oxyfuel firing has similar oxygen content as presently observed 2-3 %, however the CO_2 and H_2O increases as well as the SO_2 if recirculation of the flue gas is undertaken.

2.1 Effect of change of gas composition on corrosion

Oxyfuel combustion will result in a higher CO_2 and H_2O concentrations as well as higher SO_2 concentrations if the flue gas is recirculated before desulphurisation. This could also lead to higher CO or H_2S in areas of the furnace susceptible to reducing conditions. Since the oxygen level is similar to that in conventional firing, it could be anticipated that it should be possible to form the protective oxides formed during conventional firing as the partial pressure of oxygen would be sufficiently high. However the long term consequences of change in gas composition due to oxyfuel firing is difficult to predict and will be discussed in this section.

2.1.2. Effect of H_2O and CO_2

High CO_2 and H_2O concentrations in the gas phase result in increased oxide thickness compared to a high O_2 content. There is a vast amount of experimental and

plant data which investigates CO_2 gas phase corrosion based on advanced gas cooled reactors. Likewise there is much data on H_2O oxidation (mostly plant but also some laboratory) and H_2O oxidation with various amounts of oxygen. There is slight disagreement if oxidation in CO_2 environments is comparable to H_2O environments if the partial pressures of oxygen are the same however where comparison is made in the same laboratory, similar results are observed. However it is important to define whether the same data from pure CO_2 and H_2O is relevant or whether some synergistic or antagonistic effect occurs when these two components are mixed in the high quantities expected i.e. 30% H_2O and 60% CO_2.

Since there is relatively high oxygen content in the gas, and the percentage of water vapour is generally high in flue gas from conventional firing, the effect of slightly higher water vapour is probably not important in itself. It has been shown by many workers that increase in water vapour in air or oxygen environment results in faster oxidation rates[8]. The extensive work from steam oxidation shows that the steam environment gives faster oxidation rates than in an air environment however the oxidation rates are parabolic[9] and X20CrMoV121 has an oxidation rate an order of magnitude lower than 10CrMo910. Recent laboratory testing was undertaken at 20 atm for 500 and 1000 hours at 900°C to investigate oxidation rates in CO_2+steam[10]. A Type 304L lean stainless showed a significant increase in oxide growth compared with air but similar corrosion rates between air and 10%CO_2+ steam and they cited that CO_2+ steam was similar to experiences with steam oxidation since the partial pressure of oxygen is the same. A comparison of pure steam and steam with 10% CO_2 is given for Alloy 230 (Nickel based alloy with 14wt.% W and 22wt.% Cr) reveals an increased oxidation in the steam + CO_2 environment. Conversely, for the Alloy 214 (nickel alloy with 16wt.% Cr and 4wt.% Al), there are similar or lower oxidation rates for steam + 10% CO_2 compared with steam. The author suggests this difference could be due to the one being a chromia forming alloy and the other being an alumina forming alloy.

Parabolic rates are generally also observed for CO_2 gas[11], although corrosion rates are higher in CO_2 compared with oxygen. A comparison of a Fe-Ni alloy at 800°C for 150 hours in CO_2 shows that the oxidation rate is at least 10 times higher in carbon dioxide environments and there is much grain boundary attack[12]. Comparison of 9Cr steels shows comparable oxidation rates in steam and carbon dioxide under pressure. However it can be that CO_2 can give an additional negative contribution to corrosion. From the work in the AGR reactors in the UK in the 1970-80s, where CO_2 was used as a coolant at high temperatures and pressures[13,14], problems with 9% Cr steels were observed where a severe breakaway oxidation occurred after a long exposure time (1-5 years). Initially a normal duplex oxide was formed however carbon deposition at the metal adjacent the inner oxide occurred and when carbon started being deposited in the oxide, breakaway oxidation was initiated. High water vapour content (increase from 200 ppm to 600 ppm) increased the probability of breakaway oxidation. However it was also observed that breakaway oxidation did not occur with components under 10 atm. However in oxyfuel combustion, there is a much higher water vapour content (10% instead of ppm levels) which could really provoke this reaction. Investigation of stainless steels show that the carbon is not concentrated in the metal adjacent the oxide but diffuses into the bulk material. Thus no breakaway oxidation occurs with stainless steel.

Recent work has investigated corrosion in CO_2 + 30% H_2O conditions both in high and ambient pressures for ferritic steels with 1-11% Cr. Here the increased oxidation rate was observed for ferritic steels at high pressures due to increased

carbon deposited within the oxide[15]. Whether with longer exposures and at ambient pressures an increased carbon deposition would result in breakaway oxidation is difficult to assess.

Natesan and Rink[16] have described studies undertaken by ORNL where materials have been exposed to pure CO_2 and 50%CO_2+50%H_2O. They report some preliminary results which reveal initial oxidation rates expressed as weight gain for the mixture of CO_2+H_2O is higher at 750°C. However internal carburisation could also be an issue thus comparison of penetration and oxide thickness are required.

2.1.3. Increased SO_2 in gas phase

Much work has been conducted on the effect of SO_2 in an oxidising environment[17]. Depending on the varying compositions, this results in oxidation and sulphidation to various degrees. It is important how the phases exist in the corrosion product i.e. isolated or interconnecting throughout the corrosion product. The rates of reaction are significantly higher than with pure oxygen due to sulphides being incorporated in the scale. Sulphides are not as protective as oxides and lead to faster diffusion rates. Laboratory tests at various temperatures have been conducted in H_2-H_2S-H2O and CO-COS-CO_2 environments[18]. They concluded that carbon bearing gases could be used instead of hydrogen bearing gases to simulate variations of O_2 and SO_2 partial pressure. (They do not take account of the possible different effects due to incorporation of carbon or hydrogen species into the oxide or metal but this was perhaps not observed for their oxidation times). From 1 year laboratory exposure, the following oxidation/sulphidation rates are observed where the higher p(O_2) indicates oxidation and the lower p(O_2) indicates sulphidation (Figure 1). Penetration is a measure of corrosion rate based on parabolic behaviour) (N08810 is Alloy 800H, S44600 is AISI 446 and S67956 is INCOLOY alloy MA 956.

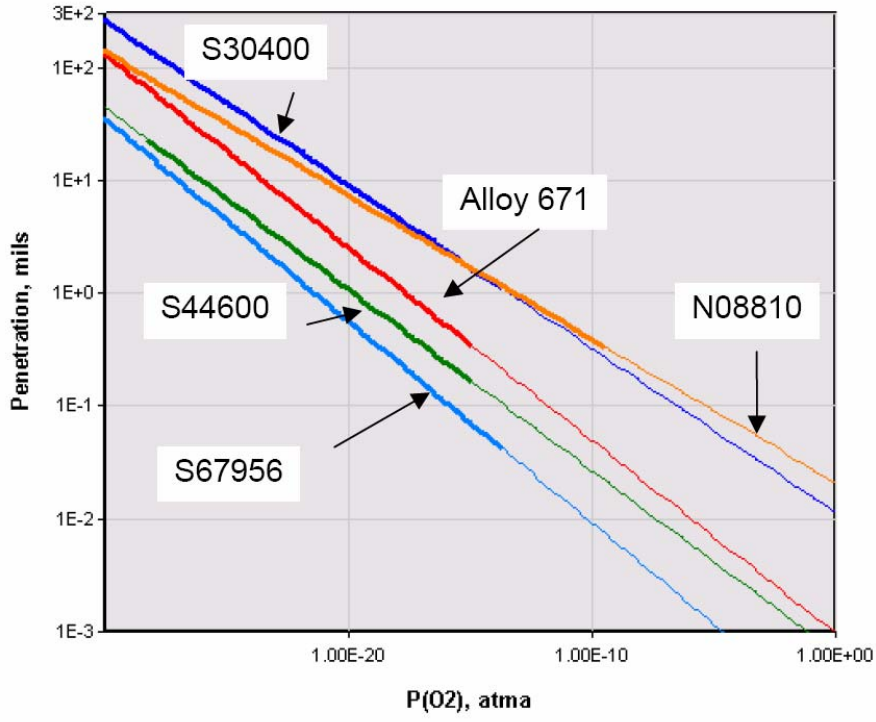

Figure 1: Effect of pO2 upon sulphidation/oxidation rates of alloys after 1 year exposure to pS_2 of 10^{-7} atama at 700°C - According to RC John Ref 18.

2.1.4. Effect of increased CO (and H_2S) in gas phase

The presence of increased CO_2 and increased SO_2 has been discussed in the previous sections with respect to oxidising conditions. However recirculation of gases and the high presence of CO_2 could give rise to reducing areas within the boiler. With conventional firing, reducing conditions have been observed on the furnace wall near the burners especially if low NOx burners and staged firing has been implemented. There are many articles foe example[19,20] on waterwall corrosion and the most important points are described. With oxidizing conditions, Fe_3O_4 forms on waterwalls. This is an effective barrier for further oxidation, and after that oxidation follows a parabolic kinetic law. If there is reducing conditions in the combustion gases, then H_2S can form from pyrite which originates from coal.

$$FeS_2 + CO + H_2O \rightarrow FeS + H_2S + CO_2$$

$$S_{org} + H_2 \rightarrow H_2S$$

As can be observed from the above equation, it would seem that a high CO_2 concentration could prevent this by pushing the equation to the left and therefore this scenario may be avoided in oxyfuel firing.

When H_2S is present in the fluegas, it reacts with iron from the protective Fe_3O_4 as follows.

$$Fe + H_2S \rightarrow FeS + H_2$$

$$Fe_3O_4 + 3H_2S + CO \rightarrow 3FeS + 3H_2O + CO_2$$

This will result in an oxide together with sulphide or only sulphide. The strength and the adherence of the corrosion layer decreases with a higher iron sulphide content and the corrosion rate increases. In addition there is a greater vulnerability to erosion in reducing gases related to the poorer adherence of sulphide compared with oxide.

On the basis of laboratory experiments using a gas content of 5-10% CO and 500-1500 ppm H_2S (rest N_2, CO_2, SO_2) corresponding to the low NOx burner, the following corrosion rate is derived[19].

$$\text{Corrosion rate} = 3.2\text{x}10^5 \text{x} \exp(-15818/1.987\text{x}(H_2S)^{0.574}\text{x}1/(\%Cr+10.5)^{1.234} \pm 2.2$$

corrosion rate in (mil/yr) (1mil=25.4μm)

T= temperature in Kelvin

H_2S = H_2S concentration in ppm

%Cr = wt.%Cr in steel.

This equation is applicable for coal with a sulphur content for coal of 0.9-1.2%. With higher sulphur content, H_2S is not the most important parameter. Deposits of unburnt carbon and FeS, which originates from FeS_2 in coal will give increased corrosion rates. From laboratory experiments, corrosion rate increases five times with the presence of FeS deposits. However it is in oxidising environments that corrosion under FeS deposit is the worst as oxidised FeS releases H_2S, COS, and CH_3SH close to the waterwall. For this reason, the article indicates that oxidising/reducing conditions should be the worst, i.e. just under OFA.

Laboratory investigations with cycling of oxidising and reducing environments have shown that a low alloyed steel has a high corrosion rate compared with a high alloyed

steel[20]. For the stainless steel, the changing oxidizing/reducing environment allowed the protective Cr_2O_3 to be formed.

Comparison of three boilers in Japan[21] with metal temperature of 400°C and air surplus ratio 0.8 showed that sulphur content resulted in high corrosion rates. In Boiler A with a high sulphur coal (6 wt %), the corrosion rate vas 0.85mm/yr. It was observed that corrosion rates were high where there was high H_2S (2100 ppm) and CO (3.9%) content in the combustion gas. In boiler B which was fired with a 3.2 % S content coal, the corrosion rate was 0.75mm/yr: It was estimated that H_2S level was 1000 ppm. Boiler C with a 2 wt.% sulphur content in coal had a corrosion rate of 0.15mm/yr and H_2S content of combustion gas was 230-270ppm.

In the UK, there have been problems with high Cl content in the coal. It has been concluded that a Cl concentration in coal of over 0.2% results in a higher corrosion rate in reducing environments[22]. This is much higher Cl content than the fuel usually utilised in Denmark.

Nava et al[23] has concluded, that for a coal type with over 1.5 wt.% S, sulphidation of low alloyed steel can be expected. Laboratory trials for T11 showed that increasing H_2S from 200ppm to 1000ppm resulted in 50% higher corrosion at 500°C. For higher Cr containing steel like a 30%Cr iron alloy, there was adequate corrosion resistance against 1000ppm H_2S. In this environment, chromium rich inner oxide is formed which reduces sulphidation attack. The article also suggests that CS_2 is more aggressive than H_2S. The corrosion rate can be predicted in mils/10000h based on H_2S content and temperature according to Figure 6 (1mil=25µm).

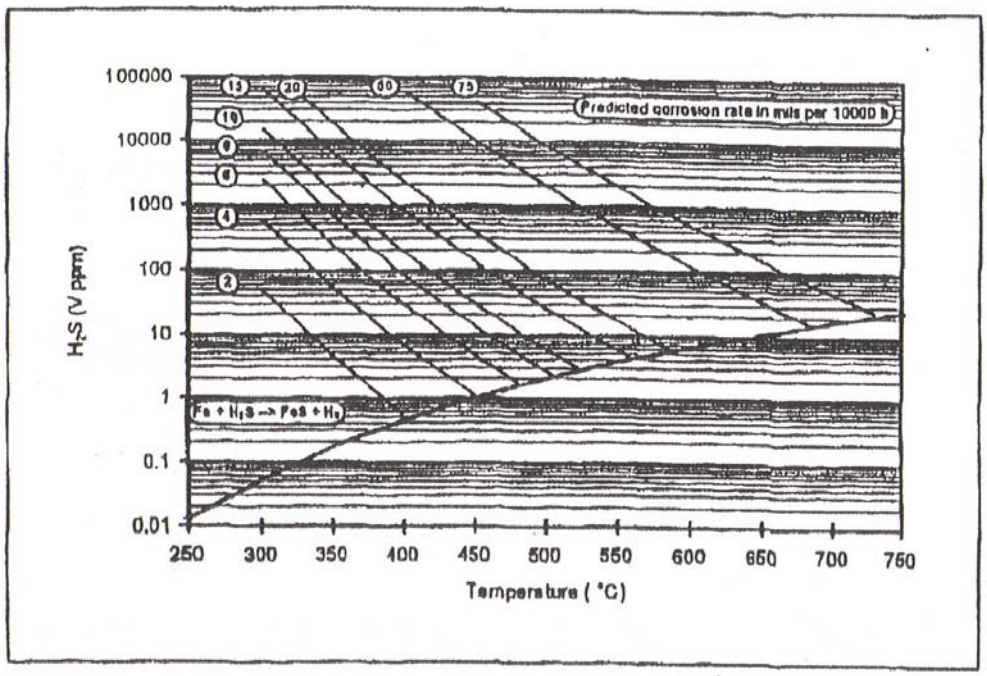

Iso-corrosion lines derived from statistical correlation of isothermal laboratory data for T-11 exposed to reducing gases typical of low-NO_x firing conditions.

Figure 2: Prediction of corrosion rate for T11 from Nava et al[23]

During low NOx combustion, there are more unburnt coal particles and iron sulphides that deposit on superheaters and reheaters. The higher content of unburnt coal in the deposit gives a localised reducing area which can give carburisation of superheater and reheaters that also result in high corrosion rate[24].

To sum up, the following factors could have an influence on waterwall corrosion in relation to oxyfuel combustion.

- Fuel: Cl, S
- Flue gas: O_2, CO, H_2S
- Deposition of FeS- and/or carbon rich (unburnt) particles
- Flame contact
- Changing between oxidising and reducing atmosphere
- Heat flux
- Metal temperature

Conceptual design studies[25] of oxyfuel combustion of Illinois coal with 75% recirculation have been undertaken by the Foster Wheeler Corporation. In an air fired furnace, the H_2S concentration was 1600ppm resulting in gas phase corrosion of 300µm/yr. In oxyfuel conditions, this increased to 6400 ppm which results in 750µm/ year. They concluded that either the flue gas should go through a FGD or that Nickel alloys as weld overlay would be needed. The CO concentrations in both systems were similar due to the use of stage firing so it is the recirculation of sulphur species that would result in the higher corrosion rate. Calculations with respect to flue gas recirculation and oxygen concentration revealed that the heat flux could increased by a factor of 1.5-2.5 resulting in wall temperature increase of 65-120°C. This would require a significant material upgrade from for example T2 (0.5Cr) to T92 (9%Cr). Even if the flue gas was run through a FGD before recirculation, there would still be a higher level of CO which may give problems.

3. Deposit composition with oxyfuel firing

Sheng and Li[26] investigated ash formation during pulverised coal combustion in O_2/CO_2 mixtures compared with O_2/N_2 mixtures. Four different coal samples were burnt with various gas compositions in a drop tube furnace. The residues ash samples were characterised by X-ray diffraction and ^{57}Fe Mössbauer spectroscopy. No significant difference was observed in the crystalline phases of the ashes. However a difference in the relative intensities of peaks was observed for some phases in the two gas environments. Mössbauer spectroscopy showed that the differing atmospheres influenced the relative percentages of iron species formed in the ashes. In O_2/CO_2 combustion resulted in more iron melting into glass silicates and less iron oxides. This could give problems with slagging and fouling.

4. Low temperature corrosion

4.1. Experiences from oil and gas industry

Low temperature corrosion with respect to oil and gas has been most recently described in the Ph.D by P. Føsbol[27] from the Chemical Engineering Dept at DTU where 202 references are given. The gas industry is concerned with natural gas, however its compositions differs somewhat from the composition that will be present due to CO_2 separation in an oxyfuel plant (Table 5). Different feed gas compositions

to the CO_2 compression unit have been calculated by Zanganeh 2007[28]. However the two major corrosive components are the mixture of CO_2 and H_2O in this environment so some of the experiences from the oil and gas industry will be relevant.

Table 5: Comparison of compositions for natural gas and CO_2 compression.

	Natural gas composition mol% cited by[27]	CO2 compression[28] vol %
CH_4	88	
Ethane	6	
Propane	2	
Butane	1	
CO_2	1.6	91.83
H_2O	0.1	3.26
SO_2		0.42
O_2		2.83
N_2	0.2	1.64
Ar		0.01

The basic corrosion reaction is that CO_2 reacts with water to form carbonic acid. Without water this reaction would not occur. Figure 3 is a schematic of the corrosion that occurs in a pipeline. Corrosion usually takes place at the bottom of the pipeline because of the water phase that condenses and drops down however this can be combated with inhibitors or additives such as NaOH. One of the problems in "Top of the Line Corrosion" and this cannot be helped by inhibitors.

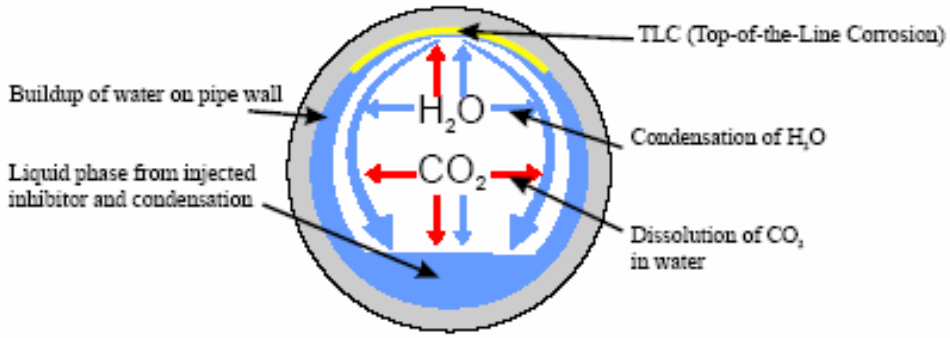

Figure 13: Cross section of pipeline showing the condensation of water which influences the corrosion process under the pipeline "roof".

Figure 3: Cross-section of pipeline showing condensation of water (Taken from ref 27).

There is much information with respect to CO_2 corrosion in the oil and gas industry and the following areas are seen as important for a materials viewpoint[30]. From reaction with carbonic acid, mild steels form $FeCO_3$ scales and it is the maintenance of the iron carbonate as a protective layer that affects corrosion rates. Important factors are as follows:

- The pH increase decreases the corrosion rate due to the stabilisation of bicarbonate and carbonate and the decreased solubility of $FeCO_3$.

- $FeCO_3$ is unstable in the presence of oxygen, and it is recommended that the oxygen content is less than 40 ppb.
- Corrosion rate increases with increase in flow velocity as $FeCO_3$ are hindered from forming or are removed.
- Corrosion rate increases with higher CO_2 partial pressure since the solution pH will decrease.
- At temperatures below 60°C, the uniform corrosion rate increases with temperature as it is not so easy to form iron carbonate. However protective films are more easily formed at a higher temperature. The optimum temperature depends on other factors such as pressure, flow rate etc. Figure 4 shows the corrosion rate of iron and a schematic of the structures formed at various temperatures where there between approx. 50-130°C, corrosion rate is highest.

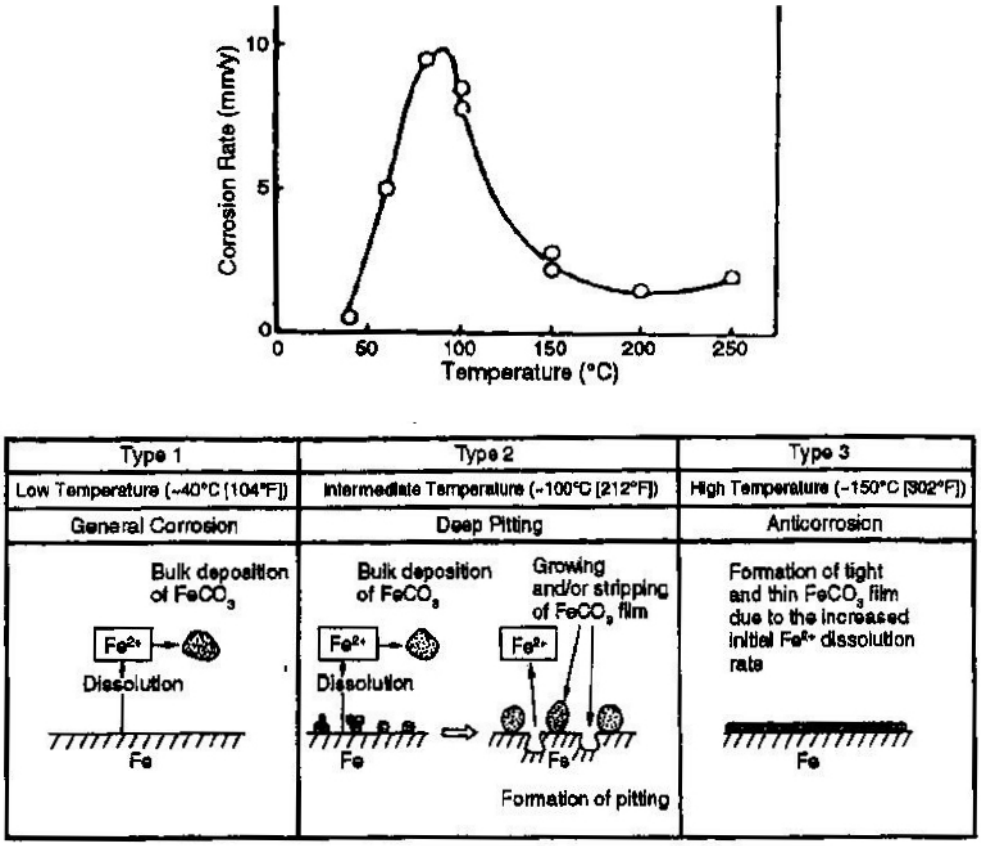

Figure 4: Corrosion rate of iron in CO_2 environments and schematic showing corrosion products at various temperatures (Taken from ref 29).

- Microstructure of alloy[30] - carbides in the steel are seen to anchor the $FeCO_3$ to the steel, however accumulation of carbides could be the cause of increasing corrosion over time for ferritic/pearlitic steels. In addition the heat treatment process also affects the corrosion resistance. Inhibitors are used widely in the industry however how they exactly improve corrosion resistance is not known and therefore evaluation tests should be conducted with the specific parameters of interest.
- Different alloys can give improved corrosion resistance in the various environments Figure 5 shows the general use of alloys depending on environment. The maximum corrosion rate (as shown in the top schematic

in Fig 4) of the steels shifts to higher temperatures with increased chromium content, however the corrosion rate also decreases significantly with increasing Cr content as Cr species are incorporated into the iron carbonate layer.

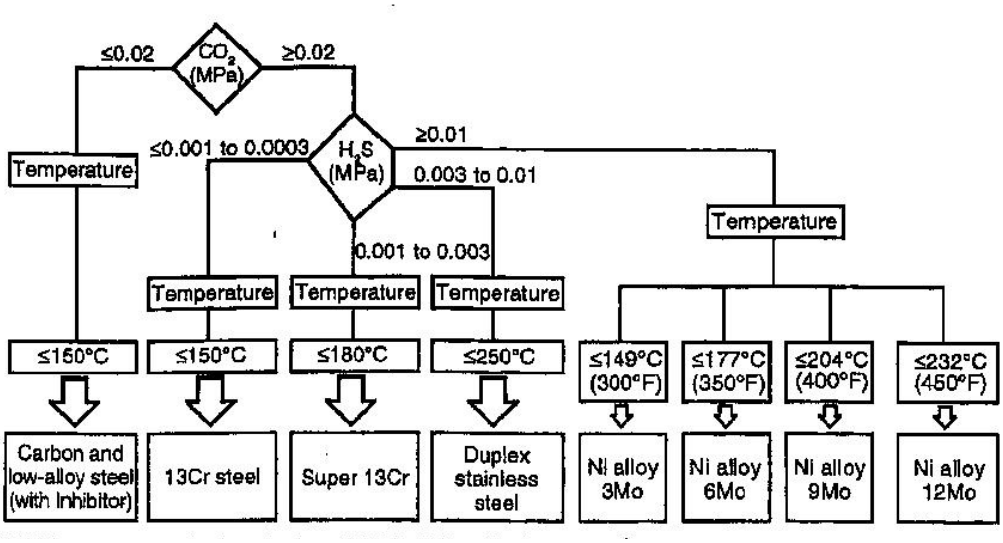

Figure 5: Flow chart for the selection corrosion resistant alloys for H_2S and/or CO_2 service (Taken from 29]

Different models have been developed where corrosion can be estimated depending on varying parameters. For example from the equation below, a corrosion rate in mm/yr can be calculated depending on t temperature °C, pCO2 as pressure in bar.

$$\log(CR) = 7.96 - \frac{2.32 \times 10^{-3}}{t + 273} - 5.55 \times 10^{-3} t + 0.67 \log p_{CO_2}$$

Nyborg[31] (2005) describes that the use of different models can give rise to significantly different corrosion rates, however $FeCO_3$ is formed to give protection, and this occurs where there is high temperature or high pH in the liquid phase. Seiersten[32] has conducted high pressure corrosion tests and shows that the accepted guidelines do not fit in with corrosion rates at the higher pressures ranges. They show the corrosion decreases with higher pressures for low alloyed steels at 40°C - for experiments up to 300 hours exposure. Where a substantial $FeCO_3$ could be formed at the lowest pressures and give some protection, however at the highest pressures, there was only a thin continuous carbonate film. Thus the corrosion rates could not be explained only based on the carbonate film formation and it was suggested that another mechanism is in play at higher pressures.

4.2. Dewpoint corrosion

Another essential difference from natural gas and the gas composition in carbon capture is that there may be higher amounts of O_2 and SO_2 or SO_3, NOx or HCl which could give additional problems. The most important is the acid dewpoint for sulphuric acid as this has a dewpoint considerably higher than water such that in an environment with SO_2 and SO_3 and water, sulphuric acid could condense out on the

tubes. SO_2 has a dewpoint below water but can react with oxygen to produce SO_3 which has a dewpoint above the waters dewpoint (Figure 6).

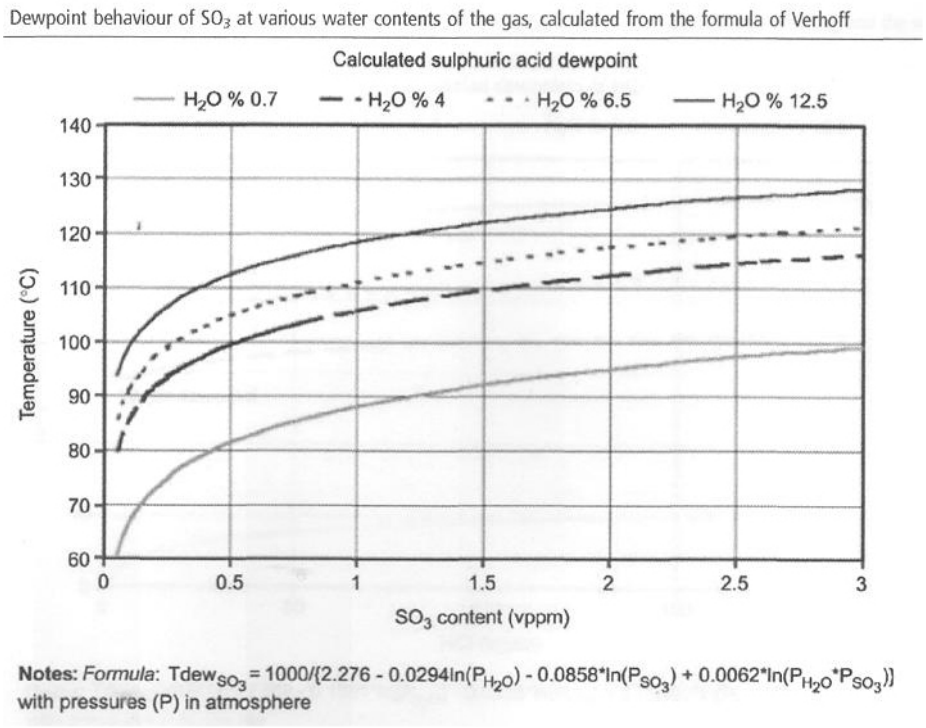

Figure 6: Dewpoint behaviour of SO_3 at various water contents of gases (calculate forVerhoff formula) Ref 33

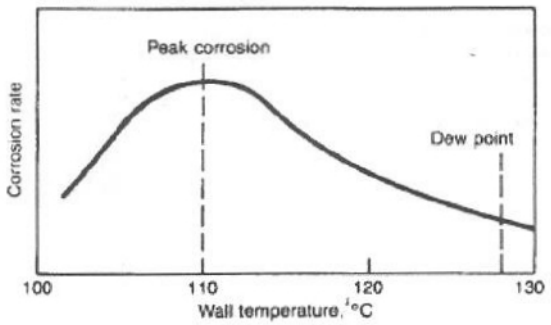

Figure 7: Corrosion rate with respect to dewpoints temperature(ref. 34).

The corrosion rate is highest just below the dew point where the SO_3 concentration is high in the condensate present as a film on metallic surfaces. As the temperature decreases, the corrosion rate decreases. The next dewpoint is hydrochloric acid (53°C depending on the amount of water content as shown in Figure 6) and water 49°C.

5. Actual corrosion results with oxyfuel conditions

Much of the literature and research cited in section 2 is based on evidence from conventional firing where N_2 is the predominant gas component and not CO_2. The literature in actual oxyfuel conditions is divided into three parts - those where there have been laboratory simulations where there is deposit on a specimen in the oxyfuel gases, and those from laboratory burner rigs, where there is heat flux from the flue gas/combustion process, and continual dynamic replenishment of the deposit in an oxyfuel environment, and those from pilot plants.

5.1. Laboratory simulations

Sroda et al[32] investigated corrosion with respect to carbon dioxide concentration both with and without ash deposits. Their experiments were not specifically concerned with oxyfuel firing as nitrogen was also present. The gas composition was 22% H_2O, 5% O2, x% CO_2 and rest N_2). However they showed for exposures of 360 hs at 535°C that an increase in CO_2 concentration from 0 to 25% resulted in an increase in weight of specimens. Weight gain was also compared in combustion gases with and without CO_2 where flyash ash was deposited on the specimens, and there was a clear weight gain when the gas composition contained 25% CO_2.

Laboratory corrosion tests (260 hours at 675°C) have been conducted with premixed gaseous mixtures to simulate conventional and oxyfuel coal combustion[36]. There was higher corrosion rates on the specimens in the oxyfuel gases where the corrosion rates in oxyfuel was double that in air-firing. In addition exposure in the same gas mixtures with the synthetic ashes which should be typical of Texas lignite and West Virginia Bituminous coal were conducted. For these tests with ash deposit, corrosion was higher in the presence of ash than with only gas environment which has been shown by many other researchers. However the authors state that there is no significant difference between oxyfuel and air (see Table 6). Actually in some cases oxyfuel had less corrosion however these are very new results and there is no mention of accuracy errors. Thus the presence of the deposit was the significant corrosive factor. It must be also noted that the same authors had previously published a paper[37] where they measured very high corrosion rates for oxyfuel firing. In the latest paper, the authors do not mention the previous results so it is assumed that there were some errors in the paper and the most recent paper should be assessed as a corrected version of the 2007 paper. At the high temperature investigated 2½ % Cr steel corrodes much faster than 9% Cr.

Table 6: Results from Reference 36 with metal loss in mm with deposits.

Alloy	Air mm	Oxyfuel mm
T22	0.97	Not tested
T92	1.11	1.29
347 SS	0.78	1.30
Inconel 617	0.85	1.02

Foster Wheeler are involved in a DOE sponsored project on oxy USC Boiler Materials Program to identify corrosive conditions in furnace and superheater/reheater. It will first be from CFD simulations to predict corrosive microclimates, and coal ashes will be produced. Based on this, 1000h laboratory tests in synthetic gas and ash conditions will be conducted[25].

Cranfield have a burner rigs which they use for investigating deposits and gas compositions and are under modification for oxyfuel. They are also doing laboratory tests in oxyfuel condition in collaboration with Eon, and results should be published next year.

5.2. Burner Rigs

There are some short-term burner rig studies from oxyfuel conditions. The ENCAP project has undertaken short-term test but no results have been published yet[39]. EON are also performing corrosion testing in oxyfuel conditions, but as yet

have not published[40]. They are involved in a Doosan Babcock led oxy-fuel firing project that is co-funded by the Technology Strategy Board, project partners and project sponsors, with DONG Energy being one of the project sponsors.

5.3. Pilot plant

Foster wheeler are modeling the effect of CO_2 combustion in CFB boilers and together with VTT which has in Jyväskylä small scale fluidized bed combustor such as 30-100kW to operate air-firing and oxygen combustion modes. Here pilot scale tests are being carried out with Polish and South African coals, however at the moment, there is no data on corrosion performance of materials[40].

Vattenfall has built a 30MW pilot plant in Scwarzepumpe, Germany. This is now running however no corrosion data is available.

There is a 30MWe Callide project in Australia.

5.4. Demo plants

Two demonstration plants are planned by Foster Wheeler - on CIUDEN in Spain - 20MWt Scheduled mid 2009 and 50MWe CFB in Jamestown, New York.

6. Specific for Studstrup plant:

Studstrup blok 3 or 4 is to be assessed with respect to retrofit. Studstrupværket has an effect of 700 MW. There are two units, units 3 and 4 which were commissioned in 1984 and 1985. Studstrupværket used oil and coal for production of heat and electricity. These have since been modernised. There is now co-firing in both units 3 and 4 in the form of 10% straw and coal.

The outlet steam temperature is 540°C in superheater 4 which is fabricated from X20CrMoV121 and TP347H. It is this component which will be assessed for corrosion. Reheater has a temperature close to the 540°C and is X20CrMoV121. From these components, this could result in surface metal temperatures of 560°C. The waterwalls are fabricated from 15Mo3 and 13CrMo44 - low chromium steels at temperatures of 370-410°C. The present flue gas composition from the plant is not known especially in the superheater and waterwall areas are not known.

6.1 Assessment of superheater corrosion:

The increased amount of SO_2 in the plant will ensure that the Cl from the straw is converted. Problems can come when reducing conditions are found on waterwalls. It is anticipated that the primary effect of more SO_2 will be a greater sulphate content in the deposit which may give increased fouling. In addition more SO_2 in the flue gas will make the sulphate more aggressive as it will give a perpetual supply of sulphur to the deposit. Co-firing of biomass and fossil fuels (both DONGs plants Avedøre 2 and Studstrup 4) has revealed high sulphate content within the deposit. The deposit at Studstrup is rich in calcium sulphate however Avedøre 2 has a greater concentration of potassium sulphate together with calcium sulphate.

In Studstrup[42] X20 sections had been exposed for 3 years (22597hs) in superheater 3, superheater 4 and the reheater. Superheater 3 had steam temperatures of 465°C and Superheater 4 had steam temperatures of 540°C however the investigated specimens were from a tube with temperature measurements to be 575°C (due to unequal distribution in the bank where the outermost tubes have a higher heat flux). The reheater had steam temperatures of 560°C. Figure 8 and 9 show the results

from Studstrup and the extrapolated corrosion rates assuming that corrosion occurs according to a linear kinetic.

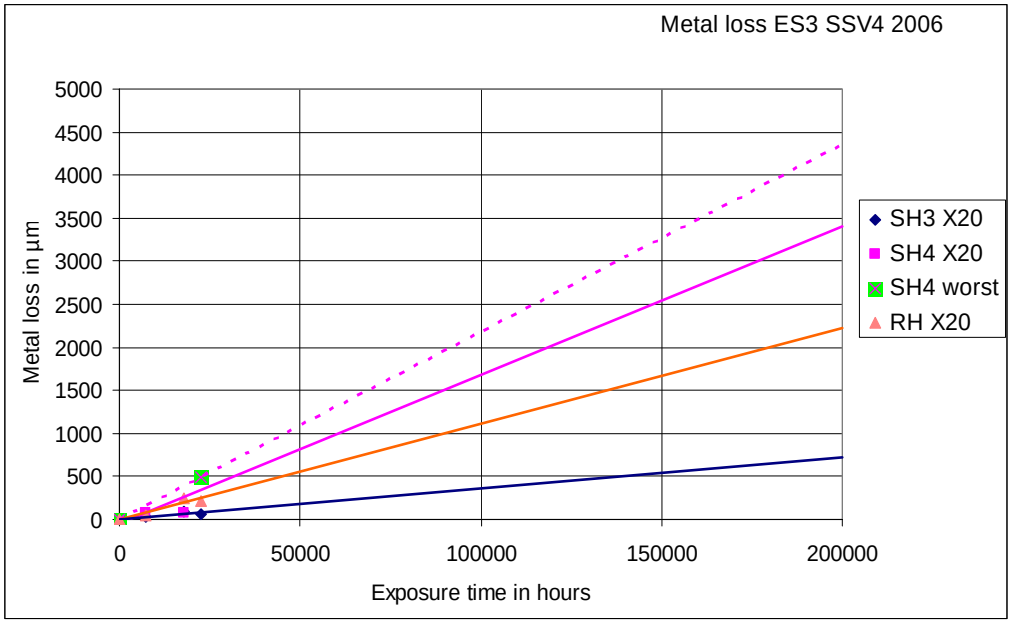

Figure 8: Corrosion rate from Studstrup unit 4 based on metal loss measurements.

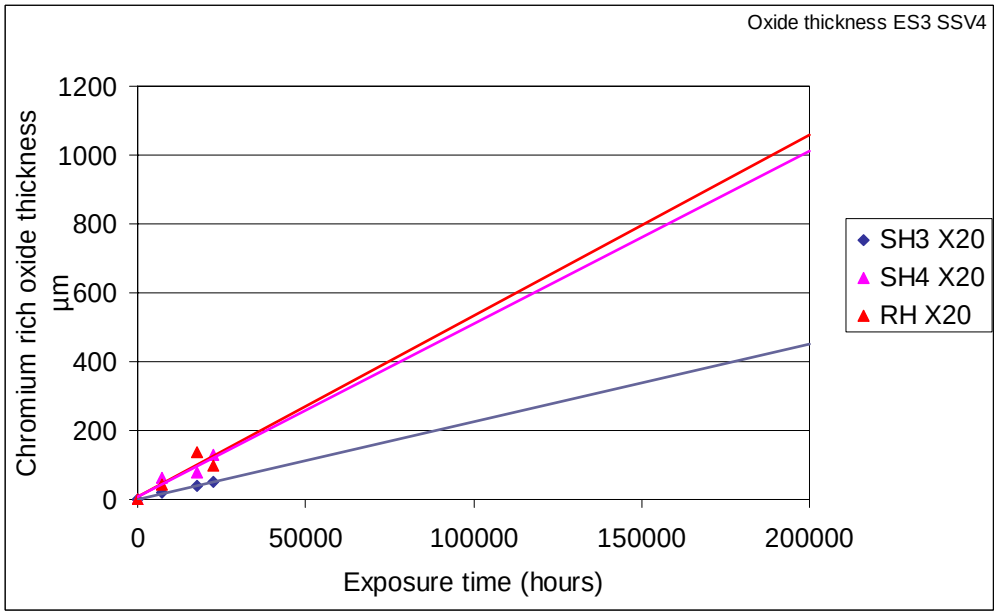

Figure 9: Corrosion rate from Studstrup unit 4 based on oxide thickness.

It is suggested that the actual corrosion rate is between metal loss measurements and oxide thickness measurements as there were some inaccuracies in metal measurements. For these data it was assumed that the oxide thickness was more accurate, thus leading to corrosion rates of 1mm after 200,000 hr exposure. The oxide appeared to be protective so a more parabolic kinetic may be the case however there will be inaccuracy in oxide thickness measurement as it assumes no spallation. In addition the specimens were machined and this could result in lower corrosion rates

than normally observed. Spallation of the oxide is inevitable after longer exposure periods. A comparison of the data is given in Figure 10 taken from reference 43.

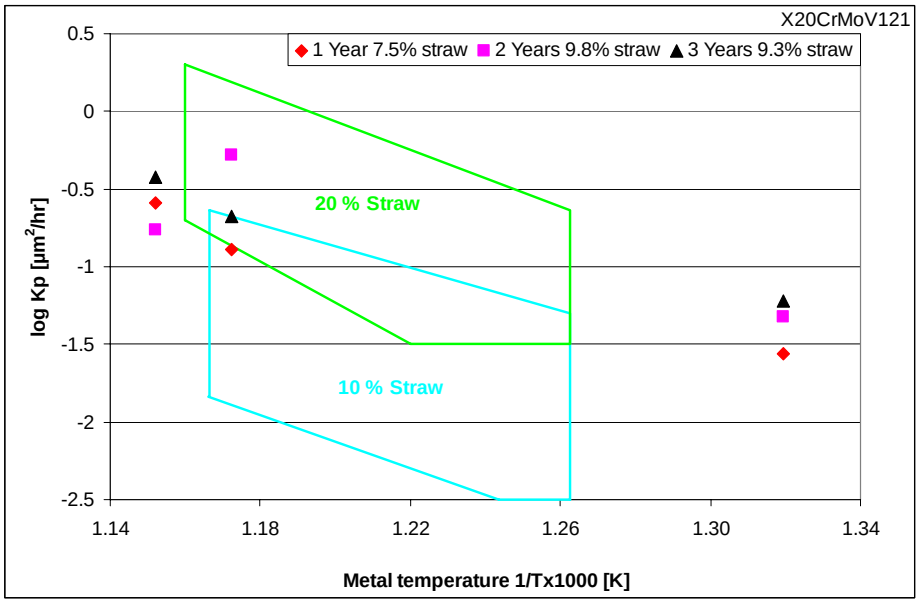

Figure 10: Corrosion rates based on oxide thickness for Avedøre 2 and Studstrup for X20CrMoV12 .

2.1.2. Data from Avedøre 2 main boiler

Avedøre 2 main boiler has been fired with gas, wood pellets and heavy fuel oil with 2% sulphur in the oil. The ratio of oil to wood is very important such that it has been decided that wood pellets will only be used with at least 10% heavy fuel oil containing 2% sulphur so that the high S neutralizes the chlorine content in wood pellets[44]. The corrosion rates for Avedøre 2 with wood pellets + heavy fuel oil + gas on a 18Cr (and 15Cr) austenitic steel at steam temperatures of 520°C and 540°C have not been alarming[44]. Figure 11 shows the corrosion rates measured at Studstrup and Avedøre 2 for TP347H FG.

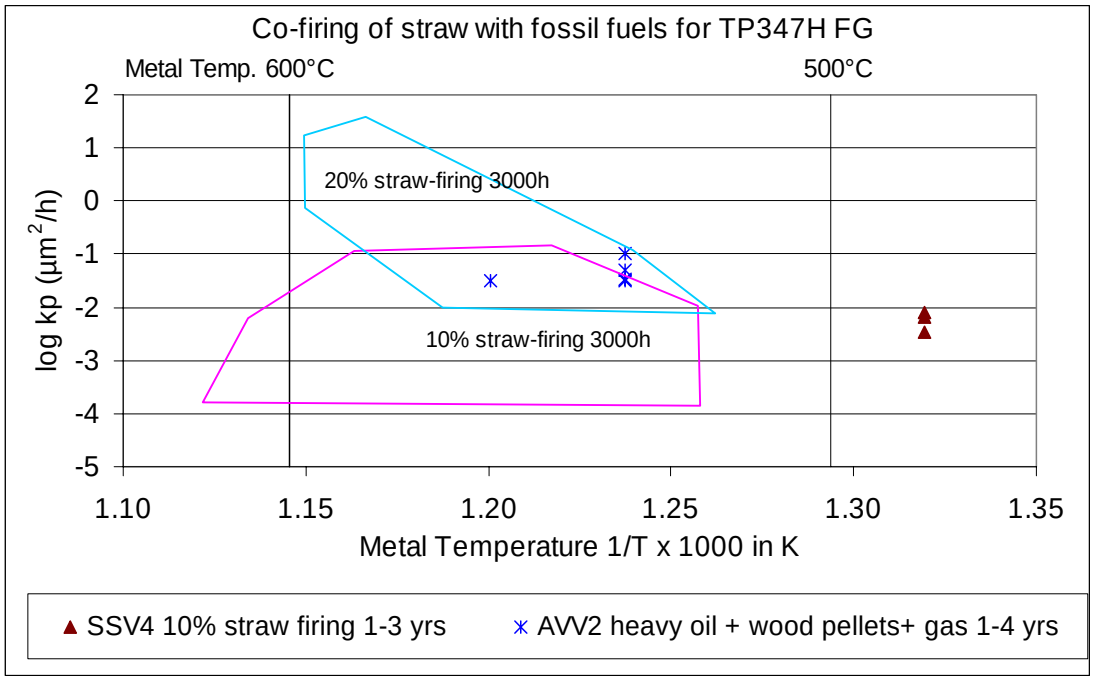

Figure 11: Corrosion rates based on oxide thickness for Avedøre 2 and Studstrup for TP347H FG.

These results are based on oxide thickness and metal loss is a more reliable measure. A test firing using coal fly ash as an additive was conducted whilst a corrosion probe was exposed. Scanning electron microscopy showed that the unspalled ash from the probes consisted of mainly potassium sulphate-calcium sulphate however in addition there was a proportion of pure calcium sulphate and also potassium aluminosilicate. In addition to this, there were many particles of iron oxide within the deposit. Thus the calcium sulphate content had decreased in this ash making it similar to a coal ash such as lignite. Figure 12 shows the results from the corrosion probe.

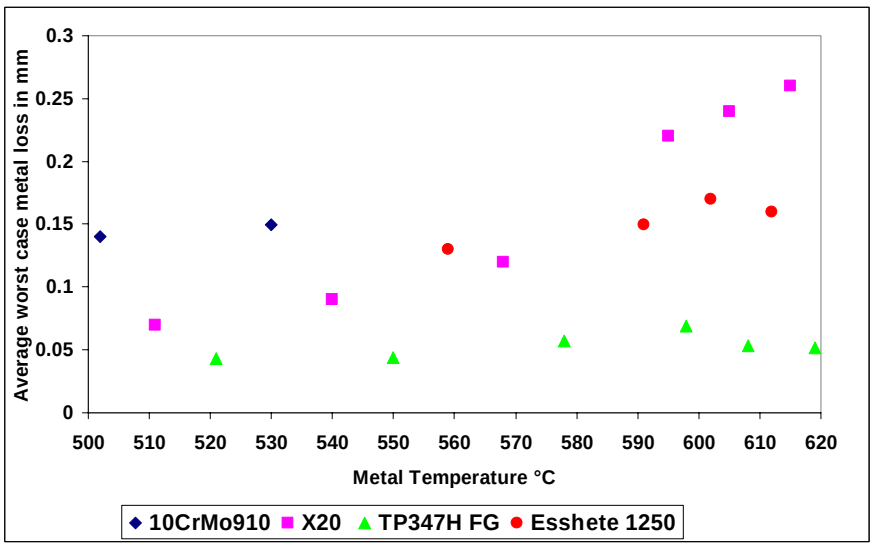

Figure 12: Metal loss for specimens exposed for 2000 hrs in Avedøre II with the use of flyash.

The alloy showing the lowest corrosion rates is TP347H FG. Compared to this, Esshete 1250 has a much higher corrosion rate although this does not increase

drastically with temperature. X20CrMoV121 (12% Cr) has a corrosion rate which is comparable to Esshete 1250 at lower temperatures (560°C), but has a much higher corrosion rate at higher temperatures. 10CrMo910 has a higher corrosion rate double that of X20CrMoV121. 10CrMo910 was not tested at the higher temperatures, however it is anticipated that its low chromium content would result in high corrosion rates at high temperatures.

Based on these results, X20 has a good corrosion rate which could be comparable to Esshete 1250, however there could be problems with 10CrMo910. However it is unadvisable to extrapolate data from a short-term test assuming a linear relationship.

In general a higher chromium content is favorable for a good corrosion resistance to sulphidation (X20 has 12% Cr and 10CrMo910 has 2.5%Cr)[47], however one reference[48] from a 10,000 hour field test in an oil-fired boiler with 2.65%S in the oil shows low metal wall losses of 0.3 mm for a 2.25 Cr steel compared to the austenitic steels.

6.2 Waterwalls

The waterwalls are fabricated from a low alloy steel and may be susceptible to waterwall corrosion. If the H_2S increases and in the lower parts of the furnace, corrosion rates could be significantly increased as cited by reference 25 and discussed in section 2.

7. Concluding remarks

This report identifies possible corrosion problems with oxyfuel combustion. Although there has been an amount of experience with steam oxidation and carbon dioxide and sulphur dioxide, the amount of experience with these components together is limited. The increased sulphur dioxide presence will probably result in sulphate rich deposits similar to those in co-firing. From data from Avedøre 2, TP347H FG performs acceptably with more sulphate rich deposits. There could be a problem with X20CrMoV121 with the more sulphate rich deposits. There is the added possibility of carbon deposition within the alloy and oxide which after long term exposure would give unexpected breakaway oxidation. Whether long term exposure is 1 year or 7 years is difficult to judge.

It is however suggested that potential problems with waterwall corrosion will be likely with the low alloyed steels used. This is based on the fact that coal firing although there are no problems in the superheater regions, the waterwalls may have problems especially if there is increased heat flux due to oxyfuel firing.

With respect to low temperature corrosion, then dewpoint corrosion may also be a problem.

8. References

1. B. Bordenet, Materials and Corrosion 2008 59 No 5 pp. 361-366.
2. D. McDonald and A. Zadiraka, 17th Annual Joint ISA POWID/EPRI Controls & Instrumentation Conference June 10-15, 2007 Pittsburgh USA
3. Y. Tan et al, Fuel, **85** (2006) pp. 507-512
4. E. Croiset, K. Thambimuthu, A. Palmer: The Canadian Journal of Chemical Engineering, **78**, (2000) pp. 402-407.
5. S.P. Khare: Fuel 87 (2008) pp 1042-1049
6. T. Ochs et al 29th International Conference on Coal Utilisation and Fuel Systems, 18-22 April 2004, Clearwater Florida
7. J. Yan, M. Anheden, G. Lindgren, L. Stromberg. 8th International Conference on Greenhouse Gas Control Technologies (GHGT-8), Trondheim, Norway. 19-22 June 2006.
8. S. Jianian, Z. Longjiang, L. Tiefan: Oxidation of Metals Vol 48 Nos. 3/4 1997 pp 347-356.
9. M.Montgomery and A. Karlsson "Bericht über die Oxidation von neuen Stahltypen in dampfseitigen Verhältnissen" VGB Kraftværkstechnik 75 (1995) H3 pp258.
10. I.G Wright et al NACE Proc 2004 Paper 04531.
11. P. Kofstad High Temperature Corrosion p 518.
12. Menzies IA, Tomlinsen WJ: British Corrosion Journal 1967 Vol 2 November pp 235-241
13. P.C Rowlands et al "The oxidation behaviour of Fe-9Cr-1Mo steels" Gas cooled reactors today, BNES London 1983.
14. P.C. Rowlands and M.I Manning "The application of TEM and STEM to the study of oxidation processes of steels in low pO2 environments" Proc NACE 1983.
15. D. Huenert and A. Kranzmann "Influence of pressure and chromium content on corrosion reactions at 600°C in CO2-H2O atmosphere" NACE Paper 08447 2008.
16. K. Natesan, DL Rink: Proc. 21st Annual Conference on Fossil Energy Materials. Knoxville Tenessee. ORNL
17. F. Gesmundo , D.J. Young, S.K. Roy High Temperature Materials and processes V8 No3 1989 pp149
18. R.C. John Proc. NACE Corrosion 2007 Paper 07465.
19. WT Bakker, SC Kung: Corrosion 2000 Paper 00246.
20. S.C. Kung and WT Bakker: Materials at High Temperatures 14(2) pp175-182 (1997).
21. S. Kihara, K. Nakagawa and I. Kajigaya: Proc. Int. Conf. On Corrosion CONCORN '97 Dec 3-6, Mumbai India.
22. P.J James L.W Pinder Materials at High Temperatures Vol 14 1997 p237

23. JC Nava-Paz, A.L. Plumley, OK Chow, W. Chen: Materials at High Temperatures 19(3) pp127-137 (2002).
24. WT Bakker, JL Blough, WW Seitz, Corrosion 2001 Paper 01168.
25. H. Hack, A. Seltzer, G. Stanko: Proc. 5th International Conference on Advances in Materials Technology for Fossil Power Plants, Marco Island, Florida. Oct 3-5 2007. EPRI Conference.
26. C. Sheng and Y. Li: Fuel 87 (2008) 1297-1305.
27. Philip L. Fosbøl: Ph.D Thesis October 2007. Dept of Chemical Engineering, DTU. Denmark.
28. K.E. Zanganeh, A. Shafeen: International Journal of Greenhouse Gas Control 1 (2007) pp47-54.
29. M. Ueda: Corrosion October 2006, pp. 856-867.
30. D.A. Lopez, T. Perez, S.N. Simison: Materials and Design 24 (2003) pp561-575.
31. R. Nyborg The oil and Gas Review 2005 Issue 2 pp70-74
32. M. Seiersten NACE Corrosion 2001 Paper 01042.
33. WMM Huijbregts, RGI Leferink “Anti-corrosion methods and materials” Vol 51 No 3 2004, pp173-188.
34. V. Ganapathy: Hydrocarbon Processing, January 1989 pp57-59.
35. S. Sroda, M. Makipaa, S. Cha, M. Spiegel: Materials and Corrosion 57 (2006) pp776-181.
36. BS Covino, S.A. Matthes, S.J. Bullard “Effect of oxyfuel combustion on superheater corrosion” NACE 2008 Paper 08456
37. BS Covino, S.A. Matthes, S.J. Bullard “Corrosion un oxyfuel/recycled flue gas-fired vs air-fired environments” 32 International Technical Conference on Coal Utilization & Fuel Systems, June 10-15 2007, Clearwater, Florida
38. Personal Communication Nigel Simms Cranfield
39. M. Montgomery and A. Hjørnhede Reports delivered to ENCAP, 2008.
40. Colin Davis - Personal communication November 2008.
41. Eriksson T, Nuortima K, Hotta A, Myöhänen K, Hyppänen T, Pikkarainen T, VGB - KELI 2008 conference, Hamburg, Germany 6-8 May 2008
42. M. Montgomery and RB Frandsen “Investigation of corrosion at Studstrup blok 4 co-firing plant: Part III - 3 years exposure.” January 2006. Part PSO 4108.
43. R.B. Frandsen, M. Montgomery, OH Larsen: Materials at High Temperatures, Vol 24, No4, Dec 2007 pp343-349.
44. J.P. Jensen, K. Nielsen, M. Montgomery, C. Andersson “Ash Chemistry, corrosion and heavy metal emissions from a 800MW wood pellet + oil + natural gas fired power plant” Proceedings 14th European Biomass conference Paris 2005.
45. M. Montgomery, T. Vilhelmsen, S.A Jensen: Materials and Corrosion 2008, 59 No 10 pp783-793

46. M. Montgomery, S.A. Jensen, O. Biede, O.H. Larsen, C. Andersson "Corrosion and oxidation experiences in Avedøre II multifuel boiler" Proc. Liege conference 2006.
47. G.Y Lai "High Temperature Corrosion and Engineering" p. 140-142.
48. J.C Parker and D.F Rosborough "High temperature corrosion trials at Marchwood Power Station - 10000 hour corrosion probe trials" J. Inst. Fuel 45 1972.

9^{th} Liege Conference : Materials for Advanced Power Engineering 2010
edited by J. Lecomte-Beckers, Q. Contrepois, T. Beck and B. Kuhn.

PRELIMINARY EXPERIENCES WITH MATERIAL TESTING AT THE OXYFUEL PILOT PLANT AT SCHWARZEPUMPE

Anders Hjörnhede[1], Melanie Montgomery[2], Martin Bjurman[3], Pamela Henderson[3], Alexander Gerhardt[4]

[1]Vattenfall Power Consultant, Sweden
[2]DTU Mekanik/Vattenfall Heat Nordic, 2800 Lyngby, Denmark
[3]Vattenfall Research and Development, Sweden
[4]Vattenfall Research and Development, Germany

Several material related issues may arise from oxyfuel combustion of coal due to the presence of CO_2 but also as an effect of the partial recirculation of the flue gas. Two examples are increased corrosion and carburisation which may limit steam data, hence limiting the efficiency.

A number of corrosion tests, in both conventional air-firing and oxyfuel mode, have been made in Vattenfalls 30 MW oxyfuel pilot plant located in Schwarze Pumpe, Germany. Internally cooled corrosion probes, equipped with ferritic, austenitic, super austenitic steels as well as Ni-based and FeCrAl alloys, simulating superheaters, economisers and air preheaters were exposed for up to 1500 hrs.

The analyses show an indication of higher material wastage in oxyfuel compared to air combustion especially at the lower exposure temperatures. This may be due to increased sulphur concentration in corrosion front, increased heat flux, carburisation or other preciptate formations on austenitic steels and Ni-based alloys.

Keywords: CCS, oxyfuel, oxyfuel pilot plant, corrosion

1. Introduction

All over the world, fossil fuels are combusted in power plants resulting in CO_2 emissions which contributes to global warming. In order to reduce CO_2 emissions from coal-fired plants, it is necessary to implement new technologies resulting in carbon capture and storage (CCS). One of the possible technologies is oxyfuel firing and capturing of CO_2. Bordenet [1] gives a survey of the material challenges with respect to oxyfuel combustion plants with CO_2 capture and post combustion plants. In oxyfuel firing, combustion occurs with oxygen such that the resulting flue gas will be mainly CO_2 and H_2O. In addition there maybe recirculation of up to 2/3 of the flue gas, thus any trace elements such as sulphur in the flue gas will build up in concentration. The higher content of CO_2 in the flue gas will make it more cost effective to recapture CO_2 after combustion. Vattenfall has constructed a 30MW oxyfuel pilot plant to validate engineering work, to learn and improve understanding of the dynamics of oxyfuel combustion and to demonstrate the capture technology, [2]. The construction of this plant started in 2007, and in late 2008 the test phase began. The pilot plant is located in Schwarze Pumpe, Germany.

Material tests are being performed both under conventional air and oxyfuel firing at various operation conditions to reveal whether the oxyfuel process gives additional materials challenges. These tests are important as the choice of suitable materials will be a key issue for the future demonstration plant. With respect to high temperature corrosion, since the actual plant has a low steam outlet temperature of 350°C, corrosion probes simulating higher steam temperatures are inserted in the plant. In addition, probes simulating waterwalls are also exposed. The three gaseous species which will increase compared to conventional firing are

CO_2, H_2O and SO_2 (due to recirculation of flue gas). However, as of yet it is unclear how this will effect corrosion rates. An initial comparison of corrosion in oxyfuel versus conventional combustion was conducted in the ENCAP programme [3]. The exposures times were below 40 hours and the results showed no significant difference between conventional firing and oxyfuel firing, indicating that there is a need for data from long-term exposures.

There are a number of different applications which are relevant for corrosion investigation:

- Demonstration plants:

Vattenfall in Germany is preparing for the erection of a 250MWe demonstration plant, purpose-built for oxyfuel firing in Jänschwalde, Germany. In the demonstration plant, the technology's commercial abilities will be proven whereas in the pilot plant the technology itself and the process are being validated. The maximum steam temperature of the demonstration plant will be 600°C. The high temperature components will be the steel types commercially available today. Knowledge of how these types of steels react in an oxyfuel environment is lacking, but the well known creep, microstructure and steam oxidation data can be used.

- Retrofit of existing USC (Ultra Super Critical) boilers:

If it appears unlikely that many new plants will be purpose-built for oxyfuel combustion in order to reduce CO_2 emissions, it is possible to retrofit already high efficiency USC boilers to oxyfuel firing. Here the steam temperature will be similar to or slightly higher than the Jänschwalde demo.

- High efficiency oxyfuel plants:

In order to recuperate the expenses of a CO_2 recapture plant, it may be necessary to increase the steam data of the plant to give the same net efficiency as the existing USC boilers. This involves employing steam temperatures of up to 700°C. At present there is no plant that runs with such high temperatures so this is challenging not only for the fireside corrosion but for steamside oxidation, microstructural stability and creep development. There are various projects that are investigating 650-700°C plants, which will give information which is also relevant for oxyfuel plants. These programs are COMET 650 (completed), AD700, COMTES 700. It is important that the steels qualified within these programs are considered as they will have already been tested with respect to welding, microstructure development and steam oxidation. So far no tests have been performed in the pilot plant at these high temperatures.

- Low Temperature and CO_2 processing unit:

Another essential part of the material testing is corrosion at low temperatures in the preheater and flue gas desulphurisation unit, flue gas condenser and CO_2 processing unit. These aspects are being investigated in the pilot plant and the knowledge is relevant for all future CCS plants irrespective of boiler outlet temperature. Low temperature corrosion is investigated by coupons installed after the boiler where corrosion problems are anticipated. In addition online corrosion sensors and corrosion probes are utilised.

2. Material testing parameters

Figure 1 shows a schematic flow sheet of the oxyfuel pilot plant in Schwarze Pumpe. It is important to note that the recirculation of the gas is before the flue gas desulphurization plant thus the content of sulphur and other impurities will increase with time. The percentage of

recirculated flue gas in the inlet gas stream is 20 - 39%. Low temperature corrosion investigations are undertaken in the areas shown on the diagram and also in the CO_2 process unit. In these areas, racks of test coupons of different materials are exposed to aid materials selection. In addition condensates are collected so that the mechanism of corrosion can be investigated and materials can be tested with similar condensates in controlled conditions in the laboratory. There are no results available from this work at present.

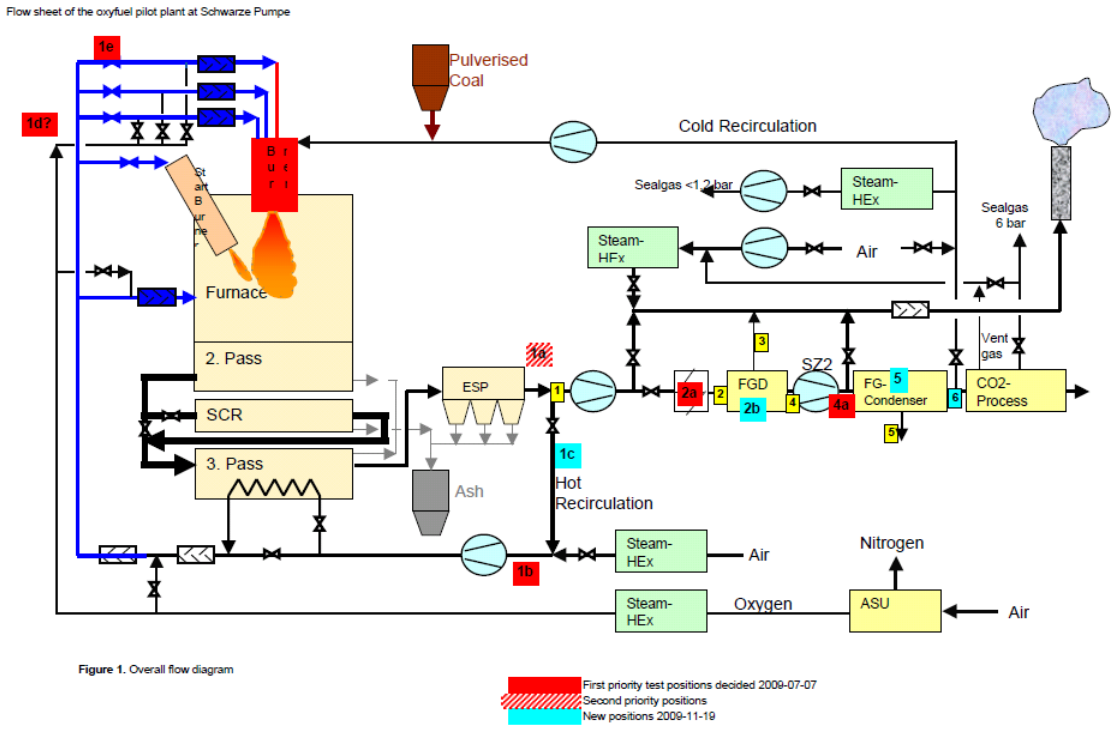

Figure 1. Overall flow diagram

Figure 1. Process flow sheet of oxyfuel plant.

Flue gas temperatures are lower when the boiler is run in oxyfuel mode compared to air-firing mode. A comparison of gas compositions measured after the electrostatic precipitator is given in Table 1. During air-firing the SO_2 levels in the flue gas varied between 1400-1800 mg/Nm^3 whereas during oxyfuel mode the SO_2 levels were about 4 times higher, being in the range 6500-8000 mg/Nm^3. Moisture as well as NOx levels were also about four times higher in oxyfuel mode. As expected the CO_2 levels are also much higher. SO_3 levels were higher in the fly ash in the oxyfuel but otherwise the compositions of the fly ash were similar between the two firing modes.

Table 1: Approximate flue gas composition after ESP and SO_3 levels in the fly-ash.

	SO_2 mg/Nm^3	O_2 Vol%	CO mg/Nm^3	CO_2 Vol%	H_2O Vol%	NOx Mg/Nm^3	Fly-ash SO_3 mg/kg
Air-firing	1600	6	7	13	8	300	46 $\pm$ 9
Oxyfuel	7000	6.8	2.5	95	30	1600	77 $\pm$ 18

Corrosion probe tests were performed both during air-firing and oxyfuel mode. Each test lasted about 250 hrs. Probes simulating superheaters, with a metal temperature of 580°C were installed before the first superheater bundle meeting the flue gas, at a gas temperature of about 760°C in oxyfuel mode and 840°C in air mode. Additional corrosion tests were performed for

1320 hrs but only in oxyfuel mode. Corrosion probes were also exposed at 650°C for 1250 hrs in oxyfuel mode only. The location was the same as for the 250 hrs exposure. Specially designed probes which simulate waterwall conditions were also used. The metal temperature was 430°C and exposure time about 1500 hrs. The alloys investigated are shown in Table 2.

The wall thicknesses and masses of the ring specimens were measured before and after exposure. In addition oxide thickness was measured and the oxide/corrosion product was investigated with LOM (Light Optical Microscope) and scanning electron microscope, SEM-EDS. Specimens were etched to reveal the presence of carbides using Murakami solution.

Table 2. Chemical composition of materials investigated.

	C	Fe	Cr	Ni	Mo	Mn	Si	Cu	*Others*
15Mo3	0.12-0.20	rest			0.25-0.35	0.10-0.35	0.40-0.90		
TP347H FG	0.04-0.10	rest	17.0-20.0	9.0-13-0		<2.00	<1.00		*Nb 0.80-1.0*
304H	0.07-0.13	rest	17.0-19.0	7.5-10.5		<1	<0.30	2.5-3.5	*Nb 0.3-0.6 N 0.05-0.12*
Kanthal APMT	<0.05	rest	22		3	0.4	0.7		*Al 5.0*
T23	0.04-0.10	rest	1.90-2.60	-	0.05-0.30	0.10-0.60	<0.50		*Nb 0.02-0.08 W 1.45-1.75*
13CrMo44	0.08-0.18	rest	0.70-1.10	-	0.40-0.60	0.40-1.00	0.10-0.35	-	
253 MA	0.05-0.10	rest	20-22	10-12		<0.8	1.1-2.0	-	*N 0.14-0.2 Ce 0.03-0.08*
X20CrMoV121	0.17-0.23	rest	10-12.5	0.3-0.8	0.8-1.2	<1	<0.5	-	
AC 66	0.04-0.08	rest	26-28	31-33		<1.0	<0.3		*Ce 0.05-0.10 Al<0.025*
Sicromal 8	0.07	rest	6.5						*Al<0.7*
P92, T92	0.07-0.13	rest	8.5-9.5	<0.4	0.3-0.6	0.3-0.6	<0.5		*V 0.15-0.25 W 1.5 – 2 Nb 0.04 -0.09 N 0.03-0.07*
TP 310	0.05	rest	24.5	21.0			0.5		
254 SMO	<0.02	rest	19.5-20.5	17.5-18.5	6.0-6.5	<1.00	<0.8	0.5-1.0	
Inconel 617	0.05-0.15	<3.0	20-24	rest	8-10	<1	<1	-	*Al 0.8-1.5, B <0.006, Ti <0.6*
C276	<0.02	4-7	14.5-16.5	rest	15-17	<1.0	<0.08		*W 3.0-4.5 Co<2.5*
Sanicro 25	0.1	rest	22.5	25		0.5	0.2		*W 3.6 Nb 0.5*
Sanicro 63	<0.10	<5.0	20-23	rest	8-10	<0.50	0.50		*Nb 3.15-4.15*

For testing in the 3rd pass (the location of economizers), gradient probes were used and the temperature is controlled along the probe such that testing of different temperatures can be undertaken with one probe. The temperature gradient of the probe was 170-70°C and the exposure time was 250 hrs in both oxyfuel fuel and air-firing mode. Two steel types were mounted on this probe, the low alloyed 15Mo3 steel and austenitic steel 304L (similar to 304H in Table 2 but with variations in C and N content). The estimated flue gas temperature was 270°C.

Another test in oxyfuel mode, with a longer exposure time of 1000 hrs, was performed at a position where the fluegas temperature was 350ºC. The probes had temperature gradients of

approximately 60-200ºC along the length of the set of sample rings and the exposed alloys were 15Mo3 and 254 SMO.

Deposit probe tests of 6 hours were performed in air and oxyfuel modes. Probes were inserted before the first superheater bundle where the flue gas temperature was 760°C in oxyfuel mode and 840°C in air mode. The probes consisted of both 10CrMo910 and 304L rings internally cooled to temperatures of 580°C, 650°C and 760°C. Rings were weighed before and after exposure to estimate deposition rates. The deposits were then analysed with SEM/EDS.

3. Results

3.1. Deposit probes

The deposition rates were generally higher in oxyfuel than in air (Figure 2). Deposition rates were also lower on the stainless steel substrate for all firing modes. It was noted that there was some deposit/dust lost during dismantling of the austenitic alloy deposit rings. With increase in probe temperature, there is an increase in deposition rate. In pre-mixed mode the oxygen is mixed with the recirculation gases without the detailed control of the blend, allowed in mode A and mode B.

The rings with the deposits were then analysed with SEM/EDX. There are no great differences for different firing modes although a slight decrease in sulphur and magnesium and an increase in calcium with increasing temperature could be noted.

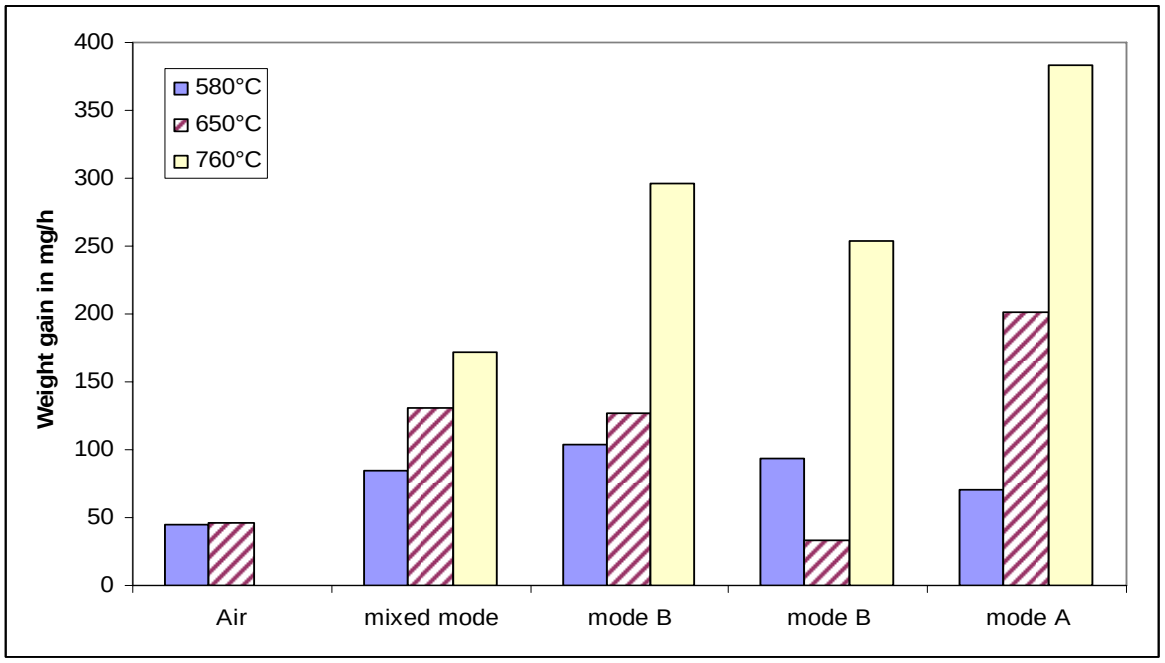

Figure 2. Deposition rates for the 10CrMo910 probe at various temperatures.

There was a difference in the distribution of the key elements around the deposit probe. In oxyfuel firing, the deposits had similar compositions on the wind- and the leeward side. However for air-firing, the calcium content was higher and the sulphur content lower on the wind side compared with the lee side.

3.2 High temperature corrosion probes

3.2.1. Waterwall probes

The corrosion results from the wall probe exposed for 1472 hours are given in Table 3. The remaining metal after exposure was measured in the SEM on cross-sections used for microstructural examination and subtracted from the average thickness measured by micrometer before testing to give a value for the metal loss. The thickness of the oxide layer was also measured with SEM. The steel with the best corrosion properties by far is Sicromal 8, EN1.4713 giving a corrosion rate of 23µm/1000hrs. The corrosion rates of the 10CrMo910, 13CrMo44 and 15Mo3 steels are unacceptably high with rates of 162, 139 and 269µm/1000hrs, respectively.

Table 3. Comparison of material loss and measured oxide thickness with SEM for the wall probe.

Material	Thickness unexposed (mm)	Metal Thickness after exposure (mm)	Material loss (µm)	Thickness of oxide (µm)	Corrosion rate in µm per 1000 h.
10 Cr Mo 9 10	2,662	2,423	239	200-250	162
13 Cr Mo 4 4	2,692	2,487	205	20-40	139
15 Mo 3	2,7165	2,321	396	300	269
1.4713	2,9295	2,896	34	40	23

3.2.2. Superheater probes 250 hrs, 580°C

The specimens from the 250 hrs exposure were measured before and after exposure, but due to the low corrosion rates, the metal loss measurements had a large degree of inaccuracy. Therefore oxide thickness measurements were used and the data is given in Figure 3. When the oxide becomes thicker there is a tendency for spallation which is revealed for results for 15Mo3.

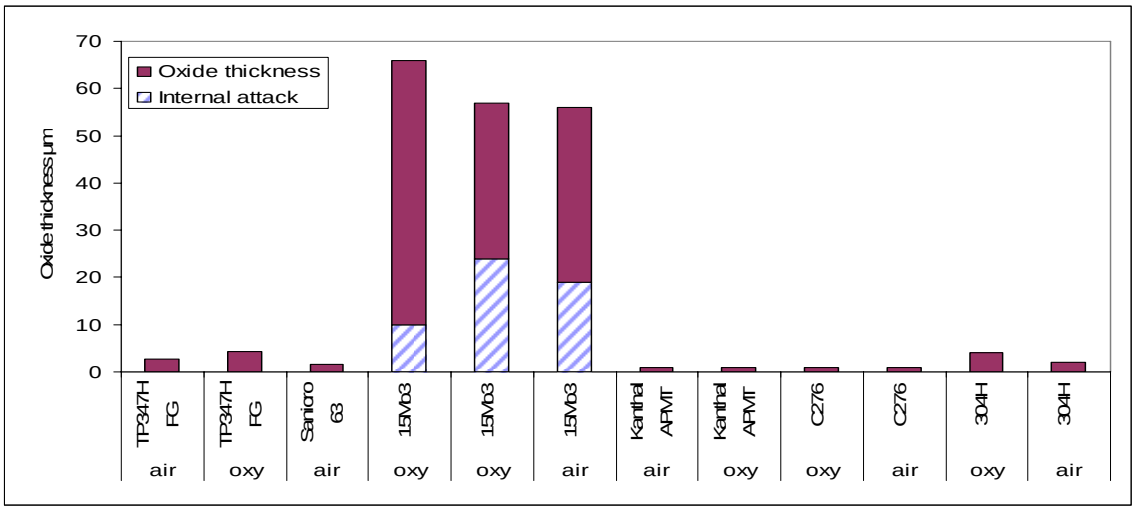

Figure 3. Measurement of oxide thickness and internal corrosion.

All specimens were etched with Murakami to reveal carbides and there was no great difference between oxyfuel and air firing. Figure 4 shows the micrographs from TP347H FG steel. The internal attack was grain boundary corrosion and not carburisation. Perhaps a slight indication of increased precipitation is observed for oxyfuel, but this was localised.

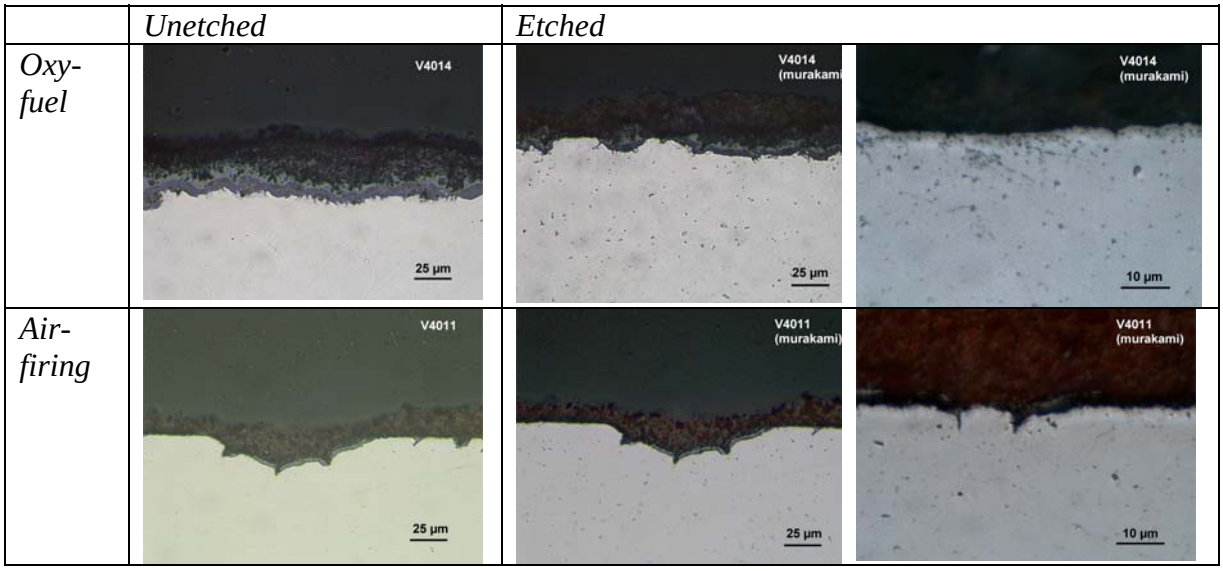

Figure 4. Light optical microscopy of TP347H FG specimens.

Specimens were also examined with SEM/EDX to analyse if there was more sulphidation for the oxyfuel specimen. No specific increase in sulphidation was revealed and sulphur was present within the oxide of both oxyfuel and air-firng specimens.

3.2.3. 1300 hrs, 580 ℃

The metal loss was measured at 24 positions around the circumference of the probe exposed for 1319 hours at 580°C and the results are shown in Figure 5. It was not possible to measure the corrosion of the Sanicro 63 alloy so its corrosion rate was estimated by comparing the oxide thickness of this specimen with a number of others and the results are shown in Figure 6. The results show that the corrosion of Sanicro 63 at 580°C is in a similar range to that of TP347 HFG and 253 MA, *i.e* under 10µm per 1000 hours. 13CrMo44, T23 and 15Mo3 all show unacceptably high corrosion rates.

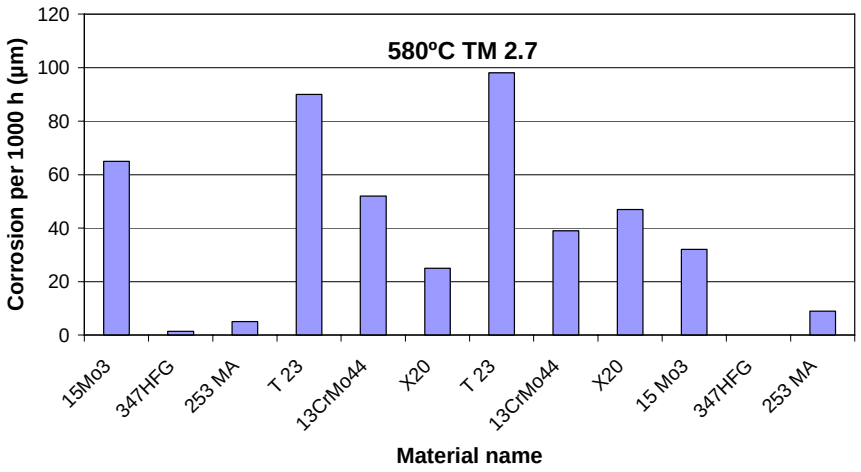

Figure 5. Average metal loss in µm per 1000 h for specimens exposed for 1319 hours at 580 ℃.

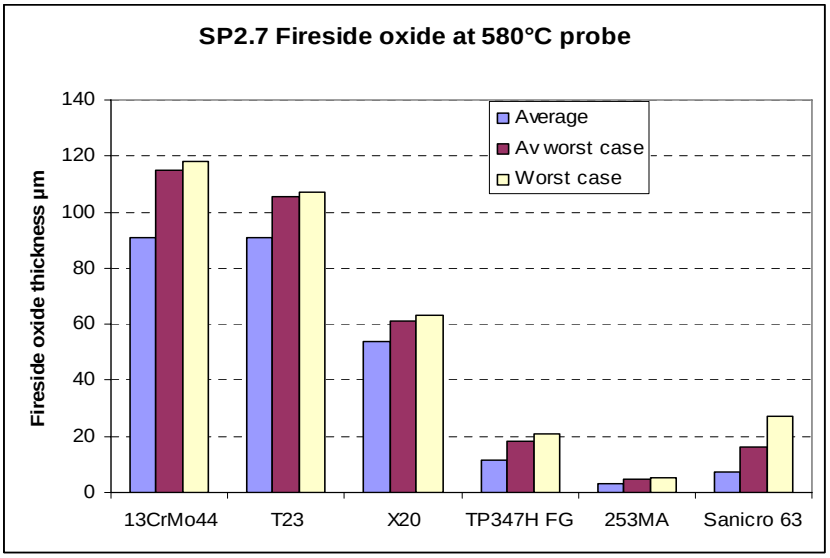

Figure 6. Oxide thicknesses on samples from 580°C probe.

3.2.4. Microstructure of samples exposed at 580°C

For the low alloy ferritic steels 13CrMo44 and T23, the outer oxide was iron rich with elements from fly ash deposit. The inner oxide was iron oxide enriched in chromium. For T23 the inner part of the oxide also contained a tungsten rich oxide. Traces of sulphur could be detected at the corrosion front especially at grain boundaries.

On the ferritic stainless steel X20CrMoV121 the outer oxide consisted of iron oxide and the inner oxide of chromium rich iron oxide. There was significant internal attack, not only at the grain boundaries at the corrosion front, but also within the grains. There are indications that both internal oxidation and internal sulphidation occurs (Figure 7). (Analysis in elemental wt.% should be used for comparison purpose only due to high inaccuracies in oxygen analysis).

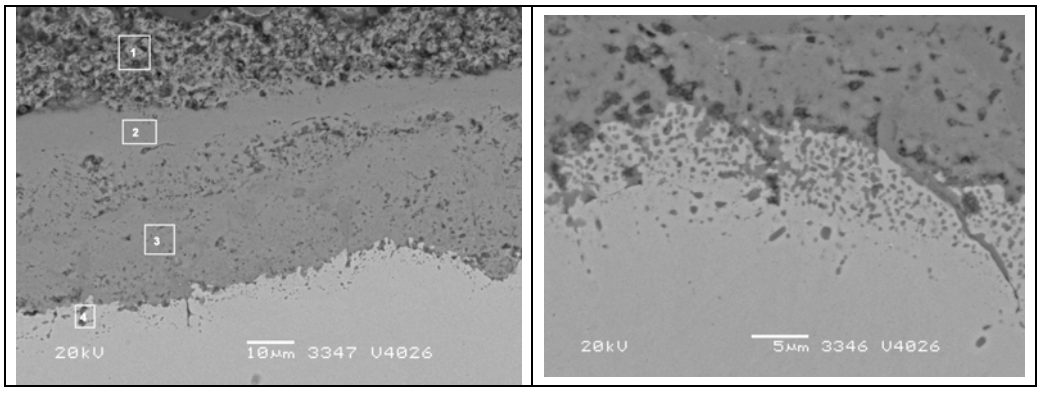

Area	O	Al	Si	S	Ca	V	Cr	Mn	Fe	Ni	Mo
1	20.15	0.59	0.45	5.87	7.17				65.77		
2	12.95						1.46	0.62	84.97		
3	9.79			0.03		0.54	20.95	1.28	64.29		3.11
4			0.83	2.06			10.54		85.01	1.57	

Figure 7. SEM-EDS analysis of fireside oxide on X20CrMoV121 exposed at 580°C.

On the austenitic TP 347H FG steel the oxide was a duplex oxide with an outer iron rich

oxide and an inner chromium rich iron oxide. There was also sulphur within the inner oxide. A very slight internal attack in the form of sulphidation at grain boundaries was observed at the corrosion front

For the 253 MA the oxide on the fireside was thin, consisting of chromium and iron rich oxide. It was observed that in some areas there was a thicker oxide of 4µm and in other areas there was a thin oxide with an underlying internal corrosion attack. The internal attack was rich in silicon and it appears that a silicon-rich phase forms at grain boundaries and then afterwards the bulk grains form oxides. There was a trace of sulphur within the oxide.

Sanicro 63 forms a relatively thick duplex oxide (15µm) where the outer oxide is nickel rich, and the inner oxide is chromium, nickel, molybdenum and niobium rich (see Figure 8). There is a strong indication that sulphur is also present in the inner layer however there are problems with overlapping EDX-signals between sulphur and molybdenum.

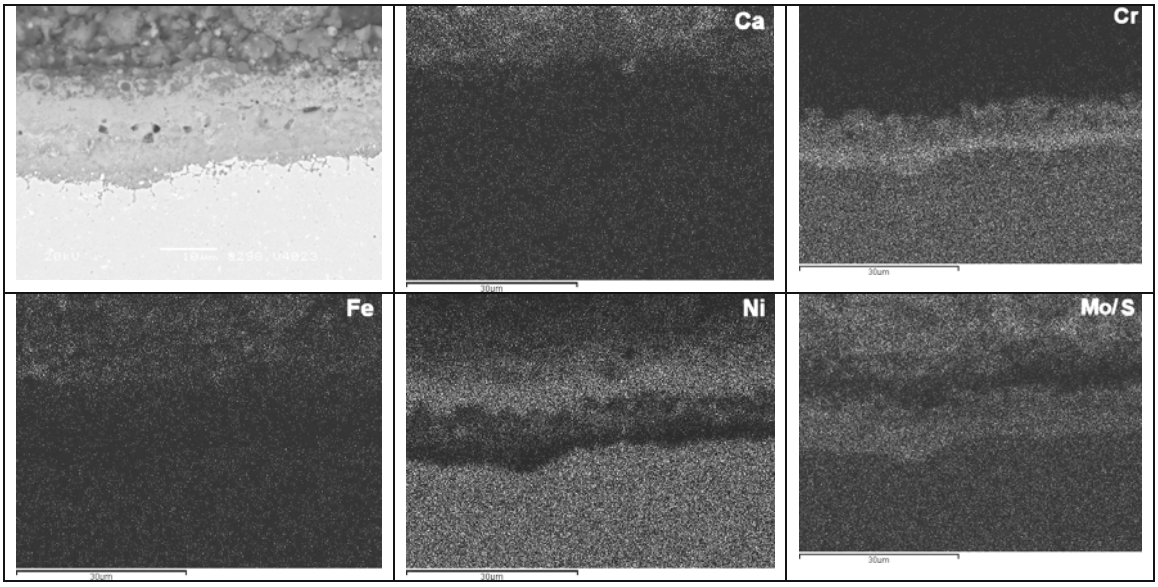

Figure 8. SEM-EDS analysis of oxide on Sanicro 63 exposed on the 580°C probe.

3.2.5. Corrosion rates from superheater probes exposed at 650ºC.
The average measured corrosion normalised to 1000 hours is shown in Figure 9. All alloys, except for the ferritic steel T92, showed a corrosion rate lower than 10µm/1000hrs. No measureable material reduction were detected on Sanicro 25 and Super 304H.

It was not possible to measure the corrosion of the Sanicro 63 and the Ni-based coatings consisting of TiAl-phase so their corrosion ratings were estimated by comparing the oxide thickness of these specimens with a number of others and the results are shown in Figure 10.

The Sanicro 63 shows an oxide growth comparable with Super 304, while the welded Ni-based TiAl phase coating showed a thinner oxide thickness.

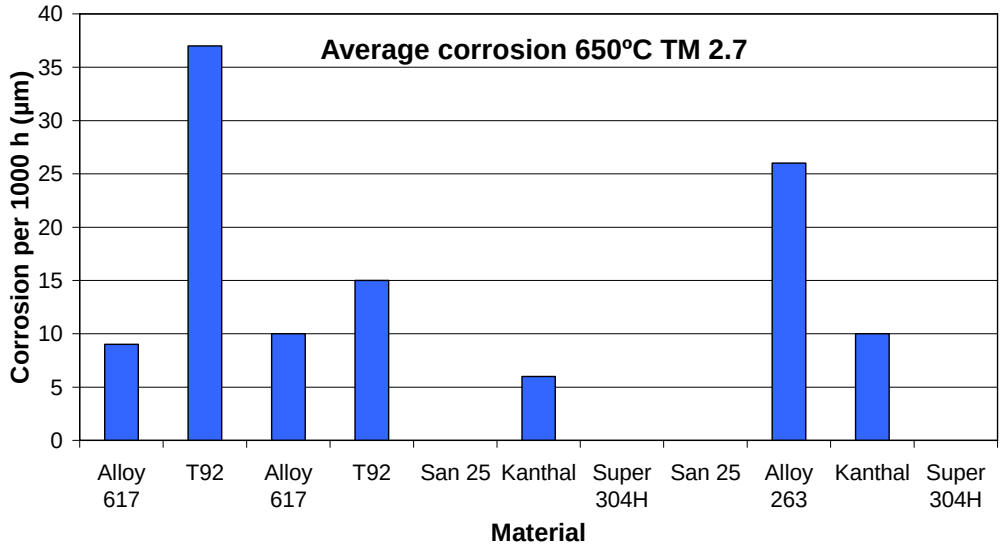

Figure 9. Average metal loss in µm per 1000 h for specimens exposed for about 1300 hrs at 650 ℃.

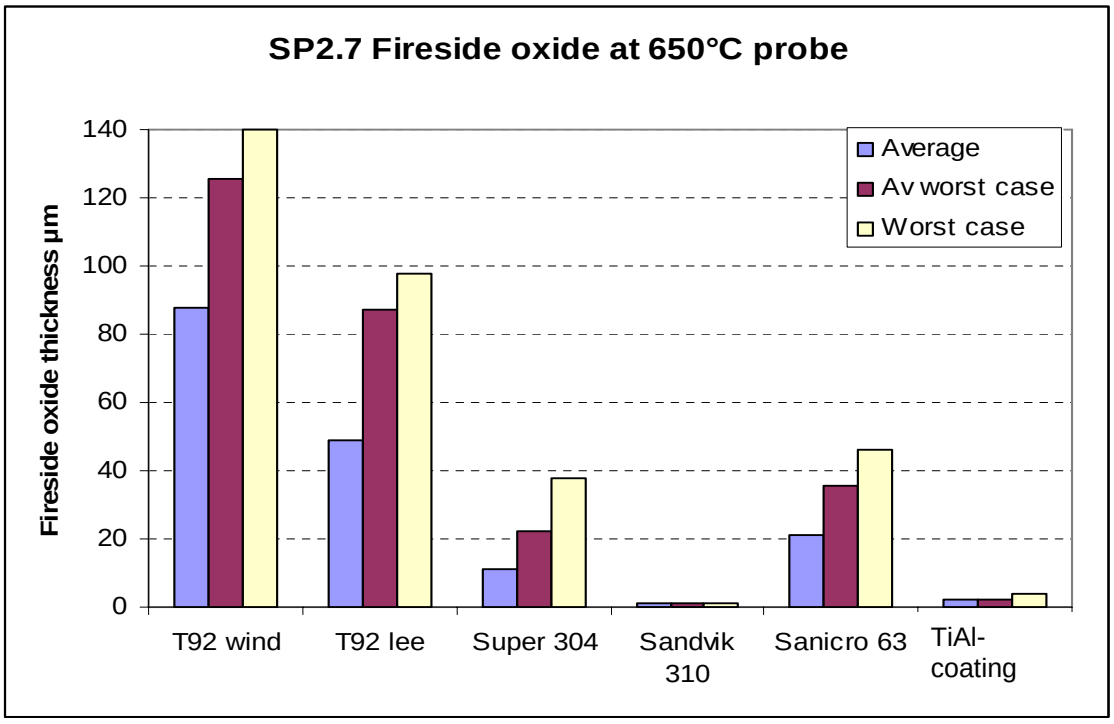

Figure 10. Oxide measurements on samples from 650 ℃ probes.

3.2.6. Microstructure of samples corroded at 650°C

For the T92 alloy the thicker oxide, located on the wind side, the outer oxide was iron rich and the inner oxide was chromium rich iron oxide. Sulphur was present in the inner oxide and especially at locations there was internal corrosion attacks in form of sulphidation.

On the Super 304 H, the fireside oxide was a thin oxide where there was occasionally a distinguishable outer oxide which was iron rich. The inner part of the oxide was a chromium rich iron oxide (Figure 11). In addition there is the slight presence of sulphides at the corrosion front especially in grain boundaries.

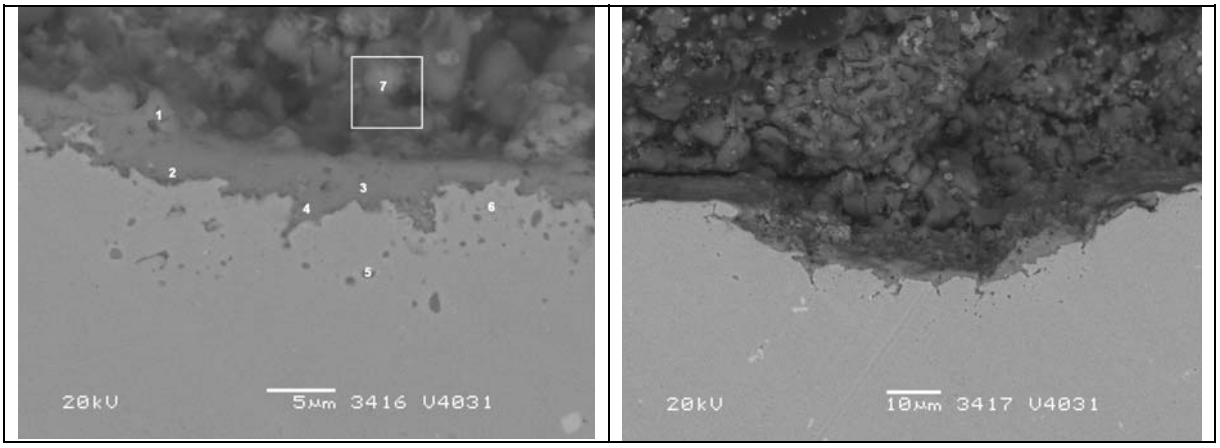

D3416	O	Al	Si	S	Ca	Cr	Mn	Fe	Ni	Cu
1	13			4	4	3		77		
2	13					80		7		
3	16		1	1		64		19		
4	13		1	2		55	3	25	2	
5				11		20	7	54	7	2
6			1	3		14		68	14	2
7	31	2	2	16	17			32		

Figure 11. SEM-EDS analysis of oxide on Super 304H exposed on the 650°C probe.

The fireside oxide for TP 310 was less than 1µm thin and gave even coverage of the surface of the specimen. The oxide was a chromium rich iron oxide also including some manganese. No significant internal attack was observed.

Similar to the 580°C probe, Sanicro 63 again formed a duplex oxide which was thicker than formed at 580°C. The outer oxide was again nickel oxide and the inner oxide consisted of elements from the bulk material (Figure 12). In this case there is a very clear indication that sulphur is present in the inner oxide and that there is also internal attack at the corrosion front.

In contrast to Sanicro 63, a Ni-based weld overlay alloyed with Ti and Al had a thin protective chromium rich oxide. Remnants of Ti and Al were found on the coataing indicating Ti and Al has promoted formation of a Cr oxide layer.

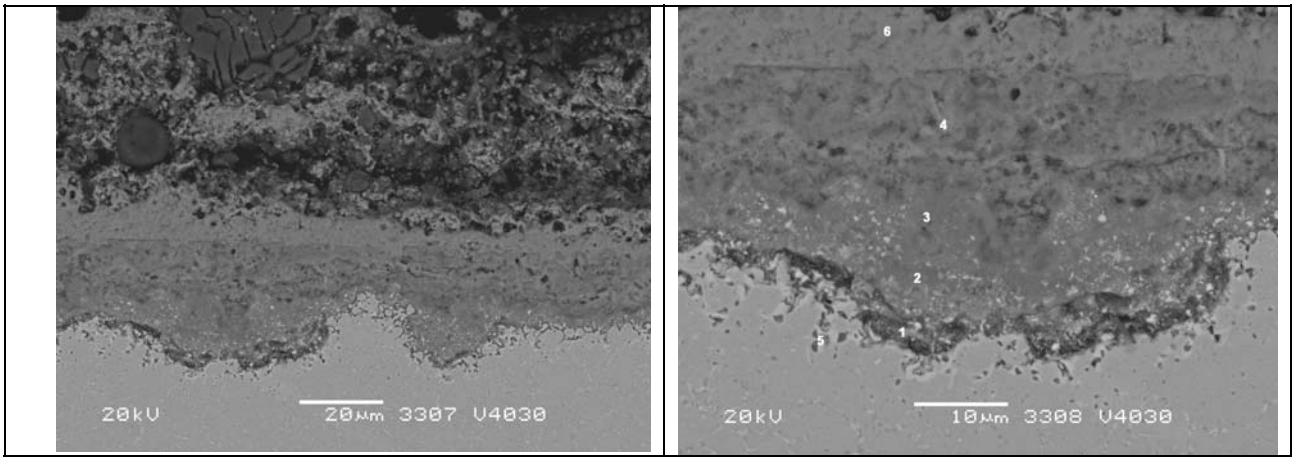

D3308	O	Al	Si	S	Ca	Ti	Cr	Fe	Ni	Nb	Mo
1	6		2	10	0	1	29	1	18	10	23
2	11		1	8		0	65		2	4	8
3	13		1	5			69		2	5	4
4	15		1	1		1	21		18	23	20
5	3	1	2	2		1	13	1	62	6	11
6	10		1	0			1	2	84	0	1

Figure 12. SEM-EDS analysis of oxide on Sanicro 63 exposed on the 650°C probe.

3.3. Low temperature corrosion temperature gradient probe tests

Both 304L and 15Mo3 were exposed on the low temperature gradient probe. The austenitic stainless steel 304L showed no corrosion after exposure in air-firing mode and minimal tarnishing in oxyfuel conditions. For the 15Mo3 specimens more corrosion was observed.

The deposits on the low temperature probes were very thin. Nevertheless it was possible to obtain samples for analysis by careful scraping of the deposits from the wind and lee sides. The results are given in Figure 13. Deposits formed during oxyfuel conditions were enriched with sulphur, especially at 170°C (20 wt% sulphur in oxyfuel compared to 4 wt% in air-firing).

The specimens were cross-sectioned and the thicknesses of the oxide layers were measured (Table 4). For all the oxyfuel specimens there was a measurable oxide, however this was only the case for the specimen at the lowest temperature for air-firing.

The chemical composition of the corrosion layer formed on 15Mo3 and 254 SMO during the 1000 hrs exposure shows that chlorine is present in the corrosion scales on the lowest temperature rings, while the amount of sulphur is higher at the higher temperatures. The high amount of carbon for the lowest temperatures indicate the presence of carbonates.

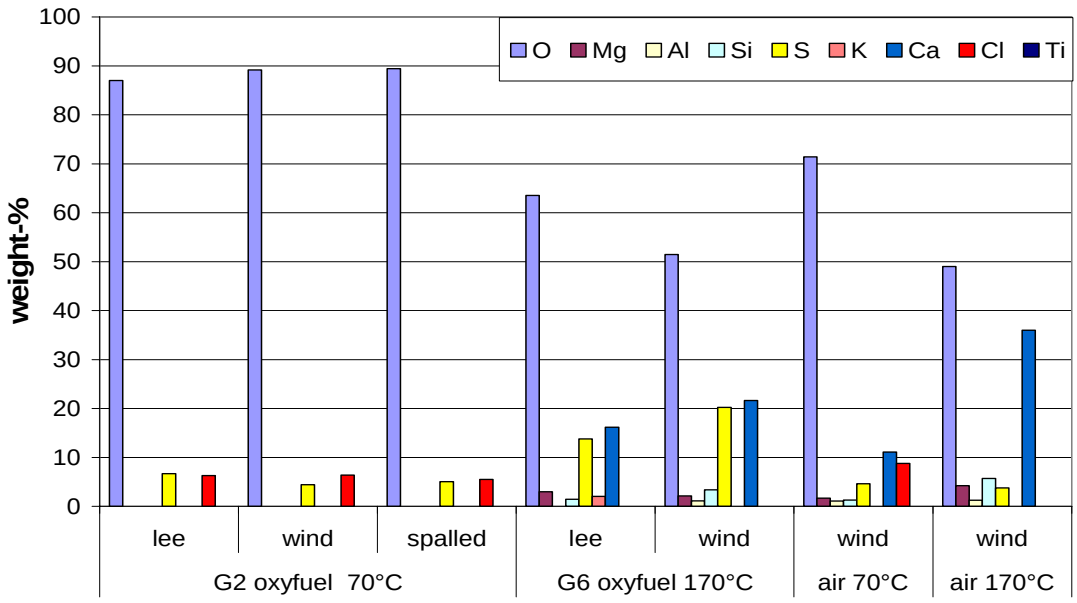

Figure 13. Chemical composition of deposits from low temperature 15Mo3 probes.

Table 4. Maximum thickness of oxide layer (µm) for the 15Mo3 on the low temperature probe exposed for 250 hrs.

	Windward side	Leeward side
Oxy-fuel 70°C	22	24
Oxy-fuel 120°C	18	<1
Oxy-fuel 170°C	17	<1
Air-firing 70°C	38	<1
Air-firing 120°C	<1	<3
Air-firing 170°C	<1	<1

Even though the exposure time is limited to 1000h all materials show measurable corrosion. 15Mo3 behaves as expected with corrosion rates up to 0,9 mm/1000h. Measurable corrosion of 254 SMO (150µm) is unexpected but it also shows the harshness of this environment, see Figure 14. The corrosion was of general type, with some local deeper pits.

SEM-EDX analysis shows that the local variations of composition in the deposits are large but that chlorides are present at the lowest temperatures. Predominantly at higher temperatures

The finding that there is no material loss at the lowest temperature and then significant loss of material from the highly alloyed 254SMO at temperatures above 90ºC is somewhat unexpected. The large material loss was localised and may be due to localized defects in the material or a localized corrosive microclimate.

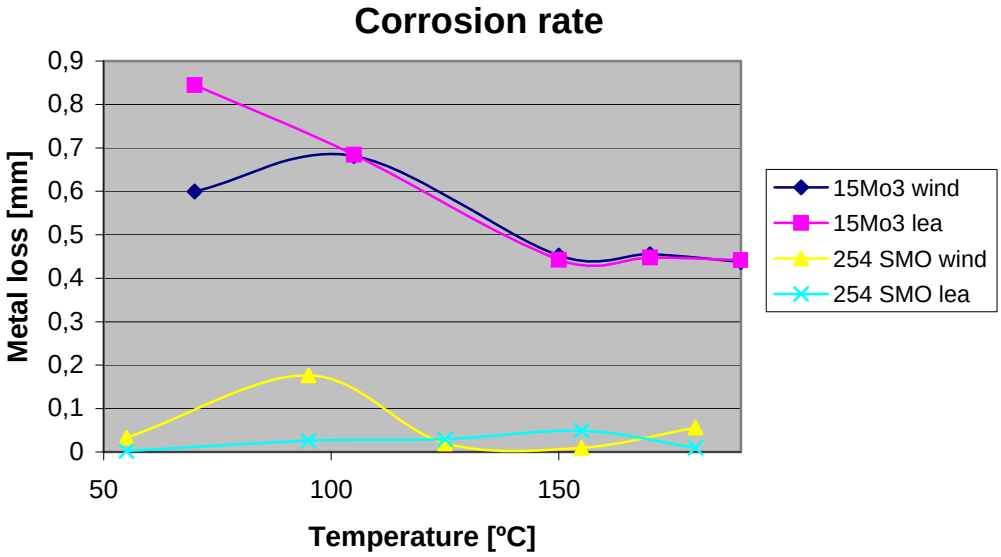

Figure 14. Corrosion rates for 15Mo3 and SMO 254 exposed on a temperature gradient probes for 1000 hrs.

4. Discussion

4.1. Deposition

There is an indication of higher deposition rate with oxyfuel than with air-firing. Further investigations need to be undertaken as only one deposit probe was used in air-firing and there were no results at the highest temperature. A higher deposition rate leads to slagging and fouling problems and decreases heat uptake of the superheaters. Sheng and Li [4] investigated ash formation during pulverised coal combustion in O_2/CO_2 mixtures compared with O_2/N_2 mixtures. Four different coal samples were burnt with various gas compositions in a drop tube furnace. The residues ash samples were characterised by X-ray diffraction and ^{57}Fe Mössbauer spectroscopy. No significant difference was observed in the crystalline phases of the ashes. However a difference in the relative intensities of peaks was observed for some phases in the two gas environments. Mössbauer spectroscopy showed that the differing atmospheres influenced the relative percentages of iron species formed in the ashes. The combustion in O_2/CO_2 resulted in more iron melting into glass silicates and less iron oxides. This could give problems with slagging and fouling.

4.1. High temperature corrosion

Similar to the results from the ENCAP studies [3] with 40 hour exposure in a burner rig, there is no significance difference in the specimens with oxyfuel and with air after 250 hrs exposure in the pilot plant. Unfortunately there are areas where we cannot make a comparison yet, for example waterwall probe testing which will be considered in future studies. Although there is an indication of high waterwall corrosion from the probe test, we have no comparison in air, and waterwall corrosion is susceptible to localised changes which may be due to boiler design/fluid dynamics and not oxyfuel combustion.

Due to the higher CO_2 and SO_2 concentration and longer exposure times, both carburisation and sulphidation may be more of a threat. The higher CO_2 may result in carbon diffusion into the material producing brittle phases and the higher SO_2 may lead to increased deposition of sulphate phases resulting in more sulphidation. Piron *et al* has exposed 9-12% martensitic steels for 1000 hrs and shown that exposure in $Ar+CO_2$ is similar to CO_2+H_2O with respect to weight gain and oxide thickness. However the carburisation depth was thinner for the CO_2+H_2O mixture than the $Ar+CO_2$. It was suggested that H_2O presence reduces the carburisation of the steel, as H_2O is easily adsorbed on the surface compared to CO_2. Ferritic steels (1-11% Cr) have been investigated in CO_2 + 30% H_2O conditions both in high and ambient pressures [6]. Increased oxidation rate was observed for ferritic steels at high pressures due to increased carbon deposited within the oxide. In oxyfuel combustion, there is a higher oxygen content in the gas which should reduce problems with carburisation.

4.2. Low temperature corrosion

The largest differences between oxyfuel and air-firing appeared on the low temperature gradient probe, installed in the economiser region, which had a temperature of 60-200°C. For the 250 hrs exposure and at the lowest temperature tested (70°C), specimens exposed in both air and oxyfuel modes revealed large amounts of corrosion. However, the specimens exposed during oxyfuel conditions were more highly corroded at higher temperatures and the deposits were enriched with sulphur, especially at 170°C (20 wt% sulphur in oxyfuel compared to 4 wt% in air-firing). Calculations show that the acid dew point (dew point for H_2SO_4) is about 30°C higher in oxyfuel mode, (124°C in air-firing and 153°C in oxyfuel mode, when firing normal lignite).

Sulfuric acid begins as small concentrations of sulfur trioxide (SO_3) in the boiler. The SO_3 is formed in the furnace and convective pass of the boiler by the reaction of SO_2 with oxygen. Among the parameters which influence the amount of SO_3 formation in the boiler are fuel sulphur content, ash content and composition, convective pass surface area, tube metal surface temperature distribution, and excess air level. As a flue gas condenses, the first temperature at which condensation begins depends on both the partial pressure of sulphur trioxide and water vapour. The initial condensate forming at the dewpoint is very corrosive but the actual deposition rate of these particles is small. As the temperature decreases, the acid concentration reduces but there is more acid available, thus high corrosion rates are generally observed 20-30°C below the actual acid dewpoint as the deposition rate of the acidic species increases. As the temperature is further reduced, then acid concentration decreases leading to decreased corrosion until it reaches the temperature where other acidic gases such as CO_2, SO_2 and NO_2 dissolve. It is clear that the amount of sulphur in the deposits increases the temperature at which downtime corrosion occurs. In addition the amount of water in the gas phase is also important [8] and the increase from 9% to 30% water vapour increases the dewpoint temperature as can be seen from Figure 15.

The squares mark the dewpoints relevant for the lignite used in this test. However a higher sulphur content in the coal would lead to a higher dewpoint temperature. This diagram is based on the assumption that 0.5% of the SO_2 is converted to SO_3. More data with longer exposure times is required to assess the corrosion rates at the various temperatures. Based on the corrosion rates and general behaviour none of the alloys withstand the environment totally but all the high alloy steels still show potential for use in these environments.

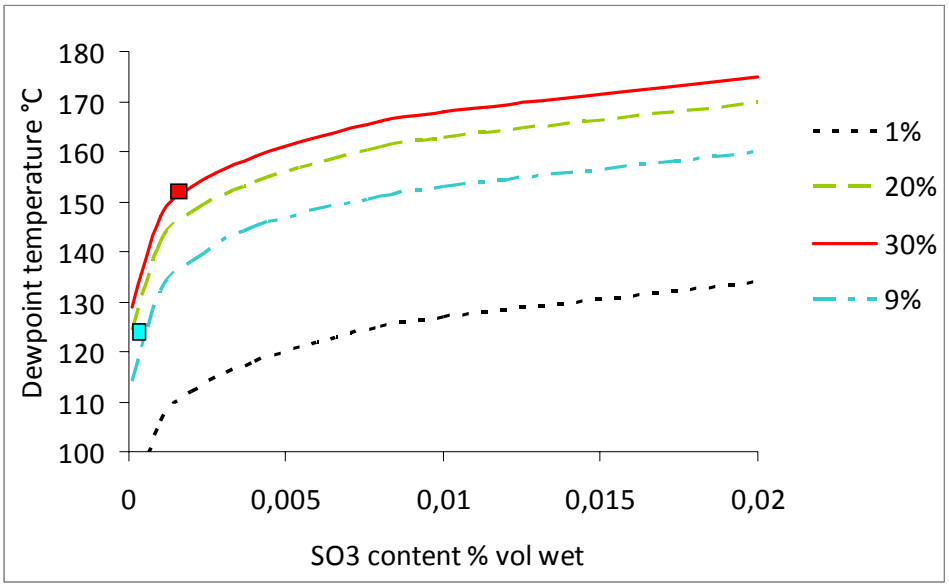

Figure 15. Dewpoint temperature with respect to SO_3 for various water contents.

5. Conclusions

The following conclusions can be drawn from this work. The chemical compositions of the high temperature (superheater) deposits from air and oxyfuel firing were found to be similar and the initial high temperature corrosion behaviour of the same steels also appeared to be similar during air and oxyfuel firing. This was an unexpected result as levels of SO_2 were approximately four times greater under oxyfuel conditions as measured after the before the ESP (Table 1). The low temperature gradient probe revealed more corrosion in oxyfuel mode and the deposits contained significantly more sulphur. Calculations show that the dewpoint temperature of SO_3 has increased due to oxyfuel combustion.

6. Acknowledgements

The authors are especially grateful to Dr. Marie Anheden, and the many other colleagues at Vattenfall who have supported this work.

7. References

[1] B. Bordenet Materials and Corrosion 59 No 5 (2008) pp. 361-366
[2] L. Strömberg et al Energy Procedia 1 (2009) pp. 581-589
[3] M. Montgomery, A. Hjörnhede, A. Gerhardt: Proceedings Eurocorr 2009 Paper 7984, Nice, France (2009)
[4] C. Sheng and Y. Li: Fuel 87 (2008) pp. 1297-1305
[5] J. Piron Abellan, T. Olszewski, H.J. Penkalla, G.H. Meier, L. Singheiser, W.J. Quadakkers WJ, Materials at High Temperatures 26 (1) (2009) pp. 63-72
[6] D. Huenert and A. Kranzmann, NACE Paper 08447 (2008)
[7] DR Holmes "Dewpoint Corrosion" pp17-34, 80-93 Published 1985 Ellis Horwood Ltd.
[8] WMM Huijbregts, RGI Leferink "Anti-corrosion methods and materials" Vol 51 No 3 (2004) pp.173-188

Oxyfuel combustion for below zero CO_2 emission

Procesteknisk rapport

Prepared	Dennis Fisker, 6 July 2010
Checked	THPED
Accepted	DENFI
Approved	KNADS

Doc. no.	768620
Project no.	3-00047

Indholdsfortegnelse

6. juli 2010
Dok. nr. 768620

1. Indledning

Formålet med det procestekniske studie er med basis i erfaring med detaljerede gennemregninger af DONG Energy's kraftværker på både kedel og turbineside at fastslå potentiale og konsekvenser af en ombygning af en eksisterende kraftværksblok til oxyfuel forbrænding (retrofit).

Nøglepunkter for undersøgelsen:

- Bestemme forventet ydelse og virkningsgrad for oxyfuel retrofit.
- Beskrive nødvendige anlægsændringer / nye komponenter
- Beskrive og gennemregne gennemførlig proceskobling
- Gennemregne fyrrum og forbrænding med CFD for validering af beregning samt forbedring af procesmodel.
- Afdække alternative proceskoblinger
- Optimere kedlens ydelse

Dette studie retter sig med retrofit af et eksisterende anlæg. Den grundlæggende opbygning af kedel med fyringsanlæg, fyrrumsstørrelse samt hedefladebestykning fastholdes derfor. Denne forudsætning er væsentlig af 2 årsager:

- Ved i størst muligt omfang at anvende eksisterende maskinkomponenter er der størst sikkerhed for at opretholde rådighed og driftsikkerhed efter retrofit til oxyfuel forbrænding.
- Procesberegningernes validitet er for eksisterende kedel eftervist gennem driftsprøver.

Da studiet baseres på et eksisterende blokanlæg, er frihedsgrader i optimeringen begrænset af anlæggets fysik og den oprindelige udlægning til kulfyring med luftforbrænding. Derfor kan resultater ikke direkte sammenlignes andre oxyfuel studier baseret på nyanlæg.

Dynamiske forhold ved oxyfuel betingelser
I det oprindelige oplæg til DONG Energy's (herefter DE) projektarbejde var der lagt op til et antal undersøgelser af dynamiske forhold ved oxyfuel retrofit. I løbet af projektet har det vist sig, at der stadig er væsentlige udfordringer i fastlæggelse af den optimale proceskobling, og derfor har projektarbejdet fokuseret på dette. De dynamiske forhold må så behandles i et konkret tilfælde med en fastlagt proceskobling.

2. Forudsætninger for beregninger

Alle procesberegninger foretages i DE's internt udviklede procesberegningsværktøj Mopeds. I Mopeds opbygges samlede modeller af både kedel- og turbinekreds, hvilket er essentielt for vurdering af konsekvenser for et blokanlægs ydelse ved væsentlige ombygninger. Mopeds har gennem en årrække vist sit værd som et pålideligt værktøj til procesberegninger, der i høj grad matcher beregninger udført af turbine- og kedelleverandører.

2.1 Randbetingelser

Det procestekniske studie fokuserer på nødvendige anlægsændringer og en vurdering af potentiale og performance ved oxyfuel forbrænding. Et antal randbetingelser er derfor på forhånd fastlagt som basis for konsistente beregninger:

Iltfabrik

Iltfabrikken som producerer den rene O_2 til oxyfuel forbrænding betragtes som en ekstern enhed og indgår ikke i procesoptimeringen. Koblingen til kedelmodellen er en gasstrøm fra iltfabrikken med følgende standard sammensætning:

	RATIO	Flow
NAME	%	kg/s
O2	0.950	35.8146
N2	0.020	0.64359
CO2	0.000	0
SO2	0.000	0
H2O	0.000	0
AR	0.031	1.43547
HCL	0.000	0
sum:	1.000	37.894
Molflow	1.1781	kmol/s

Produktionen af den rene O_2 kræver en betydelig elektrisk effekt. Dette effektbehov vises i varmebalancerne som et selvstændigt egetforbrug og fratrækkes blokanlæggets ydelse. Effektbehovet antages fast uafhængig af bloklast og er baseret på udsagn fra iltleverandører ved flere konferencer:

160 kWh/kg O_2

Dette specifikke forbrug ligger under energiforbruget på nuværende iltfabrikker, men er det forventet opnåelige, når illtfabrikken ligesom kraftværket optimeres til bedst mulig energieffektivitet. Dette forbrug gælder for 95% ren ilt, hvor resten typisk udgøres af 3% argon og 2% nitrogen.

Kul.

Alle beregninger baseres på et standard kul med nedenstående sammensætning:

COAL	MOLAR WEIGHT	WEIGHT PERCENT %
C	12.01	63.62
H	1.01	4.20
S	32.06	0.64
N	14.01	1.60
O	16.00	7.10
Cl	35.45	0.14
ASH	-1.00	11.20
H2O	18.02	11.50
sum:	100	32.876

Den nedre brændværdien for dette kul er LHV = 25.17 MJ/kg

Denne kulsammensætning er repræsentativ for de kulblandinger anlægget fyrer i dag.

Turbinekreds
Turbinekreds indgår i modelberegning, men der foretages ingen optimering til oxyfuel. Hvis udlægning til oxyfuel i væsentlig grad påvirker turbinens performance bliver de procestekniske forhold beskrevet og betydning/konsekvens vurderet. Dermed kan en efterfølgende optimering være nødvendig. Der kan også være et potentiale i integration med iltfabrikken for eksempel som delvis fødevandsforvarmning. Dette behandles ikke i dette studie.

Beregningsomfang
I samtlige beregninger vurderes kun påvirkning af blokkens ydelse og effektivitet. Ingen økonomiske forhold hverken i form af investeringer eller driftsomkostninger er medtaget.

2.2 Valg af kraftværksblok til undersøgelse

Analyserne skal generelt belyse, hvilke problemer der kan være ved en ombygning til oxy-fyring. Den valgte blok skal leve op til følgende krav:

- Bensonkedel
- Helst 2-trækskedel
- Kulstøvsfyret
- Der skal være installeret røggasrensning i form af konventionelt afsvovlings- og deNOx-anlæg
- LUFO skal være regenerativ, dvs. fx roterende Ljungstrøm
- Gode driftsdata
- Beliggenhed i forhold til CO_2-deponeringsmulighed (af mindre betydning)

SSV4 opfylder i stor grad alle opstillede krav. Blokken er ikke bestykket med målinger som en ny blok, men driftsdata kan hentes online via MIRA. Desuden eksisterer der allerede en komplet Mopeds og Fluent (CFD)-model af SSV4, hvilket giver en kick-start i projektet på den måde, at der kan spares i størrelsesorden 200 timer til modelopbygning og kalibrering. Dog kan det blive nødvendigt at kalibrere Mopedsmodellen yderligere efter driftsdata.

SSV ligger i øvrigt tæt på forskellige formationer, som GEUS har peget på som potentielle deponeringsmuligheder.

Konklusion: SSV4 vælges som test case.

3. Reference på luft

For at evaluere potentialet i en retrofit ombygning til oxyfuel forbrænding skal reference fastlægges. Derfor findes her en beskrivelse af den eksisterende proces på SSV4 både med hensyn til anlægskomponenter og performance.

3.1 Kort anlægsbeskrivelse.

Konvojblokkene Studstrup blok 3 og 4 er bygget som konventionelle udtagsanlæg. Blok 4 blev idriftssat i 1985. Blokkene er konventionelle kulfyrede dampturbineanlæg med kondensat- og fødevandsforvarmning, samt dampudtag for fjernvarmeproduktion.Der er etableret halmtilsatsfyring og blokkene er efter idriftssættelse blevet udstyret med både afsvovlingsanlæg og de-NOx anlæg.

3.2 Procesopbygning

Som baggrund for vurderingen af retrofit til oxyfuel forbrænding beskrives den samlede proces for Studstrup blok 4 (herefter SSV4). De overordnede flowveje gennemgås på modeltegninger og nøglekomponenter på kedelsiden, som berøres ved ombygning til oxyfuel beskrives teknisk.

Turbinekreds.
Figur 1 viser den samlede turbinekreds for SSV4 inklusiv kondensator, fjernvarmevekslere og fødevandsforvarmere.

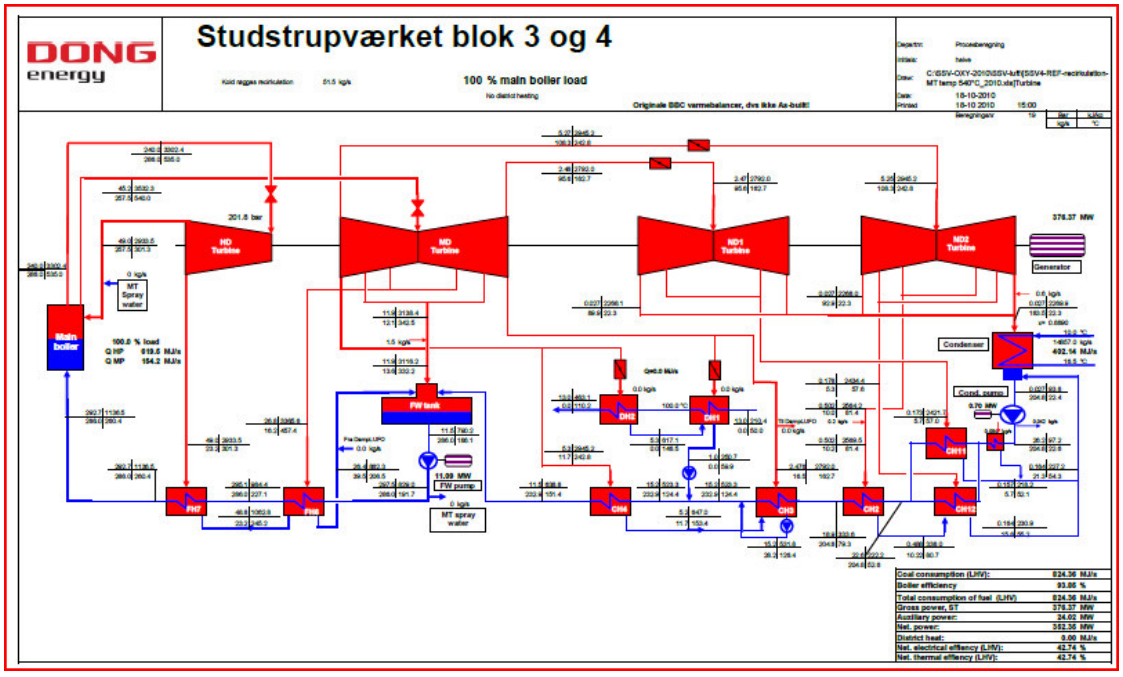

Figur 1. SSV4 turbinekreds.

Friskdamp fra hovedkedlen ledes til højtryksturbinen og ekspanderes i 100% last fra omkring 240bar til 45bar. Herefter føres dampen retur til kedlens mellemtryksdel og genoverhedes til maksimalt 540°C. Genoverhedet damp ledes til mellemtryksturbinen og herefter lavtryksturbinerne. Dampen kondenseres i kondensatoren og opvarmes trinvis i forvarmere forsynet med udtagsdamp fra turbiner. Efter forvarmer 7 er fødevandstemperaturen 260°C og det forvarmede fødevand ledes til kedlens economiser.

Blokken er et udtagsanlæg med driftsområde fra ren kondensdrift til ren modtryksdrift, dvs. maksimal fjernvarmeproduktion ved aktuel kedellast., Ved fjernvarmeproduktion tages damp til fjernvarmevekslere ud før lavtrykstur binen.

Retrofit til oxyfuel forbrænding vil ikke påvirke proceskoblingen på turbinesiden, så for SSV4 forudsættes sammen driftsområde og ændringer i turbinekredsens ydelse er en konsekvens af ændrede tryk eller temperaturforhold i kedlen. Alle beregninger foretages i kondensdrift, men blokkens mulighed for fjernvarmeproduktion vil ikke påvirkes af en konvertering til oxyfuel forbrænding.

Kedel
Kedlen er en 2-træskedel med en nominel dampydelse på 286kg/s. Kedlen har følgende nominelle data:

Dampflow	286 kg/s
Damptryk HT/MT	245 / 45 bar
Damptemperatur HT/MT	540/540 °C

Kedlen er udstyret med røggasrecirkulation, hvor kold røggas efter LUFOen blæses tilbage i fyrrummet. For at opretholde nominel MT-temperatur på 540 °C skal der recirkuleres omkring 51kg/s røggas. Det betyder, at der ved optimal regulering ikke er indsprøjtning af vand i dampen i mellemoverhederen.

Figur 2 viser kedelmodel med tilstandsstørrelser grafisk:

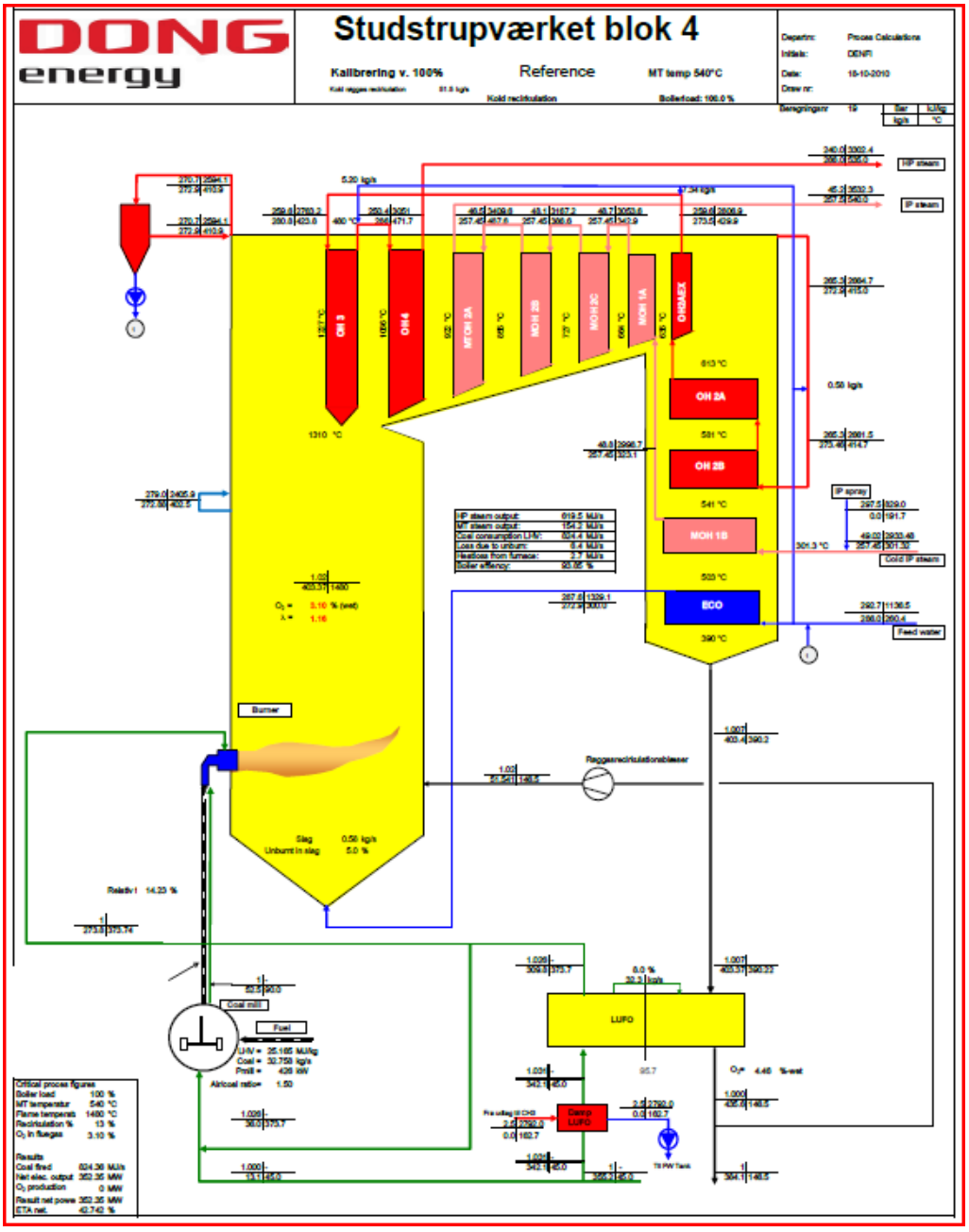

Figur 2.Kedelmodel med tilstandsstørrelser (se også bilag for klarere figur).

Fødevandet fra sidste forvarmer i turbinekredsen ledes til kedlens economiser, hvorefter vandet ledes til kedlens vikling (fordamper). Viklingen er væggen i fyrrummet. Efter fordampning i fyrrumsvægge ledes dampen til flasken (øverste venstre hjørne på Figur 2). I Benson drift passerer ren damp flasken, mens der i lavlast cirkulationsdrift udskilles ufordampet vand i flasken. Damp fra flaske ledes gennem overheder 2, 3 og slutoverheder 4. Herefter ekspanderes HT-dampen gennem HT-turbinen og ledes tilbage til kedlens mellemtrykshedeflade 1 og 2. Mellemoverhedertemperaturen reguleres med MT-indsprøjtning ved kedeltilgang.

SSV4 har Benson drift i området 100% til 35% kedellast. Ved lavere kedellast køres cirkulationsdrift, hvor en del af fødevandet ikke fordamper, men udskilles i flasken og returneres til fødevandsstrengen før ECO. Under cirkulationsdrift varierer varmeoptaget væsentligt afhængigt af tilsmudsning af fyrrumsvægge og overhedere. Det betyder varierende afgangstemperaturer på HT- og MT-siden. Ved retrofit til oxyfuel forbrænding vil beregning af optagsfordeling være behæftet ved betydelig usikkerhed. Da HT- og MT-afgangstemperaturer er afgørende for turbinekredsens performance vil vurdering af oxyfuel retrofit i cirkulationslast (lavlast) ikke være velunderbygget og udelades derfor.

3.3 Kedlens nøglekomponenter

Herunder beskrives mere detaljeret de kedelkomponenter, hvis udformning direkte influerer på proceskoblinger ved retrofit til oxyfuel forbrænding. Hermed kan de praktiske forhold omkring kommenteres og tekniske udfordringer afdækkes.

LUFO

SSV4 er udstyret med en tri-sektor lufo af Ljungstrøm typen. Figur xxx viser opbygningen:

Fugur med tri sektor lufo

Som det ses betyder dette, at primærluft og sekundærluft opvarmes i adskilte sektorer. Under normal drift skyldtes dette et væsentligt højere tryk i primærluften, som jo skal gennem kulmøllerne og bære kulstøvet igennem brænderen. Opbygningen sikrer, at den lækage fra luft til røg, som øges med trykforskellen, minimeres, idet lækage fra primærluften går i sektorer med sekundær luft. Ved retrofit til oxyfuel giver denne opbygning mulighed for at have forskellige gas sammensætninger i de eksisterende luftkanaler til kedlen.

Afsvovlingsanlæg

Afsvovlingsanlægget på SSV er af den TASP producerende spray tørringstype. Afsvovlingsanlægget indgår normalt ikke i analysen af kredsprocessens ydelse, da påvirkningen af kedlens virkningsgrad ophører efter Lufoen. Men i retrofit til oxyfuel skal både recirkulation før og efter afsvovling evalueres og opkoncentration af SO_2/SO_3 beregnes. Derfor er en simpel model af afsvovlingsanlægget opbygges med følgende kriterier

- Afsvovlingsgrad 90%
- Røggasafkøling i afsvovlingsanlæg 20°C over mætning.

Kulmøller

I kulmøllen knuses kul til kulstøv og udtørres med primærluft. Foran kulmøllen blandes varm primærluft fra LUFOen med kold luft for at opnå den temperatur ved tilgang kulmølle, som kan holde konstant temperatur i møllens afgang på omkring 90°C. Primærluften bærer det tørre kulstøv ind i kedlen.

Røggas recirkulation

SSV4 er udstyret med røggas recirkulation. Røggas recirkuleres efter LUFO og blæses kold ind i kedlen. Da recirkulation er kold påvirkes kedlens virkningsgrad af recirkulationsmængden. Under drift reguleres recirkulationsmængden efter dampens temperatur på afgang mellemtryk. Mellemtrykstemperatur lavere end 540° C reducerer turbinens ydelse og virkningsgrad. Derfor kræver en sammenligning af Oxyfuel med konventionel luftforbrænding samme MT temperatur.

Kriterier recirkulation (luft case)

- Recirkulationsmængde tilpasses med MT-afgangstemperatur på 540 °C
- Maksimal recirkulationsmængde 70kg/s.

Med blokmodellen er beregnet recirkulationsmængden af last, for at opretholde MT-temperatur 540°C.

Ved retrofit til oxyfuel forbrænding giver det ikke mening at sammenligne recirkulationsflow, da dette efter retrofit er hovedparten af flow gennem kedlen. Men flowet gennem kedlen tilpasses også ved oxyfuel, så en MT temperatur på 540-°C opnås.

3.4 Resultater – referencemodel med luftforbrænding

Med den eksisterende model for SSV4 gennemregnes lastområdet i benson drift.
I tabel nedenfor ses beregnede ydelser, virkningsgrader og indfyret effekt i 4 lastpunkter

Ydelse og virkningsgrad fra 100% til 35% last.

SSV4	Enhed	100	75	50	35
Critical process figures					
Boiler load	%	100	75	50	35
MT temperatur	°C	540	540	540	540
Flame temperature Furn	°C	1480	1394	1284	1178
Recirkulation %	%	13	16	14	22
O_2 in fluegas	%	3.10	3.34	5.00	5.00
Results					
Coal fired	MJ/s	824.4	643.5	448.1	329.6
Net elec. output	MW	352.3	274.1	187.7	133.1
O_2 production	MW	0.0	0	0.0	0.0
Result net power	MW	352.3	274.08	187.7	133.1
ETA net.	%	42.7	42.6	41.9	40.4

Ydelse

Bilag 1a og 1b viser de detaljerede varmebalancer for både kedel og turbine i 100% last med detaljer om tryk, temperaturer og flow i alle dele af både kedel og turbine.Bemærk at kedellasten er bestemt af friskdampflow (HT-damp) fra kedlen. Det betyder, at kedlen efter retrofit til oxyfuel vil levere samme dampmængde til turbinen og sammenlignelig ydelse.
Ovenstående tabel med detaljeret performance for SSV i fuldlast og dellast er udgangspunktet for vurdering af SSV4 performance efter retrofit til oxyfuel.

4. SSV4 – retrofit til oxyfuel basiskobling.

Proceskoblingen i basisløsningen ved retrofit af SSV4 er etableret med sigte på en teknisk gennemførlig løsning. Et antal mulige koblinger og variationer er evalueret for at opnå en basiskobling, som både er procesmæssig god og imødegår de væsentligste tekniske problemer. Et antal forudsætninger danner grundlag for processen:

O_2 i fyrrum.
Litteraturen og enkeltbrænderforsøg siger samstemmende, at der for at opnå en stabil flamme og rimelig udbrænding skal være en forøget O_2% i sekundærluft og primærluft til brændere. En O_2-koncentration på omkring 30%vol beskrives. Det forudsættes, at en delvis iblanding af O_2 i selve brænderen kan skabe den nødvendige O_2 lokalt omkring flammen. Derfor er O_2 i blandingen af ilt fra iltfabrik og recirkuleret røggas optimeret efter kedlen ydelse uden krav til O_2 i samlet gasstrøm til kedel.

Lokalt højere O_2 omkring brænderen vil formentlig give mulighed for at sænket iltoverskuddet i kedlen (O_2 i røggas efter forbrænding). Der er dog ikke dokumentation for at bestemme det krævede iltoverskud, hvorfor dette fastholdes som i referenceberegning med luftfyring.

I dellast øges kedlens luftoverskud. Det skyldtes hovedsageligt køleluft til inaktive brændere. Ved retrofit oxyfuel må køling af brændere forventes udført af recirkuleret røggas med samme iltindhold som røggas efter forbrænding. Derfor kan kedlens iltoverskud fastholdes på samme niveau som fuldlast i hele lastområdet. Denne forudsætning fastholdes i alle oxyfuel beregninger.

Recirkulation efter afsvovling.
I basiskoblingen recirkuleres røggas efter afsvovlingsanlægget for at undgå en opkoncentration i af svovl i kedlen. Forøget korrosion som følge af en opkoncentration er endnu ikke tilstrækkeligt afdækket, hvorfor den valgte kobling med recirkulation efter afsvovling anses for den sikre løsning. Sidst i rapporten vurderes en alternativ kobling med varm recirkulation før afsvovlingsanlæg og lufo for at vurdere potentiale for forbedring af performance.

Primærluft til kulmøller.
I oxyfuel basiskoblingen erstattes luft sekundær og primær luft med recirkuleret røggas efter LUFO. De indledende analyser af retrofit til oxyfuel viste, at det ikke er muligt at anvende recirkuleret røggas efter LUFOsom varm og kold gas til kulmøllen.Årsagen er det høje vandindhold i recirkuleret røggas, som yderligere opfugtes af kultørring i kulmøllerne og giver kondens ved kulmøllens afgang. Derfor anvendes en tørret røggas på vej mod CO_2 kompression. Komposition er hentet fra et tidligere DE oxyfuel projekt og ses på kedlens varmebalance (bilag 5a). Som tidligere beskrevet giver SSV's lufokonstruktion mulighed for forskellige gasstrømme i primær og sekundær sektor.

Røggasflow.
Både friskluftsblæser, sugetræksblæser og recirkulationsblæser skal efter retorfit til oxyfuel udskiftes eller ombygges væsentligt, da temperaturer og dermed volumenflow for alle tre ændres væsentligt. Disse komponenter begrænser derfor ikke drift under oxyfuel betingelser. De nødvendige anlægsændringer kommenteres i separat afsnit.

4.1 Basiskobling retrofit oxyfuel

Figur 3 viser en oversigtstegning af basiskoblingen for retrofit oxyfuel.

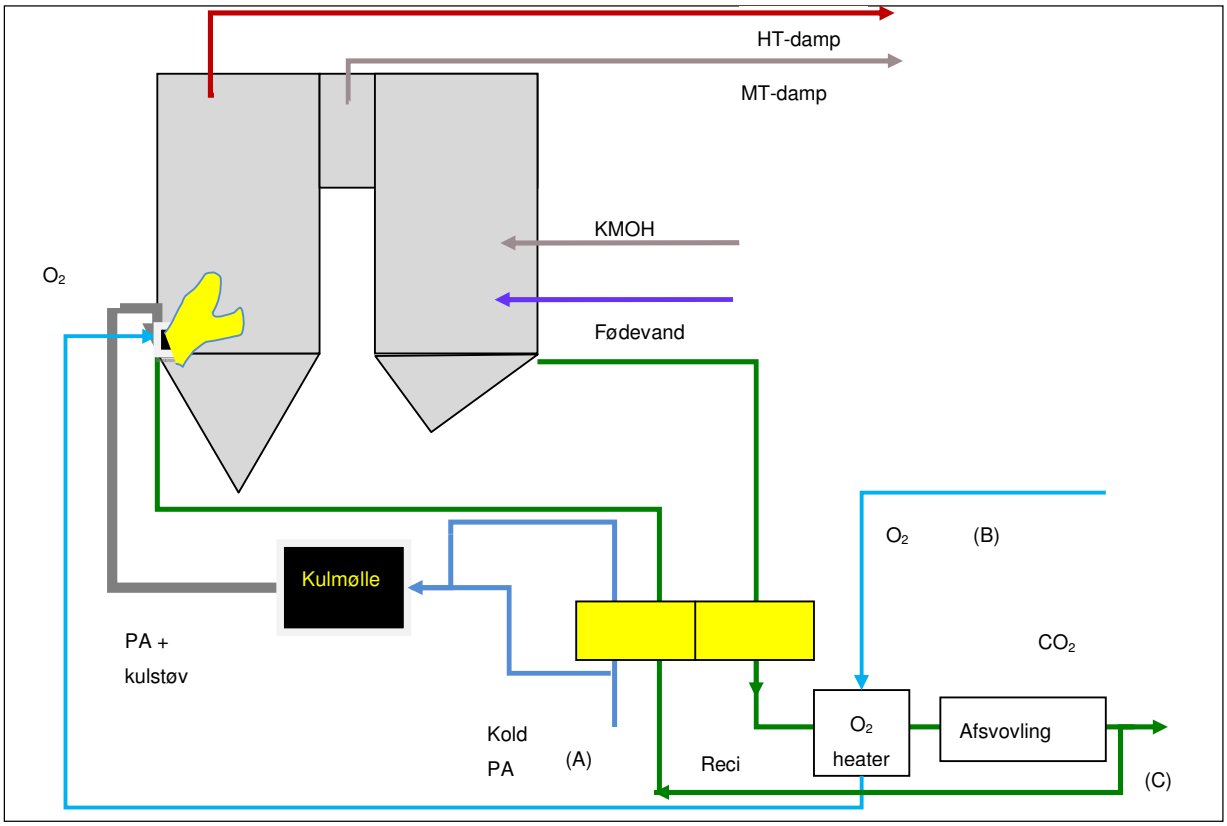

Figur 3.

Kedlens vand og dampside ændres ikke hverken konstruktionsmæssigt eller flowmæssigt. En detaljeret beskrivelse findes under gennemgang af referencemodellen.

Tør CO_2 (A) hentes før kompression og splittes, således en del opvarmes i LUFOen primærsektor og en del bypasser LUFOen. Den kolde og varme gas blandes før kulmøllen, således den ønskede temperatur (her 90 °C) opnås i afgang kulmølle. Reguleringen er i praksis sådan, at flow bestemmes af last på kulmøllen, da kul/gas forholdet er konstant. Fordelingen mellem flow til LUFO og bypass tilpasses efter afvigelse på ønsket temperatur efter mølle.

Ilt fra iltfabrikken (B) med en tilgangstemperatur på 10 °C opvarmes i en gas/gas veksler af rørtype, således lækage af ren ilt undgås. Varmen hentes fra røggassen, som herved køles før afsvovlingsanlægget. De indledende analyser med basismodellen viser, at temperaturen ved tilgang til afsvovling er høj og tæt på det tilladelige, hvorfor udnyttelse af varmen i røggassen er procesmæssigt optimalt.

Røggas (C) recirkuleres efter afsvovlingsanlæg igennem LUFOens sekundærsektor og ind i kedlen. Recirkulationsmængden bestemmes efter den ønskede MT-afgangstemperatur i kedlen. Der skal etableres en ny recirkulationsblæser, idet flowet er betydeligt større end gennem den eksisterende kolde recirkulationsblæser.

Den samlede Mopeds model af SSV4 er ombygget og tilpasset basiskoblingen beskrevet ovenfor, hvorefter lastområdet er gennemregnet. Varmebalancer for basiskobling ses i bilag 5a-8b. Resultater og sammenligning med konventionel luftforbrænding ses i tabel nedenfor.

4.2 Resultater basiskobling

Bemærk følgende nøgleforudsætninger for beregninger

- Iltoverskud i kedlen som luftforbrændig ved 100% last med 3,1% ilt i røggas.
- Recirkulationsmængde beregnes, så MT afgangstemperatur holder 540 °C.

Ydelse og virkningsgrad fra 100% til 35% last.

SSV4	Enhed	100	75	50	35
Critical process figures					
Boiler load	%	100.0	75.0	50.0	35.3
MT temperatur	°C	540.0	540.0	540.0	540.0
Flame temperature Furn	°C	1371.1	1271.0	1150.1	1069.3
Recirkulation %	%	67.5	76.2	81.2	75.9
O_2 in fluegas	%	3.1	3.1	3.1	3.1
Results					
Coal fired	MJ/s	827.6	640.4	444.1	319.3
Net elec. output	MW	352.2	270.3	183.0	125.6
O_2 production	MW	40.7	31.5	21.8	15.7
Result net power	MW	311.5	238.8	161.2	110.0
ETA net.	%	37.6	37.3	36.3	34.4

Udover denne reduktion som følge af kovertering til oxyfuel forbrænding skal omkosningen til oprensning og kompression af CO_2 medtages for at den rigtige virkningsgrad kendes. Interne DONG Energy dokumenter opgør dette til en yderligere reduktion af virkningsgraden med omkring 3,5-4,5% point.

Virkningsgranden for SSV4 efter retrofit ses i nedenstående figur sammenlignet med reference luftforbrænding:

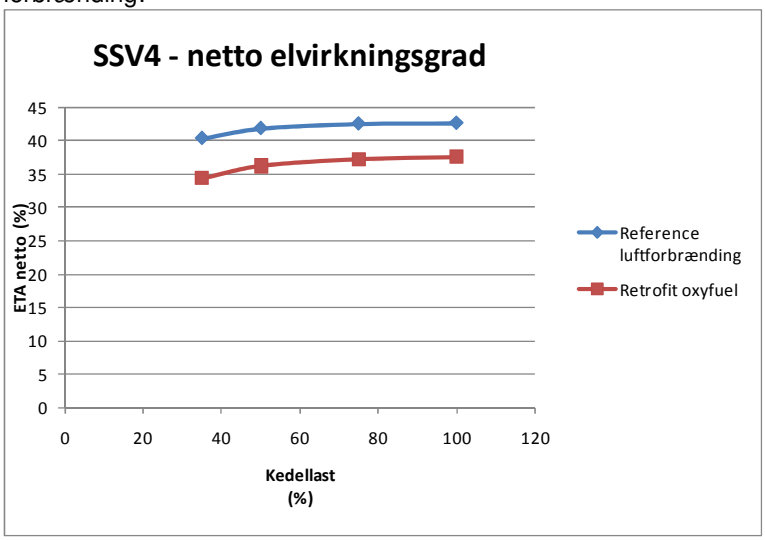

Figur 4.

Alle kendte temperaturbegrænsninger fra materialer i vægge og overhedere er overholdt i beregninger. Dog skal det bemærkes, at hvis recirkulationsmængden reduceres (MT afgangstemperaturen falder ved dette) kan temperaturer i materialer komme over det tilladelige, fordi temperaturen i fyrrummet i så fald stiger.

CFD – modellering
Mopeds kedelmodelleringen er relativt simpel omkring fyrrummet, men overhedere er detaljeret geometrisk modelleret. Derfor er pålideligheden af modelleringen vurderet med en CFD model af SSV4 kedlens fyrrum og første overhedere. Disse undersøgelser rapporteres separat, men her gengives nøglekonklusioner:

- Der opnås god overensstemmelse mellem beregnet optag i fyrrum og strålerum mellem Mopeds og CFD-modellen.
- CFD-modellen verificerer beregningen på kedlens første del med Mopeds.
- Der findes med CFD-modellen ikke ved denne analyse punkter i kedlens konstruktion, som kan forventes at give anledning til problemer ved retrofit til oxyfuel.

CFD modellering og resultater er rapporteret separat.

4.3 Kritiske punkter i basiskoblingen:

To forhold omkring den beskrevne basiskobling skal belyses nærmere i yderligere undersøgelse:

O_2 omkring brændere forudsættes højere end resulterende O_2 ved kedelafgang. Det skal i samråd med brænderleverandører afdækkes, om denne nødvendige flowkontrol kan opnås i hele driftsområdet, og at udbrænding ved oxyfuel er tilfredsstillende.

Temperatur ved tilgang afsvovling.

Mulighed for forøget køling af røggas før afsvovling skal undersøges, da nuværende høje temperaturer ligger tæt på anlæggets grænse og dermed kunne blive en begrænsning for driften. Begrænsningen kommer i form af højere svovlsyredugpunktstemperatur ved oxyfuel.

Korrosion
Det skal bemærkes, at hidtidigt oxyfuel anlæg drives med relativt lave damptemperaturer (<400°C sammenlignelige med affaldsanlæg). Forhold omkring korrosion skal afklares, idet det er afgørende for potentialet i oxyfuel at performance på turbineanlægget kan opretholdes.

Spørgsmålet er selvfølgelig afgørende ved retrofit, hvor materialer i kedlen kan være af ældre dato med begrænsede styrkeværdier. Men hvis oxyfuel også for ny anlæg af hensyn til korrosion må udlægges med lavere dampdata en konventionelle luftfyrede kedler vil det påvirke oxyfuel forbrænding sammenlignet med andre koncepter for CO_2 rensning. En sænkning af HT- og MTafgangstemperatur på 10°C reducerer typisk netto elvirkningsgraden med 0,2% point.

Korrosion belyses separat i en parallel undersøgelse i PSO projektet.

4.4 Nødvendige anlægsombygninger

Basiskoblingen til retrofit oxyfuel på SSV er baseret på størst mulig anvendelse af eksisterede komponenter og anlæg, skal et antal maskinkomponenter enten opgraderes eller udskiftes. De væsentligste er:

Blæsere:
Både suger og recirkulationsblæser skal enten ud skiftes eller totalombygges. Der beregnes et flow gennem kedlen ca. 20% højere end ved nominel last i luftforbrænding. Både kanaler til LUFO, kulmøller og kedel må forventes at skulle modificeres betydeligt.

O_2 heater
For at udnytte energien i røggassen og forvarme O_2 inden forbrænding skal en gas/gas veksler etableres. Den skal være af rørtype eller lignende, da en lækage af O_2 er kritisk for processens samlede ydelse. Der er desuden alvorlige sikkerhedsmæssige problemer med ren O_2 i forbindelse med materialer, som ikke er designet hertil.

Køling af røggas
Maksimal tilladelig tilgangstemperatur til afsvovlingsanlægget kan betyde, at der er behov for yderligere køling af røggas. Dette kunne gøres med en fjernvarmekøler eller evt. integreres med turbinekredsen som kondensat- eller fødevandsforvarmning.

Tør CO_2 til møller
Kanaler omkring LUFO og primærblæsere skal håndtere, at der er forskellig gassammensætning i primær- og sekundær-sektorer. Desuden vil risiko for kondensering i kanaler være forøget grundet recirkulationsgassens høje vandindhold. Problemet vil være størst under start/stop af blok samt eventuelt ved overgang fra luftfyring til oxyfuel.

Omfang af kanalomlægning er i høj grad afhængig af, om blokken efter retrofit kun skal køre oxyfuel eller både have mulighed for luftfyring og oxyfuel. Startforløbet er ikke beskrevet i denne analyse.

4.5 Optimering af oxyfuel basiskobling.

For at afdække potentialet en en optimering af basiskobling er der gennemført beregninger med 2 parametervariationer. Analysen er specifik for SSV kedlen, men den afdækker mulig gevinst ved optimering af retrofit koncept til valgte blok.

Sænkning af recirkulationsmængde.
Recirkulationsmængde sænkes og samlet O_2 i gas til fyrrum øges til omkring 24%. For SSV4 er grænsen for sænkning af recirkulation bestemt af beregnet temperatur ved afgang fyrrum, som hvis den hæves fra luftforbrænding vil påvirke materialebelastninger i hele kedlens 1. træk både på røg- og dampside.

		Ref luft	Kold recirkual-tion	Recirkulation efter temp furn afgang
Boiler load	%	100	100	100
MT temperatur	℃	540	540	492.3
Temperature Furn	**℃**	**1480**	**1371**	**1480**
Recirkulation %	%	13	67	60
O2 in fluegas	%	3,1	3,1	3.1
Results				
Coal fired	MJ/s	824,4	827,6	793.0
Net elec. Output	MW	352,3	352,2	338.8
O2 production	MW	0,0	40,7	38.9
Result net power	MW	352,3	311,5	299.9
ETA net.	%	42,7	37,6	37.8

Der opnås en mindre forbedring på procesvirkningsgraden. Bemærk dog at forbedringen på kedlen er væsentlig større, for MT-damptemperaturen på 492.3℃ reducerer turbinens ydelse med 11,6MW.. Beregningen viser dog, at det er muligt at forbedre den samlede Performance ved Oxy-fuel, hvis man enten fra starten optimere kedlen til Oxyfuel eller modificerer hedefladebestykningen for en eksisterende kedel væsentligt, således optimale damptemperaturer kan opretholdes med lavere recirkulationsgrad.

Iltoverskud ved forbrænding.
Som nævnt ovenfor er det nødvendig for optimal drift at kunne sikre lokalt forhøjet O_2 i de brænder-nære zoner. Hvis dette fungerer optimalt, kunne det blive muligt at sænke den totale iltprocent ud af kedlen. Iltprocenten er en nøgleparameter i oxyfuel drift og potentialet er vurderet i figur 5.

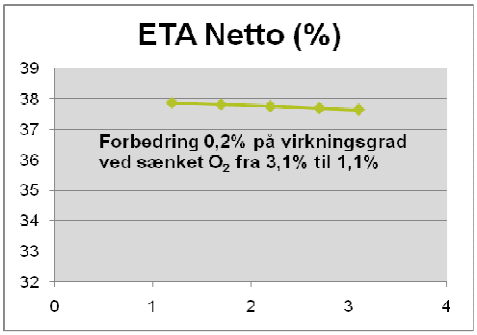

Figur 5 - Følsomhed for O_2 – potentiale ved reduktion

Det ses, at der kan opnås en forbedring ved reduktion. Først ved forsøg på en kedel af betydelig størrelse kan det afdækkes, hvilken iltprocent der er nødvendig for at opnå en rimelig forbrænding.

5. Oxyfuel forbrænding med varm recirkulation før afsvovling.

Recirkulation af røggassen før LUFO betyder en mere simpel proces og en forbedret udnyttelse af energi i røggas. Konceptet skal sammenlignes med basiskoblingen, hvor røggas recirkuleres koldt efter afsvovlingsanlægget. Sammenligning laves i 100% kedellast med følgende randbetingelser:

O_2 i fyrrum som basiskobling
Tør CO_2 til primær LUFOsektor og kulmøller
Recirkulationsmængde bestemt af MT temperatur på 540°C.

5.1 Proceskobling ved varm recirkulation

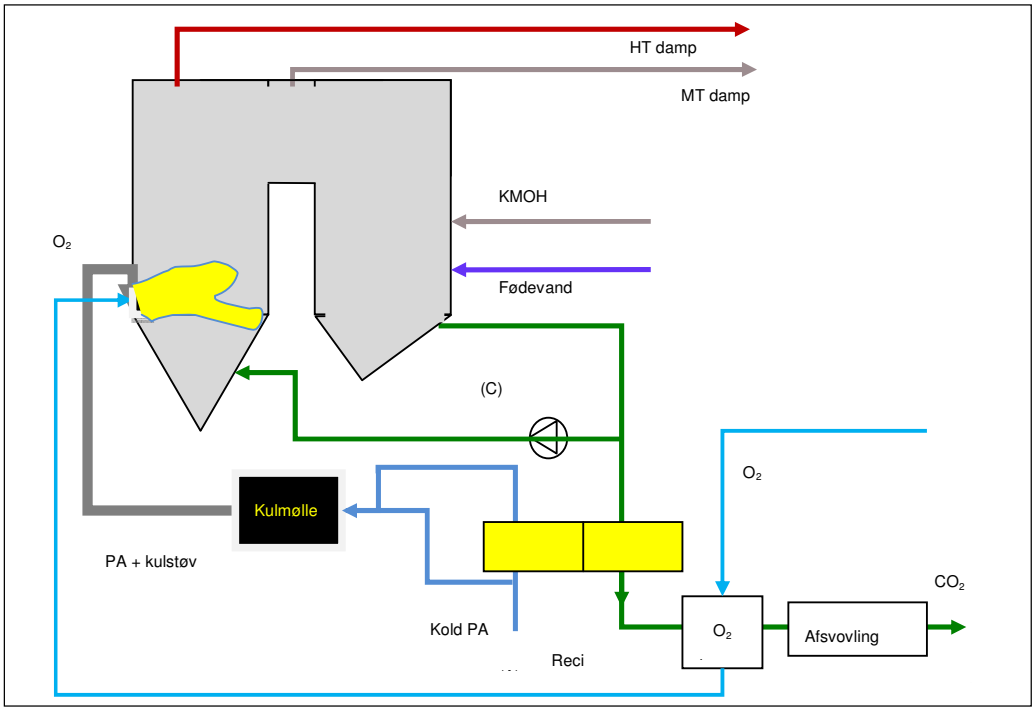

Figur 6.

Den varme røggas recirkuleres foran LUFOen med en blæser, som sidder både varmt og beskidt. Dette koncept kendes fra DE anlæg. Flow gennem LUFOen reduceres væsentligt både på varm røgside, hvor kun røggas til CO_2 rensning passerer LUFO og på den kolde side, hvor der kun opvarmes tør CO_2 til kulmøller.

5.2 Resultater

Varmebalancer for proceskoblingen med varm recirkulation ses i bilag9a og 9b. Sammenlignet med luftforbrænding opnås følgende resultater:

		Reference luft	Kold recirkualtion	Varm recirkulation
Boiler load	%	100	100	100
MT temperatur	°C	540	540	540
Temperature Furn	°C	1480	1371	1382
Recirkulation %	%	13	67	67
O2 in fluegas	%	3,1	3,1	3,,1
Results				
Coal fired	MJ/s	824,4	827,6	810,2
Net elec. output	MW	352,3	352,2	352,,8
O2 production	MW	0,0	40,7	39,,6
Result net power	MW	352,3	311,5	313,,2
ETA net,	%	42,7	37,6	38,,7

Der opnås en forbedring af procesvirkningsgraden på over 1% point. Forbedringen skyldtes hovedsageligt 2 forhold:

- Varm recirkulation øger middeltemperaturen af gas til forbrænding – hvilket reducerer indfyring
- Da indfyring reduceres, er energiforbruget til produktion af ilt også reduceret.

Disse resultater viser, at der er potentiale i at arbejde videre med en varm recirkulation, men det bemærkes at der er grundlag for yderligere optimering. Den meget varme røggas på over 200°C efter forvarmning af ilt bør udnyttes som opvarmning i kondensatkredsen alternativt til produktion af fjernvarme.

5.3 Kritiske punkter ved varm recirkulation

O_2 omkring brændere.

I blandingen af recirkuleret røggas, tør CO_2 som bæregas fra kulmøller og O_2 fra iltfabrik er O_2 i den samlede forbrændingsatmosfære 20,3% på volumenbasis. Som tidligere nævnt viser forsøg, at der for at opnå tilfredsstillende forbrænding kræves et iltindhold op mod 30%. For at opnå dette skal der være mulighed for lokal og kontrolleret indblæsning af O_2 i nærbrænderområdet.

Hvis lokalt forhøjet O_2 ikke kan opnås må recirkulationsmængden reduceres. Derved kan MT damptemperatur ikke opnås og blokkens ydelse reduceres.

Røggastemperatur før afsvovlingsanlæg.
Temperaturen i røggassen efter opvarmning fra O_2 ligger over 200°C. Ved normal luftforbænding ligger temperaturen på omkring 145°C. En kobling med varm recirkulation vil kræve ekstra køling eller en fuldstændig ombygning af afsvovlingsanlæg og kanaler.

Opkoncentration af SO_2/SO_3
I konceptet med varm recirkulation sker der en opkoncentration af SO_2/SO_3 i kedlen. Dette kan give anledning til korrosion. Følgende kan nævnes:

- Højtemperaturkorrosion i fyrrum og på første overhedere. (Belyst af separat del af PSO projekt)
- Svovlsyrekondensation i kedlens kolde ende. Varmebalance bilag 9a viser temperaturer i både LUFO og tilgang afsvovling på over 200°C, hvilket forhindrer væsentlige problemer. Dog vil røggastemperaturen falde i dellast. Ombygges kedlen til forbedret køling af røggas er dette en væsentlig udfordring. Det samme gælder under start og stop, hvor temperaturer i røggas og kanalvægge vil falde under dugpunkt.
- Under start og stop vil der være risiko for svolvsyre i kanaler og blæser til varm recirkulation. Dette problem er væsentlig større end kendt fra eksisterende DE-anlæg med varm recirkulation på grund af opkoncentration.

Ovennævnte kan nødvendiggøre væsentlige modifikationer af kedlen for at sikre, at et koncept med varm svovlholdig recirkulation skal fungere med stabil og langvarig drift.

5.4 Nødvendige anlægsombygninger.

For at etablere en kobling med varm recirkulation skal følgende komponenter tilføjes:

Recirkulationsblæser.
Ved varm recirkulation sidder den nye recirkulationsblæser varmt ved omkring 386°C og oplever flyveaske og det forøgede svovlindhold i røggasen. På andre DE-værker har vi varm recirkulation med en recirkulationsblæser på dette sted, men ved oxyfuel er den beregnede recirkulationsmængden omkring 3 gange større.
Det skal desuden bemærkes, at ved luftforbrænding holder recirkulationsblæseren MT-damptemperaturen oppe og sikre derved optimal ydelse på turbinen. Ved oxyfuel fyring er blæseren en kritisk komponent, som skal fungere for at blokken kan køre Oxyfuel drift.

For punkterne O_2 heater, Køling af røggas og Tør CO_2 tll møller er vurdering og kommentarer som under Kold recirkulation.

5.5 Optimeringsmuligheder

Der er et potentiale og nok også et behov for yderligere køling af røggassen før afsvovlingsanlægget. Effekten kan enten overføres til kondensatkredsen og dermed forøge turbinens netto ydelse eller til produktion

6. Konklusion.

2 koncepter for retrofit af SSV4 til oxyfuel forbrænding er gennemregnet med Mopeds. Modellen og resultater for forbrænding og fyrrum verificeret med en CFD-model af kedlens 1. træk.

Med de anvendte forudsætninger for proceskobling af energiforbrug til iltproduktion reduceres virkningsgraden for den samlede kraftværksblok SSV4 i fuldlast fra 42,7% til 37,6% i basiskoblingen. Det skal bemærkes, at virkningsgraden reduceres yderligere når forbrug til oprensning og kompression medtages.

Basis kobling kan gennemføres med mindst mulig usikkerhed og minimal ombygning af proces. Væsentligste udfordringer er lokal høj O_2 i brænderzone og mulighed for at opretholde damptemperaturer uden korrosionsproblemer.

Varm recirkulation af røggas giver mulighed for at forbedre den samlede performance, men der er både tekniske udfordringer og en recirkulationsblæser, der sidder varmt og udsat, og som er kritisk for oxyfuel drift. Uden egentlig optimering af den varme recirkulation opnås en forbedring på godt 1%.

Parametervariationer af recirkulationsmængden viser da også svaghederne ved retrofit til oxyfuel sammenlignet med nyanlæg optimeret til oxyfuel forbrænding. Ved at optimere kedlens hedefladebestykning og materialevalg kan formentlig opnås bedre ydelser,og en turbinekreds kan udlægges til mulige damptemperaturer. Da investeringen i iltfabrikken er betydelig selv sammenlignet med en kraftværksblok, er det nok fordelagtigt med et anlæg designet og optimeret for oxyfuel forbrænding.

7. Bilagsoversigt

Vedlagt som bilag er varmebalancer for alle lastrpunkter:

Bilag 1a:	100% kedellast, luftforbrænding, kedel
Bilag 1b:	100% kedellast, luftforbrænding, turbine
Bilag 2a:	75% kedellast, luftforbrænding, kedel
Bilag 2b:	75% kedellast, luftforbrænding, turbine
Bilag 3a:	50% kedellast, luftforbrænding, kedel
Bilag 3b:	50% kedellast, luftforbrænding, turbine
Bilag 4a:	35% kedellast, luftforbrænding, kedel
Bilag 4b:	35% kedellast, luftforbrænding, turbine
Bilag 5a:	100% kedellast, Basiskobling Oxyfuel, kedel
Bilag 5b:	100% kedellast, Basiskobling Oxyfuel turbine
Bilag 6a:	75% kedellast, Basiskobling Oxyfuel, kedel
Bilag 6b:	75% kedellast, Basiskobling Oxyfuel, turbine
Bilag 7a:	50% kedellast, Basiskobling Oxyfuel, kedel
Bilag 7b:	50% kedellast, Basiskobling Oxyfuel, turbine
Bilag 8a:	35% kedellast, Basiskobling Oxyfuel, kedel
Bilag 8b:	35% kedellast, Basiskobling Oxyfuel, turbine
Bilag 9a:	100% kedellast, Oxyfuel Varm reci. , kedel
Bilag 9b:	100% kedellast, Oxyfuel Varm reci., turbine

Studstrupværket blok 4

Kalibrering v. 100% | Reference | **MT temp 540°C**

VB 1a | **Kold recirkulation** | **Boilerload: 100.0 %**

Departm: Proces Calculations
Initials: DENFI
Date: 03-01-2011
Draw nr:

Beregningsnr ######## | Bar | kJ/kg | kg/s | °C

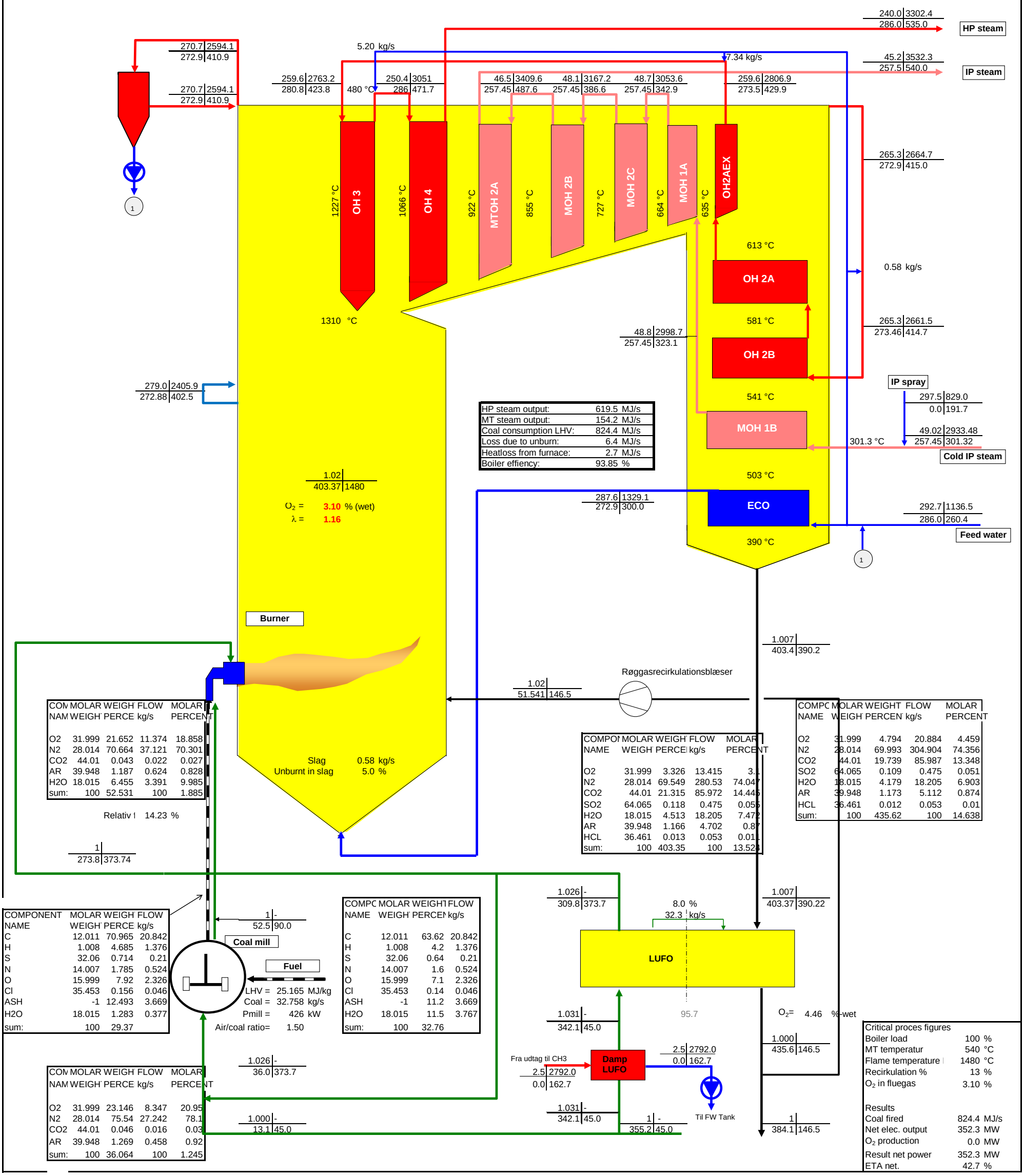

COMPONENT NAME	MOLAR WEIGHT	PERCE	FLOW kg/s	MOLAR PERCENT
O2	31.999	21.652	11.374	18.858
N2	28.014	70.664	37.121	70.301
CO2	44.01	0.043	0.022	0.027
AR	39.948	1.187	0.624	0.828
H2O	18.015	6.455	3.391	9.985
sum:	100	52.531	100	1.885

COMPONENT NAME	MOLAR WEIGHT	PERCE	FLOW kg/s	MOLAR PERCENT
O2	31.999	3.326	13.415	3.1
N2	28.014	69.549	280.53	74.047
CO2	44.01	21.315	85.972	14.445
SO2	64.065	0.118	0.475	0.056
H2O	18.015	4.513	18.205	7.472
AR	39.948	1.166	4.702	0.87
HCL	36.461	0.013	0.053	0.011
sum:	100	403.35	100	13.524

COMPONENT NAME	MOLAR WEIGHT	PERCEN	FLOW kg/s	MOLAR PERCENT
O2	31.999	4.794	20.884	4.459
N2	28.014	69.993	304.904	74.356
CO2	44.01	19.739	85.987	13.348
SO2	64.065	0.109	0.475	0.051
H2O	18.015	4.179	18.205	6.903
AR	39.948	1.173	5.112	0.874
HCL	36.461	0.012	0.053	0.01
sum:	100	435.62	100	14.638

COMPONENT NAME	MOLAR WEIGHT	PERCE	FLOW kg/s	MOLAR PERCENT
C	12.011	70.965	20.842	
H	1.008	4.685	1.376	
S	32.06	0.714	0.21	
N	14.007	1.785	0.524	
O	15.999	7.92	2.326	
Cl	35.453	0.156	0.046	
ASH	-1	12.493	3.669	
H2O	18.015	1.283	0.377	
sum:	100	29.37		

COMPONENT NAME	MOLAR WEIGHT	PERCEN	FLOW kg/s
C	12.011	63.62	20.842
H	1.008	4.2	1.376
S	32.06	0.64	0.21
N	14.007	1.6	0.524
O	15.999	7.1	2.326
Cl	35.453	0.14	0.046
ASH	-1	11.2	3.669
H2O	18.015	11.5	3.767
sum:	100	32.76	

COMPONENT NAME	MOLAR WEIGHT	PERCE	FLOW kg/s	MOLAR PERCENT
O2	31.999	23.146	8.347	20.95
N2	28.014	75.54	27.242	78.1
CO2	44.01	0.046	0.016	0.03
AR	39.948	1.269	0.458	0.92
sum:	100	36.064	100	1.245

Critical proces figures		
Boiler load	100	%
MT temperatur	540	°C
Flame temperature	1480	°C
Recirkulation %	13	%
O_2 in fluegas	3.10	%
Results		
Coal fired	824.4	MJ/s
Net elec. output	352.3	MW
O_2 production	0.0	MW
Result net power	352.3	MW
ETA net.	42.7	%

Studstrupværket blok 3 og 4

DONG energy

Kold røggas recirkulation 51.5 kg/s

100 % main boiler load

No district heating

VB 1b

Originale BBC varmebalancer, dvs ikke As-built!

Departm: Procesberegning
Initials: heive
Draw: C:\SSV-OXY-2010\SSV-luft\[SSV4-100.xls]Turbine
Date: 03-01-2011
Printed 03-01 2011 09:32
Beregningsnr 19

Bar	kJ/kg
kg/s	°C

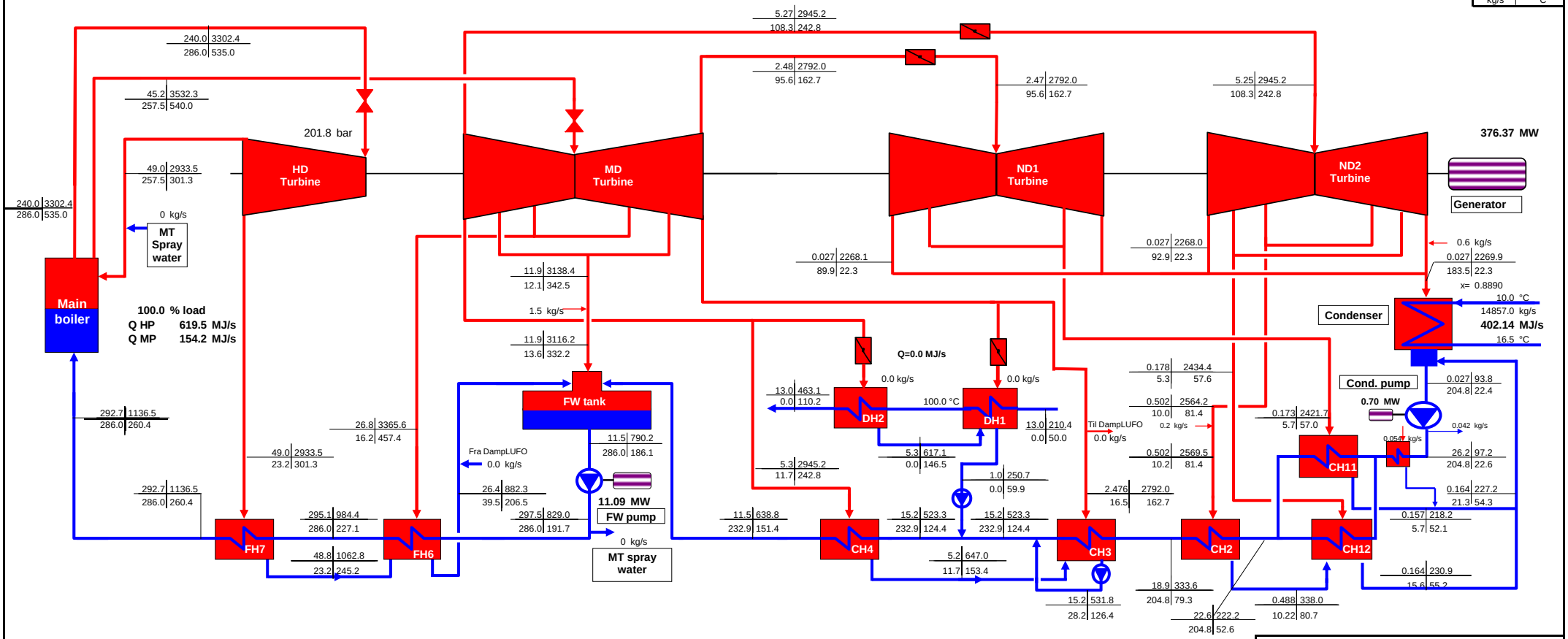

Coal consumption (LHV):	**824.36 MJ/s**
Boiler efficiency	**93.85 %**
Total consumption of fuel (LHV)	**824.36 MJ/s**
Gross power, ST	**376.37 MW**
Auxiliary power:	**24.02 MW**
Net. power:	**352.35 MW**
District heat:	**0.00 MJ/s**
Net. electrical effiency (LHV):	**42.74 %**
Net. thermal effiency (LHV):	**42.74 %**

Studstrupværket blok 4

Kalibrering v. 100% | Reference | **MT temp 540°C**

VB 2a | **Kold recirkulation** | **Boilerload: 75.0 %**

Departm: Proces Calculations
Initials: DENFI
Date: 03-01-2011
Draw nr:

Beregningsnr 121

Bar	kJ/kg
kg/s	°C

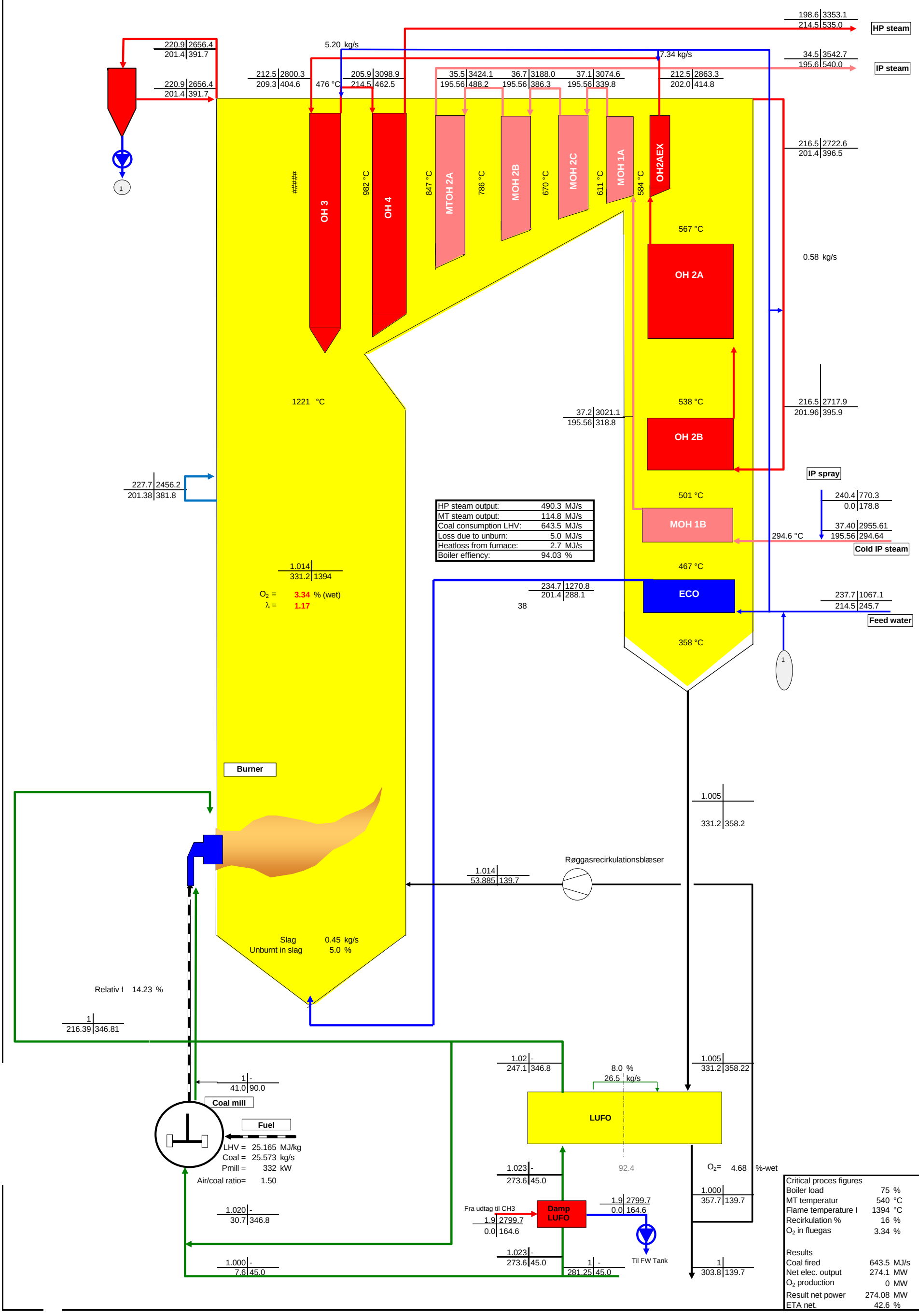

Studstrupværket blok 3 og 4

DONG energy

Kold røggas recirkulation 53.9 kg/s

75 % main boiler load

No district heating

VB 2b

Originale BBC varmebalancer, dvs ikke As-built!

Departm: Procesberegning
Initials: heive
Draw: C:\SSV-OXY-2010\SSV-luft\[SSV4-REF-75.xls]Turbine
Date: 03-01-2011
Printed 03-01 2011 09:38
Beregningsnr 121

Bar	kJ/kg
kg/s	°C

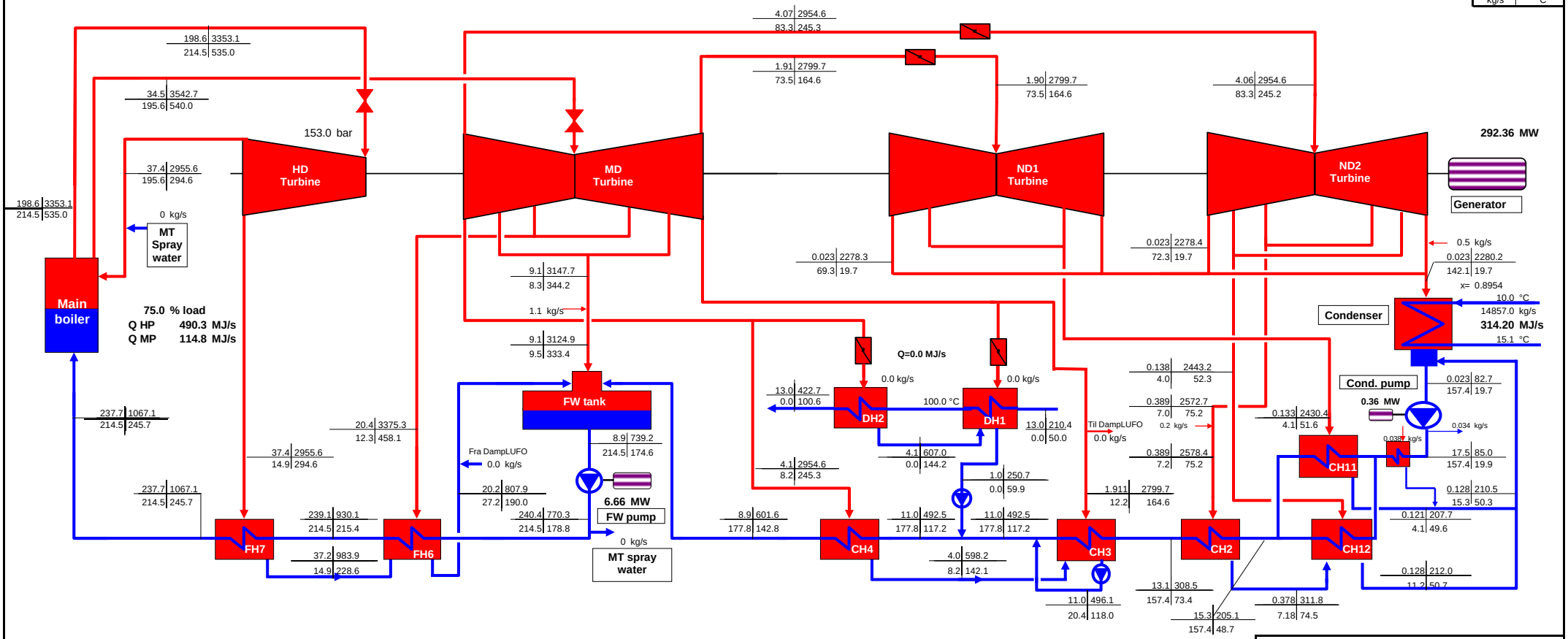

Coal consumption (LHV):	**643.54 MJ/s**
Boiler efficiency	**94.03 %**
Total consumption of fuel (LHV)	**643.54 MJ/s**
Gross power, ST	**292.36 MW**
Auxiliary power:	**18.28 MW**
Net. power:	**274.08 MW**
District heat:	**0.00 MJ/s**
Net. electrical effiency (LHV):	**42.59 %**
Net. thermal effiency (LHV):	**42.59 %**

Studstrupværket blok 4

Kalibrering v. 100% | Reference | **MT temp 540°C**

VB 3a | **Kold recirkulation** | **Boilerload: 50.0 %**

Departm:	Proces Calculations
Initials:	DENFI
Date:	03-01-2011
Draw nr:	

Beregningsnr ######## | Bar | kJ/kg | kg/s | °C

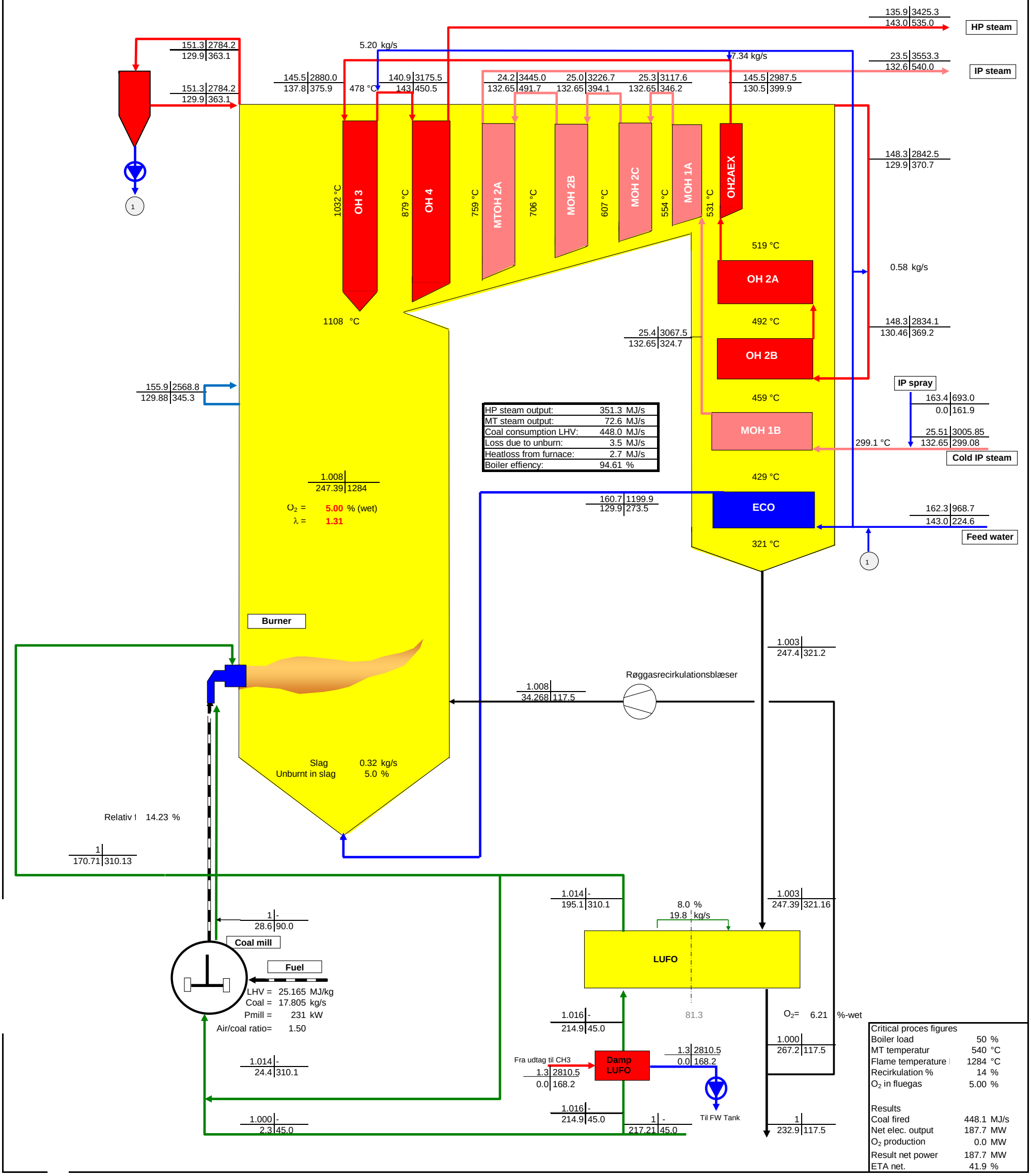

Studstrupværket blok 3 og 4

Kold røggas recirkulation 34.3 kg/s

50 % main boiler load

No district heating

VB 3b

Originale BBC varmebalancer, dvs ikke As-built!

Departm: Procesberegning
Initials: heive
Draw: C:\SSV-OXY-2010\SSV-luft\[SSV4-REF-50.xls]Turbine
Date: 03-01-2011
Printed 03-01 2011 09:39
Beregningsnr 500

Bar	kJ/kg
kg/s	°C

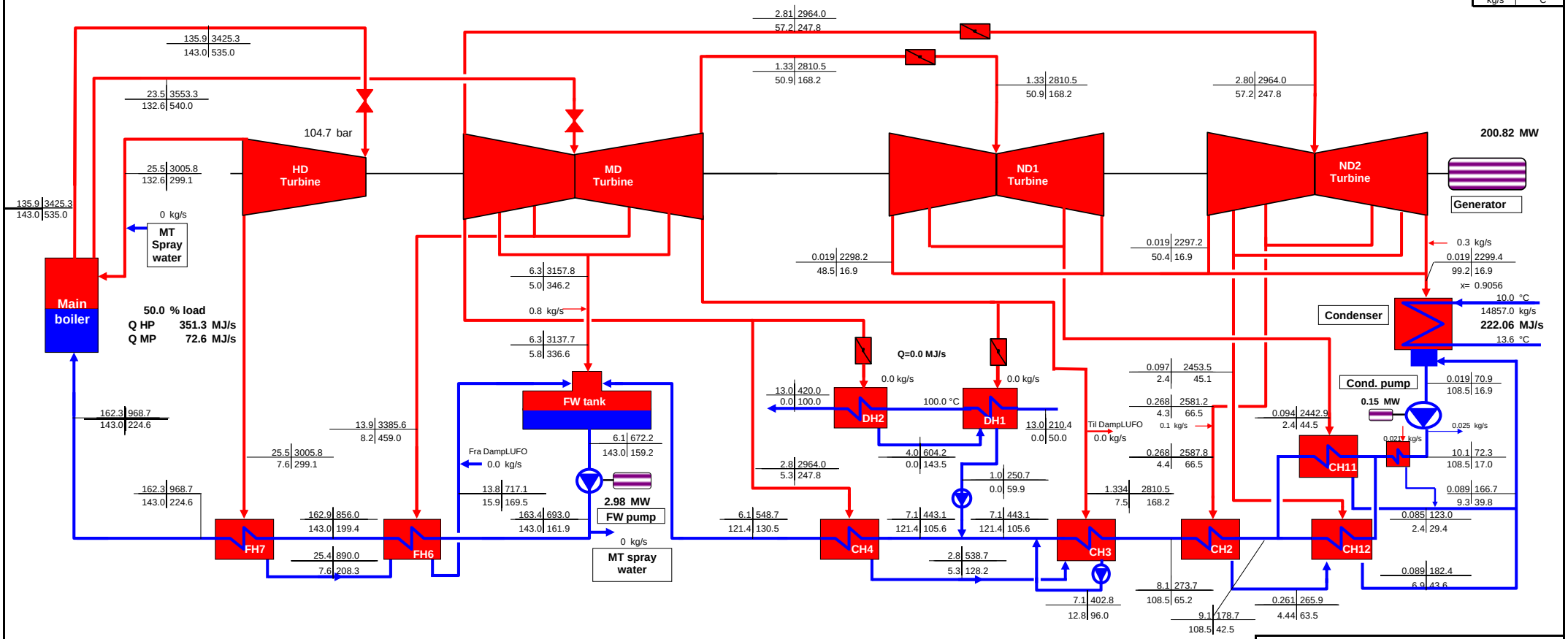

Coal consumption (LHV):	**448.05 MJ/s**
Boiler efficiency	**94.61 %**
Total consumption of fuel (LHV)	**448.05 MJ/s**
Gross power, ST	**200.82 MW**
Auxiliary power:	**13.11 MW**
Net. power:	**187.71 MW**
District heat:	**0.00 MJ/s**
Net. electrical effiency (LHV):	**41.90 %**
Net. thermal effiency (LHV):	**41.90 %**

Studstrupværket blok 4

Kalibrering v. 100% | Reference | **MT temp 540°C**

VB 4a | **Kold recirkulation** | **Boilerload: 35.3 %**

Departm: Proces Calculations
Initials: DENFI
Date: 03-01-2011
Draw nr:

Beregningsnr 121

Bar	kJ/kg
kg/s	°C

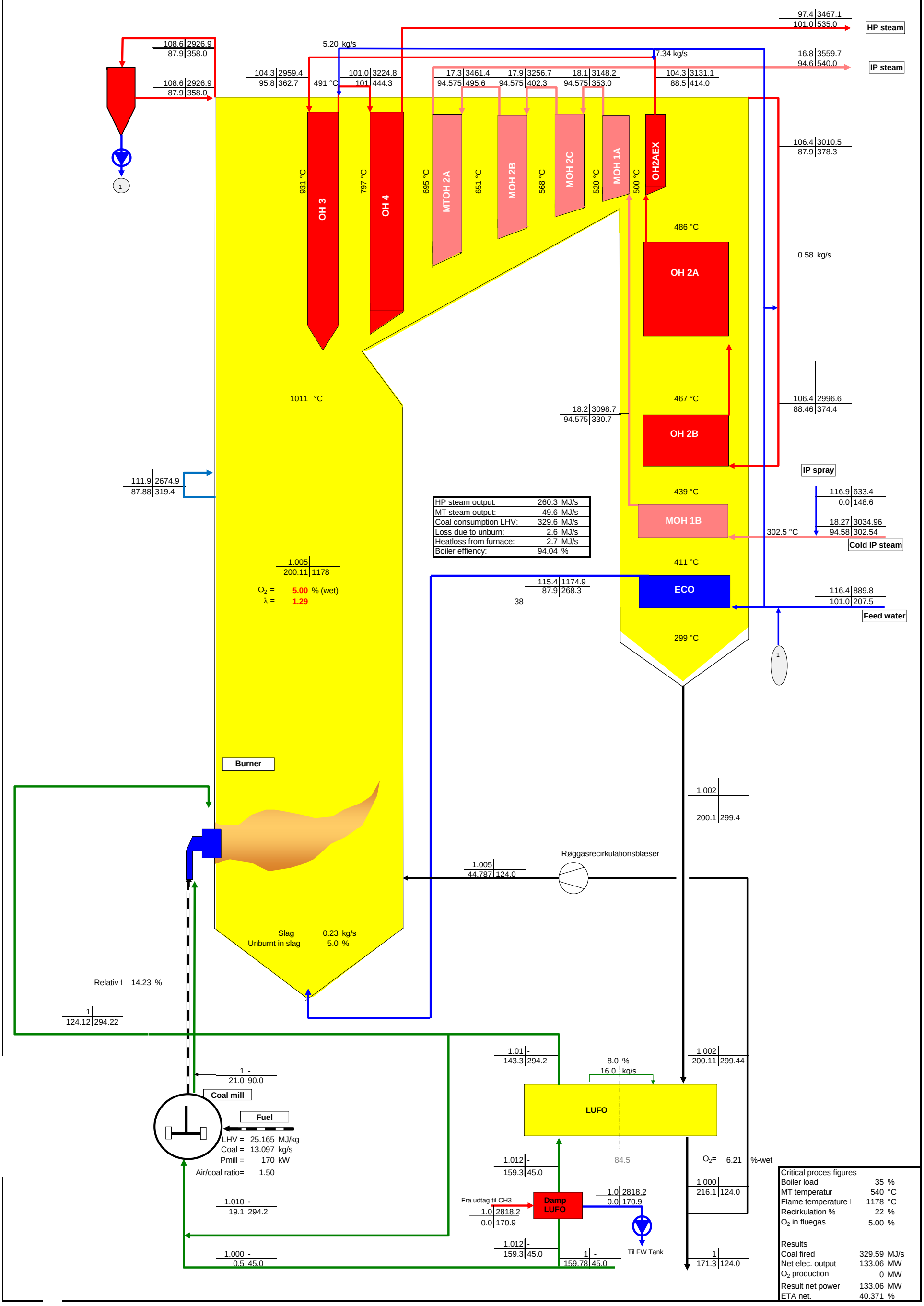

Critical proces figures		
Boiler load	35	%
MT temperatur	540	°C
Flame temperature l	1178	°C
Recirkulation %	22	%
O_2 in fluegas	5.00	%
Results		
Coal fired	329.59	MJ/s
Net elec. output	133.06	MW
O_2 production	0	MW
Result net power	133.06	MW
ETA net.	40.371	%

Studstrupværket blok 3 og 4

DONG energy

Kold røggas recirkulation 44.8 kg/s

VB 4b

35 % main boiler load

No district heating

Originale BBC varmebalancer, dvs ikke As-built!

Departm: Procesberegning
Initials: heive
Draw: C:\SSV-OXY-2010\SSV-luft\[SSV4-REF-35.xls]Turbine
Date: 03-01-2011
Printed 03-01 2011 09:44
Beregningsnr 121

Bar	kJ/kg
kg/s	°C

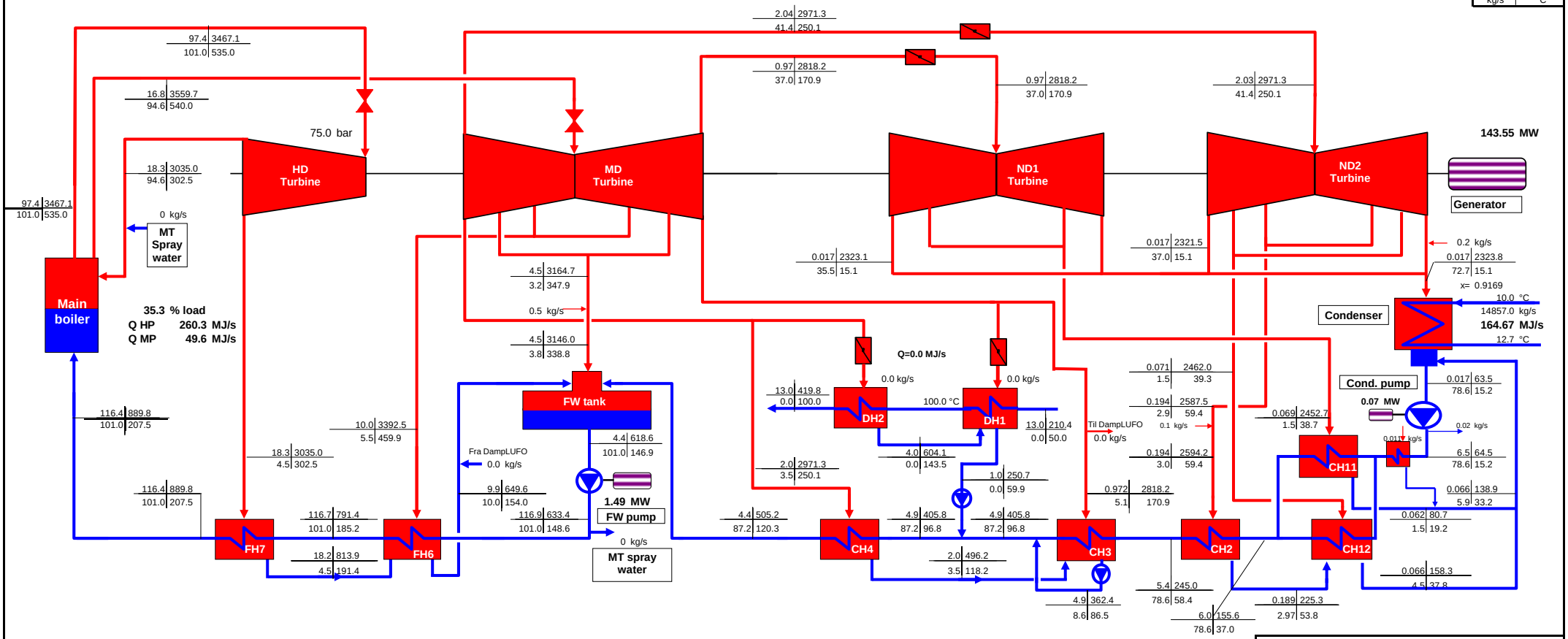

Coal consumption (LHV):	**329.58 MJ/s**
Boiler efficiency	**94.04 %**
Total consumption of fuel (LHV)	**329.58 MJ/s**
Gross power, ST	**143.55 MW**
Auxiliary power:	**10.50 MW**
Net. power:	**133.06 MW**
District heat:	**0.00 MJ/s**
Net. electrical effiency (LHV):	**40.37 %**
Net. thermal effiency (LHV):	**40.37 %**

Studstrupværket blok 3 og 4

Oxyfuel reference 100% last

"Tør CO_2 som PA luft"

VB 5a — **Boilerload: 100.0 %**

Departm:	Proces Calculations
Initials:	DENFI
Date:	22-08-2008
Draw nr:	
Beregningsnr	12

Bar | kJ/kg
kg/s | °C

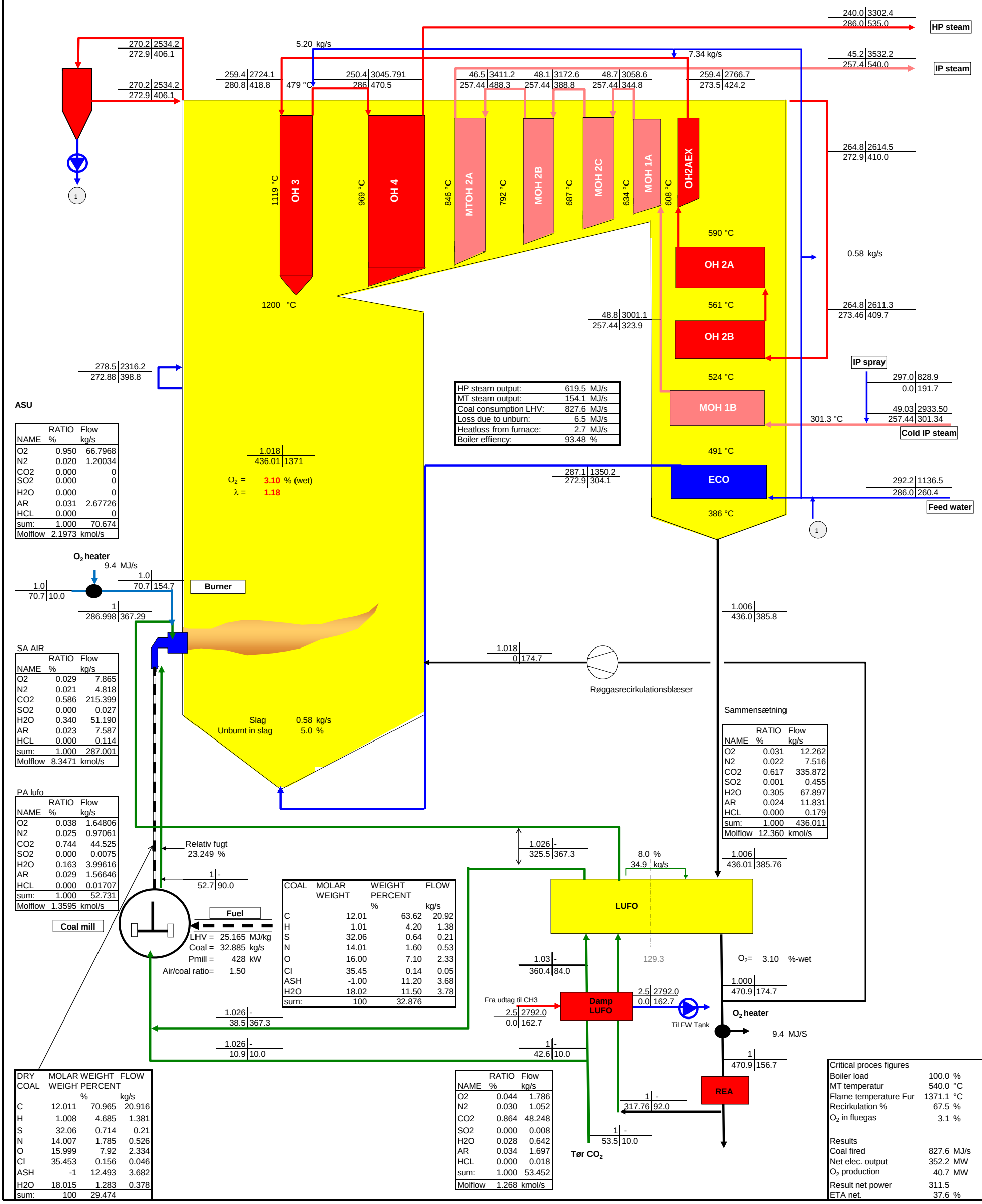

NAME	RATIO %	Flow kg/s
O2	0.950	66.7968
N2	0.020	1.20034
CO2	0.000	0
SO2	0.000	0
H2O	0.000	0
AR	0.031	2.67726
HCL	0.000	0
sum:	1.000	70.674
Molflow	2.1973	kmol/s

NAME	RATIO %	Flow kg/s
O2	0.029	7.865
N2	0.021	4.818
CO2	0.586	215.399
SO2	0.000	0.027
H2O	0.340	51.190
AR	0.023	7.587
HCL	0.000	0.114
sum:	1.000	287.001
Molflow	8.3471	kmol/s

NAME	RATIO %	Flow kg/s
O2	0.038	1.64806
N2	0.025	0.97061
CO2	0.744	44.525
SO2	0.000	0.0075
H2O	0.163	3.99616
AR	0.029	1.56646
HCL	0.000	0.01707
sum:	1.000	52.731
Molflow	1.3595	kmol/s

COAL	MOLAR WEIGHT	WEIGHT PERCENT %	FLOW kg/s
C	12.01	63.62	20.92
H	1.01	4.20	1.38
S	32.06	0.64	0.21
N	14.01	1.60	0.53
O	16.00	7.10	2.33
Cl	35.45	0.14	0.05
ASH	-1.00	11.20	3.68
H2O	18.02	11.50	3.78
sum:	100	32.876	

DRY COAL	MOLAR WEIGHT	WEIGHT PERCENT %	FLOW kg/s
C	12.011	70.965	20.916
H	1.008	4.685	1.381
S	32.06	0.714	0.21
N	14.007	1.785	0.526
O	15.999	7.92	2.334
Cl	35.453	0.156	0.046
ASH	-1	12.493	3.682
H2O	18.015	1.283	0.378
sum:	100	29.474	

NAME	RATIO %	Flow kg/s
O2	0.044	1.786
N2	0.030	1.052
CO2	0.864	48.248
SO2	0.000	0.008
H2O	0.028	0.642
AR	0.034	1.697
HCL	0.000	0.018
sum:	1.000	53.452
Molflow	1.268	kmol/s

Critical proces figures		
Boiler load	100.0	%
MT temperatur	540.0	°C
Flame temperature Fur	1371.1	°C
Recirkulation %	67.5	%
O_2 in fluegas	3.1	%
Results		
Coal fired	827.6	MJ/s
Net elec. output	352.2	MW
O_2 production	40.7	MW
Result net power	311.5	
ETA net.	37.6	%

Studstrupværket blok 3 og 4

NB. Tj(

Kold røggas recirkulation 0.0 kg/s

100 % main boiler load

No district heating

VB 5b

Originale BBC varmebalancer, dvs ikke As-built!

Departm: Procesberegning
Initials: heive
Draw: C:\SSV-OXY-2010\k-oxy\[SSV4-OXYFUEL_REF_100-ny%.xlsm]Turbine
Date: 03-01-2011
Printed 03-01 2011 09:44
Beregningsnr 12

Bar	kJ/kg
kg/s	°C

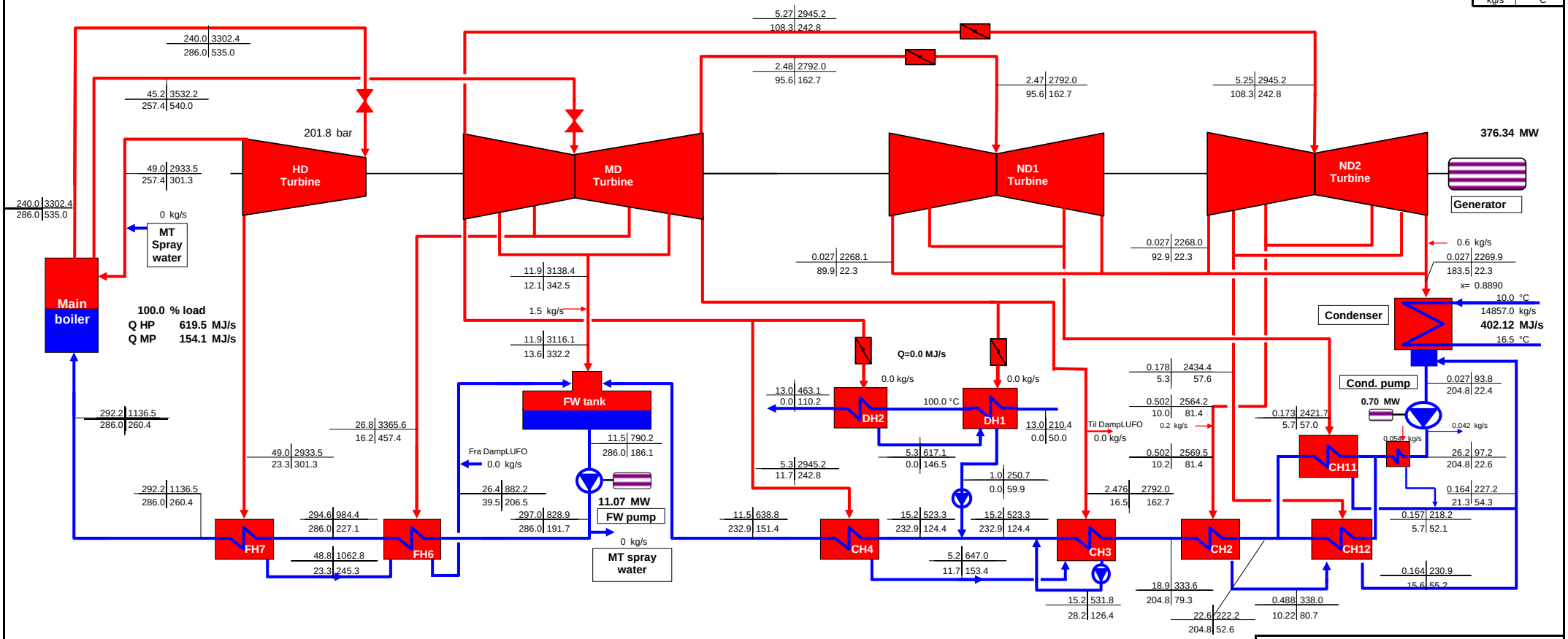

Coal consumption (LHV):	**827.55 MJ/s**
Boiler efficiency	**93.48 %**
Total consumption of fuel (LHV)	**827.55 MJ/s**
Gross power, ST	**376.34 MW**
Auxiliary power:	**24.13 MW**
Net. power:	**352.21 MW**
District heat:	**0.00 MJ/s**
Net. electrical effiency (LHV):	**42.56 %**
Net. thermal effiency (LHV):	**42.56 %**

Studstrupværket blok 4

Oxyfuel reference

"Tør CO_2 som PA luft"

VB 6a

Boilerload: 75.0 %

Departm: Proces Calculations
Initials: DENFI
Date: 22-08-2008
Draw nr:

Beregningsnr 38

Bar	kJ/kg
kg/s	°C

240.0 | 3302.4
214.5 | 535.0 — **HP steam**

34.5 | 3542.7
195.5 | 540.0 — **IP steam**

259.4 | 2546.7
201.4 | 402.1

259.4 | 2546.7
201.4 | 402.1

5.20 kg/s

7.34 kg/s

250.9 | 2711.4
209.3 | 413.2

479 °C

245.8 | 3042.534
214.5 | 467.7

35.5 | 3423.8
195.5 | 488.1

36.7 | 3181.7
195.5 | 383.6

37.1 | 3060.9
195.5 | 334.3

250.9 | 2771.2
202.0 | 420.7

254.2 | 2622.8
201.4 | 405.7

1037 °C — **OH 3**

895 °C — **OH 4**

785 °C — **MTOH 2A**

736 °C — **MOH 2B**

641 °C — **MOH 2C**

591 °C — **MOH 1A**

567 °C — **OH2AEX**

553 °C — **OH 2A**

0.58 kg/s

1110 °C

37.2 | 3000.7
195.5 | 311.0

528 °C — **OH 2B**

254.2 | 2618.3
201.96 | 405.3

IP spray

281.2 | 775.8
0.0 | 179.6

37.39 | 2923.89
195.50 | 283.51

283.5 °C

Cold IP steam

496 °C — **MOH 1B**

463 °C — **ECO**

360 °C

278.5 | 1068.0
214.5 | 245.7 — **Feed water**

275.6 | 1307.2
201.4 | 295.6

1

267.3 | 2319.5
201.38 | 394.7

HP steam output:	479.3 MJ/s
MT steam output:	121.0 MJ/s
Coal consumption LHV:	640.4 MJ/s
Loss due to unburn:	5.0 MJ/s
Heatloss from furnace:	2.7 MJ/s
Boiler effiency:	93.74 %

ASU

NAME	RATIO %	Flow kg/s
O2	0.950	51.6748
N2	0.020	0.9286
CO2	0.000	0
SO2	0.000	0
H2O	0.000	0
AR	0.031	2.07116
HCL	0.000	0
sum:	1.000	54.675
Molflow	1.6999	kmol/s

1.013
373.07 | 1271

O_2 = 3.10 % (wet)

λ = 1.20

O_2 heater

6.5 MJ/s

1.0
54.7 | 140.1

1.0
54.7 | 10.0

Burner

1
257.782 | 342.49

Slag 0.45 kg/s
Unburnt in slag 5.0 %

1.005
373.1 | 360.4

1.013
0 | 160.1

Røggasrecirkulationsblæser

Sammensætning

NAME	RATIO %	Flow kg/s
O2	0.031	10.473
N2	0.022	6.444
CO2	0.620	288.015
SO2	0.001	0.354
H2O	0.302	57.495
AR	0.024	10.144
HCL	0.000	0.153
sum:	1.000	373.077
Molflow	10.557	kmol/s

SA AIR

NAME	RATIO %	Flow kg/s
O2	0.030	7.084
N2	0.021	4.357
CO2	0.594	194.787
SO2	0.000	0.022
H2O	0.332	44.567
AR	0.023	6.860
HCL	0.000	0.103
sum:	1.000	257.781
Molflow	7.4516	kmol/s

1.02 | -
290.0 | 342.5

8.0 %
29.8 kg/s

1.005
373.07 | 360.39

PA lufo

NAME	RATIO %	Flow kg/s
O2	0.038	1.27529
N2	0.025	0.75107
CO2	0.744	34.4541
SO2	0.000	0.0058
H2O	0.163	3.09229
AR	0.029	1.21215
HCL	0.000	0.01321
sum:	1.000	40.804
Molflow	1.052	kmol/s

Relativ fugt
23.249 %

1 | -
40.8 | 90.0

Coal mill

Fuel

LHV = 25.165 MJ/kg
Coal = 25.447 kg/s
Pmill = 331 kW
Air/coal ratio= 1.50

COAL	MOLAR WEIGHT	WEIGHT PERCENT %	FLOW kg/s
C	12.01	63.62	20.92
H	1.01	4.20	1.38
S	32.06	0.64	0.21
N	14.01	1.60	0.53
O	16.00	7.10	2.33
Cl	35.45	0.14	0.05
ASH	-1.00	11.20	3.68
H2O	18.02	11.50	3.78
sum:	100	32.876	

LUFO

1.023 | -
319.9 | 83.9

122.0

O_2= 3.10 %-wet

1.000
402.9 | 160.1

1.020 | -
32.3 | 342.5

Fra udtag til CH3

1.9 | 2799.7
0.0 | 164.6

Damp LUFO

1.9 | 2799.7
0.0 | 164.6

Til FW Tank

O_2 heater

6.5 MJ/S

1.020 | -
5.9 | 10.0

1 | -
35.6 | 10.0

1
402.9 | 145.3

REA

1 | -
284.31 | 91.4

1 | -
41.5 | 10.0

Tør CO_2

DRY COAL	MOLAR WEIGHT	WEIGHT PERCENT %	FLOW kg/s
C	12.011	70.965	20.916
H	1.008	4.685	1.381
S	32.06	0.714	0.21
N	14.007	1.785	0.526
O	15.999	7.92	2.334
Cl	35.453	0.156	0.046
ASH	-1	12.493	3.682
H2O	18.015	1.283	0.378
sum:	100	29.474	

NAME	RATIO %	Flow kg/s
O2	0.044	1.386
N2	0.030	0.816
CO2	0.864	37.450
SO2	0.000	0.006
H2O	0.028	0.498
AR	0.034	1.318
HCL	0.000	0.014
sum:	1.000	41.489
Molflow	0.985	kmol/s

Critical proces figures		
Boiler load	75	%
MT temperatur	540	°C
Flame temperature Fur	1271	°C
Recirkulation %	76	%
O_2 in fluegas	3.10	%
Results		
Coal fired	640.4	MJ/s
Net elec. output	270.3	MW
O_2 production	31.5	MW
Result net power	238.8	MW
ETA net.	37.3	%

Studstrupværket blok 4

DONG energy

Kold røggas recirkulation 0.0 kg/s

75 % main boiler load

No district heating

VB 6b

Originale BBC varmebalancer, dvs ikke As-built!

Departm: Procesberegning
Initials: heive
Draw: C:\SSV-OXY-2010\k-oxy\[SSV4-OXYFUEL_REF_75%.xlsm]Turbine
Date: 03-01-2011
Printed 03-01 2011 09:51
Beregningsnr 38

Bar	kJ/kg
kg/s	°C

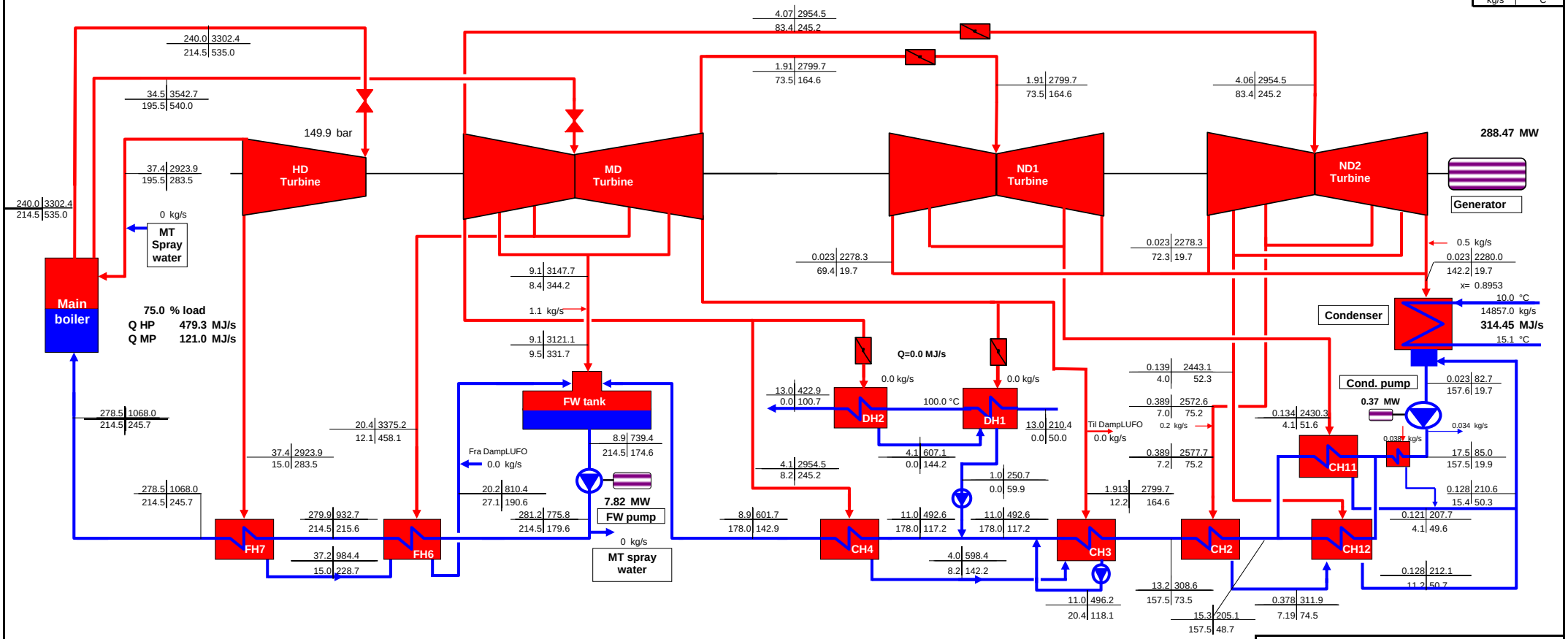

Coal consumption (LHV):	**640.37 MJ/s**
Boiler efficiency	**93.74 %**
Total consumption of fuel (LHV)	**640.37 MJ/s**
Gross power, ST	**288.47 MW**
Auxiliary power:	**18.19 MW**
Net. power:	**270.28 MW**
District heat:	**0.00 MJ/s**
Net. electrical effiency (LHV):	**42.21 %**
Net. thermal effiency (LHV):	**42.21 %**

Studstrupværket blok 4

Oxyfuel reference

"Tør CO_2 som PA luft"

VB 7a **Boilerload: 50.0 %**

Departm: Proces Calculations
Initials: DENFI
Date: 22-08-2008
Draw nr:

Beregningsnr 61

Bar	kJ/kg
kg/s	°C

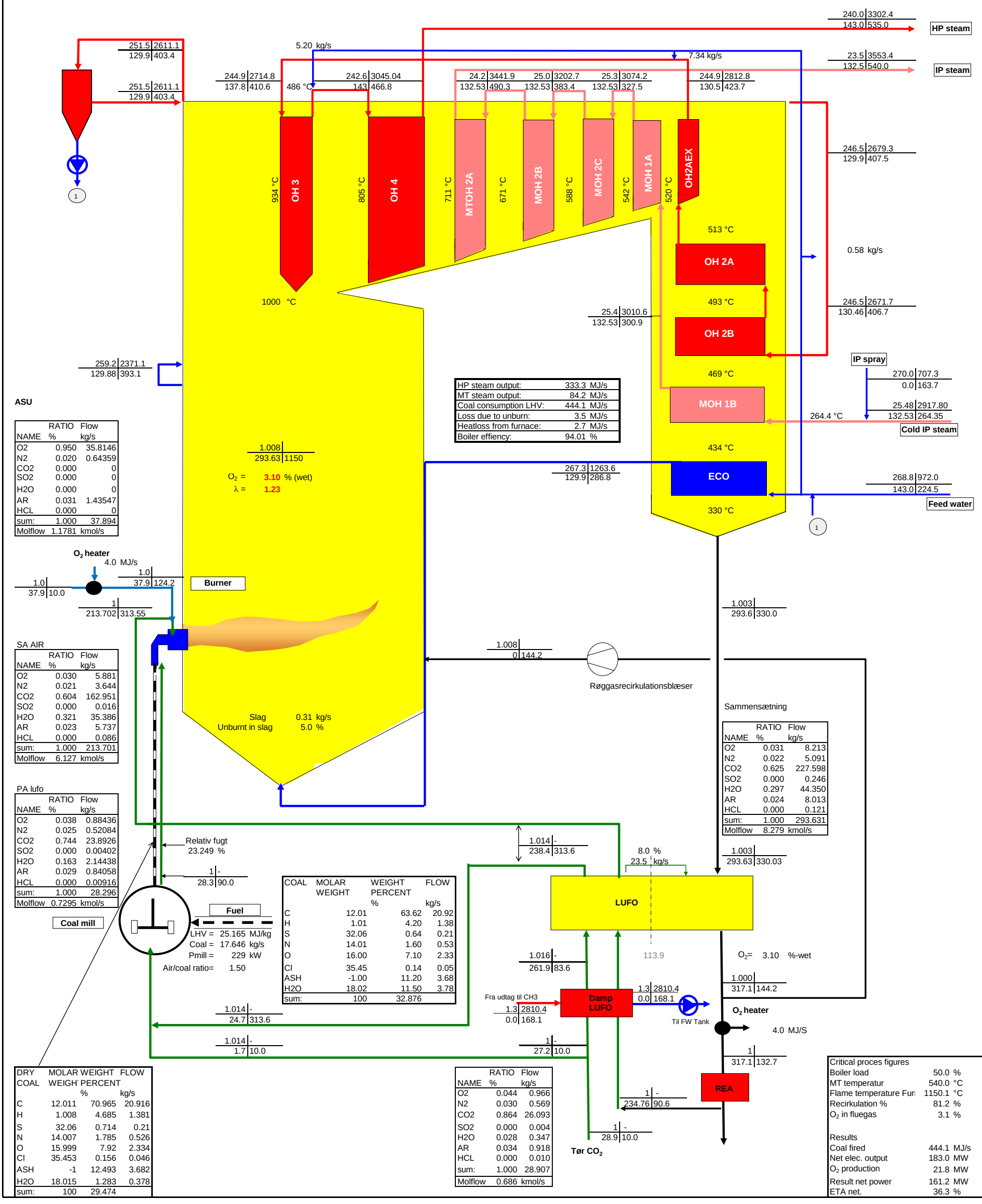

NAME	RATIO %	Flow kg/s
O2	0.950	35.8146
N2	0.020	0.64359
CO2	0.000	0
SO2	0.000	0
H2O	0.000	0
AR	0.031	1.43547
HCL	0.000	0
sum:	1.000	37.894
Molflow	1.1781	kmol/s

NAME	RATIO %	Flow kg/s
O2	0.030	5.881
N2	0.021	3.644
CO2	0.604	162.951
SO2	0.000	0.016
H2O	0.321	35.386
AR	0.023	5.737
HCL	0.000	0.086
sum:	1.000	213.701
Molflow	6.127	kmol/s

NAME	RATIO %	Flow kg/s
O2	0.038	0.88436
N2	0.025	0.52084
CO2	0.744	23.8926
SO2	0.000	0.00402
H2O	0.163	2.14438
AR	0.029	0.84058
HCL	0.000	0.00916
sum:	1.000	28.296
Molflow	0.7295	kmol/s

COAL	MOLAR WEIGHT	WEIGHT PERCENT %	FLOW kg/s
C	12.01	63.62	20.92
H	1.01	4.20	1.38
S	32.06	0.64	0.21
N	14.01	1.60	0.53
O	16.00	7.10	2.33
Cl	35.45	0.14	0.05
ASH	-1.00	11.20	3.68
H2O	18.02	11.50	3.78
sum:	100	32.876	

DRY COAL	MOLAR WEIGH	WEIGHT PERCENT %	FLOW kg/s
C	12.011	70.965	20.916
H	1.008	4.685	1.381
S	32.06	0.714	0.21
N	14.007	1.785	0.526
O	15.999	7.92	2.334
Cl	35.453	0.156	0.046
ASH	-1	12.493	3.682
H2O	18.015	1.283	0.378
sum:	100	29.474	

NAME	RATIO %	Flow kg/s
O2	0.044	0.966
N2	0.030	0.569
CO2	0.864	26.093
SO2	0.000	0.004
H2O	0.028	0.347
AR	0.034	0.918
HCL	0.000	0.010
sum:	1.000	28.907
Molflow	0.686	kmol/s

NAME	RATIO %	Flow kg/s
O2	0.031	8.213
N2	0.022	5.091
CO2	0.625	227.598
SO2	0.000	0.246
H2O	0.297	44.350
AR	0.024	8.013
HCL	0.000	0.121
sum:	1.000	293.631
Molflow	8.279	kmol/s

Critical proces figures		
Boiler load	50.0	%
MT temperatur	540.0	°C
Flame temperature Fur	1150.1	°C
Recirkulation %	81.2	%
O_2 in fluegas	3.1	%
Results		
Coal fired	444.1	MJ/s
Net elec. output	183.0	MW
O_2 production	21.8	MW
Result net power	161.2	MW
ETA net.	36.3	%

Studstrupværket blok 4

Kold røggas recirkulation 0.0 kg/s

50 % main boiler load

No district heating

VB 7b

Originale BBC varmebalancer, dvs ikke As-built!

Departm: Procesberegning
Initials: heive
Draw: C:\SSV-OXY-2010\k-oxy\[SSV4-OXYFUEL_REF_50%_ny.xlsm]Turbine
Date: 03-01-2011
Printed 03-01 2011 09:53
Beregningsnr 61

Bar	kJ/kg
kg/s	°C

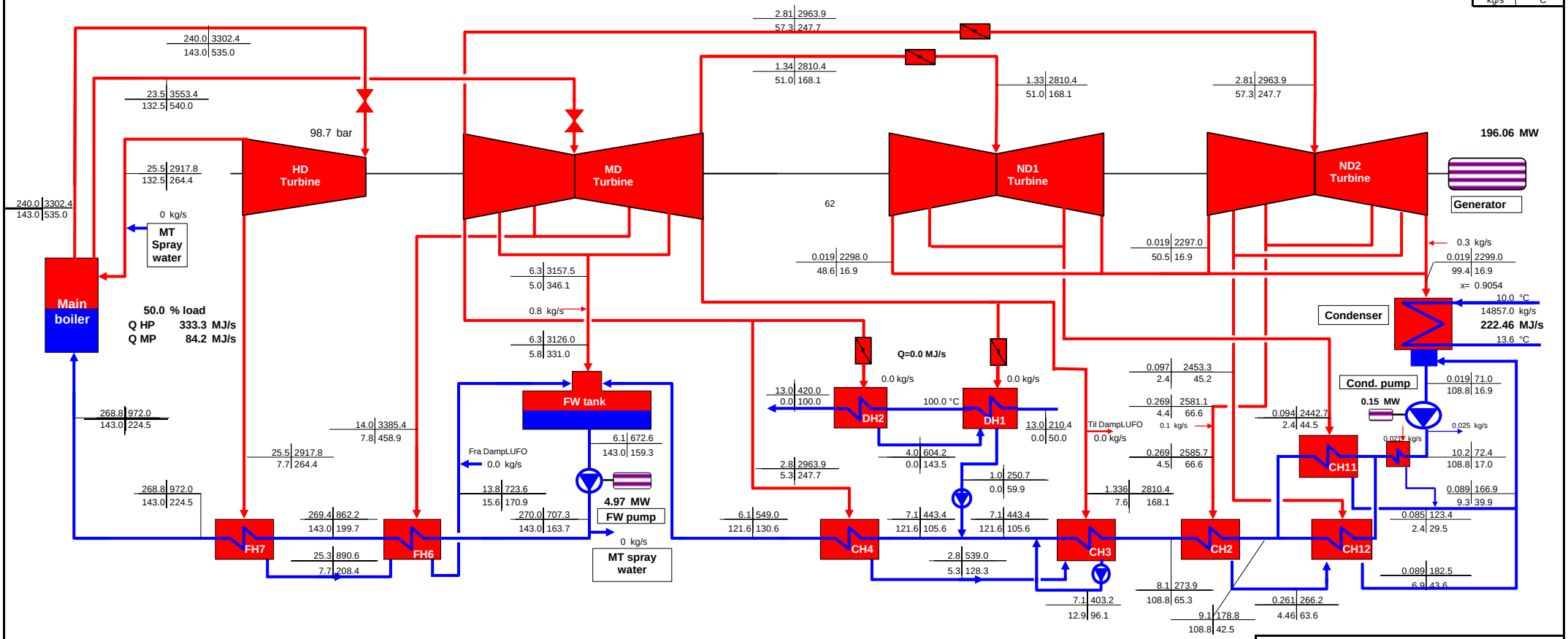

Coal consumption (LHV):	**444.06 MJ/s**
Boiler efficiency	**94.01 %**
Total consumption of fuel (LHV)	**444.06 MJ/s**
Gross power, ST	**196.06 MW**
Auxiliary power:	**13.01 MW**
Net. power:	**183.04 MW**
District heat:	**0.00 MJ/s**
Net. electrical effiency (LHV):	**41.22 %**
Net. thermal effiency (LHV):	**41.22 %**

Studstrupværket blok 4

Oxyfuel reference

"Tør CO_2 som PA luft"

Vb 8a

Boilerload: 35.3 %

Departm:	Proces Calculations
Initials:	DENFI
Date:	22-08-2008
Draw nr:	
Beregningsnr	84

Bar	kJ/kg
kg/s	°C

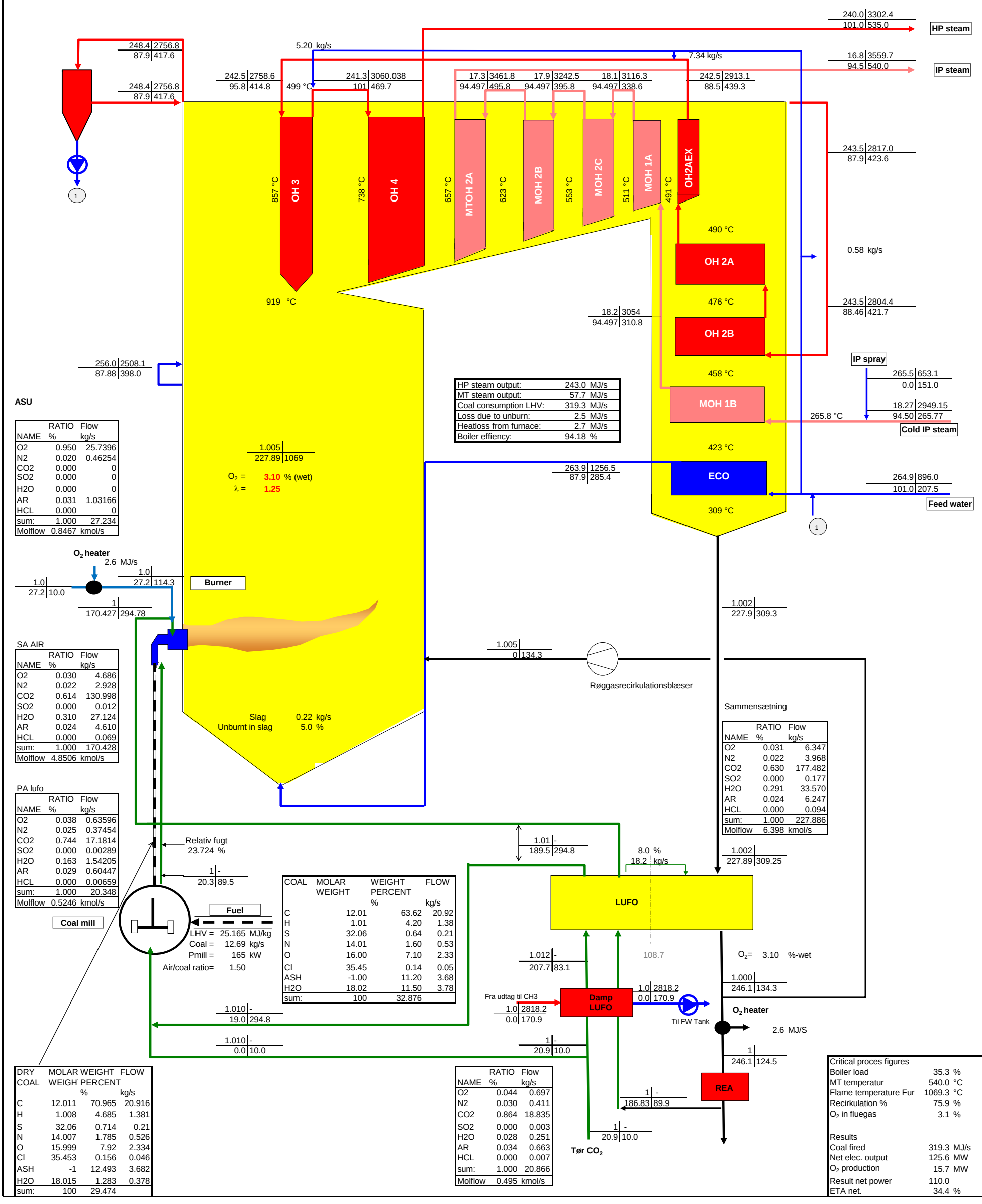

	RATIO	Flow
NAME	%	kg/s
O2	0.950	25.7396
N2	0.020	0.46254
CO2	0.000	0
SO2	0.000	0
H2O	0.000	0
AR	0.031	1.03166
HCL	0.000	0
sum:	1.000	27.234
Molflow	0.8467	kmol/s

	RATIO	Flow
NAME	%	kg/s
O2	0.030	4.686
N2	0.022	2.928
CO2	0.614	130.998
SO2	0.000	0.012
H2O	0.310	27.124
AR	0.024	4.610
HCL	0.000	0.069
sum:	1.000	170.428
Molflow	4.8506	kmol/s

	RATIO	Flow
NAME	%	kg/s
O2	0.038	0.63596
N2	0.025	0.37454
CO2	0.744	17.1814
SO2	0.000	0.00289
H2O	0.163	1.54205
AR	0.029	0.60447
HCL	0.000	0.00659
sum:	1.000	20.348
Molflow	0.5246	kmol/s

COAL	MOLAR WEIGHT	WEIGHT PERCENT %	FLOW kg/s
C	12.01	63.62	20.92
H	1.01	4.20	1.38
S	32.06	0.64	0.21
N	14.01	1.60	0.53
O	16.00	7.10	2.33
Cl	35.45	0.14	0.05
ASH	-1.00	11.20	3.68
H2O	18.02	11.50	3.78
sum:	100	32.876	

DRY COAL	MOLAR WEIGHT	WEIGHT PERCENT %	FLOW kg/s
C	12.011	70.965	20.916
H	1.008	4.685	1.381
S	32.06	0.714	0.21
N	14.007	1.785	0.526
O	15.999	7.92	2.334
Cl	35.453	0.156	0.046
ASH	-1	12.493	3.682
H2O	18.015	1.283	0.378
sum:	100	29.474	

	RATIO	Flow
NAME	%	kg/s
O2	0.044	0.697
N2	0.030	0.411
CO2	0.864	18.835
SO2	0.000	0.003
H2O	0.028	0.251
AR	0.034	0.663
HCL	0.000	0.007
sum:	1.000	20.866
Molflow	0.495	kmol/s

NAME	RATIO %	Flow kg/s
O2	0.031	6.347
N2	0.022	3.968
CO2	0.630	177.482
SO2	0.000	0.177
H2O	0.291	33.570
AR	0.024	6.247
HCL	0.000	0.094
sum:	1.000	227.886
Molflow	6.398	kmol/s

Critical proces figures		
Boiler load	35.3	%
MT temperatur	540.0	°C
Flame temperature Fur	1069.3	°C
Recirkulation %	75.9	%
O_2 in fluegas	3.1	%
Results		
Coal fired	319.3	MJ/s
Net elec. output	125.6	MW
O_2 production	15.7	MW
Result net power	110.0	
ETA net.	34.4	%

Studstrupværket blok 4

DONG energy

Kold røggas recirkulation 0.0 kg/s

VB 8b

35 % main boiler load

No district heating

Originale BBC varmebalancer, dvs ikke As-built!

Departm: Procesberegning
Initials: heive
Draw: C:\SSV-OXY-2010\k-oxy\[SSV4-OXYFUEL_REF_35%.xlsm]Turbine
Date: 03-01-2011
Printed 03-01 2011 10:03
Beregningsnr 84

Bar	kJ/kg
kg/s	°C

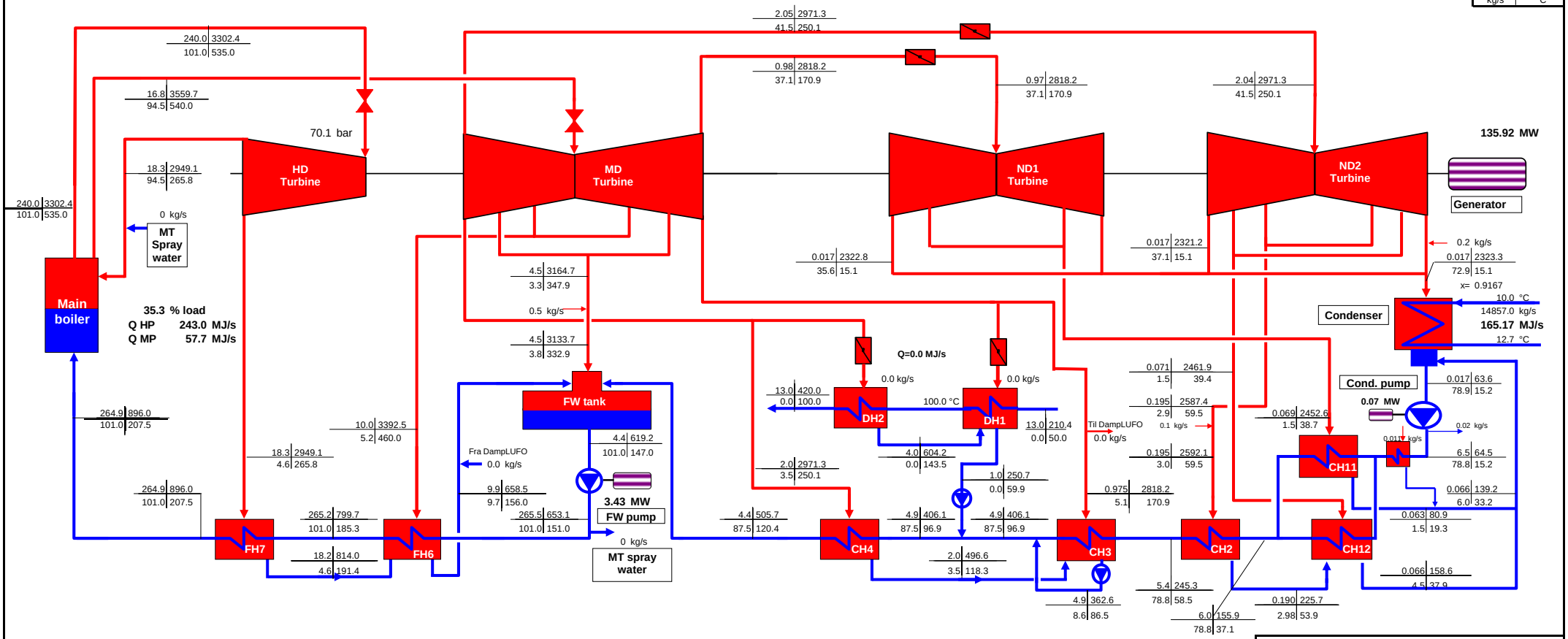

Coal consumption (LHV):	**319.33 MJ/s**
Boiler efficiency	**94.18 %**
Total consumption of fuel (LHV)	**319.33 MJ/s**
Gross power, ST	**135.92 MW**
Auxiliary power:	**10.29 MW**
Net. power:	**125.64 MW**
District heat:	**0.00 MJ/s**
Net. electrical effiency (LHV):	**39.34 %**
Net. thermal effiency (LHV):	**39.34 %**

Studstrupværket blok 4

Oxyfuel varm recirkulation 100% last

"Tør CO_2 som PA luft"

Boilerload: 100.0 %

Departm: Proces Calculations
Initials: DENFI
Date: 01-12-2010
Draw nr:

Beregningsnr 32

Bar	kJ/kg
kg/s	°C

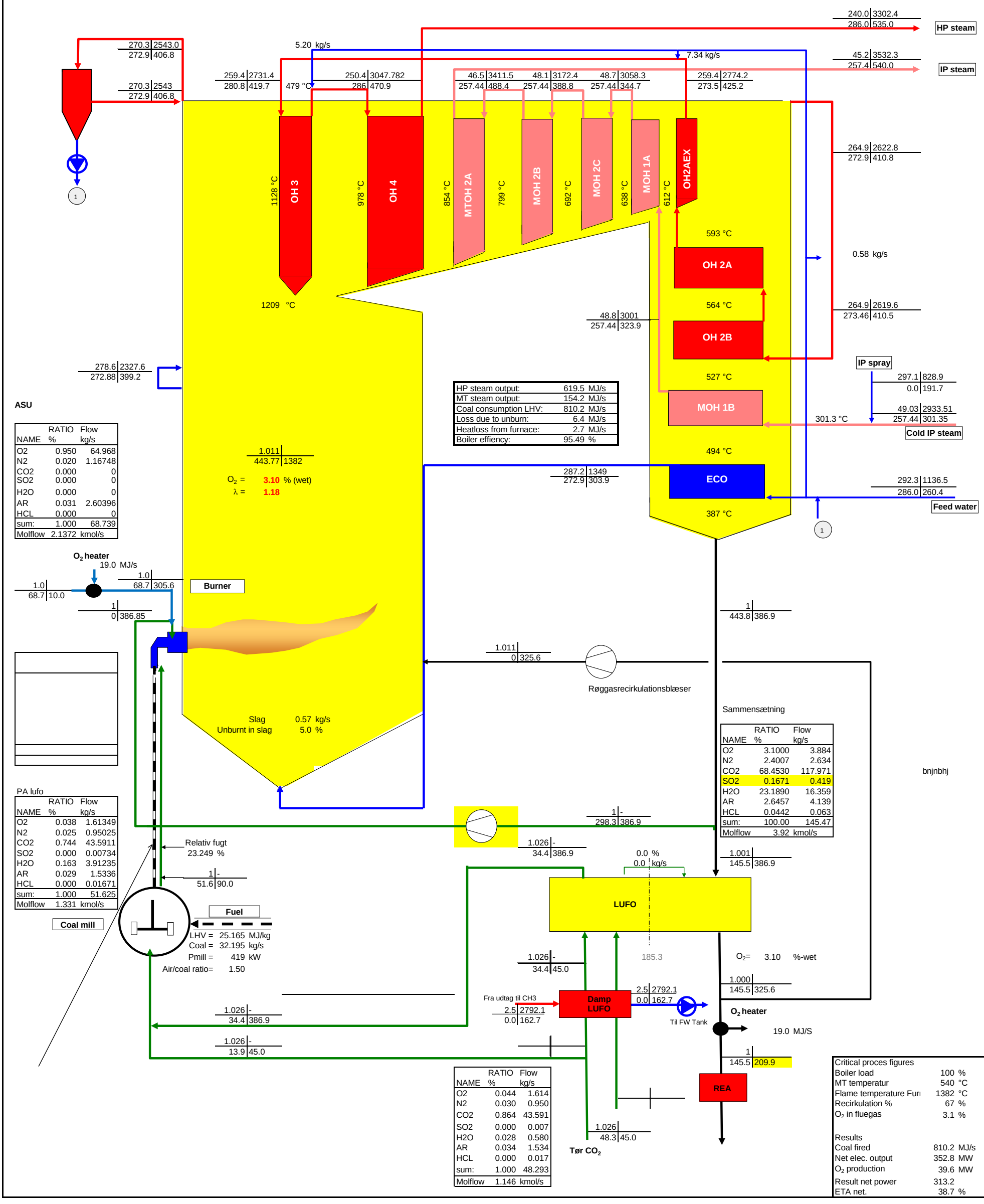

Studstrupværket blok 4

DONG energy

Kold røggas recirkulation 0.0 kg/s

100 % main boiler load

No district heating

VB 10b

Originale BBC varmebalancer, dvs ikke As-built!

Departm: Procesberegning
Initials: heive
Draw: C:\SSV-OXY-2010\Varm-reci\[SSV4-OXYFUEL_vreci.xlsm]Turbine
Date: 03-01-2011
Printed 03-01 2011 10:09
Beregningsnr 32

Bar	kJ/kg
kg/s	°C

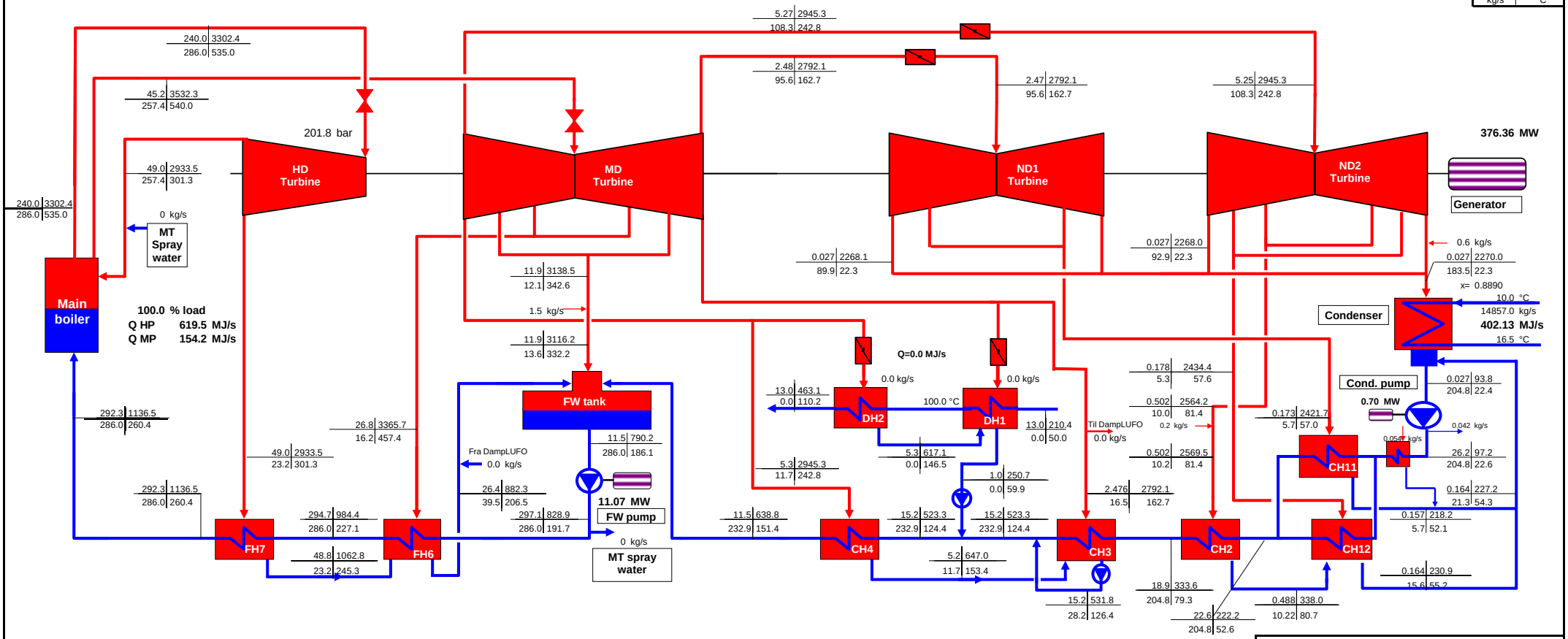

Coal consumption (LHV):	**810.18 MJ/s**
Boiler efficiency	**95.49 %**
Total consumption of fuel (LHV)	**810.18 MJ/s**
Gross power, ST	**376.36 MW**
Auxiliary power:	**23.54 MW**
Net. power:	**352.82 MW**
District heat:	**0.00 MJ/s**
Net. electrical effiency (LHV):	**43.55 %**
Net. thermal effiency (LHV):	**43.55 %**

DONG energy

PSO7171.

OxyFuel Combustion for below zero CO_2 emission

CFD report

Prepared Kim Granly Hansen, March 22, 2011
Review Søren Lovmand Hvid

Project no. 3-00047

DONG energy

Contents

DONG energy

CHAPTER 1

Introduction

As a part of the CO_2 strategy of Dong Energy, different methods of capturing CO_2 have been investigated within Dong Energy. The present report is a part of a study to determine whether a retrofit of an existing Benson type boiler to oxy-fuel combustion is a feasible way to reduce CO_2 emissions.

The main part of the study is performed using an in-house heat and mass balance calculator, MOPEDS, see Fisker (2010). Calculations are done for different boiler loads for conventional combustion of coal in atmospheric air. Calculations are then performed at oxyfuel conditions, to investigate any changes in the heat uptake within the boiler. Special emphasis is given to flue gas recirculation and reheater temperature levels. The main results from the 100 % load case can be seen in Figure 1.1 on the following page, for more details see Fisker (2010).

Since the models in MOPEDS are zero-dimensional, CFD is used to validate the models. It is expected that the better representation of the real boiler geometry in a CFD model will give better results for radiant heat transfer in the furnace.

1.1 Scope of the work

Calculations of the SSV4 boiler at conventional air combustion will be performed. The model will be calibrated to match the heat uptake in the furnace known from process calculations and operation of the plant. After calibration has been completed, calculations will be performed at oxyfuel conditions. These calculations will then be compared to MOPEDS calculations for Oxyfuel. As a part of the work, a sensitivity check of the particle model is performed.

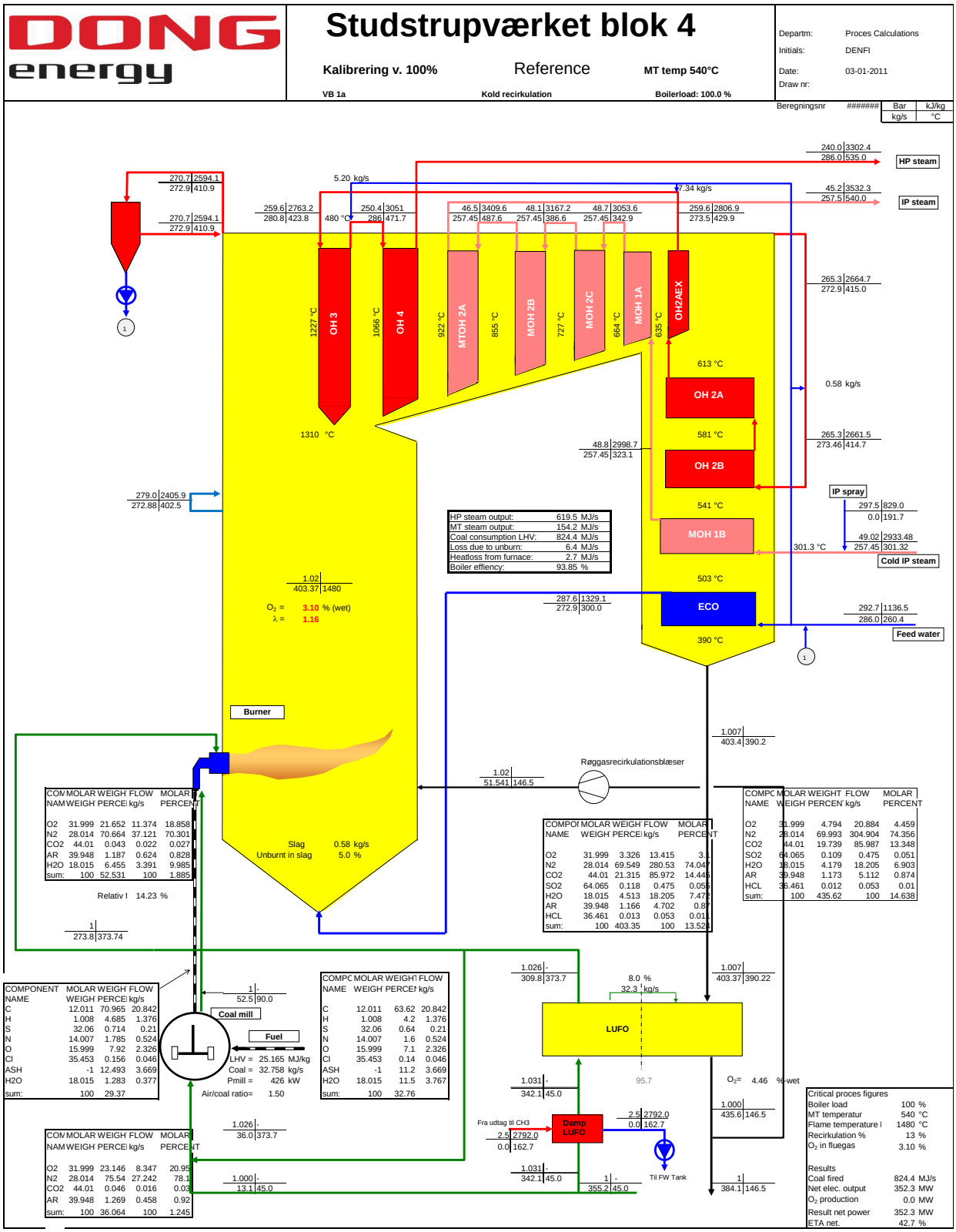

Figure 1.1: The overall results from the MOPEDS air-calculation

DONG energy

CHAPTER 2

Numerical Model

The concept of CFD is to solve a set of equations to describe the conservation of mass, momentum and energy. The type of equations solved can be illustrated by the general transport equation:

$$\underbrace{\frac{\partial}{\partial t}(\rho\phi)}_{\text{Acc}} + \underbrace{\frac{\partial}{\partial x_i}(\rho U_i \phi)}_{\text{Convection}} = \underbrace{\frac{\partial}{\partial x_i}\left(\Gamma \frac{\partial \phi}{\partial x_i}\right)}_{\text{Diffusion}} + \underbrace{S_\phi}_{\text{Source}} \tag{2.1}$$

where

ρ	is density
ϕ	is the transported quantity
U_i	is the i-directed velocity component
Γ	is the diffusion coefficient
S_ϕ	is Source term

2.1 Combustion reaction model

The chemical reaction is modelled by solving an additional set of transport equations for the species involved in reaction. The transport equation for each mass fraction of species i, Y_i, is of the form:

$$\underbrace{\frac{\partial}{\partial t}(\rho Y_i)}_{\text{Acc}} + \underbrace{\frac{\partial}{\partial x_i}(\rho U_i Y_i)}_{\text{Convection}} = \underbrace{\frac{\partial}{\partial x_i}\left[\left(\rho D_{i,m} + \frac{\mu_t}{\text{Sc}_t}\right)\frac{\partial Y_i}{\partial x_i}\right]}_{\text{Diffusion}} + \underbrace{R_i + S_i}_{\text{Source}} \tag{2.2}$$

where

$D_{i,m}$	is the laminar diffusion coefficient of species i.
μ_t	is the turbulent viscosity
Sc_t	is the turbulent Schmidt number

The first term is zero as the model is steady state and the next two are due to convective flow and diffusion respectively. The source term can be divided into two parts; the rate of production of species i, R_i, from chemical reaction and the rate of creation of species i, S_i, stemming from e.g. a dispersed phase like devolatilization or char burnout from coal.

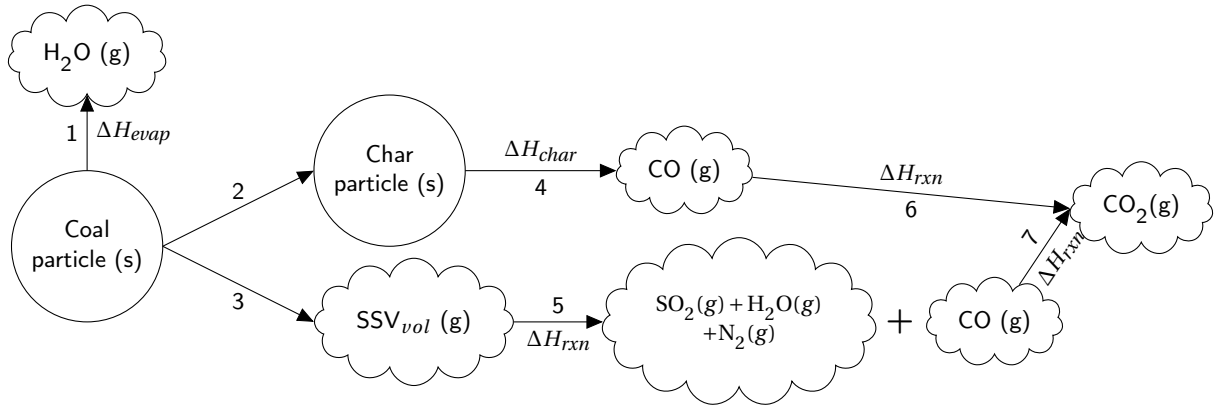

Figure 2.1: Illustration of coal combustion as it is modelled. The DPM setup results in a total of 3 source terms. From the coal particles there will be: a H_2O, a volatile (SSV_{vol}) and a CO source term to the continuous phase.

2.2 Discrete phase model

The modelling of coal combustion consists of a number of steps. An illustration of the coal combustion setup used in the model is shown in Figure 2.1. The first four steps in the figure are defined as input to the DPM model setup. The last three steps (5 to 7) are gaseous reactions specified for the continuous gas phase.

2.2.1 Euler-Lagrange model

Modelling of coal combustion is done using the Discrete Phase Model, DPM, in Fluent. The model follows an Euler-Lagrange approach where the gas phase is modelled as a continuous phase solving the Reynolds-averaged Navier-Stokes equations. The coal is modelled by a representative number of discrete particles that are tracked through the computational domain using a Lagrangian model. The two phases are coupled and interchange momentum, heat and mass, see Figure 2.2 on the facing page

The two phases are solved sequentially. The particles are injected into a fixed continuous field. The particles are tracked through the entire domain and release species and exchange heat and momentum. This will yield a source field from the discrete phase. In order to take turbulence into account a discrete random walk model is used with a Gaussian velocity distribution. Then new iterations are performed on the continuous field. particles are then again injected into a fixed continuous field etc. This continues until the overall residuals are below a given threshold and selected monitoring values level out. This is then defined as a converged solution.

Since only a representative number of particles are tracked, it is of critical importance that the distribution of the particles is representative for a real coal mixture. Previous simulations have shown that for the SSV4 boiler 6×10^5 particles give good results. In order to test the sensitivity of the model to the particle field, a number of simulations are performed where the entire particle source field in a converged solution is replaced by a new one. Iterations are then continued until a new converged solution is obtained. Such an investigation will also support evaluating the changes inside the boiler after shifting from air to oxy-fuel combustion.

The particles are modelled using the FLUENT spherical particle model together with the Rosin-Rammler size distribution with parameters as in Table 2.1 on the next page. These size parameters are defined as part of an “injection”.

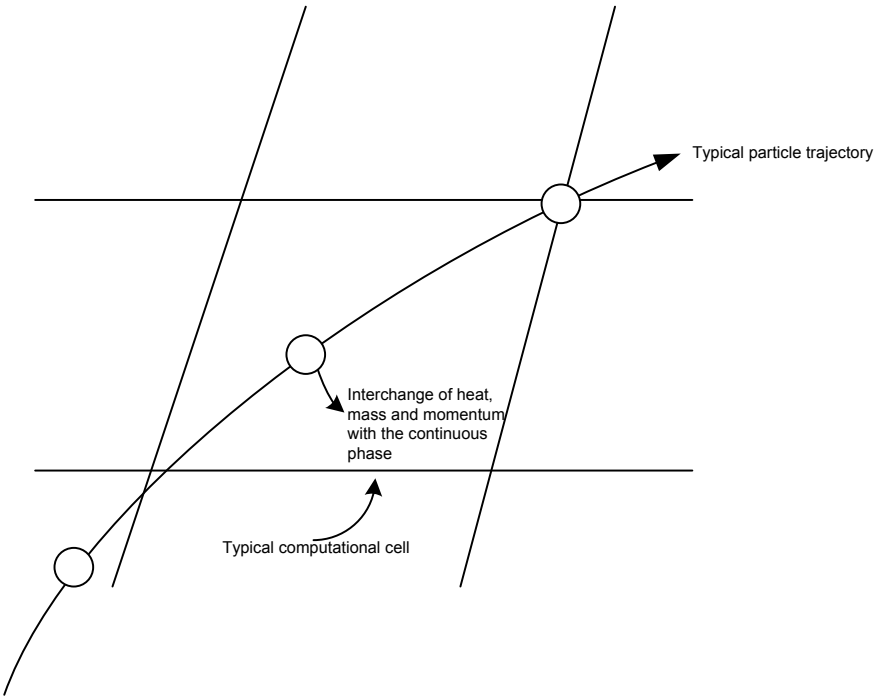

Figure 2.2: Sketch of a particle passing through a computational domain

Table 2.1: Rosin-Rammler size distribution parameters used for coal particles.

Particle type	**Min. diameter** [m]	**Max. diameter** [m]	**Mean diameter** [m]
Coal	$4 \cdot 10^{-6}$	$1.6 \cdot 10^{-4}$	$5 \cdot 10^{-5}$

2.2.2 Devolatilization and char burn out

The composition of the coal mixture is based on known data. This is converted into the input needed in the DPM, taking into account the water evaporated from coal. Data are shown in Table 2.2.

Table 2.2: Composition of the coal mixture and the straw used during the testing. Values based on "Coal database".

Comp	**Coal Mixture** (after mill, 90% H_2O evap.)	
	Dry wt %	DAF wt %
C	-	83.5319
H	-	4.5936
S	-	0.6950
N	-	2.1247
O	-	9.0548
Ash	14.38	-
Volatile	26.93	-
Fixed Carbon	58.69	-

The injection defines the properties of the particles released from a number of inlet surfaces. As shown

in Figure 2.1 on page 6 the species formed during devolatilization is an artificial gas phase species. The artificial species is afterwards "combusted" to form the normal combustion products. Including an artificial species simplifies the modelling of coal combustion. The composition of the artificial species is based on the assumption that the volatile fraction consists of all of the H, N, O and S in the particle and then some C. The model char is thereby solely C. This is a simplification as some of the N normally is bound to the char and released during char burnout, Pedersen (2009).

For oxyfuel combustion the devolatilization rate is modelled in the same way as for the air combustion. Brix et al. (2010) have reported that the devolatilization process is not significantly influenced by a shift from air to oxy-fuel combustion.

During real char burnout a mixture of CO and CO_2 is formed. To simplify the model only CO will be formed at char burnout and the CO will react further in the gas phase reactions. The DPM and the continuous phase model interact with respect to both energy and mass transfer. The DPM setup results in a total of three source terms. From the coal particles there will be: a H_2O, a volatile (SSV_{vol}) and a CO source term to the continuous phase.

The char burnout is modelled as diffusion limited, i.e. the rate of burnout is limited by the diffusion rate of oxygen in N_2 in the air case. For the oxyfuel case the burnout will be limited by the diffusion of oxygen in CO_2. This assumption has been verified experimentally by Brix et al. (2010)

2.3 Gas phase reaction setup

The combustion reaction of coal and straw is modelled as a two-step-global reaction mechanism as shown below.

$$SSV_{vol} + \left(\frac{a}{2} + \frac{b}{4} + c - \frac{e}{2}\right)O_2 \rightarrow a\mathrm{CO} + \frac{b}{2}H_2O + c\mathrm{SO}_2 + \frac{d}{2}N_2 \tag{2.3}$$

$$\mathrm{CO} + \frac{1}{2}O_2 \rightarrow \mathrm{CO}_2 \tag{2.4}$$

where

SSV_{vol} is given by $C_aH_bS_cN_dO_e$

The gas phase reaction rates are modelled using the finite-rate/eddy dissipation (FR/ED) model setup in FLUENT. In using this method it is possible to account for both conditions where a given reaction is kinetically limited and where it is mixing controlled. In turbulent combustion flames the reactions are often mixing controlled.

The kinetic controlling rates of reaction expressed below are of Arrhenius type, and the Arrhenius parameters are shown in Table 2.3 on the facing page.

$$r_i^f = k_i^f(T)[SSV_{vol}][O_2] \tag{2.5}$$

$$r_{ii}^f = k_{ii}^f(T)[\mathrm{CO}][O_2]^{\frac{1}{4}} \tag{2.6}$$

Table 2.3: The Arrhenius rate constant applied.

Reaction	Rate constant	A	B	E
(i)	k_i^f	$5.012 \cdot 10^{11}$	0	1
(ii)	k_{ii}^f	$2.239 \cdot 10^{12}$	0	$1.7 \cdot 10^8$

The eddy dissipation model relates the reaction rate to the dissipation rate of the turbulent eddies containing reactants or products.

$$r_r^{ED} = A\rho\frac{\epsilon}{\kappa}\underbrace{\min}_{R}\left(\frac{Y_R}{\nu'_{R,i}M_{w,R}}\right) \tag{2.7}$$

$$r_r^{ED} = A\rho\frac{\epsilon}{\kappa}B\left(\frac{\sum_p Y_p}{\sum_j^N \nu''_{j,r}M_{w,j}}\right) \tag{2.8}$$

The first expression is the reaction rate as a function of the eddies containing reactants and the second is a function of the product containing eddies. A and B are empirical constants. In this case A = 0.6 and B = 0.5. The FR/ED model will always assume the governing reaction rate to be the smallest of either the Arrhenius expression or one of the two mixing rates for the given reaction.

The governing parameter in the rate expressions is the large-eddy mixing scale, ℓ:

$$\ell = \frac{\kappa}{\varepsilon} \tag{2.9}$$

where

- κ is the turbulent kinetic energy
- ε is the turbulent dissipation rate

The radiation model applied is the DO radiation model by Chui and Raithby (1990), Raithby and Chui (1993), implemented in the Fluent CFD code. Likewise, turbulence closure has been modelled using the realizable variant of the κ-ε two-equation turbulence model, Shih et al. (1995) as implemented in the Fluent CFD code.

DONG energy

CHAPTER 3

Model setup

The simulations are performed using a 3D CFD model of the boiler. An overview of the geometry is shown in Figure 3.1 The boiler at SSV consists of 24 burners divided into four rows placed on the back (east) and front (west) of the boiler. The figure also shows the heaters inside the boiler.

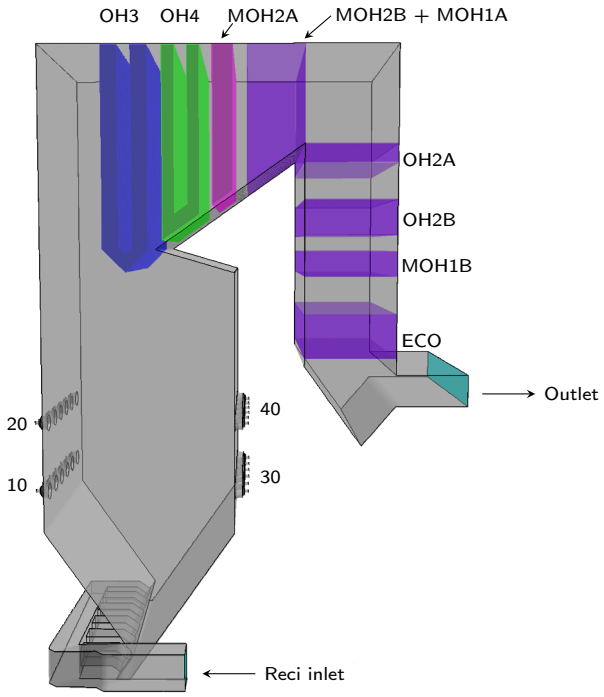

Figure 3.1: Overview of the boiler geometry. Numbers 10 to 40 refer to the four burner rows. 10 and 20 are located at the front (west) and 30 and 40 on the back (east) of the boiler. The heaters are also shown.

3.1 Heat flux setup

The heaters in the boiler have been modelled in two different ways. The first three superheaters (OH3, OH4 and MOH2A) are geometrically a part of the model defined as a set of thin plates (walls) inside the furnace to simulate the heater pipes. This is illustrated in Figure 3.2 where each colour represents one of the heaters. The heater plates are given a set of constant wall properties simulating the heater pipes. The wall temperature boundary condition is not the external pipe wall temperature but the temperature of the steam on the inside of the pipes supplemented by the thermal resistance of the pipe wall, The temperature profile is illustrated on Figure 3.3 on the next page. This means that the gas properties, especially temperature, will affect the heat flux to the heaters. The wall properties in terms of the thermal resistance are set according to known data and adjusted to fit the expected heat flux to the different heaters.

The successive heaters (including the economizer) are defined by five different volumes. The heat transfer in each of these volumes is modelled by a Source term (sink) accounting for the heat removed in the given heat exchanger. In this way the heat flux from the volume is constant and determines the temperature decrease of the flue gas as it passes the heater.

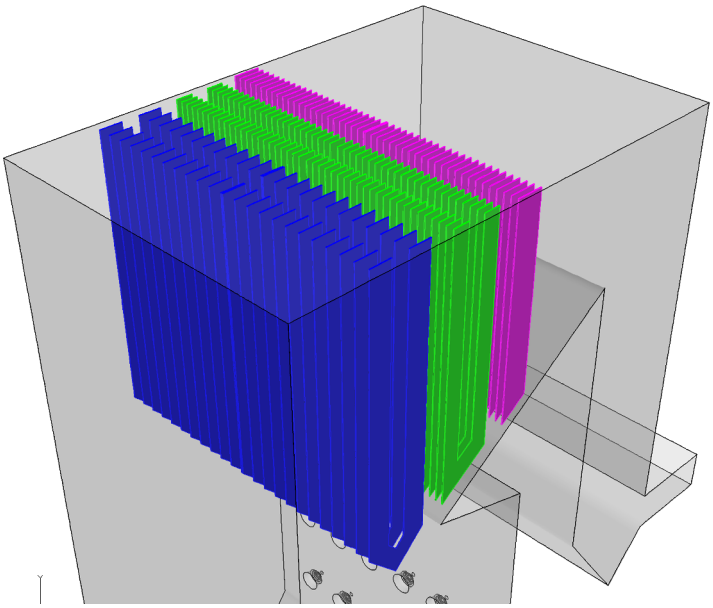

Figure 3.2: Closer look at the heaters OH3 (blue), OH4 (green) and MOH2A (pink).

The evaporator pipes are located all the way along the boiler's walls from below the burners and up to the furnace top. The heat flux to the evaporator is modelled in the same way as the first three heaters by defined wall properties and thereby letting the local temperature difference determine the heat flux. The wall temperature changes going from water to superheated steam and the temperature is defined by a user-defined profile varying only in the Y direction.

3.2 Inlet Setup

The geometry of a burner row is shown in Figure 3.4 on page 13. The row shown is row 40, which differs from the others because of the straw inlet at the centre of the four middle burners. To simplify the CFD model, the burner itself is not modelled in detail but consists of a set of inlet boundaries. The inner

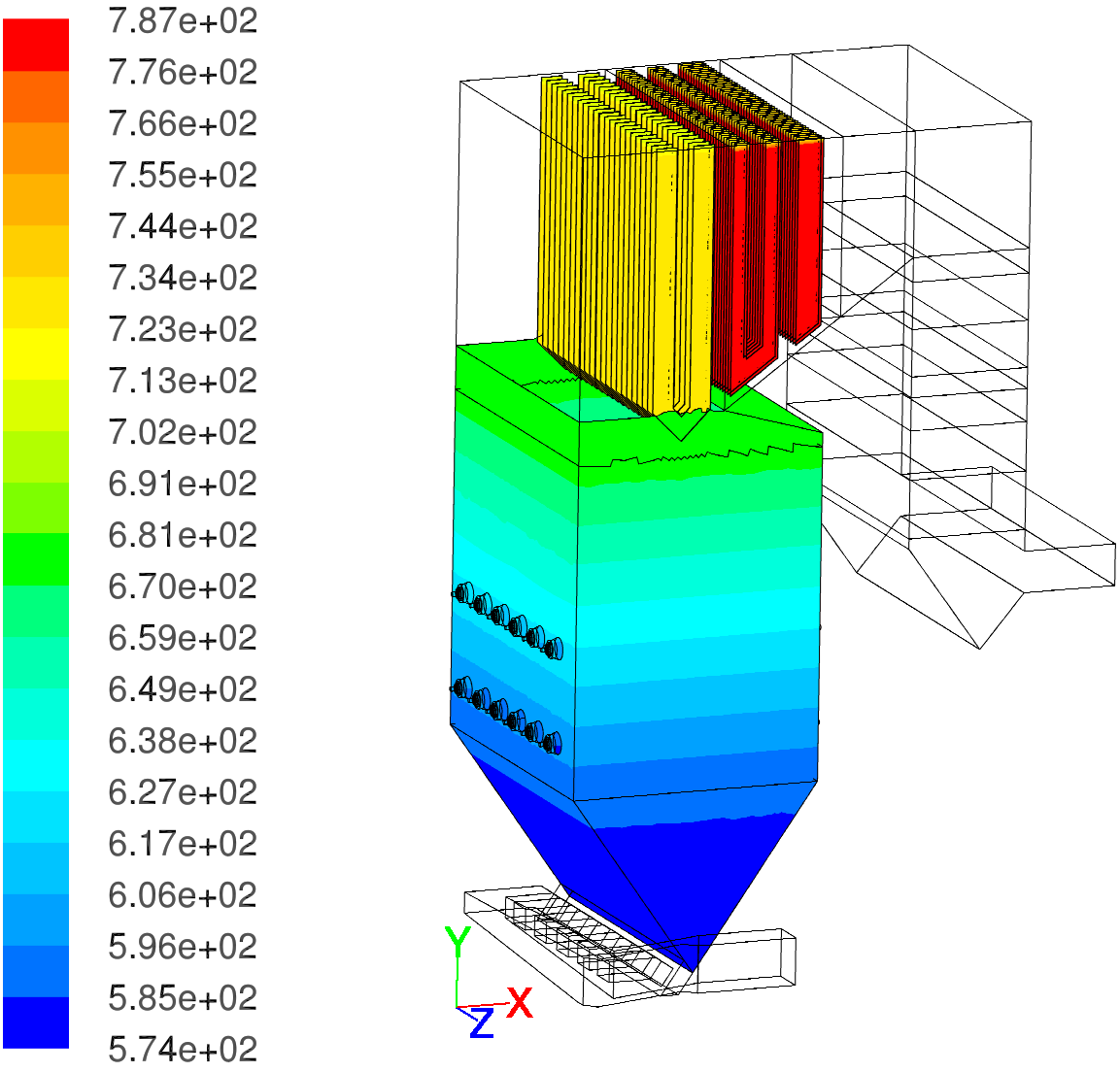

Figure 3.3: Illustration of the temperature (K) profile on the steam side in the SSV4 boiler model.

annulus (green colour) is the coal and primary air inlet. The two outer annuli are the secondary and tertiary air inlets respectively.

The CFD setup of the SSV boiler can be divided into two coupled phases; the continuous phase, which is the gas phase and the discrete phase being the particles. The following describes the inlet conditions of the continuous phase. Table 3.1 on the next page shows the input data for the calibration case, and Table 3.2 on the facing page shows the inlet conditions for the oxyfuel case. Note that the inlet conditions for the oxy-fuel case are based on the process coupling chosen in the MOPEDS calculations.

Some of the species from the MOPEDS calculations are omitted in the CFD calculations, i.e. SO_2 and Ar. These species are lumped into the mass fraction of the dominating inert species for the two cases, i.e. N_2 for the air case and CO_2 for the oxyfuel case. The species are of minor importance to the evaluation of the heat fluxes within the boiler, and leaving them out of the model will reduce the number of transport eqautions to be solved, and hence save computational time.

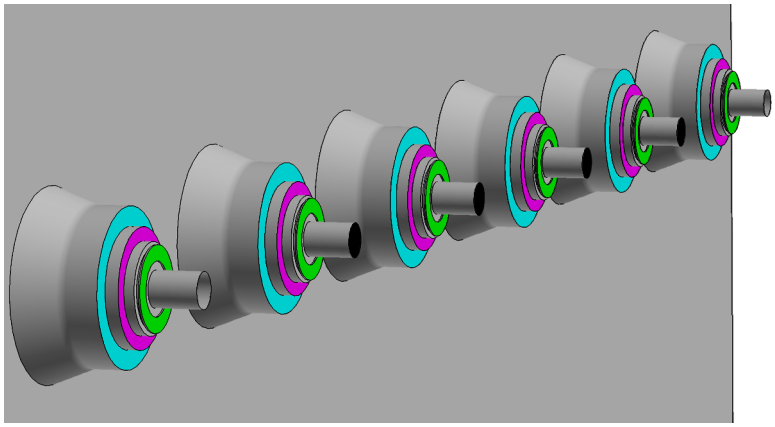

Figure 3.4: Illustration of burner row 40. Green colour is primary air and coal inlet, pink is secondary air and light blue tertiary air inlet.

Table 3.1: Inlet boundary conditions for the calibration case. Data is given for one burner.

Inlet Name	**Flow**	**Temp** [K]	**mass % (Excl. N_2)**		
			O_2	CO_2	H_2O
Primary air	2.2 kg/s	363	21.3	-	7.387
Secondary air	Ax: 25.4 m/s Tan: 30.8 m/s	646	23.0	-	0.006
Tertiary air	Ax: 55.4 m/s Tan: 88 m/s				
Recirc. flue gas	51.494 kg/s	419.65	4.794	19.739	4.179

Table 3.2: Inlet boundary conditions for the oxyfuel case. Data is given for one burner.

Inlet Name	**Flow**	**Temp** [K]	**mass % (Excl. CO_2)**		
			O_2	N_2	H_2O
Primary air	2.2 kg/s	363	3.13	4.86	7.58
Secondary air	Ax: 26.95 m/s Tan: 32.66 m/s	606.4	20.88	4.59	14.34
Tertiary air	Ax: 58.78 m/s Tan: 93.36 m/s				
Recirc. flue gas	0.5 kg/s	419.65	2.813	4.48	15.6

Apart from the overall investigation of the effects from shifting from air to oxy-fuel combustion, a calculation is performed where the oxygen levels in the burner are varied. More oxygen is added in the secondary air inlet and less is added in the tertiary inlet keeping the total amount of oxygen constant, see Table 3.3 on the next page.

3.3 Primary air

The primary air is used to transport the pulverized coal to the six burners connected to each mill, and it is assumed that 90 % of the water in the coal is evaporated into the air stream before coal and air reach the boiler. The composition of primary air used in the model is calculated based on plant data and coal

Table 3.3: Inlet boundary conditions for the oxyfuel case with oxygen staging. Data is given for one burner.

Inlet Name	**Flow**	**Temp** [K]	**mass % (Excl. CO_2)**		
			O_2	N_2	H_2O
Primary air	2.2 kg/s	363	3.13	4.86	7.58
Secondary air	Ax: 26.95 m/s Tan: 32.66 m/s	606.4	30.88	4.01	12.53
Tertiary air	Ax: 58.78 m/s Tan: 93.36 m/s	606.4	18.4	4.73	14.8
Recirc. flue gas	0.5 kg/s	419.65	2.813	4.48	15.6

composition.

3.4 Secondary and tertiary air

The secondary and tertiary air inlets are induced by swirl to stabilize the flame. In the model swirl is introduced by setting the axial and tangential velocity components for the secondary and tertiary inlets respectively. The swirl is set to a constant relation between tangential and axial velocity components for each of the two air inlets based on former simulations of the SSV burner. Furthermore, the air supply is only known as a sum of secondary and tertiary air to each burner, and the split between the two streams is also based on these former burner simulations.

The swirl is induced in alternating directions as illustrated in Figure 3.5. The swirl direction of the two air inlets is the same at a specific burner. The figure shows rows 30 and 40 at the back (east) side of the boiler. The same pattern is valid at the front side burners (rows 10 and 20).

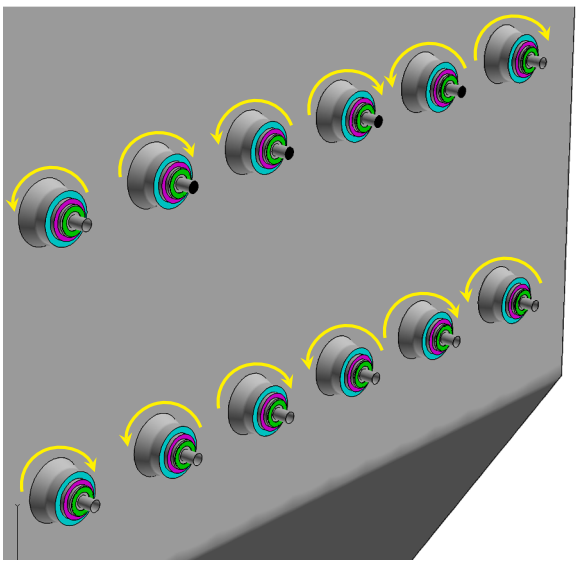

Figure 3.5: Illustration of burner row 40 (top) and row 30 (bottom). The geometry is a zoom-in at the back (east) side of the boiler. Yellow arrows indicate swirl direction at the specific burner. Secondary and tertiary inlets at the same burner are swirled in the same direction.

3.5 case overview

A total of 8 simulations are performed, see Table 3.4. The first case is a calibration case where the heat uptake in the furnace is matched to known data. The calibration is mainly performed by altering boundary properties for the boiler wall. Three separate cases based on the first simulations are then performed to estimate the model variation with a new particle source field. For one of these three cases the particle field is again changed.

Table 3.4: Overview of the simualtion cases

Case no.	**Description**
1	Calibration run with air
2	New run with changed particle source field. Based on 1
3	New run with changed particle source field. Based on 1
4	New run with changed particle source field. Based on 1
5	New run with changed particle source field Based on 3
Oxy-1	Run until monitoring points “level out”
Oxy-2	New run with changed particle source field based on Oxy-1
Oxy-3	Staging in the oxygen concentration

A first oxy-fuel calculation, Oxy-1, is then performed based on case 1, using the boundary conditions described in Table 3.2 on page 13. A new Oxyfuel calculation is then carried out with a new particle source field to check if the solution from Oxy-1 can be reproduced with a new source field.

Finally a simulation is performed where the oxygen concentration is varied between the secondary and tertiary burner inlets. The total amount of oxygen is identical to the two other oxy-fuel cases but more oxygen is added in the secondary air inlet and less in the tertiary inlet. In the real SSV4 boiler it is not possible to operate the burners with oxygen staging, but the results may have influence on possible future layouts of oxy-fuel burners.

Originally the intention was also to investigate the effect on NOx levels inside the boiler when shifting from air to oxy-fuel combustion. This has however been omitted from the investigation since Pedersen (2009) has shown that the NOx models available in Fluent are very unreliable.

DONG energy

CHAPTER 4

Results and Discussion

As mentioned in Section 2.2.1 on page 6 iterations are performed until monitoring values level out. Evolution of a solution of an oxyfuel case can be seen on Figure 4.1. As can be seen a true steady state solution is never obtained. It has been tested to keep iterating to force at steady state solution, but even several thousands of iterations do not change the fact that the solution keeps oscillating. This behaviour arises from the fact that the CFD model tries to force a steady solution on an inherently unstable flow phenomena.

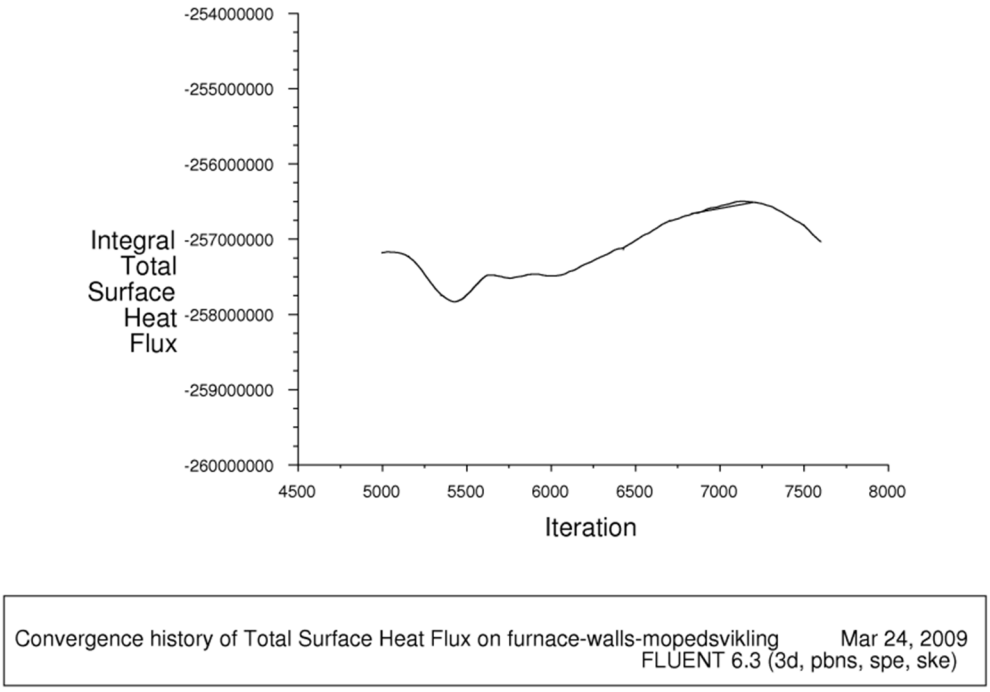

Figure 4.1: heat uptake in a part of the furnace vs. iteration number

4.1 Comparison between air combustion and oxy-fuel combustion

A contour plot of the temperature along the symmetry plane inside the boiler can be seen on Figure 4.2. As expected the temperature is highest just above the burners where the coal volatiles have been burned and the char burnout is large. The recirculated flue gas can be seen as a low temperature near the bottom of the hopper. Comparing with the oxy-fuel temperature levels in the oxy-fuel case, Figure 4.3 on the following page, it can be seen that the temperature levels are lower inside the boiler when firing at oxy-fuel conditions. The decrease in temperature is mainly an effect of the increased flue gas flow through the boiler. The increase in mass flow is a result of a number of compromises considering the temperature

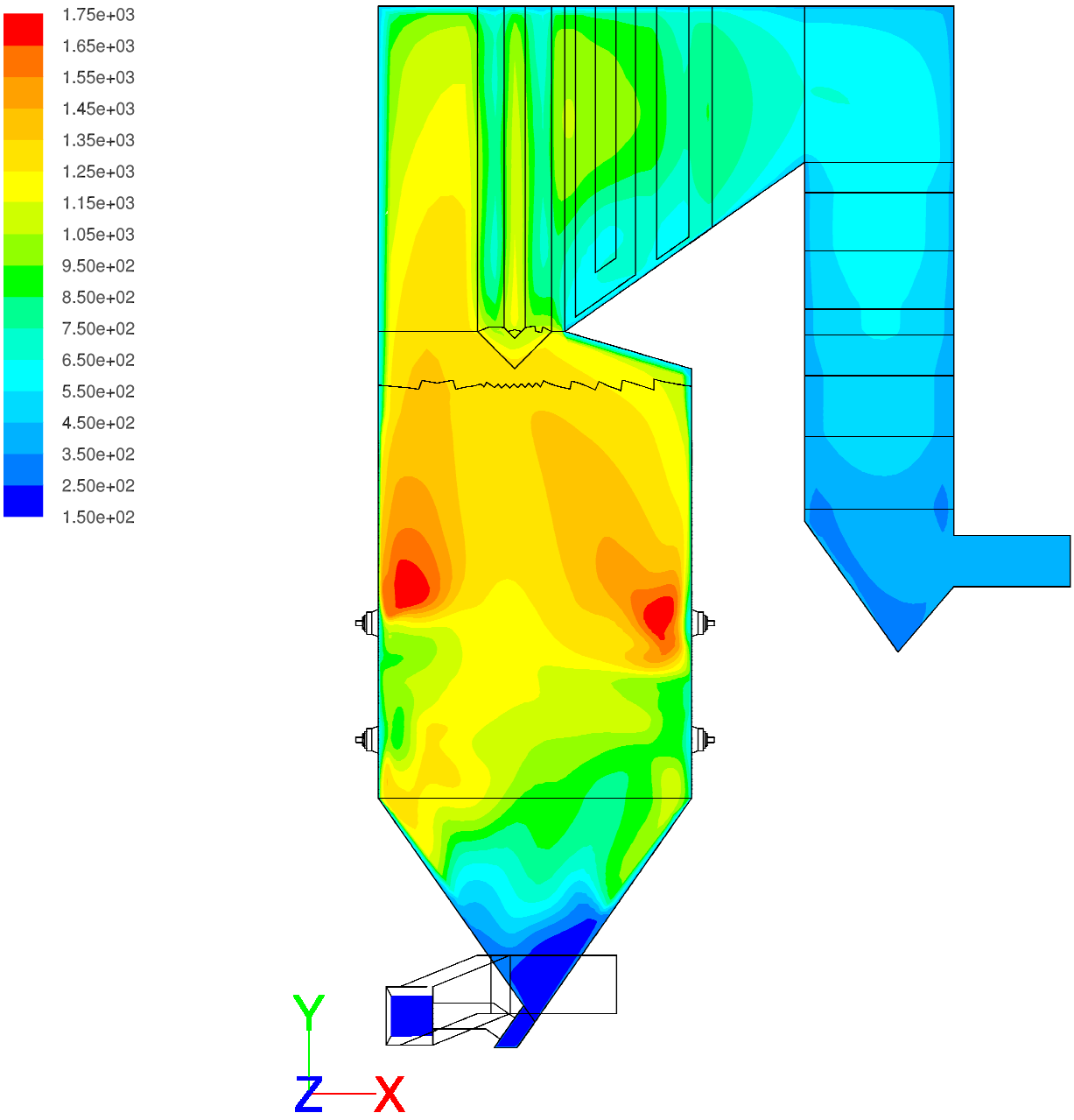

Figure 4.2: Contour plot of temperature, °C, for the air calibration case.

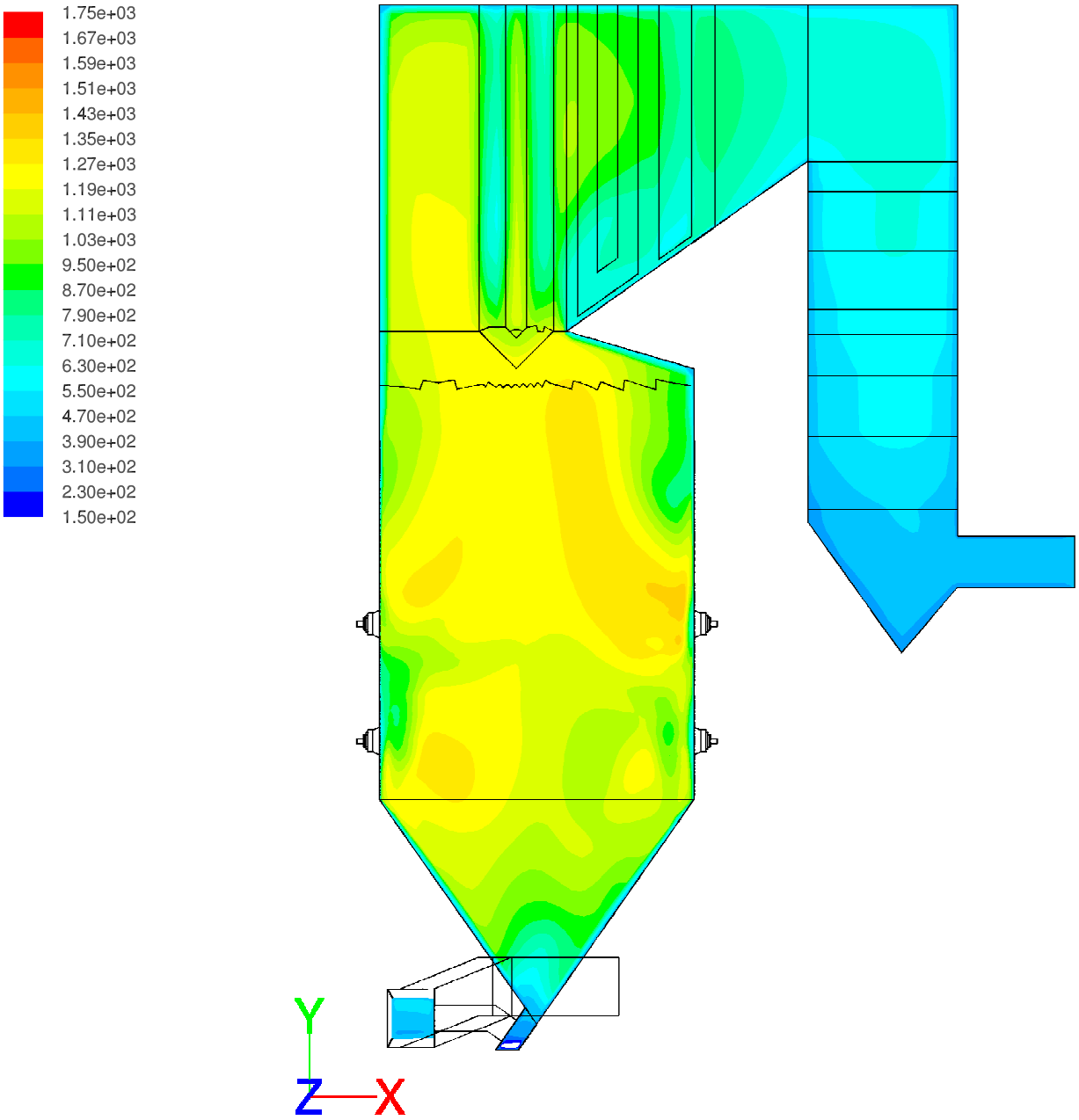

Figure 4.3: Contur plot of temperature, °C, for oxy-fuel case Oxy1.

levels inside the boiler, see Fisker (2010). Secondarily the temperature is lowered by the increase in specific heat capacity, see Table 4.1 on the next page.

Table 4.1: Volume averaged specific heat for air and oxy-fuel combustion

	Cp [kJ/(mol K)]
Air	1.234
Oxy-fuel	1.415

Looking at the first superheaters on Figure 4.5 and 4.6 it can also be seen that the temperature level just before oh3 is higher in the air case.

An overview of the results from the calculations can be seen on Figure 4.4. The total heat flux in the furnace for the air cases is approximately 300 MW with variations around 10 MW. If less variation in the flux is to be obtained, one should probably resort to using more particles in the simulation at the cost of added computational time.

The two oxy-fuel cases yield a heat flux in the furnace of around 255 MW. So it can be seen that the change in heat flux is significantly larger when shifting from air to oxy-fuel combustion than the variations seen by simply exchanging the particle source field. The staging calculation, Oxy-3 in Table 3.4 on page 15, showed no difference in heat flux compared to the two other oxy-fuel cases.

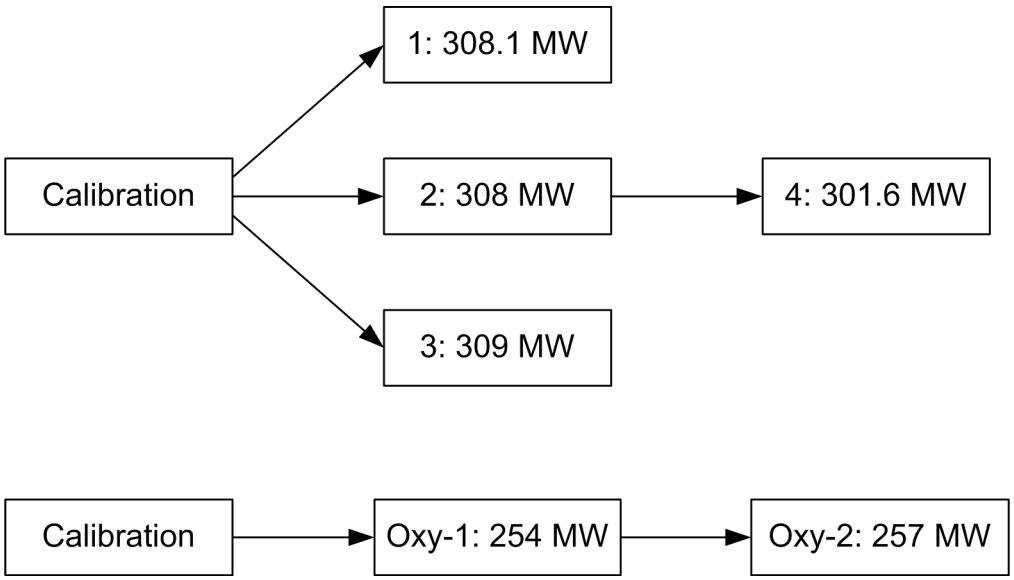

Figure 4.4: overview of the results from the different cases.

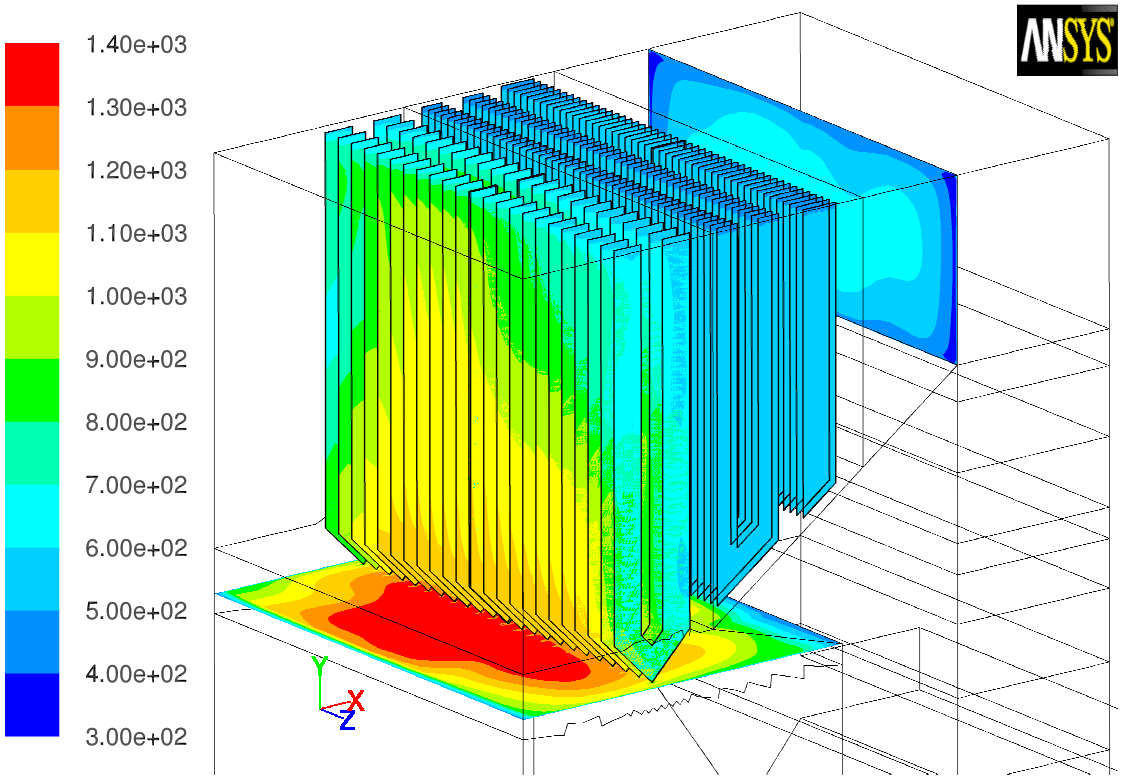

Figure 4.5: Contur plot of temperature, °C, on the first three superheaters for the calibration case.

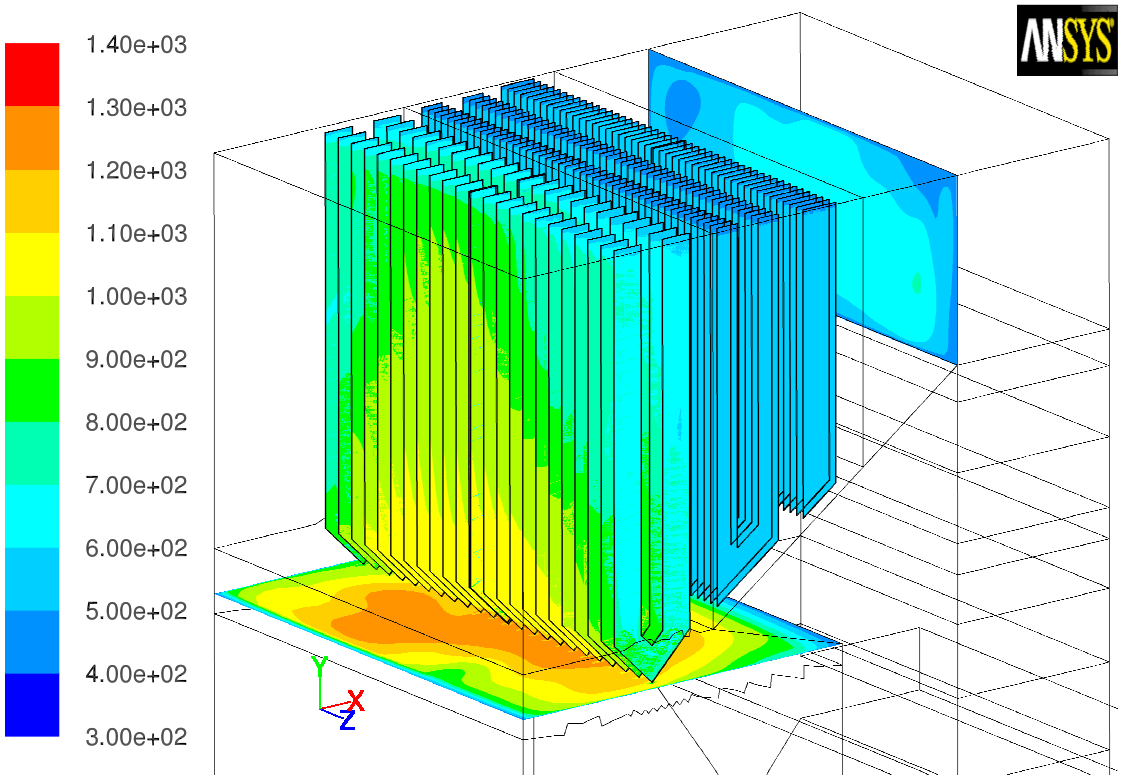

Figure 4.6: Contur plot of temperature, °C, on the first three superheaters for oxy-fuel case Oxy1.

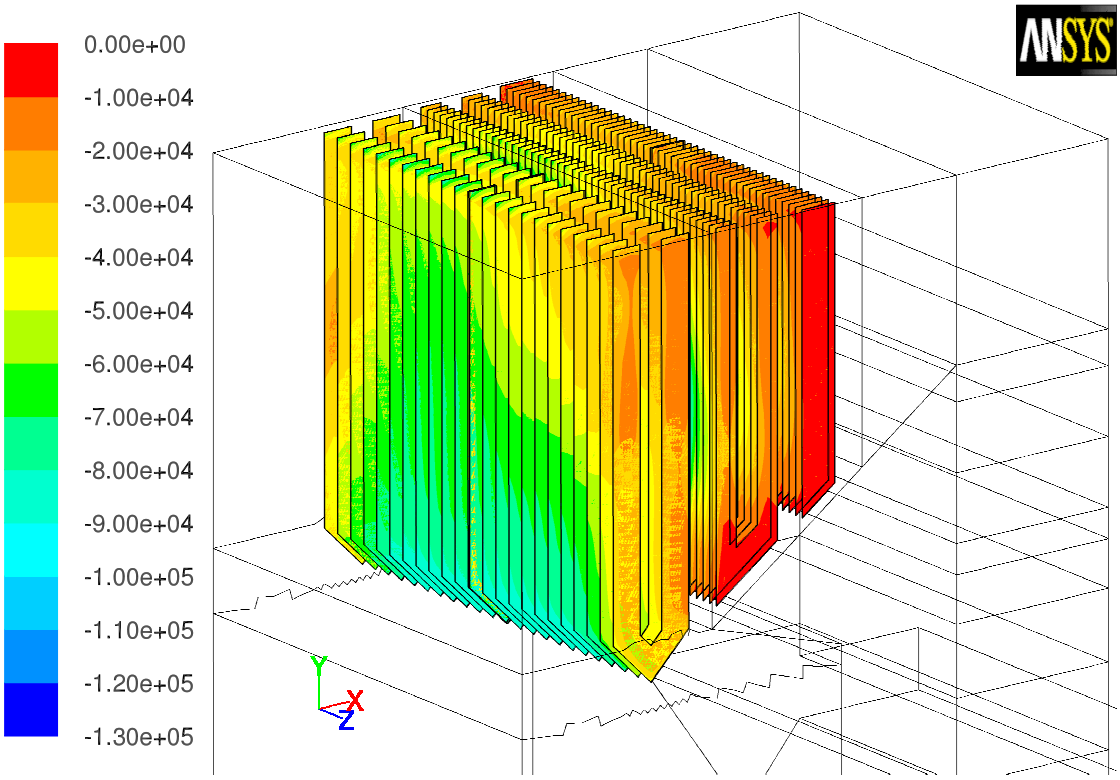

Figure 4.7: Contur plot of heat flux, on the first three superheaters for the calibration case.

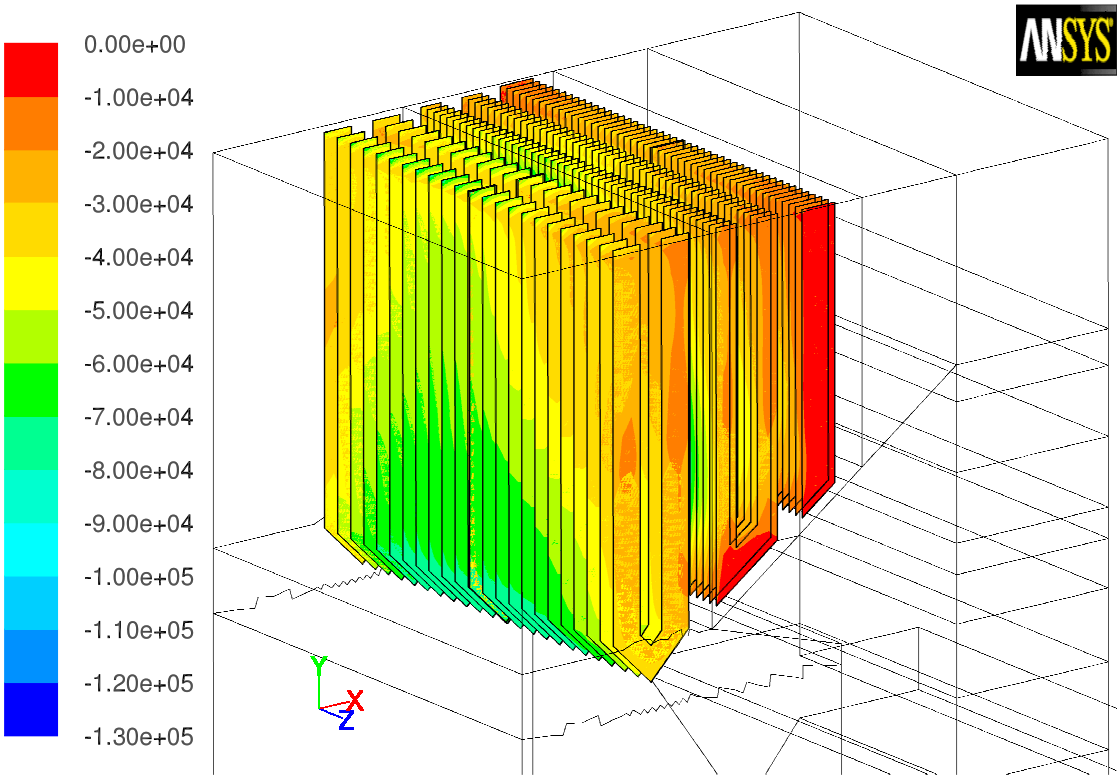

Figure 4.8: Contur plot of heat flux, on the first three superheaters for oxy-fuel case Oxy1.

4.2 Comparison with MOPEDS

A critical parameter for operation of the boiler is to maintain a constant temperature on the steam side of the superheaters. The steam side is not modelled in the CFD model but the total heatflux on the heaters is captured. It can be seen on Figure 4.7 and 4.8 that the distribution of flux is very similar in the two cases and more importantly the level of heat flux is almost identical for air combustion and oxyfuel combustion. Integrating over the three first superheaters reveals that for both air and oxyfuel combustion the total flux is 189 MW. This shows that the CFD model predicts the same trends as the MOPEDS calculations, i.e. with the boundary conditions chosen it is possible to keep the thermal load on the superheaters at the same level when shifting from air to oxyfuel combustion.

Table 4.2: Comparison of furnace heat uptake for CFD calculations and the MOPEDS calculations.

	Air	**Oxyfuel**
MOPEDS	295 MW	260 MW
CFD	300 MW	255 MW

The overall purpose of the present study is to determine whether a CFD simulation captures effects on the heat flux within the SSV4 boiler that are not captured by the MOPEDS calculations. The biggest concern in the MOPEDS calculation has been whether the model is able to capture the radiation heat transfer in the furnace correctly. A comparison can be seen in Table 4.2. As can be seen there are no significant differences in the results obtained from the two fundamentally different types of simulations for the heat flux in the boiler.

One may argue that the shift in the CFD simulation is larger than in the MOPEDS calculation. MOPEDS is however capable of capturing the same trend as the CFD simulation at a much lower computational cost. It is then recommended to use MOPEDS for retrofit calculations as long as one is mainly interested in the main temperature levels and heat fluxes within the boiler. The interaction with the water-steam process in the power plant is furthermore captured in MOPEDS without going to unrealistically long computation times as would be the case with a CFD simulation.

CHAPTER 5

Conclusions

A CFD simulation of a coal fired boiler was performed at normal conditions and at oxy-fuel conditions. A sensitivity study has been performed to test the models sensitivity to the particle model. The difference between the two cases is larger than the sensitivity of the model to the particle source field.

The difference between the two cases compared to the one predicted with MOPEDS is not significant. so MOPEDS is an adequate tool, compared to CFD, to model any changes in the combustion process when operating at oxy-fuel conditions as long as one is mainly interested in the main temperature levels and heat fluxes within the boiler.

DONG energy

Bibliography

Brix, J., P. A. Jensen, and A. D. Jensen (2010). Coal devolatilization and char conversion under suspension fired conditions in O_2/N_2 and O_2/CO_2 atmospheres. *Fuel 89*, 3373–3380.

Chui, G. D. and E. H. Raithby (1990). A finite-volume method for predicting a radiant heat transfer in enclosures with participating media. *J. Heat Transfer 112*, 415–423.

Fisker, D. (2010). Oxyfuel combustion for below zero CO_2 emission - procesteknisk rapport. Technical report, Dong Energy.

Pedersen, J. M. (2009). *CFD based NOx-modelling - PSO report.* Dong Energy A/S.

Raithby, E. H. and G. D. Chui (1993). Computation of radiant heat transfer on a non-orthogonal mesh using the finite-volume method. *Numerical Heat Transfer 23*, 269–288.

Shih, T.-H., W. W. Liou, A. Shabbir, Z. Yang, and J. Zhu (1995). A new κ-ε eddy-viscosity model for high reynolds number turbulent flows - model development and validation. *Computers and Fluids 24*, 227–238.